frontiers | Research Topics

Ocular neurodegenerative diseases: Novel mechanisms, diagnosis, and therapeutic strategies

Edited by
Dan Wen, Hetian Lei and Wensi Tao

Published in
Frontiers in Neuroscience

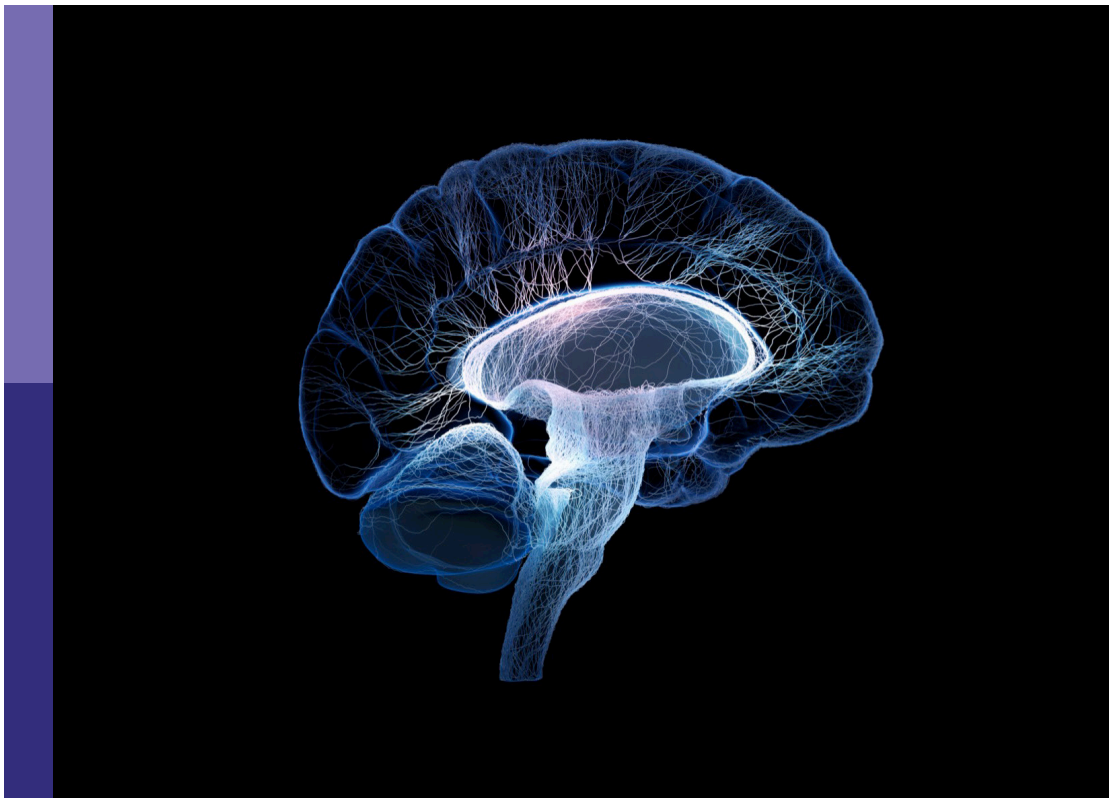

ISSN 1664-8714
ISBN 978-2-8325-3500-4
DOI 10.3389/978-2-8325-3500-4

About Frontiers

Frontiers is more than just an open access publisher of scholarly articles: it is a pioneering approach to the world of academia, radically improving the way scholarly research is managed. The grand vision of Frontiers is a world where all people have an equal opportunity to seek, share and generate knowledge. Frontiers provides immediate and permanent online open access to all its publications, but this alone is not enough to realize our grand goals.

Frontiers journal series

The Frontiers journal series is a multi-tier and interdisciplinary set of open-access, online journals, promising a paradigm shift from the current review, selection and dissemination processes in academic publishing. All Frontiers journals are driven by researchers for researchers; therefore, they constitute a service to the scholarly community. At the same time, the *Frontiers journal series* operates on a revolutionary invention, the tiered publishing system, initially addressing specific communities of scholars, and gradually climbing up to broader public understanding, thus serving the interests of the lay society, too.

Dedication to quality

Each Frontiers article is a landmark of the highest quality, thanks to genuinely collaborative interactions between authors and review editors, who include some of the world's best academicians. Research must be certified by peers before entering a stream of knowledge that may eventually reach the public - and shape society; therefore, Frontiers only applies the most rigorous and unbiased reviews. Frontiers revolutionizes research publishing by freely delivering the most outstanding research, evaluated with no bias from both the academic and social point of view. By applying the most advanced information technologies, Frontiers is catapulting scholarly publishing into a new generation.

What are Frontiers Research Topics?

Frontiers Research Topics are very popular trademarks of the *Frontiers journals series*: they are collections of at least ten articles, all centered on a particular subject. With their unique mix of varied contributions from Original Research to Review Articles, Frontiers Research Topics unify the most influential researchers, the latest key findings and historical advances in a hot research area.

Find out more on how to host your own Frontiers Research Topic or contribute to one as an author by contacting the Frontiers editorial office: frontiersin.org/about/contact

Ocular neurodegenerative diseases: Novel mechanisms, diagnosis, and therapeutic strategies

Topic editors

Dan Wen — Central South University, China

Hetian Lei — Shenzhen Eye Hospital, China

Wensi Tao — University of Miami Health System, United States

Citation

Wen, D., Lei, H., Tao, W., eds. (2023). *Ocular neurodegenerative diseases: Novel mechanisms, diagnosis, and therapeutic strategies*. Lausanne: Frontiers Media SA. doi: 10.3389/978-2-8325-3500-4

Table of contents

frontiers | Frontiers in Neuroscience

TYPE Editorial
PUBLISHED 01 September 2023
DOI 10.3389/fnins.2023.1274778

OPEN ACCESS

EDITED AND REVIEWED BY
Benjamin Thompson,
University of Waterloo, Canada

*CORRESPONDENCE
Dan Wen
✉ wendan@csu.edu.cn
Hetian Lei
✉ leihetian18@hotmail.com

RECEIVED 08 August 2023
ACCEPTED 14 August 2023
PUBLISHED 01 September 2023

CITATION
Wu W, Li Y, Hu T, Tao W, Wen D and Lei H (2023) Editorial: Ocular neurodegenerative diseases: novel mechanisms, diagnosis, and therapeutic strategies.
Front. Neurosci. 17:1274778.
doi: 10.3389/fnins.2023.1274778

Editorial: Ocular neurodegenerative diseases: novel mechanisms, diagnosis, and therapeutic strategies

Wenyi Wu[1], Yuanjun Li[1], Tu Hu[1], Wensi Tao[2], Dan Wen[1]* and Hetian Lei[3,4]*

[1]Ophthalmology of Xiangya Hospital, Central South University, Changsha, China, [2]Sylvester Comprehensive Cancer Center, University of Miami, Miami, FL, United States, [3]Department of Ophthalmology, The Third Affiliated Hospital of Xinxiang Medical University, Xinxiang, China, [4]Shenzhen Eye Hospital, Jinan University, Shenzhen Eye Institute, Shenzhen, China

KEYWORDS

neurodegeneration, high myopia, glaucoma, retinopathy, macular degeneration

Editorial on the Research Topic
Ocular neurodegenerative diseases: novel mechanisms, diagnosis, and therapeutic strategies

Ocular neurodegeneration including high myopia, glaucoma, macular degeneration, optic nerve atrophy, and retinopathy can lead to blindness without timely and appropriate treatment. As the retina is actually an extension of the brain, studies on the molecular mechanisms by which these eye diseases develop are currently one of the hottest research areas in neuroscience.

Investigations on neuronal correction of visual deficits have enriched our knowledge of functional eye diseases including ocular neurodegeneration. Nevertheless, it is urgently needed to further our understanding of how these eye diseases develop. Notably, novel therapies with superstar pharmacological intervention or new methods such as gene therapy or stem cell therapy have been attracted into this research area. The aim of this Research Topic "*Novel mechanisms, diagnostic and therapeutic strategies for ocular neurodegeneration*" is to extend our knowledge related to retina and vision disorders by bringing together work in ophthalmology, optometry, psychology, neuroscience, and vision science.

Molcak et al. have summarized the expression, distribution, functions, and interactions of purinergic receptors in the retina and included potential crosstalk with other systems. Dissection of how these processes are affected will improve our understanding of the mechanisms that drive age-related macular degeneration (AMD).

Avrutsky et al. have shown their original research data that caspase-9 inhibition has significant retinal protection from retinal vein occlusion (RVO). To be more specific, they have compared the therapeutic effect of caspase-9 inhibition with VEGF neutralization in an established mouse model of RVO, and they have conducted a series of examinations, including fundus angiography, optical coherence tomography (OCT), and electroretinography (ERG), for analyzing pathological changes.

Ye et al. have investigated the long-term safety, efficacy, and binocular balance of monovision surgery using Implantable Collamer Lens (ICL) V4c implantation and Femtosecond Laser-Assisted *in situ* Keratomileusis (FS-LASIK) for the treatment of myopic patients with presbyopia. The results show that CL V4c implantation and FS-LASIK monovision treatment have long-term safety and binocular visual acuity at various distances.

Lan et al. have demonstrated the control ability and characteristics of fixational displacement among healthy adults in a convenient method by using eye-tracking

technology. A total of 100 healthy people were recruited for this study, providing an objective view that the fixation stability decreased significantly in the group aged over 50 years old.

Chen et al. have reported a non-invasive diagnosis tool to assess blood flow perfusion in a visual pathway for ocular ischemic syndrome (OIS), which is attributable to chronic hypoperfusion caused by marked carotid stenosis. They have detected blood flow perfusion in a visual pathway by 3D pseudocontinuous ASL (3D-pCASL) using 3.0T MRI (magnetic resonance imaging). The results indicate that that there is a lower blood flow perfusion value in the visual pathway in patients with OIS.

Velmurugan et al. have summarized different gene therapy methods in Leber hereditary optic neuropathy (LHON), suggesting that a mitochondrially targeted AAV (adeno-associated virus) gene therapy is more efficient than an allotopic AAV gene therapy for rescuing the LHON phenotype.

Zheng et al. have presented a surprising treatment for restoring vision in adult amblyopia rats. By using molecular and histological approaches, they have revealed that low-frequency repetitive transcranial magnetic stimulation (rTMS) reinstates the amplitude of visual evoked potentials without influencing the impaired depth perception of amblyopic rats. They conclude that rTMS enhances functional recovery and visual plasticity in an adult amblyopic animal model.

Zhang et al. have given a bibliometric analysis of apoptosis in glaucoma. This research will broaden our comprehension about the role of apoptosis in the process of glaucoma and provide guidelines for us in basic research and disease treatment.

Zhen et al. have summarized rhodopsin-associated retinal dystrophy and its disease mechanisms and therapeutic strategies. In particular, they emphasize that innovative therapy strategies, such as gene therapy (including gene editing, neuroprotection, and optogenetics) and stem cell therapy, are promising methods for the future treatment of retina pigmentosa. Nevertheless, greater efforts are needed from basic researchers and clinicians to facilitate the translation of recent research findings from the laboratory into clinical practice.

Xiang et al. have interrogated the question of whether children with monocular myopia need to wear glasses. They consider the facts that (1) monocular myopia could lead to the accommodative dysfunction and unbalanced input of binocular visual signals, resulting in myopia progression; (2) monocular myopia may also be accompanied by stereopsis dysfunction, and long-term uncorrected monocular myopia may worsen stereopsis acuity in adulthood; (3) patients with monocular myopia could exhibit stereopsis dysfunction at an early stage; thus, they come to a conclusion that children with monocular myopia must wear glasses to restore binocular balance and visual functions, thereby delaying myopia progression.

Boal et al. have presented a study showing that retinal ganglion cells adapt to ionic stress in experimental glaucoma. Their data indicate that in response to prolonged IOP (intraocular pressure) elevation, RGCs (retinal ganglion cells) undergo an adaptive process that reduces sensitivity to changes in K+ while diminishing excitability. These experiments give insight into the RGC response to IOP stress and lay the groundwork for mechanistic investigation into targets for neuroprotective therapy.

Li et al. have systemically analyzed independent risk factors for the progression of different degrees of diabetic retinopathy and non-diabetic retinopathy among type 2 diabetic patients. They conclude that young age, short axial length, and higher levels of FBG (fasting blood glucose) and urinary albumin creatinine ratio (UACR) were the independent risk factors for the progression of diabetic retinopathy in type 2 diabetes.

Wareham et al. have presented data on collagen mimetic peptide repair of the corneal nerve bed in a mouse model of dry eye disease. Their data suggest that repair of underlying collagen in conditions that damage the ocular surface could represent a novel therapeutic avenue in treating a broad spectrum of diseases or injury.

Wang and Wang have shown a preliminary study of spectral-domain optical coherence tomography (OCT) combined with ERG in the assessment of conbercept for neovascular age-related macular degeneration (nAMD). Their data suggest that (1) conbercept is useful for the short-term treatment of nAMD; (2) it can safely improve the visual acuity of affected eyes; and (3) it can restore the structure and function of the retina.

Zhou et al. have shown that increased intraocular inflammation in retinal vein occlusion is independent of circulating immune mediators and is involved in retinal oedema. Their results suggest that (1) intraocular inflammation in RVO is driven primarily by local factors but not circulating immune mediators; (2) intraocular inflammation may promote macular oedema through the PI3K-Akt, Ras, MAPK, and Jak/STAT signaling pathways in RVO; and (3) systemic factors, including cytokines and lipid levels, may be involved in retinal microvascular remodeling.

Wang et al. have assessed the precision and reliability of a novel computerized heterophoria test (CHT). Their data suggest that (1) the CHT can be used to demonstrate excellent inter- and intra-examiner repeatability and good correlation with the POCT (prism-neutralized objective cover test); (2) the differences between the CHT and POCT are within the permissible range of error; and (3) the CHT could provide a precise and reliable measurement for clinical applications.

Altogether, this Research Topic of articles emphasizes novel diagnostic and therapeutic approaches for a variety of ocular neurodegeneration diseases, which are necessary to further explore.

Author contributions

WW: Funding acquisition, Writing—original draft. WT: Writing—review and editing. YL: Writing—review and editing. TH: Funding acquisition, Writing—review and editing. DW: Writing—review and editing. HL: Conceptualization, Funding acquisition, Writing—original draft, Writing—review and editing.

Funding

This work was supported by the National Natural Science Foundation of China (82070989 to HL and 82271109 to WW), the Introduction Plan of High-Level Foreign Experts (G2022026027L to HL), the National Natural Science Foundation of China

(81900890), Natural Science Foundation of Hunan Province (2021JJ40991), and China Postdoctoral Science Foundation Grant (2018M643004 to TH).

Conflict of interest

The authors declare that the research was conducted in the absence of any commercial or financial relationships that could be construed as a potential conflict of interest.

Publisher's note

All claims expressed in this article are solely those of the authors and do not necessarily represent those of their affiliated organizations, or those of the publisher, the editors and the reviewers. Any product that may be evaluated in this article, or claim that may be made by its manufacturer, is not guaranteed or endorsed by the publisher.

frontiers | Frontiers in Neuroscience

TYPE Original Research
PUBLISHED 19 January 2023
DOI 10.3389/fnins.2023.1109735

OPEN ACCESS

EDITED BY
Dan Wen,
Central South University, China

REVIEWED BY
Jinrong Li,
Sun Yat-sen University, China
Benjamin Thompson,
University of Waterloo, Canada

*CORRESPONDENCE
Wenqiu Zhang
✉ zhangwenqiu4541675@163.com

SPECIALTY SECTION
This article was submitted to Visual Neuroscience, a section of the journal Frontiers in Neuroscience

RECEIVED 28 November 2022
ACCEPTED 02 January 2023
PUBLISHED 19 January 2023

CITATION
Zheng J, Zhang W, Liu L and Hung Yap MK (2023) Low frequency repetitive transcranial magnetic stimulation promotes plasticity of the visual cortex in adult amblyopic rats. *Front. Neurosci.* 17:1109735. doi: 10.3389/fnins.2023.1109735

Low frequency repetitive transcranial magnetic stimulation promotes plasticity of the visual cortex in adult amblyopic rats

Jing Zheng[1,2], Wenqiu Zhang[1,2]*, Longqian Liu[1,2] and Maurice Keng Hung Yap[3]

[1]Department of Ophthalmology, West China Hospital, Sichuan University, Chengdu, China, [2]Department of Optometry and Visual Science, West China Hospital, Sichuan University, Chengdu, China, [3]School of Optometry, The Hong Kong Polytechnic University, Hong Kong SAR, China

The decline of visual plasticity restricts the recovery of visual functions in adult amblyopia. Repetitive transcranial magnetic stimulation (rTMS) has been shown to be effective in treating adult amblyopia. However, the underlying mechanisms of rTMS on visual cortex plasticity remain unclear. In this study, we found that low-frequency rTMS reinstated the amplitude of visual evoked potentials, but did not influence the impaired depth perception of amblyopic rats. Furthermore, the expression of synaptic plasticity genes and the number of dendritic spines were significantly higher in amblyopic rats which received rTMS when compared with amblyopic rats which received sham stimulation, with reduced level of inhibition and perineuronal nets in visual cortex, as observed *via* molecular and histological investigations. The results provide further evidence that rTMS enhances functional recovery and visual plasticity in an adult amblyopic animal model.

KEYWORDS

amblyopia, visual plasticity, repetitive transcranial magnetic stimulation, GABA, perineuronal nets

Introduction

The visual neural pathways are not fully developed in the early postnatal period of mammals. Besides genetic influences, the neural pathways may be adjusted and altered by visual experience. This experience-dependent visual cortex plasticity decreases rapidly in early life. Little plasticity is observed in adulthood (Hensch, 2005). Monocular and binocular abnormal visual experiences, such as form deprivation and interocular differences in retinal inputs, can cause underdevelopment of vision in the eye receiving the poorer quality input. This condition, known as amblyopia, is clinically defined as a disorder in which the eye shows decreased vision because of abnormal development of the visual pathway in childhood (Birch, 2013), without obvious organic ocular disease. Amblyopia is the most common reason for vision impairment in a single eye among children and adolescents, affecting 1–2% of the total population (Hashemi et al., 2018; Li et al., 2019). The time window when the visual cortex exhibits the greatest plasticity is termed the critical period (Hensch and Quinlan, 2018), after which the plasticity of the visual cortex is receded, making the treatment of adult amblyopia a clinical challenge (Simons, 2005). More recently, it has been shown that visual cortical plasticity in adulthood may be revived with

certain pharmacological (Maya Vetencourt et al., 2008; Silingardi et al., 2010) or environmental interventions (Greifzu et al., 2014; Erchova et al., 2017).

Emerging evidence suggests that the inhibitory neural pathways utilizing gamma-aminobutyric acid (GABA) as a neurotransmitter play a key role in the regulation of visual cortical plasticity. The level of GABAergic inhibition in the visual cortex is relatively low at birth, and the critical period begins when inhibition development reaches a certain threshold. The inhibition level is increased due to continual maturation of the pathways, following which a second threshold is reached that triggers the closure of the critical period (Spolidoro et al., 2009; Heimel et al., 2011). The inhibitory interneurons expressing the calcium-binding protein parvalbumin (PV) are the primary targets of visual input from the lateral geniculate body. As the cortex develops, perineuronal nets (PNNs) composed of extracellular matrix (ECM) are continuously deposited around the bodies and the dendrites of PV interneurons and other neurons, restricting the changes in synaptic connections and leading to the structural closure of critical periods. The artificial degradation of chondroitin sulfate proteoglycans (CSPGs), the primary component of ECM, may reactivate cortical plasticity (Pizzorusso et al., 2002; Heimel et al., 2011).

Invented in 1985, transcranial magnetic stimulation (TMS) is one of several non-invasive brain stimulation (NIBS) modalities (Polanía et al., 2018). How a magnetic pulse influences neuronal activity is described elsewhere (Hallett, 2007). Repetitive TMS (rTMS) refers to the continuous stimulation on the local cortex with a fixed frequency and intensity, which induces persistent current in the brain and promotes synaptic long-term potentiation (LTP) or long-term depression (LTD) (Hallett, 2007).

Previous studies have shown that applying different rTMS modes to particular brain regions in animals may alter neuronal activity by up or downregulating the inhibition level in the cortex, promoting the recovery of some brain-related disorders (Hoppenrath et al., 2016; Jazmati et al., 2018; Tan et al., 2018; Wu et al., 2018). The clinical application of rTMS in neuropsychiatric diseases, such as severe depression, rehabilitation exercise after stroke, schizophrenia, and drug addiction, is becoming more common. In the context of vision, it has been shown that both high- and low-frequency rTMS applied to the visual cortex temporarily improved contrast sensitivity in the adult amblyopic eye (Thompson et al., 2008). Multiple applications of continuous theta-burst stimulation (cTBS), a specific type of rTMS with high frequency and short stimulation time, over 5 days, appear to improve high spatial frequency contrast sensitivity in the adult amblyopic eye. These improvements were stable, lasting over 78 days, suggesting that rTMS may produce long-lasting effects on the amblyopic visual cortex (Clavagnier et al., 2013). Another study showed a temporary and significant improvement in visual and stereoscopic acuities in patients with amblyopia after a single application of cTBS, with decreased interocular suppression (Tuna et al., 2020). Other forms of NIBS involving low currents, such as anodal transcranial direct current stimulation (a-tDCS), have also been shown to improve contrast sensitivity in the adult amblyopic eye (Spiegel et al., 2013).

Although these studies suggest that rTMS may promote improvements in certain visual functions in the adult amblyopic eye, little is known about the mechanisms involved. We speculate that in adult amblyopia, rTMS alters the activity of the visual cortex *via* regulation of genes and inhibitory neural pathways involved in plasticity, to cause a change in visual function. We conducted a series of experiments using an adult rat amblyopia model to further our understanding of changes in the molecular and structural mechanisms associated with rTMS application.

Materials and methods

Animals

A total of 63 Wistar rats of both genders were used in this study which was approved by the Animal Ethics Committee of Sichuan University and adhered to the guidelines for the Use of Animals in Ophthalmic and Vision Research. The rats were kept in the Animal Experiment Center of West China Hospital under a 12/12 h light/dark cycle and 20–23°Cambient temperature, with *ad libitum* access to water and food. The pups lived with their mothers until weaning at P21. The animals were divided into four groups using a table of random numbers: control animals treated with sham stimulation (Con+Sham, n = 16), monocularly deprived animals treated with sham stimulation (MD+Sham, n = 16), control animals treated with rTMS (Con+rTMS, n = 15), and monocularly deprived animals treated with rTMS (MD+rTMS, n = 16). The experimental timelines of four groups are shown in **Figure 1**.

Monocular deprivation

The animals were anesthetized with 1.25% avertin (2,2,2 tribromoethanol; 10 mL/kg) by intraperitoneal injection at P12. Right upper and lower eyelid margins of 1 mm each were excised, and the eyelids were subsequently stitched shut with 6-0 silk thread. Chlortetracycline was applied on the eyelid closure every day until complete cicatrization. The eyelids were reopened at P43 followed by 24 h recovery to undergo visual function testing before the rTMS treatment. Rats showing lid reopening or infection of the eyelid during MD were excluded from the experiments and not included in the statistical analysis. Control animals also underwent anesthesia and eyelids suture with immediate opening at P12 and P43.

rTMS

A figure-of-eight coil with a diameter of 40 mm was used to deliver rTMS to conscious rats through an RT-100 Stimulator (JJWF-medicine, Chengdu, China). Following a previously described technique (Castillo-Padilla and Funke, 2016), the rat's body was wrapped with a soft towel, and its sides were held lightly by placing the index finger on its cheek gently to fix the head. The low-frequency 1 Hz mode with a total of 600 pulses for 10 min was selected, and the stimulation intensity was applied with 25% of maximal machine output below the motor threshold. The motor threshold (MT) was measured as described elsewhere (Fujiki et al., 2020). The stimulator intensity was reduced on motor cortex of rats gradually by 1% of maximum stimulator output (MSO) until half of the motor-evoked potentials under certain intensity higher than 50 μV were produced, and this intensity was recorded as the MT. The average MT of five conscious rats was 28 ± 2.24% MSO. During active stimulation, the center of the coil was placed 5 mm above the skin of the rat's occiput.

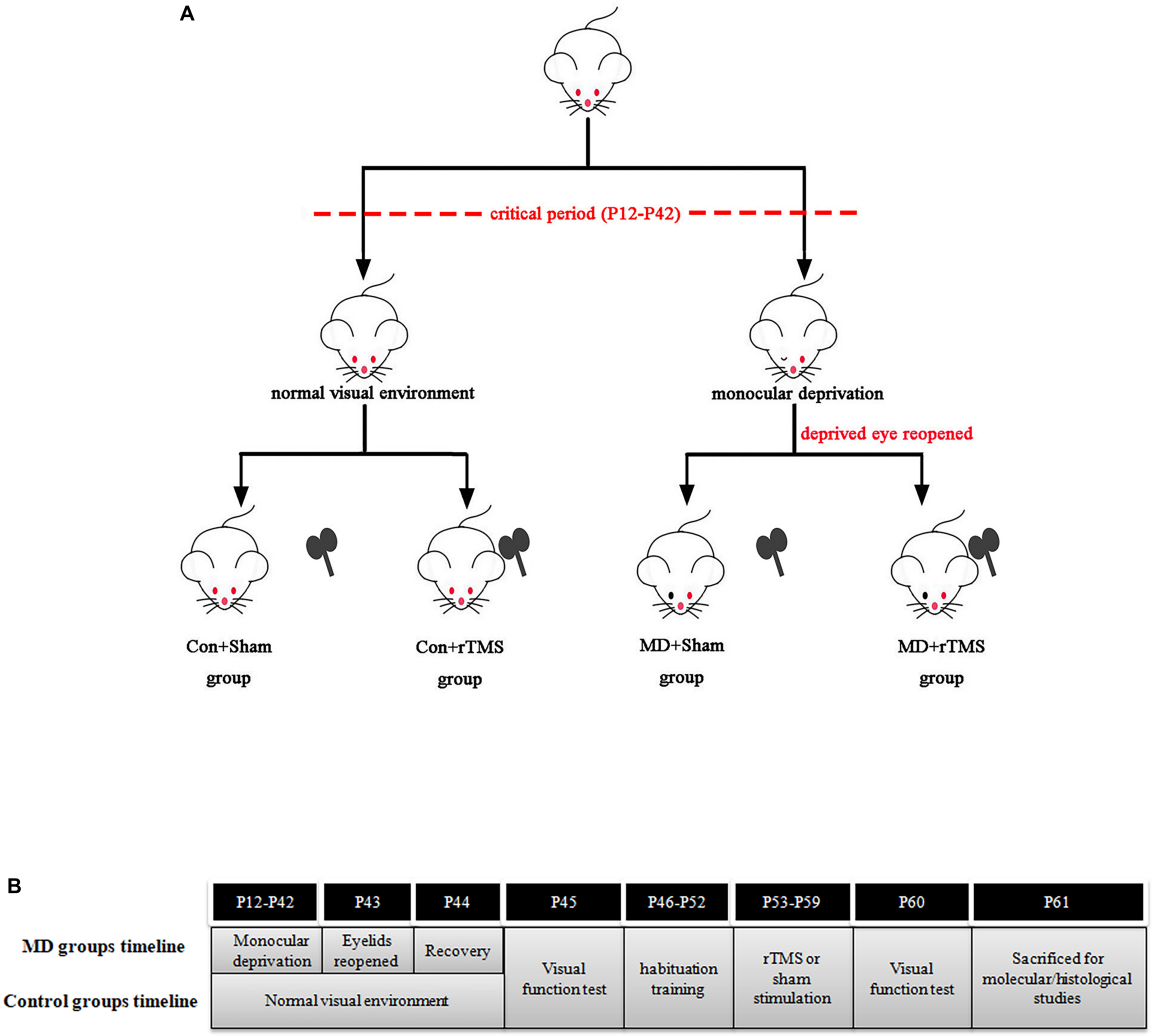

FIGURE 1
(A) The four groups in this study. **(B)** Timelines of monocular deprivation (MD) groups and control groups.

For sham stimulation, the distance between the coil and the rat's head was increased to 15 cm. The stimulation regime was conducted every day on each animal between 6:00 p.m. and 8:00 p.m. for 7 days. To aid adaptation to the environment where rTMS was applied, the animals experienced handling habituation training with the stimulation side of the coil facing the opposite direction at 6:00 p.m. for 7 days before sham or active stimulation. After acclimatization, the stressful defecation/urination in animals was noticeably reduced.

Visual evoked potentials (VEPs)

The animals in each group underwent flash VEP (fVEP) testing before and after treatment (at P45 and P60) to assess individual objective visual functions. After 30 min of dark adaptation, the animals were anesthetized with 1.25% avertin (10 mL/kg) by intraperitoneal injection. A visual electrophysiological apparatus (IRC Medical Equipment, Chongqing, China) was used following the International Society for Clinical Electrophysiology of Vision (ISCEV) standard. Electrodes were placed according to the Freeman and Sohmer (1995) and Yi et al. (2020) methods. The silver needle recording electrode was placed under the skin at the midpoint between the ears, the reference electrode was placed in the oral cavity, and the ground electrode was implanted into the tail. During flash stimulation, the unrecorded eye was occluded with a black cloth. The parameters of the flashing light were as follows: frequency of 1 Hz, flash intensity of 3.0 cd/m^2 and band-pass filtered from 1 to 100 Hz with the superposition enforced 100 times. The amplitude of P1 (from negative N1 wave through positive P1 wave peak) was recorded, and then the contralateral vs. ipsilateral value (C/I value, contralateral value: the amplitude of P1 derived from the deprived eyes in MD rats or the right eyes in control rats; ipsilateral value: the amplitude of P1 derived from the non-deprived eyes in MD rats or the left eyes in control rats) was calculated and analyzed. The C/I value reflects ocular dominance (OD) of the preferences of the neurons in the visual cortex (Sawtell et al., 2003).

Visual cliff test

A modification of the previously published cliff apparatus (Mazziotti et al., 2017; Castaño-Castaño et al., 2019) was applied to

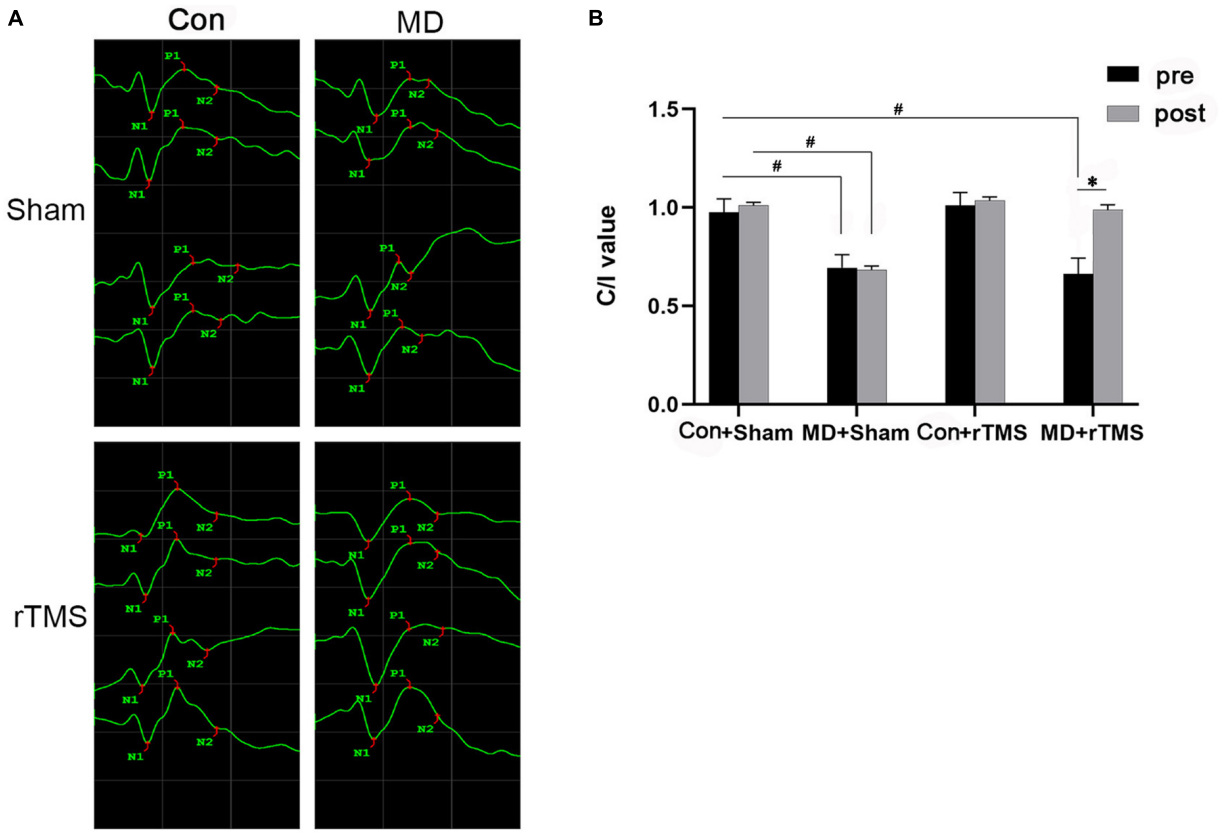

FIGURE 2
Flash visual evoked potentials (fVEP) before and after treatment in each group. **(A)** The fVEP waveform changes before and after intervention in the four groups. The waveforms from top to bottom in the Con groups were right eye, right eye after intervention, left eye, and left eye after intervention. In monocular deprivation (MD) groups, the waveforms from top to bottom were deprived eye, deprived eye after intervention, non-deprived eye, and non-deprived eye after intervention. **(B)** P1-wave amplitude of fVEP in each group was analyzed before and after intervention, and the data are presented as contralateral vs. ipsilateral value (C/I) value, as assessed by repeated-measures analysis of variance (ANOVA) with Bonferroni's correction. Following repetitive transcranial magnetic stimulation (rTMS), the C/I value of amblyopic rats improved significantly compared to the previous data. No improvement was observed in amblyopic rats exposed to sham stimulation. Data are expressed as mean ± standard error of the mean (SEM). # denotes significant comparison among MD and Con+Sham group, $p < 0.001$; *indicates significant difference between MD+rTMS pre and after rTMS, $p < 0.001$.

evaluate the depth perception of rats before and after treatment (at P45 and P60). The cliff apparatus consisted of an upper and a lower part made of polymethyl methacrylate with the open side directed upward. The four inside walls of the upper box (84 × 53 × 41 cm) were covered with black matte cardboard, and the floor was divided into two regions of equal size (42 × 53 cm). Underneath one region, a checkerboard was made up of black and white squares (3 × 3 cm), defined as the "up" zone (Figure 3A). Another transparent region was the "down" zone, and the checkerboard was placed directly under it at 30 cm to create a cliff. Two incandescent lamps were placed below two patterned checkerboards, respectively, on the bottom of the lower box (84 × 53 × 34 cm) to light up the surfaces of both zones with similar dim brightness. The luminous intensity at the height of rat eyes was measured by a luxmeter (PM6612, PeakMeter, China) set at approximately10 lux. Before the experiment, the animals were acclimated to the room for 30 min. Then, the animals were initially placed at the junction of the two zones and allowed to freely explore the surfaces for 5 min. The rats' movement track was recorded using an infrared camera (8QS3, Xiaomi, China) during the experiment. Between the trials, the zones surface was cleaned with 15% alcohol. The time spent on the respective zones was recorded manually, and then the discrimination index was calculated using the formula: $\frac{t(U)-t(D)}{t(T)}$. t(U): time on "up" zone; t(D): time on "down" zone; t(T): total time.

qRT-PCR

A total of 16 rats (n = 4/group) were sacrificed after treatment for synaptic plasticity gene array analysis. Following deep anesthesia with 1.25% avertin (10 mL/kg) by intraperitoneal injection, the rats were decapitated, and the brain was rapidly removed and placed on ice. According to the rat brain atlas (Paxinos and Watson, 2007), the binocular zone in the primary visual cortex (V1B) contralateral to the deprived eye in MD rats or contralateral to the right eye in control rats was dissected carefully. The total RNA of tissues was isolated and purified using TRIzol Plus RNA Purification Kit (Invitrogen). Subsequently, reverse transcription was conducted using the QuantiNova Reverse Transcription Kit (Qiagen). According to the manufacturer's guidelines, gene expression alterations were assessed using a synaptic plasticity gene array (RT^{2}Profiler PCR Array Rat Synaptic Plasticity, Cat. no. 249950, Qiagen) and QuantiNova SYBR Green PCR Kit (Qiagen).

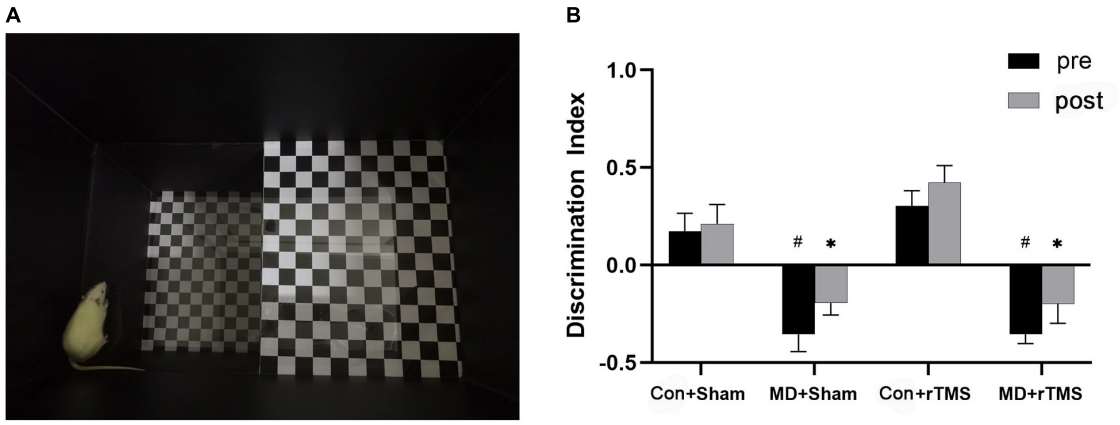

FIGURE 3
(A) An adult rat is exploring the "down" zone in the visual cliff device, while the actual light intensity during behavioral experiments is much dimmer than the environment in this picture. **(B)** Discrimination index was used to quantify the depth perception of rats by repeated-measures analysis of variance (ANOVA) with Bonferroni correction. After repetitive transcranial magnetic stimulation (rTMS), the discrimination index of monocular deprivation (MD) rats did not differ significantly from the baseline and was significantly lower than in Control rats. Data are expressed as mean ± standard error of the mean (SEM). # represents significant comparison among MD and Con+Sham group before receiving stimulation, $p < 0.05$; *indicates significant comparison among MD and Con+Sham groups after receiving the stimulation, $p < 0.05$.

The classification and gene array panels are described in Supplementary Table 1. The PCR process was performed on QuantStudio3 system (Thermo Fisher), and the data from all groups were entered into an online system[1] for analysis. Fold change (FC, gene expression relative ratio) was calculated using the classical $\Delta\Delta$Cq method. The changes in gene expression levels between the groups were considered significant if: (1) the gene expression was up- or downregulated by 50% (FC > 1.5 or FC < 1/1.5); (2) the *p*-value was <0.05 for comparison between groups.

Western blot

All the rats (n = 4/group) were anesthetized by intraperitoneal injection with 1.25% avertin (10 mL/kg) and then decapitated. The brain was carefully removed, and V1B contralateral to the deprived eye in MD rats or contralateral to the right eye in control rats was dissected. Brain tissues were immersed in RIPA lysis buffer (Beyotime), followed by lysis in an Ultrasonic Pulverizer (SCIENTZ, Ningbo, China). The protein in the lysate was quantified by BCA Protein Assay Kit (Beyotime). An equivalent of 20 μg was separated by 10% SDS-PAGE (Epizyme) and transferred to polyvinylidene difluoride (PVDF) membranes (Millipore). Subsequently, the membranes were blocked with 5% skimmed milk in TBS containing 0.1% Tween (TBST, BioFroxx) at room temperature (20–25°C) for 2 h, and incubated in primary antibody at 4°C overnight: (1) GABA synthase: GAD65, 1:1000 (ab239372, Abcam); GAD67, 1:1000 (ab213508, Abcam); (2) GABA transporters: VGAT, 1:1000 (131002, Synaptic System); (3) GABA receptors: GABAAα1, 1:1000 (ab252430, Abcam); GABAAα3, 1:2000 (12708-1-AP, Proteintech); (4) Neurotrophin: BDNF, 1:1000 (AB108319, Abcam); (5) Synapse-related proteins: Syntaxin, 1:1000 (ab272736, Abcam); PSD95, 1:2000 (ab238135, Abcam); (6) reference protein protein glyceraldehyde-3-phosphate dehydrogenase (GAPDH) (MA5-15738, Invitrogen). The blots were washed the next day with TBST (3 × 10 min), incubated with secondary antibody (anti-rabbit, 1:5000, ab6721, Abcam; anti-mouse, 1:5000, 511203, Zenbio) at room temperature for 1 h, then washed in TBST (3 × 10 min). Finally, the blots were immersed in ECL Chemiluminescent Substrate (Biosharp) and visualized using ChemiDoc MP system (Bio-Rad). The gray scale value of the proteins was analyzed using ImageJ (NIH), and the ratio of the target protein to internal reference protein GAPDH was calculated.

Immunofluorescence

After anesthesia using intraperitoneal injection with 1.25% avertin (10 mL/kg), rats were transcardially perfused with 150 mL of 0.9% saline solution, followed by 100 mL of 4% paraformaldehyde. The brains were removed and immersed in 4% paraformaldehyde at 4°C overnight, and then immersed in 30% sucrose solution until they sank to the bottom. The rats' occipital lobes were cut coronally into 20 μm-slices using a cryostat (Leica) and mounted on slides. The slices were from 2 to 4 sections of an animal, and 3–4 animals (Con+Sham, n = 4; MD+Sham, n = 4; Con+rTMS, n = 3; MD+rTMS, n = 4) were used for each group. After drying, the slides were blocked in phosphate-buffered saline (PBS) containing 0.1% Triton X-100 (Solarbio) and 5% normal goat serum (Solarbio) at room temperature (20–25°C) for 1 h and incubated with primary antibodies parvalbumin (1:100, ab181086, Abcam) and lectin from Wisteria floribunda agglutinin (1:200, L1516, Sigma) at 4°C overnight. Wisteria floribunda agglutinin (WFA) binds to glycosaminoglycans of chondroitin sulfate proteoglycans (CSPGs), the main component of PNNs (Miyata et al., 2018). The slices were washed with PBS (3 × 5 min), followed by staining with secondary antibody anti-rabbit (Cy3) (1:500, ab6939, Abcam) and streptavidin (1:200, 4800-30-14, R&D) for 1 h, and then washed in PBS (3 × 5 min). Subsequently, the nuclei were stained with DAPI (Solarbio). The images were captured under a confocal microscope (Nikon) at 4 × magnification to locate the V1B of each slice.

1 https://geneglobe.qiagen.com/us/analyze

High magnification images of V1B were patched together under a 20× objective under the scanning mode of 1 μm-step z-stack. All images were analyzed with ImageJ (NIH) for the quantification of the number of PV-positive neurons and WFA-positive cells and their colocalization by manual counting.

Golgi staining

We used FD Rapid Golgi Stain Kit (PK401, FD NeuroTechnologies) to observe the dendritic spines of V1B in all the groups. Rats (n = 4/group) were anesthetized with 1.25% avertin (10 mL/kg) by intraperitoneal injection and then decapitated. According to the manufacturer's instructions, the brains were sequentially immersed in a mixture of solution A and B for 2 weeks and then transferred to solution C for 72 h. Subsequently, the occipital lobe was cut into 150 μm-thick slices using a cryostat (Leica), which were allowed to dry naturally at room temperature, stained with a mixture of solution D and E, dehydrated using graded ethanol, clarified in xylene, and mounted with neutral balsam. The images of cerebral hemisphere sections were viewed under a bright field microscope (Nikon) with a 4× objective to locate the V1B (Figure 7A). The pyramidal neurons share typical characteristics: pyramid shape, with a thick apical dendrite extending to the meninx, and some basal dendrites from the bottom extending horizontally. The pyramidal neurons in V1B were detected under a 10× objective (Figure 7B). Finally, we used a 100× oil immersion lens to examine the dendritic spines of pyramidal neurons under the EDF plugin (NIS-Elements Viewer). The pyramidal neurons included in the statistics were from 3 to 5 sections of an animal. The secondary order basolateral dendrites >20 μm of layer II/II pyramidal neurons were captured as described elsewhere (Pizzorusso et al., 2006), and the density of spines was quantified by manual counting and analyzed using ImageJ (NIH). The headless and long filopodia were considered as the immature state of dendritic spines and not marked.

Statistical analysis

Results are presented as mean ± standard error of the mean (SEM). Repeated measures analysis of variance (ANOVA) was performed to analyze the data from fVEP and visual cliff before and after treatment, followed by the Bonferroni test for paired comparisons. Two-tailed unpaired Student's t-test of the replicate $2^{-\Delta Cq}$ values were used for each gene for comparison between two groups. Two-way ANOVA was conducted for protein and histological indicators, followed by the Bonferroni test. The Scheirer-Ray-Hare test was performed for non-parametric data (the PV-positive cell densities in layer IV among four groups). $p < 0.05$ indicated a statistically significant difference. All statistical analyses were conducted using SPSS 26.0 (IBM).

Results

rTMS promotes the recovery of objective visual function in amblyopic rats

To investigate the possible effect of rTMS on the objective visual function in rats, fVEP was measured *in vivo* before and after intervention in each group (Figure 2A). Among the four groups, the main and interaction effects on the C/I value of the duration of the treatment (time) and the group (treatment) were assessed by repeated-measures ANOVA. The treatment showed a significant main effect [F (3,48) = 80.07, $p < 0.001$], and the main effect of time was also significant [F (1,48) = 67.41, $p < 0.001$] with a significant interaction treatment × time [F (3,48) = 52.51, $p < 0.001$] (Figure 2B). For all the baseline results, the C/I value of MD+Sham and MD+rTMS groups were significantly lower than the Con+Sham group (both $p < 0.001$, repeated-measures ANOVA, Figures 2A, B), indicating that the nerve impulses from deprived eyes responding to flash were diminished in the primary visual cortex compared to the non-deprived eyes in MD rats. Sham stimulation or rTMS did not alter the C/I ratio of control rats compared to the baseline (Con+Sham group: 0.98 ± 0.02 pre vs. 1.01 ± 0.02 after sham stimulation, n = 11, $p > 0.05$; Con+rTMS group: 1.01 ± 0.02 pre vs. 1.04 ± 0.02 after rTMS, n = 13, $p > 0.05$, repeated-measures ANOVA, Figures 2A, B). The fVEP amplitudes of deprived eyes in the MD group were lower than those of non-deprived eyes before and after 7 days of sham stimulation (C/I value: 0.69 ± 0.02 at baseline, 0.68 ± 0.02 after sham stimulation, n = 13, p = 0.660). Conversely, after 7 days of rTMS, the amplitudes of deprived eyes in MD rats were similar to those of non-deprived eyes (C/I value: 0.66 ± 0.02 before and 0.99 ± 0.02 after rTMS, n = 15, $p < 0.001$). After the intervention, the C/I value of the MD+Sham group differed from the Con+Sham group significantly ($p < 0.001$), while no statistical difference was detected between the MD+rTMS and Con+rTMS groups (p = 0.71). These results suggest a promoter role of rTMS in amblyopic rats.

rTMS fails to improve the depth perception of amblyopic rats

We evaluated the depth perception of rats *via* a visual cliff device (Figure 3A), and the discrimination index of each group was calculated. The main effect on the discrimination index was statistically significant in both treatment [F (3,25) = 20.66, $p < 0.001$] and time [F (1,25) = 7.97, $p < 0.01$], without a significant interaction [F (3,25) = 0.46, p = 0.72] (Figure 3B). Regarding the baseline data, the discrimination index in the Con+Sham group was significantly higher than in the MD+Sham and MD+rTMS groups (both $p < 0.001$), indicating that the depth perception of MD rats was impaired markedly compared to control rats. Conversely, no difference was detected between the Con+Sham and Con+rTMS groups. After receiving stimulation, significant differences were detected between the Con+Sham and the two MD groups (both $p < 0.05$). Paired analysis revealed that the discrimination index in each group did not differ significantly before and after stimulation in comparison to themselves. Hence, we deduced that rTMS may not influence advanced visual functions, such as depth perception in amblyopic rats.

rTMS increases the expression of synaptic plasticity genes in the visual cortex of amblyopic rats

We used qRT-PCR to evaluate the differential expression level of the synaptic plasticity genes of each group.

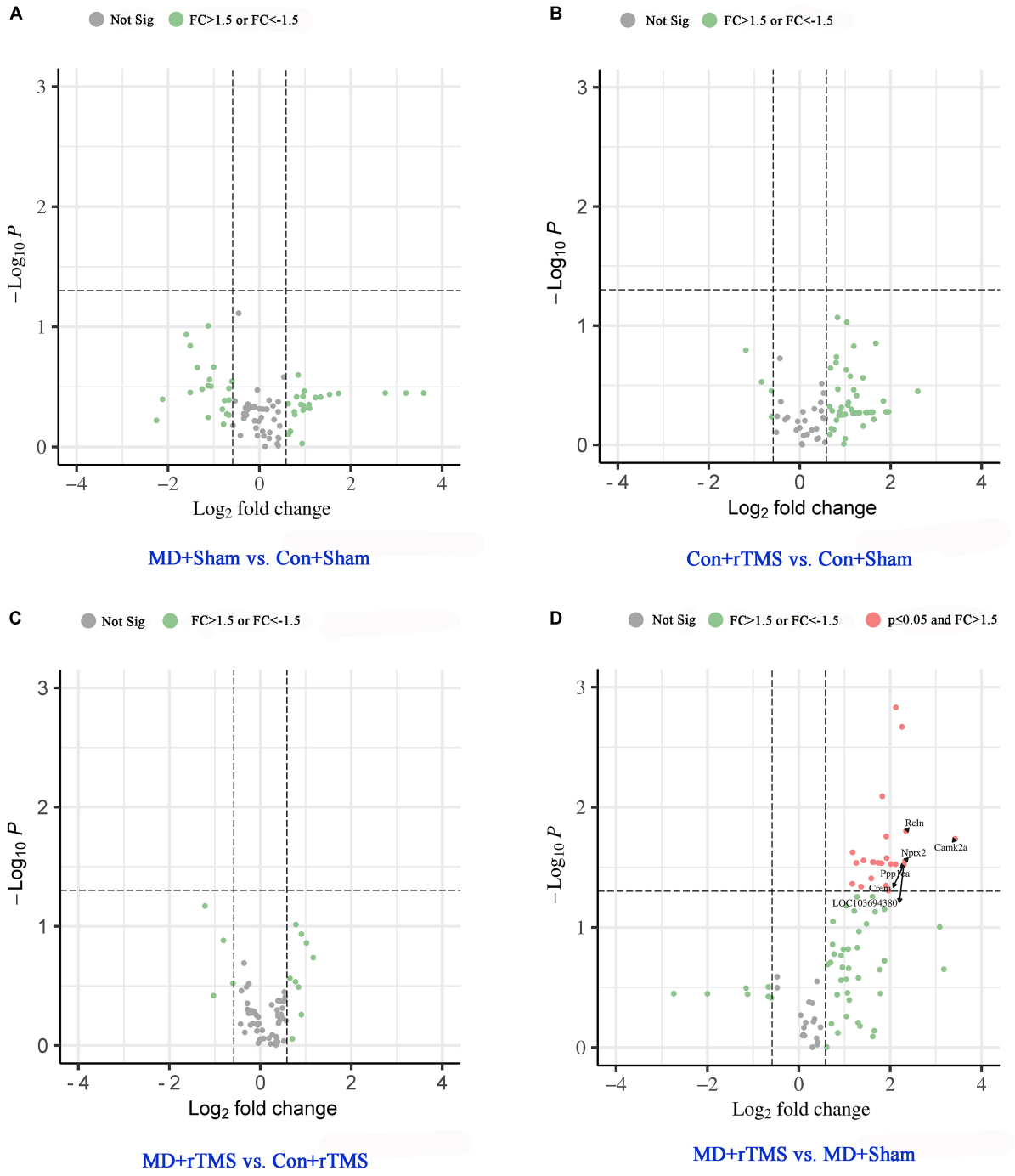

FIGURE 4
Volcano plots of gene expression changes based on chosen pairwise group comparison. Genes with >50% increased or decreased expression with no significance are shown as green-filled dot, while gray-filled dots indicate gene expression changes between −50 and +50% with no significance. The gene expression changes with $p < 0.05$ (above y = 1.30) were categorized as significant and labeled as red-filled dots. **(A)** Gene expression change between MD+Sham and Con+Sham groups. **(B)** Gene expression change between Con+rTMS and Con+Sham groups. **(C)** Gene expression change between MD+rTMS and Con+rTMS groups. In the above pairwise comparison groups, no statistically significant difference was observed in the gene expression. **(D)** Compared to the MD+Sham group, 25 synaptic plasticity genes were significantly upregulated in MD+rTMS group, and no gene was significantly downregulated. The top six increased synaptic plasticity genes are marked with black arrows. Not Sig, not significant; FC, fold change.

The relative abundance of gene expression is presented in the volcano plot (Figure 4). The abscissa axis shows the fold change in log2 model [FC = 1.5, log2(1.5) = 0.58; FC = 1/1.5, log2(1/1.5) = −0.58]. The *p*-value is converted to a −log10 model in the longitudinal axis [−log10(0.05) = 1.30]. The data points above the horizontal threshold y = 1.30 are statistically significant ($p < 0.05$), while those below the horizontal line are not significant. The green-filled dots in Figure 4 indicate 50% upregulation or downregulation in the genes with no significance, while gray-filled dots indicate gene expression changes between −50 and +50%. Genes with >50% increased expression with significant difference are shown as red-filled dots.

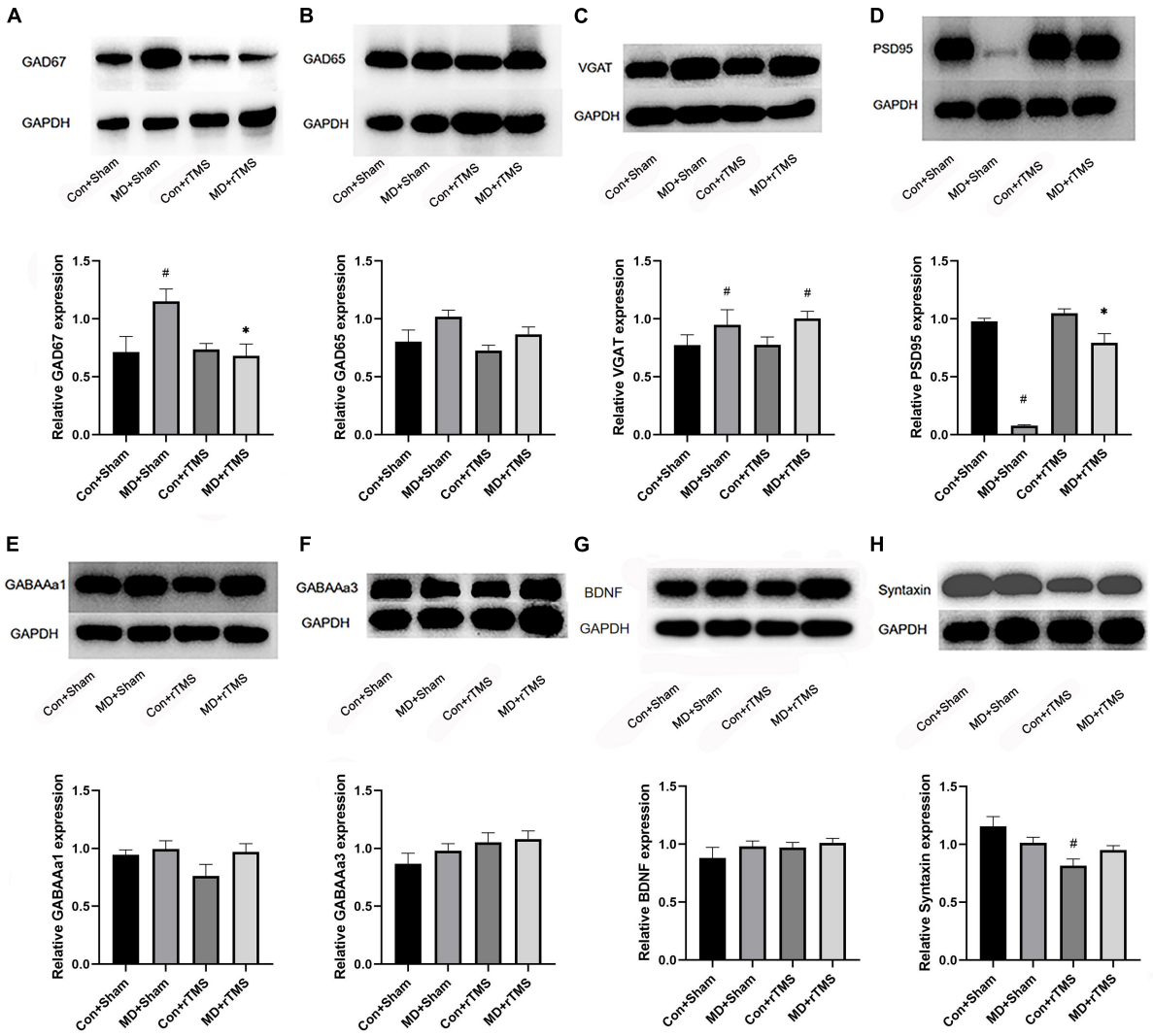

FIGURE 5
Western blot to detect the expression of the inhibitory neural pathway proteins and synapse-related protein in the binocular area of the visual cortex of rats in each group. **(A–H)** Shows the relative expression of GAD67, GAD65, VGAT, PSD95, GABAAα1, GABAAα3, BDNF, and Syntaxin, respectively. The upper panel of each figure is the electrophoresis band, and the lower is the statistical analysis diagram of the relative ratio of the target protein and the internal reference protein glyceraldehyde-3-phosphate dehydrogenase (GAPDH) in each group, as assessed by two-way analysis of variance (ANOVA). # Indicated a statistically significant difference compared to the Con+Sham group after accepting stimulation, $p < 0.05$;*indicates the significant difference compared to the MD+Sham group following receiving stimulation, $p < 0.05$.

Compared to the Con+Sham group, 22 genes were upregulated and 21 genes were downregulated in the visual cortex in the MD+Sham group, while none of them changed significantly (Figure 4A). After receiving rTMS, 53/84 genes were upregulated and 3/84 genes were downregulated compared to those experiencing sham stimulation in control rats; however, none were altered significantly (Figure 4B). Between groups receiving rTMS, eight genes were upregulated and three were downregulated in amblyopic rats compared to control rats, while none changed significantly (Figure 4C). No genes were significantly downregulated in the MD+rTMS group than in the MD+Shamgroup (Figure 4D), while 25 genes were significantly upregulated (Supplementary Table 2). Among the top six increased synaptic plasticity genes marked with arrows in Figure 4D, the one with the maximal increase in expression was *Camk2a*. Its fold change between the two groups was 10.72 (i.e., normalized expression of this gene in MD+rTMS group was over 10-fold higher than in the MD+Sham group). CAMK2α participates in long-term potentiation (LTP) *via* the regulation of ionotropic glutamate receptors (Küry et al., 2017). The second most upregulated gene was *Reln* (FC = 5.08), which codes for reelin, an ECM molecule playing a major role in layer formation and neuronal migration in the cortex (Tissir and Goffinet, 2003). *Nptx2*, the third most upregulated gene (FC = 5.01), is a member of the immediate early response gene (IEGs) family, mainly involved in glutamate signaling and synaptogenesis (Cho et al., 2008). *Crem* (CAMP-responsive element modulator) and *Ppp1ca* shared the fourth spot with *LOC103694380 (Tnf)*; the FC was 4.92 among the three genes. *Crem* encodes a bZIP transcription factor that binds to the cAMP-responsive element, which might be involved in the regulation of neural migration (Díaz-Ruiz et al., 2008). *Ppp1ca* encodes the protein which is one of the three catalytic subunits of protein phosphatase 1 (PP1) involved in LTP, long-term depression (LTD), and bidirectional plasticity in the mammalian cerebral cortex (Jouvenceau et al., 2006). *LOC103694380 (Tnf)* encodes for tumor necrosis factor-like protein which is involved

in the delayed homeostatic increase in the potentiation of open-eye during monocular deprivation (Kaneko et al., 2008), and also contributes to neurogenesis and brain development (Rockstrom et al., 2018).

rTMS reduces the level of inhibition in V1B of amblyopic rats by decreasing the synthesis of GABA

The proteins were extracted from the contralateral V1B of the deprived eye in amblyopic rats or of the right eye in control rats after treatment. The abundance of the inhibitory neural pathway proteins and synapse-related proteins was analyzed using Western blot. The difference between groups was analyzed using two-way ANOVA.

After receiving rTMS, GAD67 levels in the visual cortex of MD rats were significantly decreased compared to those receiving sham stimulation. GAD67 levels in the MD+Sham group were higher than those in the Con+Sham group (**Figure 5A**). No significant differences were detected in GAD65 levels in the visual cortex between receiving TMS and sham stimulation in MD rats (**Figure 5B**). Moreover, the VGAT levels in both MD groups were higher than those in the Con+Sham group (**Figure 5C**), indicating that the transport capacity of GABA is stronger in amblyopic rats than in control rats. rTMS significantly increased the level of PSD95 in amblyopic rats compared to sham stimulation (**Figure 5D**), indicating that a specific amount of silent state synapses have transformed into a stable state after rTMS (Xu et al., 2020). Furthermore, we determined if rTMS alters the expression of inhibitory receptors; the results showed that neither GABAAα1 nor GABAAα3 was statistically significant among the four groups (**Figures 5E, F**). Moreover, no significant difference was detected in the BDNF expression among the four groups after stimulation (**Figure 5G**). Syntaxin, a presynaptic membrane protein widely existing in the central nervous system neurons, was significantly reduced in expression following rTMS compared to sham stimulation among control rats, while no difference was observed between the two MD groups (**Figure 5H**). This result was consistent with previous studies that low-frequency stimuli may attenuate synaptic transmission efficiency in the control cortex (Fitzgerald et al., 2006). These findings emphasized that 1 Hz rTMS may reactivate the previously inhibited visual cortex in amblyopic rats by reducing the synthesis of GABA in interneurons with the maturity of stable state excitatory synapses.

rTMS promotes a juvenile-like visual cortex state by reducing the density of PNN-surrounding PV interneurons

To further determine whether rTMS promoted plasticity in the visual cortex of amblyopic rats, we assessed the density of PV interneurons and developed PNNs (Ye and Miao, 2013) by immunofluorescence (**Figure 6**). We found no difference in the density of PV-positive cells among the four groups with respect to the whole layer or the individual layers of the visual cortex (**Supplementary Figures 1A–E**). The density of WFA staining cells decreased significantly in the whole visual cortex layer in amblyopic rats receiving rTMS compared to sham stimulation and was also significantly different compared to control rats undergoing rTMS (**Supplementary Figure 2A**), while no difference was found in layer II/III (**Supplementary Figure 2B**). In layer IV, the density of WFA-positive cells decreased significantly in the MD+Sham group compared to in the Con+Sham group (**Supplementary Figure 2C**). And the tendency of WFA density in layers V and VI is similar to that in the whole layer (**Supplementary Figures 2D, E**). We also analyzed the proportion of PV/WFA double-labeled neurons in PV neurons or WFA-positive cells. In the whole layer, the ratio of WFA/PV double-positive cells to PV-positive cells reduced significantly in amblyopic rats receiving rTMS treatment compared to sham stimulation and in the Con+rTMS group (**Supplementary Figure 3A**), while no difference was found in layers II/III, IV or V (**Supplementary Figures 3B–D**). The change of the above ratio in layer VI is consistent with that in the whole layer (**Supplementary Figure 3E**). We also found no difference in the percentage of WFA-positive cells double-labeled for WFA and PV in the whole layer, layer II/III or layer IV among four groups (**Supplementary Figures 4A–C**). In layers V and VI, the percentage mentioned above increased in amblyopic rats after rTMS compared to sham stimulation (**Supplementary Figures 4D, E**). Moreover, this proportion showed a significant increase in the MD+rTMS group than in the Con+rTMS group in layer VI (**Supplementary Figure 4E**). These results suggest that rTMS promoted juvenile-like plasticity in the visual cortex, which could be attributed to reducing the density of PNNs enwrapping the PV interneurons, a typical characteristic of the immature cortex state (Liu et al., 2013).

rTMS promotes the recovery of dendritic spine density in the primary visual cortex of amblyopic rats

To evaluate whether the effects of rTMS could be mediated by the structural recovery of plasticity of dendritic spines, we assessed the density of secondary order basolateral dendrites on layers II/II pyramidal neurons in V1B contralateral to the deprived eye in MD rats or contralateral to the right eye in control rats by Golgi staining. In rats receiving sham stimulation, the average pyramidal spine density in the visual cortex of MD decreased compared to control rats (**Figures 7C, D**). After 7 days of rTMS, the dendritic spine density of visual cortical neurons increased significantly in MD rats compared to those undergoing sham stimulation and was close to that of the Con+Sham group (**Figures 7C, D**). In addition, no significant differences were detected in the spine density between the Con+Sham and Con+rTMS groups, indicating that rTMS did not affect control animals (**Figures 7C, D**).

Summaries of results indicating statistically significant differences are shown in **Tables 1**, **2**.

Discussion

This study demonstrated that low-frequency 1 Hz rTMS improved the visual function in adult amblyopic rats, along with molecular and structural changes in the visual cortex. Compared with sham stimulation, rTMS enhanced the restoration of shifted C/I value induced by long-term MD. There was no statistical difference in depth perception between the MD+Sham group and MD+rTMS group.

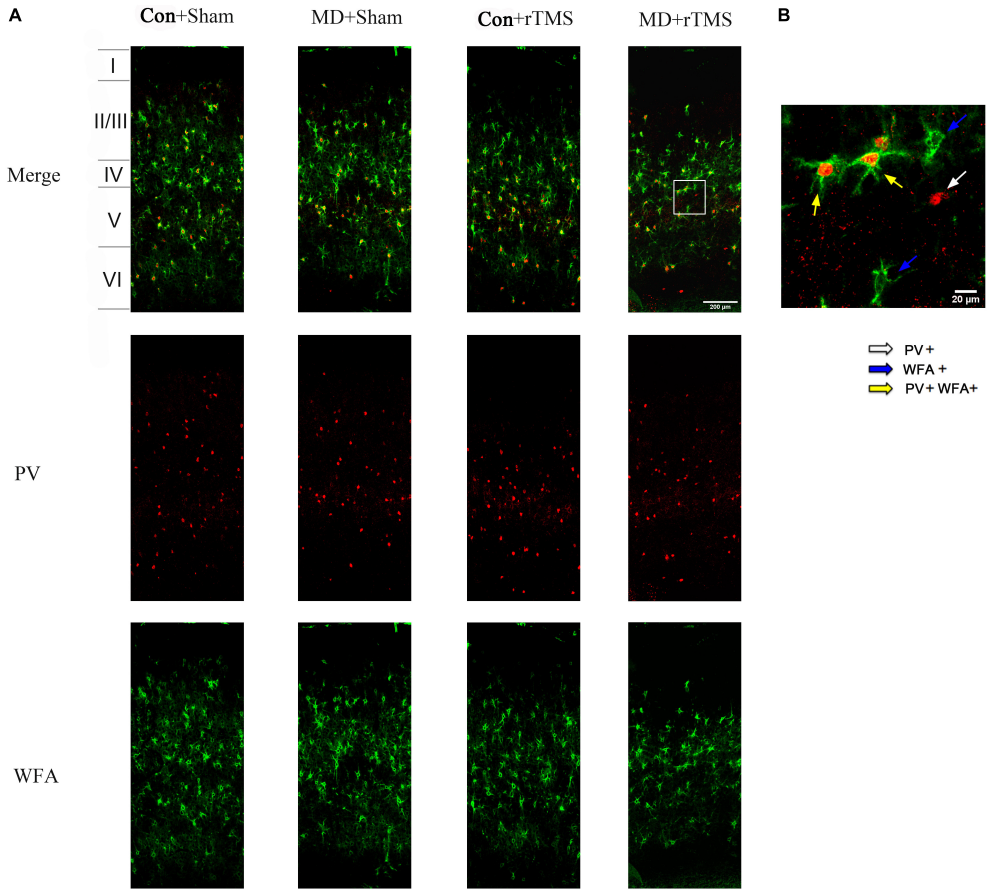

FIGURE 6
Expression of parvalbumin (PV) and wisteria floribunda agglutinin (WFA)-positive cells in the primary visual cortex (V1B) of the rats in each group. **(A)** Coronal section of V1B in each group. Laminar distribution of PV- and WFA-positive cells are stained with red and green fluorescence, respectively; scale bar: 200 μm. **(B)** A high-magnification view of the area selected by the white frame in panel **(A)**. The white arrow points to PV-positive cells; the blue arrows point to WFA-positive cells; the yellow arrows point to PV/WFA double-labeled cells; scale bar: 20 μm.

rTMS-treated MD rats demonstrated increased expression of specific synaptic plasticity genes and decreased levels of the GABA-producing protease in the visual cortex compared to the MD+sham group. This study also demonstrated that rTMS promoted a juvenile-like visual cortex in amblyopic rats by decreasing PNNs and improving the functional synaptic connections made by dendritic spines. These results suggest that rTMS has a beneficial effect on the plasticity of the visual cortex in an adult rat model of amblyopia.

Previous research has demonstrated that rTMS at low frequencies (0.2–1 Hz) induces decreases in brain excitability, while high frequency stimulation (5 Hz) activates brain (Hallett, 2007). However, the specific consequences of different stimulation frequencies on the cortex depend on the cortex's level of excitability. The adaptive changes of "regulatory threshold" (a specific level of postsynaptic response, above which LTP will be induced, and below which LTD will be induced) to synaptic activity ensure the stability of neural activity in the brain (Bienenstock et al., 1982). In other words, increased postsynaptic activity raises the regulatory threshold and causes LTD. On the contrary, LTP occurs when a sustained decline in postsynaptic activity lowers the regulatory threshold. The theory of homeostatic plasticity revolves around the deliberate modification of synaptic strength to preserve physiological balance. The application of 1 Hz rTMS to the excitatory-preconditioned cortex reduced the excitability below the baseline levels for >20 min. In contrast, cortical excitability increased for at least 20 min after 1 Hz rTMS on the inhibitory-preconditioned cortex (Siebner et al., 2004). The neurons driven by the amblyopic eye in the visual cortex are suppressed (Barnes et al., 2001). Therefore, we used a low-frequency mode of rTMS to change the ratio of excitation to inhibition in amblyopic rats. To rule out the effects of sound, thermal stimulation, and the stressful state brought on by the physical handling of the rats during the trials, we set up sham stimulation groups as controls.

Long-term MD during the critical period results in a weakened response of binocular cells to the deprived eye, followed by an increased response to the non-deprived eye, i.e., the ocular dominance shift (Hofer et al., 2006). Based on fVEP, the C/I values were significantly decreased in MD rats compared to controls in the present study, suggesting a reduced input from deprived eyes to the primary visual cortex or an increase of the non-deprived eye input. After rTMS, the C/I values increased to near normal levels in MD rats, suggesting the restoration of ocular dominance plasticity in the adult primary visual cortex. The rTMS-induced changes in the visual cortex are in line with earlier clinical studies (Thompson et al., 2008; Clavagnier et al., 2013; Tuna et al., 2020).

In addition to binocular integration, certain neurons in the visual cortex of rodents also feature binocular disparity, a function which underlies stereopsis (La Chioma et al., 2020). Stereopsis is processed by the high-order extrastriate cortex (Henriksen et al.,

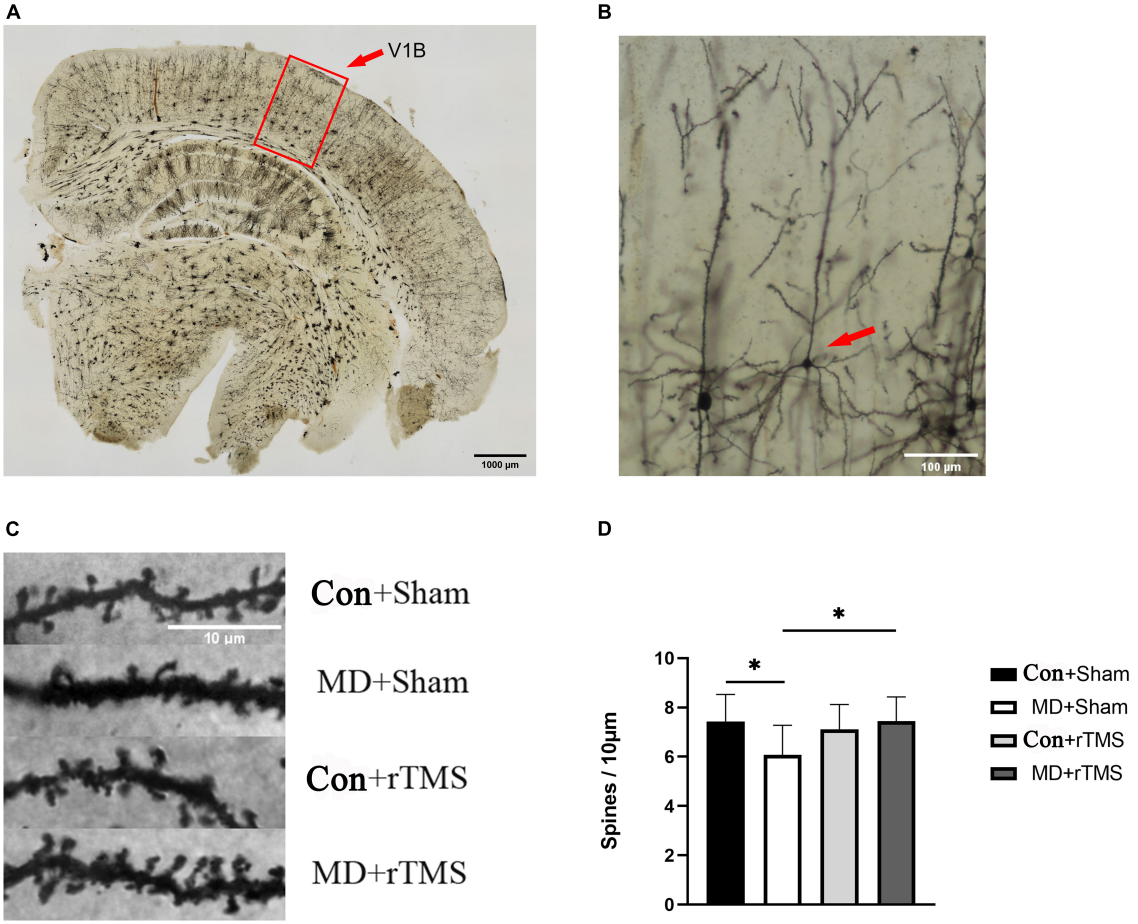

FIGURE 7
Repetitive transcranial magnetic stimulation (rTMS) effectuates a significant recovery of dendritic spine density in adult amblyopic rats. **(A)** A representative coronal section of the occipital cortex under a low magnification microscope processed *via* Golgi staining. The outline (red) delineates the primary visual cortex (V1B) where dendrites were sampled; scale bar: 1,000 μm. **(B)** A typical morphological pyramidal neuron in the visual cortex is pointed by the red arrow, scale bar: 100 μm. **(C)** Representative dendritic segments from V1B of all four groups. A marked decrease reduction in the dendritic spine density in adult monocular deprivation (MD) rats receiving sham stimulation and an increase in spine density after rTMS; scale bar: 10 μm. **(D)** Quantitative data from all the four groups were assessed by two-way analysis of variance (ANOVA). The dendritic spine density in the MD+Sham group (6.07 ± 1.21) was statistically decreased than that in the Con+Sham group (7.44 ± 1.10). The density in the MD+rTMS group (7.44 ± 0.98) was significantly increased than that in the MD+Sham group (6.07 ± 1.21). *Indicates the significant difference between the two groups, $p < 0.05$.

2016). In the treatment of amblyopia, visual acuity improvement after treatment is often not accompanied by a concurrent improvement in contrast sensitivity and stereoacuity (Wallace et al., 2011; Jia et al., 2022). In this study, depth perception was impaired in the MD rats compared to controls, as demonstrated by the visual cliff apparatus. We observed that rTMS did not affect depth perception in our MD rats. However, Tuna et al. (2020) reported that the use of continuous theta burst rTMS could improve stereopsis in adult amblyopia. Zhong et al. (2021) reported that a combination of long-term rTMS with simultaneous sensory training induced sustainable changes in plasticity in the rat's somatosensory cortex compared with a single session. We speculate that the recovery of binocular visual functions may require a longer-lasting rTMS mode such as cTBS, with supplementary treatments such as perceptual learning for instance.

Among a series of significantly elevated synaptic plasticity genes in our rTMS-treated amblyopic rats, immediate early response genes (IEGs) were predominant. IEGs respond rapidly to various extracellular stimuli, such as growth factors, mitogens, immune, and stress, and more than 100 genes are classified as IEGs (Minatohara et al., 2015). These genes also induce neuronal activity-dependent adaptive changes in downstream pathways, modulate synaptic activity, and may be a gateway controlling synaptic plasticity (de Bartolomeis et al., 2017). Other studies have also shown that rTMS enhanced cortical function by regulating the expression of IEGs in several brain-related disorders, such as Parkinson's disease (Cacace et al., 2017) and depression (Sun et al., 2015).

In this study, GAD67 was significantly decreased in the visual cortex of amblyopic adult rats receiving rTMS. Previous studies have demonstrated that reducing the synthesis and transport of GABA in the adult visual cortex is crucial for remodeling plasticity (Harauzov et al., 2010; Li et al., 2018). The administration of picrotoxin (PTX, a GABAA receptor antagonist) or 3-mercaptopropionic acid (MPA, a competitive inhibitor of GADs) to the adult rat visual cortex promoted the recovery of ocular dominance plasticity through reducing inhibitory neurotransmission pharmacologically (Harauzov et al., 2010). Cyclin-dependent kinase 5 (Cdk5) forms a complex with GAD67 in the visual cortex, and knockdown of Cdk5 may reduce GAD expression and restore juvenile-like OD plasticity in adult mice (Li et al., 2018). Trippe et al. (2009) reported that 1 Hz rTMS reduced the expression of GAD67 in the visual cortex of adult rats rapidly

TABLE 1 Results comparison between control (Con) groups and monocular deprivation (MD) groups.

	Con+Sham	Con+rTMS
MD+Sham	C/I value↓ Discrimination index↓ GAD67↑, VGAT↑, PSD95↓ PNNs density↓ Dendritic spine density↓	C/I value↓ Discrimination index↓
MD+rTMS	Discrimination index↓ VGAT↑	Discrimination index↓

The table shows how the MD groups listed in row title changed when compared with Con groups listed in column title. ↑ Indicates the significant increase / upregulation. ↓ Indicates the significant decrease / downregulation. Con, control; MD, monocular deprivation; Sham, sham stimulation; rTMS, repetitive transcranial magnetic stimulation; C/I value, contralateral vs. ipsilateral value (contralateral value: the amplitude of P1 derived from the deprived eyes in MD rats or the right eyes in control rats; ipsilateral value: the amplitude of P1 derived from the non-deprived eyes in MD rats or the left eyes in control rats); GAD67, glutamate decarboxylase 67 kDa isoform; VGAT, vesicular GABA transporter; PSD95, postsynaptic density 95; PNNs, perineuronal nets.

TABLE 2 Results comparison between sham stimulation-treated groups and repetitive transcranial magnetic stimulation (rTMS)-treated groups.

	MD+sham	Con+Sham
MD+rTMS	C/I value↑ 25 synaptic plasticity genes↑ GAD67↓, PSD95↑ PNNs density↓ Dendritic spine density↑	Discrimination index↓ PNNs density↓ Dendritic spine density
Con+rTMS	C/I value↑ Discrimination index↑	Syntaxin↓

The table shows how the rTMS-treated groups listed in row title changed when compared with sham stimulation-treated groups listed in column title. ↑ Indicates the significant increase / upregulation. ↓ Indicates the significant decrease / downregulation. Con, control; MD, monocular deprivation; Sham, sham stimulation; rTMS, repetitive transcranial magnetic stimulation; C/I value, contralateral vs. ipsilateral value (contralateral value: the amplitude of P1 derived from the deprived eyes in MD rats or the right eyes in control rats; ipsilateral value: the amplitude of P1 derived from the non-deprived eyes in MD rats or the left eyes in control rats); GAD67, glutamate decarboxylase 67 kDa isoform; PSD95, postsynaptic density 95; PNNs, perineuronal nets.

(within 2 h after the application of rTMS). The change of GAD67 reversed 1 day after rTMS and the increase lasted up to the 7th day. In Trippe et al. (2009) study, the chronic effect on GAD67 in control rats was evaluated after a 1 day single session of 1 Hz rTMS. However, our rats received consecutive stimulation for 7 days. The compromised visual cortical neurons of amblyopic rats may also respond differently to rTMS compared with control rats.

In this study, postsynaptic density 95 (PSD95) significantly decreased in amblyopia compared to controls, which was altered by rTMS. A previous study reported the upregulation of PSD95 by low-frequency rTMS in Alzheimer's Disease (Pang and Shi, 2021) and spatial cognition impairment (Ma et al., 2014). PSD95, an abundantly expressed scaffold protein, can recruit multiple components in the signaling pathway, such as neurotransmitter receptors and ion channels. Then PSD95 make these components interact or combine to form a complex to regulate signal transduction (Wegner et al., 2018). It is essential for the formation of excitatory synapses (Xu et al., 2020). This is consistent with our findings that the increase of PSD95 was accompanied by a marked increase in excitatory dendritic spine density.

Our study has several limitations. First, we used a 40 mm small coil whose field of stimulation was larger than the visual cortex of rats and might lead to multiple areas affected. It was not comparable to the regional specificity of local stimulation to the human cortex. The second limitation is that the period of observation of the treatment effects was relatively short. As a result, we do not know how persistent the changes associated with the rTMS treatment are. Furthermore, the monocular deprivation method used in this study simulates form-deprived amblyopia only. Other types of amblyopia such as strabismic and ametropic amblyopia which are more common in humans are less often studied in an animal model and could be the focus of future studies.

Our study demonstrated that rTMS promoted the reinvigoration of plasticity of the amblyopic visual cortex in a rat model. It is unknown whether rTMS has other effects on the synaptic environment besides rebalancing the excitatory and inhibitory states. Future studies should examine if other forms of plasticity could be restored by rTMS and clarify the relationship between these mechanisms and the inhibitory neural pathways. Understanding the underlying mechanisms will strengthen the evidence for the use of rTMS in the clinical treatment of adult amblyopia.

Conclusion

Application of low-frequency rTMS resulted in the recovery of visual function in an adult rat model of amblyopia, presumably arising from a reduction in the level of inhibition in the visual cortex.

Data availability statement

The original contributions presented in this study are included in this article/**Supplementary material**, further inquiries can be directed to the corresponding author.

Ethics statement

The animal study was reviewed and approved by the Animal Ethics Committee of Sichuan University.

Author contributions

JZ: conceptualization, methodology, investigation, and writing–first draft. WZ: conceptualization, data curation, and project administration. LL: writing–review and editing, data interpretation, and supervision. MH: writing–review and editing and data interpretation. All the authors have read and approved the final manuscript.

Funding

This work was supported by the National Natural Science Foundation of China (Grant Number 81800863). This work was also partially supported by Sichuan Science and Technology Program (Grant Number 2019YFS0247).

Conflict of interest

The authors declare that the research was conducted in the absence of any commercial or financial relationships that could be construed as a potential conflict of interest.

Publisher's note

All claims expressed in this article are solely those of the authors and do not necessarily represent those of their affiliated organizations, or those of the publisher, the editors and the reviewers. Any product that may be evaluated in this article, or claim that may be made by its manufacturer, is not guaranteed or endorsed by the publisher.

Supplementary material

The Supplementary Material for this article can be found online at: https://www.frontiersin.org/articles/10.3389/fnins.2023.1109735/full#supplementary-material

References

Barnes, G. R., Hess, R. F., Dumoulin, S. O., Achtman, R. L., and Pike, G. B. (2001). The cortical deficit in humans with strabismic amblyopia. *J. Physiol.* 533, 281–297. doi: 10.1111/j.1469-7793.2001.0281b.x

Bienenstock, E. L., Cooper, L. N., and Munro, P. W. (1982). Theory for the development of neuron selectivity: Orientation specificity and binocular interaction in visual cortex. *J. Neurosci.* 2, 32–48. doi: 10.1523/jneurosci.02-01-00032.1982

Birch, E. E. (2013). Amblyopia and binocular vision. *Prog. Retin. Eye Res.* 33, 67–84. doi: 10.1016/j.preteyeres.2012.11.001

Cacace, F., Mineo, D., Viscomi, M. T., Latagliata, E. C., Mancini, M., Sasso, V., et al. (2017). Intermittent theta-burst stimulation rescues dopamine-dependent corticostriatal synaptic plasticity and motor behavior in experimental parkinsonism: Possible role of glial activity. *Mov. Disord.* 32, 1035–1046. doi: 10.1002/mds.26982

Castaño-Castaño, S., Feijoo-Cuaresma, M., Paredes-Pacheco, J., Morales-Navas, M., Ruiz-Guijarro, J. A., Sanchez-Santed, F., et al. (2019). Tdcs recovers depth perception in adult amblyopic rats and reorganizes visual cortex activity. *Behav. Brain Res.* 370:111941. doi: 10.1016/j.bbr.2019.111941

Castillo-Padilla, D. V., and Funke, K. (2016). Effects of chronic itbs-rtms and enriched environment on visual cortex early critical period and visual pattern discrimination in dark-reared rats. *Dev. Neurobiol.* 76, 19–33. doi: 10.1002/dneu.22296

Cho, R. W., Park, J. M., Wolff, S. B., Xu, D., Hopf, C., Kim, J. A., et al. (2008). Mglur1/5-dependent long-term depression requires the regulated ectodomain cleavage of neuronal pentraxin npr by tace. *Neuron* 57, 858–871. doi: 10.1016/j.neuron.2008.01.010

Clavagnier, S., Thompson, B., and Hess, R. F. (2013). Long lasting effects of daily theta burst rtms sessions in the human amblyopic cortex. *Brain Stimul.* 6, 860–867. doi: 10.1016/j.brs.2013.04.002

de Bartolomeis, A., Buonaguro, E. F., Latte, G., Rossi, R., Marmo, F., Iasevoli, F., et al. (2017). Immediate-early genes modulation by antipsychotics: Translational implications for a putative gateway to drug-induced long-term brain changes. *Front. Behav. Neurosci.* 11:240. doi: 10.3389/fnbeh.2017.00240

Díaz-Ruiz, C., Parlato, R., Aguado, F., Ureña, J. M., Burgaya, F., Martínez, A., et al. (2008). Regulation of neural migration by the creb/crem transcription factors and altered dab1 levels in creb/crem mutants. *Mol. Cell. Neurosci.* 39, 519–528. doi: 10.1016/j.mcn.2008.07.019

Erchova, I., Vasalauskaite, A., Longo, V., and Sengpiel, F. (2017). Enhancement of visual cortex plasticity by dark exposure. *Philos. Trans. R. Soc. Lond. B Biol. Sci.* 372:20160159. doi: 10.1098/rstb.2016.0159

Fitzgerald, P. B., Fountain, S., and Daskalakis, Z. J. (2006). A comprehensive review of the effects of rtms on motor cortical excitability and inhibition. *Clin. Neurophysiol.* 117, 2584–2596. doi: 10.1016/j.clinph.2006.06.712

Freeman, S., and Sohmer, H. (1995). Effect of thyroxine on the development of somatosensory and visual evoked potentials in the rat. *J. Neurol. Sci.* 128, 143–150. doi: 10.1016/0022-510x(94)00229-h

Fujiki, M., Yee, K. M., and Steward, O. (2020). Non-invasive high frequency repetitive transcranial magnetic stimulation (hfrtms) robustly activates molecular pathways implicated in neuronal growth and synaptic plasticity in select populations of neurons. *Front. Neurosci.* 14:558. doi: 10.3389/fnins.2020.00558

Greifzu, F., Pielecka-Fortuna, J., Kalogeraki, E., Krempler, K., Favaro, P. D., Schlüter, O. M., et al. (2014). Environmental enrichment extends ocular dominance plasticity into adulthood and protects from stroke-induced impairments of plasticity. *Proc. Natl. Acad. Sci. U.S.A.* 111, 1150–1155. doi: 10.1073/pnas.1313385111

Hallett, M. (2007). Transcranial magnetic stimulation: A primer. *Neuron* 55, 187–199. doi: 10.1016/j.neuron.2007.06.026

Harauzov, A., Spolidoro, M., DiCristo, G., De Pasquale, R., Cancedda, L., Pizzorusso, T., et al. (2010). Reducing intracortical inhibition in the adult visual cortex promotes ocular dominance plasticity. *J. Neurosci.* 30, 361–371. doi: 10.1523/jneurosci.2233-09.2010

Hashemi, H., Pakzad, R. M., Yekta, A., Bostamzad, P., Aghamirsalim, M., Sardari, S. M., et al. (2018). Global and regional estimates of prevalence of amblyopia: A systematic review and meta-analysis. *Strabismus* 26, 168–183. doi: 10.1080/09273972.2018.1500618

Heimel, J. A., van Versendaal, D., and Levelt, C. N. (2011). The role of gabaergic inhibition in ocular dominance plasticity. *Neural Plast.* 2011:391763. doi: 10.1155/2011/391763

Henriksen, S., Tanabe, S., and Cumming, B. (2016). Disparity processing in primary visual cortex. *Philos. Trans. R. Soc. Lond. B Biol. Sci.* 371:20150255. doi: 10.1098/rstb.2015.0255

Hensch, T. K. (2005). Critical period plasticity in local cortical circuits. *Nat. Rev. Neurosci.* 6, 877–888. doi: 10.1038/nrn1787

Hensch, T. K., and Quinlan, E. M. (2018). Critical periods in amblyopia. *Vis. Neurosci.* 35:E014. doi: 10.1017/s0952523817000219

Hofer, S. B., Mrsic-Flogel, T. D., Bonhoeffer, T., and Hübener, M. (2006). Lifelong learning: Ocular dominance plasticity in mouse visual cortex. *Curr. Opin. Neurobiol.* 16, 451–459. doi: 10.1016/j.conb.2006.06.007

Hoppenrath, K., Härtig, W., and Funke, K. (2016). Intermittent theta-burst transcranial magnetic stimulation alters electrical properties of fast-spiking neocortical interneurons in an age-dependent fashion. *Front. Neural Circuits* 10:22. doi: 10.3389/fncir.2016.00022

Jazmati, D., Neubacher, U., and Funke, K. (2018). Neuropeptide y as a possible homeostatic element for changes in cortical excitability induced by repetitive transcranial magnetic stimulation. *Brain Stimul.* 11, 797–805. doi: 10.1016/j.brs.2018.02.017

Jia, Y., Ye, Q., Zhang, S., Feng, L., Liu, J., and Xu, Z. (2022). Contrast sensitivity and stereoacuity in successfully treated refractive amblyopia. *Invest. Ophthalmol. Vis. Sci.* 63:6. doi: 10.1167/iovs.63.1.6

Jouvenceau, A., Hédou, G., Potier, B., Kollen, M., Dutar, P., and Mansuy, I. M. (2006). Partial inhibition of pp1 alters bidirectional synaptic plasticity in the hippocampus. *Eur. J. Neurosci.* 24, 564–572. doi: 10.1111/j.1460-9568.2006.04938.x

Kaneko, M., Stellwagen, D., Malenka, R. C., and Stryker, M. P. (2008). Tumor necrosis factor-alpha mediates one component of competitive, experience-dependent plasticity in developing visual cortex. *Neuron* 58, 673–680. doi: 10.1016/j.neuron.2008.04.023

Küry, S., van Woerden, G. M., Besnard, T., Proietti Onori, M., Latypova, X., Towne, M. C., et al. (2017). De novo mutations in protein kinase genes camk2a and camk2b cause intellectual disability. *Am. J. Hum. Genet.* 101, 768–788. doi: 10.1016/j.ajhg.2017.10.003

La Chioma, A., Bonhoeffer, T., and Hübener, M. (2020). Disparity sensitivity and binocular integration in mouse visual cortex areas. *J. Neurosci.* 40, 8883–8899. doi: 10.1523/jneurosci.1060-20.2020

Li, Y. P., Zhou, M. W., Forster, S. H., Chen, S. Y., Qi, X., Zhang, H. M., et al. (2019). Prevalence of amblyopia among preschool children in central south china. *Int. J. Ophthalmol.* 12, 820–825. doi: 10.18240/ijo.2019.05.19

Li, Y., Wang, L., Zhang, X., Huang, M., Li, S., Wang, X., et al. (2018). Inhibition of cdk5 rejuvenates inhibitory circuits and restores experience-dependent plasticity in adult visual cortex. *Neuropharmacology* 128, 207–220. doi: 10.1016/j.neuropharm.2017.10.015

Liu, H., Xu, H., Yu, T., Yao, J., Zhao, C., and Yin, Z. Q. (2013). Expression of perineuronal nets, parvalbumin and protein tyrosine phosphatase σ in the rat visual cortex during development and after bfd. *Curr. Eye Res.* 38, 1083–1094. doi: 10.3109/02713683.2013.803287

Ma, J., Zhang, Z., Kang, L., Geng, D., Wang, Y., Wang, M., et al. (2014). Repetitive transcranial magnetic stimulation (rtms) influences spatial cognition and modulates hippocampal structural synaptic plasticity in aging mice. *Exp. Gerontol.* 58, 256–268. doi: 10.1016/j.exger.2014.08.011

Mazziotti, R., Baroncelli, L., Ceglia, N., Chelini, G., Sala, G. D., Magnan, C., et al. (2017). Mir-132/212 is required for maturation of binocular matching of orientation preference and depth perception. *Nat. Commun.* 8:15488. doi: 10.1038/ncomms15488

Minatohara, K., Akiyoshi, M., and Okuno, H. (2015). Role of immediate-early genes in synaptic plasticity and neuronal ensembles underlying the memory trace. *Front. Mol. Neurosci.* 8:78. doi: 10.3389/fnmol.2015.00078

Miyata, S., Nadanaka, S., Igarashi, M., and Kitagawa, H. (2018). Structural variation of chondroitin sulfate chains contributes to the molecular heterogeneity of perineuronal nets. *Front. Integr. Neurosci.* 12:3. doi: 10.3389/fnint.2018.00003

Pang, Y., and Shi, M. (2021). Repetitive transcranial magnetic stimulation improves mild cognitive impairment associated with alzheimer's disease in mice by modulating the mir-567/neurod2/psd95 axis. *Neuropsychiatr. Dis. Treat.* 17, 2151–2161. doi: 10.2147/ndt.S311183

Paxinos, G., and Watson, C. (2007). *The rat brain in stereotaxic coordinates*. Cambridge, MA: Academic Press.

Pizzorusso, T., Medini, P., Berardi, N., Chierzi, S., Fawcett, J. W., and Maffei, L. (2002). Reactivation of ocular dominance plasticity in the adult visual cortex. *Science* 298, 1248–1251. doi: 10.1126/science.1072699

Pizzorusso, T., Medini, P., Landi, S., Baldini, S., Berardi, N., and Maffei, L. (2006). Structural and functional recovery from early monocular deprivation in adult rats. *Proc. Natl. Acad. Sci. U.S.A.* 103, 8517–8522. doi: 10.1073/pnas.0602657103

Polanía, R., Nitsche, M. A., and Ruff, C. C. (2018). Studying and modifying brain function with non-invasive brain stimulation. *Nat. Neurosci.* 21, 174–187. doi: 10.1038/s41593-017-0054-4

Rockstrom, M. D., Chen, L., Taishi, P., Nguyen, J. T., Gibbons, C. M., Veasey, S. C., et al. (2018). Tumor necrosis factor alpha in sleep regulation. *Sleep Med. Rev.* 40, 69–78. doi: 10.1016/j.smrv.2017.10.005

Sawtell, N. B., Frenkel, M. Y., Philpot, B. D., Nakazawa, K., Tonegawa, S., and Bear, M. F. (2003). Nmda receptor-dependent ocular dominance plasticity in adult visual cortex. *Neuron* 38, 977–985. doi: 10.1016/s0896-6273(03)00323-4

Siebner, H. R., Lang, N., Rizzo, V., Nitsche, M. A., Paulus, W., Lemon, R. N., et al. (2004). Preconditioning of low-frequency repetitive transcranial magnetic stimulation with transcranial direct current stimulation: Evidence for homeostatic plasticity in the human motor cortex. *J. Neurosci.* 24, 3379–3385. doi: 10.1523/jneurosci.5316-03.2004

Silingardi, D., Scali, M., Belluomini, G., and Pizzorusso, T. (2010). Epigenetic treatments of adult rats promote recovery from visual acuity deficits induced by long-term monocular deprivation. *Eur. J. Neurosci.* 31, 2185–2192. doi: 10.1111/j.1460-9568.2010.07261.x

Simons, K. (2005). Amblyopia characterization, treatment, and prophylaxis. *Surv. Ophthalmol.* 50, 123–166. doi: 10.1016/j.survophthal.2004.12.005

Spiegel, D. P., Byblow, W. D., Hess, R. F., and Thompson, B. (2013). Anodal transcranial direct current stimulation transiently improves contrast sensitivity and normalizes visual cortex activation in individuals with amblyopia. *Neurorehabil. Neural Repair* 27, 760–769. doi: 10.1177/1545968313491006

Spolidoro, M., Sale, A., Berardi, N., and Maffei, L. (2009). Plasticity in the adult brain: Lessons from the visual system. *Exp. Brain Res.* 192, 335–341. doi: 10.1007/s00221-008-1509-3

Sun, P., Zhang, Q., Zhang, Y., Wang, F., Chen, R., Yamamoto, R., et al. (2015). Homer1a-dependent recovery from depression-like behavior by photic stimulation in mice. *Physiol. Behav.* 147, 334–341. doi: 10.1016/j.physbeh.2015.05.007

Tan, T., Wang, W., Xu, H., Huang, Z., Wang, Y. T., and Dong, Z. (2018). Low-frequency rtms ameliorates autistic-like behaviors in rats induced by neonatal isolation through regulating the synaptic gaba transmission. *Front. Cell. Neurosci.* 12:46. doi: 10.3389/fncel.2018.00046

Thompson, B., Mansouri, B., Koski, L., and Hess, R. F. (2008). Brain plasticity in the adult: Modulation of function in amblyopia with rtms. *Curr. Biol.* 18, 1067–1071. doi: 10.1016/j.cub.2008.06.052

Tissir, F., and Goffinet, A. M. (2003). Reelin and brain development. *Nat. Rev. Neurosci.* 4, 496–505. doi: 10.1038/nrn1113

Trippe, J., Mix, A., Aydin-Abidin, S., Funke, K., and Benali, A. (2009). Θ burst and conventional low-frequency rtms differentially affect gabaergic neurotransmission in the rat cortex. *Exp. Brain Res.* 199, 411–421. doi: 10.1007/s00221-009-1961-8

Tuna, A. R., Pinto, N., Brardo, F. M., Fernandes, A., Nunes, A. F., and Pato, M. V. (2020). Transcranial magnetic stimulation in adults with amblyopia. *J. Neuroophthalmol.* 40, 185–192. doi: 10.1097/wno.0000000000000828

Maya Vetencourt, J. F., Sale, A., Viegi, A., Baroncelli, L., Pasquale, R. D., O'Leary, O. F., et al. (2008). The antidepressant fluoxetine restores plasticity in the adult visual cortex. *Science* 320, 385–388. doi: 10.1126/science.1150516

Wallace, D. K., Lazar, E. L., Melia, M., Birch, E. E., Holmes, J. M., Hopkins, K. B., et al. (2011). Stereoacuity in children with anisometropic amblyopia. *J. AAPOS* 15, 455–461. doi: 10.1016/j.jaapos.2011.06.007

Wegner, W., Mott, A. C., Grant, S. G. N., Steffens, H., and Willig, K. I. (2018). In vivo sted microscopy visualizes psd95 sub-structures and morphological changes over several hours in the mouse visual cortex. *Sci. Rep.* 8:219. doi: 10.1038/s41598-017-18640-z

Wu, X. Q., Zan, G. Y., Ju, Y. Y., Chen, T. Z., Guo, L. B., Jiao, D. L., et al. (2018). Low-frequency repetitive transcranial magnetic stimulation inhibits the development of methamphetamine-induced conditioned place preference. *Behav. Brain Res.* 353, 129–136. doi: 10.1016/j.bbr.2018.07.004

Xu, W., Löwel, S., and Schlüter, O. M. (2020). Silent synapse-based mechanisms of critical period plasticity. *Front. Cell. Neurosci.* 14:213. doi: 10.3389/fncel.2020.00213

Ye, Q., and Miao, Q. L. (2013). Experience-dependent development of perineuronal nets and chondroitin sulfate proteoglycan receptors in mouse visual cortex. *Matrix Biol.* 32, 352–363. doi: 10.1016/j.matbio.2013.04.001

Yi, Z., Chen, L., Wang, X., Chen, C., and Xing, Y. (2020). Protective effects of intravitreal injection of the rho-kinase inhibitor y-27632 in a rodent model of nonarteritic anterior ischemic optic neuropathy (raion). *J. Ophthalmol.* 2020:1485425. doi: 10.1155/2020/1485425

Zhong, M., Cywiak, C., Metto, A. C., Liu, X., Qian, C., and Pelled, G. (2021). Multi-session delivery of synchronous rtms and sensory stimulation induces long-term plasticity. *Brain Stimul.* 14, 884–894. doi: 10.1016/j.brs.2021.05.005

frontiers | Frontiers in Neuroscience

TYPE Original Research
PUBLISHED 01 February 2023
DOI 10.3389/fnins.2023.1124034

OPEN ACCESS

EDITED BY
Dan Wen,
Central South University, China

REVIEWED BY
Wei Shi,
Beijing Children's Hospital, China
Xue Feng,
Beijing Jishuitan Hospital, China
Zhengzheng Wu,
University of Electronic Science and Technology of China, China
Gabriel Yang,
The Chinese University of Hong Kong (CUHK), Hong Kong SAR, China

*CORRESPONDENCE
Jin Zeng
✉ syzengjin@scut.edu.cn

†These authors have contributed equally to this work

SPECIALTY SECTION
This article was submitted to Visual Neuroscience, a section of the journal Frontiers in Neuroscience

RECEIVED 14 December 2022
ACCEPTED 11 January 2023
PUBLISHED 01 February 2023

CITATION
Lan J, Li Y, Pang S, Zhang G, Wu D, Yang C, Li J, Lin J, Yang X, Li Z, Chu H, Yan L and Zeng J (2023) Targeting displacement as an indicator of binocular fixation in normal Chinese adults. *Front. Neurosci.* 17:1124034. doi: 10.3389/fnins.2023.1124034

Targeting displacement as an indicator of binocular fixation in normal Chinese adults

Jianqing Lan[1†], Yingan Li[2†], Shasha Pang[3], Guanrong Zhang[4], Dianpeng Wu[3], Cheng Yang[1], Juan Li[1], Junyu Lin[1], Xiyang Yang[1], Zheng Li[1], Hang Chu[4], Li Yan[4] and Jin Zeng[5*]

[1]Department of Ophthalmology, Guangdong Provincial People's Hospital, Guangdong Academy of Medical Sciences, Southern Medical University, Guangzhou, China, [2]Guangdong Cardiovascular Institute, Guangdong Provincial People's Hospital, Guangdong Academy of Medical Sciences, Guangzhou, China, [3]National Engineering Research Center for Healthcare Devices, Guangzhou, China, [4]Statistics Section, Guangdong Provincial People's Hospital, Guangdong Academy of Medical Sciences, Guangzhou, China, [5]Guangdong Cardiovascular Institute, Guangdong Provincial People's Hospital, Guangdong Academy of Medical Sciences, The Second School of Clinical Medicine, Southern Medical University, Guangzhou, China

Purpose: The stability of fixation is crucial for the development of visual function. In this study, we quantify the deviation of visual target during fixational and saccadic tasks using eye-tracking technology, reflecting the control ability and characteristics of fixational displacement among healthy adults in a convenient method.

Methods: One hundred healthy participants aged between 18 and 55 years were recruited in the study. All participants underwent a complete ophthalmic assessment. The eye positions in the fixational and saccadic tasks were documented and analyzed by the Tobii eye-tracking system. Participants were grouped by age and gender. Targeting displacement (TD), defined as the average displacement between visual target and the mean of fixation points corresponding to that stimuli, was used to quantitatively observe fixational displacement in the horizontal and vertical directions.

Result: There was a strong reproducibility of TD as an indicator of fixation (ICC 0.812 to 0.891, $p < 0.001$). The TD in fixational task was significantly smaller than that of the saccadic task (3.884 ± 0.525 vs. 4.484 ± 0.509, $p < 0.001$) among normal people. Moreover, the difference of TD in the horizontal and vertical meridians was related to the nature of the task: In the fixational task, the TD in horizontal was smaller than that in the vertical ($p < 0.001$), whereas the TD in horizontal was larger than that in vertical in the saccadic task ($p = 0.003$). In the different age and gender groups: There was no significant difference between different gender and age groups in fixational task. However, during the saccadic task, males had smaller TD in the vertical direction than females (4.061 ± 0.495 vs. 4.404 ± 0.484, $p = 0.002$), and the average TD increased with age, mainly in the vertical direction (all $p < 0.05$). The fixation stability decreased significantly in the group over 50-years-old.

Conclusion: By reporting the fixational displacement of different genders and ages in fixational and saccadic tasks, as well as different longitude lines among normal people, our study might provide an objective, quantitative and convenient reference index for the evaluation of fixation stability in visual impairment diseases and aging phenomenon of visual function.

KEYWORDS

fixation stability, visual function, oculomotor system, eye movements, aging phenomenon

1. Introduction

Eye movement is an important way for the visual system to explore the external world, which plays an important role in various cognitive processes such as fixation point correction, attention shift and visual fusion (Rucci and Victor, 2015; Martinez-Conde and Macknik, 2017), and has become a research hotspot in the field of vision.

In the process of tracking the visual targets, color vision and a high level of detail are primarily encoded in the fovea centralis. As the fovea is so small at 1.5 mm in diameter (Wieland et al., 2020), with the most sensitive region only 250–300 μm in diameter that the eye must rove across the visual environment to gather information about it. In order to obtain the visual information surrounding, the eyes must move across different directions or axis. These movements are coordinated by a complex network of structures running through the cerebral cortex and brain stem, as well as the oculomotor system (OMS). Specifically, when the observer aims to see the target with details, the OMS will project the target image to the foveal vision area by eye movements in coordination with the cerebral cortex and brain stem.

Eye tracking technology is a non-invasive method for recording eye movements and gaze location across time and task. It is a common technology for observing the allocation of visual attention, a validated way for examining visual information processing and classic method to evaluate brain function in neuroscience research. It can not only measure variables that are difficult to be obtained by other methods, but also helps to evaluate visual perception function (Valsecchi et al., 2013; Imaoka et al., 2020; Wieland et al., 2020). The eye tracking technique used in this study is the mainstream method in eye movements examination as yet, which makes mass screening easier as all the examinations can be performed in a matter of minutes. Further, the finer details of eye movements are largely reflexive, while that are largely outside of conscious control, which promote the application of eye-tracking technology in children or who with poor coordination (Wieland et al., 2020).

There are three basic forms of eye movements: fixation, saccade, and pursuit eye movements. Previously, large eye movements were thought to occur only during saccades, until Ditchburn and Ginsborg, 1953 discovered that there was also a significant irregular eye movement of high frequency (30–70 c/s) and small extent (20″ arc) during fixations. Subsequently, a large number of studies have also concurred their findings. During fixation, the eye is unable to acquire high-quality information from the entire visual field in a single fixation as the fovea is small, so it is necessary for the eyes to change fixation positions constantly within a certain range. These movements are called fixational eye movements.

Since the stability of fixational eye movements is crucial for the development of visual function. Therefore, previous studies have used eye-tracking technology to focus on ophthalmic diseases related to eye movements. Notably, they reported that children with strabismus had a larger fixation instability during fixation (Kelly et al., 2019), and those with amblyopia were frequently accompanied by irregular eye movements and poor fixation (Chung et al., 2015). Children with cerebral visual impairment (CVI) exhibit, among other visual and oculomotor dysfunctions, instability of fixation (Salati et al., 2002). Similarly, in adult patients, fixation stability has been used to evaluate visual performance in amblyopia (Apaev and Tarutta, 2020). However, there are few studies studying fixational eye movements of normal adults. Moreover, most previous studies of fixation have focused on incessant fixation experiments, in which observers needed to maintain fixations on cues for a long period of time. But incessant fixation is rare in natural tasks, with most natural tasks lasting less than a second (Ditchburn and Ginsborg, 1953).

In this study, we utilized eye-tracking technology to document the target displacement (TD), which is defined as the deviation between visual target and the fixation points (Hunfalvay et al., 2021), to evaluate the fixational displacement in normal adults. Furthermore, on the basis of the fixational task, the saccadic task was performed. We aim to propose an objective, quantitative and convenient reference index for the evaluation of fixation stability, establish normative values among adults, and provide perspectives for these measurements to be added to the toolkit for visual perception function assessment in clinical practice.

2. Materials and methods

2.1. Participants

This was an observational cross-sectional study. A total of 100 healthy volunteers were enrolled from the Physical Examination Center of Guangdong Provincial People's Hospital who underwent physical examinations from January 2020 to June 2020. Participants were between the age of 18 to 52 years (M = 34.43, SD = 8.75) and the diopter range of −8.94D to +1.63D (M = 2.91, SD = 2.42); 47 were males (47%) and 53 were females (53%). Grouped by age and diopter (**Table 1**). The daily time spent in near work was ranging from 2 h to more than 12 h (M = 7.65, SD = 3.11).

The inclusion criteria for participants were as followed: (1) Age range of 18–55 years, with good comprehension and communication skills; (2) Best corrected visual acuity 20/20 or above; (3) Normal eye movement.

TABLE 1 Demographic data by age and diopter.

Group		Mean age (±SD)	Mean diopter (±SD)	Male gender (%)
Age	18–34 years old	27.54 ± 4.25	−3.45 ± 2.40	46.2%
	35–49 years old	41.74 ± 4.25	−2.40 ± 2.21	48.6%
	>50 years old	50.75 ± 0.96	−1.00 ± 3.33	46.2%
	Emmetropia: + 0.50D∼−0.50D	38.88 ± 9.15	−0.10 ± 0.44	44.8%
	Low myopia: −0.75D∼−3.00D	34.13 ± 9.57	−1.87 ± 0.71	50.0%
Diopter	Moderate myopia: −3.01D∼−6.00D	32.86 ± 7.05	−4.58 ± 0.83	47.6%
	High myopia: <−6.00D	30.43 ± 6.43	−6.80 ± 1.07	37.5%

The exclusion criteria for participants were as followed: (1) With a history of organic ocular disease or ocular surgery (except excimer laser surgery); (2) Dominant strabismus and other eye position errors detected by the 33 cm Hirschberg test and alternate cover test; (3) Those who were unable to complete the study or were required to withdraw due to any discomfort during the study.

2.2. Methods

2.2.1. General ophthalmic examination

All participants performed routine ophthalmic examinations, including visual acuity, computerized optometry, non-contact intraocular pressure, fixation nature, eye movements, anterior segment, and fundus examination. Equipment: automatic computerized optometer (Topcon, Japan), non-contact tonopachymeter (Canon, Japan), slit lamp (Topcon, Japan), fundus vascular imaging system (Optovue, USA).

2.2.2. Eye movement examination

The examinations of eye movements were carried out using the eye-tracking system, Tobii Eye Tracker 5 (Tobii Company, Sweden) at a sampling rate of 133 Hz. The eye tracker was placed below the stimulation screen (**Figure 1**). The average binocular accuracy of the eye tracker is around 0.5 to 1° of visual angle. It was non-invasive and supported free-head movements. All the tests could be consecutively performed in a matter of minutes and the tests were performed in a strictly quiet, and uniformly illuminated testing room. Subjects were seated 80 cm away from the screen with their eyes at the height of the screen, requested to look at the images, keeping their head and body steady. A three-point calibration performed before each examination to guarantee accuracy and precision of gaze tracking. Two consecutive measurements of all participants were acquired. For each measurement, the participant was asked to sit back and be realigned again. The repeatability was assessed using the intraclass correlation coefficient (ICC). This study included fixational tasks and saccadic tasks in order to evaluate fixational behavior in conditions similar to daily life activities. We introduced the term of Targeting Displacement (TD): The average displacement between visual target and the mean of fixation points corresponding to that stimuli, on X and Y-axis, and the horizontal and vertical deviation were recorded in pixels.

2.2.3. Fixational tasks (Figure 2)

A circular target (as shown in **Figure 1**) appeared above the foveal vision with the circular range of 10°. This target would surround this circle and finally return to the center, with appearing nine times in total in each trial. Every target appeared for 2 s with an interval of 0.5 s, eye tracker pursued every target in the 1° of peripheral visual field, appearing with a velocity threshold of 1°/s, and then recorded relative deviation values in the horizontal and vertical directions to the circular target. All deviation values were averaged (Valsecchi et al., 2013; Krauzlis et al., 2017; Imaoka et al., 2020).

2.2.4. Saccadic tasks (Figure 3)

A circular target (as shown in **Figure 1**) appeared in the top left corner of the screen, lasted a second and then disappeared. With an interval of 0.5 s, the circular target appeared in the top right corner of the opposite side, and disappeared after lasting 1 s. The circular target would appear eight times in total as this circulation, which would cover averagely the entire visual field range in the left and right. During this process, all subjects had saccadic movements and pursued every target, until the target disappeared. The eye tracker pursued every target in the 2° of peripheral visual field, appearing with a velocity threshold of 11°/s and an acceleration threshold of 1,900°/s^2, and then recorded relative deviation values in the horizontal and vertical directions to the circular target. All deviation values were averaged (Valsecchi et al., 2013; Krauzlis et al., 2017; Imaoka et al., 2020).

FIGURE 1
The eye tracker was placed below the stimulation screen. Tobii eye tracker 5 (Tobii Company, Sweden) at a sampling rate of 133 Hz.

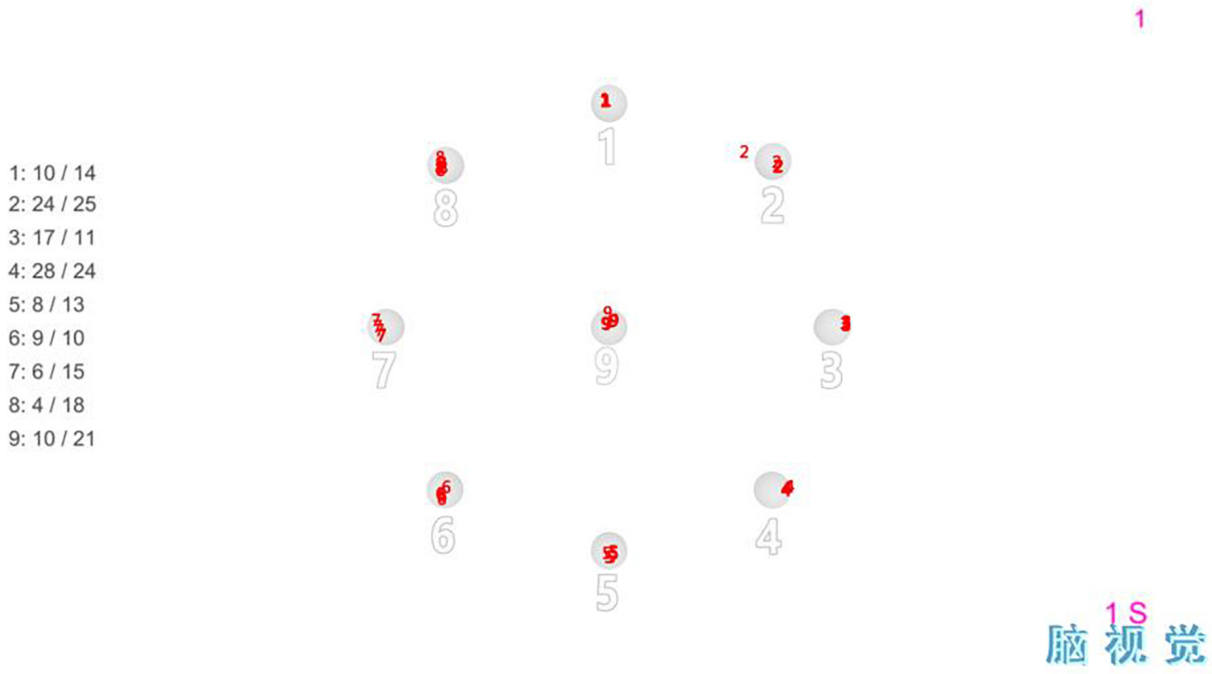

FIGURE 2
Fixational task: It consisted of fixation points of nine orientations, which were fixated in the order from 1 to 9.

3. Statistical methods

Epi-Date software was used to parallel and double input the collected data to ensure the accuracy of data input. SPSS 26.0 statistical software was used for data analysis. Since the TD data was skewed normal distribution after the normality test, we used a natural log transformation on their values to normalize data and expressed as mean ± standard deviation. The reproducibility between two measurements was evaluated using intraclass correlation coefficient (ICC). Independent sample *T* test and rank sum test were used to compare the differences of variables between the two groups, One-Way ANOVA was used to compare the differences of variables between the three groups, and linear regression analysis was performed on the basis of Pearson correlation analysis for each variable. $p < 0.05$ was considered statistically significant.

FIGURE 3
Saccadic task: It consisted of fixation points of eight orientations, which saccades were made in the order from 1 to 8.

4. Results

Table 2 is the characteristics of target displacement in fixational task and saccadic task. In the fixational task, the average TD was 3.884 ± 0.525, of which the horizontal TD was 3.602 ± 0.646, and the vertical TD was 4.060 ± 0.518. The horizontal TD was smaller than the vertical TD, and the difference was statistically significant ($p < 0.0001$). In the saccadic task, the average TD was 4.484 ± 0.509, and the horizontal TD (4.552 ± 0.664) was greater than the vertical TD (4.297 ± 0.510), and the difference was also statistically significant ($p = 0.003$). The TD in fixational task was significantly lower than that in saccadic task, and the difference was statistically significant ($p < 0.0001$).

Table 3 is the calculated measures of reproducibility of the TD by eye-tracking technology. In the eye movement examinations, two consecutive measurements of all participants were acquired. And the repeatability was assessed using the intraclass correlation coefficient (ICC). The strong ICC of TD from two measurements by eye-tracker indicated that the technology had good repeatability. The ICC values ranged from 0.812 to 0.891, $p < 0.001$.

Table 4 shows the TD of different gender and age groups under different eye movement tasks. In the fixational task, the average TD was 3.775 ± 0.566 in males and 3.934 ± 0.502 in females, and the difference was not statistically significant ($P = 0.162$). In the saccadic task, the average TD of males (4.359 ± 0.483) was lower than that of females (4.540 ± 0.512), but the difference was not statistically significant ($p = 0.094$). However, in saccadic task, the vertical TD of males was 4.061 ± 0.495, which was significantly lower than that of females (4.404 ± 0.484), $p = 0.002$.

As shown in Table 4, subjects were divided into three groups according to age: group1 (18–34 years old), group 2 (35–49 years old), and group 3 (over 50 years old). In the fixational task, the average

TABLE 2 Average magnitude of target displacement in different visual tasks (ln pixels).

Fixational task			Saccadic task		
X-axis	Y-axis	*p1*	X-axis	Y-axis	*p2*
3.602 ± 0.646	4.060 ± 0.518	*<0.001***	4.552 ± 0.664	4.297 ± 0.510	*<0.001****
3.884 ± 0.525			4.484 ± 0.509		

*p*1, comparison between TD with different directions during fixational task; *p*2, comparison between TD with different directions during saccadic task.
***$p < 0.001$; $p < 0.05$ was considered statistically significant.

TABLE 3 Calculated measures of reproducibility of the target displacements by eye-tracking technology (ICC and 95% CI).

	Fixational task			Saccadic task		
	X-axis	Y-axis	TD	X-axis	Y-axis	TD
Initial vs. second	0.815 (0.535–0.934)	0.817 (0.538–0.934)	0.891 (0.707–0.962)	0.848 (0.606–0.946)	0.812 (0.522–0.928)	0.875 (0.668–0.956)
p	*<0.001*	*<0.001*	*<0.001*	*<0.001*	*<0.001*	*<0.001*

ICC, intraclass correlation coefficient; 95% CI, 95% confidence interval.

TABLE 4 Average magnitude of target displacement in different genders and ages (ln pixels).

		Fixational task			Saccadic task		
		X-axis	Y-axis	TD	X-axis	Y-axis	TD
Genders	Males	3.490 ± 0.652	3.962 ± 0.564	3.775 ± 0.566	4.482 ± 0.687	4.061 ± 0.495	4.359 ± 0.483
	Females	3.651 ± 0.641	4.104 ± 0.494	3.934 ± 0.502	4.583 ± 0.656	4.404 ± 0.484	4.540 ± 0.512
	p	0.251	0.205	0.162	0.482	*0.002***	0.094
Age (Y)	18–34	3.568 ± 0.671	4.099 ± 0.579	3.894 ± 0.572	4.441 ± 0.615	4.307 ± 0.434	4.423 ± 0.444
	35–49	3.616 ± 0.589	4.000 ± 0.424	3.848 ± 0.456	4.633 ± 0.699	4.192 ± 0.518	4.485 ± 0.540
	≥50	3.910 ± 0.949	4.168 ± 0.627	4.136 ± 0.067	5.193 ± 0.579	5.280 ± 0.382	5.300 ± 0.290
	p	0.587	0.601	0.572	0.052	*<0.001****	*0.003***

**$p < 0.01$; ***$p < 0.001$; $p < 0.05$ was considered statistically significant.

TD was 3.894 ± 0.572 in group 1, 3.848 ± 0.456 in group 2, and 4.136 ± 0.067 in group 3. There was no significant difference between the groups ($p = 0.587$). In the saccadic task, the average TD was 4.423 ± 0.444 in group 1, 4.485 ± 0.540 in group 2, and increased to 5.300 ± 0.290 in group 3, showing an increasing trend with the increase of age, and the difference between groups was statistically significant ($p = 0.003$), and the main increase was in the vertical direction ($p < 0.001$).

5. Discussion

5.1. Eye movements during maintained fixational task

Fixational eye movement means that during maintained fixation, the gaze never comes to a complete standstill, but instead shows small displacement of the target position (Rucci and Poletti, 2015). The results of this study supported that TD always existed in the process of fixation during normal people (Table 2), and the average TD during incessant fixation was 3.884 ± 0.525 which followed a normal distribution (Figure 4). There was no gender difference ($p = 0.162$), the average TD was 3.775 ± 0.566 in males and 3.934 ± 0.502 in females (Table 4). There was no significant difference in age ($P = 0.572$), the average TD was 3.894 ± 0.572 under 35 years old, 3.848 ± 0.456 between 35 and 50 years old, and 4.136 ± 0.067 over 50 years old (Table 4). To determine the reproducibility of TD as an indicator of fixation by eye-tracking technology, two consecutive measurements of all participants were acquired in the eye movement examinations. The ICC values ranged from 0.812 to 0.891 ($p < 0.001$) indicated that the technology had good repeatability and stability in the detection of TD, which could be used in clinical examination or experimental research.

In the past, fixational eye movements have been considered as an interfering factor for a long time (Ibbotson and Krekelberg, 2011; Hafed et al., 2015), and even regarded as a representation of gaze interruption or gaze drift, which can destroy clear vision or lead to a false sense of motion. In 1804, Troxler found that during fixation, if eye movements were completely counteracted, the image in the eye would slowly disappear within a few seconds, which called "Troxler's fading" in physiology (Barrett et al., 2002). In addition, with the progress of the retinal stimulation signal research techniques, studies have pointed out that fixational eye movements play an important role in maintaining continuous perception and spatial orientation, and may be a necessary behavioral representation for maintaining normal visual tasks (Al, 1967; Ditchburn and Drysdale, 1973; Aytekin and Rucci, 2012).

Fixational eye movements are often described as involuntary movement, but some studies have shown that they can be controlled automatically at certain times, especially during the process of fine spatial vision (Poletti et al., 2013). During a virtual "needle threading" task from Ko et al., the amplitude of eye movements decreased significantly (<1°) when microsaccades precisely relocated

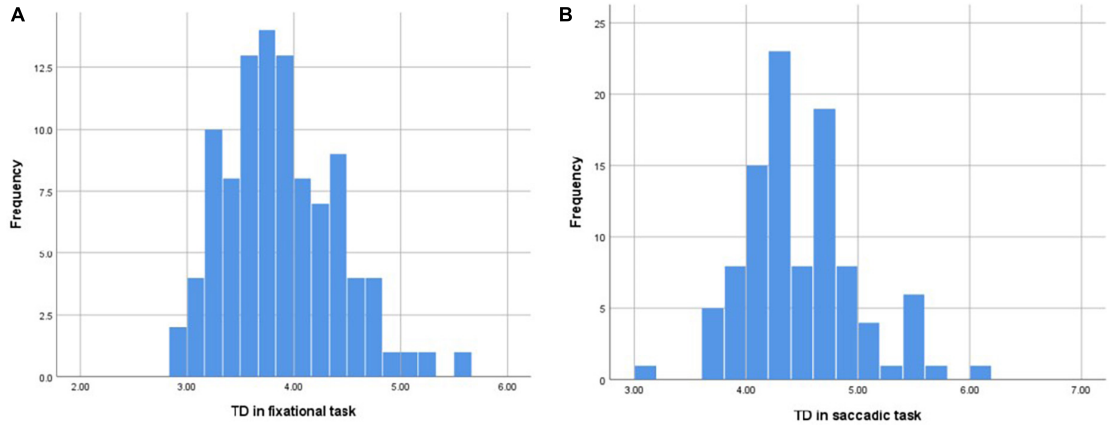

FIGURE 4
(A) The distribution of mean TD in the fixational task conformed to the normal distribution. **(B)** The distribution of mean TD in the saccadic task conformed to the normal distribution.

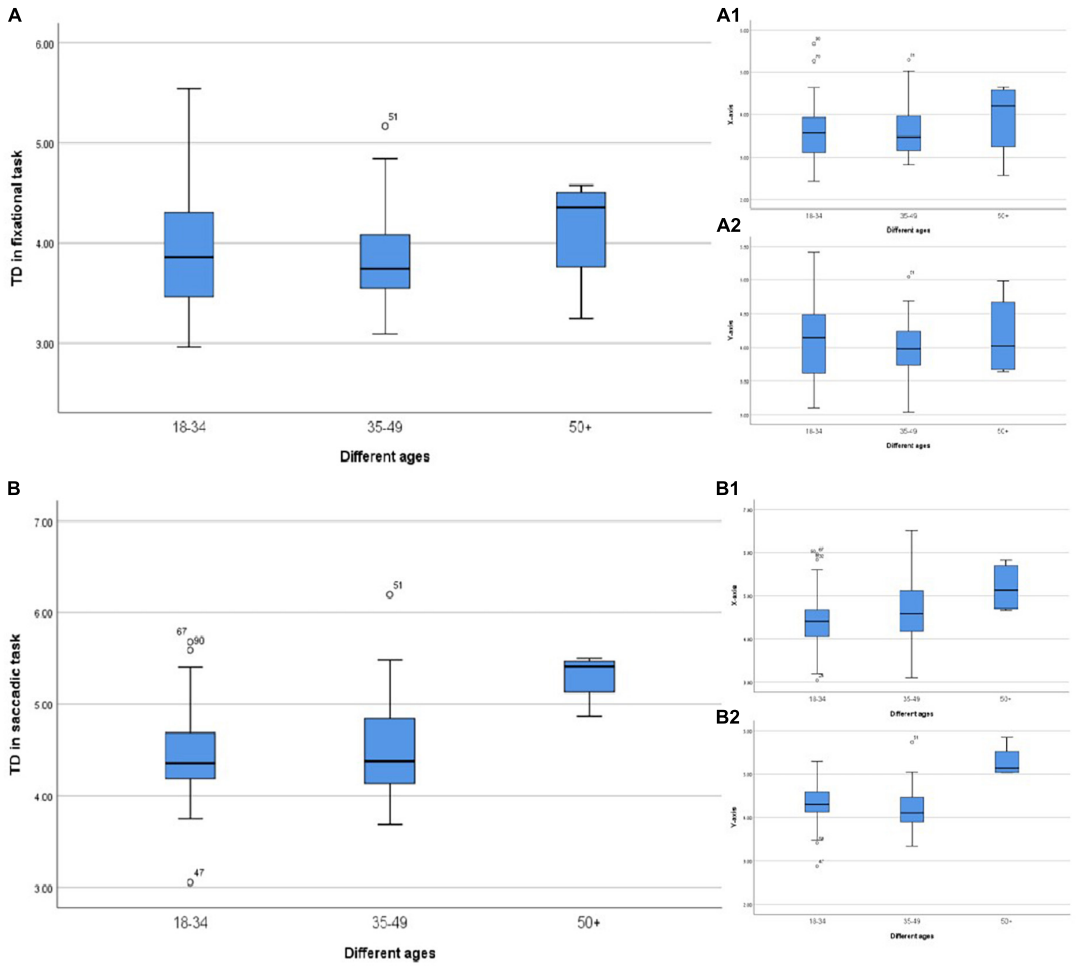

FIGURE 5
(A) TD in different ages during the fixational task. **(A1)** TD in the horizontal direction. **(A2)** TD in the vertical direction. **(B)** TD in different ages during the saccadic task. **(B1)** TD in the horizontal direction. **(B2)** TD in the vertical direction.

the line of sight alternately between the tip of the thread (Ko et al., 2010). This study found a similar phenomenon, when the eye movements induced by fixed and moving visual stimuli under different visual tasks were analyzed (Table 2), it was found that the TD was significantly decreased during fixational task compared with saccadic task ($p < 0.001$). It indicates that fixation stability depends on a variety of factors, such as the nature of the visual stimuli, the task's purpose and complexity

(Engbert and Kliegl, 2004; Cherici et al., 2012; Wieland et al., 2020).

In addition, this study was also observed the horizontal and vertical TD in the fixational eye movements. It was found that in the incessant fixational task, the TD in the horizontal direction was significantly less than that in the vertical direction (**Table 2**). We assumed that this result may related to the difference in cone densities in the horizontal and vertical meridians (Legras et al., 2018). Previous studies have shown that: in the visual process, a certain receptive field on the retina can adapt quickly after a certain period of stimulation, and no new visual signals can be generated due to the resting potential, resulting in blurred vision or even disappearance. As the only input modulation source, fixational eye movements can change the stimulated site on the retina, avoiding retinal adaptation and returning the visual function to normal (Al, 1967; Ditchburn and Drysdale, 1973; Aytekin and Rucci, 2012). Richard et al. (2018) found that the cone densities in the horizontal meridian of the macular area were higher than along the vertical meridian ($p < 0.001$). Therefore, in the process of fixation, compared with the vertical direction, less targeting displacement in the horizontal direction could change the stimulated site on the retina and avoid retinal adaptation. Therefore, in the process of fixation, less displace of visual target position in the horizontal direction can already change the stimulated site on the retina and avoid retinal adaptation, compared with the vertical direction. In fact, Andrade da Costa and Hokoç (2000) also reported that the densities of cone along the horizontal meridian of retina in the Cebus monkeys was higher, and this higher density also made the horizontal meridian maintain higher performance in the control of fixation stability, resulting in less TD during the stable fixational task.

5.2. Eye movements during saccadic task

Saccadic eye movement is a kind of rapid conjugate eye movement in the same direction of both eyes, which helps us to quickly image the target in the macular area during the saccadic tasks. Previous studies have shown that the sudden appearance of visual cues during the visual task will contribute to an increase in the amplitude of saccades (Hafed and Clark, 2002; Engbert and Kliegl, 2003; Hafed et al., 2011). In view of the results of this study, the TD in the saccadic task was significantly greater than that of the fixational task (**Table 2**), which showed that saccades induced by stimuli during the visual task can rapidly search for a new effective visual target by increasing the displacement of the visual target. However, when entering the fixation state, the TD would gradually decrease for the eyes to resume back at stable fixation state as soon as possible.

In addition, we found that the TD in the horizontal direction was significantly larger than that in the vertical direction in the saccadic task ($p = 0.003$) (**Table 2**), which may be related to the difference in the visual field range between the horizontal and vertical directions of human eyes. Previous studies have proven that the visual field range of human eyes is ranging from 188 to 200 degrees in the horizontal direction and about 120 degrees in the vertical direction (Elaine, 2012). In this study, the difference of visual targeting displacement on horizontal and vertical meridians of eye movement in saccadic task were consistent with the difference of visual field range on corresponding meridians, which might imply that the TD during the saccadic task was related to visual field searching. As mentioned above, the purpose of saccadic eye movement is to quickly move eyes in the visual field to search for a new effective visual target, while the purpose of fixation is to control the fixational position, reduce the fading of visual perception, and maintain clear vision. These two functions were quite different, which might explain our results that the TD in the horizontal direction was greater than that in the vertical direction during the saccadic task, while the TD in the horizontal direction was less than that in the vertical direction during the fixational task.

When we analyzed the TD in the saccadic task with different genders, it was found that the TD in the vertical direction of males was significantly lower than that in females (**Table 4**). Previous studies have shown that women have nearly six times visual field of men, with women having a wider visual field, while men are more likely to "stare" (Shanghai Association for Science and Technology, 2008). We speculate that females may tend to search for a wider range of visual field than males in the process of searching for targets, and this hypothesis still needs further experiments to confirm its validity.

TABLE 5 Linear regression analysis of target displacement and genders and ages.

		Fixational task			Saccadic task		
		B	95%	*P*	*B*	95%	*P*
TD	Males vs. Females	−0.166	(−0.393–0.061)	0.150	−0.166	(−0.374–0.042)	0.117
	18–34	−0.222	(−0.762–0.318)	0.417	−0.857	(−1.351–−0.363)	*0.001***
	35–49	−0.290	(−0.834–0.255)	0.294	−0.817	(−1.316–−0.319)	*0.002***
	≥50	0			0		
X-axis	Males vs. Females	−0.153	(−0.434–0.128)	0.281	−0.067	(−0.351–0.216)	0.638
	18–34	−0.324	(−0.991–0.344)	0.338	−0.743	(−1.416–−0.070)	*0.031**
	35–49	−0.296	(−0.969–0.377)	0.385	−0.561	(−1.239–0.118)	0.104
	≥50	0			0		
Y-axis	Males vs. Females	−0.159	(−0.383–0.066)	0.163	−0.356	(−0.548–−0.164)	*<0.001****
	18–34	−0.051	(−0.584–0.483)	0.851	−0.931	(−1.387–−0.475)	*<0.001****
	35–49	−0.170	(−0.708–0.368)	0.532	−1.093	(−1.553–−0.634)	*<0.001****
	≥50	0			0		

*$p < 0.05$; **$p < 0.01$; ***$p < 0.001$; $p < 0.05$ was considered statistically significant.

Furthermore, in the analysis of different age groups, we found that the TD was relatively less in the young age and middle-aged groups (<50 years old), regardless of the fixation or saccade, while the fixation stability decreased significantly in the group over 50 years old (**Figure 5**) especially in the saccadic task (**Figure 5B**). Previous studies have pointed out that saccades were mainly induced by visual information, but under some conditions, they could also be initiated after receiving information from other sources, such as mediated by vestibular. The vestibular system and other systems involved in balance have a high degree of compensatory function. There might be no clinical symptoms when the vestibular system showed aging and degeneration, but the responses declined. Lu et al. defined it as "non-pathological aging phenomenon of visual motor function." In the study of Sharpe and Sylvester (1978) saccade impairment was mainly manifested as prolonged latency, and there was a significant difference between the group aged > 40 years old and the group aged < 40 years old, suggesting that the oculomotor system was damaged in the elderly, which might be related to cerebellar atrophy. However, this study mainly showed that with the increase of age, the TD in the fixational eye movement also gradually increased, which caused fixation instability and formed visual signal noise.

At the same time, we found that the change of TD in the vertical direction was more sensitive than that in the horizontal direction during the saccadic task (**Table 5**). In previous studies on perceptual eye positions with anisometropia, we also found that patients with severe anisometropia had more obvious eye positions displacement in the vertical direction (Yang et al., 2017). The neural pathways that govern eye movements during saccadic tasks are not fully understood. However, it is generally believed that the subcortical center of the vertical gaze and its conduction pathway are located in the midbrain, while the subcortical center controlling the horizontal movement of the eye is located in the median reticular structure (Krauzlis et al., 2017). Therefore, we speculate that the visual pathways or brain regions that govern the vertical and horizontal eye movements probably different in saccadic tasks.

In conclusion, the quantitative evaluation of TD during the fixational and saccadic tasks in this study had a good repeatability. The difference of TD in different meridians was related to the nature of visual tasks: the less TD in the horizontal direction than that in the vertical direction during the fixational task might be related to the difference of cone densities in different meridians. The greater TD in the horizontal direction than that in the vertical direction during the saccadic task might be related to the difference of visual field range in different meridians. In addition, the subcortical centers that governed the horizontal and vertical direction of eye movements probably belonged to different brain regions, where dysfunction and aging of the corresponding areas would reduce the ability of the brain to control the eye muscles, resulting in a larger TD. Furthermore, our study quantified the deviation values of the visual target at nine positions in the fixational task and 10 positions in the saccadic task, and expected to establish a binocular fixation stability evaluation system based on eye tracking.

However, this study had some limitations. First, only Chinese adults were included in which the findings may not be directly applicable to other ethnic populations or to children. Second, the sample size is relatively small. In the next study, we will further improve the evaluation system by involving more subjects' data, combining clinical refraction data and binocular visual perception functions such as perceptual eye position and perceptual distortion.

Data availability statement

The original contributions presented in this study are included in the article/supplementary material, further inquiries can be directed to the corresponding author.

Author contributions

All authors listed have made a substantial, direct, and intellectual contribution to the work, and approved it for publication.

Funding

This study was supported by grants from the Science and Technology Program Project of Guangdong Province of China (2017B010110013), the Guangdong Basic and Applied Basic Research Foundation (2021A1515011822), and the Science and Technology Program of Guangzhou (202102080291).

Conflict of interest

The authors declare that the research was conducted in the absence of any commercial or financial relationships that could be construed as a potential conflict of interest.

Publisher's note

All claims expressed in this article are solely those of the authors and do not necessarily represent those of their affiliated organizations, or those of the publisher, the editors and the reviewers. Any product that may be evaluated in this article, or claim that may be made by its manufacturer, is not guaranteed or endorsed by the publisher.

References

Al, Y. (1967). *Eye movements and vision*. New York, NY: Springer Science and Business Media.

Andrade da Costa, B. L., and Hokoç, J. N. (2000). Photoreceptor topography of the retina in the new world monkey *Cebus apella*. *Vision Res.* 40, 2395–2409. doi: 10.1016/s0042-6989(00)00104-8

Apaev, A. V., and Tarutta, E. (2020). [Comparative assessment of the parameters of visual fixation in amblyopia of different origin]. *Vestn. Oftalmol.* 136, 26–31. doi: 10.17116/oftalma202013602126

Aytekin, M., and Rucci, M. (2012). Motion parallax from microscopic head movements during visual fixation. *Vision Res.* 70, 7–17. doi: 10.1016/j.visres.2012.07.017

Barrett, J. J., Mennemeier, M. S., Chatterjee, A., Fuhr, P. S., and Novack, T. A. (2002). Influence of reference frames on asymmetries in Troxler's effect. *Percept. Mot. Skills* 94, 29–38. doi: 10.2466/pms.2002.94.1.29

Cherici, C., Kuang, X., Poletti, M., and Rucci, M. (2012). Precision of sustained fixation in trained and untrained observers. *J. Vis.* 12:31. doi: 10.1167/12.6.31

Chung, S. T., Kumar, G., Li, R. W., and Levi, D. M. (2015). Characteristics of fixational eye movements in amblyopia: Limitations on fixation stability and acuity? *Vision Res.* 114, 87–99. doi: 10.1016/j.visres.2015.01.016

Ditchburn, R. W., and Drysdale, A. E. (1973). Perception of structure in flashes and in afterimages. *Vision Res.* 13, 2423–2433. doi: 10.1016/0042-6989(73)90240-X

Ditchburn, R. W., and Ginsborg, B. L. (1953). Involuntary eye movements during fixation. *J. Physiol.* 119, 1–17. doi: 10.1113/jphysiol.1953.sp004824

Elaine, N. K. N. (2012). *Human anatomy & physiology*. New York, NY: Pearson.

Engbert, R., and Kliegl, R. (2003). Microsaccades uncover the orientation of covert attention. *Vision Res.* 43, 1035–1045. doi: 10.1016/S0042-6989(03)00084-1

Engbert, R., and Kliegl, R. (2004). Microsaccades keep the eyes' balance during fixation. *Psychol. Sci.* 15, 431–436. doi: 10.1111/j.0956-7976.2004.00697.x

Hafed, Z. M., and Clark, J. J. (2002). Microsaccades as an overt measure of covert attention shifts. *Vision Res.* 42, 2533–2545. doi: 10.1016/S0042-6989(02)00263-8

Hafed, Z. M., Chen, C. Y., and Tian, X. (2015). Vision, perception, and attention through the lens of microsaccades: Mechanisms and implications. *Front. Syst. Neurosci.* 9:167. doi: 10.3389/fnsys.2015.00167

Hafed, Z. M., Lovejoy, L., and Krauzlis, R. J. (2011). Modulation of microsaccades in monkey during a covert visual attention task. *J. Neurosci.* 31, 15219–15230. doi: 10.1523/JNEUROSCI.3106-11.2011

Hunfalvay, M., Murray, N., and Carrick, F. R. (2021). Fixation stability as a biomarker for differentiating mild traumatic brain injury from age matched controls in pediatrics. *Brain Inj.* 35, 209–214. doi: 10.1080/02699052.2020.1865566

Ibbotson, M., and Krekelberg, B. (2011). Visual perception and saccadic eye movements. *Curr. Opin. Neurobiol.* 21, 553–558. doi: 10.1016/j.conb.2011.05.012

Imaoka, Y., Flury, A., and de Bruin, E. D. (2020). Assessing saccadic eye movements with head-mounted display virtual reality technology. *Front. Psychiatry* 11:572938. doi: 10.3389/fpsyt.2020.572938

Kelly, K. R., Cheng-Patel, C. S., Jost, R. M., Wang, Y., and Birch, E. E. (2019). Fixation instability during binocular viewing in anisometropic and strabismic children. *Exp. Eye Res.* 183, 29–37. doi: 10.1016/j.exer.2018.07.013

Ko, H. K., Poletti, M., and Rucci, M. (2010). Microsaccades precisely relocate gaze in a high visual acuity task. *Nat. Neurosci.* 13, 1549–1553. doi: 10.1038/nn.2663

Krauzlis, R. J., Goffart, L., and Hafed, Z. M. (2017). Neuronal control of fixation and fixational eye movements. *Philos. Trans. R. Soc. Lond. B Biol. Sci.* 372:20160205.

Legras, R., Gaudric, A., and Woog, K. (2018). Distribution of cone density, spacing and arrangement in adult healthy retinas with adaptive optics flood illumination. *PLoS One* 13:e0191141. doi: 10.1371/journal.pone.0191141

Martinez-Conde, S., and Macknik, S. L. (2017). Unchanging visions: The effects and limitations of ocular stillness. *Philos. Trans. R. Soc. Lond. B Biol. Sci.* 372:20160204. doi: 10.1098/rstb.2016.0204

Poletti, M., Listorti, C., and Rucci, M. (2013). Microscopic eye movements compensate for nonhomogeneous vision within the fovea. *Curr. Biol.* 23, 1691–1695. doi: 10.1016/j.cub.2013.07.007

Rucci, M., and Poletti, M. (2015). Control and functions of fixational eye movements. *Annu. Rev. Vis. Sci.* 1, 499–518.

Rucci, M., and Victor, J. D. (2015). The unsteady eye: An information-processing stage, not a bug. *Trends Neurosci.* 38, 195–206. doi: 10.1016/j.tins.2015.01.005

Salati, R., Borgatti, R., Giammari, G., and Jacobson, L. (2002). Oculomotor dysfunction in cerebral visual impairment following perinatal hypoxia. *Dev. Med. Child Neurol.* 44, 542–550. doi: 10.1017/s0012162201002535

Sharpe, J. A., and Sylvester, T. O. (1978). Effect of aging on horizontal smooth pursuit. *Invest. Ophthalmol. Vis. Sci.* 17, 465–468.

Valsecchi, M., Gegenfurtner, K. R., and Schütz, A. C. (2013). Saccadic and smooth-pursuit eye movements during reading of drifting texts. *J. Vis.* 13:8. doi: 10.1167/13.10.8

Wieland, B., Behringer, M., and Zentgraf, K. (2020). Withdrawal notice to: "Motor imagery and the muscle system". *Int. J. Psychophysiol.* 156, 87–92. doi: 10.1016/j.ijpsycho.2020.09.001

Shanghai Association for Science and Technology (2008). Female have 6 times the visual field of male. *Sci. Lifestyle* 80–81.

Yang, C., Li, X., Zhang, G., Lan, J., Zhang, Y., Chu, H., et al. (2017). Comparison of perceptual eye positions among patients with different degrees of anisometropia. *Medicine (Baltimore)* 96:e8119. doi: 10.1097/MD.0000000000008119

frontiers | Frontiers in Neuroscience

TYPE Original Research
PUBLISHED 06 February 2023
DOI 10.3389/fnins.2023.1105158

OPEN ACCESS

EDITED BY
Wensi Tao,
University of Miami Health System,
United States

REVIEWED BY
Fangfang Song,
Wuhan University, China
Ying Ting Sit,
Children's Hospital of Philadelphia,
United States
Hailan Zou,
The University of Hong Kong, Hong Kong SAR, China

*CORRESPONDENCE
Shu-Chao Wang
✉ wangshuchao@csu.edu.cn

†These authors have contributed equally to this work

SPECIALTY SECTION
This article was submitted to Visual Neuroscience, a section of the journal Frontiers in Neuroscience

RECEIVED 22 November 2022
ACCEPTED 09 January 2023
PUBLISHED 06 February 2023

CITATION
Zhang J-H, Wang M-J, Tan Y-T, Luo J and Wang S-C (2023) A bibliometric analysis of apoptosis in glaucoma.
Front. Neurosci. 17:1105158.
doi: 10.3389/fnins.2023.1105158

A bibliometric analysis of apoptosis in glaucoma

Jia-Heng Zhang[1,2†], Mei-Juan Wang[3†], Ya-Ting Tan[1,4], Jia Luo[5] and Shu-Chao Wang[1,6*]

[1]Center for Medical Research, The Second Xiangya Hospital of Central South University, Changsha, Hunan, China, [2]Clinical Medicine 5-Year Program, 19 Grade, Xiangya School of Medicine, Central South University, Changsha, China, [3]Medical Imaging Center, Qingdao West Coast New District People's Hospital, Qingdao, Shandong, China, [4]Department of Anatomy and Neurobiology, School of Basic Medical Sciences, Central South University, Changsha, Hunan, China, [5]Hunan Key Laboratory of the Research and Development of Novel Pharmaceutical Preparations, Changsha Medical University, Changsha, China, [6]National Clinical Research Center for Mental Disorders, The Second Xiangya Hospital of Central South University, Changsha, China

Background: Glaucoma is the first irreversible and second blindness disease, which is characterized by the death of retinal ganglion cells (RGCs) and degeneration of the optic nerve. Previous works have indicated that apoptosis is the main reason for RGC death in glaucoma. Although many studies have investigated the mechanism of apoptosis and different strategies targeting apoptosis to protect the RGCs and finally recover the impaired vision in the glaucoma. However, the global trend and hotspots of apoptosis in glaucoma have not been well illustrated and discussed.

Methods: Documents were extracted from the Web of Science Core Collection on November 2, 2022. We selected articles and reviews published in English from January 1, 1999 to November 1, 2022 to perform visual analysis and statistical analysis of countries, institutions, authors, references and keywords by VOSviewer 1.6.18 and CiteSpace 5.8.

Results: The publications about apoptosis in glaucoma show an increasing trend over time. Besides, the authors, institutions in the US and China published the most numbers of articles with the highest citation, which may be leading the research in the field of apoptosis in glaucoma. Last, series of advanced research results, technology and treatment for glaucoma, such as the discovery of key regulatory mechanisms on RGC apoptosis are emerging and will provide precise strategies for the treatment of glaucoma.

Conclusion: This research will broaden our comprehension about the role of apoptosis in the process of glaucoma, and provide guidelines for us in basic research and disease treatment in the further.

KEYWORDS

bibliometric, CiteSpace, VOSviewer, apoptosis, glaucoma, retinal ganglion cell

Introduction

Glaucoma affects 80 million people worldwide (Ju et al., 2022; Liu et al., 2022). It is characterized by the death of retinal ganglion cells (RGCs) and the degeneration of the optic nerve, ultimately leading to progressively impaired vision (Wang et al., 2017a; Chen et al., 2022b). High intraocular pressure (IOP) is thought to be the primary risk factor for RGC death (Hu et al., 2020; Ju et al., 2022). Previous studies have indicated that apoptosis is the main reason for RGC loss in glaucoma (Hu et al., 2021; Cordeiro et al., 2022). Apoptosis is a type of programmed cell death that usually occurs in developing tissues and during homeostasis in organisms (Wang et al., 2019; Yan et al., 2022, 2023). Apoptosis is characterized by chromatin condensation, nuclear fragmentation, and the formation of apoptotic bodies (Zhang et al., 2021; Wang et al., 2023). In recent decades, many studies have indicated that RGC apoptosis occurs in

glaucoma, and the mechanisms of RGC apoptosis have been widely investigated (Hu et al., 2021; Cordeiro et al., 2022). In addition, different strategies targeting apoptosis to protect RGCs and recover impaired vision in glaucoma are emerging (Chitranshi et al., 2018; Cordeiro et al., 2022). However, the global trends and research hotspots of apoptosis in glaucoma have not been well illustrated and discussed.

Compared to a review in general, bibliometric analysis is a mathematically and statistically feasible discipline to summarize and predict current and future research hotspots and trends by evaluating specific research areas based on main authors, research institutes, journals, citation frequency, keywords, etc (Hu et al., 2022; Zhang et al., 2022). CiteSpace and VOSviewer are two common and important bibliometric analysis software (Chen et al., 2022a; Zhang et al., 2022; Zhao et al., 2022). By using them alone or in combination, we obtain a better analysis of research trends and hotspots according to different specifications (Romero and Portillo-Salido, 2019; Zhao et al., 2022).

Our group focused on the research of apoptosis and necroptosis in the nervous system, which is involved in glaucoma and trauma. A bibliometric analysis broadens our understanding of existing research hotspots, future trends, and implications of apoptosis in glaucoma and other diseases, which can help to clarify the research status and identify the latest and most influential progress. In addition, a bibliometric analysis may provide us with useful tools to make clinical decisions and propose guidelines by analyzing keywords about drugs, examination, and treatment (Dai et al., 2022).

In this current study, we aimed to summarize and analyze the current research hotspots and future research trends of apoptosis in glaucoma using bibliometric analysis. This study deepens our understanding of the role of apoptosis in glaucoma and provides guidelines for basic research and disease treatment in the future.

Materials and methods

Data collection and strategy for data retrieval

The data retrieval strategy and collection process for this study are shown in Figure 1. We collected the bibliographic data in the Web of Science Core Collection (WoSCC) and download the "Full record and cited references" of the literature in "plain text" format. We screened target literature based on: (1) search formula: ALL = (glaucoma and apoptosis); (2) Document type: "Article" and "Review"; (3) Publication date: 1 January 1999 to 1 November 2022; (4) Literature Language: English. The search was completed on 2 November 2022. Our initial search for research papers on glaucoma and apoptosis was first published in 1999, so we set our search to start in 1999. We ended up with 1,674 documents that met the criteria.

Data analysis and network mapping

Bibliometrics is an efficient tool that helps researchers visualize the evolution of published literature. The analytical dimensions of bibliometrics include the year of publication, country and region, institution, journal, author, keywords, and co-citations. We imported the data from WoSCC into VOSviewer (version 1.6.18; https://www.vosviewer.com/downloavosviewer) and CiteSpace (version 5.8.R3; https://sourceforge.net/project/citespace/files/latest/do). CiteSpace and VOSviewer can be used to analyze the potential information contained in complex data, and present the structure, law, and distribution of information through visual means. Co-occurrence analysis refers to counting the frequency of occurrence of multiple phrases in the same article to determine their proximity, so as to obtain hot spots and future trends in the discipline. Co-citation analysis is used to discover the basic literature and knowledge in this research field (Romero and Portillo-Salido, 2019). The result provides information on the past, present, and future dimensions of the research field. In addition, we used Microsoft Office Excel 2021 to analyze trends in published articles over time.

In the visualization map below, each circle represents a node, and the diameter size of the circle represents how often the label appears in the co-occurrence analysis. The color of a circle is determined by the cluster of categories to which it belongs. The connection between nodes represents the association of the corresponding node, and the strength of the association between nodes is expressed in line width.

Results

Annual global publication outputs on glaucoma and apoptosis

The annual publication trend of apoptosis in glaucoma is shown in Figure 2. From 1999 to 2022, the amount of literature in this field increased from 1999 ($n = 23$, 1.37%) to 2021 ($n = 132$, 7.89%), and peaked in 2021. As of November 2022, we believe that the number of publications in 2022 will increase, following previous years' trends.

Co-authorship of countries/regions

VOSviewer was used to analyze the authors' countries, regions, and partnerships, and the results are shown in Figure 3. Table 1 lists 10 countries with the highest number of publications. China published the most literature (482 documents and 7,217 citations), but the United States was the most influential country in this field (468 documents and 24,687 citations) in terms of overall citations. A network of coauthors from 40 countries or regions with more than three studies was divided into eight cluster groups with different color representations. The largest cluster (red) consisted of nine countries centered in the United States, the United Kingdom, and Canada.

Distribution of source journals and top 10 high-cited articles

Articles on glaucoma and apoptosis were published in 435 journals. Table 2 lists the top 10 journals with the most publications, accounting for 31.7% (531 documents and 1,674 citations) of all publications, and the distribution has a strong head effect. *Investigative Ophthalmology & Visual Science* was the most prolific journal (154 documents) and the most cited (9,011 citations), followed by *Experimental Eye Research* (80 documents). Although *Progress in Retinal and Eye Research* published only four studies, it was cited 4,183 times, indicating that the journal has a high impact factor.

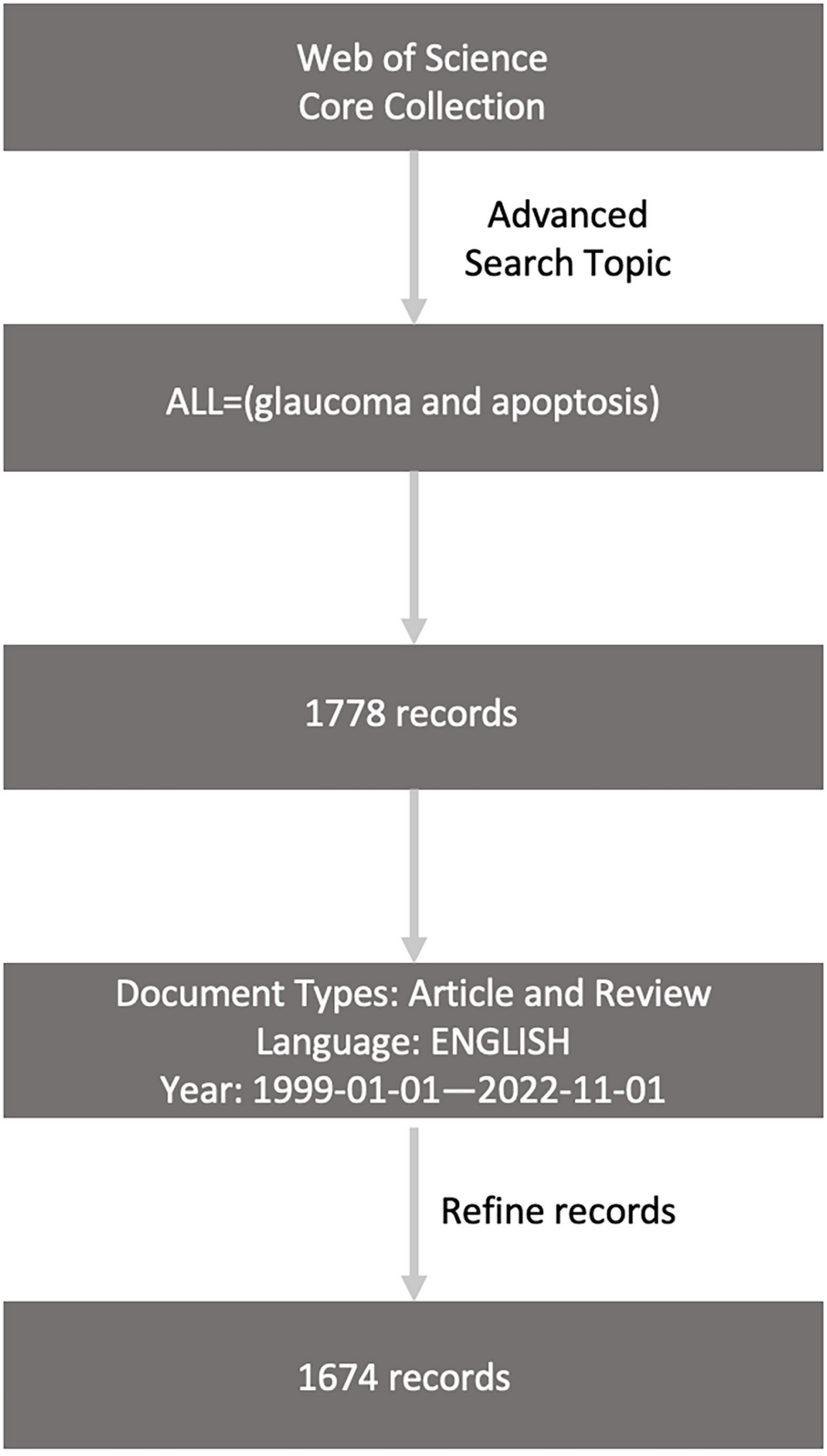

FIGURE 1
The data collection and retrieval strategy.

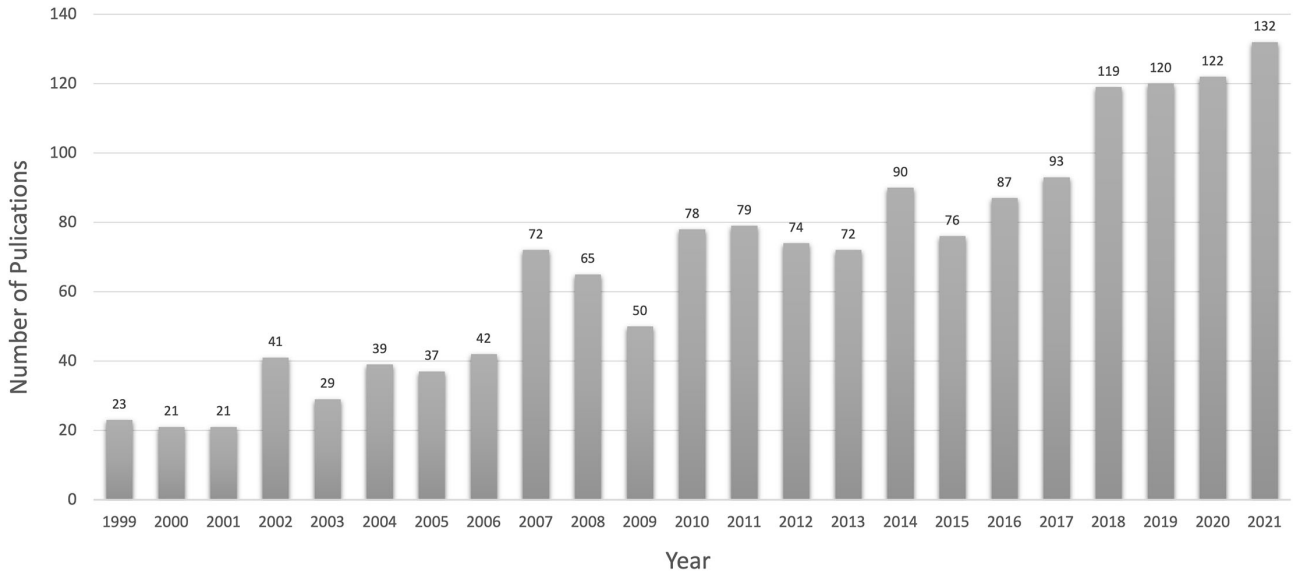

FIGURE 2
The number of articles published has grown steadily and peaked in 2021.

A total of 114 articles were cited more than 100 times. Table 3 lists the top 10 cited literature. Among them, "Muller Cells in The Healthy and Diseased Retina" (Bringmann et al., 2006), published in *Progress in Retinal and Eye Research* in 2006, was the most cited literature (1,178 citations). The lowest number of citations overall was 327.

Distribution and co-authorship of institutions

The top 10 institutions with the highest number of publications are listed in Table 4. University of Wisconsin (48 documents and 2,754 citations) appears to be the most influential institution in the field, with the second-highest number of publications and the highest number of citations. Fudan University and Shanghai Jiao Tong University, two Chinese universities, have published more literature but have lower citations (526 citations and 522 citations, respectively).

The network of coauthors from the research institutions is shown in Figure 4. Regardless of the green or red cluster, the vast majority of cooperation is limited to the country.

Distribution and co-authorship of authors

The top five authors who published the most articles were all from England, the USA, and China. Dr. Cordeiro from Imperial College London has published 22 articles over the past 31 years, ranking as the top author in the field of apoptosis in glaucoma. Table 5 lists the top 10 authors with the highest number of published articles. Cordeiro, M. Francesca (22 documents and 1,254 citations) was the most prolific, followed by Nickells, Robert W. (20 documents and 996 citations). We set the threshold to five documents and screened a total of 182 authors who met the criteria; the results are shown in Figure 5. There are nine color classifications, of which the largest is the red cluster, composed of 38 authors centered around Osborne, Neville N, Zhuo, and Yehong.

Co-citation analysis of cited references

We listed the top 10 citations in Table 6, with citations ranging from 96 to 231. As shown in Figure 6, the paper titled "Retinal ganglion cell death in experimental glaucoma and after axotomy occurs by apoptosis" (Quigley et al., 1995), published in *Ophthalmology & Visual Science* in 1995, has the most citations (231 citations).

Figure 7 shows the top 20 documents with the strongest citation outbreaks. "TUNEL-positive ganglion cells in human primary open-angle glaucoma" (Kerrigan et al., 1997), published in *Arch Ophthalmol* in 1997, had the highest impact at 19.29. The study proposes that apoptosis plays an important role in nerve cell death in primary open-angle glaucoma. "Global prevalence of glaucoma and projections of glaucoma burden through 2040: A systematic review and meta-analysis" (Tham et al., 2014), published in *Ophthalmology* in 2014, has the most citation outbreaks in recent years, with researchers predicting that the number of glaucoma cases will increase to more than 100 million by 2040. This poses a significant threat to human eye health.

The co-occurrence analysis of the keywords

Keywords can indicate the topic of the publication; therefore, by analyzing keywords, we can understand emerging trends in research. We extracted and clustered the top 50 keywords in the study using VOSviewer (Table 7). The keywords were glaucoma (526 times), apoptosis (384 times), retinal ganglion cells (341 times), neuroprotection (201 times), and oxidative stress (122 times).

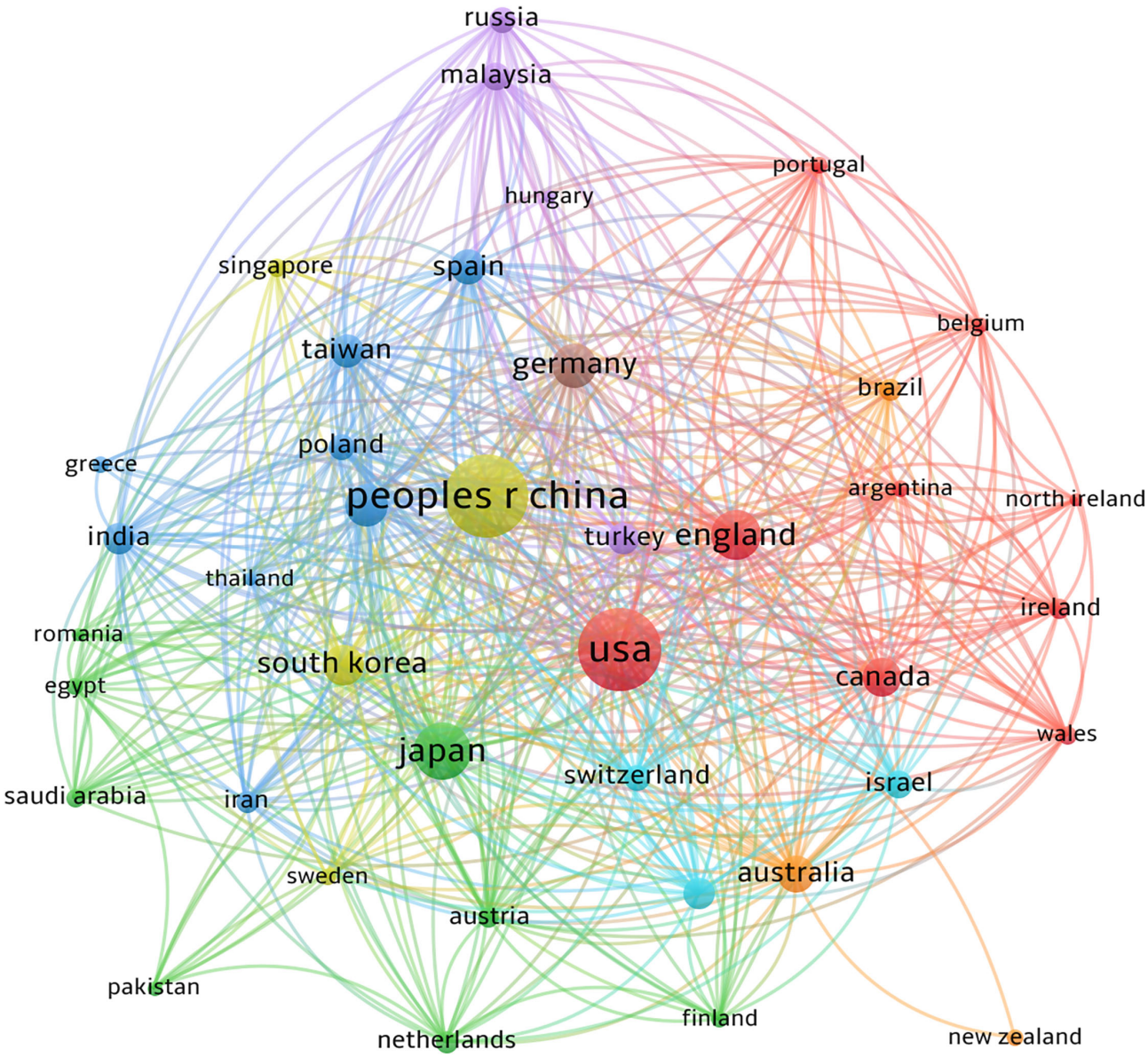

FIGURE 3
A total of 56 countries or regions have participated in the study of apoptosis in glaucoma. China and the United States are at the center of the study. The red cluster is centered in the United States. China's cooperation between countries and regions is relatively weak.

Most frequently in the author's keywords

We color-coded keywords according to the average year of occurrence (AAY) in the literature in the field, then explored the evolution trend of keywords over time, and visualized them in Figure 8. Recent keywords included mitophagy (AAY:2022.17), endoplasmic reticulum stress (AAY:2019.44), autophagy (AAY:2018.03), melatonin (AAY:2017.83), proteomics (AAY:2016.67), and epigenetics (AAY:2016.15).

Concerning glaucoma treatment progress, we listed the top 60 keywords occurring most frequently in Table 8, covering glaucoma drug treatment, surgical treatment, and eye examination. Figure 9 is a visualization of Table 8. The most frequent keyword was *N-Methyl-D-aspartate* (NMDA) receptor antagonists (59 times). NMDA-induced excitatory toxicity plays an important role in glaucoma-induced RGC death and the lack of NMDA receptor subunits in experiments can reduce the excitotoxic effect of NMDA, thereby protecting RGCs in mice (Hayashi et al., 2021). A classic treatment for glaucoma is trabeculectomy, which appeared 39 times. In addition, trabeculectomy in combination with antimetabolites, such as mitomycin-c (31 times) or 5-fluorouracil (19 times), has long been known to improve prognosis. We could see a close connection between the three keywords (Figure 9). In summary, we obtained an overview of glaucoma treatment using keyword analysis.

10.3389/fnins.2023.1105158

TABLE 1 The top 10 productive countries/regions.

Rank	Country	Documents	Citation
1	China	482	7,217
2	USA	468	24,687
3	Japan	166	5,410
4	England	114	6,788
5	Germany	85	3,412
6	Italy	75	2,859
7	South	70	1,678
8	Korea	60	2,485
9	Canada	52	1,625
10	Australia	45	1,378

TABLE 2 The top 10 journals for publications.

Journals	Documents	Citation	IF (2022)
Investigative ophthalmology and visual science	154	9,011	4.925
Experimental eye research	90	2,409	3.770
Molecular vision	60	1,598	2.711
Current eye research	52	981	2.555
Plos one	49	1,328	3.752
International journal of molecular science	28	240	6.208
Brain research	27	1,378	3.610
International journal of ophthalmology	26	154	1.645
Journal of glaucoma	24	1,019	2.290
Cell death and disease	21	783	9.685

TABLE 3 The top 10 highest cited articles.

Title	Journal	Citation	PY
Muller cells in the healthy and diseased retina	Progress in retinal and eye research	1,178	2006
Neuronal death in glaucoma	Progress in retinal and eye research	582	1999
Preservatives in eyedrops: the good, the bad and the ugly	Progress in retinal and eye research	566	2010
The role of the reactive oxygen species and oxidative stress in the pathomechanism of the age-related ocular diseases and other pathologies of the anterior and posterior eye segments in adults	Oxidative medicine and cellular longevity	563	2016
The molecular basis of retinal ganglion cell death in glaucoma	Progress in retinal and eye research	549	2012
Para-inflammation in the aging retina	Progress in retinal and eye research	459	2009
Obstructed axonal transport of BDNF and its receptor TrkB in experimental glaucoma	Investigative ophthalmology and visual science	408	2000
The role of apoptosis in age-related macular degeneration	Archives of ophthalmology	398	2002
Unexpected low-dose toxicity of the universal solvent DMSO	Faseb journal	367	2014
Neuroprotection in relation to retinal ischemia and relevance to glaucoma	Survey of ophthalmology	327	1999

PY, Published Year.

Discussion

In this current study, we used bibliometric tools to visualize and analyze current publications in the area of apoptosis in glaucoma and found that the publications on apoptosis in glaucoma increased over time. In addition, authors and universities in the US and China may be leading research in this field. It should also be noted that a series of advanced research results, technologies, and treatments for glaucoma, such as the discovery of key regulatory mechanisms of RGC apoptosis, are emerging and will provide strategies for glaucoma treatment.

In the current study, we conclude the increasing trend of publications over the years indicates the importance and progress of research in the field of apoptosis in glaucoma. Presently, China, the US, and Japan are the top three countries with the highest number of articles, implying that they are the research centers in this field. The most cited research is Dr. Quigley's (John Hopkins Hospital), "Retinal ganglion cell death in experimental glaucoma and after axotomy occurs by apoptosis (Quigley et al., 1995), which was cited 231 times. It indicated that RGCs die due to apoptosis after axotomy injury

TABLE 4 The top 10 productive institutions.

Rank	Organization	Country	Documents	Citation
1	Sun Yat Sen University	China	49	1,449
2	University Wisconsin	USA	48	2,754
3	Fudan University	China	44	526
4	Shanghai Jiao tong University	China	36	522
5	UCL	Britain	31	2,023
6	Johns Hopkins University	USA	23	2,317
7	University Calif San Diego	USA	22	1,185
8	University Oxford	Britain	22	2,572
9	University Texas	USA	22	1,084
10	Harvard University	USA	21	1,452

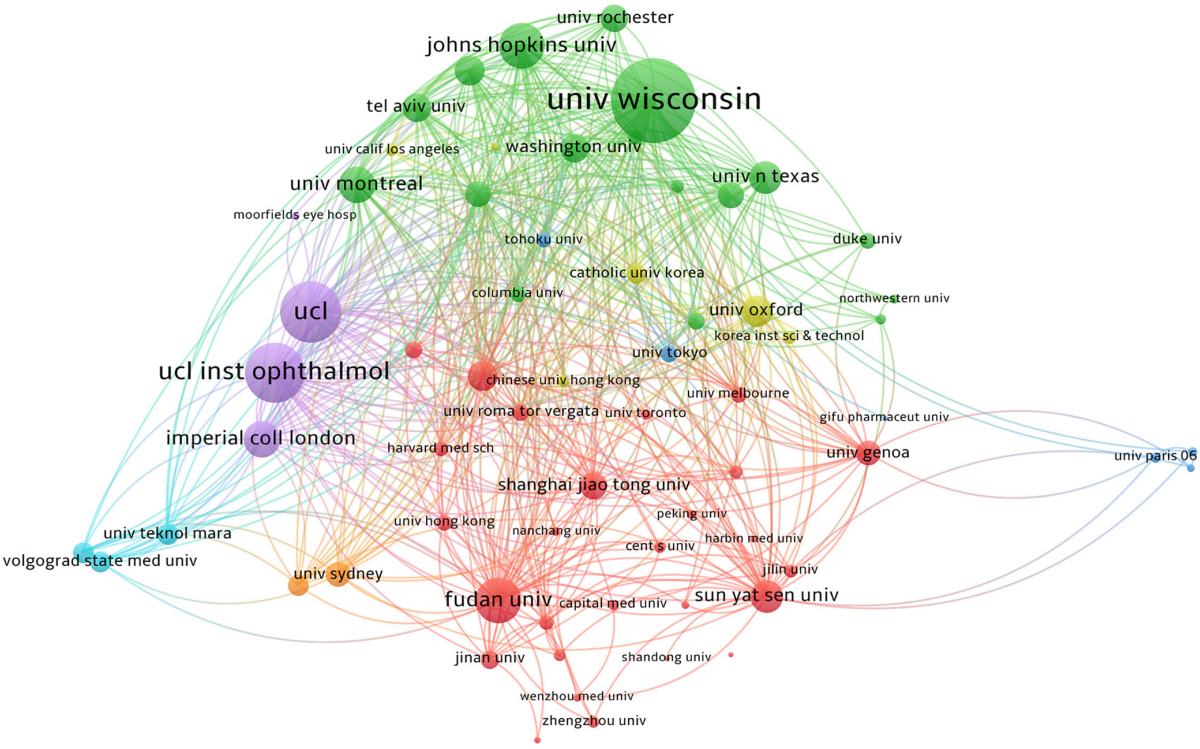

FIGURE 4
A total of 1,538 institutions participated in the study of apoptosis in glaucoma. The network of co-authors was divided into seven clusters of different colors. The green cluster is dominated by American institutions, and the University of Wisconsin had the greatest impact. The red cluster is dominated by Chinese institutions.

TABLE 5 The top 10 productive authors.

Rank	Author	Total publications	Citation	Avg citation
1	Cordeiro, M. Francesca	22	1254	57
2	Nickells, Robert W.	20	996	50
3	Guo, Li	17	820	48
4	Zhuo, Yehong	17	701	41
5	Schlamp, Cassandra L.	16	771	48
6	Pfeiffer, Norbert	16	276	17
7	Wang, Zhongfeng	15	245	16
8	Weinreb, Robert N.	15	920	61
9	Agarwal, Renu	15	149	10
10	Osborne, Neville N.	15	2095	140

and glaucoma. This provided preliminary evidence that apoptosis is the mode of RGC death and may be triggered by excitotoxins, which is important for designing strategies to protect RGCs. The journal *Ophthalmology & Visual Science* published the most articles on apoptosis in glaucoma. *Cell Death & Disease* was the journal with the highest impact factor (IF), IF 2021 = 9.685. Prof. Bringmann published a review "Muller cells in the healthy and diseased retina" (Bringmann et al., 2006) in *Progress In Retinal and Eye Research*, which is one of the top five journals (IF > 10) and is cited 1,178 times. It indicated that retinal diseases such as glaucoma are associated with Muller cell reactivation. Under normal conditions, Muller cells maintain retinal neurons by releasing neurotrophic factors and deactivating excitotoxins. After injury or disease, Muller cells may accelerate neuronal death, as they can be dysregulated leading to a disturbance in glutamate metabolism in the retina, ultimately causing neuronal cell death. A deeper understanding of Muller cell reactivation and targeting may be a useful therapeutic strategy to protect retinal neurons against apoptosis.

Furthermore, we used co-occurrence cluster analysis to produce and analyze the network graph of keywords found in studies on apoptosis in glaucoma. Based on the analysis of keyword frequencies, research hotspots could be identified. Among the top 50 most common keywords were: caspase, akt, bcl-2, and nitric oxide. The keyword results showed that research trends in glaucoma are diversifying, which is not only restricted to ophthalmology but also included progress in cell biology, biochemistry, and genetics. Based on keyword co-occurrence analysis, changes in research trends could be visualized. Initially, keywords including glaucoma, apoptosis, retinal ganglion cells, neuroprotection, and oxidative stress appeared earlier. In the analysis of frequencies and centralities of the keywords, drugs such as "benzalkonium chloride," "resveratrol," and "citicoline," and keywords related to

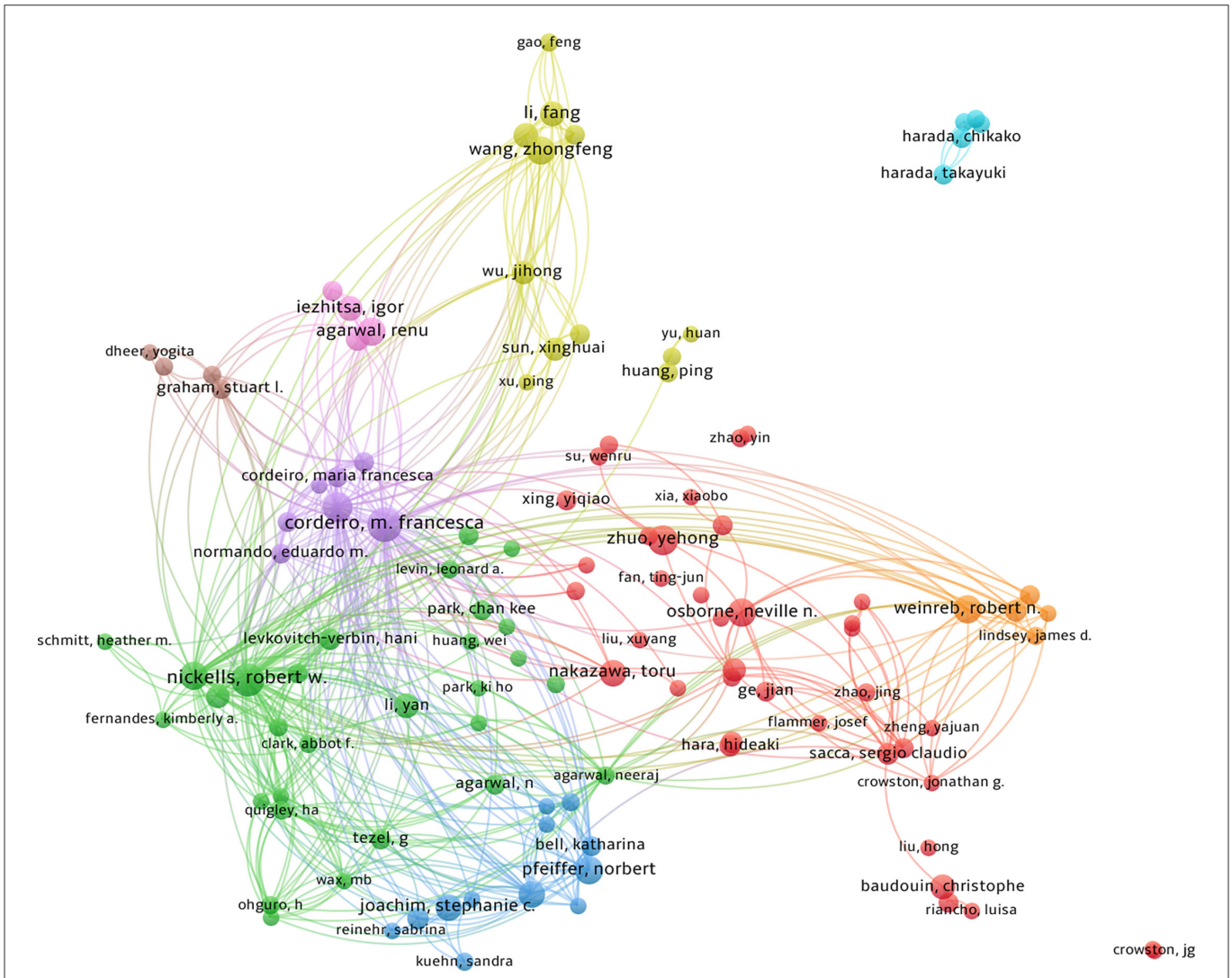

FIGURE 5
A total of 6,888 authors participated in the writing process. The Linlog/modular model was used for analysis. The weight is Total Link Strength. The size of the circle represents the amount of influence of the author. Inter-node connections represent author collaboration and the lines of connection between nodes represent the collaboration between authors.

gene research, such as "caspase," "akt," and "bcl-2," appeared earlier. These results suggest that more research on pathological mechanisms and treatment methods was carried out. In addition, after 2016, keywords such as mitophagy, endoplasmic reticulum stress, gliosis, inflammation, autophagy, melatonin, annexin, cytotoxicity, proteomics, and epigenetics were mostly retrieved and showed persistence in recent years, suggesting that this field is the next key direction and are hotspot in studies on apoptosis in glaucoma.

High IOP is the primary risk factor for glaucoma (Cheng et al., 2018). However, IOP measurement alone is not the sole diagnostic standard for glaucoma (Gedde et al., 2021; Steiner et al., 2022). Patients with any symptoms of glaucoma will progress to irreversible RGC loss and optic nerve degeneration (Wang et al., 2017b; Donahue et al., 2021). By analyzing emerging research in glaucoma treatment, some keywords related to examination and treatment have been developed in recent years. The most frequent keyword is NMDA receptor antagonists. NMDA is the most frequent and important excitatory acid in the nervous system, which induces excitatory toxicity and plays an important role in glaucoma-induced RGC death (Hayashi et al., 2021). In experimental glaucoma models, lack of NMDA receptors or NMDA inhibition can reduce the excitotoxic effects of NMDA, thereby protecting RGCs in mice (Hayashi et al., 2021; Sato et al., 2021). As a classic treatment for glaucoma (Olawoye and Etya'ale, 2021; Philippin et al., 2021), trabeculectomy appears 39 times, ranking as the second most frequent treatment keyword. In addition, trabeculectomy in combination with antimetabolites such as mitomycin-c (top three treatment keyword) or 5-fluorouracil (top 12 treatment keyword) has long been known to improve the prognosis for glaucoma treatment (Theventhiran et al., 2021; Al-Mugheiry et al., 2022; Yang et al., 2022). Ophthalmoscopy is a common technology used to detect the optic nerve head and neuronal loss (Coote, 1857; Quigley and Anderson, 1977). We also found that optical coherence tomography (OCT) appeared in 2011 and ranked among the top six treatment keywords, indicating that it is key in research on apoptosis in

TABLE 6 The top 10 most co-cited references.

Rank	First author	Year	Journal	Title	Citations
1	Quigley HA	1995	Invest ophthalmol vis sci	Retinal ganglion cell death in experimental glaucoma and after axotomy occurs by apoptosis	231
2	Quigley HA	2006	British Journal of ophthalmology	The number of people with glaucoma worldwide in 2010 and 2020	185
3	Kerrigan LA	1997	Arch ophthalmol	TUNEL-positive ganglion cells in human primary open-angle glaucoma	141
4	Garcia Valenzuela E	1995	Exp eye res	Programmed cell death of retinal ganglion cells during experimental glaucoma	139
5	Almasieh M	2012	Prog retin eye res	The molecular basis of retinal ganglion cell death in glaucoma	118
6	Tham YC	2014	Ophthalmology	Assessment of iris surface features and their relationship with iris thickness in Asian eyes	114
7	Dreyer EB	1996	Archives of ophthalmology	Elevated glutamate levels in the vitreous body of humans and monkeys with glaucoma	105
8	Tezel G	2006	Prog retin eye res	Oxidative stress in glaucomatous neurodegeneration: mechanisms and consequences	102
9	Robert N Weinreb	2014	JAMA	The pathophysiology and treatment of glaucoma: a review	98
10	Quigley HA	1996	British journal of ophthalmology	Number of people with glaucoma worldwide	96

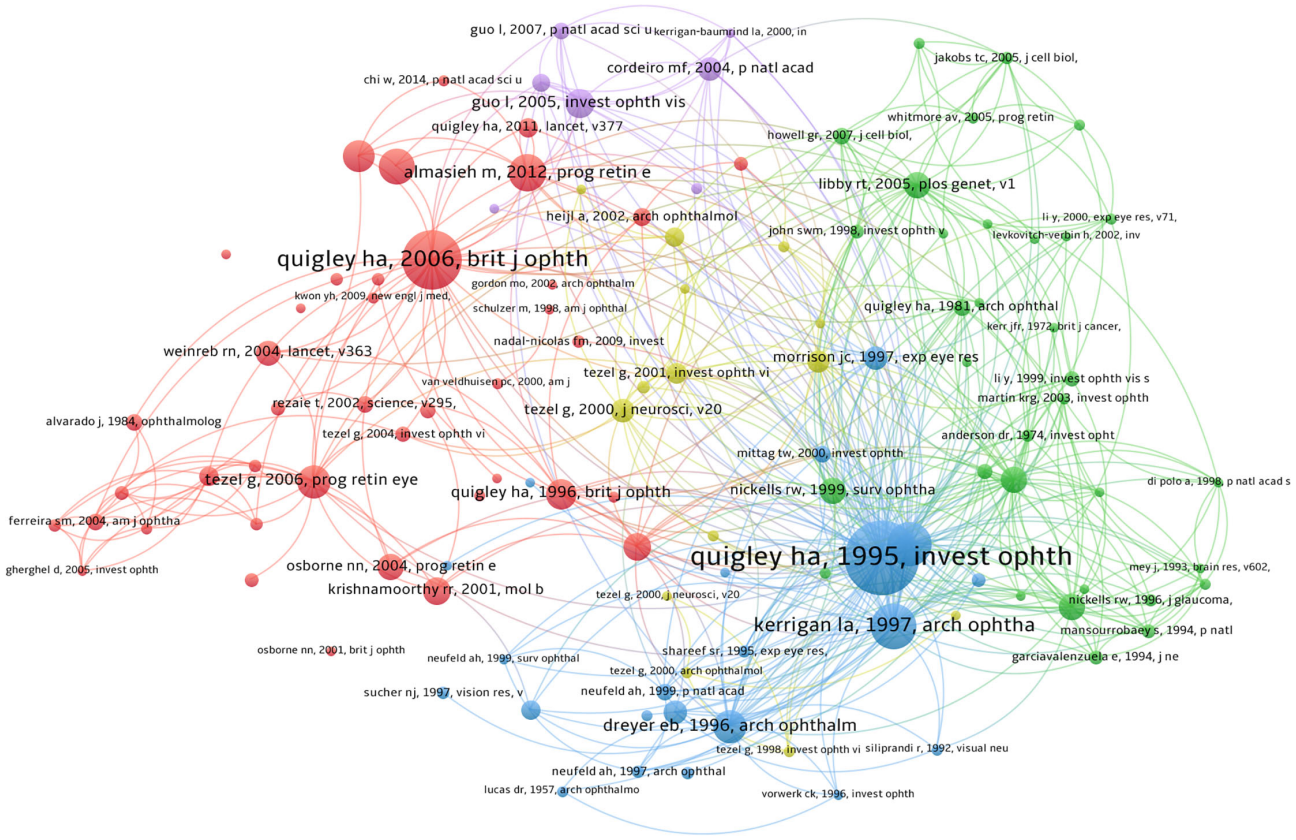

FIGURE 6
A total of 58,156 literature was cited from 1,674 retrieved literature. The two most cited articles in co-citation analysis were written by Quigley HA. The same color clusters indicate the documents are related or have some commonalities.

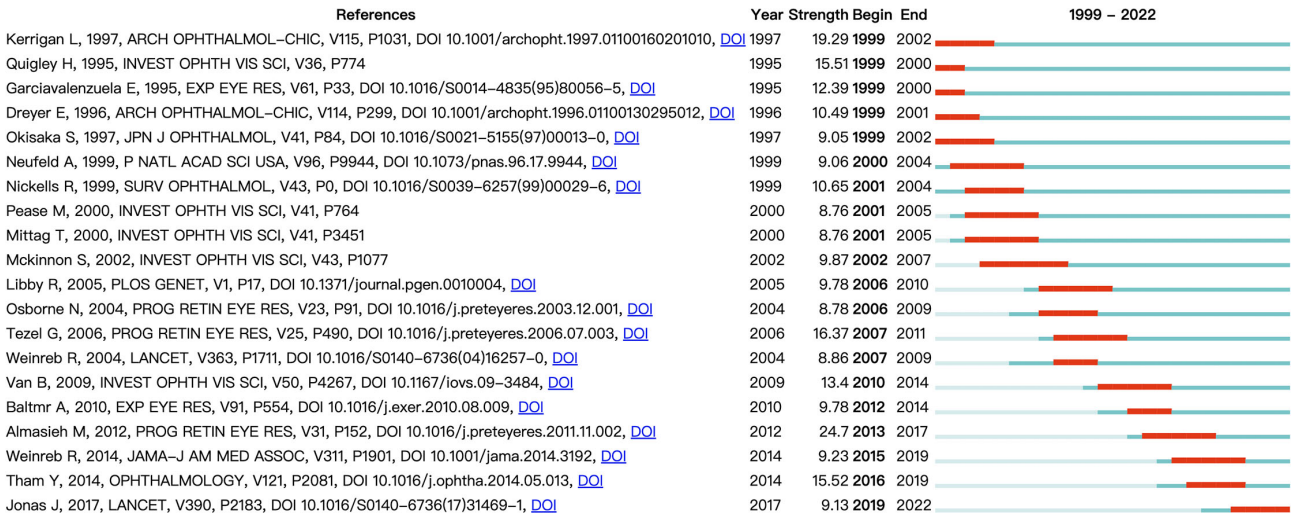

FIGURE 7
A citation burst is when the citation situation of a paper changes dramatically in a short period of time. The red line indicates the outbreak's duration, and the outbreak's intensity indicates the article's impact. The citation burst is made with CiteSpace.

TABLE 7 The top 50 Keywords.

Keywords	Counts	Rank	Keywords	Counts	Rank
Glaucoma	526	1	Neuroinflammation	17	26
Apoptosis	384	2	Optic nerve injury	17	27
Retinal ganglion cells	365	3	Hypoxia	16	28
Neuroprotection	201	4	Reactive oxygen species	16	29
Retina	123	5	Age-related macular degeneration	15	30
Oxidative stress	122	6	Cell death	15	31
Intraocular pressure	55	7	Ischemia	15	32
Neurodegeneration	54	8	Benzalkonium chloride	14	33
Optic nerve	49	9	Caspase	14	34
Autophagy	41	10	Cornea	14	35
Trabecular meshwork	41	11	Nitric oxide	14	36
Excitotoxicity	39	12	Primary open angle glaucoma	14	37
Mitochondria	36	13	Aqueous humor	13	38
Inflammation	35	14	Ganglion cell	13	39
Diabetic retinopathy	23	15	Resveratrol	13	40
Glutamate	23	16	Alzheimer's disease	12	41
Microglia	21	17	Citicoline	11	42
Rat	21	18	Eye	11	43
Retinal degeneration	21	19	Imaging	11	44
Optic neuropathy	20	20	akt	10	45
Ocular hypertension	19	21	Antioxidants	10	46
Nmda	18	22	bcl-2	10	47
Optic nerve crush	18	23	Caspase-3	10	48
Primary open-angle glaucoma	18	24	Endoplasmic reticulum stress	10	49
rgc-5	18	25	Wound healing	10	50

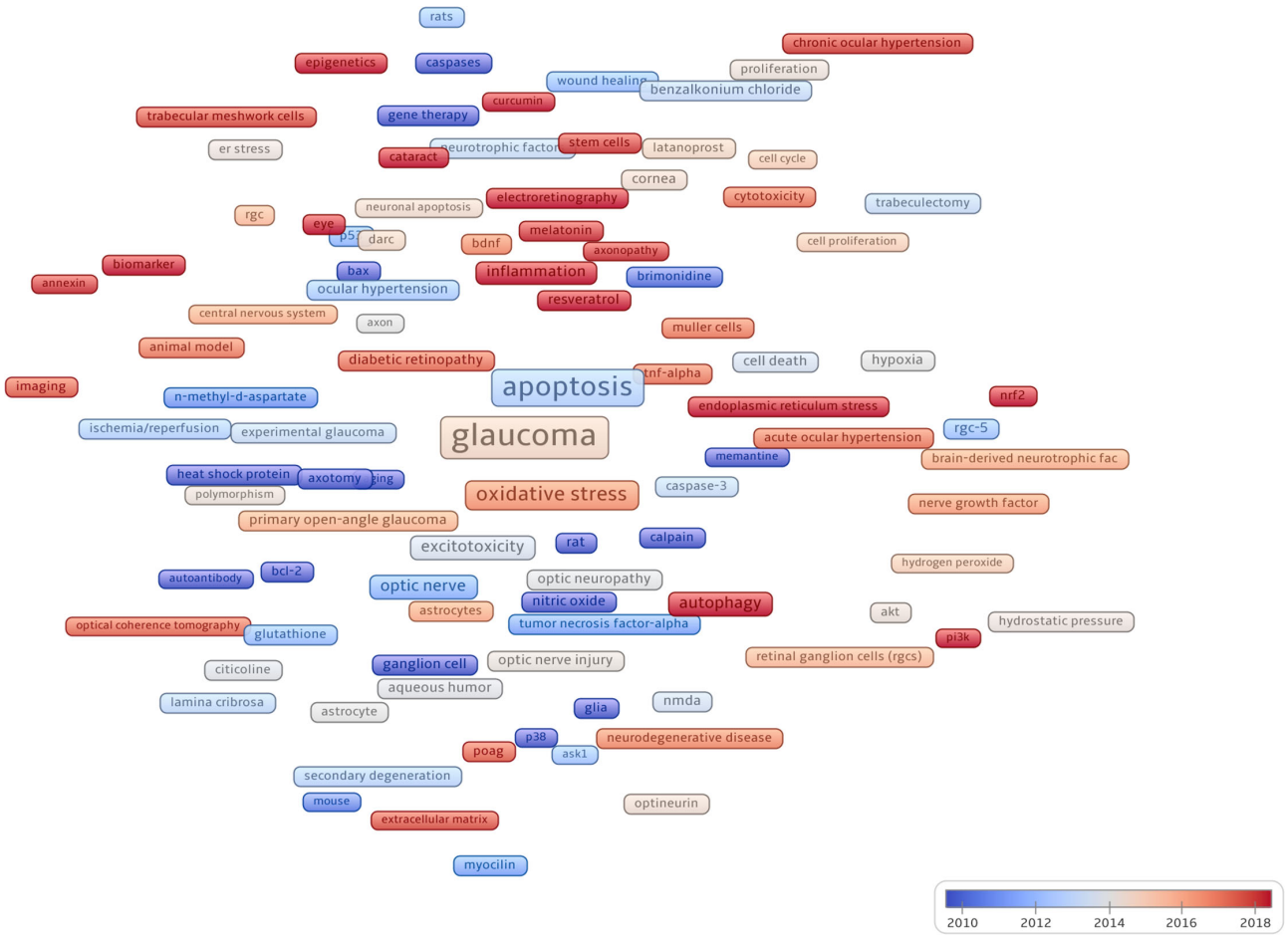

FIGURE 8
Node square sizes indicate how often keywords appear, cooler colors indicate earlier occurrences of keywords, and warmer colors indicate later occurrences.

glaucoma due to its relationship with other keywords. OCT can provide more detailed information about the loss of the optic nerve head and neurons quantitatively. However, in the early stages of glaucoma it is difficult to detect neuronal injuries, which would be permanent (Shao et al., 2022; Zhou et al., 2022). Therefore, early diagnosis and intervention to delay the progress of glaucoma and achieve a better prognosis are urgently needed. Scanning laser ophthalmoscopy, Doppler OCT, and other modified OCTs can be combined to examine capillary morphology and sensitively detect blood flow in the retina in early glaucoma (Aumann et al., 2019; Burns et al., 2019). However, at present, the only effective way to delay glaucoma progression is to reduce IOP using eye drops, surgery, or laser procedures (Schehlein and Robin, 2019; Rolim-De-Moura et al., 2022). Prostaglandins are the most common medication used to lower IOP by accelerating aqueous drainage through the uveal sclera (Jansook and Loftsson, 2022). Other drugs, such as α-adrenergic agonists, β-adrenergic blockers, and carbonic anhydrase inhibitors are second-line drugs that are ineffective in reducing IOP and have side effects (Lu et al., 2017; Nocentini and Supuran, 2019; Stoner et al., 2022). Surgical or laser procedures are recommended when medication cannot sufficiently lower IOP (Schehlein and Robin, 2019; Rolim-De-Moura et al., 2022). In recent years, advances in surgery, drug delivery, and gene therapy have led to a new field of glaucoma treatment (Wan et al., 2021; Tawfik et al., 2022). However, the impaired visual function still becomes serious after lowering the IOP in some patients (Jayanetti et al., 2020; Baudouin et al., 2021) as RGCs and the optic nerve irreversibly degenerate (Jayanetti et al., 2020; Baudouin et al., 2021). Therefore, research on the pathological mechanisms and development of neuroprotective treatments are still hotspots in glaucoma research.

Limitations

Our literature retrieval work was conducted from 1 January 1999 to 1 November 2022. Therefore, articles published after 2 November 2022 with advanced research results that met the search criteria were not included, making the number of articles in our database less than the total number today. In addition, we only included articles and reviews as we aimed to control the quality of publications as much as possible. Other types of publications, such as case reports, meta-analyses, and books were excluded, even though, they may contain valuable information. Apoptosis in glaucoma

TABLE 8 The top 60 keywords related to glaucoma treatment.

Keywords	Counts	Rank	Keywords	Counts	Rank
nmda receptor antagonists	59	1	Astaxanthin	4	31
Trabeculectomy	39	2	Beta-blockers	4	32
Mitomycin-c	31	3	Cobalt chloride	4	33
Benzalkonium chloride	27	4	Fibroblast growth-factor	4	34
Ciliary neurotrophic factor	27	5	Penetrating keratoplasty	4	35
Optical coherence tomography	25	6	Peripheral-nerve grafts	4	36
Endothelial growth-factor	24	7	Pilocarpine	4	37
C-jun	23	8	Rapamycin	4	38
Nerve growth-factor	23	9	Vitamin-c	4	39
Axotomy	21	10	Vitamin-e	4	40
Drug delivery	21	11	Statins	4	41
5-fluorouracil	19	12	Baicalin	3	42
Bdnf	19	13	Puerarin	3	43
Electroretinogram	16	14	Quercetin	3	44
Glaucoma filtration surgery	16	15	Sodium hyaluronate	3	45
Resveratrol	15	16	Valproic acid	3	46
Memantine	14	17	Aldosterone	2	47
Ginkgo-biloba extract	12	18	Aloe-emodin	2	48
Glutathione	12	19	Arbutin	2	49
Gene therapy	10	20	Calcium channel blocker	2	50
Melatonin	10	21	Loaded biodegradable microspheres	2	51
Epigallocatechin gallate	9	22	Methotrexate	2	52
Intravitreal injection	8	23	Methylprednisolone	2	53
Ceramide	7	24	Nifedipine	2	54
Magnesium acetyltaurate	7	25	Paclitaxel	2	55
Erythropoietin	6	26	Ripasudil	2	56
Minocycline	6	27	Rosiglitazone	2	57
Nanoparticles	6	28	Scutellarin	2	58
Scanning laser ophthalmoscope	6	29	Selective laser trabeculoplasty	2	59
Topical antiglaucoma medication	6	30	Lutein	2	60

encompasses several research topics. Although we made our best effort to retrieve more relevant publications, we may have overlooked important research and results using our current retrieval formula considering the limitations of bibliometric tools such as CiteSpace and VOSviewer.

Conclusion

This study aimed to determine the current and future trends and hotspots of apoptosis in glaucoma. We used bibliometric tools to visualize and analyze publications in this field and found that publications on apoptosis in glaucoma increased over time. It is an emerging series of advanced research involving technologies and treatments for glaucoma, such as the discovery of key regulatory mechanisms of RGC apoptosis, which will provide precise strategies for glaucoma treatment. In summary, this study can deepen our understanding of the trends and frontiers of apoptosis in glaucoma and provide guidelines for future research and treatment.

Data availability statement

The raw data supporting the conclusions of this article will be made available by the authors, without undue reservation.

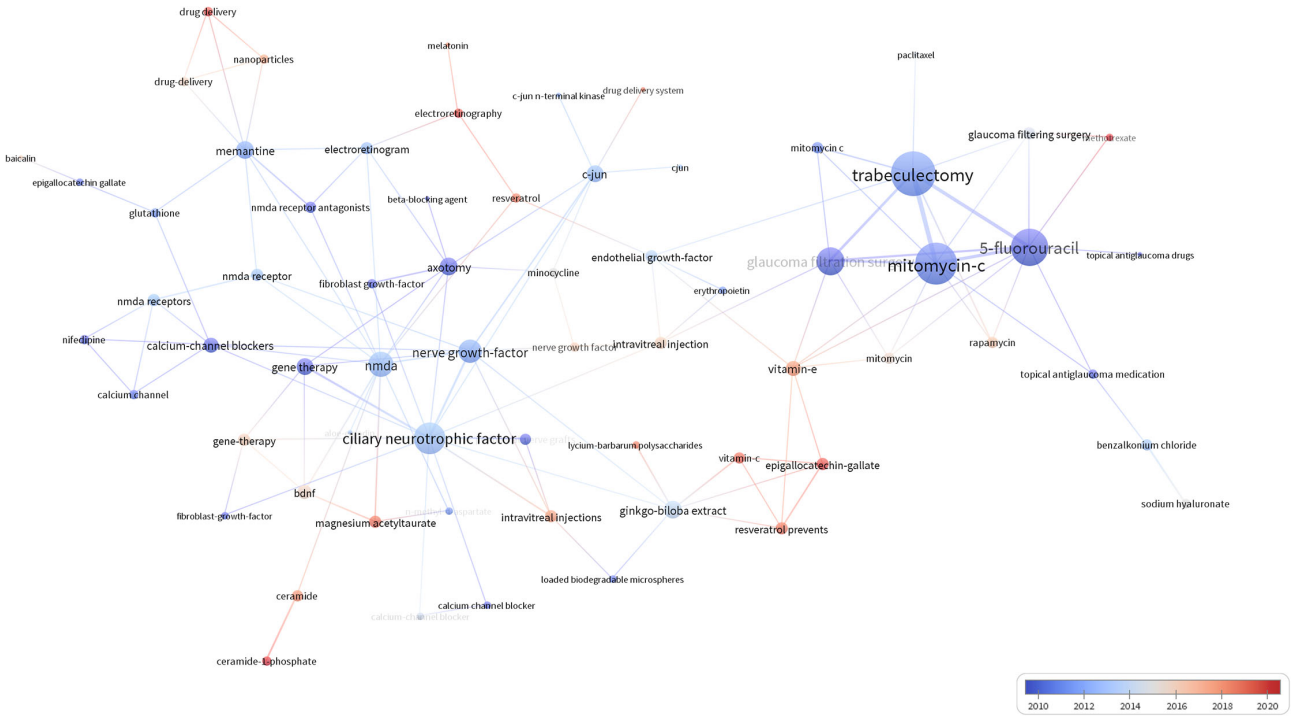

FIGURE 9
The width of the line between the nodes indicates the strength of the association between the keywords.

Author contributions

S-CW designed the experiments, interpreted the data, and revised the manuscript. J-HZ and M-JW performed the experiments, prepared the figures, and wrote the manuscript. Y-TT and JL helped to perform the experiments and prepared the figures. All authors read, discussed, and approved the final manuscript.

Funding

This study was supported by the National Natural Science Foundation of China, No. 82101126, Natural Science Foundation of Hunan Province, No. 2021JJ40873, the Hunan Provincial Natural Science Foundation of China, No. 2019JJ50696, and the Scientific Research Launch Project for new employees of the Second Xiangya Hospital of Central South University.

Conflict of interest

The authors declare that the research was conducted in the absence of any commercial or financial relationships that could be construed as a potential conflict of interest.

Publisher's note

All claims expressed in this article are solely those of the authors and do not necessarily represent those of their affiliated organizations, or those of the publisher, the editors and the reviewers. Any product that may be evaluated in this article, or claim that may be made by its manufacturer, is not guaranteed or endorsed by the publisher.

References

Al-Mugheiry, T.S., Clark, A., and Broadway, D.C. (2022). The Norwich trabeculectomy study: risk factor analysis for the development of adverse, thin cystic blebs. *Acta Ophthalmol.* 100, e1463–e1469. doi: 10.1111/aos.15193

Aumann, S., Donner, S., Fischer, J., and Muller, F. (2019). "Optical Coherence Tomography (OCT): Principle and Technical Realization," in *High Resolution Imaging in Microscopy and Ophthalmology: New Frontiers in Biomedical Optics*, ed. J.F. Bille. (Cham: CH) 59–85. doi: 10.1007/978-3-030-16638-0_3

Baudouin, C., Kolko, M., Melik-Parsadaniantz, S., and Messmer, E.M. (2021). Inflammation in Glaucoma: from the back to the front of the eye, and beyond. *Prog. Retin. Eye Res.* 83, 100916. doi: 10.1016/j.preteyeres.2020.100916

Bringmann, A., Pannicke, T., Grosche, J., Francke, M., Wiedemann, P., Skatchkov, S.N., et al. (2006). Muller cells in the healthy and diseased retina. *Prog. Retin. Eye Res.* 25, 397–424. doi: 10.1016/j.preteyeres.2006.05.003

Burns, S.A., Elsner, A.E., Sapoznik, K.A., Warner, R.L., and Gast, T.J. (2019). Adaptive optics imaging of the human retina. *Prog. Retin. Eye Res.* 68, 1–30. doi: 10.1016/j.preteyeres.2018.08.002

Chen, R., Duan, Z.Y., Duan, X.H., Chen, Q.H., and Zheng, J. (2022a). Progress in research on gut microbiota in ethnic minorities in China and consideration of intervention strategies based on ethnic medicine: a review. *Front. Cell. Infect. Microbiol.* 12, 1027541. doi: 10.3389/fcimb.2022.1027541

Chen, W., Liu, P., Liu, D., Huang, H., Feng, X., Fang, F., et al. (2022b). Maprotiline restores ER homeostasis and rescues neurodegeneration *via* Histamine Receptor H1 inhibition in retinal ganglion cells. *Nat. Commun.* 13, 6796. doi: 10.1038/s41467-022-34682-y

Cheng, S.Y., Wang, S.C., Lei, M., Wang, Z., and Xiong, K. (2018). Regulatory role of calpain in neuronal death. *Neural Regen Res* 13, 556–562. doi: 10.4103/1673-5374.228762

Chitranshi, N., Dheer, Y., Abbasi, M., You, Y., Graham, S.L., and Gupta, V. (2018). Glaucoma pathogenesis and neurotrophins: focus on the molecular and genetic basis for therapeutic prospects. *Curr. Neuropharmacol.* 16, 1018–1035. doi: 10.2174/1570159X16666180419121247

Coote, H. (1857). Clinical lecture on the employment of the ophthalmoscope in the investigation of deep-seated diseases of the eye. *Br. Med. J.* 1, 256–257. doi: 10.1136/bmj.s4-1.13.256-a

Cordeiro, M.F., Hill, D., Patel, R., Corazza, P., Maddison, J., and Younis, S. (2022). Detecting retinal cell stress and apoptosis with DARC: progression from lab to clinic. *Prog. Retin. Eye Res.* 86, 100976. doi: 10.1016/j.preteyeres.2021.100976

Dai, Z., Xu, S., Wu, X., Hu, R., Li, H., He, H., et al. (2022). Knowledge mapping of multicriteria decision analysis in healthcare: a bibliometric analysis. *Front Public Health* 10, 895552. doi: 10.3389/fpubh.2022.895552

Donahue, R.J., Fehrman, R.L., Gustafson, J.R., and Nickells, R.W. (2021). BCLXL gene therapy moderates neuropathology in the DBA/2J mouse model of inherited glaucoma. *Cell Death Dis.* 12, 781. doi: 10.1038/s41419-021-04068-x

Gedde, S. J., Vinod, K., Wright, M. M., Muir, K. W., Lind, J. T., Chen, P. P., et al. (2021). Primary open-angle glaucoma preferred practice pattern(R). *Ophthalmology* 128, P71–P150. doi: 10.1016/j.ophtha.2020.10.022

Hayashi, H., Mori, M., Harashima, M., Hashizume, T., Furiya, M., Mukaigaito, C., et al. (2021). Apolipoprotein E-containing lipoproteins and LRP1 protect From NMDA-induced excitotoxicity associated with reducing alpha2-macroglobulin in muller glia. *Invest. Ophthalmol. Vis. Sci.* 62, 23. doi: 10.1167/iovs.62.13.23

Hu, T., Wang, S., Zeng, L., Xiong, K., Chen, D., and Huang, J. (2020). Regional Expression of Act-MMP3 contributes to the selective loss of neurons in ganglion cell layers following acute retinal ischemia/reperfusion injury. *Curr. Eye Res.* 45, 591–603. doi: 10.1080/02713683.2019.1684523

Hu, X., Zhao, G. L., Xu, M. X., Zhou, H., Li, F., Miao, Y., et al. (2021). Interplay between Muller cells and microglia aggravates retinal inflammatory response in experimental glaucoma. *J. Neuroinflammation* 18, 303. doi: 10.1186/s12974-021-02366-x

Hu, X. M., Li, Z. X., Zhang, D. Y., Yang, Y. C., Zheng, S. Y., Zhang, Q., et al. (2022). Current research and clinical trends in rosacea pathogenesis. *Heliyon* 8, e10874. doi: 10.1016/j.heliyon.2022.e10874

Jansook, P., and Loftsson, T. (2022). Aqueous prostaglandin eye drop formulations. *Pharmaceutics* 14. doi: 10.3390/pharmaceutics14102142

Jayanetti, V., Sandhu, S., and Lusthaus, J. A. (2020). The latest drugs in development that reduce intraocular pressure in ocular hypertension and glaucoma. *J. Exp. Pharmacol.* 12, 539–548. doi: 10.2147/JEP.S281187

Ju, W. K., Perkins, G. A., Kim, K. Y., Bastola, T., Choi, W. Y., and Choi, S. H. (2022). Glaucomatous optic neuropathy: Mitochondrial dynamics, dysfunction and protection in retinal ganglion cells. *Prog. Retin. Eye Res.* 101136. doi: 10.1016/j.preteyeres.2022.101136

Kerrigan, L. A., Zack, D. J., Quigley, H. A., Smith, S. D., and Pease, M. E. (1997). TUNEL-positive ganglion cells in human primary open-angle glaucoma. *Arch. Ophthalmol.* 115, 1031–1035. doi: 10.1001/archopht.1997.01100160201010

Liu, S. M., Liao, L. S., Huang, J. F., and Wang, S. C. (2022). Role of CAST-Drp1 pathway in retinal neuron-regulated necrosis in experimental glaucoma. *Curr. Med. Sci.* 3, 8. doi: 10.1007/s11596-022-2639-8

Lu, L. J., Tsai, J. C., and Liu, J. (2017). Novel pharmacologic candidates for treatment of primary open-angle glaucoma. *Yale J. Biol. Med.* 90, 111–118.

Nocentini, A., and Supuran, C.T. (2019). Adrenergic agonists and antagonists as antiglaucoma agents: a literature and patent review (2013–2019). *Expert Opin. Ther. Pat.* 29, 805–815. doi: 10.1080/13543776.2019.1665023

Olawoye, O., and Etya'ale, D. (2021). Selective laser trabeculoplasty versus 0.5% timolol eye drops in the management of glaucoma in Tanzania. *Lancet Glob Health* 9, e1489–e1490. doi: 10.1016/S2214-109X(21)00402-2

Philippin, H., Matayan, E., Knoll, K.M., Macha, E., Mbishi, S., Makupa, A., et al. (2021). Selective laser trabeculoplasty vs. 0.5% timolol eye drops for the treatment of glaucoma in Tanzania: a randomised controlled trial. *Lancet Glob Health* 9, e1589–e1599. doi: 10.1016/S2214-109X(21)00348-X

Quigley, H. A., and Anderson, D. R. (1977). The histologic basis of optic disk pallor in experimental optic atrophy. *Am. J. Ophthalmol.* 83, 709–717. doi: 10.1016/0002-9394(77)90138-6

Quigley, H. A., Nickells, R. W., Kerrigan, L. A., Pease, M. E., Thibault, D. J., and Zack, D. J. (1995). Retinal ganglion cell death in experimental glaucoma and after axotomy occurs by apoptosis. *Invest. Ophthalmol. Vis. Sci.* 36, 774–786.

Rolim-De-Moura, C. R., Paranhos, A. Jr., Loutfi, M., Burton, D., Wormald, R., and Evans, J. R. (2022). Laser trabeculoplasty for open-angle glaucoma and ocular hypertension. *Cochrane Database Syst. Rev.* 8, CD003919. doi: 10.1002/14651858.CD003919.pub3

Romero, L., and Portillo-Salido, E. (2019). Trends in sigma-1 receptor research: a 25-year bibliometric analysis. *Front. Pharmacol.* 10, 564. doi: 10.3389/fphar.2019.00564

Sato, K., Sato, T., Ohno-Oishi, M., Ozawa, M., Maekawa, S., Shiga, Y., et al. (2021). CHOP deletion and anti-neuroinflammation treatment with hesperidin synergistically attenuate NMDA retinal injury in mice. *Exp. Eye Res.* 213, 108826. doi: 10.1016/j.exer.2021.108826

Schehlein, E. M., and Robin, A. L. (2019). Rho-associated kinase inhibitors: evolving strategies in glaucoma treatment. *Drugs* 79, 1031–1036. doi: 10.1007/s40265-019-01130-z

Shao, C., Li, Z., Zhang, C., Zhang, W., He, R., Xu, J., et al. (2022). Optical diagnostic imaging and therapy for thyroid cancer. *Mater Today Bio* 17, 100441. doi: 10.1016/j.mtbio.2022.100441

Steiner, S., Schwarzhans, F., Desissaire, S., Resch, H., Fischer, G., Pircher, M., et al. (2022). Birefringent properties of the peripapillary retinal nerve fiber layer in healthy and glaucoma subjects analyzed by polarization-sensitive OCT. *Invest. Ophthalmol. Vis. Sci.* 63, 8. doi: 10.1167/iovs.63.12.8

Stoner, A., Harris, A., Oddone, F., Belamkar, A., Verticchio Vercellin, A. C., Shin, J., et al. (2022). Topical carbonic anhydrase inhibitors and glaucoma in 2021: where do we stand? *Br. J. Ophthalmol.* 106, 1332–1337. doi: 10.1136/bjophthalmol-2021-319530

Tawfik, M., Chen, F., Goldberg, J. L., and Sabel, B. A. (2022). Nanomedicine and drug delivery to the retina: current status and implications for gene therapy. *Naunyn Schmiedebergs. Arch. Pharmacol.* 395, 1477–1507. doi: 10.1007/s00210-022-02287-3

Tham, Y. C., Li, X., Wong, T. Y., Quigley, H. A., Aung, T., and Cheng, C. Y. (2014). Global prevalence of glaucoma and projections of glaucoma burden through 2040: a systematic review and meta-analysis. *Ophthalmology* 121, 2081–2090. doi: 10.1016/j.ophtha.2014.05.013

Theventhiran, A. B., Kim, G., and Yao, W. (2021). Fornix-based versus limbal-based conjunctival trabeculectomy flaps for glaucoma. *Cochrane Database Syst Rev* 8, CD009380. doi: 10.1002/14651858.CD009380.pub3

Wan, C. R., Muya, L., Kansara, V., and Ciulla, T. A. (2021). suprachoroidal delivery of small molecules, nanoparticles, gene and cell therapies for ocular diseases. *Pharmaceutics* 13. doi: 10.3390/pharmaceutics13020288

Wang, S., Hu, T., Wang, Z., Li, N., Zhou, L., Liao, L., et al. (2017a). Macroglia-derived thrombospondin 2 regulates alterations of presynaptic proteins of retinal neurons following elevated hydrostatic pressure. *PLoS ONE* 12, e0185388. doi: 10.1371/journal.pone.0185388

Wang, S., Liao, L., Huang, Y., Wang, M., Zhou, H., Chen, D., et al. (2019). Pin1 is regulated by CaMKII activation in glutamate-induced retinal neuronal regulated necrosis. *Front. Cell. Neurosci.* 13, 276. doi: 10.3389/fncel.2019.00276

Wang, S., Liao, L., Wang, M., Zhou, H., Huang, Y., Wang, Z., et al. (2017b). Pin1 promotes regulated necrosis induced by glutamate in rat retinal neurons *via* CAST/Calpain2 pathway. *Front. Cell. Neurosci.* 11, 425. doi: 10.3389/fncel.2017.00425

Wang, S. C., Hu, X. M., and Xiong, K. (2023). The regulatory role of Pin1 in neuronal death. *Neural Regen Res* 18, 74–80. doi: 10.4103/1673-5374.341043

Yan, W. T., Yang, Y. D., Hu, X. M., Ning, W. Y., Liao, L. S., Lu, S., et al. (2022). Do pyroptosis, apoptosis, and necroptosis (PANoptosis) exist in cerebral ischemia? Evidence from cell and rodent studies. *Neural Regen Res* 17, 1761–1768. doi: 10.4103/1673-5374.331539

Yan, W. T., Zhao, W. J., Hu, X. M., Ban, X. X., Ning, W. Y., Wan, H., et al. (2023). PANoptosis-like cell death in ischemia/reperfusion injury of retinal neurons. *Neural. Regen. Res.* 18, 357–363. doi: 10.4103/1673-5374.346545

Yang, H. Y., Chi, S. C., Ko, Y. C., Chen, M. J., Kuang, T. M., Chang, Y. F., et al. (2022). Bleb-related infection after primary trabeculectomy: medical chart reviews from 1993 to 2021. *Br. J. Ophthalmol.* 3, 1429. doi: 10.1136/bjo-2022-321429

Zhang, J. H., Ni, S. Y., Tan, Y. T., Luo, J., and Wang, S. C. (2022). A bibliometric analysis of PIN1 and cell death. *Front. Cell Dev. Biol.* 10, 1043725. doi: 10.3389/fcell.2022.1043725

Zhang, Q., Wan, X. X., Hu, X. M., Zhao, W. J., Ban, X. X., Huang, Y. X., et al. (2021). Targeting programmed cell death to improve stem cell therapy: implications for treating diabetes and diabetes-related diseases. *Front Cell Dev Biol.* 9, 809656. doi: 10.3389/fcell.2021.809656

Zhao, L., Li, J., Feng, L., Zhang, C., Zhang, W., Wang, C., et al. (2022). Depicting developing trend and core knowledge of primary open-angle glaucoma: a bibliometric and visualized analysis. *Front. Med.* 9, 922527. doi: 10.3389/fmed.2022.922527

Zhou, C., Lin, Z., Huang, S., Li, B., and Gao, A. (2022). Progress in probe-based sensing techniques for *in vivo* diagnosis. *Biosensors* 12, 943. doi: 10.3390/bios12110943

frontiers | Frontiers in Neuroscience

TYPE Original Research
PUBLISHED 13 February 2023
DOI 10.3389/fnins.2023.1121490

OPEN ACCESS

EDITED BY
Dan Wen,
Central South University, China

REVIEWED BY
Han Zhang,
The First Affiliated Hospital of China Medical University, China
Toshiaki Goseki,
Atami Hospital, Japan
Ping Xie,
Nanjing Medical University, China

*CORRESPONDENCE
Xiaolei Zhang
✉ rain19822@qq.com
Yanling Wang
✉ doctorwyl2020@sina.com

†These authors have contributed equally to this work and share first authorship
‡These authors have contributed equally to this work

SPECIALTY SECTION
This article was submitted to Visual Neuroscience, a section of the journal Frontiers in Neuroscience

RECEIVED 11 December 2022
ACCEPTED 19 January 2023
PUBLISHED 13 February 2023

CITATION
Chen Y, Feng X, Huang Y, Zhao L, Chen X, Qin S, Sun J, Jing J, Zhang X and Wang Y (2023) Blood flow perfusion in visual pathway detected by arterial spin labeling magnetic resonance imaging for differential diagnosis of ocular ischemic syndrome.
Front. Neurosci. 17:1121490.
doi: 10.3389/fnins.2023.1121490

Blood flow perfusion in visual pathway detected by arterial spin labeling magnetic resonance imaging for differential diagnosis of ocular ischemic syndrome

Yanan Chen[1†], Xue Feng[2†], Yingxiang Huang[1], Lu Zhao[1], Xi Chen[1], Shuqi Qin[1], Jiao Sun[1], Jing Jing[3], Xiaolei Zhang[1*‡] and Yanling Wang[1*‡]

[1]Department of Ophthalmology, Beijing Friendship Hospital, Capital Medical University, Beijing, China, [2]Department of Ophthalmology, Beijing Jishuitan Hospital, The Fourth Clinical Medical College of Peking University, Beijing, China, [3]Department of Neurology, Beijing Tiantan Hospital, Capital Medical University, Beijing, China

Background: Ocular ischemic syndrome (OIS), attributable to chronic hypoperfusion caused by marked carotid stenosis, is one of the important factors that cause ocular neurodegenerative diseases such as optic atrophy. The current study aimed to detect blood flow perfusion in a visual pathway by arterial spin labeling (ASL) and magnetic resonance imaging (MRI) for the differential diagnosis of OIS.

Methods: This diagnostic, cross-sectional study at a single institution was performed to detect blood flow perfusion in a visual pathway based on 3D pseudocontinuous ASL (3D-pCASL) using 3.0T MRI. A total of 91 participants (91 eyes) consisting of 30 eyes with OIS and 61 eyes with noncarotid artery stenosis-related retinal vascular diseases (39 eyes with diabetic retinopathy and 22 eyes with high myopic retinopathy) were consecutively included. Blood flow perfusion values in visual pathways derived from regions of interest in ASL images, including the retinal-choroidal complex, the intraorbital segments of the optic nerve, the tractus optics, and the visual center, were obtained and compared with arm-retinal circulation time and retinal circulation time derived from fundus fluorescein angiography (FFA). Receiver operating characteristic (ROC) curve analyses and the intraclass correlation coefficient (ICC) were performed to evaluate the accuracy and consistency.

Results: Patients with OIS had the lowest blood flow perfusion values in the visual pathway (all $p < 0.05$). The relative intraorbital segments of optic nerve blood flow values at post-labeling delays (PLDs) of 1.5 s (area under the curve, AUC = 0.832) and the relative retinal–choroidal complex blood flow values at PLDs of 2.5 s (AUC = 0.805) were effective for the differential diagnosis of OIS. The ICC of the blood flow values derived from the retinal–choroidal complex and the intraorbital segments of the optic nerve between the two observers showed satisfactory concordance (all ICC > 0.932, $p < 0.001$). The adverse reaction rates of ASL and FFA were 2.20 and 3.30%, respectively.

Conclusion: 3D-pCASL showed that the participants with OIS had lower blood flow perfusion values in the visual pathway, which presented satisfactory accuracy, reproducibility, and safety. It is a noninvasive and comprehensive differential diagnostic tool to assess blood flow perfusion in a visual pathway for the differential diagnosis of OIS.

KEYWORDS

blood flow perfusion, visual pathway, arterial spin labeling, ocular ischemic syndrome, carotid stenosis, ocular neurodegeneration, optic atrophy

Introduction

Marked stenosis or occlusion of the common or internal carotid arteries may cause ocular hypoperfusion (Lee et al., 2022) and/or cerebral hypoperfusion (Lineback et al., 2022). Ocular ischemic syndrome (OIS), attributable to chronic ocular hypoperfusion, is one of the important factors that cause ocular neurodegenerative diseases (Mester et al., 2009), such as optic atrophy (Battista et al., 2022). Ocular ischemic syndrome (OIS) describes ocular symptoms and signs attributable to ocular hypoperfusion caused by marked stenosis or occlusion of the common or internal carotid arteries (Terelak-Borys et al., 2012). It was first described by Hedges (1962), with their findings such as peripheral dot and blot hemorrhages and dilated retinal veins attributed to retinal hypoxia induced by carotid artery insufficiency (Casalino et al., 2017). It is a blinding and disabling disease (Hung and Chang, 2017) and has diverse clinical manifestations accompanied by asymptomatic injury (Mendrinos et al., 2010). It is usually asymptomatic but has potentially blinding abilities (Hung and Chang, 2017). The diagnosis of OIS can portend life-threatening cerebrovascular and cardiovascular complications (Mendrinos et al., 2010). The mortality rate of patients with OIS is 40% within 5 years from onset (Mills, 1989), and the most common causes of death are cardiac disease and stroke (Avery et al., 2019). The diagnosis of OIS is critical for saving visual function and improving the chances of survival.

The identification of the OIS and its various clinical manifestations presents an interdisciplinary challenge. In addition to OIS, there are also ischemic mechanisms present in retinal vascular diseases related to noncarotid artery stenosis, such as diabetic retinopathy (DR) and high myopia (HM) retinopathy (Steigerwalt et al., 2009). It was reported that the thinning of the choroid contributes more to the measured decreased chorioretinal perfusion than slowed arterial filling time (Vaghefi et al., 2017). Previous studies confirmed the ischemic mechanisms in DR and HM retinopathy. DR is a well-recognized ocular ischemic disease which is a microvascular complication of diabetes (Stolte and Fang, 2020). Mudaliar et al. reported that hyperglycemia causes retinal damage through complex metabolic pathways, leading to vascular damage, oxidative stress, capillary ischemia, and retinal tissue hypoxia. A growing body of evidence (Steigerwalt et al., 2009) suggests that HM is associated with decreased ocular blood flow (BF), the complications of which may contribute to severe visual loss. A recent study has shown that the aberrant blood perfusion of the cerebellum detected by ASL in patients with HM indicates a new understanding of brain abnormalities and brain plasticity (Wang et al., 2020).

Identifying a clinical distinction between OIS, which can potentially imply being affected by lethal disease and noncarotid artery stenosis-related retinal vascular disease, is essential and difficult. Therefore, reliable diagnostic biomarkers are needed. The traditional imaging modality for assessing ocular blood perfusion is fundus fluorescein angiography (FFA) (Terelak-Borys et al., 2012). Its invasive examination process relies on sodium fluorescein, an orange water-soluble dye, which is not applicable to all patients. Arterial spin labeling (ASL) magnetic resonance imaging (MRI) has been widely used in cerebrovascular disease (Scelsi et al., 2018). ASL allows magnetically labeled water protons from arterial blood as an endogenous diffusible tracer that disperses from the vascular system into neighboring tissues (Kitajima and Uetani, 2023). Voxel blood flow was quantified in mL/100 mL/min (Valentin et al., 2022). Anatomy and functionality are all important factors affecting tissue perfusion (Vaghefi et al., 2017). Therefore, we set the DR group in terms of arterial filling time and the HM group in terms of tissue volume.

This diagnostic test study was designed to detect blood flow perfusion in a visual pathway by ASL-MRI and explore an accurate, reproducible, and safe diagnostic tool for the differential diagnosis of OIS.

Materials and methods

Study design and participants

In this cross-sectional study, 91 participants (91 eyes) with retinal vascular diseases were prospectively and consecutively enrolled from November 2018 to November 2021. Participants included 30 patients with carotid artery stenosis (30 eyes with OIS) and 61 controls with noncarotid artery stenosis-related retinal vascular diseases (39 eyes with DR and 22 eyes with high myopic retinopathy).

The diagnostic criteria of OIS (Luo et al., 2018) are as follows: (1) the stenosis of the ipsilateral (to the affected eye) internal carotid artery (ICA) was >50%; (2) abnormal ocular symptoms and/or signs which cannot be explained by other ocular diseases; (3) FFA with the following signs: arm-choroidal circulation time>15 s, arm-retinal circulation time (ARCT) >18 s, and retinal circulation time (RCT) >11 s. The subjects that satisfied the first criterion and any of the two criteria in (2) or (3) led to a diagnosis of OIS (Lauria et al., 2020). The diagnostic criteria for DR (Fransen et al., 2002) are based on the international clinical DR severity grading standard established by the American Academy of Ophthalmology in 2002 (Nawaz et al., 2019; Flaxel et al., 2020). The diagnostic criteria for high myopic retinopathy are based on three key factors: atrophy (A), traction (T), and neovascularization (N), which is named the ATN classification system (Ruiz-Medrano et al., 2019).

The inclusion criteria were defined as follows: (1) patients with OIS; (2) patients with DR with severity greater than or equal to mild non-proliferative diabetic retinopathy; (3) patients with high myopic retinopathy with severity graded as A0-A4/T0-T3/N0-N2s.

The exclusion criteria were defined as follows: a history of other ocular diseases: glaucoma, uveitis, ocular trauma, or intraocular surgery; other types of retinal vascular diseases: retinal artery occlusion, retinal vein occlusion, retinal macroaneurysms, hypertensive retinopathy; MRI ineligibility (de Keizer and te Strake, 1986): claustrophobia or the presence of a cardiac pacemaker, joint replacement, or other implanted metal devices; MR images with visible artifacts; FFA ineligibility (Awan and Yang, 2006): hypersensitivity to sodium fluorescein and liver and kidney dysfunction; ocular diseases that diminished the quality of fundus image: serious cataract and vitreous hemorrhage. We excluded those who were implanted with metal devices ($n = 1$), had hypersensitivity to sodium fluorescein ($n = 1$), and whose MR and FFA images were of poor quality ($n = 2$).

The study was approved by the Medical Research Ethics Committee of Beijing Friendship Hospital, Capital Medical University (NO.2018-P2-185-02). All participants provided informed consent according to the Declaration of Helsinki.

Clinical ophthalmic examination

All subjects underwent slit-lamp, optical coherence tomography (OCT, Heidelberg Spectralis), and FFA (Spectralis hra) examinations (Figure 1). OCT was used to measure the central macular retinal thickness in conventional mode. OCT measured the central macular choroidal thickness in the enhanced depth imaging (EDI) mode. FFA examinations were performed according to the requirements of the patient's condition. Allergy tests were carried out, and the subjects with negative results underwent a puncture of the median cubital vein and were injected with sodium fluorescein contrast medium. We collected the ARCT, RCT, capillary non-perfusion (NP) area, neovascularization (NV), retinal vascular staining, microaneurysms, and other fluorescein angiography signs. The same experienced technician completed each examination.

ASL image acquisition

All subjects underwent a 3.0T MRI scan using a Philips Ingenia 3.0T scanner equipped with a 16-channel head coil. T1 and T2 weighted images, diffusion-weighted images, and 3D time-of-flight MR angiography images were obtained before the ASL sequence, and scanning time summed up to 20 min. Foam pads were placed at the sides of the subject's head to minimize head motion, and earplugs were used to reduce noise. During the MRI scan, subjects were instructed to close their eyes and stay relaxed to reduce eye movement.

The BF in the visual pathway was determined using the 3D pseudo-continuous ASL (3D-pCASL) technique, with the scan parameters as follows: gradient and spin echo sequence, post-labeling delay (PLD) = 1.5 s (repetition time [TR] = 3903 ms, echo time [TE] = 11 ms), PLD = 2.5 s (TR = 4903 ms, TE = 11 ms), bandwidth in echo-planar imaging = 2899.7 Hz, label distance = 90 mm, flip angle (FA) = 90°, slice thickness = 6 mm, number of slices = 20, slice gap = 0, slice orientation=transverse, field of view (FOV) = 240 × 240 mm, acquisition matrix = 64 × 64, number of excitations (NEX) = 3.

ASL data quantification

Blood perfusion maps were automatically obtained using the default process by the dedicated workstation (IntelliSpace Portal Release v.7.0.4.20175, Philips), and the data were derived from the blood perfusion maps. The regions of interest (ROIs) derived from the retinal-choroidal complex, the intraorbital segments of the optic nerve, the tractus opticus, and the visual center (Figure 2) were drawn by a neurologist (10 years of experience) and an ophthalmologist (10 years of experience), respectively, and clinical information was reviewed in a blinded fashion. The specific location of the retina-choroid complex, the orbital segment of the optic nerve, the optic tract, and the visual center were based on T1 and T2 weighted images. The unified criteria for drawing ROIs were as follows: The ROIs were all subrounded. The area of ROI of the retinal-choroidal complex, the intraorbital segments of the optic nerve, and the tractus opticus were 0.3 cm^2; the area of ROI of the gyrus lingual, the cuneus, and the occipital lobe was 2 cm^2, and the average BF value was taken as the BF of the visual center. The relative BF (rBF) value was defined as rBF = affected BF/healthy BF (Muir and Duong, 2011). The results of the measurements were retrieved from the two observers and calculated as the average value.

Statistical analysis

Sample size considerations included the rarity of the OIS. This study hypothesizes that the area under the curve (AUC) of the BF perfusion values in a visual pathway is >0.5. Our pre-test showed that the AUC was >0.8. According to the following parameters, $\alpha = 0.05$, $\beta = 0.1$, the power was calculated using PASS11.0 software, which was >90%, proving that the sample size was adequate.

Statistical analyses were performed using SPSS statistical software (version 26.0, SPSS) and GraphPad Prism software (version 6.0c, GraphPad Inc). Continuous variables were presented as mean ± standard deviation. A one-way ANOVA was used to analyze the differences among groups. Categorical variables were analyzed using Chi-square tests. Receiver operating characteristic (ROC) curve analyses were performed, and the AUC was applied to evaluate accuracy. A intraclass correlation coefficient (ICC) was performed to evaluate the consistency of BF values reported by the two observers; an ICC of >0.75 indicated satisfactory concordance. Statistical significance was accepted as a two-sided test with an alpha level of 0.05. A *P*-value of <0.05 was considered statistically significant.

Results

Demographics and ocular characteristics

A total of 91 participants (mean [SD] age, 61.0 [10.0] years; 37 [40.7%] women) had 91 eyes with retinal vascular diseases, including 30 patients (30 eyes) with OIS after carotid artery stenosis and 61 controls with noncarotid artery stenosis-related retinal vascular diseases, which included 39 patients (39 eyes) with DR and 22 patients (22 eyes) with high myopic retinopathy. There were differences in age ($F = 8.97$, $p < 0.001$), with the predominant gender being male ($\chi 2 = 16.54$, $p < 0.001$) among the three groups. Subjects with OIS and high myopic retinopathy showed thinner central macular retinal thickness ($F = 4.98$, $p = 0.009$); subjects with high myopic retinopathy showed the thinnest central macular choroidal thickness ($F = 42.65$, $p < 0.001$). There were no significant differences in ARCT among the three groups ($F = 1.40$, $p = 0.253$). The differences among the three groups in the RCT were significant. The subjects with OIS showed the highest RCT values ($F = 3.75$, $p = 0.027$). The differences in the rates of capillary non-perfusion and neovascularization among the three groups were significant. The subjects with DR showed the highest rates of capillary non-perfusion ($\chi^2 = 27.66$, $p < 0.001$) and neovascularization ($\chi^2 = 22.00$, $p < 0.001$). The demographics and clinical characteristics of each group are represented in Table 1.

ASL characteristics based on ROI analysis

There were significant differences among the three groups in detectable BF values of the visual pathway at PLDs of 1.5 and 2.5 s, including the BF values of the retinal–choroidal complex ($F = 4.065$, $p = 0.020$; $F = 4.923$, $p = 0.009$), the intraorbital segments of the

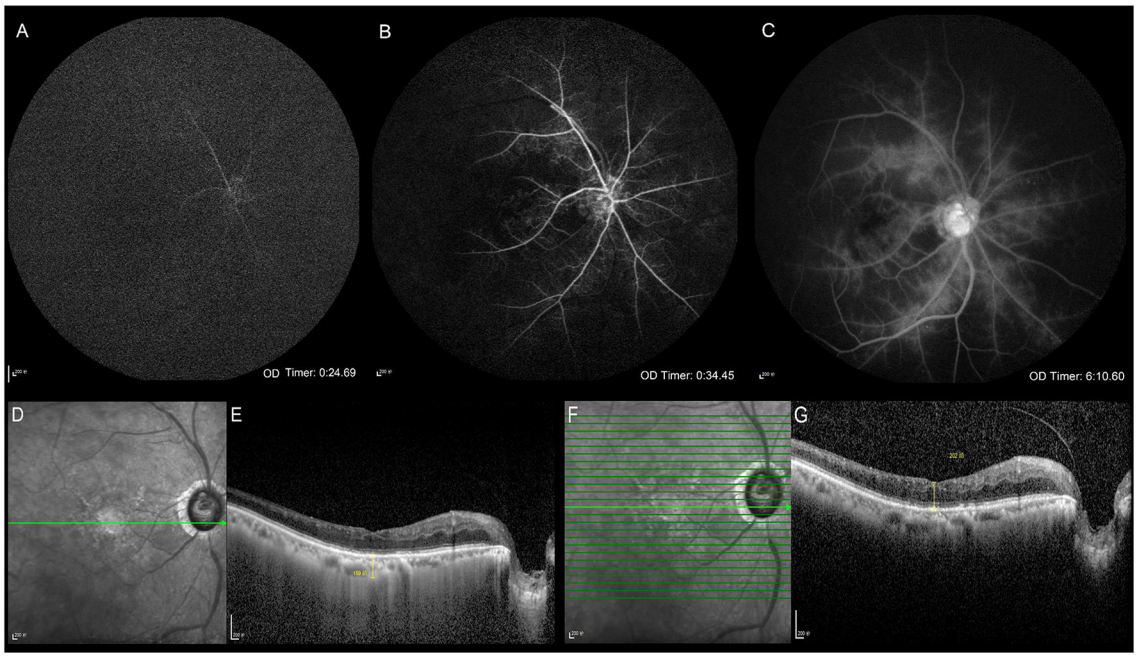

FIGURE 1
Clinical ophthalmic examinations. Fundus fluorescein angiography **(A–C)**. Optical coherence tomography **(D–G)**. The arm-retinal circulation time is 24.69 s showing the delayed retinal arierial filling **(A)**. The venous phase starts at 34.45 s, showing delayed retinal venous filling, which indicates that the retinal circulation time is 9.76 s **(B)**. Late retinal vascular staining **(C)**. The infrared image and the central macular choroidal thickness in enhanced depth imaging mode **(D, E)**. The infrared image and the central macular retinal thickness in conventional mode **(F, G)**.

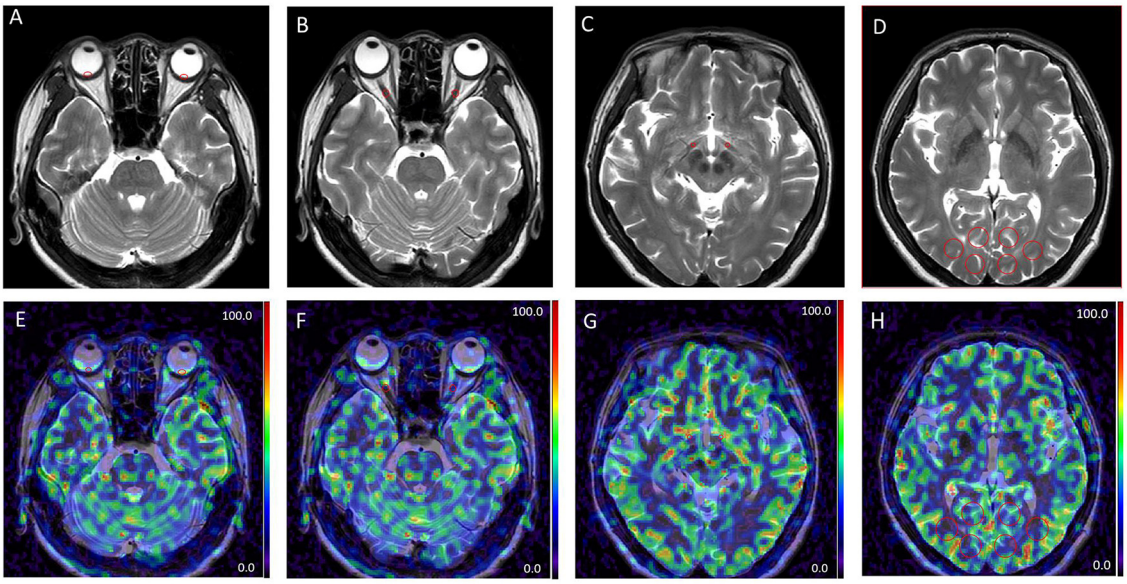

FIGURE 2
Examples of different patterns in MRI images. T2 weighted images **(A–D)**. Arterial spin labeling (ASL) images at post-labeling delay (PLD) of 1.5 s **(E–H)**. Regions of interest derived from the retinal-choroidal complex **(A, E)**; the intraorbital segments of the optic nerve **(B, F)**; the tractus opticus **(C, G)**; the visual center **(D, H)**; ROIs were all marked by red circles.

optic nerve ($F = 10.873$, $p < 0.001$; $F = 3.907$, $p = 0.024$), the tractus opticus ($F = 13.617$, $p < 0.001$; $F = 3.738$, $p = 0.028$), and the visual center ($F = 11.057$, $p < 0.001$; $F = 4.012$, $p = 0.022$) (Table 2). Subjects with OIS had the lowest BF perfusion values in the visual pathway at PLD of 1.5 and 2.5 s among the three groups (all $p < 0.05$). Subjects with DR were presented with lower BF perfusion values in the intraorbital segments of the optic nerve, the tractus opticus, and the visual center at a PLD of 1.5 s (all $p < 0.05$). Subjects with high myopic retinopathy were presented with lower BF perfusion values in the retinal–choroidal complex at a PLD of 2.5 s (all $p < 0.05$). Most

TABLE 1 Demographics and ocular characteristics.

Variable	Total ($n = 91$)	OIS ($n = 30$)	DR ($n = 39$)	HM ($n = 22$)	p-value
Gender, female/male, n (%)	37(40.7)/54(59.3)	5(16.7)/25(83.3)	16(41.0)/23(59.0)	16(72.7)/6(27.3)	< 0.001
Age, years, mean (SD)	61.0 (10.0)	66.6 (8.3)	59.3 (7.8)	56.3 (12.3)	< 0.001
OCT					
Central macular retinal thickness, μm, mean (SD)	265.90 (122.81)	223.47 (30.12)	309.33 (142.75)	242.50(145.31)	0.009
Central macular choroidal thickness, μm, mean (SD)	211.84 (93.55)	243.41 (61.80)	252.61 (73.53)	94.48 (60.43)	< 0.001
FFA					
ARCT, seconds, mean (SD)	18.00 (5.51)	19.30 (6.60)	17.61 (4.68)	16.87 (5.12)	0.253
RCT, seconds, mean (SD)	3.87 (4.37)	5.60 (7.18)	3.06 (1.19)	2.89 (0.89)	0.027
Capillary non-perfusion, n (%)	22 (24.2)	2 (6.7)	20 (51.3)	0 (0)	< 0.001
Neovascularization, n (%)	24 (26.4)	3(10)	20(51.3)	1(4.5)	< 0.001

OIS, ocular ischemic syndrome; DR, diabetic retinopathy; HM, high myopia; OCT, optical coherence tomography; FFA, fundus fluorescein angiography; ARCT, arm-retinal circulation time; RCT, retinal circulation time; SD, standard deviation.
p-values for comparisons among OIS, DR, and HM.
p <0.05 was considered statistically significant.

TABLE 2 ASL characteristics based on ROI analysis.

Variable	Total (n= 91)	OIS ($n = 30$)	DR ($n = 39$)	HM ($n = 22$)	p value
ASL: BF (PLD = 1.5 s)					
Retinal–choroidal complex, ml/100 g/min, mean (SD)	14.15 (9.17)	10.43 (10.88)	15.52 (8.07)	16.77 (6.99)	0.020
Intraorbital segments of optic nerve, ml/100 g/min, mean (SD)	14.52 (11.62)	12.29 (9.33)	11.12 (7.73)	23.59 (15.36)	< 0.001
Tractus opticus, ml/100 g/min, mean (SD)	14.27 (8.69)	13.87 (7.20)	10.62 (7.13)	21.28 (9.14)	< 0.001
Visual center, ml/100 g/min, mean (SD)	16.50 (9.93)	15.68 (9.91)	12.87 (7.72)	24.03 (9.70)	< 0.001
ASL: BF (PLD = 2.5 s)					
Retinal–choroidal complex, ml/100 g/min, mean (SD)	16.46 (10.66)	12.99 (10.95)	20.29 (11.03)	14.40 (7.22)	0.009
Intraorbital segments of optic nerve, ml/100 g/min, mean (SD)	17.74 (11.77)	13.15 (9.18)	19.18 (13.09)	21.46 (10.91)	0.024
Tractus opticus, ml/100 g/min, mean (SD)	22.23 (9.52)	19.05 (10.10)	22.48 (9.21)	26.12 (7.97)	0.028
Visual center, ml/100 g/min, mean (SD)	28.40 (8.81)	24.81 (10.15)	29.87 (8.09)	30.67 (6.65)	0.022

ASL, arterial spin labeling; ROI, region of interest; OIS, ocular ischemic syndrome; DR, diabetic retinopathy; HM, high myopia; BF, blood flow; PLD, postlabeling delay; SD, standard deviation.
p-values for comparisons among OIS, DR, and HM.
p <0.05 was considered statistically significant.

of the perfusion values in the visual pathway increased from PLD 1.5 s to PLD 2.5 s (Figure 3).

Accuracy of ASL in the differential diagnosis of OIS

The accuracy of ASL in the diagnosis of OIS was evaluated using the ROC curve analysis (Figure 4). The BF values of the retinal–choroidal complex at a PLD of 1.5 s [AUC:0.669; 95% confidence interval (CI) 0.55–0.79; $p = 0.01$] were estimated by comparison with the ARCT of the gold standard FFA-based diagnosis of delayed retinal arterial filling. The relative intraorbital segments of optic nerve BF values at PLDs of 1.5 s (AUC:0.832; 95%CI 0.74–0.93; $p < 0.001$), with a cutoff point of 0.79 (sensitivity:76.7%; specificity:85.2%), and the relative retinal–choroidal complex BF values at PLDs of 2.5 s (AUC:0.805; 95%CI 0.70–0.92; $p < 0.001$), with a cutoff point of 0.78 (sensitivity:73.3%; specificity:83.6%), were effective predictors for the differential diagnosis of OIS.

Concordance between observers in ASL

There was concordance between the two observers, with an ICC of 0.932 (95% CI 0.897–0.955, $p < 0.001$) at PLDs of 1.5 s and 0.974 (95%CI 0.956–0.984, $p < 0.001$) at PLDs of 2.5 s for the retinal–choroidal complex. The ICC of the BF values of the intraorbital segments of optic nerve BF between the two observers was 0.972 (95%CI 0.956–0.982, $p < 0.001$) at PLDs of 1.5 s and 0.984 (95%CI 0.974–0.990, $p < 0.001$) at PLDs of 2.5 s. The ICC of the BF values of the optic tract and the visual center at PLDs of 1.5 s and PLD of 2.5 s were all more than 0.984 (all $p < 0.001$).

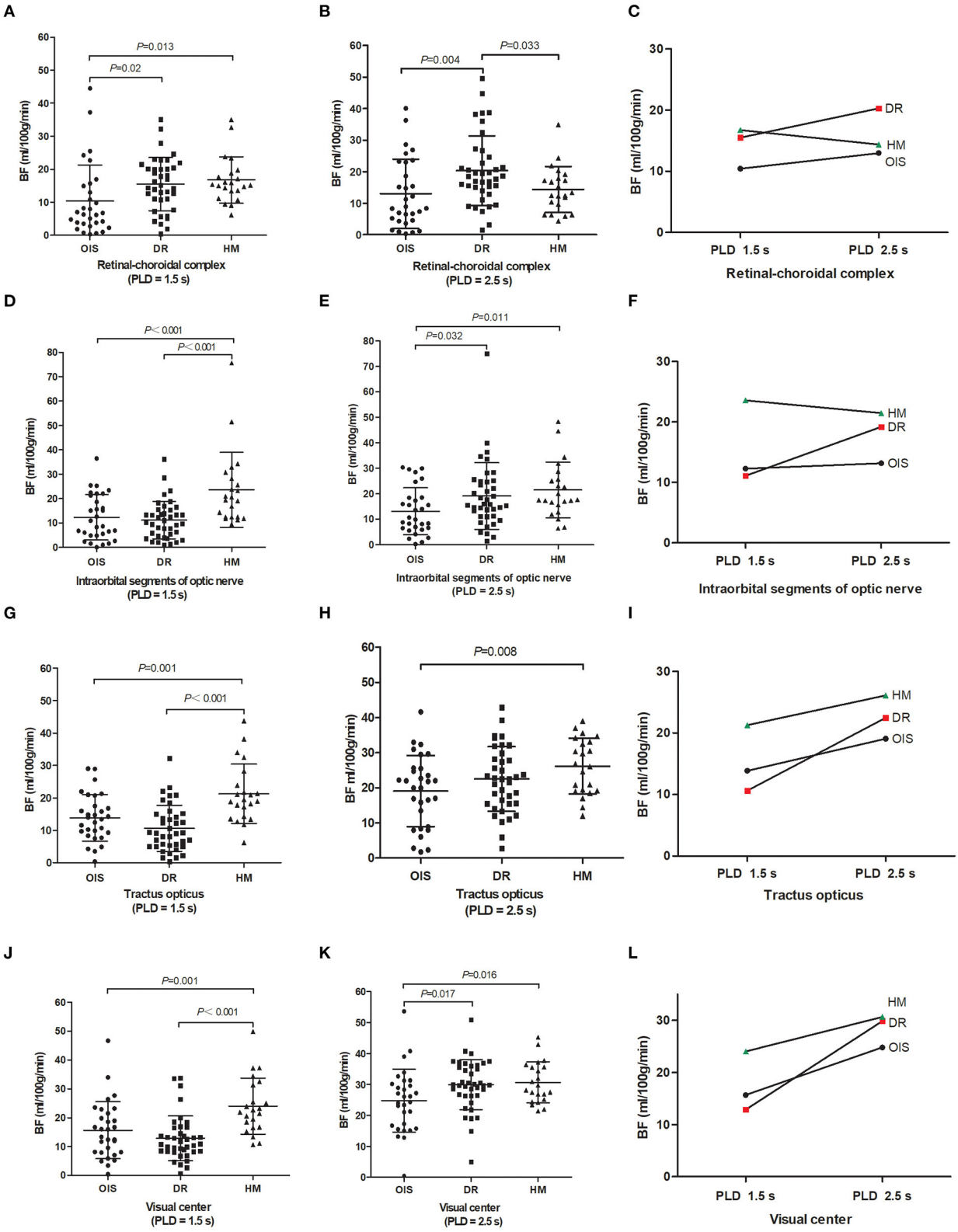

FIGURE 3
Between-group comparison. Magnetic resonance imaging metrics for each subject are shown as raw data with lines for mean and standard deviation **(A, B, D, E, G, H, J, K)**. Images showing blood flow perfusion values changed from PLD 1.5–2.5 s **(C, F, I, L)**. BF, blood flow; PLD, post-labeling delay; OIS, ocular ischemic syndrome; DR, diabetic retinopathy; HM, high myopia.

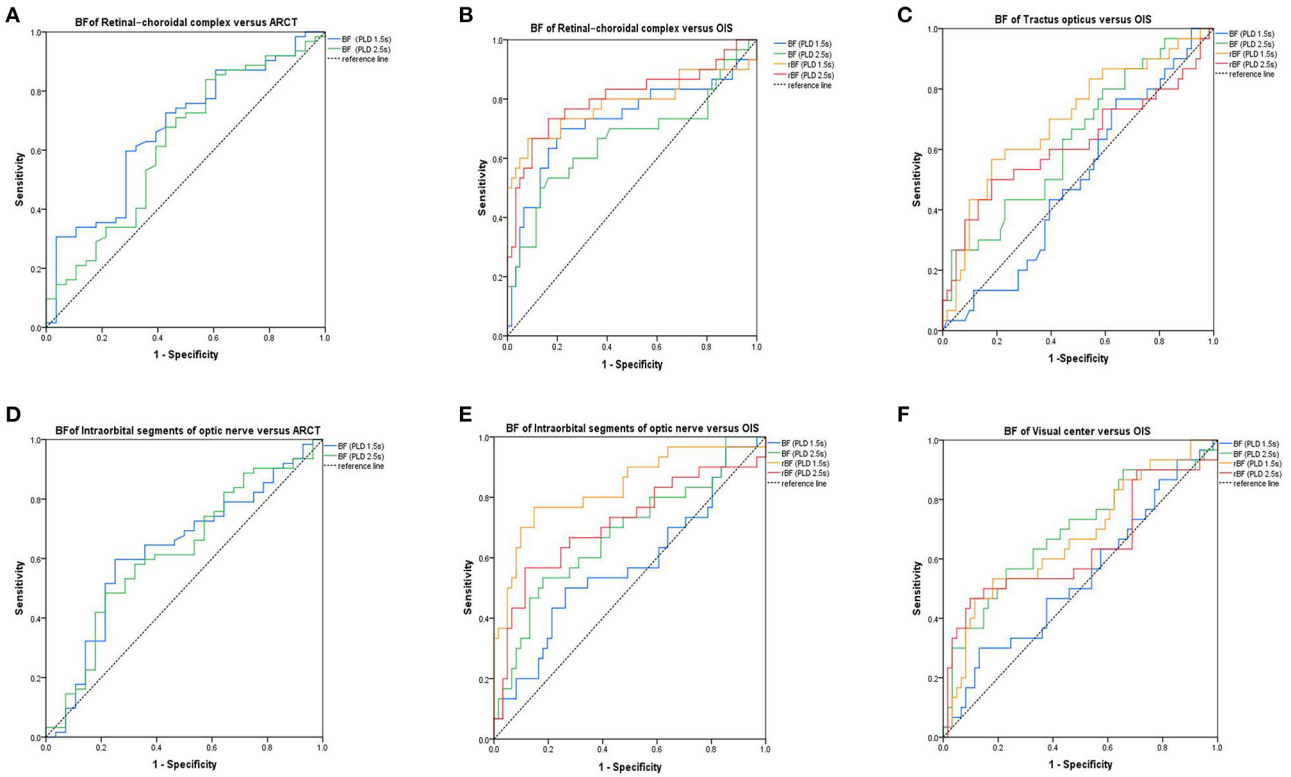

FIGURE 4
Receiver operating characteristic curves. The area under curve (AUC) showing the accuracy of the values of blood flow perfusion in the visual pathway, identified using arterial spin labeling (ASL) for diagnosis of the delayed retinal arterial filling **(A, D)**. The AUC shows the accuracy of the values of blood flow perfusion in the visual pathway, identified using ASL for diagnosis of OIS **(B, C, E, F)**. BF, blood flow; rBF, relative blood flow; ARCT, arm-retinal circulation time; OIS, ocular ischemic syndrome.

Safety of ASL and FFA

Of the 91 subjects, two patients felt uncomfortable due to the claustrophobic space of the MRI, and three patients developed a mild rash due to the sodium fluorescein contrast agent. The adverse reaction rates of ASL and FFA were 2.20 and 3.30%, respectively. There was no significant difference in the safety between ASL and FFA ($p < 0.001$), but ASL was noninvasive and, independent of contrast media, showed better convenience.

Discussion

In our study, subjects with OIS tended to be older, with a male predominance, keeping with characteristics described in the literature (Xiang and Zou, 2020). The characteristics of the disease made complete matching impossible. Previous studies (Vaghefi et al., 2017) showed that, in addition to the rate of BF, the volume of the vascular tissue may be one of the important factors that will influence the perfusion of the eye in ASL. Central macular retinal and choroidal thickness measured by EDI-OCT can be the surrogate biomarker of the vascular tissue, which is known to decrease with increasing age (Ikuno et al., 2011). Our study showed that subjects with OIS and high myopic retinopathy showed thinner central macular retinal thickness compared to subjects with DR, which was consistent with the characteristics of the disease reported in the earlier literature (Brito et al., 2015). Another finding was that subjects with HM presented with the thinnest central macular choroidal thickness compared with the other two groups, which was in keeping with previous studies (Fang et al., 2019). The blood supply of the visual pathway is from the ophthalmic artery, the middle cerebral artery, and the posterior cerebral artery (Abhinav et al., 2020). A study (Dan et al., 2019) assessed resting cerebral blood flow changes in patients with retinitis pigmentosa using a pseudo-continuous ASL and found that altered cerebral BF may cause trans-synaptic retrograde degeneration of the visual pathway in patients with retinitis pigmentosa. We also found some interesting results: The subjects with DR were presented with lower BF perfusion values in the intraorbital segments of the optic nerve, the tractus opticus, and the visual center at PLDs of 1.5 s. A previous study (Wong et al., 2020) showed the association between DR and an increased risk of stroke, which indicated that the larger cerebrovascular implications are caused by the microvascular pathology inherent to DR. Therefore, we speculated that the BF perfusion of the visual pathway in patients with DR was affected by systemic diseases. The results of the present study also showed that the subjects with high myopic retinopathy presented with lower BF perfusion values in the retinal–choroidal complex at PLDs of 2.5 s, which further confirmed that the volume of the vascular tissue is another factor that will affect the perfusion of the posterior pole in ASL. ASL is used to evaluate the tissue perfusion rate. Tissue perfusion—the exchange of water and nutrients with tissues—occurs over the entire length of capillaries (Zhu et al., 2022). ASL basically

"tracks" the water molecules in the blood from the arterial cavity to the tissue capillary bed and treats the water molecules as a freely diffusible tracer. ASL can easily occur through magnetization reversal or saturation of blood and water molecules in the blood supply artery along the *Z*-axis (Moran et al., 2022). After labeling, the time to wait for the blood to enter the tissue is called the PLD time or the reversal time of some specific ASL technology. Select the delay time so that the image can be obtained, ideally when the water molecules and tissues are magnetized and exchanged. Arterial blood labeling is realized through the combination of pulse and gradient to reverse the longitudinal magnetization of blood-water protons (Iutaka et al., 2023).

The accuracy of ASL perfusion evaluation is essential to diagnosing OIS. As the primary cause of OIS, the stenosis or occlusion of the common or internal carotid arteries is easy to ignore, and it is a necessary condition for diagnosing OIS (Mendrinos et al., 2010). The most specific (but not the most sensitive) fluorescein angiography sign of OIS is prolonged retinal filling time, known as ARCT, which is present in approximately 60% of patients with OIS (Terelak-Borys et al., 2012). The most sensitive (but not the most specific) fluorescein angiography sign of OIS is prolonged RCT, which is present in 95% of patients with OIS (Brown and Magargal, 1988). The BF values of the retinal–choroidal complex at PLDs of 1.5 s were estimated by comparison with the ARCT of the gold standard FFA-based diagnosis of delayed retinal arterial filling in our study. The result of an AUC of 0.669 was not satisfactory. However, the results of the rBF value were satisfactory. In previous studies of cerebral blood flow perfusion, the relative cerebral perfusion value (Iutaka et al., 2023) was more concerning than the absolute value (Salisbury et al., 2022). However, a delayed arterial filling time is not diagnostic for ocular ischemia (Hung and Chang, 2017). In Vaghefi's report (Vaghefi et al., 2017), they attempted to quantify the chorioretinal blood perfusion in patients with a clinical diagnosis of retinal ischemia using ASL. They speculated that ocular ischemia may be due to tissue volume and arterial flow, but only four participants without blood perfusion of the visual pathway were evaluated in their study.

The reproducibility of ASL perfusion evaluation is necessary for clinical application in diagnosing OIS. In our study, the ICC of the BF values derived from the retinal–choroidal complex and the intraorbital segments of the optic nerve between the two observers at PLDs of 1.5 and 2.5 s showed satisfactory concordance. A previous study (Khanal et al., 2019) demonstrated the high intraday and interday repeatability in the quantitative ASL-MRI measurements of retinal–choroidal complex blood perfusion. However, their study did not evaluate other blood perfusion values in the visual pathway. When we suspect that the patient has ocular hypoperfusion, we should combine ASL with FFA to make a comprehensive judgment. When ASL is applied in the eye, the blood perfusion in the posterior part of the eye will be measured, and the low perfusion of the visual pathway can be presented, which will help to understand the factors affecting the changes in the blood perfusion of the visual pathway and the changes in the blood perfusion of the eye caused by carotid artery stenosis.

The safety and convenience of the clinical application of ASL in the differential diagnosis of OIS may be attractive to ophthalmologists compared with traditional ophthalmic examinations. However, FFA is the gold standard for diagnosing retinal vascular diseases. The limitations of FFA in itself affect the clinical application. In our study, two patients felt uncomfortable due to the claustrophobic space of the MRI, and three patients developed a mild rash due to the sodium fluorescein contrast agent. Although there was no significant difference in the safety of ASL and FFA, ASL was noninvasive and showed more advantages, independent of contrast media.

Conclusion

In conclusion, 3D-pCASL showed the participants with OIS had lower blood flow perfusion values in the visual pathway, which presented satisfactory accuracy, reproducibility, and safety. It is a noninvasive and comprehensive diagnostic tool to assess blood flow perfusion in a visual pathway for the differential diagnosis of OIS.

Limitations

The limitations of this study are as follows. The spatial resolution of images is larger than the areas of intraorbital ROIs and the tractus opticus, which are determined by the size of the study organ. ASL of white matter, particularly small white matter tracts, has always been problematic, even when this study used the contralateral side as an internal reference. However, we attempted to include complete clinical data for analysis to explore OIS's noninvasive differential diagnosis strategy.

Data availability statement

The original contributions presented in the study are included in the article/supplementary material, further inquiries can be directed to the corresponding authors.

Ethics statement

The studies involving human participants were reviewed and approved by the Medical Research Ethics Committee of Beijing Friendship Hospital, Capital Medical University (NO.2018-P2-185-02). The patients/participants provided their written informed consent to participate in this study.

Author contributions

XZ and YW supervised the present study. YC and XF performed the analysis and wrote the manuscript. YH, LZ, XC, SQ, and JS helped to collect the clinical data. JJ contributed to the image processing. All authors contributed to the article and approved the submitted version.

Funding

The study was supported by the National Natural Science Foundation of China (81870686), the Research Foundation of Beijing Friendship Hospital, Capital Medical University (yyqdkt

2019-29), and Capital's Funds for Health Improvement and Research (2018-1-2021).

Conflict of interest

The authors declare that the research was conducted in the absence of any commercial or financial relationships that could be construed as a potential conflict of interest.

Publisher's note

References

Abhinav, K., Gimenez, P., Tyler, M., Patel, Z. M., and Fernandez-Miranda, J. C. (2020). Endoscopic endonasal approach for resection of suprasellar hemangioblastoma: selective pituitary sacrifice and use of indocyanine dye: 2-dimensional operative video. *Oper Neurosurg. (Hagerstown)* 20, E46–E47. doi: 10.1093/ons/opaa250

Avery, M. B., Magal, I., Kherani, A., and Mitha, A. P. (2019). Risk of stroke in patients with ocular arterial occlusive disorders: a retrospective Canadian study. J. *Am Heart Assoc* 8, e010509. doi: 10.1161/JAHA.118.010509

Awan, A., and Yang, Y. C. (2006). Shellfish allergy: a contraindication for fundus fluorescein angiography; misconception or reality. *Eye (Lond)* 20, 1383–1384. doi: 10.1038/sj.eye.6702220

Battista, M., Cascavilla, M. L., Grosso, D., Borrelli, E., Frontino, G., Amore, G., et al. (2022). Retinal vascular impairment in Wolfram syndrome: an optical coherence tomography angiography study. *Sci. Rep.* 12, 2103. doi: 10.1038/s41598-022-06150-6

Brito, P. N., Rosas, V. M., Coentrao, L. M., Carneiro, A. V., Rocha-Sousa, A., Brandao, E., et al. (2015). Evaluation of visual acuity, macular status, and subfoveal choroidal thickness changes after cataract surgery in eyes with diabetic retinopathy. *Retina* 35, 294–302. doi: 10.1097/IAE.0000000000000298

Brown, G. C., and Magargal, L. E. (1988). The ocular ischemic syndrome. Clinical, fluorescein angiographic and carotid angiographic features. *Int. Ophthalmol.* 11, 239–251. doi: 10.1007/BF00131023

Casalino, G., Bandello, F., and Chakravarthy, U. (2017). An unusual cause of unilateral vision loss. *JAMA Ophthalmol.* 135, 69–70. doi: 10.1001/jamaophthalmol.2016.2730

Dan, H., Shen, Y., Huang, X., Zhou, F., and Xing, Y. (2019). Arterial spin labeling perfusion magnetic resonance imaging reveals resting cerebral blood flow alterations specific to retinitis pigmentosa patients. *Curr Eye Res* 44, 1353–1359. doi: 10.1080/02713683.2019.1649702

de Keizer, R. J., and te Strake, L. (1986). Intraocular lens implants (pseudophakoi) and steelwire sutures: a contraindication for MRI? *Doc. Ophthalmol.* 61, 281–284. doi: 10.1007/BF00142354

Fang, Y., Du, R., Nagaoka, N., Yokoi, T., Shinohara, K., Xu, X., et al. (2019). OCT-based diagnostic criteria for different stages of myopic maculopathy. *Ophthalmology* 126, 1018–1032. doi: 10.1016/j.ophtha.2019.01.012

Flaxel, C. J., Adelman, R. A., Bailey, S. T., Fawzi, A., Lim, J. I., Vemulakonda, G. A., et al. (2020). Diabetic retinopathy preferred practice pattern(R). *Ophthalmology*. 127, 66–P145. doi: 10.1016/j.ophtha.2019.09.025

Fransen, S. R., Leonard-Martin, T. C., Feuer, W. J., Hildebrand, P. L., and Inoveon Health Research, G. (2002). Clinical evaluation of patients with diabetic retinopathy: accuracy of the Inoveon diabetic retinopathy-3DT system. *Ophthalmology* 109, 595–601. doi: 10.1016/S0161-6420(01)00990-3

Hedges, T. R. (1962). Ophthalmoscopic findings in internal carotid artery occlusion. *Bull. Johns Hopkins Hosp*. 111, 89–97.

Hung, J. H., and Chang, Y. S. (2017). Ocular ischemic syndrome. *CMAJ* 189, E804. doi: 10.1503/cmaj.160459

Ikuno, Y., Maruko, I., Yasuno, Y., Miura, M., Sekiryu, T., Nishida, K., et al. (2011). Reproducibility of retinal and choroidal thickness measurements in enhanced depth imaging and high-penetration optical coherence tomography. *Invest. Ophthalmol. Vis. Sci.* 52, 5536–5540. doi: 10.1167/iovs.10-6811

Iutaka, T., De Freitas, M. B., Omar, S. S., Scortegagna, F. A., Nael, K., Nunes, R. H., et al. (2023). Arterial spin labeling: techniques, clinical applications, and interpretation. *Radiographics* 43, e220088. doi: 10.1148/rg.220088

Khanal, S., Turnbull, P. R. K., Vaghefi, E., and Phillips, J. R. (2019). Repeatability of arterial spin labeling mri in measuring blood perfusion in the human eye. J. *Magn. Reson. Imaging* 49, 966–974. doi: 10.1002/jmri.26323

Kitajima, M., and Uetani, H. (2023). Arterial spin labeling for pediatric central nervous system diseases: techniques and clinical applications. *Magn. Reson. Med. Sci.* 22, 27–43. doi: 10.2463/mrms.rev.2021-0118

Lauria, A. L., Koelling, E. E., Houghtaling, P. M., and White, P. W. (2020). Carotid endarterectomy for ocular ischemic syndrome: a case report and review of the literature. *Ann. Vasc. Surg. 67* 567. e9-567 e12. doi: 10.1016/j.avsg.2020.03.005

Lee, D., Tomita, Y., Yang, L., Negishi, K., and Kurihara, T. (2022). Ocular Ischemic Syndrome and Its Related Experimental Models. *Int. J. Mol Sci.* 23, 5249. doi: 10.3390/ijms23095249

Lineback, C. M., Stamm, B., Sorond, F., and Caprio, F. Z. (2022). Carotid disease, cognition, and aging: time to redefine asymptomatic disease? *Geroscience* 15, 1–7. doi: 10.1007/s11357-022-00688-z

Luo, J., Yan, Z., Jia, Y., and Luo, R. (2018). Clinical analysis of 42 cases of ocular ischemic syndrome. *J. Ophthalmol.* 2018, 2606147. doi: 10.1155/2018/2606147

Mendrinos, E., Machinis, T. G., and Pournaras, C. J. (2010). Ocular ischemic syndrome. *Surv. Ophthalmol.* 55, 2–34. doi: 10.1016/j.survophthal.2009.02.024

Mester, L., Szabo, A., Atlasz, T., Szabadfi, K., Reglodi, D., Kiss, P., et al. (2009). Protection against chronic hypoperfusion-induced retinal neurodegeneration by PARP inhibition via activation of PI-3-kinase Akt pathway and suppression of JNK and p38 MAP kinases. *Neurotox. Res.* 16, 68–76. doi: 10.1007/s12640-009-9049-6

Mills, R. P. (1989). Anterior segment ischemia secondary to carotid occlusive disease. J. *Clin NeuroOphthalmol.* 9, 200–204.

Moran, C., Xu, Z. Y., Mehta, H., Gillies, M., Karayiannis, C., Beare, R., et al. (2022). Neuroimaging and cognitive correlates of retinal Optical Coherence Tomography (OCT) measures at late middle age in a twin sample. *Sci. Rep.* 12, 9562. doi: 10.1038/s41598-022-13662-8

Muir, E. R., and Duong, T. Q. (2011). MRI of retinal and choroidal blood flow with laminar resolution. *NMR BioMed.* 24, 216–223. doi: 10.1002/nbm.1576

Nawaz, I. M., Rezzola, S., Cancarini, A., Russo, A., Costagliola, C., Semeraro, F., et al. (2019). Human vitreous in proliferative diabetic retinopathy: characterization and translational implications. *Prog. Retin. Eye Res.* 72, 100756. doi: 10.1016/j.preteyeres.2019.03.002

Ruiz-Medrano, J., Montero, J. A., Flores-Moreno, I., Arias, L., Garcia-Layana, A., Ruiz-Moreno, J. M., et al. (2019). Myopic maculopathy: Current status and proposal for a new classification and grading system (ATN). *Prog. Retin. Eye Res.* 69, 80–115. doi: 10.1016/j.preteyeres.2018.10.005

Salisbury, D. F., Curtis, M., Longenecker, J., Yeh, F. C., Kim, T., Coffman, B. A., et al. (2022). Pathological resting-state executive and language system perfusion in first-episode psychosis. *Neuroimage Clin.* 36, 103261. doi: 10.1016/j.nicl.2022.103261

Scelsi, M. A., Khan, R. R., Lorenzi, M., Christopher, L., Greicius, M. D., Schott, J. M., et al. (2018). Genetic study of multimodal imaging Alzheimer's disease progression score implicates novel loci. *Brain* 141, 2167–2180. doi: 10.1093/brain/awy141

Steigerwalt, R. D., Cesarone, M. R., Belcaro, G., Pascarella, A., Rapagnetta, L., Angelis, M. D., et al. (2009). Ocular ischemia in high myopia treated with intravenous prostaglandin e1. *Retin Cases Brief Rep.* 3, 379–382. doi: 10.1097/ICB.0b013e31817f2c80

Stolte, S., and Fang, R. (2020). A survey on medical image analysis in diabetic retinopathy. *Med. Image Anal.* 64, 101742. doi: 10.1016/j.media.2020.101742

Terelak-Borys, B., Skonieczna, K., and Grabska-Liberek, I. (2012). Ocular ischemic syndrome - a systematic review. *Med. Sci. Monit.* 18, RA138–144. doi: 10.12659/MSM.883260

Vaghefi, E., Kauv, K., Pan, W., and Squirrell, D. (2017). Application of arterial spin labelling in detecting retinal ischemia. *Case Rep. Ophthalmol.* 8, 545–557. doi: 10.1159/000485316

Valentin, B., Stabinska, J., Reurik, F., Tell, C., Mewes, A. D., Muller-Lutz, A., et al. (2022). Feasibility of renal perfusion quantification by Fourier decomposition MRI. *Magn. Reson. Imaging* 85, 3–9. doi: 10.1016/j.mri.2021.10.003

Wang, H., Li, S., Chen, X., Wang, Y., Li, J., Wang, Z., et al. (2020). Cerebral blood flow alterations in high myopia: an arterial spin labeling study. *Neural. Plast*. 2020, 6090262. doi: 10.1155/2020/6090262

Wong, K. H., Hu, K., Peterson, C., Sheibani, N., Tsivgoulis, G., Majersik, J. J., et al. (2020). Diabetic retinopathy and risk of stroke: a secondary analysis of the ACCORD eye study. *Stroke* 51, 3733–3736. doi: 10.1161/STROKEAHA.120.030350

Xiang, Z. Y., and Zou, H. D. (2020). Recent epidemiology study data of myopia. *J. Ophthalmol.* 2020, 4395278. doi: 10.1155/2020/4395278

Zhu, X., Zhu, J., Wang, Y., Chu, Z., Wang, R. K., Xu, Y., et al. (2022). A moderate dosage of coffee causes acute retinal capillary perfusion decrease in healthy young individuals. *BMC Ophthalmol.* 22, 460. doi: 10.1186/s12886-022-02638-x

frontiers | Frontiers in Neuroscience

TYPE Original Research
PUBLISHED 22 March 2023
DOI 10.3389/fnins.2023.1135991

OPEN ACCESS

EDITED BY
Jiawei Zhou,
Wenzhou Medical University, China

REVIEWED BY
Yao Zhimo,
Wenzhou Medical University, China
Jibo Zhou,
Shanghai Ninth People's Hospital, China

*CORRESPONDENCE
Dan Wen
✉ wendan@csu.edu.cn

SPECIALTY SECTION
This article was submitted to Visual Neuroscience, a section of the journal Frontiers in Neuroscience

RECEIVED 02 January 2023
ACCEPTED 06 March 2023
PUBLISHED 22 March 2023

CITATION
Xiang A, Du K, Fu Q, Zhang Y, Zhao L, Yan L and Wen D (2023) Do monocular myopia children need to wear glasses? Effects of monocular myopia on visual function and binocular balance.
Front. Neurosci. 17:1135991.
doi: 10.3389/fnins.2023.1135991

Do monocular myopia children need to wear glasses? Effects of monocular myopia on visual function and binocular balance

Aiqun Xiang[1,2,3], Kaixuan Du[1,2,3], Qiuman Fu[1,2,3], Yanni Zhang[1,2,3], Liting Zhao[1,2,3], Li Yan[4] and Dan Wen[1,2,3]*

[1]Eye Center of Xiangya Hospital, Central South University, Changsha, Hunan, China, [2]Hunan Key Laboratory of Ophthalmology, Changsha, Hunan, China, [3]National Clinical Research Center for Geriatric Disorders, Xiangya Hospital, Central South University, Changsha, Hunan, China, [4]National Engineering Research Center for Healthcare Devices, Guangzhou, China

Objective: This study aims to compare the binocular visual functions and balance among monocular myopic adolescents and adults and binocular low myopic adolescents and explore whether monocular myopia requires glasses.

Methods: A total of 106 patients participated in this study. All patients were divided into three groups: the monocular myopia children group (Group 1 = 41 patients), the monocular myopia adult group (Group 2 = 26 patients) and the binocular low myopia children group (Group 3 = 39 patients). The refractive parameters, accommodation, stereopsis, and binocular balance were compared.

Results: The binocular refractive difference in Group 1, Group 2, and Group 3 was −1.37 ± 0.93, −1.94 ± 0.91, and −0.32 ± 0.27 D, respectively. Moreover, uncorrected visual acuity (UCVA), spherical equivalent (SE) and monocular accommodative amplitude (AA) between myopic and emmetropic eyes in Group 1 and Group 2 were significantly different (all $P < 0.05$). There was a significant difference in the accommodative facility (AF) between myopic and emmetropic eyes in Group 2 ($t = 2.131$, $P = 0.043$). Furthermore, significant differences were found in monocular AA ($t = 6.879$, $P < 0.001$), binocular AA ($t = 5.043$, $P < 0.001$) and binocular AF ($t = -3.074$, $P = 0.003$) between Group 1 and Group 2. The normal ratio of stereopsis according to the random dots test in Group 1 was higher than in Group 2 ($\chi 2 = 14.596$, $P < 0.001$). The normal ratio of dynamic stereopsis in Group 1 was lower than in Group 3 ($\chi 2 = 13.281$, $P < 0.001$). The normal signal-to-noise ratio of the binocular balance point in Group 1 was lower than Group 3 ($\chi 2 = 4.755$, $P = 0.029$).

Conclusion: First, monocular myopia could lead to accommodative dysfunction and unbalanced input of binocular visual signals, resulting in myopia progression. Second, monocular myopia may also be accompanied by stereopsis dysfunction, and long-term uncorrected monocular myopia may worsen stereopsis acuity in adulthood. In addition, patients with monocular myopia could

exhibit stereopsis dysfunction at an early stage. Therefore, children with monocular myopia must wear glasses to restore binocular balance and visual functions, thereby delaying myopia progression.

KEYWORDS

monocular myopia, visual function, binocular balance, stereopsis, accommodation

1. Introduction

Myopia is a global public health problem (Li et al., 2016). In recent years, the incidence of myopia has increased, and the age of onset has become younger. Monocular myopia is common in school-aged children. Moreover, an inter-ocular difference of 1.00 D or more in cycloplegic spherical equivalent (SE) was considered anisometropia (Afsari et al., 2013; Hu et al., 2016). Myopia changes the refractive status, structure and function of the eyes (Mitchell and Sengpiel, 2009; Sengpiel, 2011). Due to the difference in refractive power between the two eyes, anisometropia will result in different retinal image sizes in each eye, resulting in dysfunctional monocular and binocular vision (Huang et al., 2011). Monocular myopic patients usually do not wear glasses because of their good monocular vision. Does the uncorrected monocular myopia affect the balance between two eyes? This is one of the issues we explored.

Moreover, the visual function of monocular myopia is frequently disregarded. In clinical settings, stereopsis and accommodative functions are normally used to evaluate binocular visual functions (Wilson, 2017; Niechwiej-Szwedo et al., 2020). However, the random dots stereopsis is used to detect only close-range and static stereopsis, limiting the evaluation and accuracy of stereopsis. Therefore, we applied the virtual reality platform to test the binocular vision functions of patients from different dimensions. We employed methods mentioned earlier to observe the changes in visual functions of children and adults with monocular myopia and guide monocular myopia patients on whether they need glasses.

2. Materials and methods

2.1. Patients

A total of 106 patients were enrolled in the Laser Center of Ophthalmology, Xiangya Hospital of Central South University, from April 2021 to December 2021. The exclusion criteria were as follows: strabismus, amblyopia, organic and congenital ophthalmopathy, nystagmus, history of ocular trauma and surgery. Patients were divided into three groups, 41 children with monocular myopia (Group 1: 23 males and 18 females), 26 adults with monocular myopia (Group 2: 9 males and 17 females), and 39 children with binocular low myopia (Group 3: 21 males and 18 females). Specific inclusion criteria were as follows: in the monocular myopia group, the spherical correction of one eye was −0.5 to −3.00 D, the cylinder was less than −1.50 D, the best corrected visual acuity was 20/20 or better, and the naked eye visual acuity of the other eye was 20/20 or better, the difference of SE between two eyes was greater than or equal to 1.00 D. In binocular low myopia group, the spherical correction ranged from −0.5 to −3.00 D and the cylinder was less than −1.50 D, the best corrected visual acuity of both eyes was 20/20 or better, the difference of SE between two eyes was less than 1.00 D. Children and adults with monocular myopia do not routinely wear glasses, whereas children with binocular low myopia do. Informed consent was obtained from the patients and the parents or legal guardians of the underaged patients. All study protocols were approved by the Medical Ethics Committee of Xiangya Hospital of Central South University and carried out in adherence to the Declaration of Helsinki regarding ethical principles for research involving human subjects.

2.2. Measurement of refractive parameters

Cycloplegic eye drops (atropine twice daily) was given for 1 week for children under 8 years. Compound tropicamide eye drops were administered for patients over 8 years, once every 10 min for four times. Computer optometry, ophthalmoscopy combined with subjective refraction to determine spherical and cylinder.

2.3. Measurement of accommodative functions

2.3.1. Accommodative amplitude

The AA was measured using Donders' push-up method. Patients were instructed to focus on the line second from the bottom on a reduced vision chart at a distance of approximately 40 cm and indicate when the target blurred as the chart moved slowly toward the eye. The distance from the target to the spectacle plane was measured with a millimeter ruler and converted to diopters. During monocular measurements, the untested eye was covered with an occluder.

2.3.2. Accommodative facility

The AF was measured with a ±2.00 D flipper. The participants were instructed to read each of the 20/30 letters in order immediately after recognition. First, through the −2.00 DS lens and then the +2.00 DS lens, the number of flips per minute was recorded and converted to cycles per minute (cpm). During monocular measurement, the untested eye was covered with an occluder.

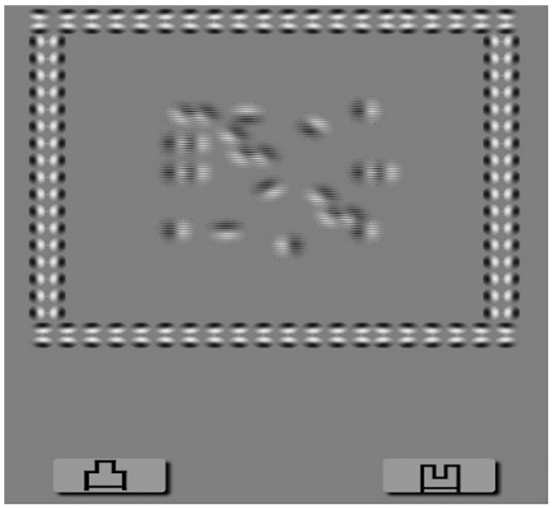

FIGURE 1
Dynamic stereopsis. Patients wearing 3D polarized glasses are required to recognize that the outlines of letter "N" were elevated from or flat on the screen taking the square as a reference. There are four grades, and the result reach to grade 4 can be recorded as normal.

2.4. Random dots stereopsis

According to the patients' daily refractive correction status, monocular myopia patients were tested without glasses, and low myopia patients were tested with glasses. Subjects were measured at a distance of 40 cm. There are two inspection boards, each with four stereoacuity inspection pictures, decreasing from 800–40 arcsec in order of parallax. The result less than or equal to 60 arcsec is normal.

2.5. Dynamic stereopsis

All subjects wore polarized glasses after refractive correction to observe the stimulus on a screen with a gray background (44 cd/m^2). Stimulus was a square containing 16 Gobar spots generated by a random-dot kinematogram (RDK) algorithm with a monitor frame rate of 10 Hz. Gobar spots formed two outlines of the letter "N" according to the motion definition structure and were displayed to the two eyes through the polarized glasses. Two letters had binocular parallax and could be fused to form stereoacuity. Subjects were asked to use the square as a reference to recognize whether the outlines of the letter "N" were elevated or flat relative to the screen. There are four grades, and the result reaching grade 4 is normal (Figure 1).

2.6. Binocular rivalry signal-noise ratio

All subjects wore polarized glasses after refractive correction to observe the stimulus on a screen with a gray background (44 cd/m^2). Stimulus was the moving signal dots and noise dots in the square. Patients were instructed to watch the signal dots with the right eye and the noise dots with the left eye. The signal dots moved in all directions uniformly, while the noise points moved erratically. The examinee was required to identify the movement direction of the signal points. After detecting the correct direction each time, the ratio of the signal dots to the noise dots was changed until the patient could not recognize the movement direction of the signal dots; finally, the binocular balance was obtained. The ratio of signal and noise dots can be divided into eight levels. The ratio of signal dots is 100% at level 1. At level 2, the ratio of signal dots is 85%, and noise dots is 15%. At level 3, the signal and noise dots ratios are 70 and 30%, respectively. Subsequently, the number of signal dots is decreased by 10%, the number of noise dots is increased by 10% at each level, and the ratio of signal dots is 20% at level 8. Each level was tested three times and promoted if it was correct. After examining the right eye, the patient was instructed to follow the signal dots with the left eye, and the right eye should watch the noise dots; we recorded the levels of both eyes, respectively. It is considered normal when the monocular is greater than or equal to grade 6, and the difference between two eyes is less than two grades (Figure 2).

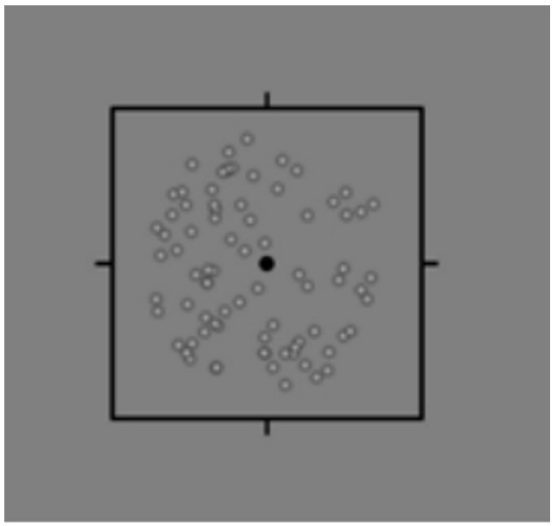

FIGURE 2
Binocular rivalry signal-noise ratio. Patients wear 3D polarized glasses and watch the moving signal dots and noise dots on the screen. The signal dots moved in all directions uniformly, while the noise points moved erratically. The examinee was required to identify the movement direction of the signal points. After detecting the correct direction each time, the ratio of the signal dots to the noise dots was changed until the patient could not recognize the movement direction of the signal dots; finally, the binocular balance was obtained.

2.7. Statistical analysis

Statistical analysis was performed using Statistical Product and Service Solutions (SPSS) (Ver. 23.0.; IBM Corp.; Armonk, NY, USA). The measurement data were expressed as mean ± standard deviation, and the counting data were expressed by rate (%). Comparison of refractive parameters and accommodative functions between emmetropia and myopic in the monocular myopia group were examined by the paired sample *t*-test, and the

TABLE 1 Demographic and biometric measures (mean ± SD) for the subjects'.

	Group 1	Group 2	Group 3
Number	41 (82 eyes)	26 (52 eyes)	39 (78 eyes)
Sex (male/female)	23/18	9/17	21/18
Age (range)	10.59 ± 2.24 (6–15)	24.08 ± 1.98 (19–27)	9.67 ± 2.30 (6–15)
BRD (D)	−1.37 ± 0.93	−1.94 ± 0.91	−0.32 ± 0.27
UCVA (logMAR)	0.25 ± 0.37	0.27 ± 0.42	0.49 ± 0.22
BCVA (logMAR)	−0.11 ± 0.05	−0.12 ± 0.05	−0.11 ± 0.04

TABLE 2 Results of biometric measures and accommodative functions between myopic and emmetropic eyes in Group 1 and Group 2.

Group	UCVA (logMAR)	BCVA (logMAR)	SE (D)	AA (D)	AF (cpm)
Group 1					
Myopic eyes	0.57 ± 0.26	−0.11 ± 0.05	−1.49 ± 0.78	11.56 ± 2.45	6.16 ± 2.83
Emmetropic eyes	−0.06 ± 0.07	−0.11 ± 0.05	−0.12 ± 0.36	11.04 ± 2.69	5.71 ± 2.87
t	14.447	0.628	−9.404	2.108	1.372
P	<0.001	0.534	<0.001	0.041	0.178
Group 2					
Myopia eyes	0.64 ± 0.28	−0.12 ± 0.05	−1.87 ± 0.79	9.19 ± 1.58	6.69 ± 2.36
Emmetropic eyes	−0.09 ± 0.07	−0.12 ± 0.05	−0.07 ± 0.42	8.58 ± 1.35	5.60 ± 2.45
t	12.354	−0.717	−10.943	2.557	2.131
P	<0.001	0.480	<0.001	0.017	0.043

independent two-sample *t*-test was used to compare the monocular myopia children group and the other two groups, respectively. The comparison between the adolescent monocular myopia group and the other two groups was tested by two independent sample *t*-test. The random dot stereopsis, dynamic stereopsis, and signal-to-noise ratio were analyzed by $\chi 2$ test. A *P* value of < 0.05 was considered a statistically significant difference.

3. Results

This study comprised 106 patients, 41 (23 men and 18 women) in the monocular myopia children group (Group 1), 26 (9 men and 17 women) in the monocular myopia adult group (Group 2), and 39 (21 men and 18 women) in the binocular low myopia children group (Group 3). The mean age was 10.59 ± 2.24 years (6–15 years), 24.08 ± 1.98 years (19–27 years), and 9.67 ± 2.30 years (6–15 years), respectively. The biometric data of each group are listed in Table 1.

Table 2 represents the results of biometric measurements and accommodative functions between myopic and emmetropic eyes in Group 1 and Group 2. There was a significant difference in UCVA ($t = 14.447$, $P < 0.001$), SE ($t = -9.404$, $P < 0.001$), and AA ($t = 2.108$, $P = 0.041$) between myopic and emmetropic eyes in Group 1. There was no significant difference in BCVA ($t = 0.628$, $P = 0.534$) and AF ($t = 1.372$, $P = 0.178$) between myopic and emmetropic eyes in Group 1. In Group 2, there was a significant difference in UCVA ($t = 12.354$, $P < 0.001$), SE ($t = -10.943$, $P < 0.001$), AA ($t = 2.557$, $P = 0.017$), and AF ($t = 2.131$, $P = 0.043$) between myopic and emmetropic eyes but there was no significant difference in BCVA ($t = -0.717$, $P = 0.480$).

A comparison of the accommodative functions of Group 1 and the other two groups is presented in Figure 3. There was a significant difference in monocular AA ($t = 6.879$, $P < 0.001$), binocular AA ($t = 5.043$, $P < 0.001$) and binocular AF ($t = -3.074$, $P = 0.003$). Furthermore, there was no significant difference in accommodative functions between Group 1 and Group 3 (all *P* values > 0.05).

Figure 4 shows the results of random dots stereopsis in Group 1, Group 2, and Group 3. The normal rate of random dots stereopsis in Group 1 was higher than in Group 2 ($\chi 2 = 14.596$, $P < 0.001$). The results of dynamic stereopsis are given in Figure 5. The normal rate of dynamic stereopsis in Group 1 was lower than in Group 3 ($\chi 2 = 13.281$, $P < 0.001$). The results of the binocular rivalry signal-noise ratio are provided in Figure 6. The normal ratio of signal-to-noise ratio in Group 1 was lower than in Group 3 ($\chi 2 = 4.755$, $P = 0.029$).

5. Discussion

Monocular myopia is very common in clinical practice; such patients, particularly children with monocular myopia, are an indispensable part of the myopic population. Patients with monocular myopia have good vision without glasses and can maintain the needs of daily life (such as writing, reading, and walking). Consequently, many parents and even some adults believe that monocular myopia does not require glasses. They believe using corrective lenses could detract from the beauty, cause inconvenience, and accelerate myopia development. Do patients with monocular myopia need to wear glasses?

However, there is no unified conclusion about the pathogenesis of myopia. Many scholars hypothesized that accommodation is involved in myopia progression (Myrowitz, 2012; Koomson et al., 2016). There is a strong correlation between AA and age (Augusteyn et al., 2011). According to the formula of minimum AA and AF of the corresponding age, the monocular AA and monocular and binocular AF of Group 1 and Group 2 were lower than the normal values. While in Group 3, only the AF was abnormal. These results indicated that the decreased AA and AF might be involved in myopia development. Its mechanism may be that the decreased AA and AF keep the retina in hyperopic defocus for an extended period, thus promoting myopia (Read et al., 2010). Usually, both eyes have symmetrical accommodation. This study analyzed the accommodation function between the two eyes in each group and found no significant difference in AA and accommodative facility between the two eyes in the binocular myopia group. However, in Group 1, the AA of myopic eyes was lower than emmetropic eyes. Furthermore, in Group 2, the AA and AF of the myopic eyes were lower than the emmetropic eyes. These suggested that there was no obvious difference in binocular accommodative function in myopic patients with the same refractive state, but some degree of inequality in the binocular accommodative function of patients with anisometropia was found,

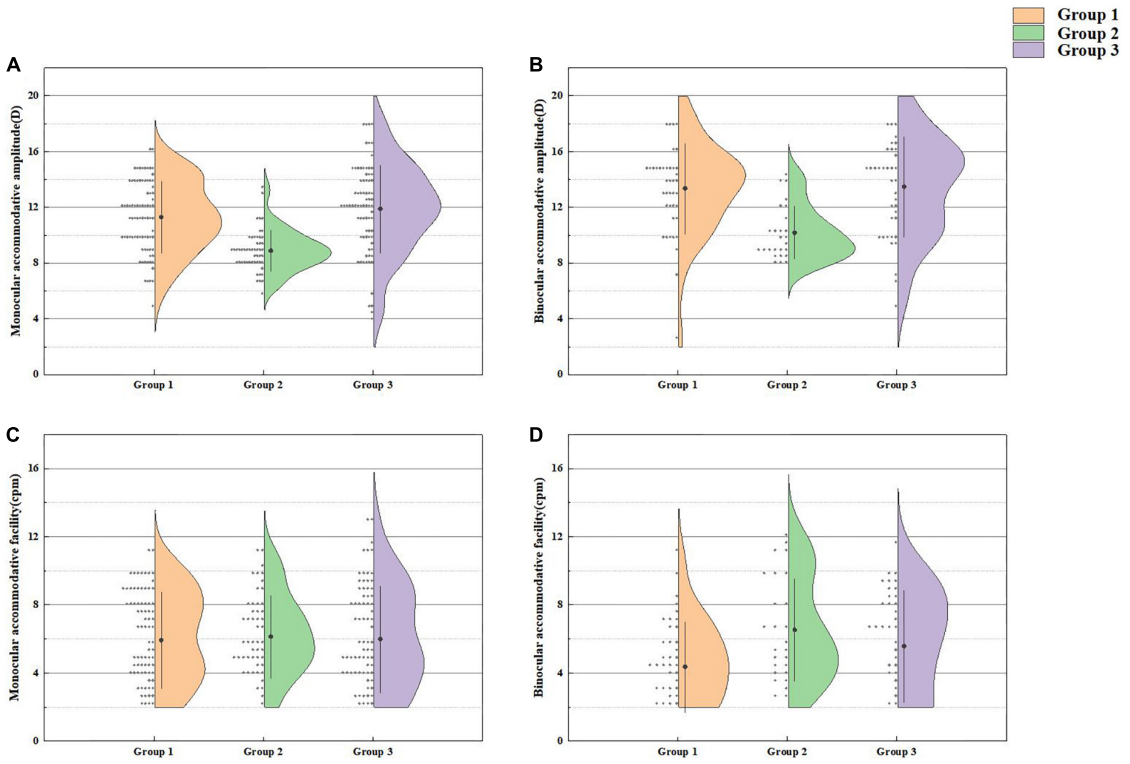

FIGURE 3
Monocular accommodative amplitude **(A)**, binocular accommodative amplitude **(B)**, monocular accommodative facility **(C)**, and binocular accommodative facility **(D)** in Group 1 and the other two groups.

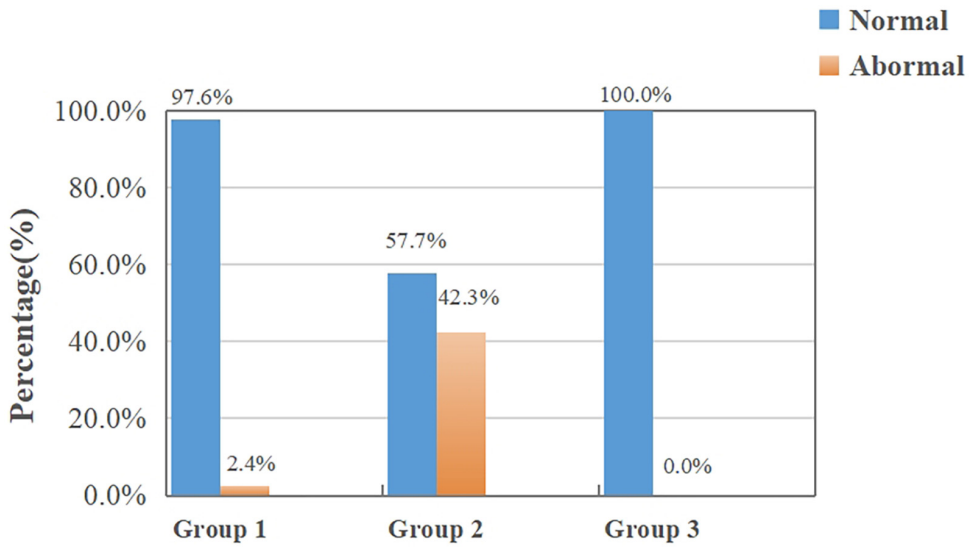

FIGURE 4
Results of random dots stereopsis in Group 1 and the other two groups.

consistent with the previous research results (Toor et al., 2019). Hence, this study's findings proposed that anisometropia could lead to abnormal accommodative function, accelerating the development of anisometropia or binocular myopia.

Previous studies have found a correlation between anisometropia and the progression of binocular myopia (Parssinen, 1990; Tong et al., 2006; Deng and Gwiazda, 2012). Children with monocular myopia may still be monocular myopia in adulthood, which shows that the degree of binocular anisometropia increases, while another part may develop into binocular myopia without obvious pathological anisometropia. Moreover, form deprivation and lens-induced myopia are two classic experimental models of

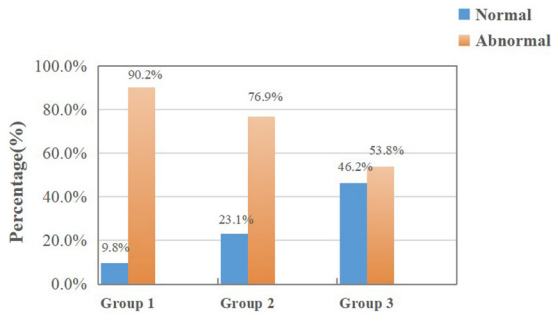

FIGURE 5
Results of dynamic stereopsis in Group 1 and the other two groups.

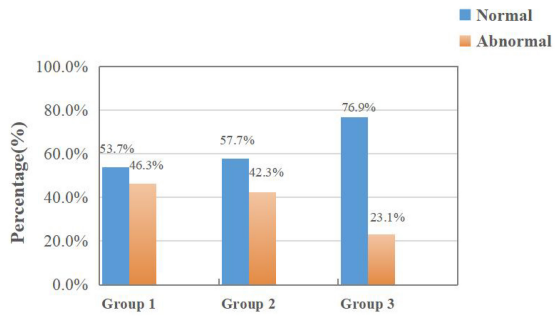

FIGURE 6
Results of binocular rivalry signal-noise ratio in Group 1 and the other two groups.

myopia (Bowrey et al., 2015; Fu et al., 2015; Wang et al., 2015). Both models demonstrate that abnormal visual input in one eye could cause the eye axis to lengthen, resulting in a difference in the refractive state of both eyes; thus, an increase in the eye axis is an important reason for myopia progression (Terasaki et al., 2017). First, uncorrected monocular myopia is comparable to form deprivation, causing the eye axis to elongate and accelerate the progression of myopia. Accordingly, some children with monocular myopia may develop greater anisometropia in adulthood. Second, the structural difference influences the refractive state and the efficiency of image processing by the visual pathway, suppressing low-quality images and prioritizing high-quality images (Westendorf et al., 1982; Zheleznyak et al., 1982; Larsson and Holmstrom, 2006; Hashemi et al., 2011). Binocular balance might have a role in this mechanism. Li et al. (2013) and Hess and Thompson (2015) proposed the concept of the binocular balance point and developed a method for detecting the binocular balance point. According to the study's results, the rate of binocular imbalance in Group 1 was significantly higher than in Group 3. The most important function of vision is to collect external information to guide sports behavior, which necessitates normal visual perception and fine motor control. Binocular visual information depends on the brain's sensitivity to the spatial and temporal frequencies of binocular retinal images. Therefore, binocular balance can only be achieved when binocular retinal images' spatial and temporal frequencies are identical (Levi et al., 1979; Vassilev et al., 2002; Vera-Diaz et al., 2018). Binocular vision input by binocular vision imbalance due to strabismus, anisometropia or amblyopia in the early stage (when normal contralateral eyes are used for viewing) could result in eye movement disorders such as unstable gaze and abnormal saccades (Birch et al., 2019). Zhou et al. (2016) also found that the two eyes of patients with anisometropia were significantly imbalanced. The early binocular imbalance may impede the development of the motor area (MT or V5) of the brain, thereby impairing the contralateral eye's motor processing ability (Zeki, 2015). If the gaze time is prolonged or abnormal saccade may directly affect the visual function, symptoms such as visual dysfunction and fatigue will be produced when performing long-term visual tasks. This influence could be a potential factor for the contralateral eye to become myopic, causing some adolescents with monocular myopia to develop nearsightedness over time. In the progression of myopia, whether it is lens-induced, form deprivation or abnormal accommodation, the clarity of monocular signal input is limited (Kee and Deng, 2008; Siegwart and Norton, 2010). Refractive adaption might be a treatment for binocular imbalance (Zhou et al., 2016), timely correction of monocular myopia can produce consistent images, balance the information processing efficiency in both eyes, and reduce the impact on the normal contralateral eye during visual development.

Stereopsis is an advanced function of binocular vision that refers to the capacity of the visual organs to perceive three-dimensional (3D) space. The index to evaluate stereopsis is the minimum parallax that can be distinguished by both eyes. Stereopsis will be impaired if monocular vision, binocular monocular vision, or binocular fusion are abnormal (Read and Cumming, 2017; Na and Yoo, 2018). Random dots map is a widely used stereopsis detection method in clinical practice. This study showed no significant difference in the random dots' stereopsis between Group 1 and Group 3, but Group 2 was worse than Group 1. Stereopsis is based on binocular stimulation and fusion and requires the visual perception of the brain's neural network (Wilson, 2017). With age, more and more neural network connections are formed between the eyes and the brain (Oberer et al., 2018). This structure's maturity facilitates the maturation of visual functions such as vision and depth perception. During visual development in monocular myopic patients who do not wear corrective lenses, cones and rods of the myopic eye might receive less visual stimulation, and the transmission of nerve impulses from the optic nerve to the visual cortex is also diminished. Under this dual mechanism of binocular competition and inhibition of activation of the cerebral cortex, the fusion function of both eyes deteriorates, thereby diminishing the stereoscopic function in adults (Campos and Enoch, 1980).

Random dots stereopsis is only a sketchy examination in clinic practice. In addition, we used virtual reality platform to detect the dynamic stereopsis of patients more comprehensively. Dynamic stereopsis refers to the difference in the direction, speed and size of binocular retinal images caused by external moving objects, which stimulates the perception of relatively selective neurons in the central direction (Hosokawa et al., 2013; Jain and Zaidi, 2013). The stimulus used in this study was a random and deformable 3D shape composed of binocular parallax. This design allowed us to detect and quantify the parallax in the movement process, equivalent to a simplified version of the real-world object and more consistent with daily life scenarios. Our results showed that all three

groups were impaired in dynamic stereopsis, and the normal rate of dynamic stereopsis of Group 1 was lower than Group 3. Thus, it can be suggested that myopic children may result in abnormal visual function in the early stage; however, there are no widely utilized clinical detection tools. More advanced and sensitive methods are required. The dynamic stereopsis of children with monocular myopia is worse than that of binocular low myopia. We think that asymmetric signal input has a greater influence on stereopsis. To some extent, the imaging quality of the myopic retina is blurred in symmetry, and there are still the same amount of visual nerve impulses in the visual cortex in the state of refractive correction, so it has a slight impact on stereopsis. However, the asymmetric signal input in monocular myopic patients has a greater impact on stereopsis. Stereopsis affects our observation of definition, distance, and contrast (Vedamurthy et al., 2016). Once the monocular myopia detection, corrective glasses should be used to correct it in its early stages and maintain the same level of visual signal stimulation.

This study was limited by the fact that in the adult control group, only patients with monocular myopia were chosen. In fact, many children who have recently developed monocular myopia will eventually develop myopia in both eyes. Therefore, future research must include additional samples to demonstrate that uncorrected monocular myopia may contribute to the development of binocular myopia.

In conclusion, monocular myopia could lead to abnormal accommodative function and unbalanced input of binocular visual signals, accelerating myopia. In addition, monocular myopia may cause stereopsis dysfunction, and long-term uncorrected monocular myopia may impair stereopsis acuity in adulthood. Furthermore, patients with monocular myopia may have abnormal stereopsis at an early stage. The commonly used random dots stereopsis test could not reflect the stereopsis in real time. Hence, it is recommended to adopt dynamic stereopsis detection. Generally speaking, children with monocular myopia must wear glasses for timely correction and to rebuild binocular balance and binocular vision function, and delay the development of myopia.

Data availability statement

The raw data supporting the conclusions of this article will be made available by the authors, without undue reservation.

Ethics statement

The studies involving human participants were reviewed and approved by the Ethics Committee of the Xiangya Hospital of Central South University. Written informed consent to participate in this study was provided by the participants' legal guardian/next of kin.

Author contributions

DW and AX conceived and designed the study. AX, KD, and QF performed the experiments. AX wrote the main manuscript text. YZ and LZ prepared the figures and tables. DW revised the manuscript. LY provided technical support. All authors read and approved the manuscript.

Funding

This work was supported by grants from the Science and Technology Bureau of Changsha (2021JJ70147).

Conflict of interest

The authors declare that the research was conducted in the absence of any commercial or financial relationships that could be construed as a potential conflict of interest.

Publisher's note

All claims expressed in this article are solely those of the authors and do not necessarily represent those of their affiliated organizations, or those of the publisher, the editors and the reviewers. Any product that may be evaluated in this article, or claim that may be made by its manufacturer, is not guaranteed or endorsed by the publisher.

References

Afsari, S., Rose, K., Gole, G., Philip, K., Leone, J., French, A., et al. (2013). Prevalence of anisometropia and its association with refractive error and amblyopia in preschool children. *Br. J. Ophthalmol.* 97, 1095–1099. doi: 10.1136/bjophthalmol-2012-302637

Augusteyn, R. C., Mohamed, A., Nankivil, D., Veerendranath, P., Arrieta, E., Taneja, M., et al. (2011). Age-dependence of the optomechanical responses of ex vivo human lenses from India and the USA, and the force required to produce these in a lens stretcher: the similarity to in vivo disaccommodation. *Vis. Res.* 51, 1667–1678. doi: 10.1016/j.visres.2011.05.009

Birch, E., Kelly, K., and Giaschi, D. (2019). Fellow eye deficits in amblyopia. *J. Binocul. Vis. Ocul. Motil.* 69, 116–125.

Bowrey, H. E., Metse, A. P., Leotta, A. J., Zeng, G., and McFadden, S. A. (2015). The relationship between image degradation and myopia in the mammalian eye. *Clin. Exp. Optom.* 98, 555–563.

Campos, E. C., and Enoch, J. M. (1980). Amount of aniseikonia compatible with fine binocular vision: some old and new concepts. *J. Pediatr. Ophthalmol. Strabismus* 17, 44–47. doi: 10.3928/0191-3913-19800101-11

Deng, L., and Gwiazda, J. (2012). Anisometropia in children from infancy to 15 years. *Invest Ophthalmol. Vis. Sci.* 53, 3782–3787.

Fu, X. Y., Zhang, X., Xia, W., Zhong, L., Wang, Y., Sun, Z., et al. (2015). Effects of 530 nm monochromatic light on basic fibroblast growth factor and transforming growth factor-beta1 expression in Muller cells. *Int. J. Ophthalmol.* 8, 904–909. doi: 10.3980/j.issn.2222-3959.2015.05.09

Hashemi, H., Khabazkhoob, M., Yekta, A., Mohammad, K., and Fotouhi, A. (2011). Prevalence and risk factors for anisometropia in the Tehran eye study, Iran. *Ophthalmic Epidemiol.* 18, 122–128.

Hess, R., and Thompson, B. (2015). Amblyopia and the binocular approach to its therapy. *Vis. Res.* 114, 4–16.

Hosokawa, K., Maruya, K., and Sato, T. (2013). Temporal characteristics of depth perception from motion parallax. *J. Vis.* 13:16. doi: 10.1167/13.1.16

Hu, Y., Wu, J., Lu, T., Wu, H., Sun, W., Guo, D., et al. (2016). Prevalence and associations of anisometropia in children. *Invest. Ophthalmol. Vis. Sci.* 57, 979–988.

Huang, C., Zhou, J., Lu, Z., and Zhou, Y. (2011). Deficient binocular combination reveals mechanisms of anisometropic amblyopia: signal attenuation and interocular inhibition. *J. Vis.* 11:10.1167/11.6.4 4. doi: 10.1167/11.6.4

Jain, A., and Zaidi, Q. (2013). Efficiency of extracting stereo-driven object motions. *J. Vis.* 13:18. doi: 10.1167/13.1.18

Kee, C. S., and Deng, L. (2008). Astigmatism associated with experimentally induced myopia or hyperopia in chickens. *Invest. Ophthalmol. Vis. Sci.* 49, 858–867.

Koomson, N., Amedo, A., Opoku-Baah, C., Ampeh, P., Ankamah, E., and Bonsu, K. (2016). Relationship between reduced accommodative lag and myopia progression. *Optometry Vis. Sci.* 93, 683–691.

Larsson, E. K., and Holmstrom, G. E. (2006). Development of astigmatism and anisometropia in preterm children during the first 10 years of life: a population-based study. *Arch. Ophthalmol.* 124, 1608–1614. doi: 10.1001/archopht.124.11.1608

Levi, D. M., Harwerth, R. S., and Manny, R. E. (1979). Suprathreshold spatial frequency detection and binocular interaction in strabismic and anisometropic amblyopia. *Invest. Ophthalmol. Vis. Sci.* 18, 714–725.

Li, J., Hess, R., Chan, L., Deng, D., Chen, X., Yu, M., et al. (2013). How best to assess suppression in patients with high anisometropia. *Optom. Vis. Sci.* 90, e47–e52. doi: 10.1097/OPX.0b013e31827d072c

Li, M., Cheng, H., Yuan, Y., Wang, J., Chen, Q., Me, R., et al. (2016). Change in choroidal thickness and the relationship with accommodation following myopic excimer laser surgery. *Eye (Lond)* 30, 972–978. doi: 10.1038/eye.2016.75

Mitchell, D. E., and Sengpiel, F. (2009). Neural mechanisms of recovery following early visual deprivation. *Philos. Trans. R. Soc. Lond. B Biol. Sci.* 364, 383–398.

Myrowitz, E. H. (2012). Juvenile myopia progression, risk factors and interventions. *Saudi J. Ophthalmol.* 26, 293–297.

Na, M., and Yoo, A. (2018). The effect of orthokeratology on axial length elongation in children with myopia: contralateral comparison study. *Jpn J. Ophthalmol.* 62, 327–334. doi: 10.1007/s10384-018-0573-x

Niechwiej-Szwedo, E., Thai, G., and Christian, L. (2020). Contribution of stereopsis, vergence, and accommodative function to the performance of a precision grasping and placement task in typically developing children age 8-14 years. *Hum. Mov. Sci.* 72:102652. doi: 10.1016/j.humov.2020.102652

Oberer, N., Gashaj, V., and Roebers, C. M. (2018). Executive functions, visual-motor coordination, physical fitness and academic achievement: longitudinal relations in typically developing children. *Hum. Mov. Sci.* 58, 69–79. doi: 10.1016/j.humov.2018.01.003

Parssinen, O. (1990). Anisometropia and changes in anisometropia in school myopia. *Optom. Vis. Sci.* 67, 256–259.

Read, J., and Cumming, B. (2017). Visual perception:neural networks for stereopsis. *Curr. Biol.* 27, R594–R596.

Read, S. A., Collins, M., Woodman, E., and Cheong, S. (2010). Axial length changes during accommodation in myopes and emmetropes. *Optom. Vis. Sci.* 87, 656–662.

Sengpiel, F. (2011). Experimental models of amblyopia: insights for prevention and treatment. *Strabismus* 19, 87–90. doi: 10.3109/09273972.2011.600419

Siegwart, J. T. Jr., and Norton, T. T. (2010). Binocular lens treatment in tree shrews: effect of age and comparison of plus lens wear with recovery from minus lens-induced myopia. *Exp. Eye Res.* 91, 660–669. doi: 10.1016/j.exer.2010.08.010

Terasaki, H., Yamashita, T., Yoshihara, N., Kii, Y., and Sakamoto, T. (2017). Association of lifestyle and body structure to ocular axial length in Japanese elementary school children. *BMC Ophthalmol.* 17:123. doi: 10.1186/s12886-017-0519-y

Tong, L., Chan, Y., Gazzard, G., Tan, D., and Saw, S. (2006). Longitudinal study of anisometropia in Singaporean school children. *Invest. Ophthalmol. Vis. Sci.* 47, 3247–3252. doi: 10.1167/iovs.05-0906

Toor, S., Horwood, A., and Riddell, P. (2019). The effect of asymmetrical accommodation on anisometropic amblyopia treatment outcomes. *J. AAPOS* 23, 203.e1–203.e5. doi: 10.1016/j.jaapos.2019.05.010

Vassilev, A., Mihaylova, M., and Bonnet, C. (2002). On the delay in processing high spatial frequency visual information: reaction time and VEP latency study of the effect of local intensity of stimulation. *Vis. Res.* 42, 851–864. doi: 10.1016/s0042-6989(01)00300-5

Vedamurthy, I., Knill, D., Huang, S., Yung, A., Ding, J., Kwon, O., et al. (2016). Recovering stereo vision by squashing virtual bugs in a virtual reality environment. *Philos. Trans. R. Soc. Lond. B Biol. Sci.* 371:20150264. doi: 10.1098/rstb.2015.0264

Vera-Diaz, F. A., Bex, P., Ferreira, A., and Kosovicheva, A. (2018). Binocular temporal visual processing in myopia. *J. Vis.* 18:17.

Wang, J. C., Chun, R., Zhou, Y., Zuo, B., Li, K., Liu, Q., et al. (2015). Both the central and peripheral retina contribute to myopia development in chicks. *Ophthalmic Physiol. Opt.* 35, 652–662.

Westendorf, D. H., Blake, R., Sloane, M., and Chambers, D. (1982). Binocular summation occurs during interocular suppression. *J. Exp. Psychol. Hum. Percept. Perform.* 8, 81–90.

Wilson, H. R. (2017). Binocular contrast, stereopsis, and rivalry: toward a dynamical synthesis. *Vis. Res.* 140, 89–95. doi: 10.1016/j.visres.2017.07.016

Zeki, S. (2015). Area V5-a microcosm of the visual brain. *Front. Integr. Neurosci.* 9:21. doi: 10.3389/fnint.2015.00021

Zheleznyak, L., Sabesan, R., Oh, J., MacRae, S., and Yoon, G. (1982). Modified monovision with spherical aberration to improve presbyopic through-focus visual performance. *Invest. Ophthalmol. Vis. Sci.*. 54, 3157–3165.

Zhou, J., Feng, L., Lin, H., and Hess, R. (2016). On the maintenance of normal ocular dominance and a possible mechanism underlying refractive adaptation. *Invest. Ophthalmol. Vis. Sci.* 57, 5181–5185. doi: 10.1167/iovs.16-19696

frontiers | Frontiers in Neuroscience

TYPE Original Research
PUBLISHED 27 March 2023
DOI 10.3389/fnins.2023.1142668

OPEN ACCESS

EDITED BY
Wensi Tao,
University of Miami Health System,
United States

REVIEWED BY
Guy Perkins,
University of California, San Diego,
United States
Tonking Bastola,
University of California, San Diego,
United States

*CORRESPONDENCE
David J. Calkins
✉ david.j.calkins@vumc.org

SPECIALTY SECTION
This article was submitted to
Visual Neuroscience,
a section of the journal
Frontiers in Neuroscience

RECEIVED 11 January 2023
ACCEPTED 10 March 2023
PUBLISHED 27 March 2023

CITATION
Boal AM, McGrady NR, Holden JM,
Risner ML and Calkins DJ (2023) Retinal
ganglion cells adapt to ionic stress in
experimental glaucoma.
Front. Neurosci. 17:1142668.
doi: 10.3389/fnins.2023.1142668

Retinal ganglion cells adapt to ionic stress in experimental glaucoma

Andrew M. Boal, Nolan R. McGrady, Joseph M. Holden, Michael L. Risner and David J. Calkins*

Department of Ophthalmology and Visual Sciences, Vanderbilt Eye Institute, Vanderbilt University Medical Center, Nashville, TN, United States

Introduction: Identification of early adaptive and maladaptive neuronal stress responses is an important step in developing targeted neuroprotective therapies for degenerative disease. In glaucoma, retinal ganglion cells (RGCs) and their axons undergo progressive degeneration resulting from stress driven by sensitivity to intraocular pressure (IOP). Despite therapies that can effectively manage IOP many patients progress to vision loss, necessitating development of neuronal-based therapies. Evidence from experimental models of glaucoma indicates that early in the disease RGCs experience altered excitability and are challenged with dysregulated potassium (K^+) homeostasis. Previously we demonstrated that certain RGC types have distinct excitability profiles and thresholds for depolarization block, which are associated with sensitivity to extracellular K^+.

Methods: Here, we used our inducible mouse model of glaucoma to investigate how RGC sensitivity to K^+ changes with exposure to elevated IOP.

Results: In controls, conditions of increased K^+ enhanced membrane depolarization, reduced action potential generation, and widened action potentials. Consistent with our previous work, 4 weeks of IOP elevation diminished RGC light-and current-evoked responses. Compared to controls, we found that IOP elevation reduced the effects of increased K^+ on depolarization block threshold, with IOP-exposed cells maintaining greater excitability. Finally, IOP elevation did not alter axon initial segment dimensions, suggesting that structural plasticity alone cannot explain decreased K^+ sensitivity.

Discussion: Thus, in response to prolonged IOP elevation RGCs undergo an adaptive process that reduces sensitivity to changes in K^+ while diminishing excitability. These experiments give insight into the RGC response to IOP stress and lay the groundwork for mechanistic investigation into targets for neuroprotective therapy.

KEYWORDS

neurodegeneration, retinal ganglion cells, glaucoma, excitability, potassium, physiology, action potential

1. Introduction

Glaucoma is the leading cause of irreversible vison loss worldwide (Tham et al., 2014). The disease involves progressive degeneration of retinal ganglion cells (RGCs) and their axons, which carry visual information from the eye to central targets in the brain. Aging is the leading risk factor, though sensitivity to intraocular pressure (IOP) is the only modifiable risk factor. In glaucoma, stress evolving from sensitivity to IOP challenges RGC axons as they pass unmyelinated through the optic nerve head of the retina. Many patients continue to lose vision despite efforts to manage IOP with topical and surgical hypotensive therapies (Heijl et al., 2002),

underscoring the need to identify new therapeutics based on mechanistic understanding of how RGCs and their axons respond to glaucomatous stress.

Development of neuronal-based therapies for the treatment of glaucoma requires identification of targets involved in pathophysiology, target-specific therapeutics, and biomarkers to assay outcomes (Calkins, 2021). Early progression in experimental glaucoma involves enhanced RGC excitability with a concurrent reduction in axon function (Risner et al., 2018). Prolonged stress ultimately overcomes the adaptive mechanisms and leads to RGC degeneration (Sappington et al., 2010; Naguib et al., 2021; Risner et al., 2021, 2022). The RGC population is heterogeneous (Sanes and Masland, 2015; Baden et al., 2016; Bae et al., 2018; Tran et al., 2019), with RGC-intrinsic factors shaping their individual response properties (Emanuel et al., 2017; Werginz et al., 2020; Wienbar and Schwartz, 2022). Importantly, such intrinsic differences may predispose certain RGC types to be particularly sensitive to IOP-related stress (Della Santina et al., 2013; El-Danaf and Huberman, 2015; Ou et al., 2016; Risner et al., 2021). Previously, we established that different RGC subtypes exhibit varied sensitivities to elevated extracellular potassium (Boal et al., 2022). Dysregulation of potassium ion (K^+) homeostasis and channel expression contribute to altered excitability in neurodegenerative diseases, including glaucoma, and represent potential targets for early diagnosis and treatment (Hall et al., 2015; Frazzini et al., 2016; Cacace et al., 2019; Fischer et al., 2019a,b; Kim et al., 2021).

Here, we utilized our inducible mouse model of glaucoma (Sappington et al., 2010; Calkins et al., 2018) to investigate how prolonged exposure to elevated IOP changes RGC sensitivity to acutely elevated extracellular K^+. Following 4 weeks of IOP elevation, alpha ON-sustained (αON-S) and alpha OFF-sustained (αOFF-S) RGCs had reduced responses to light and depolarizing current stimulation, consistent with previous results (Risner et al., 2021, 2022). In controls with normal IOP, challenging RGCs with high extracellular K^+ led to membrane depolarization, blunted spike rate, and action potential (AP) widening in both αON-S and αOFF-S cells. IOP elevation reduced the effects of elevated K^+ in both RGC types. Compared to controls, RGCs exposed to elevated IOP were less depolarized and maintained greater current-evoked spiking during acute K^+ elevation. Furthermore, K^+-dependent AP widening was decreased, though the impact of IOP on AP widths differed for αON-S and αOFF-S cells. Immunolabeling of the axon initial segment (AIS), the site of AP initiation in neurons, revealed that IOP elevation did not structurally alter AIS scaffolding for either RGC type.

These results suggest that, after 4 weeks of IOP elevation, RGCs undergo an adaptive process that reduces sensitivity to acutely elevated K^+ while diminishing their excitability. Differences between αON-S and αOFF-S in how AP widths vary with IOP exposure and K^+ conditions support evidence for cell-type specific responses to stress. This adaptation involves altered AP generation, indicating an axogenic process, but it is not solely reflective of axonal structural plasticity.

2. Materials and methods

2.1. Animals

We obtained 15 C57Bl6/J mice (8 males, 7 females, 12–20 weeks old) from Jackson Laboratories (Bar Harbor, ME). These numbers were determined, based upon our previous experience with this model and recording strategy (Risner et al., 2018, 2021; Boal et al., 2022), to provide a sufficient number of each cell type for statistical comparisons. Mice were housed at the Vanderbilt University Division of Animal Care and maintained on 12-h light/dark cycle. Animals were allowed water and standard rodent chow *ad libitum*. All animal experiments were reviewed and approved by the Vanderbilt University Medical Center Institutional Animal Care and Use Committee.

2.2. Intraocular pressure elevation and measurement

Mice were anesthetized with isoflurane (2.5%) and administered tropicamide (1%), proparacaine (0.5%), and lubricating drops in both eyes. For the 4 week intraocular pressure (IOP) elevation group (4wk IOP) we bilaterally injected 1.5 µL of 15 µm polystyrene microbeads (Invitrogen, Carlsbad, CA) into the anterior chamber of the eye (Sappington et al., 2010) using borosilicate glass pipette attached to a micromanipulator (M3301R, WPI, Sarasota, FL), driven by a microsyringe pump (DMP, WPI, Sarasota, FL). For the 4wk saline control group (4wk Ctrl) we bilaterally injected an equal volume of sterile phosphate-buffered saline (PBS) into the anterior chamber using the same system. Mice were injected in cohorts of five at a time. For 4wk Ctrl, a second cohort of five was done because an insufficient number of cells of interest were recorded from the first. Animals of both sexes were evenly split between experimental groups ($p = 0.5581$, Chi-squared test).

For IOP measurements, mice were lightly anesthetized with isoflurane (2%) and pressures were measured using rebound tonometry (iCare Tonolab; Vantaa, Finland). IOP for each eye was determined as the mean of 15 consecutive measurements. For the 2 days preceding anterior chamber injections we measured IOP for each group and averaged these values to determine baseline IOP. Beginning 2 days post-injection, IOP was measured three times per week for the duration of the 4 week experimental period.

2.3. Electrophysiology

Approximately 4 weeks (±2 days) following anterior chamber injection mice were euthanized *via* cervical dislocation and decapitation, eyes were enucleated, and the retinas were dissected out under long-wavelength illumination (630 nm, 800 µW/cm^2, FND/FG, Ushio, Cypress, CA). Retinas were placed in carbogen-saturated Ames' medium (US Biologic, Memphis, TN) supplemented with 20 mM D-glucose and 22.6 mM $NaHCO_3$ (pH 7.4, 290 Osm). Each retina was mounted flat onto a physiological chamber, inner retina facing upwards, and perfused at a rate of 2 mL/min with Ames' medium maintained at 35°C (Model TC-344C, Warner Instruments, Hamden, CT).

Retinal ganglion cells (RGCs) were viewed under differential interference contrast (DIC) using an Andor CCD camera attached to an Olympus BX50 upright microscope at 40x magnification. RGCs with large somas were targeted for intracellular recording with pipettes pulled from borosilicate glass (I.D. 0.86 mm, O.D. 1.5 mm; Sutter Instruments, Novato, CA) and filled with (in mM): 125 K-gluconate, 10 KCl, 10 HEPES, 10 EGTA, 4 Mg-ATP, 1 Na-GTP, and 0.1 ALEXA 555 dye (Invitrogen, Carlsbad, CA). The intracellular solution pH was

7.35 and osmolarity was 285 Osm. Recording pipettes filled with intracellular solution had a resistance between 4 and 8 MΩ. Whole-cell current-clamp signals were amplified (Multiclamp 700B, Molecular Devices, San Jose, CA) and digitized at 10 kHz (Digidata 1550A, Molecular Devices, San Jose, CA). Access resistance was monitored periodically during recordings and maintained ≤ 30 MΩ.

We measured resting membrane potential (RMP), spontaneous spiking, light-evoked spike activity (full-field 365 + 460 nm, 3.4 mW/cm^2, 3-s duration, CoolLED, pE-4,000, Andover, United Kingdom), and current-evoked spiking while clamping the cell at 0 pA. Current-evoked spiking was measured during stepwise application of 1 s depolarizing current pulses, ranging from 0 to +300 pA in 10 pA increments, with a 2 s inter-stimulus interval. Current was clamped at 0 pA between pulses.

2.4. High extracellular potassium recordings

A second batch of Ames' medium was prepared as described above, but with an additional 5 mM of KCl (i.e., high K^+), bringing the total K^+ concentration to 8 mM. Following completion of baseline recordings, high K^+ medium was washed into the recording chamber while RGC membrane voltage was continuously recorded. Prior to high K^+ experimental recordings, we allowed a wash on period of 5–6 min, allowing RGC membrane potential to stabilize. Recordings (RMP, spontaneous activity, light-evoked spiking, current-evoked spiking) were then performed as described above. After high K^+ experiments the extracellular medium was switched back to the baseline solution and RGC membrane voltage was continuously measured during a wash off period of 10–20 min, allowing RGCs to recover baseline RMP and spontaneous activity. Full recovery typically took 10–15 min, although it occasionally required up to 20 min. We limited the number of experimental protocols to reduce the time of high K^+ exposure. Furthermore, to limit potential cumulative effects of K^+ wash on/off, we limited the total number of cells that were recorded under high K^+ to no more than 3 from each retina.

2.5. RGC physiology analysis

Raw data files from electrophysiologic recordings were analyzed in Python 3.9 using the pyABF 2.3.5 (Harden, 2022) and SciPy 1.7.1 modules (Virtanen et al., 2020). Action potentials (APs) were detected from membrane voltage data using the SciPy "find_peaks" function with parameters of 20 mV minimum prominence and a distance threshold of 1.5 ms. Spike rates for current-evoked spiking protocols were reported as the average rate for 2 adjacent 10 pA increments of stimulation (20 pA bins). For AP width measurements, a cubic spline function was fit to each AP waveform and half-width was measured as the duration, in ms, where the membrane potential was above the midway point between AP peak and minimum after-hyperpolarization.

2.6. Immunohistochemistry and imaging

Immediately following recordings, retinas were fixed in 4% paraformaldehyde and incubated at 4°C for 24 h. After fixation, retinas were immunolabeled for choline acetyltransferase (ChAT, 1:100; Millipore, Burlington, MA, Cat. #AB144P) and ankyrin-G (AnkG, 1:200; NeuroMab N106/36; Antibodies, Inc. Cat. # 75-146). Tissue was blocked in 5% normal donkey serum for 2 h, then incubated in primary antibodies for 3 d at 4°C, and finally incubated for 2 h at room temperature with donkey anti-goat Alexa 405 and donkey anti-mouse Alexa 488 secondary antibodies (Jackson ImmunoResearch, West Grove, PA). Z-stack images of dye-filled RGCs were obtained using an Olympus FV1000 inverted microscope at 40x magnification. Image analysis, including creating orthogonal projections used for visualization of dendritic stratification depth, was performed using ImageJ (NIH, Bethesda, MD).

2.7. Axon initial segment analysis

We evaluated 11 4wk IOP cells (5 αON-S and 6 αOFF-S) and 18 4wk Ctrl cells (9 αON-S and 9 αOFF-S) with identifiable axon initial segments (AISs) as defined by a segment of ankyrin-G (AnkG) labeling that colocalized to a filled RGC axon. AnkG fluorescence was measured in ImageJ starting from the edge of the soma along the axon in a max-intensity Z projection limited to the extent of the axonal process. Background fluorescence was subtracted from AnkG intensity profiles using a rolling ball filter with a radius equal to approximately 15% of the data length. Smoothed AnkG profiles were generated using a Savitzky–Golay filter with a first order polynomial fit. Axon initial segment (AIS) bounds were algorithmically defined as the extent where smoothed AnkG values were greater than 50% of the difference between baseline and maximum intensity.

2.8. Data analysis and statistical tests

All data are reported as mean ± standard error of the mean (SEM) unless otherwise indicated. All statistical tests were performed in GraphPad Prism 9 (Graphpad Software, San Diego, CA). All data sets were checked for normality. Where appropriate, parametric statistical tests (unpaired *t*-test, paired *t*-test, 2-way ANOVA, simple linear regression) were performed. When data were not normally distributed, appropriate nonparametric tests (e.g., Mann–Whitney test) were performed. For ANOVA tests, *p*-values were corrected for multiple comparisons. Where noted, determination of the influence of sex on high K^+-induced change in RMP was determined by multiple linear regression modeling (ΔRMP ~ Intercept + Cell Type + Experimental Group + Sex). We defined statistical significance as a *p*-value of 0.05 or less. Exact *p*-values and the specific statistical test used for each analysis are listed in the figure legends or results text.

3. Results

3.1. Elevated IOP alters RGC electrophysiology

We performed bilateral injections of either polystyrene microbeads to occlude the anterior chamber ($n = 5$ animals, 10 eyes) or sterile phosphate-buffered saline ($n = 10$ animals, 20 eyes) and measured intraocular pressure (IOP) for 4 weeks (Figure 1). Following

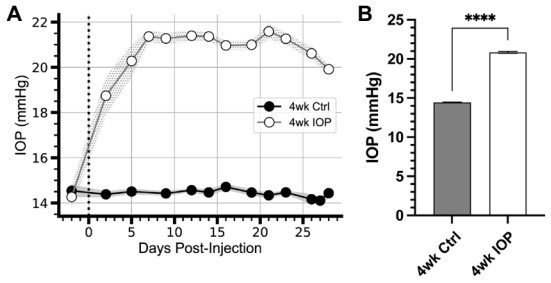

FIGURE 1
IOP elevation due to microbead occlusion of the anterior chamber. **(A)** Intraocular pressure (IOP) of microbead-injected eyes (4wk IOP) increases rapidly following injection (vertical dotted line) and remain elevated for the duration of the 4 weeks. The IOP of saline-injected eyes (4wk Ctrl) remains unchanged from baseline. Shaded region: ± standard error of the mean. **(B)** Mean IOP for each eye across all days following microbead injection significantly elevates compared to Ctrl (p=0.000046, unpaired t-test). Error bars: ± standard error of the mean. ****p<0.0001.

injections, IOP in saline-injected eyes remained unchanged from baseline (Figure 1A). Following microbead occlusion, IOP increased 46% above their baseline (Figure 1A), exceeding IOP in saline control eyes by 44% (Figure 1B, $p < 0.0001$). IOP elevation in microbead eyes was sustained for the duration of the experiment (Figure 1A).

After 4 weeks mice were sacrificed and retinas prepared for electrophysiologic recordings. As previously described (Risner et al., 2018, 2020a, 2021, 2022; Boal et al., 2022), we targeted αRGCs for recording by identifying large cell bodies and confirmed cell types by characterizing soma size, dendritic stratification within the inner plexiform layer (Famiglietti and Kolb, 1976; Galli-Resta et al., 2000), and light-evoked responses (Figure 2). We focused analysis on two well-characterized and readily identifiable αRGC types: αON-Sustained (αON-S) and αOFF-Sustained (αOFF-S; Krieger et al., 2017). In the saline (4wk Ctrl) group we recorded 10 αON-S RGCs (7 eyes, 4 mice; 8 cells from males, 2 from females) and 10 αOFF-S RGCs (8 eyes, 7 mice; 5 male, 5 female). In the microbead group (4wk IOP) we recorded 10 αON-S RGCs (9 eyes, 5 mice; 4 male, 6 female) and 7 αOFF-S RGCs (7 eyes, 5 mice; 3 male, 4 female). Cells from mice of both sexes were evenly represented among αON-S and αOFF-S for 4wk Ctrl (p=0.1596, Chi-squared test) and 4wk IOP (p=0.9062, chi-squared test).

Four weeks of IOP elevation altered the resting membrane and light-evoked spiking characteristics of both RGC types. RGCs from the 4wk IOP group had a depolarized resting membrane potential (RMP) relative to controls (Figure 2C, p=0.0572; αON-S + 2.25 mV, αOFF-S + 2.41 mV). Spontaneous spiking in the absence of light also appeared altered (Figure 2D), with αON-S cells trending toward greater spiking (p=0.0507) and αOFF-S cells trending toward less spiking (p=0.1613). The membrane voltage response to light stimulation for αON-S was significantly blunted after IOP elevation (Figures 2E,F), with cells from the 4wk IOP group exhibiting diminished mean (p=0.0202) and peak (p=0.0251) spike rates in response to light onset. Light-evoked spiking also appeared altered in αOFF-S cells (Figures 2G,H), although not quite as overtly as αON-S cells. Mean and peak spike rates were not significantly different between experimental groups (Figure 2H), though the histogram of mean spike rates (Figure 2G) appeared qualitatively altered by 4wk IOP, with spiking at light offset tending to be less sustained.

3.2. 4wk IOP RGCs are less sensitive to elevated extracellular potassium

Since potassium homeostasis may be altered in glaucoma (Fischer et al., 2019a,b), we next sought to investigate how 4 weeks of IOP elevation alters the sensitivity of RGCs to acutely elevated extracellular potassium. As previously described (Boal et al., 2022), we performed a within-subjects experimental design with recordings before and after application of extracellular medium containing additional KCl (extra 5 mM, high K^+, Figure 3A). For both αON-S and αOFF-S high K^+ depolarized the RMP, regardless of experimental group (Figure 3B, $p < 0.0001$ for both cell types). However, there was a statistically significant interaction between IOP group and potassium effect on RMP for both cell types (p=0.0002, αON-S; p=0.0063, αOFF-S). Comparison of the high K^+-evoked depolarization of RMP (ΔRMP) between experimental groups demonstrated that 4wk IOP RGCs were significantly less depolarized by the acutely elevated potassium (Figure 3C, $p < 0.0001$). The sex of the mouse from which an RGC came was not significantly associated with ΔRMP (p=0.1572, multiple linear regression model).

αON-S and αOFF-S RGCs have distinct responses to depolarizing current (Twyford et al., 2014; Kameneva et al., 2016), which are in part related to their different sensitivities to extracellular potassium (Boal et al., 2022). We measured the spiking response of αRGCs to 1 s depolarizing current injections ranging from 0 to +300 pA, before and after washing on high K^+ medium (Figure 4), to determine how 4wk IOP exposure alters these properties. In saline controls, high K^+ appreciably altered the current-spiking relationship of both αON-S and αOFF-S cells. In baseline extracellular media control αON-S RGCs (Figures 4A,C) exhibited little spiking at low depolarizations but spike rates increased as the strength of depolarization increased. After high K^+ wash on, spike rates were higher at small depolarizations but began to plateau and then slow as the strength of depolarization was increased. Control αOFF-S RGCs (Figures 4E,G) exhibited a different pattern of current-evoked spiking than αON-S, but were also appreciably impacted by high K^+. In baseline media control αOFF-S cells had relatively high spike rates that initially increased with increasing stimulation, but reached a peak and began to subsequently decrease beyond about 100 pA of depolarization. High K^+ considerably decreased spike rates, which quickly fell to 0 Hz with increasing magnitudes of depolarization. In 4wk IOP αRGCs, high K^+ appeared to have a lesser effect on current-evoked spiking than in controls. For αON-S cells (Figures 4B,D), 4wk IOP excitability was diminished at baseline relative to controls, exhibiting less of an increase in spike rate with increasing stimulation ($p < 0.001$, simple linear regression). High K^+ again blunted spike rates (p=0.0002), though not to the same degree as in controls. 4wk IOP exposure likewise diminished αOFF-S excitability at baseline (Figures 4F,H), with peak firing rates trending lower (p=0.0639, unaired t test), and lessened the impact of high K^+ on spiking, with cells appearing to maintain the ability to fire at greater magnitudes of depolarization than in controls. Across both cell types, the absolute difference in firing rates between high K^+ and baseline conditions was less in the 4wk IOP group than in the 4wk control group (p=0.0317).

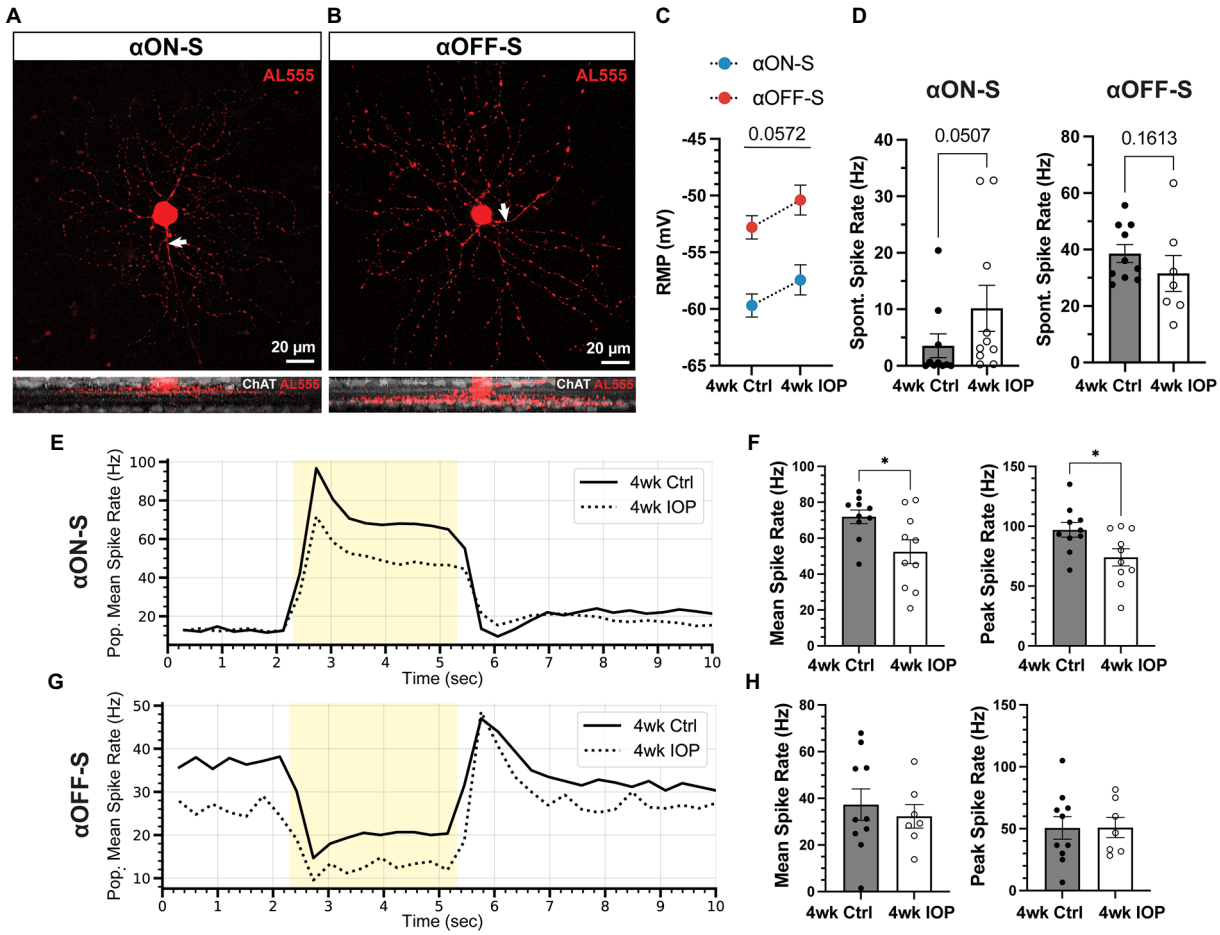

FIGURE 2
Elevated IOP alters membrane and light-evoked spiking characteristics in αON-S and αOFF-S RGCs. **(A,B)** Morphologic and physiologic characterization of retinal ganglion cells (RGCs). Patched cells were filled with Alexa-fluor 555 dye (AL555, red) and morphologically reconstructed with confocal microscopy. Representative maximum intensity projections of alpha ON-sustained (αON-S, **A**) and alpha OFF-sustained (αOFF-S, **B**) RGCs demonstrate characteristic soma size and dendritic branching patterns (upper). White arrows indicate the axonal projection. Orthogonal projections of representative AL555-filled cells co-labeled for choline acetyltransferase (ChAT, white) demonstrate the branching of αON-S and αOFF-S dendrites in the ON- and OFF-sublaminas of the inner plexiform layer, respectively (lower). **(C)** Resting membrane potentials (RMP) for both cell types from 4wk Ctrl and IOP groups. RGC RMPs in the 4wk IOP group are more depolarized than controls (p=0.0572, 2-way ANOVA). **(D)** Spontaneous spiking rates for αON-S and αOFF-S RGCs. αON-S cells in the 4wk IOP group trend toward greater spontaneous spiking (p=0.0507, Mann–Whitney test), whereas 4wk IOP αOFF-S cells trend toward less spontaneous spiking (p=0.1613, Mann–Whitney test). **(E)** Mean firing rates of αON-S cells in the 4wk Ctrl and 4wk IOP groups binned into 200ms intervals during light stimulation (yellow). **(F)** Mean (left) and peak (right) light-evoked spike rates for αON-S cells. 4wk IOP decreases both measures (mean: p=0.0202, unpaired t-test; peak: p=0.0251, unpaired t-test). **(G)** Mean firing rates of αOFF-S cells in the 4wk Ctrl and 4wk IOP groups binned into 200ms intervals during light stimulation (yellow). **(H)** Mean (left) and peak (right) light-evoked spike rates for αOFF-S cells. Error bars: ± standard error of the mean. *p<0.05.

We previously found differences in excitability between αON-S and αOFF-S were reflected in the shape of their action potentials (APs), and that high K^+ promoted rate-dependent AP widening (Boal et al., 2022). We measured AP half-widths in both experimental groups to determine if decreased potassium sensitivity in 4wk IOP RGCs was reflected at the level of AP generation (Figure 5). Control αON-S cells (Figures 5A,C) exhibited minimal AP widening with increased stimulation at baseline. High K^+ media widened αON-S APs and increased rate-dependent widening. Control αOFF-S cells (Figures 5E,G) had a moderate degree of rate-dependent AP widening at baseline, and high K^+ caused further widening. After 4wk IOP elevation, αON-S APs (Figures 5B,D) had slightly wider APs at baseline than controls (p=0.0133, unpaired t test). However, 4wk IOP αON-S APs appeared less widened in high K^+ medium relative to baseline. 4wk IOP αOFF-S cells (Figures 5F,H) did not have appreciably different AP shapes at baseline compared to controls (p=0.6867). Further, they too had less K^+ induced AP widening than control αOFF-S cells. In total, the mean change in AP half-width after high K^+ application for all cells was significantly less for 4wk IOP RGCs than for controls (p=0.0061).

Finally, we explored a potential mechanism for the observed differences in RGC excitability and potassium sensitivity. Scaling of the axon initial segment (AIS) is implicated in mediating intrinsic excitability of RGCs (Raghuram et al., 2019; Werginz et al., 2020; Wienbar and Schwartz, 2022). The AIS, marked by labeling for scaffolding protein ankyrin-G (AnkG), is a complex that clusters voltage-gated ion channels in the proximal portion of the axon and serves as the site of AP generation (Zhou et al., 1998; Gasser et al.,

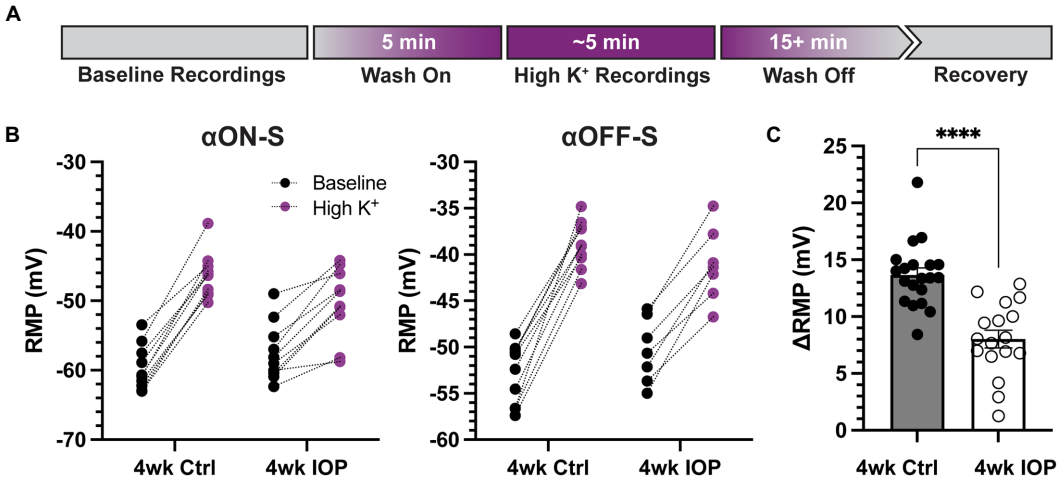

FIGURE 3
Elevated IOP reduces the influence of extracellular potassium on RGC depolarization. **(A)** Timeline illustrating the design of acutely elevated extracellular potassium (High K^+) experiments. Following baseline recordings, extracellular medium with an extra 5mM KCl is washed on for 5min until membrane potentials stabilized. High K^+ recordings are done, and then high K^+ is washed off with regular extracellular medium until full recovery of membrane potential and spontaneous spiking, at least 15min. **(B)** Resting membrane potentials (RMPs) for αON-S and αOFF-S cells in both experimental groups before and after high K^+ wash on. There is a significant interaction effect between K^+ and IOP for both αON-S (p=0.0002; 2-way repeated measures ANOVA) and αOFF-S (0.0063) cells. **(C)** The change in RMP following high K^+ wash on for each cell, separated by experimental group. Cells exposed to 4wk IOP elevation are significantly less depolarized by high K^+ (p=0.00000091, Mann–Whitney test). Error bars: ± standard error of the mean. ****p<0.0001.

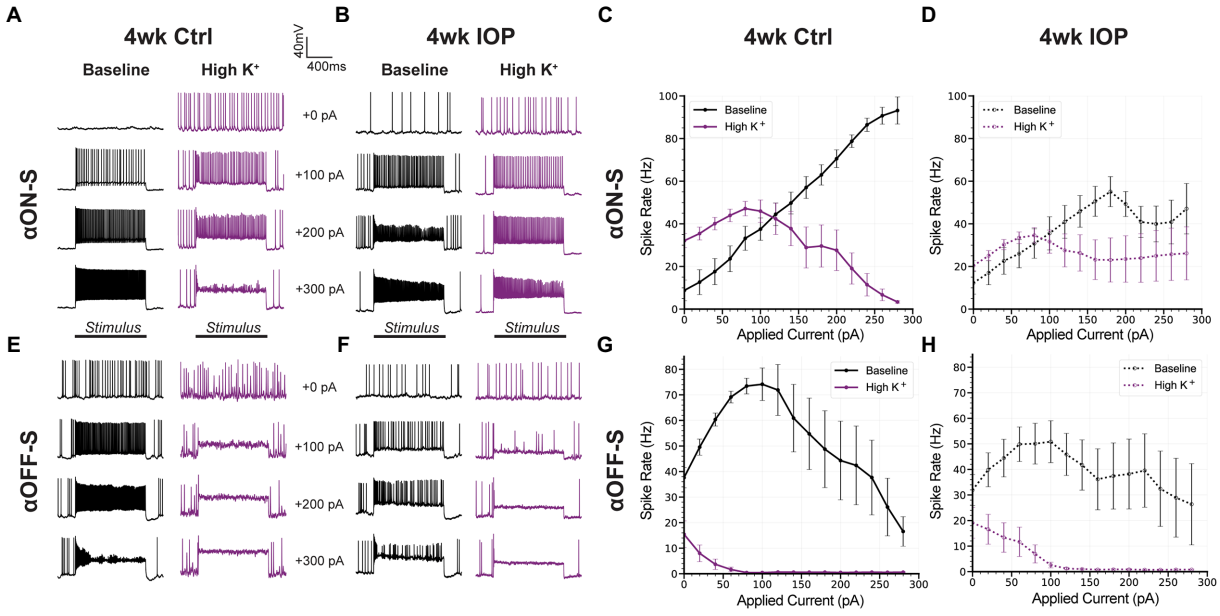

FIGURE 4
Current-evoked spiking is less depressed by high K^+ after IOP elevation. **(A,B)** Representative current-clamp responses of αON-S cells from both experimental groups to 0, 100, 200, and 300 pA pulses, before and after washing on high K^+. **(C,D)** The spiking responses of αON-S cells to depolarizing current pulses ranging from 0 to 300 pA, before and after high K^+. **(E,F)** Representative current-clamp responses of αOFF-S cells from both experimental groups before and after washing on high K^+. **(G,H)** The spiking responses of αON-S cells to depolarizing current pulses, before and after high K^+. The difference in spike rates between baseline and high K^+ groups for all cells is lower in the 4wk IOP group than in the 4wk Ctrl (p=0.0317, unpaired t-test). Error bars: ± standard error of the mean.

2012; Huang and Rasband, 2018; Leterrier, 2018). The dimensions of the AIS are plastic and can change in response to stimuli, such as chronically elevated extracellular potassium (Grubb and Burrone, 2010) and sustained sensory input (Jamann et al., 2021), in order to modulate neuronal excitability. Because changes to the AIS have been implicated in neurodegenerative disease (Sun et al., 2014; Marin et al., 2016; Hatch et al., 2017), we investigated whether altered AIS dimensions were associated with the decreased RGC potassium

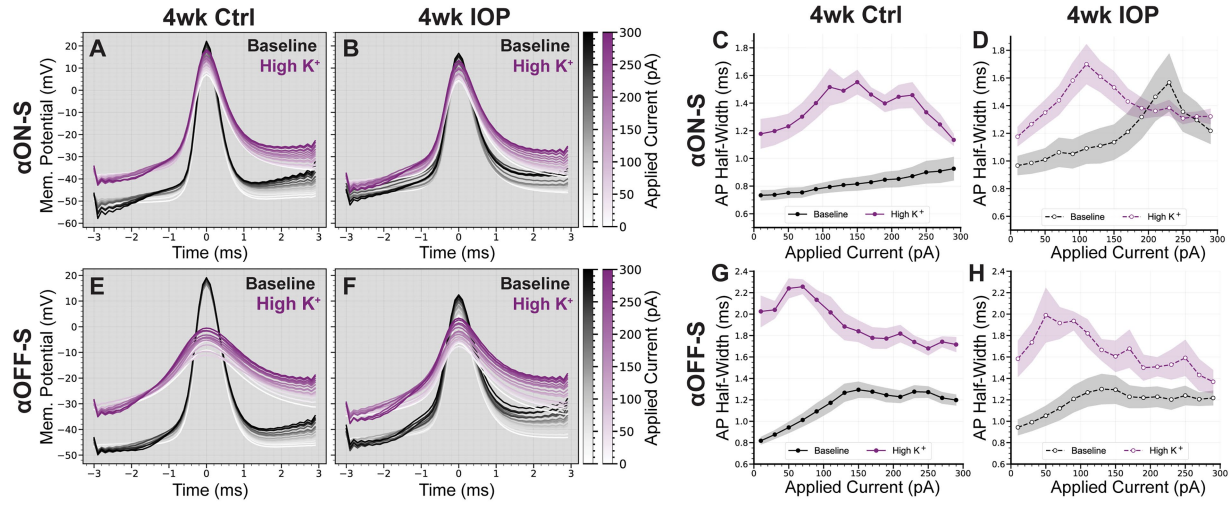

FIGURE 5
IOP elevation reduces the influence of high K^+ on action potential shape. **(A,B)** Mean action potential (AP) shapes of αON-S cells in baseline and high K^+ conditions at each current step, for 4wk Ctrl **(A)** and 4wk IOP **(B)** groups. **(C,D)** Action potential half-widths of αON-S cells in baseline and high K^+ conditions at each current step, for 4wk Ctrl **(C)** and 4wk IOP **(D)** groups. **(E,F)** Mean action potential (AP) shapes of αOFF-S cells in baseline and high K^+ conditions at each current step, for 4wk Ctrl **(E)** and 4wk IOP **(F)** groups. **(G,H)** Action potential half-widths of αOFF-S cells in baseline and high K^+ conditions at each current step, for 4wk Ctrl **(C)** and 4wk IOP **(D)** groups. The potassium-induced widening of action potentials is lessened after 4wks IOP elevation (p=0.0061, unpaired t-test). Shaded regions: ± standard error of the mean.

sensitivity in our microbead model. We labeled filled RGCs for AnkG and measured the AIS distance from the soma and length (Figure 6A) for each RGC axon. There were 11 4wk IOP cells (5 αON-S and 6 αOFF-S) and 18 4wk Ctrl cells (9 αON-S and 9 αOFF-S) with identifiable axon initial segments. The AIS distance (Figure 6B) and length (Figure 6C) from 4wk IOP RGCs was not statistically different than those of control RGCs.

4. Discussion

4.1. Blunted RGC excitability occurs alongside a reduced sensitivity to high K^+ conditions

The data presented here support evidence of RGC excitability changes with prolonged exposure to elevated IOP and offer insight into how RGCs respond to the acute stress of elevated extracellular potassium. We hypothesized intrinsic differences in K^+ sensitivity between αON-S and αOFF-S RGCs may drive a preferential susceptibility to elevated IOP-induced degeneration. In the present study we did not evaluate the degree of RGC death by counting somas in the retina or axons in the optic nerve. Previous work in the same model has established at the four-week timepoint there is some degeneration of axons but minimal loss of RGC somas in the retina (Ward et al., 2014; Bond et al., 2016; Risner et al., 2021, 2022). As in previous experiments at the four-week time point (Risner et al., 2021, 2022) we observed reduced light-and current-evoked RGC spiking (Figures 2, 4). Though the excitabilities of both αRGC types appear altered in the 4wk IOP group relative to controls, there appears to be a marginally larger effect size on the αON-S cells. These findings could represent a preferential susceptibility to IOP-related stress; however, excitability changes may also be an adaptive response.

We challenged RCGs with acutely elevated extracellular K^+ to determine how sensitivity to ionic stress changes with prolonged IOP elevation and how this impacts excitability. As expected, high K^+ media depolarized RGC membranes for both cell types and both experimental groups (Figure 3). Remarkably, 4wk IOP elevation significantly diminished this effect, suggesting that there is decreased RGC sensitivity to acute ionic stress. We examined the impact of potassium on RGC excitability to determine if this difference was related to intrinsic changes, such as altered axonal K^+ ion channel expression or function (Figure 4). Stepwise application of depolarizing currents reflected previously determined cell type (Twyford et al., 2014; Kameneva et al., 2016; Yang et al., 2018; Boal et al., 2022) and IOP dependent (Risner et al., 2022) differences in RGC excitability, and high K^+ conditions significantly impacted spiking. Strikingly, RGCs in the 4wk IOP group were less impacted by high K^+, maintaining sustained spiking at greater magnitudes of depolarizing current before reaching the threshold for depolarization block. These findings support the notion that decreased RGC excitability and altered K^+ sensitivity are related to RGC-intrinsic changes.

To further probe these effects, we measured AP half-width during evoked spiking (Figure 5). Differences in this measure may reflect changes to the mechanisms of AP generation, as AP shape is impacted by K+ currents (Geiger and Jonas, 2000; Kole et al., 2007; Kuznetsov et al., 2012; Gonzalez Sabater et al., 2021; Alexander et al., 2022). Again, there was a dramatic difference in the effect of K^+ between the 4wk IOP and control groups: for both αON-S and αOFF-S, APs were less widened by high K^+. This further supports the hypothesis that elevated IOP is affecting RGC-intrinsic excitability and suggests that there may be altered structure or function of voltage gated K^+ channels. Interestingly, however, there was cell type specificity in how AP widths differed with IOP exposure and K^+ conditions. αON-S cells exhibited a widening of APs following 4wk IOP elevation, even

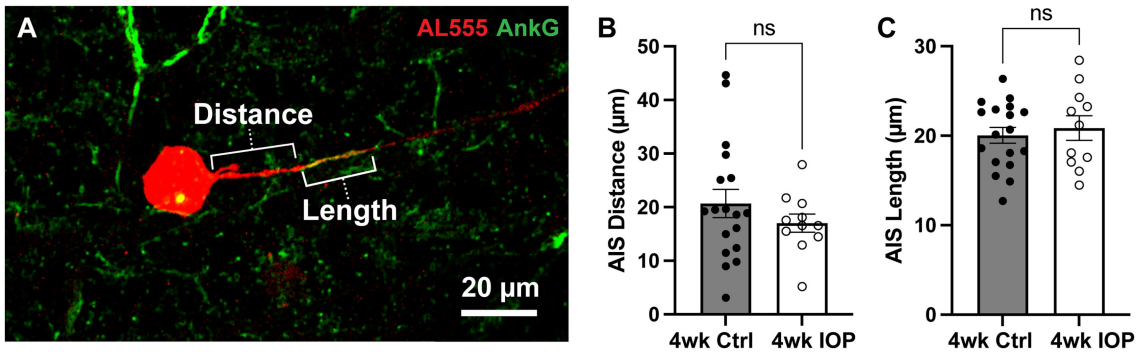

FIGURE 6
Axon initial segment dimensions are unchanged by IOP elevation. **(A)** Representative image of Alexa 555 (AL555, red) dye-filled RGC labeled for the axon initial segment (AIS) scaffolding protein ankyrin-G (AnkG, green). Annotations demonstrate the dimensions of AIS distance from soma and length which are quantified. **(B,C)** The AIS distance from the soma **(B)** and length **(C)** for all RGCs with AnkG-labeled axons. 4wk IOP does not significantly alter either of these dimensions (Distance: p=0.3194, unpaired t-test; Length: p=0.6007, unpaired t-test). Error bars: ± standard error of the mean.

in baseline, normal K^+ conditions. On the contrary, αOFF-S AP widths were similar for both the 4wk IOP and the control groups under normal K^+. Both cell types had less change in AP width following high K^+ wash on, but this difference was driven largely by the IOP-induced baseline shift for the αON-S RGCs. This is perhaps a function of cell type-specific responses to stress, paralleling the differences seen in Figure 2. αON-S RGCs had significantly diminished light-evoked spiking, while αOFF-S light spiking was mostly preserved. It remains to be determined whether these changes prove to be protective or maladaptive for the RGCs with continued stress.

4.2. Retinal ganglion cell adaptation to prolonged stress

The significant differences in the impact of high K^+ conditions on RGC responses are suggestive of an adaptive process, whereby RGCs alter their physiology to preserve function and/or mitigate further degenerative stress. Hyperexcitability at 2 weeks following IOP elevation is driven by axogenic processes (Risner et al., 2018, 2020b), and these studies further support evidence of axonal changes at 4 weeks. RGC axonal excitability and AP generation is dependent upon and shaped by the AIS, a dynamic structure, thus we focused our mechanistic exploration on alterations to the AIS dimensions. We hypothesized that, similar to *in vitro* chronic depolarization (Grubb and Burrone, 2010), prolonged glaucomatous stress from K^+ dysregulation and early hyperexcitability would lead to a distal shift in the AIS away from the soma. Yet, the results shown in Figure 6 do not demonstrate any differences in AIS dimensions between 4wk IOP cells and controls. Though this interpretation is limited by sample size and the lack of topographic location of cells, since AIS dimensions scale with retinal topography (Raghuram et al., 2019), this finding indicates that our observed differences in excitability and K^+ sensitivity are likely not solely reflective of AIS structural plasticity.

Rather, changes in voltage-gated ion channel and interacting protein expression, alongside larger scale alterations in glial regulation of the extracellular milieu (Nwaobi et al., 2016; Murphy-Royal et al., 2017; Fischer et al., 2019b; Theparambil et al., 2020; Boal et al., 2021), may underly a multifactorial adaptive process to minimize metabolic and excitotoxic stress. Retinal regulation of extracellular K^+ is largely accomplished by Müller glia (Newman et al., 1984; Karwoski et al., 1989; Kofuji and Newman, 2004), which undergo reactive changes in glaucoma and exhibit physiologic deficits in K^+ buffering capacity (Bolz et al., 2008; Fischer et al., 2019b). RGC hyperexcitability driving increased K^+ flux may compound with impaired glial buffering capacity, amplifying axonal stress. Furthermore, depressed excitability may reflect interactions between dysregulated potassium and alterations in other ions, such as calcium, which modulates neuronal excitability and can contribute to cell death (Jones and Smith, 2016; Segal, 2018). Investigation of changes to expression and function of calcium-activated potassium channels in this model may further elucidate ion-mediated mechanisms of glaucomatous degeneration (Stirling and Stys, 2010; Crish and Calkins, 2011; Van Hook et al., 2019).

Glaucoma is a chronic and insidious disease, where the interaction between vulnerable RGCs and physiologic stress can lead to dysfunction and cell death over the course of many years. It often takes a significant degree of axon degeneration for many patients notice the resultant vision changes (Hu et al., 2014). While this emphasizes the importance of early diagnosis, it also suggests a resilience of visual function in the face of prolonged stress. Discoveries in animal models of glaucoma have illuminated the variety of adaptive responses that RGCs undergo in the face of oxidative, metabolic, and inflammatory challenges (Calkins, 2021). The experiments presented here explore an important facet of RGC adaptation, giving insight into the modulation of RGC excitability, and lay the groundwork for mechanistic investigation into potential diagnostic and therapeutic targets in early glaucomatous neurodegeneration.

Data availability statement

The raw data supporting the conclusions of this article will be made available by the authors, without undue reservation.

Ethics statement

The animal study was reviewed and approved by Vanderbilt University Medical Center Institutional Animal Care and Use Committee.

Author contributions

AB, MR, and DC designed research. AB and NM performed research. AB, NM, and JH analyzed data. AB and DC wrote the paper. All authors contributed to the article and approved the submitted version.

Funding

This work was supported by the Potocsnak Family Vision Research Center, a departmental unrestricted award by the Research to Prevent Blindness Inc., Research to Prevent Blindness Inc. Stein Innovation Award to DC, and National Institutes of Health grants EY017427, EY024997, and EY008126 to DC. AB was supported in part by NEI and NIGMS of the National Institutes of Health under award numbers 1F30EY033627-01A1 and T32GM007347. MR was supported in part by BrightFocus Foundation Award G2022011S. Imaging supported through the Vanderbilt University Medical Center Cell Imaging Shared Resource core facility and NIH grants CA68485, DK20593, DK58404, and DK59637.

Acknowledgments

We would like to thank Brian Carlson for general laboratory assistance.

Conflict of interest

The authors declare that the research was conducted in the absence of any commercial or financial relationships that could be construed as a potential conflict of interest.

Publisher's note

References

Alexander, T. D., Muqeem, T., Zhi, L., Tymanskyj, S. R., and Covarrubias, M. L. (2022). Tunable action potential repolarization governed by Kv3.4 channels in dorsal root ganglion neurons. *J. Neurosci.* 42, 8647–8657. doi: 10.1523/JNEUROSCI.1210-22.2022

Baden, T., Berens, P., Franke, K., Roman Roson, M., Bethge, M., and Euler, T. (2016). The functional diversity of retinal ganglion cells in the mouse. *Nature* 529, 345–350. doi: 10.1038/nature16468

Bae, J. A., Mu, S., Kim, J. S., Turner, N. L., Tartavull, I., Kemnitz, N., et al. (2018). Digital Museum of Retinal Ganglion Cells with dense anatomy and physiology. *Cell* 173, 1293–1306.e19. doi: 10.1016/j.cell.2018.04.040

Boal, A. M., McGrady, N. R., Risner, M. L., and Calkins, D. J. (2022). Sensitivity to extracellular potassium underlies type-intrinsic differences in retinal ganglion cell excitability. *Front. Cell. Neurosci.* 16:966425. doi: 10.3389/fncel.2022.966425

Boal, A. M., Risner, M. L., Cooper, M. L., Wareham, L. K., and Calkins, D. J. (2021). Astrocyte networks as therapeutic targets in glaucomatous neurodegeneration. *Cells* 10:1368. doi: 10.3390/cells10061368

Bolz, S., Schuettauf, F., Fries, J. E., Thaler, S., Reichenbach, A., and Pannicke, T. (2008). K(+) currents fail to change in reactive retinal glial cells in a mouse model of glaucoma. *Graefes Arch. Clin. Exp. Ophthalmol.* 246, 1249–1254. doi: 10.1007/s00417-008-0872-x

Bond, W. S., Hines-Beard, J., GoldenMerry, Y. L., Davis, M., Farooque, A., Sappington, R. M., et al. (2016). Virus-mediated EpoR76E therapy slows optic nerve Axonopathy in experimental glaucoma. *Mol. Ther.* 24, 230–239. doi: 10.1038/mt.2015.198

Cacace, R., Heeman, B., Van Mossevelde, S., De Roeck, A., Hoogmartens, J., De Rijk, P., et al. (2019). Loss of DPP6 in neurodegenerative dementia: a genetic player in the dysfunction of neuronal excitability. *Acta Neuropathol.* 137, 901–918. doi: 10.1007/s00401-019-01976-3

Calkins, D. J. (2021). Adaptive responses to neurodegenerative stress in glaucoma. *Prog. Retin. Eye Res.* 84:100953. doi: 10.1016/j.preteyeres.2021.100953

Calkins, D. J., Lambert, W. S., Formichella, C. R., McLaughlin, W. M., and Sappington, R. M. (2018). The microbead occlusion model of ocular hypertension in mice. *Methods Mol. Biol.* 1695, 23–39. doi: 10.1007/978-1-4939-7407-8_3

Crish, S. D., and Calkins, D. J. (2011). Neurodegeneration in glaucoma: progression and calcium-dependent intracellular mechanisms. *Neuroscience* 176, 1–11. doi: 10.1016/j.neuroscience.2010.12.036

Della Santina, L., Inman, D. M., Lupien, C. B., Horner, P. J., and Wong, R. O. (2013). Differential progression of structural and functional alterations in distinct retinal ganglion cell types in a mouse model of glaucoma. *J. Neurosci.* 33, 17444–17457. doi: 10.1523/JNEUROSCI.5461-12.2013

El-Danaf, R. N., and Huberman, A. D. (2015). Characteristic patterns of dendritic remodeling in early-stage glaucoma: evidence from genetically identified retinal ganglion cell types. *J. Neurosci.* 35, 2329–2343. doi: 10.1523/JNEUROSCI.1419-14.2015

Emanuel, A. J., Kapur, K., and Do, M. T. H. (2017). Biophysical variation within the M1 type of ganglion cell photoreceptor. *Cell Rep.* 21, 1048–1062. doi: 10.1016/j.celrep.2017.09.095

Famiglietti, E. V. Jr., and Kolb, H. (1976). Structural basis for ON-and OFF-center responses in retinal ganglion cells. *Science* 194, 193–195. doi: 10.1126/science.959847

Fischer, R. A., Risner, M. L., Roux, A. L., Wareham, L. K., and Sappington, R. M. (2019a). Impairment of membrane repolarization accompanies axon transport deficits in glaucoma. *Front. Neurosci.* 13:1139. doi: 10.3389/fnins.2019.01139

Fischer, R. A., Roux, A. L., Wareham, L. K., and Sappington, R. M. (2019b). Pressure-dependent modulation of inward-rectifying K(+) channels: implications for cation homeostasis and K(+) dynamics in glaucoma. *Am. J. Physiol. Cell Physiol.* 317, C375–C389. doi: 10.1152/ajpcell.00444.2018

Frazzini, V., Guarnieri, S., Bomba, M., Navarra, R., Morabito, C., Mariggio, M. A., et al. (2016). Altered Kv2.1 functioning promotes increased excitability in hippocampal neurons of an Alzheimer's disease mouse model. *Cell Death Dis.* 7:e2100. doi: 10.1038/cddis.2016.18

Galli-Resta, L., Novelli, E., Volpini, M., and Strettoi, E. (2000). The spatial organization of cholinergic mosaics in the adult mouse retina. *Eur. J. Neurosci.* 12, 3819–3822. doi: 10.1046/j.1460-9568.2000.00280.x

Gasser, A., Ho, T. S., Cheng, X., Chang, K. J., Waxman, S. G., Rasband, M. N., et al. (2012). An ankyrinG-binding motif is necessary and sufficient for targeting Nav1.6 sodium channels to axon initial segments and nodes of Ranvier. *J. Neurosci.* 32, 7232–7243. doi: 10.1523/JNEUROSCI.5434-11.2012

Geiger, J. R., and Jonas, P. (2000). Dynamic control of presynaptic ca(2+) inflow by fast-inactivating K(+) channels in hippocampal mossy fiber boutons. *Neuron* 28, 927–939. doi: 10.1016/s0896-6273(00)00164-1

Gonzalez Sabater, V., Rigby, M., and Burrone, J. (2021). Voltage-gated potassium channels ensure action potential shape Fidelity in distal axons. *J. Neurosci.* 41, 5372–5385. doi: 10.1523/jneurosci.2765-20.2021

Grubb, M. S., and Burrone, J. (2010). Activity-dependent relocation of the axon initial segment fine-tunes neuronal excitability. *Nature* 465, 1070–1074. doi: 10.1038/nature09160

Hall, A. M., Throesch, B. T., Buckingham, S. C., Markwardt, S. J., Peng, Y., Wang, Q., et al. (2015). Tau-dependent Kv4.2 depletion and dendritic hyperexcitability in a mouse

model of Alzheimer's disease. *J. Neurosci.* 35, 6221–6230. doi: 10.1523/JNEUROSCI.2552-14.2015

Harden, S. W. (2022). pyABF 2.3.5. Available at: https://swharden.com/pyabf/ (Accessed 12 March 2022).

Hatch, R. J., Wei, Y., Xia, D., and Gotz, J. (2017). Hyperphosphorylated tau causes reduced hippocampal CA1 excitability by relocating the axon initial segment. *Acta Neuropathol.* 133, 717–730. doi: 10.1007/s00401-017-1674-1

Heijl, A., Leske, M. C., Bengtsson, B., Hyman, L., and Hussein, M. (2002). Reduction of intraocular pressure and glaucoma progression: results from the early manifest glaucoma trial. *Arch. Ophthalmol.* 120, 1268–1279. doi: 10.1001/archopht.120.10.1268

Hu, C. X., Zangalli, C., Hsieh, M., Gupta, L., Williams, A. L., Richman, J., et al. (2014). What do patients with glaucoma see? Visual symptoms reported by patients with glaucoma. *Am. J. Med. Sci.* 348, 403–409. doi: 10.1097/MAJ.0000000000000319

Huang, C. Y., and Rasband, M. N. (2018). Axon initial segments: structure, function, and disease. *Ann. N. Y. Acad. Sci.* 1420, 46–61. doi: 10.1111/nyas.13718

Jamann, N., Dannehl, D., Lehmann, N., Wagener, R., Thielemann, C., Schultz, C., et al. (2021). Sensory input drives rapid homeostatic scaling of the axon initial segment in mouse barrel cortex. *Nat. Commun.* 12:23. doi: 10.1038/s41467-020-20232-x

Jones, B. L., and Smith, S. M. (2016). Calcium-sensing receptor: a key target for extracellular calcium signaling in neurons. *Front. Physiol.* 7:116. doi: 10.3389/fphys.2016.00116

Kameneva, T., Maturana, M. I., Hadjinicolaou, A. E., Cloherty, S. L., Ibbotson, M. R., Grayden, D. B., et al. (2016). Retinal ganglion cells: mechanisms underlying depolarization block and differential responses to high frequency electrical stimulation of ON and OFF cells. *J. Neural Eng.* 13:016017. doi: 10.1088/1741-2560/13/1/016017

Karwoski, C. J., Lu, H. K., and Newman, E. A. (1989). Spatial buffering of light-evoked potassium increases by retinal Muller (glial) cells. *Science* 244, 578–580. doi: 10.1126/science.2785716

Kim, K. R., Kim, Y., Jeong, H. J., Kang, J. S., Lee, S. H., Kim, Y., et al. (2021). Impaired pattern separation in Tg2576 mice is associated with hyperexcitable dentate gyrus caused by Kv4.1 downregulation. Mol. *Brain* 14:62. doi: 10.1186/s13041-021-00774-x

Kofuji, P., and Newman, E. A. (2004). Potassium buffering in the central nervous system. *Neuroscience* 129, 1043–1054. doi: 10.1016/j.neuroscience.2004.06.008

Kole, M. H., Letzkus, J. J., and Stuart, G. J. (2007). Axon initial segment Kv1 channels control axonal action potential waveform and synaptic efficacy. *Neuron* 55, 633–647. doi: 10.1016/j.neuron.2007.07.031

Krieger, B., Qiao, M., Rousso, D. L., Sanes, J. R., and Meister, M. (2017). Four alpha ganglion cell types in mouse retina: function, structure, and molecular signatures. *PLoS One* 12:e0180091. doi: 10.1371/journal.pone.0180091

Kuznetsov, K. I., Grygorov, O. O., Maslov, V. Y., Veselovsky, N. S., and Fedulova, S. A. (2012). Kv3 channels modulate calcium signals induced by fast firing patterns in the rat retinal ganglion cells. *Cell Calcium* 52, 405–411. doi: 10.1016/j.ceca.2012.06.007

Leterrier, C. (2018). The axon initial segment: an updated viewpoint. *J. Neurosci.* 38, 2135–2145. doi: 10.1523/JNEUROSCI.1922-17.2018

Marin, M. A., Ziburkus, J., Jankowsky, J., and Rasband, M. N. (2016). Amyloid-beta plaques disrupt axon initial segments. *Exp. Neurol.* 281, 93–98. doi: 10.1016/j.expneurol.2016.04.018

Murphy-Royal, C., Dupuis, J., Groc, L., and Oliet, S. H. R. (2017). Astroglial glutamate transporters in the brain: regulating neurotransmitter homeostasis and synaptic transmission. *J. Neurosci. Res.* 95, 2140–2151. doi: 10.1002/jnr.24029

Naguib, S., Backstrom, J. R., Gil, M., Calkins, D. J., and Rex, T. S. (2021). Retinal oxidative stress activates the NRF2/ARE pathway: an early endogenous protective response to ocular hypertension. *Redox Biol.* 42:101883. doi: 10.1016/j.redox.2021.101883

Newman, E. A., Frambach, D. A., and Odette, L. L. (1984). Control of extracellular potassium levels by retinal glial cell K+ siphoning. *Science* 225, 1174–1175. doi: 10.1126/science.6474173

Nwaobi, S. E., Cuddapah, V. A., Patterson, K. C., Randolph, A. C., and Olsen, M. L. (2016). The role of glial-specific Kir4.1 in normal and pathological states of the CNS. *Acta Neuropathol.* 132, 1–21. doi: 10.1007/s00401-016-1553-1

Ou, Y., Jo, R. E., Ullian, E. M., Wong, R. O., and Della Santina, L. (2016). Selective vulnerability of specific retinal ganglion cell types and synapses after transient ocular hypertension. *J. Neurosci.* 36, 9240–9252. doi: 10.1523/JNEUROSCI.0940-16.2016

Raghuram, V., Werginz, P., and Fried, S. I. (2019). Scaling of the AIS and Somatodendritic compartments in alpha S RGCs. *Front. Cell. Neurosci.* 13:436. doi: 10.3389/fncel.2019.00436

Risner, M. L., McGrady, N. R., Boal, A. M., Pasini, S., and Calkins, D. J. (2020a). TRPV1 supports Axogenic enhanced excitability in response to neurodegenerative stress. *Front. Cell. Neurosci.* 14:603419. doi: 10.3389/fncel.2020.603419

Risner, M. L., McGrady, N. R., Pasini, S., Lambert, W. S., and Calkins, D. J. (2020b). Elevated ocular pressure reduces voltage-gated sodium channel NaV1.2 protein expression in retinal ganglion cell axons. *Exp. Eye Res.* 190:107873. doi: 10.1016/j.exer.2019.107873

Risner, M. L., Pasini, S., Cooper, M. L., Lambert, W. S., and Calkins, D. J. (2018). Axogenic mechanism enhances retinal ganglion cell excitability during early progression in glaucoma. *Proc. Natl. Acad. Sci. U. S. A.* 115, E2393–E2402. doi: 10.1073/pnas.1714888115

Risner, M. L., Pasini, S., McGrady, N. R., and Calkins, D. J. (2022). Bax contributes to retinal ganglion cell dendritic degeneration during glaucoma. *Mol. Neurobiol.* 59, 1366–1380. doi: 10.1007/s12035-021-02675-5

Risner, M. L., Pasini, S., McGrady, N. R., D'Alessandro, K. B., Yao, V., Cooper, M. L., et al. (2021). Neuroprotection by Wld(S) depends on retinal ganglion cell type and age in glaucoma. *Mol. Neurodegener.* 16:36. doi: 10.1186/s13024-021-00459-y

Sanes, J. R., and Masland, R. H. (2015). The types of retinal ganglion cells: current status and implications for neuronal classification. *Annu. Rev. Neurosci.* 38, 221–246. doi: 10.1146/annurev-neuro-071714-034120

Sappington, R. M., Carlson, B. J., Crish, S. D., and Calkins, D. J. (2010). The microbead occlusion model: a paradigm for induced ocular hypertension in rats and mice. *Invest. Ophthalmol. Vis. Sci.* 51, 207–216. doi: 10.1167/iovs.09-3947

Segal, M. (2018). Calcium stores regulate excitability in cultured rat hippocampal neurons. *J. Neurophysiol.* 120, 2694–2705. doi: 10.1152/jn.00447.2018

Stirling, D. P., and Stys, P. K. (2010). Mechanisms of axonal injury: internodal nanocomplexes and calcium deregulation. *Trends Mol. Med.* 16, 160–170. doi: 10.1016/j.molmed.2010.02.002

Sun, X., Wu, Y., Gu, M., and Zhang, Y. (2014). miR-342-5p decreases ankyrin G levels in Alzheimer's disease transgenic mouse models. *Cell Rep.* 6, 264–270. doi: 10.1016/j.celrep.2013.12.028

Tham, Y. C., Li, X., Wong, T. Y., Quigley, H. A., Aung, T., and Cheng, C. Y. (2014). Global prevalence of glaucoma and projections of glaucoma burden through 2040: a systematic review and meta-analysis. *Ophthalmology* 121, 2081–2090. doi: 10.1016/j.ophtha.2014.05.013

Theparambil, S. M., Hosford, P. S., Ruminot, I., Kopach, O., Reynolds, J. R., Sandoval, P. Y., et al. (2020). Astrocytes regulate brain extracellular pH via a neuronal activity-dependent bicarbonate shuttle. *Nat. Commun.* 11:5073. doi: 10.1038/s41467-020-18756-3

Tran, N. M., Shekhar, K., Whitney, I. E., Jacobi, A., Benhar, I., Hong, G., et al. (2019). Single-cell profiles of retinal ganglion cells differing in resilience to injury reveal Neuroprotective genes. *Neuron* 104, 1039–1055.e12. doi: 10.1016/j.neuron.2019.11.006

Twyford, P., Cai, C., and Fried, S. (2014). Differential responses to high-frequency electrical stimulation in ON and OFF retinal ganglion cells. *J. Neural Eng.* 11:025001. doi: 10.1088/1741-2560/11/2/025001

Van Hook, M. J., Nawy, S., and Thoreson, W. B. (2019). Voltage-and calcium-gated ion channels of neurons in the vertebrate retina. *Prog. Retin. Eye Res.* 72:100760. doi: 10.1016/j.preteyeres.2019.05.001

Virtanen, P., Gommers, R., Oliphant, T. E., Haberland, M., Reddy, T., Cournapeau, D., et al. (2020). SciPy 1.0: fundamental algorithms for scientific computing in python. *Nat. Methods* 17, 261–272. doi: 10.1038/s41592-019-0686-2

Ward, N. J., Ho, K. W., Lambert, W. S., Weitlauf, C., and Calkins, D. J. (2014). Absence of transient receptor potential vanilloid-1 accelerates stress-induced axonopathy in the optic projection. *J. Neurosci.* 34, 3161–3170. doi: 10.1523/JNEUROSCI.4089-13.2014

Werginz, P., Raghuram, V., and Fried, S. I. (2020). Tailoring of the axon initial segment shapes the conversion of synaptic inputs into spiking output in OFF-alpha T retinal ganglion cells. *Sci. Adv.* 6:37. doi: 10.1126/sciadv.abb6642

Wienbar, S., and Schwartz, G. W. (2022). Differences in spike generation instead of synaptic inputs determine the feature selectivity of two retinal cell types. *Neuron* 110, 2110–2123.e4. doi: 10.1016/j.neuron.2022.04.012

Yang, C. Y., Tsai, D., Guo, T., Dokos, S., Suaning, G. J., Morley, J. W., et al. (2018). Differential electrical responses in retinal ganglion cell subtypes: effects of synaptic blockade and stimulating electrode location. *J. Neural Eng.* 15:046020. doi: 10.1088/1741-2552/aac315

Zhou, D., Lambert, S., Malen, P. L., Carpenter, S., Boland, L. M., and Bennett, V. (1998). AnkyrinG is required for clustering of voltage-gated Na channels at axon initial segments and for normal action potential firing. *J. Cell Biol.* 143, 1295–1304. doi: 10.1083/jcb.143.5.1295

frontiers | Frontiers in Neuroscience

TYPE Original Research
PUBLISHED 27 March 2023
DOI 10.3389/fnins.2023.1119724

OPEN ACCESS

EDITED BY
Dan Wen,
Central South University, China

REVIEWED BY
Jiajia Yuan,
Renmin Hospital of Wuhan University, China
David Mackey,
The University of Western Australia, Australia
Congwu He,
Wuhan Neophth Biotechnology Co., Ltd., China

*CORRESPONDENCE
Vittorio Porciatti
✉ vporciatti@med.miami.edu
Hong Yu
✉ hyu3@med.miami.edu

†Deceased

SPECIALTY SECTION
This article was submitted to Visual Neuroscience, a section of the journal Frontiers in Neuroscience

RECEIVED 09 December 2022
ACCEPTED 13 January 2023
PUBLISHED 27 March 2023

CITATION
Velmurugan S, Chou T-H, Eastwood JD, Porciatti V, Liu Y, Hauswirth WW, Guy J and Yu H (2023) Comparison of different gene-therapy methods to treat Leber hereditary optic neuropathy in a mouse model.
Front. Neurosci. 17:1119724.
doi: 10.3389/fnins.2023.1119724

Comparison of different gene-therapy methods to treat Leber hereditary optic neuropathy in a mouse model

Sindhu Velmurugan[1], Tsung-Han Chou[1], Jeremy D. Eastwood[1], Vittorio Porciatti[1]*, Yuan Liu[1], William W. Hauswirth[2], John Guy[1†] and Hong Yu[1]*

[1]Bascom Palmer Eye Institute, University of Miami Miller School of Medicine, Miami, FL, United States, [2]Department of Ophthalmology, College of Medicine, University of Florida, Gainesville, FL, United States

Introduction: Therapies for Leber hereditary optic neuropathy (LHON), in common with all disorders caused by mutated mitochondrial DNA, are inadequate. We have developed two gene therapy strategies for the disease: mitochondrial-targeted and allotopic expressed and compared them in a mouse model of LHON.

Methods: A LHON mouse model was generated by intravitreal injection of a mitochondrialtargeted Adeno-associated virus (AAV) carrying mutant human NADH dehydrogenase 4 gene (*hND4/m.11778G>A*) to induce retinal ganglion cell (RGC) degeneration and axon loss, the hallmark of the human disease. We then attempted to rescue those mice using a second intravitreal injection of either mitochondrial-targeted or allotopic expressed wildtype human *ND4*. The rescue of RGCs and their axons were assessed using serial pattern electroretinogram (PERG) and transmission electron microscopy.

Results: Compared to non-rescued LHON controls where PERG amplitude was much reduced, both strategies significantly preserved PERG amplitude over 15 months. However, the rescue effect was more marked with mitochondrial-targeted therapy than with allotopic therapy (p = 0.0128). Post-mortem analysis showed that mitochondrial-targeted human *ND4* better preserved small axons that are preferentially lost in human LHON.

Conclusions: These results in a pre-clinical mouse model of LHON suggest that mitochondrially-targeted AAV gene therapy, compared to allotopic AAV gene therapy, is more efficient in rescuing the LHON phenotype.

KEYWORDS

gene therapy, mitochondrial-targeted, allotopic expression, Leber hereditary optic neuropathy (LHON), mitochondrial-targeted therapy

Introduction

Mitochondrial dysfunction affects almost every tissue in the body, especially those with high energy requirements such as the brain, heart, nervous system, and eye (Desler and Rasmussen, 2012). Leber Hereditary Optic Neuropathy (LHON) is the most common primary genetic mitochondrial disease characterized by losing retinal ganglion cells (RGCs) and optic nerve atrophy (Ellouze et al., 2008). More than 90% of LHON cases are caused by one of the three point mutations in mitochondrial DNA (m. 11778G > A, m.3460G > A, and m.14484 T > C) that encode subunits ND4, ND1, and ND6 of respiration complex I, respectively (Yu-Wai-Man and Chinnery, 1993; Karaarslan, 2019; Zuccarelli et al., 2020).

Pharmacological therapies for LHON, as in most mitochondrial diseases, are inadequate. Gene therapy approaches for LHON have been proposed (Yu et al., 2012; Bacman et al., 2013; Chadderton et al., 2013); However allotopic expression is the only approach that has reached human testing for m. 11778G > A mutation in China (NCT01267422) (Liu et al., 2020), in France (NCT02064569) (Yu-Wai-Man et al., 2020), and in the USA (NCT02161380) (Feuer et al., 2016; Guy et al., 2017; Lam et al., 2022). The French clinical trial is currently in phase 3 trials in the USA and Europe.

The allotopic expression approach involves expressing a nuclear version of a mitochondrial gene in the nucleus and importing the expressed protein back to the mitochondria with the help of the N-terminal fused mitochondrial targeting sequence (MTS) (Koilkonda R. D. et al., 2014; Artika, 2020). Guy et al. (2002) studied the allotopic method extensively in (1) expressing wildtype ND4 in cybrid cells and (2) generating animal models for LHON using mutant human ND4 (R340H) (Qi et al., 2007; Koilkonda R. et al., 2014). Studies proving the use of a second AAV as a vector to carry allotopic wildtype ND4 (Baracca et al., 2005; Qi et al., 2007; Koilkonda R. et al., 2014; Cwerman-Thibault et al., 2015) to rescue RGC degeneration and loss of vision frames the basis for performing gene therapy using allotopically expressed human ND4 in patients carrying m.11778G > A mutation (NCT02161380) (Koilkonda and Guy, 2011; Cwerman-Thibault et al., 2014; Guy et al., 2014, 2017; Koilkonda R. et al., 2014; Feuer et al., 2016; Yu-Wai-Man et al., 2020).

Although visual improvement was observed in patients in those clinical trials, most participants still have low vision, and are still classified as being legally blind, especially for those with the visual loss for more than 1 year (Guy et al., 2014, 2017; Yu-Wai-Man et al., 2020; Yuan et al., 2020). Additionally, the hydrophobicity of ND4 protein limits its ability to cross the mitochondrial membrane and maintain stable long-term gene expression (Oca-Cossio et al., 2003; Perales-Clemente et al., 2011). The entire process, from practical protein synthesis to successful integration into mitochondrial respiration complex, is challenging.

Viruses have the ability to traverse the mitochondrial double membrane to access the inner matrix and deliver DNA inside the organelle (Maul et al., 1978; Kaeppel et al., 2013). Yu et al. (2012) have observed that fusing a MTS to the capsid of adeno-associated virus (MTS-AAV) can redirect the virus to mitochondria rather than the nucleus. When the MTS-AAV-carried *ND4* gene was introduced into the LHON cybrids, ATP synthesis was rescued and when injected into LHON rodents, visual loss and optic atrophy improved post gene therapy. It was also proven using next-generation sequencing that the transferred gene remains episomal, making mito-targeted gene transfer a long-term platform for the treatment of LHON and other primary genetic mitochondrial diseases (Ellouze et al., 2008; Yu et al., 2018).

In this study, we used mito-targeted and allotopic expressed wildtype hND4 to treat LHON mice induced by MTSAAV delivered *hND4G11778A* and compare their therapeutic efficacy to protect the RGCs and axons from dysfunction and degeneration in those mice.

Materials and methods

Animals

All animal procedures were performed abiding by the National Institutes of Health Guide for Care and Use of Laboratory Animals and the ARVO Statement for the use of Animals in Ophthalmic and Vision Research. Intraocular injections of recombinant AAV were performed on 3-month-old DBA/1J mice post sedation by inhalation of 1.5–2% isoflurane, right after baseline tests. A local anesthetic (proparacaine HCl) was topically applied to the cornea, and then a 32-gauge needle attached to a Hamilton syringe was inserted through the pars plana. 1 μl of AAVs carrying the gene of interest was injected into the eyes at the interval of 2 days, including MTSAAV/mutant ND4 (4.32 E9 vg/eye), MTSAAV/mCherry (4.52 E8 vg/eye), MTSAAV/wild-type ND4 (4.4 E8 vg/eye), AAV/p1ND4 (4.5 E9 vg/eye), and AAV/Cherry (3.72 E9 vg/eye) as showed in **Table 1**. For the treatment, the mice were first injected with mutant human ND4, and 2 days later were injected with wildtype human ND4 (Rescued) or m/Cherry (un-rescued). The injection controls received two injections of mCherry. Pattern electroretinograms (PERGs) were performed longitudinally at 3-, 6-, 9-, and 12-month after injections for the allotopic group and baseline, 1-, 3-, 6-, and 12-month after injection for the mito-targeted group.

Plasmids and AAVs

Plasmids including sc-HSP-ND4G11778A, sc-HSP-wtND4, sc-HSP-mCherry, sc-smCBA-P1ND4, and sc-smCBA-Cherry were constructed as previously described (Koilkonda R. et al., 2014; Yu et al., 2018). In brief, for mito-constructs, human *ND4 G11778A* or wildtype *ND4* gene fused in frame with *FLAG* and mitochondrial-encoded *Cherry*(mCherry) were cloned into scAAV backbones under the control of the mitochondrial heavy strand promoter (*HSP*), where *ND4FLAG* is followed by *mCherry* with a stop codon between two genes (sc-HSP-ND4G11778A or sc-HSP-wtND4). *mCherry* cloned into the same scAAV backbone was used as a control (sc-HSP-mCherry). For allotopic constructs, human *ND4* in standard code was fused with the MTS of ATP synthase subunit C (*p1ND4*) and cloned into scAAV backbones under the control of chicken b-actin promoter (sc-*smCBA-P1ND4*). Also, mCherry in standard code was cloned in the same scAAV backbone and used as a control (sc-*smCBA-Cherry*). The resultant plasmids were purified using Qiagen endotoxin free megprep. Then, the mito-constructs were packaged by the University of Florida into MTSAAV2 using VP2COX8, VP1, VP3 (Y444, 500, 730F), and helper plasmid PXX6, and the allotopic constructs were packaged into AAV2 using PDG2mut (Y444, 500, 730F) by National Heart, Lung and Blood Institute's GTRP AAV facility at Children's Hospital of Philadelphia (CHOP).

TABLE 1 Summary of experiments.

Study groups	Naïve control	Injection control	Unrescued	Rescued
Mito-targeted (1st)	*n* = 5	MTSAAV/ mCherry	MTSAAV/ mutND4	MTSAAV/ mutND4
		MTSAAV/ mCherry	MTSAAV/ mCherry	MTSAAV/ wtND4
		n = 10	*n* = 10	*n* = 10
Allotopic (2nd)	*n* = 10	*n* = 0	MTSAAV/ mutND4	MTSAAV/ mutND4
			AAV/Cherry	AAV/p1ND4
			n = 10	*n* = 10

MTS, mitochondrial targeted sequence; mut, mutant; wt, wildtype; mCherry, mcherry in mito-code.
Cherry, mcherry in standard code.

PERG

Pattern electroretinograms (Chou et al., 2014) were obtained from mice at various time points. In brief, mice were weighed and anesthetized intraperitoneally (IP) using a mixture of ketamine (80 mg/kg body weight) and xylazine (10 mg/kg body weight). A feedback-controlled heating pad was used to maintain the body temperature of individual animals at 37.6°C. PERG signals were recorded from a common subcutaneous needle (Grass Technologies, West Warwick, RI, USA) placed in the snout and referenced to a similar electrode placed in the back of the head. A third subcutaneous electrode placed at the root of the tail served as a ground. Pupils were natural without dilation. A small drop of balanced saline solution was applied topically as necessary to prevent corneal dryness. Visual stimuli consisting of horizontal gratings (95% contrast, 0.06 cycles/degree spatial frequency), 700 cd/m^2 mean luminance were generated on two (15 cm × 15 cm) LED tablet displays (Jorvec Corp, Miami, FL, USA) and presented at each eye separately at a distance of 10 cm. Gratings reverse in contrast at slightly different temporal frequency (OD, 0.984 Hz; OS, 0.992 Hz) to allow deconvolution of the signal and retrieval of PERG from each eye. PERG signals were fed to an Opti-Amp bioamplifier (Intelligent Hearing Systems Inc., Miami, FL, USA) amplified (10,000-fold), filtered (1–300 Hz, 6 dB/oct), and averaged (OD, 372 epochs of 492 ms; OS, 372 epochs of 496 ms) using a Universal Smart Box acquisition system (Intelligent Hearing Systems Inc., Miami, FL, USA).

Optic nerve diameter and axon count

A total of 15 months post-injection, optic nerves were dissected from 1 mm behind the ocular bulbs. For quantifying the axon counts, transmission electron micrographs were photographed by a masked observer at a magnification of 1500X for each optic nerve specimen (n = 3 in each group). The diameter and number of axons were manually counted by a masked observer. In the mito-targeted group, a total of 2,226 axons were counted for the un-rescued group, 3,049 axons for the rescued group, and 3,320 axons for mcherry double injected control group. In the allotopic group, a total of 4,695 axons were counted for the un-rescued group, 6,445 axons for the rescued group, and 5,229 axons for the I group.

Statistical analysis

GraphPad Prism software was used to perform univariate statistical analysis. To compare PERG amplitude changes over time between controls and treated mice, the method of Generalized Estimating Equations (GEE) was used (IBM SPSS statistics Ver. 26). GEE is an unbiased non-parametric method to analyze longitudinal correlated data, accounting for the inclusion of both eyes in the design. In the analysis, PERG amplitude was the dependent variable, and age at testing period and treatment group (Controls, Treated) were predictor variables. Main effects (Age, Group) and interaction between age and treatment group were computed, as well as pairwise comparisons between age and treatment group. PERG latency tended to increase with age in all groups. As the differences between groups were relatively small, latency changes were not specifically analyzed but were included as covariates. P-values of < 0.05 were considered statistically significant. Values were expressed as means ± standard deviation (SD).

Results

Mito targeted wildtype ND4 mediates a rapid and more efficient vision rescue than allotopic expressed ND4

To compare the therapeutic efficacy of the mito-targeted- and allotopic- gene therapy, we performed two experiments in which a LHON mouse model was first generated by intravitreal injection of MTSAAV carrying mutant human *ND4G11778A*(*mutND4*) and then rescued using a second injection of either mito-targeted or allotopic wildtype human *ND4* (wtND4) (**Table 1**). The mito-targeted *wtND4* was in mitochondrial genetic code, while, allotopic expressed *wtND4* was recoded in nuclear (standard) code and fused in-frame with MTS of the ATP synthase subunit C (p1ND4) (Guy et al., 2002). Unrescued mice received a second injection of *mCHERRY* encoded in either mitochondrial (mito-targeted) or standard (allotopic) genetic code. Both experiments included a group of non-injected mice as naive controls. The rescue efficacy of the two strategies was assessed using longitudinal PERGs, a sensitive electrophysiological measure for RGC function *in vivo*.

To detect if double injections *per se* impaired the RGC function, we compared the PERG amplitude between naïve and mcherry_mcherry double injected mice from baseline to 1-, 3-, and 12-month after injection (**Figure 1A**). No significant decrease was found in PERG amplitude with age for both naïve and mcherry double- injected mice (P = 0.096). We did not find a statistically significant difference in PERG amplitude between the two groups (P = 0.082) or any interaction between age and group (P = 0.322) (**Figure 1B**).

Next, we wanted to detect whether mito-targeted *wtND4* rescued the RGC dysfunction induced by *mutND4* in the injected mice. Compared to age matched un-rescued control mice (MTND4_mcherry), mice in both groups had a similar baseline PERG amplitude before injection (**Figure 2A**); however, a significant decrease in PERG amplitude was found at 1 month after injection in both groups (**Figure 2B**). The rescued mice (MTND4_WT_rescued) regained the PERG amplitude at 3 months (p = 0.055, **Figure 2C**), and the difference between the rescued and unrescued mice became statistically significant at 6 (p = 0.018, **Figure 2D**) and 12 months (p = 0.042, **Figure 2E**) after injection. GEE analysis showed a significant change starting at the age of 6 months (3 months after injection) and persisted to 9 (6 months after injection) and 15 months after birth (12 months after injection). The mean PERG amplitude significantly decreased with age (<0.001); specifically, the effect between the two groups was statistically significant (p = 0.039), suggesting mito-targeted wildtype ND4 efficiently reverts RGC loss in LHON mice (**Figure 2F**).

Then, we wanted to see if the allotopically expressed wtND4 rescued RGC dysfunction in the injected mice. For this experiment, data were available for the post-injection period (3, 6, 9,12 months of age, 6, 9, 12, 15 months after injection) as a confirmation of our previous studies using allotopic vector in the same mouse strain of the same age range (Koilkonda R. et al., 2014; Koilkonda R. D. et al., 2014). Compared to unrescued mice (Allo-unrescued), the rescued

10.3389/fnins.2023.1119724

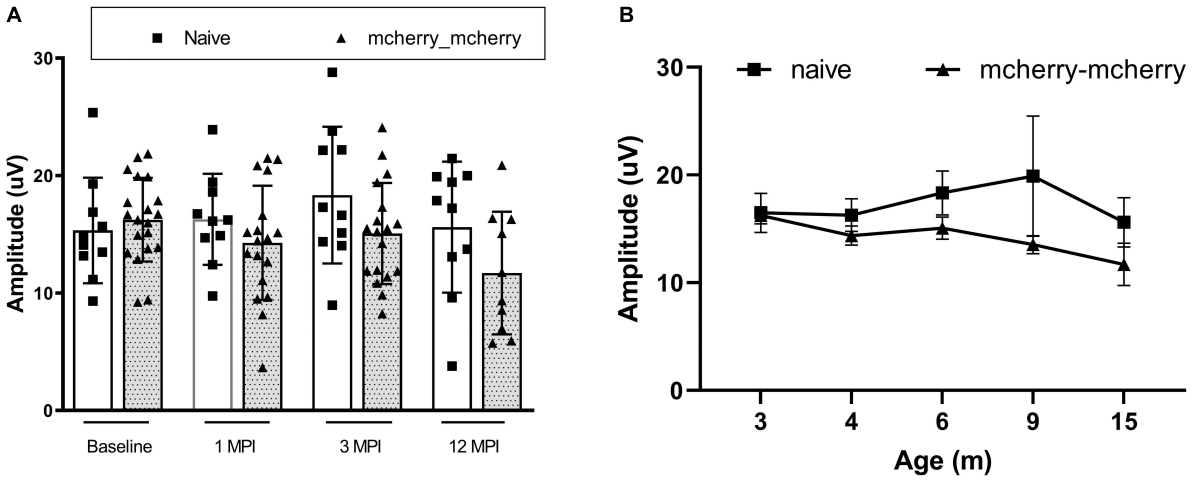

FIGURE 1
Double injection does not impair the RGC function. **(A)** Scatterplot of PERG amplitudes (average of both eyes) of all mice tested in each group shows no significant difference between naïve and mcherry-double injected mice from baseline, 1-, 3-, and 12-month post-injection. **(B)** A line graph shows the mean PERG amplitude of the mice in both groups did not decrease significantly with age from 3 to 15 months after birth (from baseline to 12 months after injection).

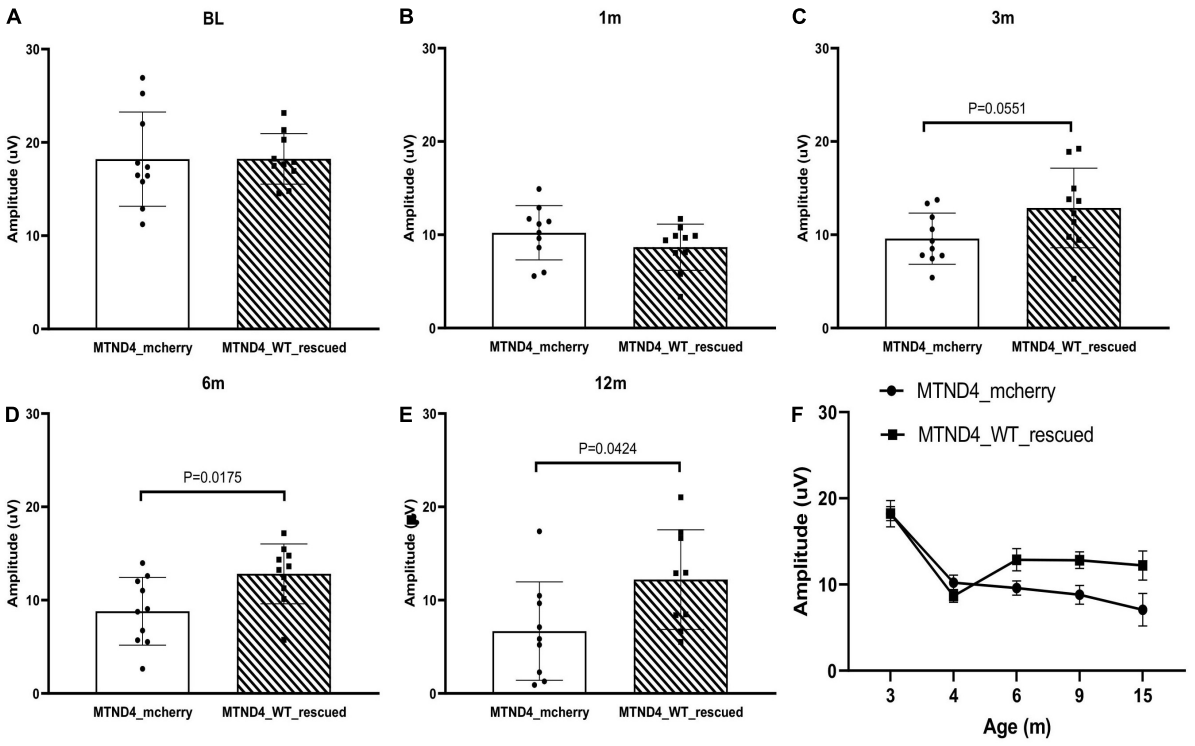

FIGURE 2
Mito-targeted *wtND4* rescue mutND4-induced RGC dysfunction. **(A)** Scatterplot of PERG amplitudes (average of both eyes) of all mice tested in each group showed no significant difference at the baseline (BL) between un-rescued (MTND4_mcherry) and rescued mice (MTND4_WT_rescued). **(B)** Mutant ND4 injection induced a significant decrease in PERG amplitude at 1 month after injection. Wildtype ND4 reverse the reduction PERG from 3 months **(C)**, 6 months **(D)**, to 12 months **(E)** after injection. **(F)** A line graph shows the mean PERG amplitude for un-rescued mice significantly decreased with age relative to rescued mice from 6 to 15 months after birth.

mice (Allo-rescued) showed an overall increase in PERG amplitude of about 15% ($P = 0.017$) that was more marked in 9–12 months after injection (Figures 3A–E), suggesting that allotopic expressed wtND4 mediates a moderate and delayed rescue in LHON mice.

Lastly, to determine if any difference exists in rescue effects of RGC dysfunction in LHON mice between mito-targeted and allotopic gene therapy, data was analyzed as mean PERG amplitude change between the rescue group and its corresponding non-rescued control (MTND4_WT_rescued and MTND4_mcherry vs. Allo-rescued and Allo-unrescued). As no baseline PERG data were collected for the allotopic group, rescue-induced PERG changes could not be compared relative to baseline. However, we were able

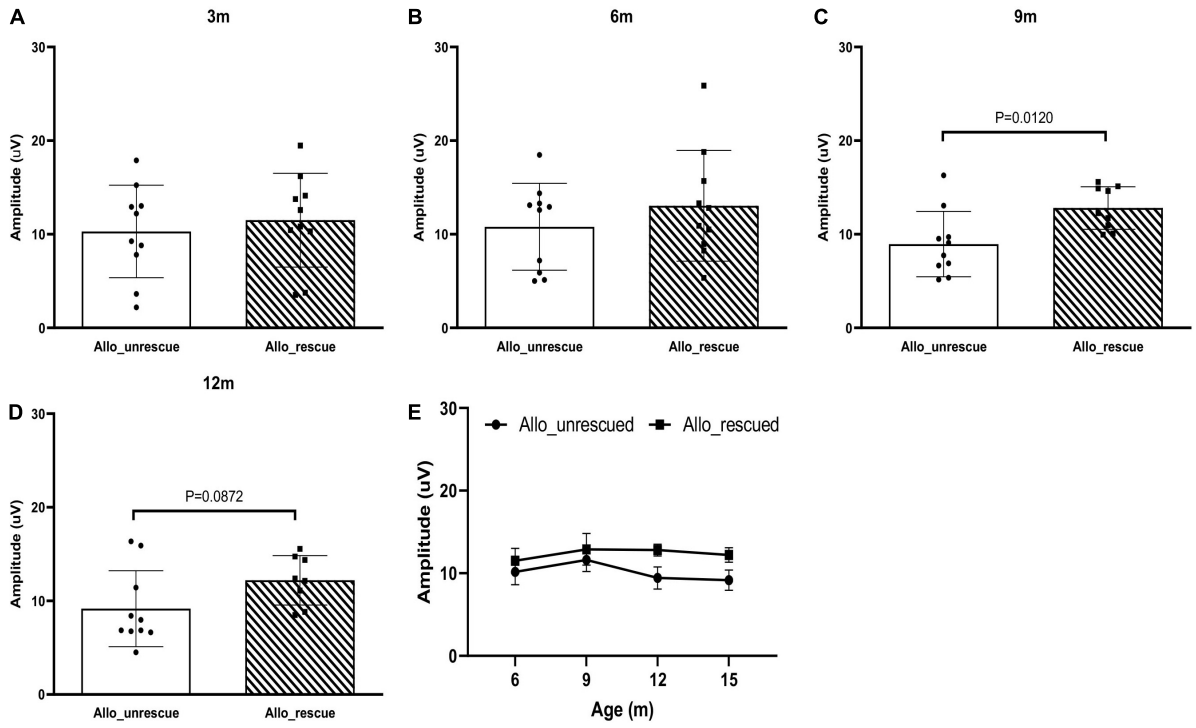

FIGURE 3
Allotopic expressed wtND4 rescue mutND4-induced RGC dysfunction. Scatterplots of PERG amplitudes (average of both eyes) of all mice tested in each group showed PERG amplitude of unrescued (Allo−unrescue) and rescued (Allo_rescue) mice at 3 months **(A)**, 6 months **(B)**, 9 months **(C)**, and 12 months **(D)** post-injection. **(E)** A line graph shows the mean PERG amplitude for un-rescued mice significantly decreased with age relative to rescued mice from 9 to 15 months after birth.

to analyze rescue effects by comparing post-injection data with corresponding post-injection data of unrescued mice. Namely, we subtracted individual rescued PERG amplitudes from the grand mean of corresponding unrescued data over a comparable age ranges (3, 6, 12 MPI). Kolmolgorov-Smirnoff tests showed that the distributions of both allotopic and mito-targeted approach data points were different from zero, indicating both strategies were effective in rescue; however, the rescue effect was more robust with the mito-targeted approach ($p = 0.0128$) (Figure 4).

Mito targeted wildtype ND4 mediates a more efficient rescue of axons in the optic nerve compared to allotopic expressed ND4

To evaluate the rescue efficacy of optic atrophy induced by mutant ND4 in mice, we performed post-mortem ultrastructural analysis 15 months after intravitreal injections. The optic nerves of the mutant *ND4* injected untreated mice (MTND4_mcherry, Figure 5A) had many cystic spaces and electron-dense debris where axons were degraded. In contrast, age-matched control (mcherry_mcherry, Figure 5B) and mito-targeted *ND4* treated mice (MTND4_WT_rescued, Figure 5C) exhibited numerous axons. Quantitative analysis revealed 33% axons loss in untreated mice compared to controls (186995 ± 33784 vs. 278898 ± 14203, axons/mm^2, $p = 0.009$), while wildtype *ND4* treatment increased the axons by 37% (256132 ± 22452, axons/mm^2, $p = 0.033$, Figure 5D). Consistently, the optic nerves of unrescued mice (Allo-unrescue, Figure 5E) in the allotopic group also had more cystic spaces compared to naïve (Figure 5F) and rescued mice (Allo-rescue) (Figure 5G). Axon quantification revealed an increase of 37.5% in Allo-rescue mice (216577 ± 20351 vs. 157768 ± 25500, axons/mm^2) compared to unrescued mice (Figure 5H). Although the sample size for the axon density measurement was small ($n = 3$ per group), there was a significant difference between mice rescued with the mito-targeted strategy ($p = 0.0095$) compared to mice rescued with the allotopic strategy ($p = 0.158$).

To compare the distribution of axons diameters in unrescued and rescued LHON mice, we manually measured the diameter of every axon that was imaged as described in the methods. The proportion of axons of different diameters was calculated relative to the total existing axons counted for each eye. Compared to age-matched unrescued mice, the axon distribution of MTND4-rescued mice tended to shift toward small axons (Figure 5I), whereas no apparent shift was evident in Allo-rescued mice (Figure 5J). The data suggests that mito -targeted delivery systems for gene therapy may preserve small axons that are preferentially lost in human LHON (Sadun et al., 2000).

Discussion

Mammalian mtDNA is present as thousands of copies per cell in most cells and mutations can occur in all (homoplasmy) or a fraction of them (heteroplasmy) (Frazier et al., 2019; Naeem and Sondheimer, 2019; Jackson et al., 2020; Filograna et al., 2021). Virtually all pathogenic mutations in mtDNA are functionally recessive

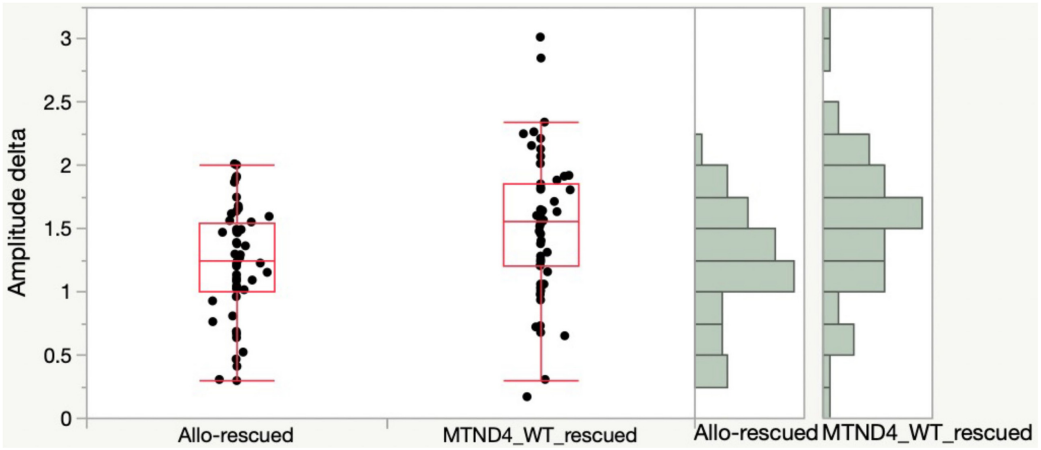

FIGURE 4
Mito-targeted approach mediates a stronger rescue than allotopic strategy. PERG amplitude differences between rescued and unrescued mice are different from zero for both allotopic and mito-targeted approaches (both are effective in rescue) but the rescue effect is stronger with the mito-targeted approach (the distributions are significantly different for the two approaches, $p = 0.0128$).

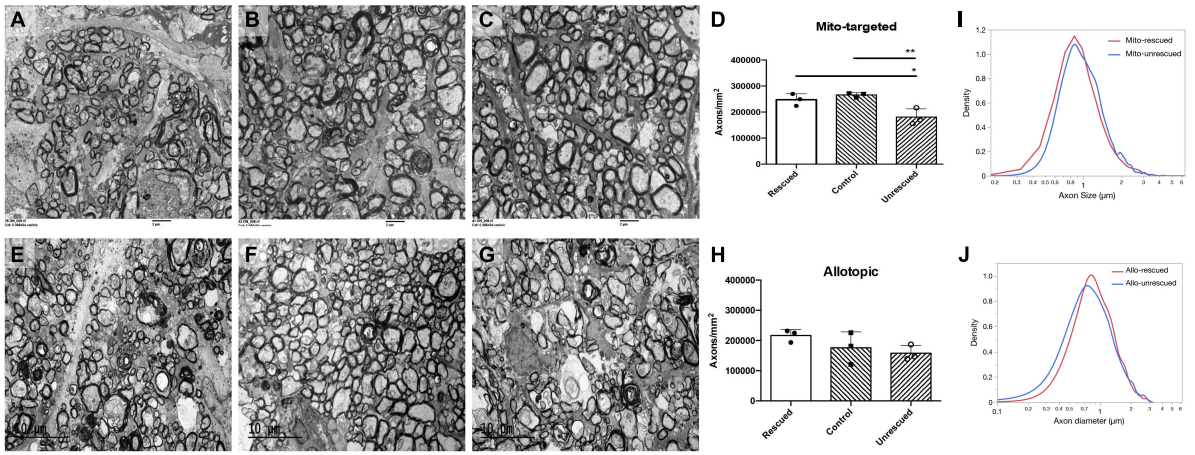

FIGURE 5
Wild type ND4 protect optic nerve degeneration. Transmission electron micrographs of the retrobulbar optic nerve were performed 15 months post-injection. More cystic spaces are observed in un-rescued mice **(A,E)** when compared to mcherry double-injected control **(B)**, mito-targeted ND4 rescued **(C)**, naïve **(F)**, and allotopic expressed ND4 rescued **(G)** mice. Quantification of axons in the mice of mito-targeted **(D)** and allotopic **(H)** rescue experiments. Only mito-targeted ND4 significantly preserved axons compared to its corresponding non-rescued controls. In contrast, allotopic expressed ND4 did not. Analysis of the distribution of axonal diameters showed that mito-targeted ND4 **(I)** preserved small axons with a shift to larger diameter axons in the corresponding non-rescued compared to the allotopic group **(J)**.

(Filograna et al., 2021), including mutant ND4 (m.11778G > A). The impact of pathogenic mutations will not be biochemically and clinically manifest until the ratio of mutated to wildtype mtDNA exceeds a certain upper limit (Shoffner et al., 1990; Rossignol et al., 2003; Falabella et al., 2022). A load of heteroplasmy, defined as the relative amount of mutated to wildtype mtDNA, corresponds to timing and symptom severity (Naeem and Sondheimer, 2019; Jackson et al., 2020). Thus, shifting the heteroplasmic equilibrium without correcting all, or perhaps even most mtDNA mutations, can lead to a shift in disease onset and symptom severity due to complementation of wildtype molecules for the effects of the mutation (DiMauro and Schon, 2003; Desquiret-Dumas et al., 2012; Naeem and Sondheimer, 2019; Jackson et al., 2020). Heteroplasmic shifting can be induced at different levels of mitochondrial gene expression, such as the Mito-targeted strategy induces the shift at DNA level while allotopic strategy induces at protein level.

This study compared rescue effects of two gene-therapy strategies—allotopic and mito-targeted—using a LHON mouse model induced by MTSAAV-delivered *hND4G11778A*. RGC function was investigated in response to coarse patterns of high-contrast (0.05 c/deg = 2.77 logMAR) (Yu et al., 2012; Chadderton et al., 2013; Liu et al., 2020) to detect severe visual deficits that are also characteristic of human LHON and potential reversal of visual loss after gene-therapy. We found that both allotopic and mito-targeted gene therapy strategies were effective in improving visual function compared to age-matched unrescued mice. However, the rescue effect of mito-targeted gene therapy appeared to occur earlier than that of allotopic strategy.

Mitochondria retain only a small number of genes, which encode highly hydrophobic proteins throughout evolutionary history (Johnston and Williams, 2016). One of the most common hypotheses about this phenomenon is the difficulty of importing and sorting

those proteins across the mitochondrial membrane if produced remotely (Adams and Palmer, 2003; Allen, 2015; Johnston and Williams, 2016). The allotopic approach delivers the *ND4* gene in standard genetic code into the nucleus and then translocates the expressed ND4 protein from cytosol back to mitochondria. In contrast, mito-targeted strategy delivers *ND4* gene directly inside mitochondria using a mitochondrial targeting AAV (MTSAAV), and the ND4 protein is expressed inside mitochondria, making this strategy more likely to have a higher delivery efficacy and an earlier rescue than the allotopic approach.

The difference in rescue between these two strategies is in agreement with our previous observation. An allotopic test article, produced by the University of Florida, initiated significant rescue 12 months after injection in the same LHON mouse model as in this study (Koilkonda R. et al., 2014). Instead, mito-targeted wildtype ND4 mediated a marked reversal of visual function loss in mutant ND4 transgenic mitomice started from 1 month and sustained up to 12 months after injection (Yu et al., 2018).

Delayed therapeutic effects of the allotopic vector were also evident in the clinical trials for LHON. In the clinical trial we performed, a substantial improvement of > = 15ETDRS (Early Treatment Diabetic Retinopathy Study) letters was noted from 12- to 24-month post-injection (Feuer et al., 2016; Guy et al., 2017; Lam et al., 2022). Similarly, the French Gensight study group reported that a mean (SD) improvement in BCVA of −0.308 (0.068) LogMAR, equivalent to a gain of 15 ETDRS letters for changes from the baseline, was evident at 96 weeks after the treatment with the allotopic expressed ND4 in their phase 3 clinical trial (Yu-Wai-Man et al., 2020; Newman et al., 2021).

Rapid rescue is clinically relevant in treating LHON patients, especially for those who have bilateral simultaneous onset of acute visual loss or unilateral cases with acute visual loss in one eye 6–8 weeks before vision loss in the second eye. Rapid rescue of RGCs using gene therapy might prevent optic nerve degeneration or prevent visual loss in the second eye, even though oxidative injury and apoptosis may already be irreversible at this time. Also, the enhanced survival of RGCs might mediate vision improvement in both eyes as we have observed in the current LHON clinical trials where vision improved bilaterally with unilateral gene therapy injection.

In conclusion, our data shows that the severe visual loss induced by a mitochondrial disease may be reversed for most of the lifespan of laboratory mice using both mito-targeted and allotopic expressed gene therapy. However, mito-targeted therapy likely mediates a quicker and more efficient rescue than the allotopic strategy. This study has certain limitations, such as the experiments were performed in different time periods and under conditions that were similar but not identical, including the test articles that were produced from different facilities. The allotopic vector was made in a GMP lab using two plasmids for the package, while the mito-target vector was produced in a non-GMP lab using five plasmids for the package. This might induce some difference in the titer, purity, and empty/full capsid ratio of the two vectors. Besides, the mouse number, gender, and gene therapy protocols used to rescue the animals were similar within a protocol but not identical among different groups. Further investigations will be needed to confirm the findings. Still, this study provides preliminary experimental evidence supporting mito-targeted gene therapy as a long-term platform for treating human mitochondrial optic neuropathies such as LHON.

Data availability statement

The original contributions presented in this study are included in the article/supplementary material, further inquiries can be directed to the corresponding authors.

Ethics statement

The animal study was reviewed and approved by the Institutional Animal Care and Use Committee, University of Miami.

Author contributions

JG and HY designed the research. SV, T-HC, JE, YL, and HY performed the research. WWH contributed to new reagents/analytic tools. SV, T-HC, VP, and HY analyzed the data. SV, VP, and HY wrote the manuscript. All authors contributed to the article and approved the submitted version.

Funding

This study was supported by the National Eye Institute R01 EY 027414, R01 EY017141, R24 EY028785, and P30 EY014801.

Acknowledgments

We acknowledge the defining contributions of JG (deceased), who invented mito-targeting AAV and LHON gene therapy investigational product (allotopic expression system) and designed the research. His tireless efforts made this study possible. We also gratefully acknowledge Dr. Alfred S. Lewin and Mr. Vince A. Chiodo at the University of Florida for the MTSAAV package and the support of the and National Heart, Lung and Blood Institute's GTRP AAV facility at CHOP in manufacturing the allotopic AAV.

Conflict of interest

The authors declare that the research was conducted in the absence of any commercial or financial relationships that could be construed as a potential conflict of interest.

Publisher's note

References

Adams, K. L., and Palmer, J. D. (2003). Evolution of mitochondrial gene content: gene loss and transfer to the nucleus. *Mol. Phylogenet. Evol.* 29, 380–395. doi: 10.1016/S1055-7903(03)00194-5

Allen, J. F. (2015). Why chloroplasts and mitochondria retain their own genomes and genetic systems: colocation for redox regulation of gene expression. *Proc. Natl. Acad. Sci. U.S.A.* 112, 10231–10238. doi: 10.1073/pnas.1500012112

Artika, I. M. (2020). Allotopic expression of mitochondrial genes: basic strategy and progress. *Genes Dis.* 7, 578–584. doi: 10.1016/j.gendis.2019.08.001

Bacman, S. R., Williams, S. L., Pinto, M., Peralta, S., and Moraes, C. T. (2013). Specific elimination of mutant mitochondrial genomes in patient-derived cells by mitoTALENs. *Nat. Med.* 19, 1111–1113. doi: 10.1038/nm.3261

Baracca, A., Solaini, G., Sgarbi, G., Lenaz, G., Baruzzi, A., Schapira, A. H., et al. (2005). Severe impairment of complex I-driven adenosine triphosphate synthesis in Leber hereditary optic neuropathy cybrids. *Arch. Neurol.* 62, 730–736. doi: 10.1001/archneur.62.5.730

Chadderton, N., Palfi, A., Millington-Ward, S., Gobbo, O., Overlack, N., Carrigan, M., et al. (2013). Intravitreal delivery of AAV-NDI1 provides functional benefit in a murine model of Leber hereditary optic neuropathy. *Eur. J. Hum. Genet.* 21, 62–68. doi: 10.1038/ejhg.2012.112

Chou, T. H., Bohorquez, J., Toft-Nielsen, J., Ozdamar, O., and Porciatti, V. (2014). Robust mouse pattern electroretinograms derived simultaneously from each eye using a common snout electrode. *Invest. Ophthalmol. Vis. Sci.* 55, 2469–2475. doi: 10.1167/iovs.14-13943

Cwerman-Thibault, H., Augustin, S., Ellouze, S., Sahel, J. A., and Corral-Debrinski, M. (2014). Gene therapy for mitochondrial diseases: Leber hereditary optic neuropathy as the first candidate for a clinical trial. *C. R. Biol.* 337, 193–206. doi: 10.1016/j.crvi.2013.11.011

Cwerman-Thibault, H., Augustin, S., Lechauve, C., Ayache, J., Ellouze, S., Sahel, J. A., et al. (2015). Nuclear expression of mitochondrial ND4 leads to the protein assembling in complex I and prevents optic atrophy and visual loss. *Mol. Ther. Methods Clin. Dev.* 2:15003. doi: 10.1038/mtm.2015.3

Desler, C., and Rasmussen, L. J. (2012). Mitochondria in biology and medicine. *Mitochondrion* 12, 472–476. doi: 10.1016/j.mito.2012.06.008

Desquiret-Dumas, V., Gueguen, N., Barth, M., Chevrollier, A., Hancock, S., Wallace, D. C., et al. (2012). Metabolically induced heteroplasmy shifting and l-arginine treatment reduce the energetic defect in a neuronal-like model of MELAS. *Biochim. Biophys. Acta* 1822, 1019–1029. doi: 10.1016/j.bbadis.2012.01.010

DiMauro, S., and Schon, E. A. (2003). Mitochondrial respiratory-chain diseases. *N. Engl. J. Med.* 348, 2656–2668. doi: 10.1056/NEJMra022567

Ellouze, S., Augustin, S., Bouaita, A., Bonnet, C., Simonutti, M., Forster, V., et al. (2008). Optimized allotopic expression of the human mitochondrial ND4 prevents blindness in a rat model of mitochondrial dysfunction. *Am. J. Hum. Genet.* 83, 373–387. doi: 10.1016/j.ajhg.2008.08.013

Falabella, M., Minczuk, M., Hanna, M. G., Viscomi, C., and Pitceathly, R. D. S. (2022). Gene therapy for primary mitochondrial diseases: experimental advances and clinical challenges. *Nat. Rev. Neurol.* 18, 689–698. doi: 10.1038/s41582-022-00715-9

Feuer, W. J., Schiffman, J. C., Davis, J. L., Porciatti, V., Gonzalez, P., Koilkonda, R. D., et al. (2016). Gene therapy for Leber hereditary optic neuropathy: initial results. *Ophthalmology* 123, 558–570. doi: 10.1016/j.ophtha.2015.10.025

Filograna, R., Mennuni, M., Alsina, D., and Larsson, N. G. (2021). Mitochondrial DNA copy number in human disease: the more the better? *FEBS Lett.* 595, 976–1002. doi: 10.1002/1873-3468.14021

Frazier, A. E., Thorburn, D. R., and Compton, A. G. (2019). Mitochondrial energy generation disorders: genes, mechanisms, and clues to pathology. *J. Biol. Chem.* 294, 5386–5395. doi: 10.1074/jbc.R117.809194

Guy, J., Feuer, W. J., Davis, J. L., Porciatti, V., Gonzalez, P. J., Koilkonda, R. D., et al. (2017). Gene therapy for Leber hereditary optic neuropathy: low- and medium-dose visual results. *Ophthalmology* 124, 1621–1634. doi: 10.1016/j.ophtha.2017.05.016

Guy, J., Feuer, W. J., Porciatti, V., Schiffman, J., Abukhalil, F., Vandenbroucke, R., et al. (2014). Retinal ganglion cell dysfunction in asymptomatic G11778A: Leber hereditary optic neuropathy. *Invest. Ophthalmol. Vis. Sci.* 55, 841–848. doi: 10.1167/iovs.13-13365

Guy, J., Qi, X., Pallotti, F., Schon, E. A., Manfredi, G., Carelli, V., et al. (2002). Rescue of a mitochondrial deficiency causing Leber hereditary optic neuropathy. *Ann. Neurol.* 52, 534–542. doi: 10.1002/ana.10354

Jackson, C. B., Turnbull, D. M., Minczuk, M., and Gammage, P. A. (2020). Therapeutic manipulation of mtDNA Heteroplasmy: a shifting perspective. *Trends Mol. Med.* 26, 698–709. doi: 10.1016/j.molmed.2020.02.006

Johnston, I. G., and Williams, B. P. (2016). Evolutionary inference across eukaryotes identifies specific pressures favoring mitochondrial gene retention. *Cell Syst.* 2, 101–111. doi: 10.1016/j.cels.2016.01.013

Kaeppel, C., Beattie, S. G., Fronza, R., van Logtenstein, R., Salmon, F., Schmidt, S., et al. (2013). A largely random AAV integration profile after LPLD gene therapy. *Nat. Med.* 19, 889–891. doi: 10.1038/nm.3230

Karaarslan, C. (2019). Leber's hereditary optic neuropathy as a promising disease for gene therapy development. *Adv. Ther.* 36, 3299–3307. doi: 10.1007/s12325-019-01113-2

Koilkonda, R., Yu, H., Talla, V., Porciatti, V., Feuer, W. J., Hauswirth, W. W., et al. (2014). LHON gene therapy vector prevents visual loss and optic neuropathy induced by G11778A mutant mitochondrial DNA: biodistribution and toxicology profile. *Invest. Ophthalmol. Vis. Sci.* 55, 7739–7753. doi: 10.1167/iovs.14-15388

Koilkonda, R. D., and Guy, J. (2011). Leber's hereditary optic neuropathy-gene therapy: from benchtop to bedside. *J. Ophthalmol.* 2011:179412. doi: 10.1155/2011/179412

Koilkonda, R. D., Yu, H., Chou, T. H., Feuer, W. J., Ruggeri, M., Porciatti, V., et al. (2014). Safety and effects of the vector for the Leber hereditary optic neuropathy gene therapy clinical trial. *JAMA Ophthalmol.* 132, 409–420. doi: 10.1001/jamaophthalmol.2013.7630

Lam, B. L., Feuer, W. J., Davis, J. L., Porciatti, V., Yu, H., Levy, R. B., et al. (2022). Leber hereditary optic neuropathy gene therapy: adverse events and visual acuity results of all patient groups. *Am. J. Ophthalmol.* 241, 262–271. doi: 10.1016/j.ajo.2022.02.023

Liu, H. L., Yuan, J. J., Zhang, Y., Tian, Z., Li, X., Wang, D., et al. (2020). Factors associated with rapid improvement in visual acuity in patients with Leber's hereditary optic neuropathy after gene therapy. *Acta Ophthalmol.* 98, e730–e733. doi: 10.1111/aos.14379

Maul, G. G., Rovera, G., Vorbrodt, A., and Abramczuk, J. (1978). Membrane fusion as a mechanism of simian virus 40 entry into different cellular compartments. *J. Virol.* 28, 936–944. doi: 10.1128/jvi.28.3.936-944.1978

Naeem, M. M., and Sondheimer, N. (2019). Heteroplasmy shifting as therapy for mitochondrial disorders. *Adv. Exp. Med. Biol.* 1158, 257–267. doi: 10.1007/978-981-13-8367-0_14

Newman, N. J., Yu-Wai-Man, P., Carelli, V., Moster, M. L., Biousse, V., Vignal-Clermont, C., et al. (2021). Efficacy and safety of intravitreal gene therapy for Leber hereditary optic neuropathy treated within 6 months of disease onset. *Ophthalmology* 128, 649–660. doi: 10.1016/j.ophtha.2020.12.012

Oca-Cossio, J., Kenyon, L., Hao, H., and Moraes, C. T. (2003). Limitations of allotopic expression of mitochondrial genes in mammalian cells. *Genetics* 165, 707–720. doi: 10.1093/genetics/165.2.707

Perales-Clemente, E., Fernandez-Silva, P., Acin-Perez, R., Perez-Martos, A., and Enriquez, J. A. (2011). Allotopic expression of mitochondrial-encoded genes in mammals: achieved goal, undemonstrated mechanism or impossible task? *Nucleic Acids Res.* 39, 225–234. doi: 10.1093/nar/gkq769

Qi, X., Sun, L., Lewin, A. S., Hauswirth, W. W., and Guy, J. (2007). The mutant human ND4 subunit of complex I induces optic neuropathy in the mouse. *Invest. Ophthalmol. Vis. Sci.* 48, 1–10. doi: 10.1167/iovs.06-0789

Rossignol, R., Faustin, B., Rocher, C., Malgat, M., Mazat, J. P., and Letellier, T. (2003). Mitochondrial threshold effects. *Biochem. J.* 370, 751–762. doi: 10.1042/bj20021594

Sadun, A. A., Win, P. H., Ross-Cisneros, F. N., Walker, S. O., and Carelli, V. (2000). Leber's hereditary optic neuropathy differentially affects smaller axons in the optic nerve. *Trans. Am. Ophthalmol. Soc.* 98, 223–232.

Shoffner, J. M., Lott, M. T., Lezza, A. M., Seibel, P., Ballinger, S. W., and Wallace, D. C. (1990). Myoclonic epilepsy and ragged-red fiber disease (MERRF) is associated with a mitochondrial DNA tRNA(Lys) mutation. *Cell* 61, 931–937. doi: 10.1016/0092-8674(90)90059-N

Yu, H., Koilkonda, R. D., Chou, T. H., Porciatti, V., Ozdemir, S. S., Chiodo, V., et al. (2012). Gene delivery to mitochondria by targeting modified adenoassociated virus suppresses Leber's hereditary optic neuropathy in a mouse model. *Proc. Natl. Acad. Sci. U.S.A.* 109, E1238–E1247. doi: 10.1073/pnas.1119577109

Yu, H., Porciatti, V., Lewin, A., Hauswirth, W., and Guy, J. (2018). Longterm reversal of severe visual loss by mitochondrial gene transfer in a mouse model of Leber hereditary optic neuropathy. *Sci. Rep.* 8:5587. doi: 10.1038/s41598-018-23836-y

Yuan, J., Zhang, Y., Liu, H., Wang, D., Du, Y., Tian, Z., et al. (2020). Seven-year follow-up of gene therapy for Leber's hereditary optic neuropathy. *Ophthalmology* 27, 1125–1127. doi: 10.1016/j.ophtha.2020.02.023

Yu-Wai-Man, P., and Chinnery, P. F. (1993). "Leber hereditary optic neuropathy," in *GeneReviews (®)* (Seattle, WA: University of Washington, Seattle).

Yu-Wai-Man, P., Newman, N. J., Carelli, V., Moster, M. L., Biousse, V., Sadun, A. A., et al. (2020). Bilateral visual improvement with unilateral gene therapy injection for Leber hereditary optic neuropathy. *Sci. Transl. Med.* 12:eaaz7423. doi: 10.1126/scitranslmed.aaz7423

Zuccarelli, M., Vella-Szijj, J., Serracino-Inglott, A., and Borg, J. J. (2020). Treatment of Leber's hereditary optic neuropathy: an overview of recent developments. *Eur. J. Ophthalmol.* 30, 1220–1227. doi: 10.1177/1120672120936592

frontiers | Frontiers in Neuroscience

TYPE Review
PUBLISHED 03 April 2023
DOI 10.3389/fnins.2023.1132179

OPEN ACCESS

EDITED BY
Hetian Lei,
Shenzhen Eye Hospital,
China

REVIEWED BY
Xue Feng,
Beijing Jishuitan Hospital,
China
Xinhua Shu,
Glasgow Caledonian University,
United Kingdom
Valentin Gordeliy,
UMR5075 Institut de Biologie Structurale (IBS),
France
Paul Park,
Case Western Reserve University,
United States

*CORRESPONDENCE
Shuqian Dong
✉ dongshuqian2006@163.com
Houbin Zhang
✉ houbin_zhang@yahoo.com

†These authors have contributed equally to this work

SPECIALTY SECTION
This article was submitted to Visual Neuroscience, a section of the journal Frontiers in Neuroscience

RECEIVED 27 December 2022
ACCEPTED 13 March 2023
PUBLISHED 03 April 2023

CITATION
Zhen F, Zou T, Wang T, Zhou Y, Dong S and Zhang H (2023) Rhodopsin-associated retinal dystrophy: Disease mechanisms and therapeutic strategies.
Front. Neurosci. 17:1132179.
doi: 10.3389/fnins.2023.1132179

Rhodopsin-associated retinal dystrophy: Disease mechanisms and therapeutic strategies

Fangyuan Zhen[1,2†], Tongdan Zou[2†], Ting Wang[2], Yongwei Zhou[1], Shuqian Dong[1*] and Houbin Zhang[2,3*]

[1]Department of Ophthalmology, The First Affiliated Hospital of Zhengzhou University, Henan Provincial Ophthalmic Hospital, Zhengzhou, China, [2]The Key Laboratory for Human Disease Gene Study of Sichuan Province and Institute of Laboratory Medicine, Sichuan Provincial People's Hospital, University of Electronic Science and Technology of China, Chengdu, Sichuan, China, [3]Research Unit for Blindness Prevention, Chinese Academy of Medical Sciences (2019RU026), Sichuan Academy of Medical Sciences and Sichuan Provincial People's Hospital, Chengdu, Sichuan, China

Rhodopsin is a light-sensitive G protein-coupled receptor that initiates the phototransduction cascade in rod photoreceptors. Mutations in the rhodopsin-encoding gene *RHO* are the leading cause of autosomal dominant retinitis pigmentosa (ADRP). To date, more than 200 mutations have been identified in *RHO*. The high allelic heterogeneity of *RHO* mutations suggests complicated pathogenic mechanisms. Here, we discuss representative *RHO* mutations as examples to briefly summarize the mechanisms underlying rhodopsin-related retinal dystrophy, which include but are not limited to endoplasmic reticulum stress and calcium ion dysregulation resulting from protein misfolding, mistrafficking, and malfunction. Based on recent advances in our understanding of disease mechanisms, various treatment methods, including adaptation, whole-eye electrical stimulation, and small molecular compounds, have been developed. Additionally, innovative therapeutic treatment strategies, such as antisense oligonucleotide therapy, gene therapy, optogenetic therapy, and stem cell therapy, have achieved promising outcomes in preclinical disease models of rhodopsin mutations. Successful translation of these treatment strategies may effectively ameliorate, prevent or rescue vision loss related to rhodopsin mutations.

KEYWORDS

rhodopsin, retinitis pigmentosa, retinal degeneration, gene therapy, stem cell therapy

1. Introduction

Photoreceptors are the cells in the retina where light signals are converted to neural visual signals through the phototransduction cascade. The human retina contains two types of photoreceptors: rods and cones (Molday and Moritz, 2015). Rods account for 95% of all photoreceptors, and cones account for the remaining 5% (Molday and Moritz, 2015).

Rods are distinct from cones in structure and function. Rods expressing rhodopsin that are highly sensitive to light are responsible for scotopic vision, whereas cones contain cone opsins and are responsible for photopic vision and color vision. The loss of rods, cones or both in the retina causes devastating vision disorders that are collectively called retinal degeneration. Retinitis pigmentosa (RP) is the most common inherited retinal disorder, affecting 1/3,000 to 1/4,000 individuals worldwide (Hartong et al., 2006; Zhang, 2016; Perea-Romero et al., 2021). RP affects rod cell function and peripheral vision at the beginning of the disease. The patients

experience night blindness. As the disease progresses, it also affects cones and impairs central vision. The patients develop tunnel vision and may become completely blind at its advanced stage. To date, over 70 genes have been identified to cause nonsyndromic RP that does not affect other organs or tissues (RetNet[1]). RP can be inherited in an autosomal dominant, autosomal recessive, or X-linked manner. Although rare, RP can also be inherited in mitochondrial or digenic forms (Kim et al., 2012; Wu et al., 2014; Zhang, 2016; Wu et al., 2019). This review aims to summarize the progress in studies on the mechanism and therapy for retinal disorders related to rhodopsin mutations, including RP and CSNB.

In rod photoreceptors, rhodopsin, a visual pigment, is formed by the conjugation of 11-*cis*-retinaldehyde to opsin proteins. Rhodopsin belongs to the G protein-coupled receptor family, and its activation initiates the very first step of phototransduction in rod photoreceptors upon the absorption of photons. Rhodopsin is synthesized in the inner segment of the rod and then processed and transported to the outer segment (Athanasiou et al., 2018). The capture of the photon by the chromophore in rhodopsin causes the isomerization of 11-*cis*-retinaldehyde to all-trans-retinaldehyde and a conformational change in the protein, leading to the activation of the downstream phototransduction cascade, which occurs within the photoreceptor outer segment.

The *RHO* gene, encoding the opsin protein and mapped to the long arm of chromosome 3 at 3q22.1, consists of 5 exons. The open reading frame is composed of nucleotides encoding 348 amino acid residues with a calculated molecular weight of ~39 kDa (Rosenfeld et al., 1992; Athanasiou et al., 2018). Rhodopsin constitutes ~85% of the protein mass of rod outer segment plasma membranes (Palczewski, 2014). As the most abundant protein in photoreceptors, rhodopsin is densely packed on the disc membrane (Molday and Moritz, 2015). Atomic force microscopy (AFM) and cryo-electron tomography has revealed that rhodopsin is organized in the disc membrane *via* a four-tier hierarchy—monomers, dimers, rows of dimers, and row pairs—which is critical for outer segment morphogenesis (Fotiadis et al., 2003; Gunkel et al., 2015; Ploier et al., 2016). Approximately half of the surface of each disc is occupied by rhodopsin, with the remainder filled mostly with lipids, cholesterol, and less abundant proteins (Palczewski, 2014; Molday and Moritz, 2015; Athanasiou et al., 2017).

Rhodopsin is irreplaceable and vital in the process of vision; one small mistake in the process of gene transcription, translation, folding processing, or delivery to designated places may lead to vision damage. Mutations in rhodopsin are the most common cause of autosomal dominant retinitis pigmentosa (ADRP; Wilson and Wensel, 2003; Malanson and Lem, 2009; Ferrari et al., 2011; Athanasiou et al., 2017). While about 20–30% of RP cases are ADRP (Daiger et al., 2014), *RHO* mutations account for 30–40% of ADRP cases. Although uncommon, rhodopsin mutations may cause dominant congenital stationary night blindness (CSNB; Singhal et al., 2013) and recessive RP (Kumaramanickavel et al., 1994; Kartasasmita et al., 2011). Over 200 mutations in *RHO*, including over 170 missense and nonsense mutations, have been associated with RP[2] (Table 1). These mutations, varying from point mutations, insertions, and deletions to complex rearrangements, impair rhodopsin functions, ultimately leading to RP or CSNB symptoms through a variety of mechanisms, some of which will be described in detail in the following paragraphs. While the mechanisms underlying rhodopsin-related retinal dystrophy have been systemically reviewed previously (Athanasiou et al., 2018), here, we focus more on well-studies mechanisms that have been utilized for the development of potential therapeutic approaches. This review also integrates and updates the information on pharmacological intervention, optogenetics, gene therapy and gene editing, and stem cell therapy for rhodopsin-related retinal disorders that were reviewed previously (Athanasiou et al., 2018; Ikelle et al., 2020; Meng et al., 2020; Ortega and Jastrzebska, 2021; Piri et al., 2021; Ortega and Jastrzebska, 2022). Many of these therapeutical approaches are not gene-specific and can be also applied to retinal degeneration caused by other gene mutations.

2. Mechanisms of rhodopsin-related retinal disorders

Since the first rhodopsin mutation was identified in RP patients (Dryja et al., 1990), tremendous progress has been made toward understanding the mechanisms of retinal degeneration arising from rhodopsin mutations. Rhodopsin mutants exhibit a range of deficiencies in the 11-*cis*-retinaldehyde interaction (Liu et al., 1996; Iannaccone et al., 2006; Gragg and Park, 2018). There are two classes of rhodopsin mutations that have been designated based on their ability to bind the chromophore 11-*cis*-retinaldehyde when they are expressed in cultured cells (Kaushal and Khorana, 1994; Woods and Pfeffer, 2020). Class I mutants can reconstitute with 11-*cis*-retinaldehyde to form normal rhodopsin and are transported to the cell surface. Class II mutants are localized in the ER and cannot reconstitute with 11-*cis*-retinaldehyde to form functional rhodopsin, or binds 11-*cis*-retinaldehyde poorly. Rhodopsin mutations may cause protein misfolding and ER retention, mistrafficking, altered post-translational modifications and reduced stability, and constitutive action, which lead to photoreceptor death or dysfunction through divergent mechanisms. Dominant rhodopsin mutations with known features have been categorized into seven groups (Athanasiou et al., 2018). The following are the pathogenic mechanisms for representative rhodopsin mutations from four different groups whose mechanisms have been relatively well studied, including protein misfolding and ER retention (P23H), altered post-translational modifications and reduced stability (T17M), mistrafficking (Q344ter), and constitutive activation (G90D). More systemic description of these mechanisms can be found in a previous review (Athanasiou et al., 2018).

2.1. P23H

P23H, the first mutation reported in ADRP (Dryja et al., 1991), is the most common mutation found in rhodopsin in the United States (Wu et al., 2019; Woods and Pfeffer, 2020). P23H rhodopsin is a typical example of a class II mutation.

The pathogenesis of the P23H mutation has been extensively studied in a variety of animal models and *in vitro* cultured cells. The P23H mutation affects the adjacent H-bonding network in the chromophore binding region critical for the activity of the

1 https://sph.uth.edu/retnet

2 https://www.hgmd.cf.ac.uk/ac/

10.3389/fnins.2023.1132179

TABLE 1 Identified missense and nonsense mutations in rhodopsin.

Mutant	Codon change	a.a change	Codon number	Mutant	Codon change	a.a change	Codon number
T4K	ACR-AAA	Thr-Lys	4	G106W	GGG-TGG	Gly-Trp	106
P12R	CCC-CGC	Pro-Arg	12	G109R	GGA-AGA	Gly-Arg	109
N15S	AAT-AGT	Asn-Ser	15	C110R	TGC-CGC	Cys-Arg	110
T17M	ACG-ATG	Thr-Met	17	C110Y	TGC-TAC	Cys-Tyr	110
G18D	GGT-GRT	Gly-Asp	18	C110S	TGC-TCC	Cys-Ser	110
V20G	GTR-GGA	Val-Gly	20	C110F	TGC-TTC	Cys-Phe	110
R21C	CGC-TGC	Arg-Cys	21	E113K	GAG-AAG	Glu-Lys	113
P23H	CCC-CAC	Pro-His	23	G114D	GGC-GAC	Gly-Asp	114
P23L	CCC-CTC	Pro-Leu	23	G114V	GGC-GTC	Gly-Val	114
P23A	CCC-GCC	Pro-Ala	23	E122G	GAA-GGR	Glu-Gly	122
Q28H	CAG-CAC	Gln-His	28	L125R	CTG-CGG	Leu-Arg	125
Q28H	CAG-CAT	Gln-His	28	W126Ter	TGG-TGA	Trp-Term	126
Q28R	CAG-CGG	Gln-Arg	28	W126L	TGG-TTG	Trp-Leu	126
M39R	ATG-AGG	Met-Arg	39	S127F	TCC-TTC	Ser-Phe	127
L40R	CTG-CGG	Leu-Arg	40	L131P	CTG-CCG	Leu-Pro	131
M44T	ATG-ACG	Met-Thr	44	R135P	CGG-CCG	Arg-Pro	135
F45L	TTT-CTT	Phe-Leu	45	R135L	CGG-CTG	Arg-leu	135
L46R	CTG-CGG	Leu-Arg	46	R135G	CGG-GCG	Arg-Gly	135
L47R	CTG-CGG	Leu-Arg	47	R135W	CGG-TGG	Arg-Trp	135
G51R	GGC-CGC	Gly-Arg	51	Y136Ter	TAC-TAA	Tyr-Term	136
G51A	GGC-GCC	Gly-Ala	51	V137M	GTG-ATG	Val-Met	137
G51V	GGC-GTC	Gly-Val	51	C140S	TGT-TCT	Cys-Ser	140
F52V	TTC-GTC	Phe-Val	52	R147C	CGC-TGC	Arg-Cys	147
F52Y	TTC-TAC	Phe-Tyr	52	Q150K	GAG-AAG	Glu-Lys	150
P53R	CCC-CGC	Pro-Arg	53	T160T	ACC-ACA	Thr-Thr	160
F56Y	TTC-TAC	Phe-Tyr	56	W161R	TGG-CGG	Trp-Arg	161
L57R	CTC-CGC	Leu-Arg	57	W161Ter	TGG-TAG	Trp-Term	161
T58R	ACG-AGG	Thr-Arg	58	M163T	ATG-ACG	Met-Thr	163
T58M	ACG-ATG	Thr-Met	58	A164E	GCG-GAG	Ala-Glu	164
Y60Ter	TAC-TAA	Tyr-Ter	60	A164V	GCG-GTG	Ala-Val	164
Q64Ter	CAG-TAG	Gln-Ter	64	C167R	TGC-CGC	Cys-Arg	167
R69H	CGC-CAC	Arg-His	69	C167Y	TGC-TAC	Cys-Tyr	167
N78I	AAC-ATC	Asn-Ile	78	C167W	TGC-TGG	Cys-Trp	167
L79P	CTR-CCR	Leu-Pro	79	A169P	GCA-CCA	Ala-Pro	169
V87L	GTC-CTC	Val-Leu	87	P170H	CCC-CAC	Pro-His	170
V87D	GTC-GAC	Val-Asp	87	P170R	CCC-CGC	Pro-Arg	170
L88P	CTA-CCR	Leu-Pro	88	P171Q	CCA-CAA	Pro-Gln	171
G89R	GGT-CGT	Gly-Arg	89	P171L	CCA-CTA	Pro-Leu	171
G89D	GGT-GAT	Gly-Asp	89	P171S	CCA-TCA	Pro-Ser	171
G90D	GGC-GAC	Gly-Asp	90	G174S	GGC-AGC	Gly-Ser	174
G90V	GGC-GTC	Gly-Val	90	S176F	TCC-TTC	Ser-Phe	176
T92I	ACC-ATC	Thr-Ile	92	Y178N	TAC-AAC	Tyr-Asn	178
T94I	ACC-ATC	Thr-Ile	94	Y178D	TAC-GAC	Tyr-Asp	178

(Continued)

TABLE 1 (Continued)

Mutant	Codon change	a.a change	Codon number	Mutant	Codon change	a.a change	Codon number
T97I	ACC-ATC	Thr-Ile	97	Y178C	TAC-TGC	Tyr-Cys	178
G101E	GGA-GAA	Gly-Glu	101	I179F	ATC-TTC	Ile-Phe	179
G101V	GGA-GTR	Gly-Val	101	P180A	CCC-GCC	Pro-Ala	180
V104I	GTC-ATC	Val-Ile	104	P180S	CCC-TCC	Pro-Ser	180
V104F	GTC-TTC	Val-Phe	104	E181K	GAG-AAG	Glu-Lys	181
G106R	GGG-AGG	Gly-Arg	106	G182S	GGC-AGC	Gly-Ser	182
G182V	GGC-GTC	Gly-Val	182	P291R	CCA-CGA	Pro-Arg	291
Q184P	CAG-CCG	Gln-Pro	184	A292T	GCG-ACG	Ala-Thr	292
C185R	TGC-CGC	Cys-Arg	185	A292E	GCG-GAG	Ala-Glu	292
S186P	TCG-CCG	Ser-Pro	186	A295V	GCC-GTC	Ala-Val	295
S186W	TCG-TGG	Ser-Trp	186	K296N	AAG-AAT	Lys-Asn	296
C187R	TGT-CGT	Cys-Arg	187	K296M	AAG-ATG	Lys-Met	296
C187G	TGT-GGT	Cys-Gly	187	K296E	AAG-GAG	Lys-Glu	296
C187Y	TGT-TAT	Cys-Tyr	187	S297R	AGC-AGA	Ser-Arg	297
G188R	GGA-AGA	Gly-Arg	188	A298D	GCC-GAC	Ala-Asp	298
G188E	GGA-GAA	Gly-Glu	188	A299T	GCC-AAC	Ala-Thr	299
D190N	GAC-AAC	Asp-Asn	190	V304D	GTC-GAC	Val-Asp	304
D190G	GAC-GGC	Asp-Gly	190	K311E	AAG-GAG	Lys-Glu	311
D190Y	GAC-TAC	Asp-Tyr	190	Q312Ter	CAG-TAG	Gln-Term	312
Y191C	TAC-TGC	Tyr-Cys	191	N315K	AAC-AAG	Asn-Lys	315
T193M	ACG-ATG	Thr-Met	193	T320N	ACC-AAC	Thr-Asn	320
N200K	AAC-AAG	Asn-Lys	200	L328P	CTG-CCG	Leu-Pro	328
F203S	TTT-TCT	Phe-Ser	203	A333V	GCC-GTC	Ala-Val	333
M207K	ATG-AAG	Met-Lys	207	T340M	ACG-ATG	Thr-Met	340
M207R	ATG-AGG	Met-Arg	207	E341K	GAG-AAG	Glu-Lys	341
V209M	GTG-ATG	Val-Met	209	E341Ter	GAG-TAG	Glu-Ter	341
V210F	GTC-TTC	Val-Phe	210	T2342M	ACG-ATG	Thr-Met	342
H211P	CAC-CCC	His-Pro	211	S343N	AGC-AAC	Ser-Asn	343
H211R	CAC-CGC	His-Arg	211	S343C	AGC-TGC	Ser-Cys	343
H211L	CAC-CTC	His-Leu	211	Q344P	CAG-CCG	Gln-Pro	344
I214N	ATC-AAC	Ile-Asn	214	Q344R	CAG-CGG	Gln-Arg	344
P215T	CCC-ACC	Pro-Thr	215	Q344Ter	CAG-TAG	Gln-Term	344
P215L	CCC-CTC	Pro-Leu	215	V345M	GTG-ATG	Val-Met	345
M216K	ATG-AAG	Met-Lys	216	V345L	GTG-CTG	Val-Leu	345
M216R	ATG-AGG	Met-Arg	216	V345G	GTG-GGG	Val-Gly	345
M216L	ATG-TTG	Met-Leu	216	V345L	GTG-TTG	Val-Leu	345
F220C	TTT-TGT	Phe-Cys	220	A346P	GCC-CCC	Ala-Pro	346
C222R	TGC-CGC	Cys-Arg	222	P347T	CCG-ACG	Pro-Thr	347
E249Ter	GAG-TAG	Glu-Term	249	P347Q	CCG-CAG	Pro-Gln	347
R252P	CGC-CCC	Arg-Pro	252	P347R	CCG-CGG	Pro-Arg	347
M253I	ATG-ATT	Met-Ile	253	P347L	CCG-CTG	Pro-Leu	347
P267R	CCC-CGC	Pro-Arg	267	P347A	CCG-GCG	Pro-Ala	347
P267L	CCC-CTC	Pro-Leu	267	P347S	CCG-TCG	Pro-Ser	347

(Continued)

TABLE 1 (Continued)

Mutant	Codon change	a.a change	Codon number	Mutant	Codon change	a.a change	Codon number
S270R	AGC-AGA	Ser-Arg	270	Ter349Q	TAA-CAA	Term-Gln	349
G284S	GGT-AGT	Gly-Ser	284	Ter349E	TAA-GAA	Term-Glu	349
T289P	ACC-CCC	Thr-Pro	289				

a.a: amino acid.

chromophore in rhodopsin expressed cultured HEK293 cells (Woods and Pfeffer, 2020). Additionally, it also alters the overall structure and activity of rhodopsin (Woods and Pfeffer, 2020). The monomer of mutant P23H is not functional, and it is unstable by itself and tends to adopt a specific homodimer arrangement (Woods and Pfeffer, 2020). P23H also exerts a destructive effect on disk membranes—likely through a homodimerization process—even at very low concentrations (Woods and Pfeffer, 2020). Another proposed possible pathogenic mechanism is related to activation of the UPR resulting from misfolding of the mutant protein as demonstrated in culture cells and transgenic mice (Frederick et al., 2001; Lin et al., 2007). UPR-mediated endoplasmic reticulum stress (ERS) triggers Ca^{2+} release from the ER, leading to activation of calpains and caspase-12 (Kitamura, 2008; Choudhury et al., 2013). Activated calpain can cleave the mitochondrial protein AIF (apoptosis-inducing factor), promoting AIF exit from the mitochondria through a pore formed by BAX and translocation into the nucleus, where AIF recruits cyclophilin A for chromatin condensation and fragmentation (Candé et al., 2004; Moubarak et al., 2007). AIF has been demonstrated to be present in the nuclei of most dying photoreceptor cells in P23H transgenic and knock-in mouse models (Comitato et al., 2016, 2020). Blocking calpain activity effectively protects the retina from degeneration in P23H knock-in mice (Comitato et al., 2020), suggesting calpain activation as one of the major causes of P23H mutant rhodopsin-induced photoreceptor degeneration.

2.2. T17M

The T17M mutation in *RHO* results in methionine replacing threonine at position 17 (Choudhury et al., 2013). This mutation is another class II mutantion that causes rhodopsin protein msifolding (Krebs et al., 2010), as described above. The mutation affects the binding of opsin proteins to 11-*cis*-retinaldehyde, resulting in ADRP (Li et al., 1998; Mendes et al., 2005; Krebs et al., 2010; Choudhury et al., 2013). The T17M rhodopsin mutant expressed in cultured cells is abnormally mislocalized in the endoplasmic reticulum (Li et al., 1998; Krebs et al., 2010; Jiang et al., 2014), with no colocalization with the Golgi apparatus as normal rhodopsin (Deretic and Papermaster, 1991), which may activate UPR and upregulating ERS-related proteins, such as BIP, GRP94, CHOP, peIF-2a/eIF-2a, and activating ATF-6a (Baumeister et al., 2005; Wang et al., 2009). Upregulation of ERS-related genes has been documented in the retina of T17M transgenic mice (Kunte et al., 2012). *In vitro* evidence suggests the mutant protein is unstable and susceptible to degradation by the proteasome system (Jiang et al., 2014). The demise of photoreceptors caused by T17M is partially attributed to the activation of caspase-7. Ablation of the gene encoding caspase-7 protects photoreceptors in T17M transgenic mice, likely through UPR reprogramming and inhibition of TRAF2-JNK apoptosis (Choudhury et al., 2013).

ROS are also suggested to play an important role in T17M-related retinal degeneration. ROS are the byproducts of aerobic metabolism, including oxygen ions, peroxides, and oxygen-containing free radicals (Jiang et al., 2014). High levels of ROS may damage lipids, proteins, and nucleic acids and affect the functions of organelles (Halliwell, 2011). Mitochondria are the main source of ROS. Increased ROS levels have been observed in cells expressing mutant T17M rhodopsin (Jiang et al., 2014), as ERS promotes chaperone activities that require more energy. Treatment of cells expressing T17M rhodopsin with ROS scavengers reduces cell death.

2.3. G90D

The G90D mutation, which is due to the substitution of aspartic acid for glycine at position 90 in rhodopsin, destabilizes a crucial ionic bond between E113 and K296 (Singhal et al., 2013; Silverman et al., 2020). *In vitro* data suggest that the G90D mutant belongs to a group of constitutively active mutants (including K29E) that can activate transducin in the dark (Rao et al., 1994; Robinson et al., 1994; Toledo et al., 2011; Park, 2014), resulting in a light-adapted state and the desensitization of rod photoreceptor cells in the dark (Sieving et al., 2001; Jin et al., 2003; Naash et al., 2004; Dizhoor et al., 2008). The mutation of neutral G to charged D alters the water-mediated H-bond network at the Schiff base region of the chromophore and the central transmembrane region, which may cause slow binding of the chromophore during pigment regeneration and constitutive activation of transducin (Rao et al., 1994; Gross et al., 2003). Persistent rhodopsin activation can cause retinal degeneration in both a transducin-dependent manner and a transducin-independent manner (Hao et al., 2002). Earlier studies showed that mutation of this gene causes congenital night blindness (Dizhoor et al., 2008). Patients with the G90D mutation have shown decreased light sensitivity of rod cells and night vision dysfunction. Most patients with the G90D mutation express normal amounts of rhodopsin, and the structure of the rods is well preserved (Sieving et al., 1995), while others exhibit the typical RP manifestation, in which the loss of rods is accompanied by the subsequent death of the cone cells and blindness (Berson, 1993). A cohort study comprised of 15 patients showed that 20 and 53.3% of patients with the G90D mutation displayed CSNB and classic RP, respectively, with no obvious sex differences (Kobal et al., 2021). Recently, slow retinal degeneration was also found in homozygous G90D transgenic mice (Colozo et al., 2020). From this point of view, the human G90D mutation may be right at the boundary between dysfunction and degenerative disease, providing an opportunity to

further explore the mechanism by which the spontaneous activation of the visual transduction cascade leads to rod structure damage and cell death (Dizhoor et al., 2008).

2.4. Q344ter

The Q344ter mutation in rhodopsin causes the glutamine-encoding codon 344 to be replaced by a stop codon, resulting in early termination of the polypeptide and loss of the signature C-terminal motif sequence QVAPA. Rhodopsin is synthesized in the rough ER of the inner segment, processed by the Golgi apparatus, and then transported across the connecting cilium to the outer segment where phototransduction occurs. The C-terminal motif of rhodopsin is sufficient and necessary for rhodopsin to be correctly transported to outer segments. It has been shown that the carboxy-terminal cytoplasmic tail of the rhodopsin protein is involved in the post-Golgi transport of rhodopsin (Sung and Tai, 1999). The Q334Ter mutant expressed in transgenic animal models is mislocalized to the plasma membrane of the inner segments and subsequently translocated to the lysosome for degradation (Ropelewski and Imanishi, 2019). Degradation of mislocalized mutant rhodopsin causes disruption of plasma membrane protein homeostasis and downregulation of the sodium-potassium ATPase α-subunit (NKA). Compromised NKAα function is sufficient to cause shortening and loss of rod outer segments, which may underpin the mechanism of retinal degeneration related to the Q334Ter mutation (Ropelewski and Imanishi, 2019). A recent transcriptomic analysis of retinas from Q334Ter knock-in mice revealed alterations in the expression of chromatin complex genes such as histone genes (Bales et al., 2018). A more recent study showed that the upregulation of proinflammatory cytokines and pathways is involved the pathogenesis of retinal degeneration in this knock-in mouse model (Hollingsworth et al., 2021).

These mechanisms represent a summary of representative pathogenesis related to rhodopsin mutations (Figure 1). Information for the mechanisms associated with other types of rhodopsin mutation can be found in several great earlier reviews (Athanasiou et al., 2018). Given the complexity of the interaction between all physiological processes and the wide spectrum of rhodopsin mutations, as well as the unique genetic background of each individual, we are still far from a complete understanding of these pathogenic mechanisms.

3. Strategies for therapy of rhodopsin-related retinal disorders

RP-related rhodopsin mutations are highly heterogeneous, with over 200 mutations identified (Loewen et al., 2020). Conventional treatments have little effect in terms of the cure and prevention of retinal degeneration as a result of the wide spectrum of rhodopsin mutations. In the past two decades, enormous efforts have been directed toward developing innovative treatment methods or drugs to protect vision from retinal degeneration caused by RP, particularly rhodopsin mutations. Here, we summarize the developed strategies that potentially delay the degeneration of retinal photoreceptor cells and preserve vision (Figure 2). Some of these strategies, such as gene therapy and stem cell therapy, can be applied to RP caused by mutations in genes other than *RHO*.

3.1. Whole-eye electrical stimulation

Electrical stimulation therapy (EST), as a classic physical therapy, can improve muscle and nerve function. As early as the 19th century, the rehabilitative effects of electrical stimulation on the eyes were observed (Dor, 1873). The administration of low-level electric current by various approaches has been demonstrated to improve visual function, validating the feasibility of this therapeutic strategy in the treatment of eye diseases (Hanif et al., 2016). Using methods such as subretinal implants or transcorneal electrical stimulation (TES), low-level electrical stimulation of the eye has been shown to have neuroprotective effects on retinal degeneration in humans and animal subjects (Ciavatta et al., 2013; Hanif et al., 2016; Yu et al., 2020).

RHO P23H transgenic rats receiving 30 min of low-level electrical stimulation at a frequency of twice a week (4 μA at 5 Hz; $n = 10$) from 4 to 24 weeks of age exhibited significant improvements in visual function, as exemplified by better responses in the electroretinography (ERG) test (Hanif et al., 2016). The underlying mechanism could be due to increased expression of neuroprotective factors, such as ciliary nerve trophic factor (CNTF) and brain-derived neurotrophic factor (BDNF), in Müller cells (MCs; Ferrari et al., 2011; Gall et al., 2011; Hanif et al., 2016). Transcorneal electrical stimulation therapy in 21 patients with RP showed that TES might cause trivial symptoms such as foreign body sensation, burning, and itching, which, however, were mild and controllable (Demir et al., 2022). In the future, EST can be combined with other treatment methods to increase its efficacy.

3.2. Pharmacological therapy

Pharmacological compounds are often used to alleviate or treat various types of RP due to their various beneficial factors, such as their wide variety and easy availability. Several types of pharmacological compounds have been experimentally and clinically tested to treat retinal dystrophies caused by rhodopsin mutations.

3.2.1. Flavonoids

GPCR activities can be modulated by exogenous or endogenous molecules. Flavonoids are functional modifiers that can alter conformation and strengthen the expression of visual receptors (Ortega et al., 2019, 2021). Flavonoids are a group of yellow pigments with flavonoids (2-phenylchromones) as the parent compound, including isomers of flavonoids and their hydrogenated reduction products. Flavonoids are commonly found in fruits and vegetables. Due to their antioxidant, anti-inflammatory, and anti-apoptotic properties, flavonoids have been documented to improve vision in various ophthalmic diseases (Majumdar and Srirangam, 2010; Ortega et al., 2019). They also help stabilize ligand-free opsin, which promotes retinal degeneration when present in excess in the retina (Ortega et al., 2021). The binding of flavonoids to the P23H mutant rhodopsin changes the protein conformation and partially restores its intracellular transport, which slows photoreceptor degeneration in a mouse model (Ortega et al., 2019, 2022). The flavonoid quercetin can

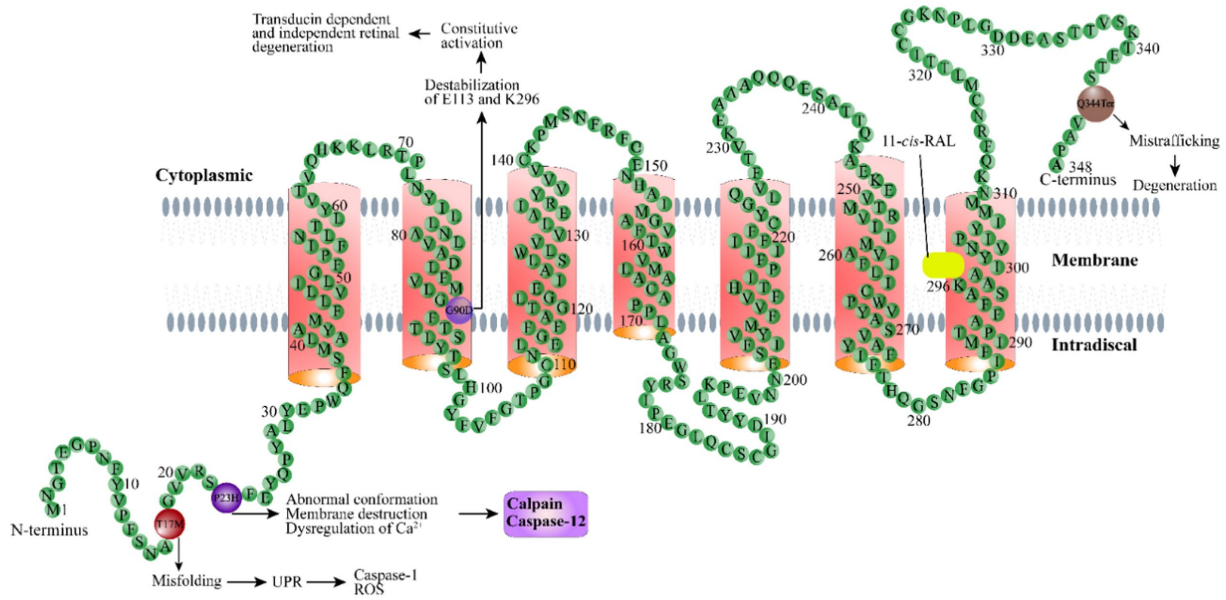

FIGURE 1
Schematic illustration of the rhodopsin structure. Rhodopsin is a G protein-coupled receptor with seven typical transmembrane domains. Representative rhodopsin mutations, including T17M, P23H, G90D, and Q344Ter, as well as the disease mechanisms related to these mutations, are shown. 11-*cis*-RAL: 11-*cis*-retinaldehyde.

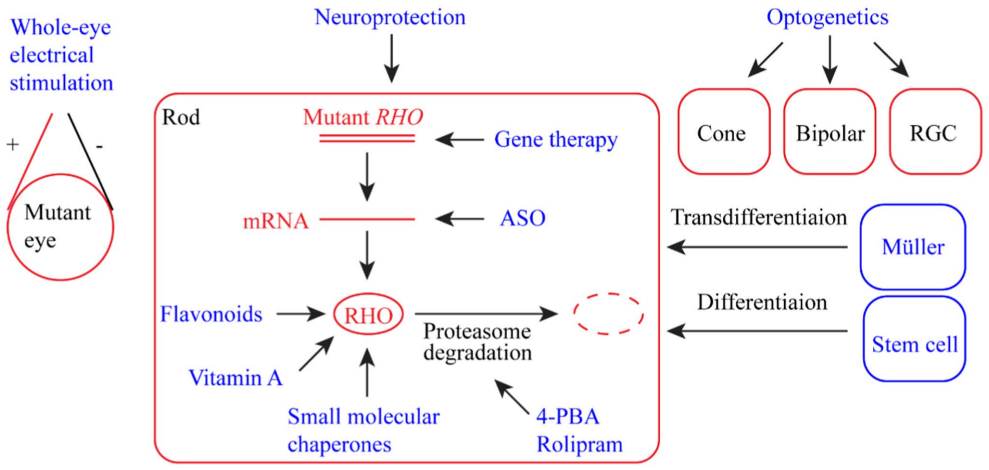

FIGURE 2
Summary of therapeutic strategies for retinal dystrophy (RD) associated with rhodopsin mutations. The strategies include whole-eye electric stimulation, pharmacological therapy (flavonoids, vitamin A, small molecular chaperones, 4-PBA (4-phenyl butyric acid), and rolipram), ASO (antisense oligonucleotide) therapy, gene therapy, neuroprotection, optogenetic therapy, and stem cell therapy (including photoreceptor regeneration from Müller cells).

allosterically modulate opsin regenerated with 9-*cis*-retinaldehyde and enhance the stability and conformational properties of the G90V mutant (Herrera-Hernandez et al., 2017). Therefore, flavonoids can potentially be used as primary compounds to design nonretinoids for the treatment of retinal degeneration associated with rhodopsin mutations (Herrera-Hernandez et al., 2017; Ortega et al., 2019, 2022).

3.2.2. Vitamin A

Retinaldehyde (or retinal), also known as vitamin A aldehyde, is a derivative of retinol after oxidation or is produced by the oxidative cleavage of β-carotene. Retinaldehyde is a prosthetic group of rhodopsin. Retinaldehyde is mainly converted from vitamin A supplemented from the blood. One study showed that vitamin A supplementation helps preserve rod photoreceptors and visual function in a T17M (class II mutation) transgenic mouse (Li et al., 1998) but has little beneficial effect on P347S (class I mutation) mutant mice (Li et al., 1998). More importantly, a recent study showed that the D190N transgenic mice on the vitamin A diet exhibited higher levels of autofluorescence and lipofuscin metabolites, raising concerns about the potential detrimental effect of vitamin A supplementation

on the retina expressing D190N (Cui et al., 2022). As the vitamin A method depends on the context of mutations, when this therapeutic method is translated from the laboratory to clinical treatment, the patients should be genotyped for the mutation in rhodopsin to determine whether this treatment method should be initiated.

3.2.3. 4-PBA (4-phenyl butyric acid) and rolipram

Misfolded proteins caused by the P23H mutation activate ERS responses, which may trigger imbalanced activation of autophagy relative to the proteasome (Qiu et al., 2019), leading to activation of protein degradation and cell death pathways in photoreceptor cells. The autophagy and ubiquitin–proteasome degradation pathways are two important methods of intracellular quality control and recycling that are responsible for cellular homeostasis in eukaryotes. The misfolded proteins caused by genetic mutations may lead to the persistent activation of the autophagy pathway. The autophagy pathway cannot completely deal with misfolded proteins, which may lead to secondary proteasome degradation and proteasome deficiency or decreased proteasome activity. A recent study showed that reducing ERS-induced autophagy activation while simultaneously increasing proteasome activity improves photoreceptor survival (Qiu et al., 2019), which suggests a potential new therapeutic strategy for the treatment of ADRP caused by protein folding defects.

This idea has also been validated in experiments using 4-phenyl butyric acid (4-PBA) and rolipram. While 4-PBA is a chemical partner that improves protein folding and protein shuttling to the proteasome pathway, rolipram is a selective phosphodiesterase-4 inhibitor that can directly increase proteasome activity (Zeitlin et al., 2002; Malo et al., 2013; Qiu et al., 2019). Both compounds have shown decreased ERS metabolism, decreased activation of the cell death pathway, and improvements in terms of photoreceptor morphology and visual function in a P23H mouse model (Powers et al., 2009; Qiu et al., 2019). Concomitantly, the transcription levels of the proapoptotic genes Fas and caspase 8 are downregulated (Yao J. et al., 2018; Qiu et al., 2019). Decreased phosphorylation of MLKL and RIPK3, which are two markers of necroptosis activation, was also observed in 4-PBA-treated mice. Therefore, 4-PBA rescues photoreceptors by suppressing both apoptotic and necroptotic cell death. In addition, a recent study using P23H knock-in mice suggests that 4-PBA may protect photoreceptors by modulating the mitochondrial function through epigenetic regulation (Ozawa et al., 2022). Despite the encouraging evidence in the preclinical animal model, the application of these compounds to treat inherited retinal diseases (IRDs) should be performed with caution, as neuroprotective therapies for IRDs failed to yield positive results in a clinical trial (Birch et al., 2016). The main reason could be that blocking one death pathway may activate other potential death pathways (Qiu et al., 2019).

3.2.4. SRD005825, YC-001, and TUDCA

To address the pathogenesis caused by protein misfolding, pharmacological compounds, such as small molecule chaperones, have been developed to help stabilize the protein structure. This is another strategy for the treatment of RP. SRD005825, YC-001, and TUDCA are three representative compounds that are used in this regard. While SRD005825 and YC-001 are two recently developed compounds, TUDCA is a natural compound that has been extensively studied.

3.2.4.1. SRD005825

SRD005825, also known as SHP630, is an analog of 9-*cis*-retinaldehyde but does not covalently bind to opsin as a chromophore (Ahmed et al., 2019). *In vitro* assays showed that SRD005825 competes for 9-*cis*-retinaldehyde binding for purified rhodopsin. SRD005825 facilitates the reconstitution of mutant rhodopsin proteins and promotes T17M mutant rhodopsin translocation to the plasma membrane (Ahmed et al., 2019). Treatment with SRD005825 significantly slows the rate of rapid retinal degeneration in T17M mutant mice. SRD005825 also induces mutant rhodopsin to adopt a normal conformation and improves the light response following treatment in T17M mice. SRD005825 is a promising candidate for the treatment of RP caused by misfolded mutant rhodopsin.

3.2.4.2. YC-001

YC-001 is a novel nonretinoid pharmacological chaperone of rod photoreceptor opsin (Chen et al., 2018). Compared with 9-*cis*-retinaldehyde, YC-001 exhibits micromolar potency and greater efficacy but with a lower cytotoxicity. The chaperone activity of YC-001 is demonstrated by its ability to rescue multiple rhodopsin mutants in mammalian cells. By binding to rhodopsin, YC-001 antagonizes opsin signaling in a noncompetitive manner. YC-001 regulates the synthesis of the P23H mutant protein and stabilizes its structure in the ROS disk upon bleaching by light. Additionally, YC-001 is able to rescue the transport of other class II rhodopsin mutants, such as G106R, D190N, and P267L, but not P53R or C110Y, suggesting variation in folding defects among different class II mutants. Of importance, the metabolism of YC-001 in mice is significantly different from that in humans. Hence, the application of YC-001 for the treatment of human RP requires additional testing and evaluation (Chen et al., 2018).

3.2.4.3. TUDCA

TUDCA is a natural compound found in bear bile that has been used in Asia for over 3,000 years to treat visual disorders (Boatright et al., 2006). TUDCA protects neurons from apoptosis in neurodegenerative diseases (Duan et al., 2002; Keene et al., 2002), possibly by reducing ERS and inflammatory responses (Beuers et al., 1992; Özcan et al., 2006). TUDCA treatment is capable of preserving cone and rod structure and function and the connections between photoreceptor cells and postsynaptic neurons in a P23H rat model (Fernandez-Sanchez et al., 2011, 2015). In parallel, TUDCA reduces the number of microglia in P23H transgenic rats and prevents their activation (Noailles et al., 2014). Additionally, TUDCA reduces the presence of macrophages. Thus, the neuroprotective effect of TUDCA is mediated by its anti-inflammatory properties. Although TUDCA has proven to be effective in the protection of retinal neurons in P23H rats, its application in clinical trials is limited by the fact that high systemic concentrations are required to achieve local neuroprotective effects. Technically, it is difficult to maintain a high concentration of the drug in the eye for the long term. A persistently high concentration of the drug can be achieved by systemic high-concentration administration or frequent intraocular injections, which, however, may cause pharmacological toxicity and physical damage, respectively (Fernández-Sánchez et al., 2017). One potential solution could be loading the drug into a biodegradable microsphere that enables a slow and sustained release (Fernández-Sánchez et al., 2017); however, the feasibility of this concept requires further testing.

3.3. Antisense oligonucleotide therapy

Antisense-mediated gene suppression was first reported in 1978 (Zamecnik and Stephenson, 1978). In recent years, antisense oligonucleotides (ASOs) have emerged as a potential strategy for the treatment of inherited retinal diseases (Collin and Garanto, 2017). ASOs are small DNA or RNA molecules that are complementary to their target mRNAs. Therapeutic ASOs can be chemically synthesized oligonucleotides 18–30 nucleotides in length. The binding of ASOs to targeted RNAs promotes RNA fragmentation and degradation. They may also inhibit the expression of target RNA by blocking the translation machinery. One study showed that intravitreal administration of second-generation ASOs effectively and specifically reduces the level of allele-specific mutant rhodopsin in a transgenic rat that expresses a murine P23H rhodopsin gene (Murray et al., 2015). In this study, the treated eyes also exhibited improved photoreceptor morphologies, function, and cell survival. ASOs have several apparent advantages over other gene-silencing agents (Murray et al., 2015), such as high selectivity for alleles with single-base mutations and simple delivery in a water-based formulation (Østergaard et al., 2013). A first-generation ASO for the treatment of cytomegalovirus (CMV) retinitis has been approved by the FDA (Group, 2002; Jabs and Griffiths, 2002). The half-life of second-generation ASOs is notably longer than that of first-generation ASOs. Thus, the treatment cycle will also be longer without the need for frequent injections (Murray et al., 2015). These advantages make ASOs great candidates for the treatment of retinal degeneration caused by rhodopsin mutations.

3.4. Gene therapy

Gene therapy enables the addition of exogenous genes to correct pathogenic symptoms. Depending on the mutation type, several strategies have been developed to treat RP. Gene augmentation is a simple and straightforward strategy featuring the transfer and expression of wild-type exogenous genes into host cells. This approach has proven to be successful in the treatment of autosomal recessive RP both experimentally and clinically (Kumar et al., 2016; Bennett, 2017). However, this strategy had limited success in treating ADRP. Although gene augmentation may improve pathogenic symptoms by diluting mutant proteins, the gain-of-function or dominant-negative mutant proteins that remain within the cells will still exert their toxic effects. Therefore, researchers are striving to develop alternative strategies to treat ADRP, particularly rhodopsin-associated RP, which accounts for over 25% of all ADRP cases (Dryja et al., 1991; Sullivan et al., 2013).

3.4.1. Mutation-independent strategies

One of these alternative strategies is to nonselectively knock down both the mutant and WT *RHO* with the concomitant expression of resistant WT *RHO* as a replacement. This resistant WT *RHO* is achieved by using synonymous codons at the target site. Ribozyme, zinc-finger–based artificial transcription factors, and RNAi have been utilized to suppress the expression of endogenous target genes (LaVail et al., 2000; Jiang et al., 2011; Mussolino et al., 2011). A recent study showed that a single vector expressing both shRNA and a human *RHO* replacement cDNA made resistant to RNA interference was successful in treating a naturally occurring canine model of RHO-ADRP with the T4R mutation (Cideciyan et al., 2018). The highly potent shRNA nearly completely suppressed the endogenous canine *RHO* RNA, and the replacement cDNA expressed 30% of the normal RHO protein. Treatment of P23H transgenic mice using the same shRNA and shRNA-resistant human slowed retinal degeneration during the 9-month study period (Ahmed et al., 2023). An apparent advantage of this mutation-independent strategy is that one single construct can be applied to the treatment of ADRP caused by different rhodopsin mutations, with over 200 identified, which will be much more cost-friendly for potential patients. Several clinical trials using this treatment strategy have been launched and planned to be initiated (Meng et al., 2020).

Nevertheless, this strategy is not free of disadvantages, as knockdown of endogenous rhodopsin RNA with siRNA may cause cell toxicity (Grimm et al., 2006). Moreover, the toxicity of overexpressed rhodopsin in the photoreceptors should also be taken into account. The off-target effect of shRNA should be another concern to be considered. To circumvent these disadvantages of shRNA, a novel approach using artificial mirtrons has been tested. Mirtrons are derived from spliced-out introns that regulate gene expression in a way similar to classic microRNAs (miRNAs; Curtis et al., 2012). A strategy using mirtron-based knockdown in combination with gene replacement has been shown to reduce disease severity in a P23H knock-in mouse model (Orlans et al., 2021). An alternative strategy is using a CRISPR-mediated system to ablate the endogenous *RHO* gene in combination with the optimized *RHO* replacement. This strategy has achieved promising results in P23H and D190N mouse models (Tsai et al., 2018). Similarly, EDIT-3, developed to target human *RHO*-assoicated ADRP, is currently undergoing preclinical trials (Meng et al., 2020).

3.4.2. Gene editing

Another concern related to the knockdown/replacement strategy is the duration of its efficacy. The recently emerging CRISPR/CAS9 technique is a solution to this concern. CRISPR/CAS9-mediated gene editing can correct the mutation and restore the normal function of the targeted gene (Rasoulinejad and Maroufi, 2021). A report showed that this technique was capable of correcting ~45% of the mutant allele at the DNA level in a P23H mouse model, significantly delaying the progression of photoreceptor degeneration in the treated area (Li et al., 2018). Allele-specific editing also effectively ameliorates dominant RP in an *RHO* P347S transgenic mouse model (Patrizi et al., 2021). A recently developed CRISPR-mediated DNA base editors enable corrections of pathogenic single nucleotide variants (SNVs) in rhodopsin (Komor et al., 2016), whereas the CRISPR-based primer editing system is even more versatile, potentially installing any combination of point mutations, small insertions or small deletions (Anzalone et al., 2019). Targeting of the CAS9 protein to the desired genomic position requires the presence of a construct-specific protospacer adjacent motif (PAM) and a guide RNA molecule. A systemic survey of 247 reported pathogenic *RHO* variants for suitable PAM sites for currently available base editors showed that 55% of those SNVs are editable with base editors and only 32% of them harbor PAM sites (Kaukonen et al., 2022). CAS9 variants have been developed to overcome the restriction of PAMs (Miller et al., 2020; Huang et al., 2023), which may greatly expand the use of base editors. The safety of this allele-specific editing and base editing strategies requires further research for validation.

3.5. Neuroprotection by trophic factors

Trophic factors are secreted small proteins that regulate cell proliferation, maturation, and viability (Snider and Johnson, 1989; von Bartheld, 1998). Some trophic factors have been documented to effectively delay retinal degeneration in various animal models (Faktorovich et al., 1990; LaVail et al., 1992; Unoki and LaVail, 1994; Green et al., 2001; Miyazaki et al., 2003; Buch et al., 2006). Basic fibroblast factor (bFGF) was the first factor to demonstrate neuroprotective effects on degenerative photoreceptors in light-damaged rats, and RCS rats suffer from a mutation in the MERKT gene (Faktorovich et al., 1990). Since then, more neurotrophic factors, including brain-derived neurotrophic factor (BDNF; LaVail et al., 1992), ciliary neurotrophic factor (CNTF; Unoki and LaVail, 1994), glial cell line-derived neurotrophic factor (GDNF; Buch et al., 2006), and pigment epithelium-derived factor (PEDF; Miyazaki et al., 2003), have been found to effectively counter retinal degeneration.

As neurotrophic factors are proteins, they are susceptible to degradation by proteases. Consequently, they have a relatively short half-life and can only provide short-term protection. Viral vector-mediated delivery of genes encoding neurotrophic factors has been shown to achieve sustained expression of these factors and offer long-term protection. One study showed that FGF-15 and FGF-18 expressed from the recombinant AAV virus notably delayed retinal degeneration caused by transgenic rats expressing a P23H or Q334ter rhodopsin mutation (Green et al., 2001). FGF-15 and FGF-18 are two members of the fibroblast factor family. In addition, AAV-mediated expression of CNTF prolongs photoreceptor survival in mutant rhodopsin mice (Liang et al., 2001). A recent study showed that treatment of P23H rats using neurotrophic factors in combination with suppression of microglia by minocycline achieved better results than using neurotrophic factors alone. Thus, neurotrophic factors are promising candidates for the treatment of retinal degeneration related to rhodopsin mutations.

Although CNTF and PEDF have been shown to rescue photoreceptor morphologies and prolong photoreceptor survival in rodent models of retinal degeneration, they may suppress retinal function, as determined by ERG recoding (Liang et al., 2001; Miyazaki et al., 2003; Buch et al., 2006). Additionally, translation of this approach into clinical applications encountered a major setback, based on one clinical study showing that RP patients treated with CNTF released continuously from an intravitreal implant had a greater loss of total visual field sensitivity in the treated eyes than in the sham-treated eyes (Birch et al., 2016). The reason for the contradictory results between animal models and human patients is unknown. Therefore, the use of neurotrophic factors for treating RP requires further evaluation.

3.6. Optogenetic therapy

During the process of RP, the progressive death of rod photoreceptors is followed by cone cell death. After photoreceptor cells die in advanced RP, the structure and function of the remaining cells, such as retinal ganglion cells and bipolar cells, remain intact. Therefore, it is possible to convert these remaining light-insensitive cells into photosensitive cells using an optogenetic therapy approach, thereby partially restoring vision (Pan et al., 2015). Channelrhodopsin 2 (ChR2) is a widely used optogenetic protein for this purpose. ChR2, originally cloned from *Chlamydomonas reinhardtii* (Nagel et al., 2003), is a direct light-gated cation ion channel that opens rapidly upon the absorption of photons and depolarizes the cell membrane (Nagel et al., 2002; Busskamp et al., 2010; Mutter et al., 2014). Restoration of vision using an optogenetic strategy was achieved in preclinical mouse and rat models of RP (Bi et al., 2006; Tomita et al., 2007, 2010). In addition to optogenetic proteins, chemical photoswitchs, such as DENAQ, AAQ and diethylamino-azo-diethylamino (DAD), have been shown to restore retinal responses to light in mice with degenerated photoreceptors (Polosukhina et al., 2012; Tochitsky et al., 2014; Laprell et al., 2017). A recent clinical study showed that a blind patient partially recovered visual function after optogenetic therapy using the channelrhodopsin protein ChrimsonR fused to the red fluorescent protein tdTomato (Sahel et al., 2021). The patient recovered to the extent that he could recognize the location of objects and reach out to locate them with the help of goggle-assisted-light stimulation. As optogenetic therapy is a gene and mutation-independent approach, it is conceivable that optogenetic therapy is quite promising to restore partial vision for advanced RP patients with rhodopsin mutations.

3.7. Stem cell therapy

With the improvement of our understanding of stem cells, stem cell therapy has emerged as a promising treatment method for RP, particularly RP at an advanced stage when most photoreceptors are lost and gene therapy is difficult. There are two major strategies for treating RP using stem cell therapy: (1) the transplantation of exogenous stem cells into the retina and the induction of the differentiation of the cells into desired cell types and (2) the induction of transdifferentiation of MCs into other types of neural cells.

3.7.1. Transplantation of exogenous stem cells

As early as 1988, retinal pigment epithelium (RPE) transplantation was tested for the treatment of RCS rats with defective RPEs (Li and Turner, 1988). In addition to RPE, transplantation of stem cells or cells differentiated from stem cells has been explored to protect or substitute for neurons in retinal disorders, particularly for late-stage retinal degeneration. Stem cells for treatment purposes include embryonic stem cells (Lund et al., 2006; Idelson et al., 2009; Lu et al., 2009), induced and reprogrammed stem cells (Sun et al., 2015), and adult tissue stem cells (Kicic et al., 2003; Arnhold et al., 2007; Xiong et al., 2011). Embryonic stem cells are derived from a developing embryo. However, the source of embryonic stem cells, in particular human embryonic stems, is limited and may raise ethical concerns (Ikelle et al., 2020). With the advent of induced pluripotent stem cells (iPSCs) that are reprogrammed from adult somatic cells by the transfection of defined critical transcription factors, such as SOX2, Klf4, c-Myc, and Oct4 (Takahashi and Yamanaka, 2006), the supply of stem cells is essentially unlimited without ethical restriction. Nevertheless, the use of iPSCs is limited, as they tend to result in immune rejection and teratogenicity (Holan et al., 2021). Adult tissue

stem cells include mesenchymal stem cells (MSCs) and neural stem cells (NSCs).

In the past decade, human adult bone marrow mesenchymal stem cells (BM-MSCs) have gained exclusive attention for the treatment of retinal degeneration due to their unique properties (Zaverucha-do-Valle et al., 2011; Tzameret et al., 2014; Weiss and Levy, 2020). BM-MSCs are easily expandable, with a broad differentiation potential into other cell types (Ferrari et al., 1998; Kopen et al., 1999; Kicic et al., 2003; Vandervelde et al., 2005; Oh et al., 2008), such as neurons and astrocytes. They can be used for autologous transplantation. Thus, they are safer than embryonic stem cells. Moreover, autologous transplantation may promote survival and enhanced therapeutic effects. Mesenchymal stem cells can be introduced into the eyes *via* the intraocular injection of cell suspension and cell patches. Upon the *in vitro* stimulation of growth and differentiation factors, including FGF2, taurine, retinoic acid, and IGF-1, MSCs can differentiate into precursor photoreceptor cells depending on their surface markers, such as specific antigens (Jayaram et al., 2014). Once differentiated, the photoreceptor cells integrate into the photoreceptor layer in the degenerated retina, and they can improve retinal function and restore vision. BM-MSCs have been demonstrated to restore lost visual function in animal models with retinal dystrophies (Lu et al., 2010; Zaverucha-do-Valle et al., 2011). Subretinal transplantation of BM-MSCs has been demonstrated to rescue photoreceptors in rhodopsin knockout mice (Arnhold et al., 2007), suggesting the possibility of using BM-MSCs to treat human RP caused by rhodopsin dysfunction.

Currently, several limitations of stem therapy need to be overcome before it becomes a practical clinical therapeutic approach. A technical obstacle faced by stem cell therapy is how to homogeneously disperse the transplanted cells into the retina to cover a large area. Another limitation is that it is difficult for the transplanted cells to migrate and integrate into the existing neural network to function correctly, although a recent study showed that the degradation of the extracellular matrix with chondroitinase ABC promotes cell migration (Ding et al., 2019). Another major issue is that the induction rate of the differentiation of the transplanted cells into the target cells is relatively low. According to reports, one team successfully differentiated photoreceptor cells *in vitro* under EPO treatment conditions (Ding et al., 2019). Another group performed intravitreal bone marrow mesenchymal stem cell transplantation in three patients with advanced RP, with adverse effects observed in two of them after transplantation. Between 2 weeks and 3 months after transplantation, patients reported an improvement in their perception of light. Another patient was observed to have severe fibrous tissue proliferation, resulting in tractional retinal detachment (Satarian et al., 2017). Simple bone marrow MSC transplantation is currently imperfect, and animal studies are recommended before implementation of clinical trials (Satarian et al., 2017).

3.7.2. Autologous stem cell induction therapy

In addition to transplantation of exogenous cells, emerging evidence shows that diseases due to photoreceptor cell loss can be treated by inducing the differentiation of MCs present in the eye into destination cells. MCs are the primary retinal glial cells with protrusions that span the entire thickness of the retina (Bringmann and Reichenbach, 2001). MCs in the human retina are thought to be dormant retinal precursor cells that can regenerate retinal neurons when the retinal tissue is damaged (Karl and Reh, 2010; Yu et al., 2014; Jorstad et al., 2017; Yao K. et al., 2018). Thus, awakening the regenerative potential of the retina is a promising way to repair degenerated retinas (Yu et al., 2014).

A recent study showed that the absence of Ephrin-A2/A3 promoted retinal regenerative potential of MCs in mice lacking rhodopsin (Zhu et al., 2021). The Ephrin family and its receptor, Eph, are the key regulators of CNS development, neural cell migration, and MC proliferation. Ephrin-A2/A3 and its receptor, Ephrin-A4, are both expressed in the retina, especially in MCs, but under physiological conditions, Ephrin signaling inhibits the neurogenic potential of MCs. The expression of Ephrin-A2/A3 and its receptor Ephrin-A4 increases with retinal maturation and proliferation, while the neurogenic potential of progenitor cells decreases, and Ephrin-A2/A3 is a negative regulator of MC proliferation and neurogenic potential. Controlling Ephrin-A2/A3 expression promotes the migration of proliferating cells to the photoreceptor cell layer for regeneration and the replacement of lost cells (Zhu et al., 2021). In *Rho*$^{-/-}$/*Ephrin A2*$^{-/-}$/*Ephrin A3*$^{-/-}$ triple knockout mice, significantly more MCs were detected in the inner nuclear layer than in *Rho* knockout mice, and proliferating MCs could also be detected to have migrated to the outer nuclear layer (Zhu et al., 2021).

4. Conclusion

Retinal dystrophy associated with rhodopsin mutations is an inherited disease with a pathogenesis that largely stems from cellular autophagy induced by abnormal retinoid binding to mutant proteins leading to cytotoxicity. A growing body of laboratory and clinical evidence suggests that the dysregulation of calcium homeostasis and unfolded protein responses play vital roles in retinal degeneration as independent or combined pathogenic mechanisms. The development of drugs targeting molecules these pathways may provide new therapeutic approaches for retinal degeneration. In recent decades, vitamin A supplementation has become the main therapy method; however, its use in clinical practice is limited because the effects do not significantly improve or delay the rate of retinal degeneration, especially in patients with advanced RP. Innovative therapy strategies, such as gene therapy (including gene editing, neuroprotection, and optogenetics) and stem cell therapy, are promising methods for the future treatment of RP. Greater efforts are needed from researchers and clinicians to facilitate the translation of recent research findings from the laboratory into clinical practice.

Author contributions

FZ and TZ wrote the manuscript. TW and YZ made the figures. SD and HZ edited the manuscript. All authors contributed to the article and approved the submitted version.

Funding

This work was supported by the grants from the National Natural Science Foundation of China (nos. 81770935 to HZ and 81800830 to SD), the Department of Science and Technology of Sichuan Province (no. 2023JDZH0002 to HZ), Young and Middle-aged Health Science and Technology Innovation Talent Training Project (Outstanding Young Persons) of Henan Province (no. YXKC2022025 to SD), Medical Science and Technology Project (the Key Project Jointly Built by the Province and the Ministry) of Henan Province (no. SBGJ202102167 to SD), and the Key Research and Development and Promotion Project (Science and Technology) program of Henan Province (no. 192102310077 to SD).

Conflict of interest

The authors declare that the research was conducted in the absence of any commercial or financial relationships that could be construed as a potential conflict of interest.

Publisher's note

References

Ahmed, C. M., Dwyer, B. T., Romashko, A., van Adestine, S., Park, E. H., Lou, Z., et al. (2019). SRD005825 acts as a pharmacologic chaperone of opsin and promotes survival of photoreceptors in an animal model of autosomal dominant retinitis Pigmentosa. *Transl. Vis. Sci. Technol.* 8:30. doi: 10.1167/tvst.8.6.30

Ahmed, C. M., Massengill, M. T., Ildefonso, C. J., Jalligampala, A., Zhu, P., Li, H., et al. (2023). Binocular benefit following monocular subretinal AAV injection in a mouse model of autosomal dominant retinitis pigmentosa (adRP). *Vis. Res.* 206:108189. doi: 10.1016/j.visres.2023.108189

Anzalone, A. V., Randolph, P. B., Davis, J. R., Sousa, A. A., Koblan, L. W., Levy, J. M., et al. (2019). Search-and-replace genome editing without double-strand breaks or donor DNA. *Nature* 576, 149–157. doi: 10.1038/s41586-019-1711-4

Arnhold, S., Absenger, Y., Klein, H., Addicks, K., and Schraermeyer, U. (2007). Transplantation of bone marrow-derived mesenchymal stem cells rescue photoreceptor cells in the dystrophic retina of the rhodopsin knockout mouse. *Graefes Arch. Clin. Exp. Ophthalmol.* 245, 414–422. doi: 10.1007/s00417-006-0382-7

Athanasiou, D., Aguila, M., Bellingham, J., Li, W., McCulley, C., Reeves, P. J., et al. (2018). The molecular and cellular basis of rhodopsin retinitis pigmentosa reveals potential strategies for therapy. *Prog. Retin. Eye Res.* 62, 1–23. doi: 10.1016/j.preteyeres.2017.10.002

Athanasiou, D., Aguila, M., Opefi, C. A., South, K., Bellingham, J., Bevilacqua, D., et al. (2017). Rescue of mutant rhodopsin traffic by metformin-induced AMPK activation accelerates photoreceptor degeneration. *Hum. Mol. Genet.* 26, ddw387–ddw319. doi: 10.1093/hmg/ddw387

Bales, K. L., Ianov, L., Kennedy, A. J., Sweatt, J. D., and Gross, A. K. (2018). Autosomal dominant retinitis pigmentosa rhodopsin mutant Q344X drives specific alterations in chromatin complex gene transcription. *Mol. Vis.* 24, 153–164.

Baumeister, P., Luo, S., Skarnes, W. C., Sui, G., Seto, E., Shi, Y., et al. (2005). Endoplasmic reticulum stress induction of the Grp78/BiP promoter: activating mechanisms mediated by YY1 and its interactive chromatin modifiers. *Mol. Cell. Biol.* 25, 4529–4540. doi: 10.1128/MCB.25.11.4529-4540.2005

Bennett, J. (2017). Taking stock of retinal gene therapy: looking Back and moving forward. *Mol. Ther.* 25, 1076–1094. doi: 10.1016/j.ymthe.2017.03.008

Berson, E. L. (1993). Retinitis pigmentosa. The Friedenwald lecture. *Invest. Ophthalmol. Vis. Sci.* 34, 1659–1676.

Beuers, U., Spengler, U., Kruis, W., Aydemir, U., Wiebecke, B., Heldwein, W., et al. (1992). Ursodeoxycholic acid for treatment of primary sclerosing cholangitis: a placebo-controlled trial. *Hepatology* 16, 707–714. doi: 10.1002/hep.1840160315

Bi, A., Cui, J., Ma, Y. P., Olshevskaya, E., Pu, M., Dizhoor, A. M., et al. (2006). Ectopic expression of a microbial-type rhodopsin restores visual responses in mice with photoreceptor degeneration. *Neuron* 50, 23–33. doi: 10.1016/j.neuron.2006.02.026

Birch, D. G., Bennett, L. D., Duncan, J. L., Weleber, R. G., and Pennesi, M. E. (2016). Long-term follow-up of patients with retinitis Pigmentosa receiving intraocular ciliary neurotrophic factor implants. *Am J. Ophthalmol.* 170, 10–14. doi: 10.1016/j.ajo.2016.07.013

Boatright, J. H., Moring, A. G., McElroy, C., Phillips, M. J., Do, V. T., Chang, B., et al. (2006). Tool from ancient pharmacopoeia prevents vision loss. *Mol. Vis.* 12, 1706–1714.

Bringmann, A., and Reichenbach, A. (2001). Role of Muller cells in retinal degenerations. *Front. Biosci.* 6, E72–E92. doi: 10.2741/bringman

Buch, P. K., MacLaren, R. E., Durán, Y., Balaggan, K. S., MacNeil, A., Schlichtenbrede, F. C., et al. (2006). In contrast to AAV-mediated Cntf expression, AAV-mediated Gdnf expression enhances gene replacement therapy in rodent models of retinal degeneration. *Mol. Ther.* 14, 700–709. doi: 10.1016/j.ymthe.2006.05.019

Busskamp, V., Duebel, J., Balya, D., Fradot, M., Viney, T. J., Siegert, S., et al. (2010). Genetic reactivation of cone photoreceptors restores visual responses in retinitis pigmentosa. *Science* 329, 413–417. doi: 10.1126/science.1190897

Candé, C., Vahsen, N., Kouranti, I., Schmitt, E., Daugas, E., Spahr, C., et al. (2004). AIF and cyclophilin a cooperate in apoptosis-associated chromatinolysis. *Oncogene* 23, 1514–1521. doi: 10.1038/sj.onc.1207279

Chen, Y., Chen, Y., Jastrzebska, B., Golczak, M., Gulati, S., Tang, H., et al. (2018). A novel small molecule chaperone of rod opsin and its potential therapy for retinal degeneration. *Nat. Commun.* 9:1976. doi: 10.1038/s41467-018-04261-1

Choudhury, S., Bhootada, Y., Gorbatyuk, O., and Gorbatyuk, M. (2013). Caspase-7 ablation modulates UPR, reprograms TRAF2-JNK apoptosis and protects T17M rhodopsin mice from severe retinal degeneration. *Cell Death Dis.* 4:e528. doi: 10.1038/cddis.2013.34

Ciavatta, V. T., Mocko, J. A., Kim, M. K., and Pardue, M. T. (2013). Subretinal electrical stimulation preserves inner retinal function in RCS rat retina. *Mol. Vis.* 19, 995–1005.

Cideciyan, A. V., Sudharsan, R., Dufour, V. L., Massengill, M. T., Iwabe, S., Swider, M., et al. (2018). Mutation-independent rhodopsin gene therapy by knockdown and replacement with a single AAV vector. *Proc. Natl. Acad. Sci. U. S. A.* 115, E8547–E8556. doi: 10.1073/pnas.1805055115

Collin, R. W., and Garanto, A. (2017). Applications of antisense oligonucleotides for the treatment of inherited retinal diseases. *Curr. Opin. Ophthalmol.* 28, 260–266. doi: 10.1097/ICU.0000000000000363

Colozo, A. T., Vasudevan, S., and Park, P. S. (2020). Retinal degeneration in mice expressing the constitutively active G90D rhodopsin mutant. *Hum. Mol. Genet.* 29, 881–891. doi: 10.1093/hmg/ddaa008

Comitato, A., di Salvo, M. T., Turchiano, G., Montanari, M., Sakami, S., Palczewski, K., et al. (2016). Dominant and recessive mutations in rhodopsin activate different cell death pathways. *Hum. Mol. Genet.* 25, ddw137–ddw2812. doi: 10.1093/hmg/ddw137

Comitato, A., Schiroli, D., Montanari, M., and Marigo, V. (2020). Calpain activation is the major cause of cell death in photoreceptors expressing a rhodopsin Misfolding mutation. *Mol. Neurobiol.* 57, 589–599. doi: 10.1007/s12035-019-01723-5

Cui, X., Kim, H. J., Cheng, C. H., Jenny, L. A., Lima de Carvalho, J. R., Chang, Y. J., et al. (2022). Long-term vitamin a supplementation in a preclinical mouse model forRhoD190N-associated retinitis pigmentosa. *Hum. Mol. Genet.* 31, 2438–2451. doi: 10.1093/hmg/ddac032

Curtis, H. J., Sibley, C. R., and Wood, M. J. (2012). Mirtrons, an emerging class of atypical miRNA. *Wiley Interdiscip. Rev. RNA* 3, 617–632. doi: 10.1002/wrna.1122

Daiger, S. P., Bowne, S. J., and Sullivan, L. S. (2014). Genes and mutations causing autosomal dominant retinitis Pigmentosa. *Cold Spring Harb. Perspect. Med.* 5:a017129. doi: 10.1101/cshperspect.a017129

Demir, M. N., Acar, U., Sobaci, G., and Goksuluk, D. (2022). Outcomes of transcorneal electrical stimulation therapy in the early stages of retinitis pigmentosa. *Turk. J. Med. Sci.* 52, 741–746. doi: 10.55730/1300-0144.5368

Deretic, D., and Papermaster, D. S. (1991). Polarized sorting of rhodopsin on post-Golgi membranes in frog retinal photoreceptor cells. *J. Cell Biol.* 113, 1281–1293. doi: 10.1083/jcb.113.6.1281

Ding, S. L. S., Koh, A. E., Kumar, S., Ali Khan, M. S., Alzahrani, B., and Mok, P. L. (2019). Genetically-modified human mesenchymal stem cells to express erythropoietin enhances differentiation into retinal photoreceptors: an in-vitro study. *J. Photochem. Photobiol. B* 195, 33–38. doi: 10.1016/j.jphotobiol.2019.04.008

Dizhoor, A. M., Woodruff, M. L., Olshevskaya, E. V., Cilluffo, M. C., Cornwall, M. C., Sieving, P. A., et al. (2008). Night blindness and the mechanism of constitutive signaling

of mutant G90D rhodopsin. *J. Neurosci.* 28, 11662–11672. doi: 10.1523/JNEUROSCI.4006-08.2008

Dor, H. (1873). Beiträge zur Electrotherapie der Augenkrankheiten. *Albr. Graefes. Arch. Ophthalmol.* 19, 316–352.

Dryja, T. P., Hahn, L. B., Cowley, G. S., McGee, T. L., and Berson, E. L. (1991). Mutation spectrum of the rhodopsin gene among patients with autosomal dominant retinitis pigmentosa. *Proc. Natl. Acad. Sci. U. S. A.* 88, 9370–9374. doi: 10.1073/pnas.88.20.9370

Dryja, T. P., McGee, T. L., Reichel, E., Hahn, L. B., Cowley, G. S., Yandell, D. W., et al. (1990). A point mutation of the rhodopsin gene in one form of retinitis pigmentosa. *Nature* 343, 364–366. doi: 10.1038/343364a0

Duan, W. M., Rodrigues, C. M., Zhao, L. R., Steer, C. J., and Low, W. C. (2002). Tauroursodeoxycholic acid improves the survival and function of nigral transplants in a rat model of Parkinson's disease. *Cell Transplant.* 11, 195–205. doi: 10.3727/096020198389960

Faktorovich, E. G., Steinberg, R. H., Yasumura, D., Matthes, M. T., and LaVail, M. M. (1990). Photoreceptor degeneration in inherited retinal dystrophy delayed by basic fibroblast growth factor. *Nature* 347, 83–86. doi: 10.1038/347083a0

Fernández-Sánchez, L., Bravo-Osuna, I., Lax, P., Arranz-Romera, A., Maneu, V., Esteban-Pérez, S., et al. (2017). Controlled delivery of tauroursodeoxycholic acid from biodegradable microspheres slows retinal degeneration and vision loss in P23H rats. *PLoS One* 12:e0177998. doi: 10.1371/journal.pone.0177998

Fernandez-Sanchez, L., Lax, P., Noailles, A., Angulo, A., Maneu, V., and Cuenca, N. (2015). Natural compounds from saffron and bear bile prevent vision loss and retinal degeneration. *Molecules* 20, 13875–13893. doi: 10.3390/molecules200813875

Fernandez-Sanchez, L., Lax, P., Pinilla, I., Martin-Nieto, J., and Cuenca, N. (2011). Tauroursodeoxycholic acid prevents retinal degeneration in transgenic P23H rats. *Invest. Ophthalmol. Vis. Sci.* 52, 4998–5008. doi: 10.1167/iovs.11-7496

Ferrari, G., Cusella–, G., Angelis, D., Coletta, M., Paolucci, E., Stornaiuolo, A., et al. (1998). Muscle regeneration by bone marrow-derived myogenic progenitors. *Science* 279, 1528–1530. doi: 10.1126/science.279.5356.1528

Ferrari, S., Di Iorio, E., Barbaro, V., Ponzin, D., Sorrentino, F. S., and Parmeggiani, F. (2011). Retinitis pigmentosa: genes and disease mechanisms. *Curr. Genomics* 12, 238–249. doi: 10.2174/138920211795860107

Fotiadis, D., Liang, Y., Filipek, S., Saperstein, D. A., Engel, A., and Palczewski, K. (2003). Atomic-force microscopy: rhodopsin dimers in native disc membranes. *Nature* 421, 127–128. doi: 10.1038/421127a

Frederick, J. M., Krasnoperova, N. V., Hoffmann, K., Church-Kopish, J., Ruther, K., Howes, K., et al. (2001). Mutant rhodopsin transgene expression on a null background. *Invest. Ophthalmol. Vis. Sci.* 42, 826–833.

Gall, C., Sgorzaly, S., Schmidt, S., Brandt, S., Fedorov, A., and Sabel, B. A. (2011). Noninvasive transorbital alternating current stimulation improves subjective visual functioning and vision-related quality of life in optic neuropathy. *Brain Stimul.* 4, 175–188. doi: 10.1016/j.brs.2011.07.003

Gragg, M., and Park, P. S. (2018). Misfolded rhodopsin mutants display variable aggregation properties. *Biochim Biophys Acta Mol Basis Dis* 1864, 2938–2948. doi: 10.1016/j.bbadis.2018.06.004

Green, E. S., Rendahl, K. G., Zhou, S., Ladner, M., Coyne, M., Srivastava, R., et al. (2001). Two animal models of retinal degeneration are rescued by recombinant adeno-associated virus-mediated production of FGF-5 and FGF-18. *Mol. Ther.* 3, 507–515. doi: 10.1006/mthe.2001.0289

Grimm, D., Streetz, K. L., Jopling, C. L., Storm, T. A., Pandey, K., Davis, C. R., et al. (2006). Fatality in mice due to oversaturation of cellular microRNA/short hairpin RNA pathways. *Nature* 441, 537–541. doi: 10.1038/nature04791

Gross, A. K., Xie, G., and Oprian, D. D. (2003). Slow binding of retinal to rhodopsin mutants G90D and T94D. *Biochemistry* 42, 2002–2008. doi: 10.1021/bi020612r

Group, V. S. (2002). Safety of intravitreous fomivirsen for treatment of cytomegalovirus retinitis in patients with AIDS. *Am J. Ophthalmol.* 133, 484–498. doi: 10.1016/s0002-9394(02)01332-6

Gunkel, M., Schöneberg, J., Alkhaldi, W., Irsen, S., Noé, F., Kaupp, U. B., et al. (2015). Higher-order architecture of rhodopsin in intact photoreceptors and its implication for phototransduction kinetics. *Structure* 23, 628–638. doi: 10.1016/j.str.2015.01.015

Halliwell, B. (2011). Free radicals and antioxidants – quo vadis? *Trends Pharmacol. Sci.* 32, 125–130. doi: 10.1016/j.tips.2010.12.002

Hanif, A. M., Kim, M. K., Thomas, J. G., Ciavatta, V. T., Chrenek, M., Hetling, J. R., et al. (2016). Whole-eye electrical stimulation therapy preserves visual function and structure in P23H-1 rats. *Exp. Eye Res.* 149, 75–83. doi: 10.1016/j.exer.2016.06.010

Hao, W., Wenzel, A., Obin, M. S., Chen, C. K., Brill, E., Krasnoperova, N. V., et al. (2002). Evidence for two apoptotic pathways in light-induced retinal degeneration. *Nat. Genet.* 32, 254–260. doi: 10.1038/ng984

Hartong, D. T., Berson, E. L., and Dryja, T. P. (2006). Retinitis pigmentosa. *Lancet* 368, 1795–1809. doi: 10.1016/S0140-6736(06)69740-7

Herrera-Hernandez, M. G., Ramon, E., Lupala, C. S., Tena-Campos, M., Perez, J. J., and Garriga, P. (2017). Flavonoid allosteric modulation of mutated visual rhodopsin associated with retinitis pigmentosa. *Sci. Rep.* 7:11167. doi: 10.1038/s41598-017-11391-x

Holan, V., Palacka, K., and Hermankova, B. (2021). Mesenchymal stem cell-based therapy for retinal degenerative diseases: experimental models and clinical trials. *Cells* 10:588. doi: 10.3390/cells10030588

Hollingsworth, T. J., Hubbard, M. G., Levi, H. J., White, W., Wang, X., Simpson, R., et al. (2021). Proinflammatory pathways are activated in the human Q344X rhodopsin Knock-in mouse model of retinitis Pigmentosa. *Biomol. Ther.* 11:1163. doi: 10.3390/biom11081163

Huang, T. P., Heins, Z. J., Miller, S. M., Wong, B. G., Balivada, P. A., Wang, T., et al. (2023). High-throughput continuous evolution of compact Cas9 variants targeting single-nucleotide-pyrimidine PAMs. *Nat. Biotechnol.* 41, 96–107. doi: 10.1038/s41587-022-01410-2

Iannaccone, A., Man, D., Waseem, N., Jennings, B. J., Ganapathiraju, M., Gallaher, K., et al. (2006). Retinitis pigmentosa associated with rhodopsin mutations: Correlation between phenotypic variability and molecular effects. *Vision Res* 46, 4556–4567. doi: 10.1016/j.visres.2006.08.018

Idelson, M., Alper, R., Obolensky, A., Ben-Shushan, E., Hemo, I., Yachimovich-Cohen, N., et al. (2009). Directed differentiation of human embryonic stem cells into functional retinal pigment epithelium cells. *Cell Stem Cell* 5, 396–408. doi: 10.1016/j.stem.2009.07.002

Ikelle, L., Al-Ubaidi, M. R., and Naash, M. I. (2020). Pluripotent stem cells for the treatment of retinal degeneration: current strategies and future directions. *Front. Cell Dev. Biol.* 8:743. doi: 10.3389/fcell.2020.00743

Jabs, D. A., and Griffiths, P. D. (2002). Fomivirsen for the treatment of cytomegalovirus retinitis. *Am J. Ophthalmol.* 133, 552–556. doi: 10.1016/s0002-9394(02)01325-9

Jardon-Valadez, E., Bondar, A. N., and Tobias, D. J. (2010). Coupling of retinal, protein, and water dynamics in squid rhodopsin. *Biophys. J.* 99, 2200–2207. doi: 10.1016/j.bpj.2010.06.067

Jayaram, H., Jones, M. F., Eastlake, K., Cottrill, P. B., Becker, S., Wiseman, J., et al. (2014). Transplantation of photoreceptors derived from human Müller glia restore rod function in the P23H rat. *Stem Cells Transl. Med.* 3, 323–333. doi: 10.5966/sctm.2013-0112

Jiang, H., Xiong, S., and Xia, X. (2014). Retinitis pigmentosaassociated rhodopsin mutant T17M induces endoplasmic reticulum (ER) stress and sensitizes cells to ER stress-induced cell death. *Mol. Med. Rep.* 9, 1737–1742. doi: 10.3892/mmr.2014.1987

Jiang, L., Zhang, H., Dizhoor, A. M., Boye, S. E., Hauswirth, W. W., Frederick, J. M., et al. (2011). Long-term RNA interference gene therapy in a dominant retinitis pigmentosa mouse model. *Proc. Natl. Acad. Sci. U. S. A.* 108, 18476–18481. doi: 10.1073/pnas.1112758108

Jin, S., Cornwall, M. C., and Oprian, D. D. (2003). Opsin activation as a cause of congenital night blindness. *Nat. Neurosci.* 6, 731–735. doi: 10.1038/nn1070

Jorstad, N. L., Wilken, M. S., Grimes, W. N., Wohl, S. G., VandenBosch, L. S., Yoshimatsu, T., et al. (2017). Stimulation of functional neuronal regeneration from Müller glia in adult mice. *Nature* 548, 103–107. doi: 10.1038/nature23283

Karl, M. O., and Reh, T. A. (2010). Regenerative medicine for retinal diseases: activating endogenous repair mechanisms. *Trends Mol. Med.* 16, 193–202. doi: 10.1016/j.molmed.2010.02.003

Kartasasmita, A., Fujiki, K., Iskandar, E., Sovani, I., Fujimaki, T., and Murakami, A. (2011). A novel nonsense mutation in rhodopsin gene in two Indonesian families with autosomal recessive retinitis pigmentosa. *Ophthalmic Genet.* 32, 57–63. doi: 10.3109/13816810.2010.535892

Kaukonen, M., McClements, M. E., and MacLaren, R. E. (2022). CRISPR DNA Base editing strategies for treating retinitis Pigmentosa caused by mutations in rhodopsin. *Genes (Basel)* 13:1327. doi: 10.3390/genes13081327

Kaushal, S., and Khorana, H. G. (1994). Structure and function in rhodopsin. 7. Point mutations associated with autosomal dominant retinitis pigmentosa. *Biochemistry* 33, 6121–6128. doi: 10.1021/bi00186a011

Keene, C. D., Rodrigues, C. M., Eich, T., Chhabra, M. S., Steer, C. J., and Low, W. C. (2002). Tauroursodeoxycholic acid, a bile acid, is neuroprotective in a transgenic animal model of Huntington's disease. *Proc. Natl. Acad. Sci. U. S. A.* 99, 10671–10676. doi: 10.1073/pnas.162362299

Kicic, A., Shen, W. Y., Wilson, A. S., Constable, I. J., Robertson, T., and Rakoczy, P. E. (2003). Differentiation of marrow stromal cells into photoreceptors in the rat eye. *J. Neurosci.* 23, 7742–7749. doi: 10.1523/JNEUROSCI.23-21-07742.2003

Kim, C., Kim, K. J., Bok, J., Lee, E. J., Kim, D. J., Oh, J. H., et al. (2012). Microarray-based mutation detection and phenotypic characterization in Korean patients with retinitis pigmentosa. *Mol. Vis.* 18, 2398–2410.

Kimata, N., Pope, A., Eilers, M., Opefi, C. A., Ziliox, M., Hirshfeld, A., et al. (2016). Retinal orientation and interactions in rhodopsin reveal a two-stage trigger mechanism for activation. *Nat. Commun.* 7:12683. doi: 10.1038/ncomms12683

Kitamura, M. (2008). Endoplasmic reticulum stress and unfolded protein response in renal pathophysiology: Janus faces. *Am. J. Physiol. Renal Physiol.* 295, F323–F334. doi: 10.1152/ajprenal.00050.2008

Kobal, N., Krašovec, T., Šuštar, M., Volk, M., Peterlin, B., Hawlina, M., et al. (2021). Stationary and progressive phenotypes caused by the p.G90D mutation in rhodopsin gene. *Int. J. Mol. Sci.* 22:2133. doi: 10.3390/ijms22042133

Komor, A. C., Kim, Y. B., Packer, M. S., Zuris, J. A., and Liu, D. R. (2016). Programmable editing of a target base in genomic DNA without double-stranded DNA cleavage. *Nature* 533, 420–424. doi: 10.1038/nature17946

Kopen, G. C., Prockop, D. J., and Phinney, D. G. (1999). Marrow stromal cells migrate throughout forebrain and cerebellum, and they differentiate into astrocytes after injection into neonatal mouse brains. *Proc. Natl. Acad. Sci. U. S. A.* 96, 10711–10716. doi: 10.1073/pnas.96.19.10711

Krebs, M. P., Holden, D. C., Joshi, P., Clark, C. L. 3rd, Lee, A. H., and Kaushal, S. (2010). Molecular mechanisms of rhodopsin retinitis pigmentosa and the efficacy of pharmacological rescue. *J. Mol. Biol.* 395, 1063–1078. doi: 10.1016/j.jmb.2009.11.015

Kumar, S. R., Markusic, D. M., Biswas, M., High, K. A., and Herzog, R. W. (2016). Clinical development of gene therapy: results and lessons from recent successes. *Mol. Ther. Methods Clin. Dev.* 3:16034. doi: 10.1038/mtm.2016.34

Kumaramanickavel, G., Maw, M., Denton, M. J., John, S., Srikumari, C. R., Orth, U., et al. (1994). Missense rhodopsin mutation in a family with recessive RP. *Nat. Genet.* 8, 10–11. doi: 10.1038/ng0994-10

Kunte, M. M., Choudhury, S., Manheim, J. F., Shinde, V. M., Miura, M., Chiodo, V. A., et al. (2012). ER stress is involved in T17M rhodopsin-induced retinal degeneration. *Invest. Ophthalmol. Vis. Sci.* 53, 3792–3800. doi: 10.1167/iovs.11-9235

Laprell, L., Tochitsky, I., Kaur, K., Manookin, M. B., Stein, M., Barber, D. M., et al. (2017). Photopharmacological control of bipolar cells restores visual function in blind mice. *J. Clin. Invest.* 127, 2598–2611. doi: 10.1172/JCI92156

LaVail, M. M., Unoki, K., Yasumura, D., Matthes, M. T., Yancopoulos, G. D., and Steinberg, R. H. (1992). Multiple growth factors, cytokines, and neurotrophins rescue photoreceptors from the damaging effects of constant light. *Proc. Natl. Acad. Sci. U. S. A.* 89, 11249–11253. doi: 10.1073/pnas.89.23.11249

LaVail, M. M., Yasumura, D., Matthes, M. T., Drenser, K. A., Flannery, J. G., Lewin, A. S., et al. (2000). Ribozyme rescue of photoreceptor cells in P23H transgenic rats: long-term survival and late-stage therapy. *Proc. Natl. Acad. Sci. U. S. A.* 97, 11488–11493. doi: 10.1073/pnas.210319397

Li, P., Kleinstiver, B. P., Leon, M. Y., Prew, M. S., Navarro-Gomez, D., Greenwald, S. H., et al. (2018). Allele-specific CRISPR-Cas9 genome editing of the Single-Base P23H mutation for rhodopsin-associated dominant retinitis Pigmentosa. *CRISPR J.* 1, 55–64. doi: 10.1089/crispr.2017.0009

Li, T., Sandberg, M. A., Pawlyk, B. S., Rosner, B., Hayes, K. C., Dryja, T. P., et al. (1998). Effect of vitamin a supplementation on rhodopsin mutants threonine-17 --> methionine and proline-347 --> serine in transgenic mice and in cell cultures. *Proc. Natl. Acad. Sci. U. S. A.* 95, 11933–11938. doi: 10.1073/pnas.95.20.11933

Li, L. X., and Turner, J. E. (1988). Inherited retinal dystrophy in the RCS rat: prevention of photoreceptor degeneration by pigment epithelial cell transplantation. *Exp. Eye Res.* 47, 911–917. doi: 10.1016/0014-4835(88)90073-5

Liang, F. Q., Dejneka, N. S., Cohen, D. R., Krasnoperova, N. V., Lem, J., Maguire, A. M., et al. (2001). AAV-mediated delivery of ciliary neurotrophic factor prolongs photoreceptor survival in the rhodopsin knockout mouse. *Mol. Ther.* 3, 241–248. doi: 10.1006/mthe.2000.0252

Lin, J. H., Li, H., Yasumura, D., Cohen, H. R., Zhang, C., Panning, B., et al. (2007). IRE1 signaling affects cell fate during the unfolded protein response. *Science* 318, 944–949. doi: 10.1126/science.1146361

Liu, X., Garriga, P., and Khorana, H. G. (1996). Structure and function in rhodopsin: correct folding and misfolding in two point mutants in the intradiscal domain of rhodopsin identified in retinitis pigmentosa. *Proc Natl Acad Sci. USA* 93, 4554–4559. doi: 10.1073/pnas.93.10.4554

Loewen, A. D., Tam, B. M., Scharbach, R. T., Chiu, C. N., and Moritz, O. L. (2020). "Mutant rhodopsins associated with sector RP primarily localize to rod photoreceptor outer segments in transgenic Xenopus laevis," in *ARVO Annual Meeting Abstract*.

Lu, B., Malcuit, C., Wang, S., Girman, S., Francis, P., Lemieux, L., et al. (2009). Long-term safety and function of RPE from human embryonic stem cells in preclinical models of macular degeneration. *Stem Cells* 27, 2126–2135. doi: 10.1002/stem.149

Lu, B., Wang, S., Girman, S., McGill, T., Ragaglia, V., and Lund, R. (2010). Human adult bone marrow-derived somatic cells rescue vision in a rodent model of retinal degeneration. *Exp. Eye Res.* 91, 449–455. doi: 10.1016/j.exer.2010.06.024

Lund, R. D., Wang, S., Klimanskaya, I., Holmes, T., Ramos-Kelsey, R., Lu, B., et al. (2006). Human embryonic stem cell-derived cells rescue visual function in dystrophic RCS rats. *Cloning Stem Cells* 8, 189–199. doi: 10.1089/clo.2006.8.189

Majumdar, S., and Srirangam, R. (2010). Potential of the bioflavonoids in the prevention/treatment of ocular disorders. *J. Pharm. Pharmacol.* 62, 951–965. doi: 10.1211/jpp.62.08.0001

Malanson, K. M., and Lem, J. (2009). Rhodopsin-mediated retinitis pigmentosa. *Prog. Mol. Biol. Transl. Sci.* 88, 1–31. doi: 10.1016/S1877-1173(09)88001-0

Malo, A., Kruger, B., Goke, B., and Kubisch, C. H. (2013). 4-Phenylbutyric acid reduces endoplasmic reticulum stress, trypsin activation, and acinar cell apoptosis while increasing secretion in rat pancreatic acini. *Pancreas* 42, 92–101. doi: 10.1097/MPA.0b013e318259f6ca

Mendes, H. F., van der Spuy, J., Chapple, J. P., and Cheetham, M. E. (2005). Mechanisms of cell death in rhodopsin retinitis pigmentosa: implications for therapy. *Trends Mol. Med.* 11, 177–185. doi: 10.1016/j.molmed.2005.02.007

Meng, D., Ragi, S. D., and Tsang, S. H. (2020). Therapy in rhodopsin-mediated autosomal dominant retinitis Pigmentosa. *Mol. Ther.* 28, 2139–2149. doi: 10.1016/j.ymthe.2020.08.012

Miller, S. M., Wang, T., Randolph, P. B., Arbab, M., Shen, M. W., Huang, T. P., et al. (2020). Continuous evolution of SpCas9 variants compatible with non-G PAMs. *Nat. Biotechnol.* 38, 471–481. doi: 10.1038/s41587-020-0412-8

Miyazaki, M., Ikeda, Y., Yonemitsu, Y., Goto, Y., Sakamoto, T., Tabata, T., et al. (2003). Simian lentiviral vector-mediated retinal gene transfer of pigment epithelium-derived factor protects retinal degeneration and electrical defect in Royal College of surgeons rats. *Gene Ther.* 10, 1503–1511. doi: 10.1038/sj.gt.3302028

Molday, R. S., and Moritz, O. L. (2015). Photoreceptors at a glance. *J. Cell Sci.* 128, 4039–4045. doi: 10.1242/jcs.175687

Moubarak, R. S., Yuste, V. J., Artus, C., Bouharrour, A., Greer, P. A., Menissier-de Murcia, J., et al. (2007). Sequential activation of poly(ADP-ribose) polymerase 1, calpains, and Bax is essential in apoptosis-inducing factor-mediated programmed necrosis. *Mol. Cell. Biol.* 27, 4844–4862. doi: 10.1128/MCB.02141-06

Murray, S. F., Jazayeri, A., Matthes, M. T., Yasumura, D., Yang, H., Peralta, R., et al. (2015). Allele-specific inhibition of rhodopsin with an antisense oligonucleotide slows photoreceptor cell degeneration. *Invest. Ophthalmol. Vis. Sci.* 56, 6362–6375. doi: 10.1167/iovs.15-16400

Mussolino, C., Sanges, D., Marrocco, E., Bonetti, C., di Vicino, U., Marigo, V., et al. (2011). Zinc-finger-based transcriptional repression of rhodopsin in a model of dominant retinitis pigmentosa. *EMBO Mol. Med.* 3, 118–128. doi: 10.1002/emmm.201000119

Mutter, M., Swietek, N., and Munch, T. A. (2014). Salvaging ruins: reverting blind retinas into functional visual sensors. *Methods Mol. Biol.* 1148, 149–160. doi: 10.1007/978-1-4939-0470-9_10

Naash, M. I., Wu, T. H., Chakraborty, D., Fliesler, S. J., Ding, X. Q., Nour, M., et al. (2004). Retinal abnormalities associated with the G90D mutation in opsin. *J. Comp. Neurol.* 478, 149–163. doi: 10.1002/cne.20283

Nagel, G., Ollig, D., Fuhrmann, M., Kateriya, S., Musti, A. M., Bamberg, E., et al. (2002). Channelrhodopsin-1: a light-gated proton channel in green algae. *Science* 296, 2395–2398. doi: 10.1126/science.1072068

Nagel, G., Szellas, T., Huhn, W., Kateriya, S., Adeishvili, N., Berthold, P., et al. (2003). Channelrhodopsin-2, a directly light-gated cation-selective membrane channel. *Proc. Natl. Acad. Sci. U. S. A.* 100, 13940–13945. doi: 10.1073/pnas.1936192100

Noailles, A., Fernandez-Sanchez, L., Lax, P., and Cuenca, N. (2014). Microglia activation in a model of retinal degeneration and TUDCA neuroprotective effects. *J. Neuroinflammation* 11:186. doi: 10.1186/s12974-014-0186-3

Oh, J. Y., Kim, M. K., Shin, M. S., Lee, H. J., Ko, J. H., Wee, W. R., et al. (2008). The anti-inflammatory and anti-angiogenic role of mesenchymal stem cells in corneal wound healing following chemical injury. *Stem Cells* 26, 1047–1055. doi: 10.1634/stemcells.2007-0737

Orlans, H. O., McClements, M. E., Barnard, A. R., Martinez-Fernandez de la Camara, C., and MacLaren, R. E. (2021). Mirtron-mediated RNA knockdown/replacement therapy for the treatment of dominant retinitis pigmentosa. *Nat. Commun.* 12:4934. doi: 10.1038/s41467-021-25204-3

Ortega, J. T., and Jastrzebska, B. (2021). Neuroinflammation as a therapeutic target in retinitis Pigmentosa and quercetin as its potential modulator. *Pharmaceutics* 13:1935. doi: 10.3390/pharmaceutics13111935

Ortega, J. T., and Jastrzebska, B. (2022). Rhodopsin as a molecular target to mitigate retinitis Pigmentosa. *Adv. Exp. Med. Biol.* 1371, 61–77. doi: 10.1007/5584_2021_682

Ortega, J. T., Parmar, T., Carmena-Bargueno, M., Perez-Sanchez, H., and Jastrzebska, B. (2022). Flavonoids improve the stability and function of P23H rhodopsin slowing down the progression of retinitis pigmentosa in mice. *J. Neurosci. Res.* 100, 1063–1083. doi: 10.1002/jnr.25021

Ortega, J. T., Parmar, T., Golczak, M., and Jastrzebska, B. (2021). Protective effects of flavonoids in acute models of light-induced retinal degeneration. *Mol. Pharmacol.* 99, 60–77. doi: 10.1124/molpharm.120.000072

Ortega, J. T., Parmar, T., and Jastrzebska, B. (2019). Flavonoids enhance rod opsin stability, folding, and self-association by directly binding to ligand-free opsin and modulating its conformation. *J. Biol. Chem.* 294, 8101–8122. doi: 10.1074/jbc.RA119.007808

Østergaard, M. E., Southwell, A. L., Kordasiewicz, H., Watt, A. T., Skotte, N. H., Doty, C. N., et al. (2013). Rational design of antisense oligonucleotides targeting single nucleotide polymorphisms for potent and allele selective suppression of mutant huntingtin in the CNS. *Nucleic Acids Res.* 41, 9634–9650. doi: 10.1093/nar/gkt725

Ozawa, Y., Toda, E., Homma, K., Osada, H., Nagai, N., Tsubota, K., et al. (2022). Effects of epigenetic modification of PGC-1α by a chemical chaperon on mitochondria biogenesis and visual function in retinitis Pigmentosa. *Cells* 11:1497. doi: 10.3390/cells11091497

Özcan, U., Yilmaz, E., Özcan, L., Furuhashi, M., Vaillancourt, E., Smith, R. O., et al. (2006). Chemical chaperones reduce ER stress and restore glucose homeostasis in a mouse model of type 2 diabetes. *Science* 313, 1137–1140. doi: 10.1126/science.1128294

Palczewski, K. (2014). Chemistry and biology of the initial steps in vision: the Friedenwald lecture. *Invest. Ophthalmol. Vis. Sci.* 55, 6651–6672. doi: 10.1167/iovs.14-15502

Pan, Z. H., Lu, Q., Bi, A., Dizhoor, A. M., and Abrams, G. W. (2015). Optogenetic approaches to restoring vision. *Annu. Rev. Vis. Sci.* 1, 185–210. doi: 10.1146/annurev-vision-082114-035532

Park, P. S. (2014). Constitutively active rhodopsin and retinal disease. *Adv. Pharmacol.* 70, 1–36. doi: 10.1016/B978-0-12-417197-8.00001-8

Patrizi, C., Llado, M., Benati, D., Iodice, C., Marrocco, E., Guarascio, R., et al. (2021). Allele-specific editing ameliorates dominant retinitis pigmentosa in a transgenic mouse model. *Am. J. Hum. Genet.* 108, 295–308. doi: 10.1016/j.ajhg.2021.01.006

Perea-Romero, I., Gordo, G., Iancu, I. F., del Pozo-Valero, M., Almoguera, B., Blanco-Kelly, F., et al. (2021). Genetic landscape of 6089 inherited retinal dystrophies affected cases in Spain and their therapeutic and extended epidemiological implications. *Sci. Rep.* 11:1526. doi: 10.1038/s41598-021-81093-y

Piri, N., Grodsky, J. D., and Kaplan, H. J. (2021). Gene therapy for retinitis pigmentosa. *Taiwan J. Ophthalmol.* 11, 348–351. doi: 10.4103/tjo.tjo_47_21

Ploier, B., Caro, L. N., Morizumi, T., Pandey, K., Pearring, J. N., Goren, M. A., et al. (2016). Dimerization deficiency of enigmatic retinitis pigmentosa-linked rhodopsin mutants. *Nat. Commun.* 7:12832. doi: 10.1038/ncomms12832

Polosukhina, A., Litt, J., Tochitsky, I., Nemargut, J., Sychev, Y., de Kouchkovsky, I., et al. (2012). Photochemical restoration of visual responses in blind mice. *Neuron* 75, 271–282. doi: 10.1016/j.neuron.2012.05.022

Powers, E. T., Morimoto, R. I., Dillin, A., Kelly, J. W., and Balch, W. E. (2009). Biological and chemical approaches to diseases of proteostasis deficiency. *Annu. Rev. Biochem.* 78, 959–991. doi: 10.1146/annurev.biochem.052308.114844

Qiu, Y., Yao, J., Jia, L., Thompson, D. A., and Zacks, D. N. (2019). Shifting the balance of autophagy and proteasome activation reduces proteotoxic cell death: a novel therapeutic approach for restoring photoreceptor homeostasis. *Cell Death Dis.* 10:547. doi: 10.1038/s41419-019-1780-1

Rao, V. R., Cohen, G. B., and Oprian, D. D. (1994). Rhodopsin mutation G90D and a molecular mechanism for congenital night blindness. *Nature* 367, 639–642. doi: 10.1038/367639a0

Rasoulinejad, S. A., and Maroufi, F. (2021). CRISPR-based genome editing as a new therapeutic tool in retinal diseases. *Mol. Biotechnol.* 63, 768–779. doi: 10.1007/s12033-021-00345-4

Robinson, P. R., Buczylko, J., Ohguro, H., and Palczewski, K. (1994). Opsins with mutations at the site of chromophore attachment constitutively activate transducin but are not phosphorylated by rhodopsin kinase. *Proc. Natl. Acad. Sci. U. S. A.* 91, 5411–5415. doi: 10.1073/pnas.91.12.5411

Ropelewski, P., and Imanishi, Y. (2019). Disrupted plasma membrane protein homeostasis in a Xenopus Laevis model of retinitis Pigmentosa. *J. Neurosci.* 39, 5581–5593. doi: 10.1523/JNEUROSCI.3025-18.2019

Rosenfeld, P. J., Cowley, G. S., McGee, T. L., Sandberg, M. A., Berson, E. L., and Dryja, T. P. (1992). A null mutation in the rhodopsin gene causes rod photoreceptor dysfunction and autosomal recessive retinitis pigmentosa. *Nat. Genet.* 1, 209–213. doi: 10.1038/ng0692-209

Sahel, J. A., Boulanger-Scemama, E., Pagot, C., Arleo, A., Galluppi, F., Martel, J. N., et al. (2021). Partial recovery of visual function in a blind patient after optogenetic therapy. *Nat. Med.* 27, 1223–1229. doi: 10.1038/s41591-021-01351-4

Satarian, L., Nourinia, R., Safi, S., Kanavi, M. R., Jarughi, N., Daftarian, N., et al. (2017). Intravitreal injection of bone marrow mesenchymal stem cells in patients with advanced retinitis Pigmentosa; a safety study. *J. Ophthalmic Vis. Res.* 12, 58–64. doi: 10.4103/2008-322X.200164

Sieving, P. A., Fowler, M. L., Bush, R. A., Machida, S., Calvert, P. D., Green, D. G., et al. (2001). Constitutive "light" adaptation in rods from G90D rhodopsin: a mechanism for human congenital nightblindness without rod cell loss. *J. Neurosci.* 21, 5449–5460. doi: 10.1523/JNEUROSCI.21-15-05449.2001

Sieving, P. A., Richards, J. E., Naarendorp, F., Bingham, E. L., Scott, K., and Alpern, M. (1995). Dark-light: model for nightblindness from the human rhodopsin Gly-90-->asp mutation. *Proc. Natl. Acad. Sci. U. S. A.* 92, 880–884. doi: 10.1073/pnas.92.3.880

Silverman, D., Chai, Z., Yue, W. W. S., Ramisetty, S. K., Bekshe Lokappa, S., Sakai, K., et al. (2020). Dark noise and retinal degeneration from D190N-rhodopsin. *Proc. Natl. Acad. Sci. U. S. A.* 117, 23033–23043. doi: 10.1073/pnas.2010417117

Singhal, A., Ostermaier, M. K., Vishnivetskiy, S. A., Panneels, V., Homan, K. T., Tesmer, J. J., et al. (2013). Insights into congenital stationary night blindness based on the structure of G90D rhodopsin. *EMBO Rep.* 14, 520–526. doi: 10.1038/embor.2013.44

Snider, W. D., and Johnson, E. M. Jr. (1989). Neurotrophic molecules. *Ann. Neurol.* 26, 489–506. doi: 10.1002/ana.410260402

Sullivan, L. S., Bowne, S. J., Reeves, M. J., Blain, D., Goetz, K., NDifor, V., et al. (2013). Prevalence of mutations in eyeGENE probands with a diagnosis of autosomal dominant retinitis pigmentosa. *Invest. Ophthalmol. Vis. Sci.* 54, 6255–6261. doi: 10.1167/iovs.13-12605

Sun, J., Mandai, M., Kamao, H., Hashiguchi, T., Shikamura, M., Kawamata, S., et al. (2015). Protective effects of human iPS-derived retinal pigmented epithelial cells in comparison with human mesenchymal stromal cells and human neural stem cells on the degenerating retina inrd1mice. *Stem Cells* 33, 1543–1553. doi: 10.1002/stem.1960

Sung, C.-H., and Tai, A. W. (1999). Rhodopsin trafficking and its role in retinal dystrophies. *Int. Rev. Cytol* 195, 215–267. doi: 10.1016/s0074-7696(08)62706-0

Takahashi, K., and Yamanaka, S. (2006). Induction of pluripotent stem cells from mouse embryonic and adult fibroblast cultures by defined factors. *Cells* 126, 663–676. doi: 10.1016/j.cell.2006.07.024

Tochitsky, I., Polosukhina, A., Degtyar, V. E., Gallerani, N., Smith, C. M., Friedman, A., et al. (2014). Restoring visual function to blind mice with a photoswitch that exploits electrophysiological remodeling of retinal ganglion cells. *Neuron* 81, 800–813. doi: 10.1016/j.neuron.2014.01.003

Toledo, D., Ramon, E., Aguilà, M., Cordomí, A., Pérez, J. J., Mendes, H. F., et al. (2011). Molecular mechanisms of disease for mutations at Gly-90 in rhodopsin. *J. Biol. Chem.* 286, 39993–40001. doi: 10.1074/jbc.M110.201517

Tomita, H., Sugano, E., Isago, H., Hiroi, T., Wang, Z., Ohta, E., et al. (2010). Channelrhodopsin-2 gene transduced into retinal ganglion cells restores functional vision in genetically blind rats. *Exp. Eye Res.* 90, 429–436. doi: 10.1016/j.exer.2009.12.006

Tomita, H., Sugano, E., Yawo, H., Ishizuka, T., Isago, H., Narikawa, S., et al. (2007). Restoration of visual response in aged dystrophic RCS rats using AAV-mediated channelopsin-2 gene transfer. *Invest. Ophthalmol. Vis. Sci.* 48, 3821–3826. doi: 10.1167/iovs.06-1501

Tsai, Y. T., Wu, W. H., Lee, T. T., Wu, W. P., Xu, C. L., Park, K. S., et al. (2018). Clustered regularly interspaced short palindromic repeats-based genome surgery for the treatment of autosomal dominant retinitis Pigmentosa. *Ophthalmology* 125, 1421–1430. doi: 10.1016/j.ophtha.2018.04.001

Tzameret, A., Sher, I., Belkin, M., Treves, A. J., Meir, A., Nagler, A., et al. (2014). Transplantation of human bone marrow mesenchymal stem cells as a thin subretinal layer ameliorates retinal degeneration in a rat model of retinal dystrophy. *Exp. Eye Res.* 118, 135–144. doi: 10.1016/j.exer.2013.10.023

Unoki, K., and LaVail, M. M. (1994). Protection of the rat retina from ischemic injury by brain-derived neurotrophic factor, ciliary neurotrophic factor, and basic fibroblast growth factor. *Invest. Ophthalmol. Vis. Sci.* 35, 907–915.

Vandervelde, S., van Luyn, M. J., Tio, R. A., and Harmsen, M. C. (2005). Signaling factors in stem cell-mediated repair of infarcted myocardium. *J. Mol. Cell. Cardiol.* 39, 363–376. doi: 10.1016/j.yjmcc.2005.05.012

von Bartheld, C. S. (1998). Neurotrophins in the developing and regenerating visual system. *Histol. Histopathol.* 13, 437–459. doi: 10.14670/HH-13.437

Wang, M., Wey, S., Zhang, Y., Ye, R., and Lee, A. S. (2009). Role of the unfolded protein response regulator GRP78/BiP in development, cancer, and neurological disorders. *Antioxid. Redox Signal.* 11, 2307–2316. doi: 10.1089/ARS.2009.2485

Weiss, J. N., and Levy, S. (2020). Stem cell ophthalmology treatment study (SCOTS): bone marrow-derived stem cells in the treatment of age-related macular degeneration. *Medicines (Basel)* 7:16. doi: 10.3390/medicines7040016

Wilson, J. H., and Wensel, T. G. (2003). The nature of dominant mutations of rhodopsin and implications for gene therapy. *Mol. Neurobiol.* 28, 149–158. doi: 10.1385/MN:28:2:149

Woods, K. N., and Pfeffer, J. (2020). Conformational perturbation, allosteric modulation of cellular signaling pathways, and disease in P23H rhodopsin. *Sci. Rep.* 10:2657. doi: 10.1038/s41598-020-59583-2

Woods, K. N., Pfeffer, J., and Klein-Seetharaman, J. (2017). Chlorophyll-derivative modulation of rhodopsin signaling properties through evolutionarily conserved interaction pathways. *Front. Mol. Biosci.* 4:85. doi: 10.3389/fmolb.2017.00085

Wu, J., Chen, L., Tam, O. S., Huang, X. F., Pang, C. P., and Jin, Z. B. (2014). Whole exome sequencing reveals genetic predisposition in a large family with retinitis pigmentosa. *Biomed. Res. Int.* 2014:302487. doi: 10.1155/2014/302487

Wu, Y., Guo, Y., Yi, J., Xu, H., Yuan, L., Yang, Z., et al. (2019). HeterozygousRHOp.R135W missense mutation in a large Han-Chinese family with retinitis pigmentosa and different refractive errors. *Biosci. Rep.* 39:BSR20182198. doi: 10.1042/BSR20182198

Xiong, N., Zhang, Z., Huang, J., Chen, C., Zhang, Z., Jia, M., et al. (2011). VEGF-expressing human umbilical cord mesenchymal stem cells, an improved therapy strategy for Parkinson's disease. *Gene Ther.* 18, 394–402. doi: 10.1038/gt.2010.152

Yao, J., Qiu, Y., Frontera, E., Jia, L., Khan, N. W., Klionsky, D. J., et al. (2018). Inhibiting autophagy reduces retinal degeneration caused by protein misfolding. *Autophagy* 14, 1226–1238. doi: 10.1080/15548627.2018.1463121

Yao, K., Qiu, S., Wang, Y. V., Park, S. J. H., Mohns, E. J., Mehta, B., et al. (2018). Restoration of vision after de novo genesis of rod photoreceptors in mammalian retinas. *Nature* 560, 484–488. doi: 10.1038/s41586-018-0425-3

Yu, H., Enayati, S., Chang, K., Cho, K., Lee, S. W., Talib, M., et al. (2020). Noninvasive electrical stimulation improves photoreceptor survival and retinal function in mice with inherited photoreceptor degeneration. *Invest. Ophthalmol. Vis. Sci.* 61:5. doi: 10.1167/iovs.61.4.5

Yu, H., Vu, T. H., Cho, K. S., Guo, C., and Chen, D. F. (2014). Mobilizing endogenous stem cells for retinal repair. *Transl. Res.* 163, 387–398. doi: 10.1016/j.trsl.2013.11.011

Zamecnik, P. C., and Stephenson, M. L. (1978). Inhibition of Rous sarcoma virus replication and cell transformation by a specific oligodeoxynucleotide. *Proc. Natl. Acad. Sci. U. S. A.* 75, 280–284. doi: 10.1073/pnas.75.1.280

Zaverucha-do-Valle, C., Gubert, F., Bargas-Rega, M., Coronel, J. L., Mesentier-Louro, L. A., Mencalha, A., et al. (2011). Bone marrow mononuclear cells increase retinal ganglion cell survival and axon regeneration in the adult rat. *Cell Transplant.* 20, 391–406. doi: 10.3727/096368910X524764

Zeitlin, P. L., Diener-West, M., Rubenstein, R. C., Boyle, M. P., Lee, C. K., and Brass-Ernst, L. (2002). Evidence of CFTR function in cystic fibrosis after systemic administration of 4-phenylbutyrate. *Mol. Ther.* 6, 119–126. doi: 10.1006/mthe.2002.0639

Zhang, Q. (2016). Retinitis Pigmentosa: Progress and perspective. *Asia Pac. J. Ophthalmol. (Phila)* 5, 265–271. doi: 10.1097/APO.0000000000000227

Zhu, R. L., Fang, Y., Yu, H. H., Chen, D. F., Yang, L., and Cho, K. S. (2021). Absence of ephrin-A2/A3 increases retinal regenerative potential for Muller cells in rhodopsin knockout mice. *Neural Regen. Res.* 16, 1317–1322. doi: 10.4103/1673-5374.301034

frontiers | Frontiers in Neuroscience

TYPE Original Research
PUBLISHED 06 April 2023
DOI 10.3389/fnins.2023.1143476

OPEN ACCESS

EDITED BY
Wensi Tao,
University of Miami Health System, United States

REVIEWED BY
Jie Zhang,
Huazhong University of Science and Technology, Wuhan, China
Yan Yan,
Shanghai Jiao Tong University, China

*CORRESPONDENCE
Jia Tan
✉ jasmintj@126.com
Guoping Kuang
✉ kgp@163.com

†These authors have contributed equally to this work

SPECIALTY SECTION
This article was submitted to Visual Neuroscience, a section of the journal Frontiers in Neuroscience

RECEIVED 13 January 2023
ACCEPTED 17 March 2023
PUBLISHED 06 April 2023

CITATION
Li Z, Tong J, Liu C, Zhu M, Tan J and Kuang G (2023) Analysis of independent risk factors for progression of different degrees of diabetic retinopathy as well as non-diabetic retinopathy among type 2 diabetic patients. *Front. Neurosci.* 17:1143476. doi: 10.3389/fnins.2023.1143476

Analysis of independent risk factors for progression of different degrees of diabetic retinopathy as well as non-diabetic retinopathy among type 2 diabetic patients

Zheng Li[1,2†], Jie Tong[3,4†], Chang Liu[5], Mingqiong Zhu[1,2], Jia Tan[6*] and Guoping Kuang[1,2*]

[1]Department of Ophthalmology, The First People's Hospital of Chenzhou, Chenzhou, Hunan, China, [2]Department of Ophthalmology, The Affiliated Chenzhou Hospital, Hengyang Medical School, University of South China, Chenzhou, Hunan, China, [3]Department of Spinal Surgery, The First People's Hospital of Chenzhou, Chenzhou, Hunan, China, [4]Department of Spinal Surgery, The Affiliated Chenzhou Hospital, Hengyang Medical School, University of South China, Chenzhou, Hunan, China, [5]Department of Endocrinology, The First People's Hospital of Chenzhou, Chenzhou, Hunan, China, [6]Department of Ophthalmology, Xiangya Hospital of Central South University, Changsha, Hunan, China

Purpose: To study the independent risk factors for development of different degrees of diabetic retinopathy (DR) as well as non-DR (NDR) among type 2 diabetic patients.

Methods: This cross-sectional study included 218 patients with type 2 diabetes between January 2022 and June 2022. All the patients were divided into two groups: the DR group and the NDR group. The DR group was subdivided into the mild, moderate and severe non-proliferative DR (NPDR) group and the proliferative DR (PDR) group. Data recorded for all patients included age, gender, duration of diabetes, blood pressure, glycated hemoglobin (HbA1c), fasting blood glucose (FBG), blood lipids, best corrected visual acuity (BCVA), intraocular pressure (IOP), axial length (AL), anterior chamber depth (ACD), and renal function. Logistic regression methods were used to analyze the risk factors for DR.

Results: The prevalence of DR in type 2 diabetes was 28.44%. The duration of diabetes, age, mean arterial pressure (MAP), HbA1c, FBG, urinary albumin/creatinine ratio (UACR), BCVA, AL, and ACD were significantly different between the DR and the NDR groups (p <0.05). Multivariate logistic regression analysis identified age, FBG, UACR, and AL as the independent risk factors for DR (OR=0.843, 2.376, 1.049, 0.005; p=0.034, 0.014, 0.016, p <0.001).

Conclusion: Young age, short AL, higher levels of FBG and UACR were the independent risk factors for the progression of DR in type 2 diabetes.

KEYWORDS

diabetes mellitus, retinopathy, progression, risk factor, cross-sectional study

Introduction

The International Diabetes Federation (IDF) estimated the global burden of diabetes mellitus (DM) to be 463 million in 2019 and projected it to be 700 million by 2045. Diabetic retinopathy (DR) is a common and severe microvascular complication of DM, and one of the major diseases causing blindness in adults. In recent years, the prevalence and blindness rate of DR have

significantly increased, seriously threatening the quality of life of patients with diabetes. With a rapidly aging global population, increasing lifespan of people living with DM, and lifestyle changes leading to an increased risk for DM, a higher burden of DR and demand for eye care and treatment are expected (Ting et al., 2016; Teo et al., 2021).

Several studies have shown that the risks of DR onset and its progression are modified by a variety of systemic and ocular factors. Age, male sex, hypertension, duration of diabetes, diabetic neuropathy, diabetic nephropathy, fasting blood glucose, serum total cholesterol, serum triglyceride, and glycated hemoglobin (HbA1c) are risk factors for diabetic retinopathy (Ting et al., 2016; Yin et al., 2020). Longer duration of diabetes has a higher likelihood of predicting DR. However, few studies have addressed the issue of whether there are differences in the risk factors for the duration of diabetes and age between the groups with different degrees of DR. We suppose that the risk factors of DR may be inconsistent under different courses of T2DM. Currently, the treatment of DR is mainly to prevent or delay disease progression. Early detection and intervention of risk factors can reduce the progression of DR. Hence, it is of great significance to focus on the risk factors of DR at an early stage of T2DM.

In addition, more attention should be paid to the relationship between Myopia and DR. High myopia has been suggested to have a protective effect against DR (Lin et al., 2020). However, it remains unclear whether the protective association of myopia with DR is related to the long axial length or to other components, such as ACD. Hence, it is critical to explore the independent risk factors for progression of different degrees of DR as well as NDR and target the high-risk factors for active and effective prevention.

Materials and methods

Materials

This cross-sectional study analyzed 218 consecutive patients with type 2 diabetes admitted to the Endocrinology Department of the First People's Hospital of Chenzhou between January 2022 and June 2022. The study was conducted in accordance with the tenets of the Declaration of Helsinki and was approved by the hospital ethics committee (No. 2022025). Written informed consent was provided by all patients before joining the study.

Inclusion criteria were as follows: (1) age $\geq$ 18 years. (2) Patients with type 2 diabetes who met the diagnostic criteria (Chinese Diabetes Society, 2020) of the Chinese guidelines for the prevention and treatment of type 2 diabetes (2020 Edition) as follows: typical diabetes symptoms plus plasma glucose level $\geq$ 11.1 mmol·L^{-1} at any time, or fasting plasma glucose level $\geq$ 7.0 mmol · L^{-1}, or blood glucose level $\geq$ 11.1 mmol · L^{-1} 2 h after glucose load. (3) Patients or family members gave informed consent.

Exclusion criteria were as follows: (1) patients with type 1 diabetes mellitus (DM), gestational DM, ketoacidosis and hyperosmolar diabetic acidosis. (2) Patients with complications such as DM with iatrogenic Cushing's syndrome, Sheehan syndrome, acute purulent tonsillitis, and granulocytopenia that could affect the results of the risk factor analysis. (3) Fundus examination was affected by refractive media opacities such as retinal detachment, keratopathy, and cataract. (4) Non-diabetes mellitus-induced renal dysfunction disease. (5) A history of glaucoma, ocular trauma, or ocular surgery was present.

Methods

Data recorded for all patients included: (1) Name, gender, age, diabetes duration, glycemic control, etc. (2) Blood pressure: systolic blood pressure (SBP), diastolic blood pressure (DBP) at rest. Mean arterial pressure (MAP) was calculated as: MAP = (SBP + 2 × DBP)/3. (3) Early morning fasting blood samples were collected to measure serum triglycerides (TG), low-density lipoprotein cholesterol (LDL-C), glycated hemoglobin (HbA1c), and fasting blood glucose (FBG). (4) Twenty four hour urine samples were collected from patients to determine urinary albumin/creatinine ratio (UACR). (5) Blood sample and ocular examinations were performed on the same day in this study. Ophthalmic examination included best corrected visual acuity (BCVA), non-contact tonometry (model CT-80A; TOPCON, Japan), slit-lamp examination, ocular biological measurements (ocular axis, anterior chamber depth). Anterior chamber depth (ACD) and axial length (AL) of the globe using an IOLMaster (version 5.02; Carl Zeiss Meditec, Germany), Fundus examination after dilated pupils as well as fundus photography (model CR-2AF; Canon, Japan), fluorescein fundus angiography (FFA) (model HRA-II; Heidelberg, Germany) was performed on patients with confirmed DR as permitted by voluntary and systemic conditions.

Criteria for DR diagnosis and staging were according to the 2017 SED/SERV consensus guidelines (Corcóstegui et al., 2017). Those with no DR in both eyes were classified as the non-DR (NDR) group, those with DR diagnosed in one or both eyes were classified as the DR group, and those with discordant lesion degrees in both eyes were grouped by more severe lesion degrees. The DR group was further divided into the mild, moderate and severe non-proliferative DR (NPDR) group as well as the proliferative DR (PDR) group.

Statistical analysis

Descriptive statistical results are presented as mean ± standard deviation (SD). Counting data were expressed as frequencies and percentages, and comparisons between groups were performed using chi-squared test. Continuous variables were reported as means and standard deviations, which were compared between groups using independent samples *t*-tests. Comparisons of means between more than two groups were performed by one-way analysis of variance (ANOVA). Univariate logistic regression analysis was used to evaluate the related risk factors for the occurrence of DR. After controlling the confounding bias, multivariate logistic regression analysis was performed to clarify the independent risk factors for the occurrence of DR. A *value of p* <0.05 was considered statistically significant. Statistical analysis was performed using SPSS 16.0.

Results

General characteristics of study participants

The general characteristics of the 218 patients are shown in Table 1. In this study, a total of 51 patients (51 eyes) with DR received FFA examination and a total of 30 patients (30 eyes) with DR received previous retina laser treatment. The prevalence of DR among the 218

patients was found to be 28.44%. The prevalence of NPDR was 50.3% (5.50% mild, 7.80% moderate and 8.26% severe), and the prevalence of PDR was 6.88%. Diabetes duration (DD) and age were compared between the NDR and DR groups, and the difference was statistically significant ($t = 9.171, -4.276, p < 0.01$). The MAP, HbA1c, FBG, BCVA, and UACR were significantly higher in the DR group than in the NDR group, while the AL and ACD were significantly lower in the DR group than in the NDR group ($p < 0.05$).

Association between age, diabetes duration, and DR

Comparison of the duration of diabetes and age between the groups with different degrees of NPDR and PDR showed that with the duration of diabetes increases, the younger the age of onset, the higher the risk of progression of DR; the patients in the PDR group had a longer mean duration of diabetes and a younger mean age than the patients in the NPDR group ($F = 9.111, 3.352, p < 0.001, p = 0.025$, respectively), as shown in Table 2 and Figure 1.

Risk factor analysis for DR

Univariate logistic regression analysis showed that DD, age, MAP, HbA1c, FBG, UACR, AL, and ACD were significantly associated with the development of DR ($p < 0.05$). TG and LDL-C were not associated with the occurrence of DR ($p > 0.05$), as shown in Table 3.

The risk factors for DR such as DD, age, MAP, HbA1c, FBG, UACR, TG, LDL-C, AL, and ACD were included as independent variables in the multivariate logistic regression analysis. The results showed that age, FBG, UACR, and AL were independent risk factors for the progression of DR ($p = 0.034$, 0.014, 0.016, and $p < 0.001$, respectively), as shown in Table 4.

Discussion

In this study, the results showed that the prevalence of DR was 28.44%, with predominance of moderate and severe NPDR. As the duration of diabetes increases, the younger the age of onset, the higher the risk of progression of DR. The patients in the PDR group had a longer mean duration of diabetes and a younger mean age than the patients in the NPDR group. The severity and prevalence of disease increased with Diabetes duration (DD), which was similar to the results of previous studies (Song et al., 2018; Yin et al., 2020). Numerous studies have shown that DR results from a combination of multiple factors, mainly related to blood glucose, blood pressure, lipids, DD, age, renal function and other factors (Song et al., 2018; Teo et al., 2021). Our results showed that DD, age, MAP, HbA1c, FBG, UACR, AL, and ACD were significantly different between the DR group and the NDR group. Patients in the NDR group had better BCVA than those in the DR group, which was related to the fundus disease in the DR Group. Moreover, age, FBG, UACR, and AL were independent risk factors for concurrent DR in patients with type 2 diabetes by multivariate logistic regression analysis. Hence, younger age, shorter AL, higher FBG and UACR levels were associated with a higher risk of concurrent DR.

TABLE 1 Comparison of various clinical parameters between the DR group and the NDR group.

	DR group (n=62)	NDR group (n=156)	t/χ^2	P
DD, year (mean ± SD)	10.10 ± 3.59	5.94 ± 2.76	9.171	<0.001*
Age, year (mean ± SD)	60.69 ± 9.70	66.65 ± 9.09	−4.276	<0.001*
Gender (male/femle, n)	37/25	91/65	0.033	0.856†
MAP (mmHg)	90.82 ± 9.58	86.20 ± 8.07	3.605	<0.001*
HbA1c (%)	7.64 ± 0.90	6.50 ± 0.79	9.150	<0.001*
FBG (mmol·L^{-1})	9.74 ± 1.32	7.78 ± 1.38	9.510	<0.001*
TG (mmol·L^{-1})	1.89 ± 0.16	1.86 ± 0.14	1.820	0.070*
LDL-C (mmol·L^{-1})	3.64 ± 0.33	3.57 ± 0.31	1.621	0.106*
UACR (mg·g^{-1})	260.29 ± 45.44	190.99 ± 14.08	17.139	<0.001*
AL (mm)	22.85 ± 0.41	24.12 ± 1.06	−9.159	<0.001*
ACD (mm)	2.79 ± 0.21	2.90 ± 0.17	−3.977	<0.001*
Mean IOP (mmHg)	14.74 ± 3.01	14.86 ± 2.76	−0.275	0.784*
Hypertension [n (%)]	30 (48.38)	42 (26.92)	9.241	0.002†
BCVA [n (%)]			7.887	0.019†
>0.1	40 (64.52)	120 (76.92)		
0.02 ~ 0.1	17 (27.42)	34 (21.79)		
<0.02	5 (8.06)	2 (1.28)		

*Independent sample t-test.
†Chi-squared test.
DD, Diabetes duration; MAP, mean arterial pressure; HbA1c, glycated hemoglobin; FBG, fasting blood glucose; TG, triglycerides; LDL-C, low-density lipoprotein cholesterol; UACR, urinary albumin/creatinine ratio; AL, axial length; ACD, anterior chamber depth; IOP, intraocular pressure; BCVA, best corrected visual acuity.

TABLE 2 Comparison of the basic data of each subgroup of DR patients.

	Number of cases	DD, year (mean±SD)	Age, year (mean ± SD)
NPDR group			
Mild	12	7.17 ± 2.29	64.50 ± 4.70
Moderate	17	8.76 ± 2.19	64.29 ± 7.63
Severe	18	11.17 ± 3.93	59.11 ± 9.04
PDR group	15	12.67 ± 3.15	55.47 ± 12.90
F-value		9.111	3.352
p-value		<0.001	0.025

NPDR, non-proliferative DR; PDR, proliferative DR.

Long AL may be protective against the development of DR. He et al. (2017) conducted an epidemiological investigation and found that type 2 diabetic patients with long AL had a low risk of developing DR. Man et al. (2012) stated that long AL is protective for mild, moderate, and severe DR. The mechanism of the protective effect of

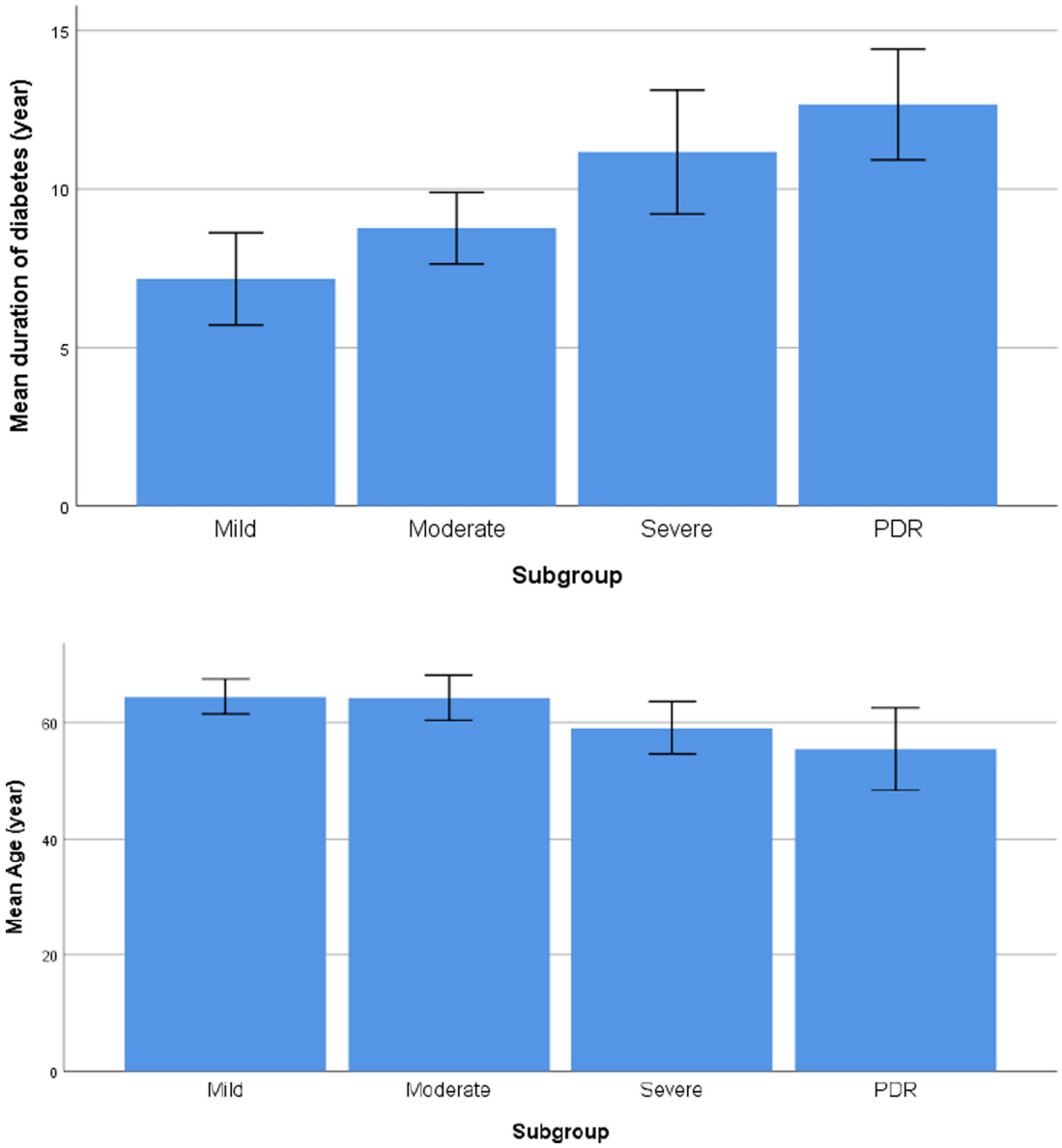

FIGURE 1
Comparison of the duration of diabetes and age between the groups with different degrees of NPDR and PDR.

long AL and myopia on the development and progression of DR remains unknown, and the possible reasons are as follows: (1) Patients with longer AL have reduced retinal blood flow, slower blood velocity, and reduced vessel wall pressure, thus limiting the occurrence and progression of DR (Lim et al., 2011; Kim et al., 2018). (2) Disruption of retinal and choroidal blood vessels occurs earlier in patients with high myopia, and the drop in retinal blood perfusion prevents the formation of an abnormal hyperperfusion state that induces DR, thus reducing the risk of developing DR (Benavente-Pérez et al., 2010; Kim et al., 2018). (3) The choroid and retina become thinner with the growth of the ocular axis, and the retinal metabolic rate and oxygen demand decrease, thereby reducing the release of some inflammatory factors due to hypoxia as well as VEGF production (Sawada et al., 2011). (4) Patients with long AL and high myopia often have earlier onset of vitreous liquefaction and posterior vitreous detachment, lack of scaffolds in the vitreous that are needed for neovascular proliferation, easier diffusion of oxygen through the liquefied vitreous, reduced aggregation of promoting neovascular factors to achieve the degree of neovascularization, and therefore slowing the progression of DR (Lin et al., 2020).

Previous studies have shown that high levels of UACR, as a marker of endothelial dysfunction, may affect renal and retinal microangiopathy, and are associated with type 1 DR pathogenesis, not with type 2 DR (Pedro et al., 2010). Our results showed that UACR levels could not only assess the risk of concurrent DR in patients with type 2 diabetes but also were positively correlated with the prevalence of DR. Both glomerular and retinal vessels of the microcirculation system that share similar physiological features, with hyperglycemia driving the production of glycosylation end products, resulting in functional impairment of the vascular endothelium, enhanced oxidative stress and release of inflammatory mediators, causing disruption of the glomerular filtration membrane barrier and blood

TABLE 3 Univariate logistic regression analysis of risk factors for DR.

	Partial regression coefficients	SD	Wald statistic	*OR*	95% *CI*	*P*
DD	0.410	0.063	42.144	1.506	1.331 ~ 1.705	<0.001
Age	−0.067	0.017	15.310	0.935	0.904 ~ 0.967	<0.001
MAP	0.059	0.017	11.607	1.060	1.025 ~ 1.097	0.001
HbA1c	1.543	0.234	43.379	4.679	2.956 ~ 7.406	<0.001
FBG	0.912	0.138	43.787	2.490	1.900 ~ 3.262	<0.001
TG	1.817	1.010	3.239	6.155	0.851 ~ 44.539	0.072
LDL-C	0.762	0.473	2.597	2.142	0.848 ~ 5.412	0.107
UACR	0.065	0.010	41.991	1.067	1.046 ~ 1.088	<0.001
AL	−7.053	1.036	46.396	0.001	0 ~ 0.007	<0.001
ACD	−2.939	0.788	13.921	0.053	0.011 ~ 0.248	<0.001

DD, Diabetes duration; MAP, mean arterial pressure; HbA1c, glycated hemoglobin; FBG, fasting blood glucose; TG, triglycerides; LDL-C, low-density lipoprotein cholesterol; UACR, urinary albumin/creatinine ratio; AL, axial length; ACD, anterior chamber depth.

TABLE 4 Multivariate logistic regression analysis of risk factors for DR.

Independent variable	*OR*	95% *CI*	*P*
DD	1.293	0.778 ~ 2.149	0.321
Age	0.843	0.720 ~ 0.987	0.034
MAP	1.057	0.930 ~ 1.202	0.397
HbA1c	1.199	0.293 ~ 4.914	0.801
FBG	2.376	1.193 ~ 4.731	0.014
TG	0.002	0 ~ 12.360	0.165
LDL-C	0.300	0.005 ~ 17.730	0.563
UACR	1.049	1.009 ~ 1.091	0.016
AL	0.005	0 ~ 0.078	<0.001
ACD	0.295	0.001 ~ 103.532	0.683

DD, Diabetes duration; MAP, mean arterial pressure; HbA1c, glycated hemoglobin; FBG, fasting blood glucose; TG, triglycerides; LDL-C, low-density lipoprotein cholesterol; UACR, urinary albumin/creatinine ratio; AL, axial length; ACD, anterior chamber depth.

retinal barrier (Liu et al., 2022). Therefore, diabetic patients with high UACR levels should be screened for DR by fundus examination as early as possible.

Previous studies have shown that DR severity in type 2 diabetes is significantly positively correlated with TG, and LDL-C is an independent risk factor for retinopathy (Agroiya et al., 2013; Tan et al., 2018). On the contrary, some studies suggest that LDL-C has nothing to do with DR (Pang et al., 2012; Wang et al., 2012). Chang and Wu (2013) speculated that blood lipids may not directly damage endothelial tissue, only in the later stages are they pathogenic by damaging retinal vessels. Therefore, it is believed that dyslipidemia is more involved in its pathogenesis in the severe stages of DR than in the early stages. Considering the low prevalence of PDR (6.88%), our results showed that TG and LDL-C were not associated with the progression of DR.

Studies have shown that obesity, medications, and oxygen therapy are also contributing factors to DR (Thomas et al., 2012; Mcmonnies, 2015; Raum et al., 2015; Li et al., 2022). Raum et al. (2015) prospectively identified obesity (BMI ≥ 30) as a risk factor for eyesight loss in DR. However, in this cross-sectional study, the included subjects were consecutive patients hospitalized during a certain period, which was limited by geographical, dietary and lifestyle habits, with fewer patients with obesity. Therefore, a study specifically focused on the correlation between obesity and DR is needed to supplement the future study.

This study only selected UACR as an indicator to evaluate renal function, which has limitations. Studies have shown a significant association between GFR and DR in Caucasian T2DM patients, with reduced GFR increasing the risk of DR, but both associations have been inconsistently reported in Asian populations (Grunwald et al., 2012; Perol et al., 2012; Man et al., 2015; Guo et al., 2016). A cross-sectional study that included 3,301 T2DM patients showed that both proteinuria and GFR decline were significantly associated with the development of DR (Guo et al., 2016). Therefore, it may be more helpful to include indicators such as GFR and Cr in future studies to discover independent risk factors for the progression of DR.

Conclusion

In this study, we evaluated the association between DR and systemic influencing factors, and found that young age, short axial length, and high levels of FBG and UACR were independent risk factors for the progression of DR in type 2 diabetes. Although the conclusions of this study provide a basis for clinicians to identify high-risk factors for developing DR, whether it can be used for screening DR needs to be confirmed by further large sample, multi-center studies.

Data availability statement

The raw data supporting the conclusions of this article will be made available by the authors, without undue reservation.

Ethics statement

The studies involving human participants were reviewed and approved by the Ethics Committee of the First People's Hospital of Chenzhou. The patients/participants provided their written informed consent to participate in this study.

Author contributions

ZL and JeT designed the study and drafted the manuscript. CL and MZ collected the data and carried out statistical analyses and data interpretation. GK participated in the study design and contributed to the editing of the manuscript. JaT performed the computational analysis and contributed to the preparation of the manuscript. All authors contributed to the interpretation of the data and approved the final version of the manuscript.

Funding

This research was supported by the Science and Technology Planning Project of Chenzhou, China (No. CZKJ2016053).

Conflict of interest

The authors declare that the research was conducted in the absence of any commercial or financial relationships that could be construed as a potential conflict of interest.

Publisher's note

All claims expressed in this article are solely those of the authors and do not necessarily represent those of their affiliated organizations, or those of the publisher, the editors and the reviewers. Any product that may be evaluated in this article, or claim that may be made by its manufacturer, is not guaranteed or endorsed by the publisher.

References

Agroiya, P., Philip, R., Saran, S., Gutch, M., Tyagi, R., and Gupta, K. K. (2013). Association of serum lipids with diabetic retinopathy in type 2 diabetes. *Indian J. Endocrinol. Metab.* 17, 335–S337. doi: 10.4103/2230-8210.119637

Benavente-Pérez, A., Hosking, S. L., Logan, N. S., and Broadway, D. C. (2010). Ocular blood flow measurements in healthy human myopic eyes. *Graefes Arch. Clin. Exp. Ophthalmol.* 248, 1587–1594. doi: 10.1007/s00417-010-1407-9

Chang, Y., and Wu, W. (2013). Dyslipidemia and diabetic retinopathy. *Rev. Diabet. Stud.* 10, 121–132. doi: 10.1900/RDS.2013.10.121

Chinese Diabetes Society (2020). Guideline for the prevention and treatment of type 2 diabetes mellitus in China. *Chin J Endocrinol Metab* 37, 2–51. doi: 10.3760/cma.j.cn311282-20210304-00142

Corcóstegui, B., Durán, S., González-Albarrán, M. O., Hernández, C., Ruiz-Moreno, J. M., Salvador, J., et al. (2017). Update on diagnosis and treatment of diabetic retinopathy: A consensus guideline of the working group of ocular health (Spanish society of diabetes and Spanish vitreous and retina society). *J. Ophthalmol.* 2017, 1–10. doi: 10.1155/2017/8234186

Grunwald, J. E., Alexander, J., Ying, G. S., Maguire, M., Daniel, E., Whittock-Martin, R., et al. (2012). Retinopathy and chronic kidney disease in the chronic renal insufficiency cohort (CRIC) study. *Arch. Ophthalmol.* 130, 1136–1144. doi: 10.1001/archophthalmol.2012.1800

Guo, K., Zhang, L., Zhao, F., Lu, J., Pan, P., Yu, H., et al. (2016). Prevalence of chronic kidney disease and associated factors in Chinese individuals with type 2 diabetes: Cross-sectional study. *J. Diabetes Complicat.* 30, 803–810. doi: 10.1016/j.jdiacomp.2016.03.020

He, J., Xu, X., Zhu, J., Zhu, B., Zhang, B., Lu, L., et al. (2017). Lens power, axial length-to-corneal radius ratio, and association with diabetic retinopathy in the adult population with type 2 diabetes. *Ophthalmology* 124, 326–335. doi: 10.1016/j.ophtha.2016.10.041

Kim, D. Y., Song, J. H., Kim, Y. J., Lee, J. Y., Kim, J., Yoon, Y. H., et al. (2018). Asymmetric diabetic retinopathy progression in patients with axial anisometropia. *Retina* 38, 1809–1815. doi: 10.1097/IAE.0000000000002109

Li, Y., Gappy, S., Liu, X., Sassalos, T., Zhou, T., Hsu, A., et al. (2022). Metformin suppresses pro-inflammatory cytokines in vitreous of diabetes patients and human retinal vascular endothelium. *PLoS One* 17:e268451:e0268451. doi: 10.1371/journal.pone.0268451

Lim, L. S., Cheung, C. Y., Lin, X., Mitchell, P., Wong, T. Y., and Mei-Saw, S. (2011). Influence of refractive error and axial length on retinal vessel geometric characteristics. *Invest. Ophthalmol. Vis. Sci.* 52, 669–678. doi: 10.1167/iovs.10-6184

Lin, Z., Li, D., Zhai, G., Wang, Y., Wen, L., Ding, X. X., et al. (2020). High myopia is protective against diabetic retinopathy via thinning retinal vein: A report from Fushun Diabetic Retinopathy Cohort Study (FS-DIRECT). *Diab. Vasc. Dis. Res.* 17:147916412094098. doi: 10.1177/1479164120940988

Liu, W., Du, J., Ge, X., Jiang, X., Peng, W., Zhao, N., et al. (2022). The analysis of risk factors for diabetic kidney disease progression: A single-centre and cross-sectional experiment in Shanghai. *BMJ Open* 12:e60238. doi: 10.1136/bmjopen-2021-060238

Man, R. E. K., Sasongko, M. B., Sanmugasundram, S., Nicolaou, T., Jing, X., Wang, J. J., et al. (2012). Longer axial length is protective of diabetic retinopathy and macular edema. *Ophthalmology* 119, 1754–1759. doi: 10.1016/j.ophtha.2012.03.021

Man, R. E. K., Sasongko, M. B., Wang, J. J., MacIsaac, R., Wong, T. Y., Sabanayagam, C., et al. (2015). The association of estimated glomerular filtration rate with diabetic retinopathy and macular edema. *Invest. Ophthalmol. Vis. Sci.* 56, 4810–4816. doi: 10.1167/iovs.15-16987

Mcmonnies, C. W. (2015). Hyperbaric oxygen therapy and the possibility of ocular complications or contraindications. *Clin. Exp. Optom.* 98, 122–125. doi: 10.1111/cxo.12203

Pang, C., Jia, L., Jiang, S., Liu, W., Hou, X., Zuo, Y., et al. (2012). Determination of diabetic retinopathy prevalence and associated risk factors in Chinese diabetic and pre-diabetic subjects: Shanghai diabetic complications study. *Diabetes Metab. Res. Rev.* 28, 276–283. doi: 10.1002/dmrr.1307

Pedro, R., Ramon, S., Marc, B., Juan, F., and Isabel, M. (2010). Prevalence and relationship between diabetic retinopathy and nephropathy, and its risk factors in the North-East of Spain, a population-based study. *Ophthalmic Epidemiol.* 17, 251–265. doi: 10.3109/09286586.2010.498661

Perol, J., Balkau, B., Guillausseau, P. J., and Massin, P. (2012). A study of the 3-year incidence of diabetic retinopathy in a French diabetic population seen at Lariboisière Hospital, Paris. *Diabetes Metab.* 38, 225–229. doi: 10.1016/j.diabet.2012.01.001

Raum, P., Lamparter, J., Ponto, K. A., Peto, T., Hoehn, R., Schulz, A., et al. (2015). Correction: Prevalence and cardiovascular associations of diabetic retinopathy and maculopathy: Results from the gutenberg health study. *PLoS One* 10:e139527. doi: 10.1371/journal.pone.0139527

Sawada, O., Miyake, T., Kakinoki, M., Sawada, T., Kawamura, H., and Ohji, M. (2011). Negative correlation between aqueous vascular endothelial growth factor levels and axial length. *Jpn. J. Ophthalmol.* 55, 401–404. doi: 10.1007/s10384-011-0027-1

Song, P., Yu, J., Chan, K. Y., Theodoratou, E., and Rudan, I. (2018). Prevalence, risk factors and burden of diabetic retinopathy in China: A systematic review and meta-analysis. *J. Glob. Health* 8:010803. doi: 10.7189/jogh.08.010803

Tan, G. S., Gan, A., Sabanayagam, C., Tham, Y. C., Neelam, K., Mitchell, P., et al. (2018). Ethnic differences in the prevalence and risk factors of diabetic retinopathy. *Ophthalmology* 125, 529–536. doi: 10.1016/j.ophtha.2017.10.026

Teo, Z. L., Tham, Y., Yu, M., Chee, M. L., Rim, T. H., Cheung, N., et al. (2021). Global prevalence of diabetic retinopathy and projection of burden through 2045. *Ophthalmology* 128, 1580–1591. doi: 10.1016/j.ophtha.2021.04.027

Thomas, R. L., Dunstan, F., Luzio, S. D., Roy Chowdury, S., Hale, S. L., North, R. V., et al. (2012). Incidence of diabetic retinopathy in people with type 2 diabetes mellitus attending the Diabetic Retinopathy Screening Service for Wales: Retrospective analysis. *BMJ* 344:e874. doi: 10.1136/bmj.e874

Ting, D. S. W., Cheung, G. C. M., and Wong, T. Y. (2016). Diabetic retinopathy: Global prevalence, major risk factors, screening practices and public health challenges: A review. *Clin. Exp. Ophthalmol.* 44, 260–277. doi: 10.1111/ceo.12696

Wang, S., Xu, L., Jonas, J. B., You, Q. S., Wang, Y. X., and Yang, H. (2012). Dyslipidemia and eye diseases in the adult Chinese population: The Beijing eye study. *PLoS One* 7:e26871. doi: 10.1371/journal.pone.0026871

Yin, L., Zhang, D., Ren, Q., Su, X., and Sun, Z. (2020). Prevalence and risk factors of diabetic retinopathy in diabetic patients. *Medicine* 99:e19236. doi: 10.1097/MD.0000000000019236

frontiers | Frontiers in Neuroscience

TYPE Original Research
PUBLISHED 25 April 2023
DOI 10.3389/fnins.2023.1179421

OPEN ACCESS

EDITED BY
Wensi Tao,
University of Miami Health System,
United States

REVIEWED BY
Lei Fang,
Sun Yat-sen University, China
Run Tian,
Second People's Hospital of Yunnan Province,
China

*CORRESPONDENCE
Peng Wang
✉ luckywp2000@aliyun.com

RECEIVED 04 March 2023
ACCEPTED 31 March 2023
PUBLISHED 25 April 2023

CITATION
Wang X and Wang P (2023) Spectral-domain optical coherence tomography combined with electroretinography in the assessment of conbercept for neovascular age-related macular degeneration: a preliminary study. *Front. Neurosci.* 17:1179421. doi: 10.3389/fnins.2023.1179421

Spectral-domain optical coherence tomography combined with electroretinography in the assessment of conbercept for neovascular age-related macular degeneration: a preliminary study

Xing Wang and Peng Wang*

Chongqing Key Laboratory of Ophthalmology, Department of Ophthalmology, Chongqing Eye Institute, The First Affiliated Hospital of Chongqing Medical University, Chongqing, China

Objective: To observe the effect of three consecutive intravitreal injections of conbercept in the treatment of neovascular age-related macular degeneration (nAMD), to investigate the correlation between retinal anatomy and retinal function by spectral-domain optical coherence tomography (SD-OCT) and electroretinography (ERG), to evaluate the short-term clinical efficacy of conbercept in the treatment of nAMD, and to explore the value of ERG as a predictor of treatment efficacy.

Method: A retrospective investigation was conducted on 36 patients (36 eyes) treated with intravitreal injections of conbercept at 0.5mg a month for three consecutive courses. Data collected included the best corrected visual acuity (BCVA), central retinal thickness (CRT), retinal pigment epithelium (RPE) elevation volume in 1mm-diameter (1RV), 3mm-diameter (3RV), and 6mm-diameter circles around the fovea (6RV), amplitude density and latency of the P1 wave in the multifocal electroretinography (mf-ERG) R1 ring and amplitude and latency in full-field electroretinography (ff-ERG) at baseline and monthly. The paired t test was used to compare the difference between pre- and posttreatment. Pearson correlation analysis was used to analyze the correlation between macular retinal structure and function. The difference was significant when $p<0.05$.

Results: At 12weeks, the BCVA, CRT, 1RV, 3RV, 6RV, the P1 wave amplitude density of the mf-ERG R1 ring and the ff-ERG amplitude parameters were all significantly improved ($p<0.001$). The BCVA in logMAR was positively correlated with CRT; 1RV, 3RV, and 6RV were negatively correlated with the amplitude density and latency of the mf-ERG R1 ring P1 wave. There were no severe ocular or systemic complications during the follow-up period.

Conclusion: Conbercept is useful for the short-term treatment of nAMD. It can safely improve the visual acuity of affected eyes and restore the structure and function of the retina. ERG could serve as an objective indicator of function for evaluating the efficacy of and determining the need for retreatment during nAMD treatment.

KEYWORDS

neovascular age-related macular degeneration, multifocal electroretinogram, full-field electroretinogram, spectral-domain optical coherence tomography, conbercept

Introduction

Neovascular age-related macular degeneration (nAMD) is a common blinding disease manifested as chronic and progressive aging of the macula (Ambati and Fowler, 2012). Several factors are associated with the development of nAMD, including age, environment, smoking, lifestyle, genetics (ultraviolet radiation-induced) chronic photodamage, hypertension, metabolic disorders, oxygen damage, and inflammatory reactions (Sakurada et al., 2013).

In recent years, a series of imaging examinations such as spectral-domain optical coherence tomography (SD-OCT), fundus fluorescein angiography (FFA), indocyanine green angiography (ICGA), multifocal electroretinography (mf-ERG) and full-field electroretinography (ff-ERG) have been widely used in ophthalmology (Castillo et al., 2014). SD-OCT is a high-resolution, 3D reconstruction-capable examination that can display the retinal tissue structure at different layers, measure the thickness of the retina and its different layers, accurately locate retinopathy, and be subjected to multilevel analysis (Wilde et al., 2015). Visual electrophysiological examinations are commonly used to evaluate various clinical macular diseases, these objective, specific and noninvasive examinations can also be used for the early detection of subclinical and undetected dysfunction (Renner et al., 2005). Invented by Sutter and Tran (1992) in the early 1990s, mf-ERG is a technique for objectively assessing visual cell function in the macula by obtaining the local retinal response to different stimulation units simultaneously. Its main advantages are its ability to identify lesions and assess disease severity (Moschos and Nitoda, 2018).

Anti-vascular endothelial growth factor (VEGF) is among the priority therapies for the treatment of nAMD. The efficacy and safety of anti-VEGF agents in eliminating choroidal neovascularization (CNV) have been clearly demonstrated. Anti-VEGF agents can effectively improve visual acuity, reduce blindness, and improve quality of life (Funk et al., 2009; Scott et al., 2015). Among anti-VEGF agents, conbercept is China's first novel biological drug, mainly targeting nAMD (Li et al., 2014). Conbercept is a fully human-derived protein that binds tightly to VEGF-A, VEGF-B, and placental growth factor (PIGF) (Lu et al., 2015). With high affinity and long half-life, it effectively inhibits the proliferation and migration of vascular endothelial cells and angiogenesis (Cui et al., 2018). Additionally, the unique structure of conbercept prolongs its effective duration of action and exposure, reducing the number and risk of injections and easing the burden of treatment (Nguyen and Guymer, 2015).

The criteria for evaluating the efficacy of anti-VEGF therapy and the need for retreatment rely on OCT, FFA, ICGA, mf-ERG, and other methods, such as microperimetry (Rai et al., 2021) and pupillographic objective perimetry (Rai et al., 2022). The only functional indicator currently in use is vision loss of more than five letters, which is subjective. Additionally, many hospitals do not have Early Treatment Diabetic Retinopathy Study (ETDRS) charts. Therefore, we intend to combine changes in best corrected visual acuity (BCVA), SD-OCT, and ERG to evaluate the clinical efficacy of conbercept in the treatment of nAMD and to understand the correlation between retinal anatomy and retinal function. We also sought to assess the value of ERG in anti-VEGF therapy and determine whether it could serve as an objective indicator of function in evaluating the efficacy of treatment and determining the need for retreatment.

Methods

Research design

This study is a retrospective clinical observation conducted according to the tenets of the Declaration of Helsinki. Thirty-six subjects (36 eyes) diagnosed with nAMD by fundus examination, SD-OCT, FFA, and ICGA were recruited from June 2017 to October 2018 from the Department of Ophthalmology of the First Affiliated Hospital of Chongqing Medical University, Chongqing, China. All patients received an intravitreal injection of 0.5 mg conbercept once a month for three consecutive courses. The injections were performed in strict accordance with the clinical trial data of conbercept (Zhang et al., 2011; Li et al., 2014). The inclusion criteria were as follows: (1) age $\geq$ 50 years, BCVA 0.05–0.5, and the nAMD diagnostic criteria (Adrean et al., 2018); (2) FFA/ICGA suggesting the presence of macular neovascularization; and (3) no previous treatment (e.g., triamcinolone, anti-VEGF, photodynamic therapy). Anyone with one of the following conditions was excluded: (1) allergy to local anesthetics, mydriatic eye drops, and contrast agents; (2) moderate refractive opacity that affects imaging, aphakic eyes; (3) history of internal eye surgery, trauma or previous fundus laser photocoagulation; (4) glaucoma or high intraocular pressure; (5) fundus diseases such as pathological myopia, diabetic retinopathy, retinal vein occlusion, proliferative vitreoretinopathy, MH, idiopathic or autoimmune uveitis; and (6) scleromalacia.

Assessment

BCVA was assessed with the international logarithmic visual acuity scale. Intraocular pressure (IOP) was measured by a noncontact automatic tonometer (NIDEK NT-510, Japan). Slit-lamp examination and fundus photography (TOPCON TRC-NW8 fundus camera, Japan), SD-OCT, and ERG were performed at baseline and 4 weeks after each intravitreal injection. FFA and ICGA were performed at baseline by a Heidelberg Spectralis HRA illuminator. At baseline and at each visit, we carefully examined the anterior segment (including the cornea, anterior chamber, iris, lens), vitreous chamber, and IOP and recorded the opacity of the refractive media. We also tested the subject for infection or uveal inflammatory reactions before and after intravitreal injection and, if present, assessed and recorded the severity of the reactions.

SD-OCT was performed with a spectral-domain OCT instrument (SPECTRALIS HRA OCT, Heidelberg, Germany). The overlapping mode was used for the same patient for each measurement. Central retinal thickness (CRT) was delineated as the average thickness of the neurosensory retina within a central 1 mm-diameter area. The retinal pigment epithelium (RPE) layer strips were manually fine-tuned to obtain a more accurate measurement. The lesion volume within 1 mm-, 3 mm-, and 6 mm-diameter circles around the macular fovea was measured using macular topographic analysis software. The CRT and the RPE elevation volume in the 1 mm-diameter (1RV), 3 mm-diameter (3RV) and 6 mm-diameter circles around the macular fovea (6RV) were recorded.

ERG was performed with a RETI-Port/Scan 21 system (Roland Consult Gmbh, Wiesbaden, Germany). Prior to the examination,

0.5% topiramate ophthalmic solution was administered to fully dilate the pupil to approximately 7 mm in diameter, and cocaine hydrochloride ophthalmic solution was given for surface anesthesia. Reference electrodes were attached to each side of the crotch, and recording electrodes were hung on the conjunctiva surface of the lower third of the eyes and then fixed with tape. The patient's pupil was tested for dilatation according to the standards of the International Society for Clinical Electrophysiology of Vision (Berezovsky et al., 2003). Dark-adapted 0.01 ERG (rod response), dark-adapted 3.0 ERG (combined response), dark-adapted 3.0 oscillatory potentials, light-adapted 3.0 ERG (cone response), and light-adapted 3.0 flicker response (cone-pathway response) were recorded. mf-ERG was performed in 61 stimulation unit modes. Since the amplitude density of the P1 waves mainly corresponds to the distribution range of visual cells, with the highest density at the fovea and gradually decreasing toward the periphery, the measured R1 ring mainly represents the retinal function of the fovea (Chen et al., 2005). The mf-ERG recordings were thus analyzed by measuring the amplitude density and latency of the P1 wave of the R1 ring. During the recording, abnormalities such as electrode detachment, baseline drift, and interference were observed to avoid shifting of eye position. All examinations were completed by the same physician.

Statistical analysis

We used SPSS 22.0 software (SPSS, IBM, Armonk, NY) for statistical analysis. The mean ± standard deviation represents the measurements. All data were verified to be normally distributed using the Kolmogorov–Smirnov test. The means of the BCVA, CRT, 1RV, 3RV, 6RV, and the mf-ERG (the amplitude density and latency of the P1 wave of the R1 ring) and ff-ERG parameters (amplitude and latency of the dark-adapted 0.01 b wave, dark adapted 3.0 a/b wave, dark-adapted 3.0 oscillatory potentials, light-adapted 3.0 a/b wave and light-adapted 3.0 flicker responses b wave) were compared between baseline and 12 weeks. We used the two paired-samples *t* test for all comparisons. Correlations between the BCVA and SD-OCT, mf-ERG, and ff-ERG parameters were analyzed using the Pearson correlation. $p < 0.05$ indicated statistical significance.

Results

Patient characteristics

The average age of the 36 subjects was 71.28 ± 9.16 years. Among them, 19 (52.78%) were male, and 17 (47.22%) were female. There were 15 (41.67%) cases of nAMD in the right eye and 21 (58.33%) cases in the left eye. Other details are available in Table 1. In our study, all 36 patients had monocular nAMD.

TABLE 1 Baseline characteristics of patients with AMD.

N		36
Age, *y*		71.28 ± 9.16
Sex	Male, *n*	19 (52.78%)
	Female, *n*	17 (47.22%)
Side	Right, *n*	15 (41.67%)
	Left, *n*	21 (58.33%)
Duration of AMD, *m*		6.28 ± 2.76
MNV Type I/II/III, *n*		15/19/2

AMD, age-related macular degeneration; MNV, macular neovascularization; n, number; m, month. Values are mean ± SD.

BCVA

Twelve weeks after the first injection, the mean BCVA (0.85 ± 0.34) improved by 2–3 lines (0.56 ± 0.29), and the difference from baseline was statistically significant ($t = 8.6524$, $p = 3.2 \times 10^{-10}$) (Table 2).

SD-OCT

The SD-OCT examinations showed that the 36 eyes had a loss of normal morphology of the macular area at baseline with intraretinal cysts, subretinal fluid (SRF), retinal thickening, pigment epithelial detachment (PED), subretinal hyperreflective material (SHRM) and intraretinal hyperreflective foci (IHFs). The specific percentages of these alterations are detailed in Table 2. The mean CRT (472.14 ± 181.53) significantly decreased to 311.61 ± 95.67 at 12 weeks ($p = 1.2 \times 10^{-8}$); the mean 1RV (0.36 ± 0.14) significantly decreased to 0.25 ± 0.08 at 12 weeks ($p = 1.0 \times 10^{-7}$); the mean 3RV (3.04 ± 0.98) significantly decreased to 2.17 ± 0.72 at 12 weeks ($p = 3.5 \times 10^{-8}$); and the mean 6RV (8.17 ± 2.91) significantly decreased to 4.90 ± 2.49 at 12 weeks ($p = 2.6 \times 10^{-9}$) (Table 2; Figure 1A).

ERG

Comparison of the P1 wave data of the mf-ERG R1 ring at baseline (36.47 ± 14.25) and after 12 weeks (58.36 ± 13.45) indicated a considerable increase in amplitude density ($p = 5.0 \times 10^{-11}$) but not in the P1 latency (38.13 ± 9.75 vs. 39.21 ± 9.63, $p = 0.22$) (Table 3; Figure 1B). Comparisons of the ff-ERG parameters showed that all but latency significantly increased after 12 weeks. The details are shown in Table 3.

Correlation analysis

Pearson correlation analysis was conducted between the BCVA (logMAR) and OCT and ERG measurements at baseline and 12 weeks separately for all 36 nAMD eyes, and the corresponding scatter plots were generated. The analyzes indicated that the BCVA was positively and significantly correlated with the CRT, 1RV, 3RV, and 6RV, negatively and significantly correlated with the amplitude density and latency of the P1 wave of the mfERG R1 ring and negatively but not significantly correlated with the ff-ERG parameters.

Notably, at 12 weeks, the BCVA and CRT were positively correlated, but not significantly ($p = 0.06$) (Tables 4, 5; Figures 2A,B).

Complications and adverse reactions

The IOP was within the normal range (10 to 21 mmHg) in all 36 eyes before and after treatment during the follow-up period; any

TABLE 2 Changes in BCVA, fundus findings, and SD-OCT after intravitreal injection of Conbercept.

	Baseline (0week)	4 weeks	8 weeks	12 weeks	End vs. Pre	
					T value	*p* value
BCVA (logMAR)	0.85 ± 0.34	0.69 ± 0.30	0.58 ± 0.30	0.56 ± 0.29	8.6524	3.2×10^{-10}
CRT (μm)	472.14 ± 181.53	389.5 ± 126.57	332.19 ± 102.43	311.61 ± 95.67	7.4002	1.2×10^{-8}
1RV (mm^3)	0.36 ± 0.14	0.31 ± 0.11	0.26 ± 0.07	0.25 ± 0.08	6.6614	1.0×10^{-7}
3RV (mm^3)	3.04 ± 0.98	2.59 ± 0.71	2.23 ± 0.65	2.17 ± 0.72	7.0254	3.5×10^{-8}
6RV (mm^3)	8.17 ± 2.91	6.66 ± 2.42	5.36 ± 2.53	4.90 ± 2.49	7.9148	2.6×10^{-9}
Retinal						
Hemorrhages (%)	66 ± 1.78	56 ± 1.23	42 ± 1.29	21 ± 1.09	7.4002	3.5×10^{-8}
Hard						
Exsudates (%)	58 ± 1.12	54 ± 1.97	32 ± 1.22	27 ± 1.90	6.8924	2.1×10^{-8}
IRC (%)	15 ± 2.21	14 ± 1.45	13 ± 1.34	10 ± 1.32	7.0981	2.5×10^{-8}
SRF (%)	17 ± 1.01	15 ± 1.21	13 ± 1.11	9 ± 1.21	7.2223	1.9×10^{-8}
PED (%)	22 ± 1.67	20 ± 0.97	17 ± 1.01	15 ± 0.87	6.5671	1.6×10^{-8}
IHF (%)	29 ± 2.03	25 ± 1.78	23 ± 1.56	20 ± 1.21	7.1261	2.4×10^{-8}
SHRM (%)	16 ± 1.77	14 ± 1.01	12 ± 1.71	9 ± 0.87	7.2212	2.6×10^{-8}

BCVA, best corrected visual acuity; CRT, central retinal thickness; 1RV, 1 mm round in circle of RPE uplift volume; 3RV, 3 mm round in circle of RPE uplift volume; 6RV, 6 mm round in circle of RPE uplift volume; IRC, intraretinal cysts; SRF, subretinal fluid; PED, pigment epithelial detachment; IHF, intraretinal hyperreflective foci; SHRM, subretinal hyperreflective material. Values are mean ± SD.

variations in the IOP were small and nonsignificant ($p > 0.05$). Two eyes with corneal epithelial defects and four eyes with subconjunctival hemorrhage after injection eventually recovered. None of the 36 eyes had severe ocular or systemic complications (e.g., secondary glaucoma, iatrogenic cataract, vitreous hemorrhage, endophthalmitis, retinal tears). None of the patients had even mild inflammation.

Discussion

Currently, we still do not fully understand nAMD. Untreated patients are prone to central visual distortion, fixed black shadow, and central visual impairment (Sikorav et al., 2017). Older age at diagnosis, poor vision, high severity, and longer duration of the disease are strongly associated with poor prognosis (Nguyen et al., 2018). A variety of factors lead to the development of nAMD, which is mainly characterized as the formation of CNV via the action of multiple cytokines (such as VEGF, angiopoietin, inflammatory factors, insulin-like growth factor1, cyclooxygenase-2, chemokine receptor-3, and primary fibroblast growth factor). Any of these cytokines causes damage to Bruch's membrane, which in turn is accompanied by a relative or absolute increase in VEGF and aggregation of inflammatory factors, leading to the occurrence of CNV (Cheung et al., 2017; Chen et al., 2018).

Studies have shown that the formation of CNV is mainly due to the high expression of VEGF (Klettner et al., 2013; Liu et al., 2017). VEGF-A, VEGF-B, VEGF-C, VEGF-D, and PIGF are five members of the VEGF family. VEGF is essentially a glycoprotein, which is a type of polypeptide growth factor (Tarallo and De Falco, 2015). Under hypoxic and inflammatory conditions, VEGF increases plasminogen activator (PA) activity by increasing the mRNA expression of PA and plasminogen activator inhibitor-l (PAI-1), resulting in denaturation of the extracellular matrix, increased vascular permeability, vascular endothelial cell migration, blood–retinal barrier impairment, proliferation and neovascularization (Shibuya, 2013). Fundus manifestations usually include retinal drusen, frequent bleeding, exudation, and oedema. The bleeding further results in scar development, leading to the irreversible loss of central vision (Zhang and Ma, 2007). Anti-VEGF products such as bevacizumab, ranibizumab, aflibercept, and conbercept all act to reduce VEGF activity, bringing hope to nAMD patients (Yazdi et al., 2015; Moreno et al., 2016; Avery et al., 2017; Liu et al., 2019). Among them, conbercept is a new generation of fusion protein drugs developed independently in China that can fully bind VEGF-A isoforms, VEGF-B and PIGF, with higher affinity than aflibercept and bevacizumab (Yu et al., 2012; Ventrice et al., 2013). It effectively reaches all layers of the fundus and has a long half-life. Fifteen days after injection, the retinal concentration of conbercept is still 1,000 times higher than retinal VEGF exposure, allowing extension of the injection interval and reducing the financial burden for the patient (Zhang et al., 2009). Some multicenter, large sample randomized controlled clinical registry studies (HOPE, AURORA, PHOENIX) have confirmed the superiority and safety of the multitarget antagonistic effects of conbercept (Zhang et al., 2011; Li et al., 2014; Liu et al., 2019).

In this study, after 36 patients received three core treatments with conbercept, the BCVA demonstrated 2 to 3 rows of improvement over the baseline visual acuity ($p < 0.001$), suggesting that conbercept can effectively stabilize and improve vision in the treatment of nAMD. Furthermore, the CRT, 1RV, 3RV, and 6RV decreased significantly, confirming the specific effect of conbercept on reducing the retinal thickness and lesion volume in the macula. These findings indicate that conbercept can inhibit CNV leakage, promote fluid absorption, and restore normal retina morphology, which provides theoretical support for the improvement of BCVA from the anatomical structure. ERG, a noninvasive, highly specific and highly sensitive

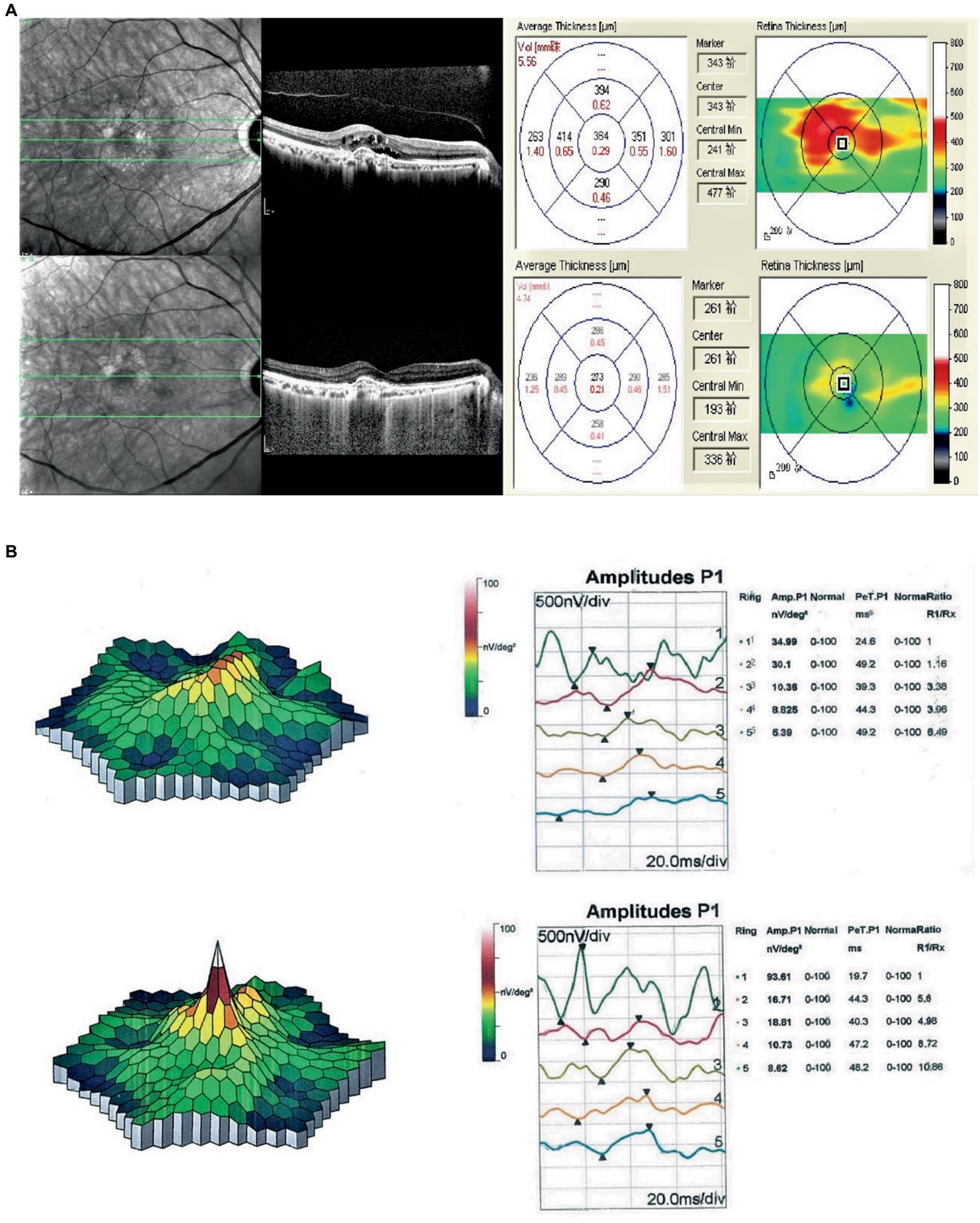

FIGURE 1
(A) Compared with the first OCT, OCT at the final follow-up for the nAMD patients essentially showed recovery of the macular area. The CRT decreased by 91µm, the 1RV decreased by 0.08mm^3, the 3RV decreased by 0.58mm^3, and the 6RV decreased by 0.82mm^3. **(B)** Comparison of the first mf-ERG in nAMD patients at the last follow-up showed a significant increase in the P1 wave amplitude density of the R1 ring (58.62nV/deg^2), and no substantial change in the P1 wave latency.

examination, can objectively reflect the function of the retina (Robson et al., 2018). Maturi et al. (2006) studied the amplitude density of macular function on mfERG in 9 patients with nAMD before and one month after bevacizumab treatment. The results showed a significant improvement in the electrophysiological response of the macula after treatment, suggesting the need to assess the degree of recovery of

TABLE 3 Changes in the mf-ERG R1 ring and ff-ERG after intravitreal injection of Conbercept.

	Baseline (0week)	12 weeks	End vs. Pre	
			T value	*p* value
mf-ERG R1 ring				
P1 amplitude density (nv/deg^2)	36.47 ± 14.25	58.36 ± 13.45	−9.3533	5.0×10^{-11}
P1 latency (ms)	38.13 ± 9.75	39.21 ± 9.63	−1.2568	0.22
ff-ERG				
Dark-adapted				
Scotopic b-wave amplitude (μV)	35.48 ± 27.31	79.49 ± 45.32	−7.6377	5.9×10^{-9}
Scotopic b-wave latency (ms)	45.88 ± 4.80	46.33 ± 4.38	−0.8031	0.43
Combined maximal a-wave amplitude (μV)	89.46 ± 46.39	145.01 ± 65.02	−6.1812	4.46×10^{-7}
Combined maximal a-wave latency (ms)	21.61 ± 2.26	22.56 ± 1.77	−3.1490	3.33×10^{-3}
Combined maximal b-wave amplitude (μV)	165.49 ± 78.36	267.62 ± 99.07	−7.4794	9.29×10^{-9}
Combined maximal b-wave latency (ms)	44.32 ± 3.51	46.23 ± 2.25	−3.2089	2.85×10^{-3}
Oscillatory potentials amplitude (μV)	17.87 ± 12.53	24.50 ± 13.88	−3.7067	7.22×10^{-4}
Oscillatory potentials latency (ms)	25.36 ± 0.69	25.55 ± 0.49	−1.8335	0.07
Light-adapted				
Cone response a-wave amplitude (μV)	41.45 ± 27.39	65.48 ± 39.06	−6.7436	8.21×10^{-8}
Cone response a-wave latency (ms)	25.83 ± 4.51	26.72 ± 3.63	−1.6999	0.10
Cone response b-wave amplitude (μV)	22.42 ± 15.01	38.11 ± 20.91	−5.3081	6.31×10^{-6}
Cone response b-wave latency (ms)	32.84 ± 3.54	33.38 ± 3.95	−1.4808	0.15
30-Hz flicker amplitude (μV)	57.71 ± 23.95	79.93 ± 39.83	−3.9114	4.03×10^{-4}
30-Hz flicker latency (ms)	67.14 ± 15.43	67.81 ± 16.17	−0.2912	0.77

mf-ERG, multifocal electroretinogram; ff-ERG, full-field electroretinogram. Values are mean ± SD.

TABLE 4 Correlation analysis between BCVA (logMAR) and OCT measurements.

	Baseline (0week)		12weeks	
	r value	*p* value	*r* value	*p* value
CRT	0.3824	0.02	0.314501	0.06
1RV	0.4322	0.85×10^{-2}	0.476404	0.33×10^{-2}
3RV	0.5361	0.08×10^{-2}	0.488476	0.25×10^{-2}
6RV	0.3831	0.02	0.389903	0.02

CRT, central retinal thickness; 1RV, 1 mm round in circle of RPE uplift volume; 3RV, 3 mm round in circle of RPE uplift volume; 6RV, 6 mm round in circle of RPE uplift volume.

visual function in conjunction with mf-ERG indicator when treating patients with nAMD. The study claimed that in early AMD the rods degenerate earlier than the cones and that the decrease in rod-mediated photopic sensitivity is more pronounced than that in cone-mediated photopic sensitivity (Jackson et al., 2002; Feigl et al., 2005). We found that the amplitude density of the P1 wave of the mf-ERG R1 ring and the amplitude of the ff-ERG parameters increased significantly following conbercept treatment, while the ERG latency did not change significantly from baseline. These increases are thought to be the result of partial recovery of visual cell function. However, the latency on ERG reflects the speed of visual cell propagation, which varies from site to site. Due to the lack of regularity in the distribution of nAMD lesions, latency does not accurately reflect visual cell function impairment. Combining the results for the BCVA and the OCT and ERG parameters, we conclude that conbercept is helpful for the short-term treatment of nAMD.

The BCVA in logMAR was significantly positively correlated with the SD-OCT measurements but negatively correlated with the P1 wave measurements of the mf-ERG R1 ring. This is consistent with previous studies showing that the mf-ERG response objectively predicts future vision loss and has a high sensitivity in assessing the effects of intravitreal injections of anti-VEGF agents (Pedersen et al., 2010; Wu et al., 2014; de Oliveira Dias et al., 2017). In our study, one eye (without PED) showed no significant changes in the BCVA or P1 wave density after three courses of treatment but did show significant decreases in the CRT, 1RV, 3RV, and 6RV; this may be related to the long course of the disease. In nAMD, some of the visual cell functions are permanently lost and cannot be restored; consequently, there was no significant improvement in visual acuity even after the anatomy improved. This suggests that the morphological changes revealed by SD-OCT do not fully equate with the changes in visual cell function. Gonzalez-Garcia et al. (2016) found that mf-ERG can detect electrophysiological changes in the retina prior to vision loss during AMD. This suggests that mf-ERG is more sensitive in diagnosing and monitoring disease progression and changes than OCT, although both OCT and mf-ERG can be effective in this regard. Similarly, Ambrosio et al. (2015) noted that mf-ERG allows a more direct assessment of macular function than other measures. In AMD, it shows high specificity and sensitivity in detecting early retinal dysfunction and could serve as a predictor of vision loss. Other studies have reported that ff-ERG can be used as a functional tool to assess the retina after

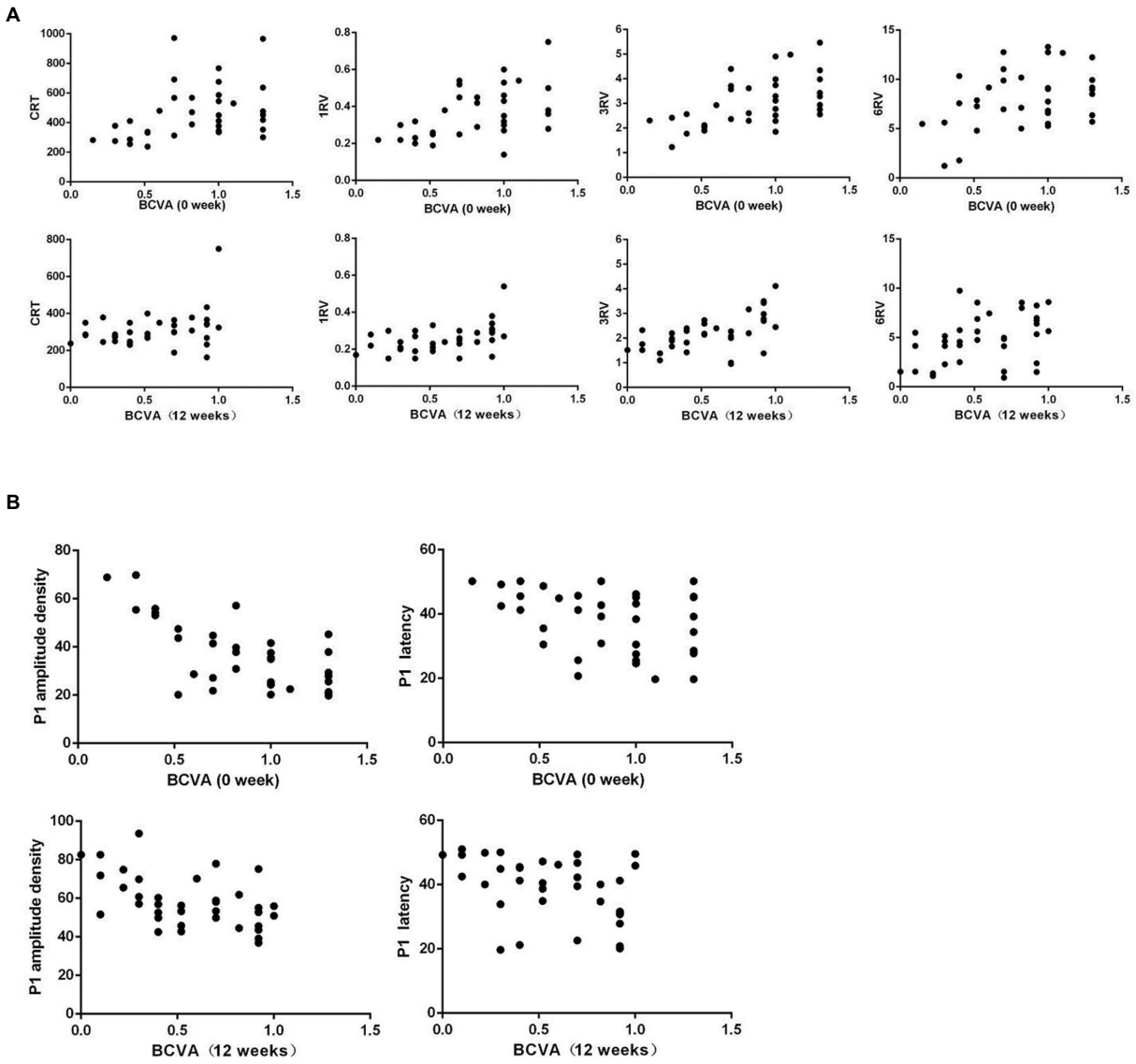

FIGURE 2
(A) Scatter plots of the first and last BCVA (logMAR) and OCT measurements for nAMD patients show a significant, positive correlation between the first BCVA (logMAR) and CRT, but the final, positive correlation is not significant. The first and last BCVAs (logMAR) is significantly, positively correlated with 1RV, 3RV, and 6RV. **(B)** The first and last BCVA (logMAR) and mf-ERG correlation scatter plots of nAMD patients show a significant, negative correlation between the BCVA (logMAR) and P1 wave amplitude density and latency.

intravitreal injections (Skaat et al., 2011; Andrade et al., 2016). Our results showed an increased amplitude in ff-ERG parameters but no significant correlation with the BCVA. We believe this may have occurred due to our sample size and short follow-up period.

In addition, the clinical application of microperimetry has further expanded the psychophysical study of retinal function in recent years. Similar to ERG, microperimetry can detect retinal function through light stimulation in different regions and of varying intensity (Meleth et al., 2011). Similar to ERG, microperimetry can be used to assess visual dysfunction in the reticular pseudodrusen (RPD) in the macula. Forte et al. (2014) found that compared with those with early AMD, patients with only RPD changes in the fundus and normal vision had decreased visual sensitivity on microperimetry. However, in patients with mid-term atrophic AMD, changes in RPD did not affect the visual sensitivity on microperimetry. The RPD plays an important role in the progression of AMD. In the future, further studies of the effects of RPD on atrophic AMD and visual function using microperimetry are needed (Querques et al., 2014).

In conclusion, to our knowledge, our investigation is the first report on BCVA combined with ERG and SD-OCT to evaluate the therapeutic efficacy of conbercept in nAMD. In the short term, conbercept can safely and significantly improve and stabilize vision in the treatment of nAMD, which contributes to the functional and structural recovery of the macula. Our sample size was limited, and only three treatments were analyzed. More multicenter, large-sample, prospective, randomized clinical controlled trials are needed to explore the long-term efficacy, drug safety, treatment regimen, and course of treatment of conbercept.

Our investigation showed that BCVA, SD-OCT, and ERG can be combined to morphologically and functionally assess the

TABLE 5 Correlation analysis between BCVA (logMAR) and ERG measurements.

	Baseline (0week)		12weeks	
	r value	*p* value	*r* value	*p* value
mf-ERG R1 ring				
P1 amplitude density	−0.6774	5.68×10^{-2}	−0.4953	0.21×10^{-2}
P1 latency	−0.3432	0.04	−0.3729	0.03
ff-ERG				
Dark-adapted				
Scotopic b-wave amplitude	−0.2348	0.17	−0.0524	0.76
Scotopic b-wave latency	−0.3090	0.07	−0.4729	0.36×10^{-2}
Combined maximal a-wave amplitude	−0.3018	0.07	−0.3938	0.02
Combined maximal a-wave latency	−0.1657	0.33	−0.4621	0.45×10^{-2}
Combined maximal b-wave amplitude	−0.1050	0.54	−0.2886	0.09
Combined maximal b-wave latency	0.0107	0.95	0.1376	0.43
Oscillatory potentials amplitude	0.2297	0.18	0.2136	0.21
Oscillatory potentials latency	−0.0724	0.67	−0.1641	0.35
Light-adapted				
Cone response a-wave amplitude	0.0791	0.65	0.0764	0.66
Cone response a-wave latency	−0.0011	0.99	−0.2671	0.43
Cone response b-wave amplitude	−0.2903	0.09	−0.5707	0.03×10^{-2}
Cone response b-wave latency	−0.1953	0.25	0.1678	0.34
30-Hz flicker amplitude	0.0466	0.79	−0.1043	0.55
30-Hz flicker latency	−0.1128	0.51	−0.0024	0.99

mf-ERG, multifocal electroretinogram; ff-ERG, full-field electroretinogram.

condition of the eye. The ability to use the results obtained by ERG and further predict subsequent functional deterioration could be valuable in developing treatment protocols and designing clinical trials. Further research is needed to predict the prognostic value for nAMD and other macular diseases based on the ERG response. Although ERG is not currently used routinely in patient testing, a combined assessment would be more objective and comprehensive in assessing the clinical efficacy of conbercept for nAMD. During nAMD treatment, ERG could serve as an objective functional indicator for assessing treatment efficacy and determining the need for retreatment.

Data availability statement

The original contributions presented in the study are included in the article/supplementary material, further inquiries can be directed to the corresponding author.

Ethics statement

Ethical review and approval was not required for the study on human participants in accordance with the local legislation and institutional requirements. Written informed consent for participation was not required for this study in accordance with the national legislation and the institutional requirements.

Author contributions

XW and PW contributed to the conception of the study. XW collected data and wrote the manuscript. PW extracted the data and revised the manuscript text. All authors reviewed the manuscript and approved it for publication.

Acknowledgments

Our deepest gratitude goes first and foremost to Hui Peng for her constant encouragement and guidance. Second, we would like to express our heartfelt appreciation to the doctors and nurses in our department for their help.

Conflict of interest

The authors declare that the research was conducted in the absence of any commercial or financial relationships that could be construed as a potential conflict of interest.

Publisher's note

All claims expressed in this article are solely those of the authors and do not necessarily represent those of their affiliated

organizations, or those of the publisher, the editors and the reviewers. Any product that may be evaluated in this article, or claim that may be made by its manufacturer, is not guaranteed or endorsed by the publisher.

References

Adrean, S. D., Chaili, S., Ramkumar, H., Pirouz, A., and Grant, S. (2018). Consistent long-term therapy of Neovascular age-related macular degeneration managed by 50 or more anti-VEGF injections using a treat-extend-stop protocol. *Ophthalmology* 125, 1047–1053. doi: 10.1016/j.ophtha.2018.01.012

Ambati, J., and Fowler, B. J. (2012). Mechanisms of age-related macular degeneration. *Neuron* 75, 26–39. doi: 10.1016/j.neuron.2012.06.018

Ambrosio, L., Ambrosio, G., Nicoletti, G., de Crecchio, G., and Falsini, B. (2015). The value of multifocal electroretinography to predict progressive visual acuity loss in early AMD. *Doc. Ophthalmol.* 131, 125–135. doi: 10.1007/s10633-015-9507-9

Andrade, G. C., Dias, J. R., Maia, A., Farah, M. E., Meyer, C. H., and Rodrigues, E. B. (2016). Intravitreal injections of ZIV-aflibercept for diabetic macular edema: a pilot study. *Retina* 36, 1640–1645. doi: 10.1097/IAE.0000000000001000

Avery, R. L., Castellarin, A. A., Steinle, N. C., Dhoot, D. S., Pieramici, D. J., See, R., et al. (2017). Systemic pharmacokinetics and pharmacodynamics of Intravitreal Aflibercept, Bevacizumab, and Ranibizumab. *Retina* 37, 1847–1858. doi: 10.1097/IAE.0000000000001493

Berezovsky, A., Moraes, N. S., Nusinowitz, S., and Salomao, S. R. (2003). Standard full-field electroretinography in healthy preterm infants. *Doc. Ophthalmol.* 107, 243–249. doi: 10.1023/B:DOOP.0000005333.76622.c2

Castillo, M. M., Mowatt, G., Lois, N., Elders, A., Fraser, C., Amoaku, W., et al. (2014). Optical coherence tomography for the diagnosis of neovascular age-related macular degeneration: a systematic review. *Eye* 28, 1399–1406. doi: 10.1038/eye.2014.214

Chen, X. L., Hu, Q. R., Bai, Y. J., Deng, Y., Wang, H. W., Liu, S., et al. (2018). A comparison of risk factors for agerelated macular degeneration and polypoidal choroidal vasculopathy in Chinese patients. *Graefes Arch. Clin. Exp. Ophthalmol.* 256, 1449–1457. doi: 10.1007/s00417-018-4020-y

Chen, C., Zuo, C., Piao, C., and Miyake, Y. (2005). Recording rod ON and OFF responses in ERG and multifocal ERG. *Doc. Ophthalmol.* 111, 73–81. doi: 10.1007/s10633-005-4267-6

Cheung, C. M., Laude, A., Yeo, I., Tan, S. P., Fan, Q., Mathur, R., et al. (2017). Systemic, ocular and genetic risk factors for age-related macular degeneration and Polypoidal Choroidal vasculopathy in Singaporeans. *Sci. Rep.* 7:41386. doi: 10.1038/srep41386

Cui, J., Sun, D., Lu, H., Dai, R., Xing, L., Dong, H., et al. (2018). Comparison of effectiveness and safety between conbercept and ranibizumab for treatment of neovascular age-related macular degeneration. A retrospective case-controlled non-inferiority multiple center study. *Eye* 32, 391–399. doi: 10.1038/eye.2017.187

de Oliveira Dias, J. R., de Andrade, G. C., Kniggendorf, V. F., Novais, E. A., Maia, A., Meyer, C., et al. (2017). Clinical and electrophysiological evaluation after Intravitreal Ziv-Aflibercept for exudative age-related macular degeneration. *Retina* 37, 1499–1507. doi: 10.1097/IAE.0000000000001385

Feigl, B., Brown, B., Lovie-Kitchin, J., and Swann, P. (2005). Cone- and rod-mediated multifocal electroretinogram in early age-related maculopathy. *Eye* 19, 431–441. doi: 10.1038/sj.eye.6701503

Forte, R., Cennamo, G., de Crecchio, G., and Cennamo, G. (2014). Microperimetry of subretinal drusenoid deposits. *Ophthalmic Res.* 51, 32–36. doi: 10.1159/000354117

Funk, M., Karl, D., Georgopoulos, M., Benesch, T., Sacu, S., Polak, K., et al. (2009). Neovascular age-related macular degeneration: intraocular cytokines and growth factors and the influence of therapy with ranibizumab. *Ophthalmology* 116, 2393–2399. doi: 10.1016/j.ophtha.2009.05.039

Gonzalez-Garcia, E., Vilela, C., Navea, A., Arnal, E., Muriach, M., and Romero, F. J. (2016). Electrophysiological and clinical tests in dry age-related macular degeneration follow-up: differences between mfERG and OCT. *Doc. Ophthalmol.* 133, 31–39. doi: 10.1007/s10633-016-9545-y

Jackson, G. R., Owsley, C., and Curcio, C. A. (2002). Photoreceptor degeneration and dysfunction in aging and age-related maculopathy. *Ageing Res. Rev.* 1, 381–396. doi: 10.1016/S1568-1637(02)00007-7

Klettner, A., Kauppinen, A., Blasiak, J., Roider, J., Salminen, A., and Kaarniranta, K. (2013). Cellular and molecular mechanisms of age-related macular degeneration: from impaired autophagy to neovascularization. *Int. J. Biochem. Cell Biol.* 45, 1457–1467. doi: 10.1016/j.biocel.2013.04.013

Li, X., Xu, G., Wang, Y., Xu, X., Liu, X., Tang, S., et al. (2014). Safety and efficacy of conbercept in neovascular age-related macular degeneration: results from a 12-month randomized phase 2 study: AURORA study. *Ophthalmology* 121, 1740–1747. doi: 10.1016/j.ophtha.2014.03.026

Liu, K., Song, Y., Xu, G., Ye, J., Wu, Z., Liu, X., et al. (2019). Conbercept for treatment of Neovascular agerelated macular degeneration: results of the randomized phase 3 PHOENIX study. *Am J. Ophthalmol.* 197, 156–167. doi: 10.1016/j.ajo.2018.08.026

Liu, C. H., Wang, Z., Sun, Y., and Chen, J. (2017). Animal models of ocular angiogenesis: from development to pathologies. *FASEB J.* 31, 4665–4681. doi: 10.1096/fj.201700336R

Lu, H., Cui, J., Dong, H., Luo, B., Xiu, W., and Li, H. (2015). Clinical observation of a new anti-VEGF drugs conbercept for wet age-related macular degeneration. *Zhonghua Yan Ke Za Zhi* 51, 818–821.

Maturi, R. K., Bleau, L. A., and Wilson, D. L. (2006). Electrophysiologic findings after intravitreal bevacizumab (Avastin) treatment. *Retina* 26, 270–274. doi: 10.1097/00006982-200603000-00003

Meleth, A. D., Mettu, P., Agrón, E., Chew, E. Y., Sadda, S. R., Ferris, F. L., et al. (2011). Changes in retinal sensitivity in geographic atrophy progression as measured by microperimetry. *Invest. Ophthalmol. Vis. Sci.* 52, 1119–1126. doi: 10.1167/iovs.10-6075

Moreno, M. R., Tabitha, T. S., Nirmal, J., Radhakrishnan, K., Yee, C. H., Lim, S., et al. (2016). Study of stability and biophysical characterization of ranibizumab and aflibercept. *Eur. J. Pharm. Biopharm.* 108, 156–167. doi: 10.1016/j.ejpb.2016.09.003

Moschos, M. M., and Nitoda, E. (2018). The role of mf-ERG in the diagnosis and treatment of age-related macular degeneration: electrophysiological features of AMD. *Semin. Ophthalmol.* 33, 461–469. doi: 10.1080/08820538.2017.1301496

Nguyen, V., Daien, V., Guymer, R. H., McAllister, I. L., Morlet, N., Barthelmes, D., et al. (2018). Clinical and social characteristics associated with reduced visual acuity at presentation in Australian patients with neovascular age-related macular degeneration: a prospective study from a long-term observational data set. The fight retinal blindness! P. *Clin. Exp. Ophthalmol.* 46, 266–274. doi: 10.1111/ceo.13038

Nguyen, T. T., and Guymer, R. (2015). Conbercept (KH-902) for the treatment of neovascular age-related macular degeneration. *Expert. Rev. Clin. Pharmacol.* 8, 541–548. doi: 10.1586/17512433.2015.1075879

Pedersen, K. B., Moller, F., Sjolie, A. K., and Andreasson, S. (2010). Electrophysiological assessment of retinal function during 6 months of bevacizumab treatment in neovascular age-related macular degeneration. *Retina* 30, 1025–1033. doi: 10.1097/IAE.0b013e3181cafc8f

Querques, G., Massamba, N., Srour, M., Boulanger, E., Georges, A., and Souied, E. H. (2014). Impact of reticular pseudodrusen on macular function. *Retina* 34, 321–329. doi: 10.1097/IAE.0b013e3182993df1

Rai, B. B., Essex, R. W., Sabeti, F., Maddess, T., Rohan, E. M. F., van Kleef, J. P., et al. (2021). An objective Perimetry study of central versus peripheral sensitivities and delays in age-related macular degeneration. *Transl. Vis. Sci. Technol.* 10:24. doi: 10.1167/tvst.10.14.24

Rai, B. B., Sabeti, F., Carle, C. F., Rohan, E. M., van Kleef, J. P., Essex, R. W., et al. (2022). Rapid objective testing of visual function matched to the ETDRS grid and its diagnostic power in age-related macular degeneration. *Ophthalmol. Sci.* 2:100143. doi: 10.1016/j.xops.2022.100143

Renner, A. B., Kellner, U., Tillack, H., Kraus, H., and Foerster, M. H. (2005). Recording of both VEP and multifocal ERG for evaluation of unexplained visual loss electrophysiology in unexplained visual loss. *Doc. Ophthalmol.* 111, 149–157. doi: 10.1007/s10633-005-5362-4

Robson, A. G., Nilsson, J., Li, S., Jalali, S., Fulton, A. B., Tormene, A. P., et al. (2018). ISCEV guide to visual electrodiagnostic procedures. *Doc. Ophthalmol.* 136, 1–26. doi: 10.1007/s10633-017-9621-y

Sakurada, Y., Yoneyama, S., Imasawa, M., and Iijima, H. (2013). Systemic risk factors associated with polypoidal choroidal vasculopathy and neovascular age-related macular degeneration. *Retina* 33, 841–845. doi: 10.1097/IAE.0b013e31826ffe9d

Scott, L. J., Chakravarthy, U., Reeves, B. C., and Rogers, C. A. (2015). Systemic safety of anti-VEGF drugs: a commentary. *Expert Opin. Drug Saf.* 14, 379–388. doi: 10.1517/14740338.2015.991712

Shibuya, M. (2013). Vascular endothelial growth factor and its receptor system: physiological functions in angiogenesis and pathological roles in various diseases. *J. Biochem.* 153, 13–19. doi: 10.1093/jb/mvs136

Sikorav, A., Semoun, O., Zweifel, S., Jung, C., Srour, M., Querques, G., et al. (2017). Prevalence and quantification of geographic atrophy associated with newly diagnosed and treatment-naive exudative age-related macular degeneration. *Br. J. Ophthalmol.* 101, 438–444. doi: 10.1136/bjophthalmol-2015-308065

Skaat, A., Solomon, A., Moroz, I., Hai, O. V., Rechtman, E., Vishnevskia Dai, V., et al. (2011). Increased electroretinogram a-wave amplitude after intravitreal bevacizumab injection for neovascular agerelated macular degeneration. *Acta Ophthalmol.* 89, e269–e273. doi: 10.1111/j.1755-3768.2010.02005.x

Sutter, E. E., and Tran, D. (1992). The field topography of ERG components in man—I. The photopic luminance response. *Vision Res.* 32, 433–446. doi: 10.1016/0042-6989(92)90235-B

Tarallo, V., and De Falco, S. (2015). The vascular endothelial growth factors and receptors family: up to now the only target for anti-angiogenesis therapy. *Int. J. Biochem. Cell Biol.* 64, 185–189. doi: 10.1016/j.biocel.2015.04.008

Ventrice, P., Leporini, C., Aloe, J. F., Greco, E., Leuzzi, G., Marrazzo, G., et al. (2013). Anti-vascular endothelial growth factor drugs safety and efficacy in ophthalmic diseases. *J. Pharmacol. Pharmacother.* 4, S38–S42. doi: 10.4103/0976-500X.120947

Wilde, C., Patel, M., Lakshmanan, A., Amankwah, R., Dhar-Munshi, S., Amoaku, W., et al. (2015). The diagnostic accuracy of spectral-domain optical coherence tomography for neovascular age-related macular degeneration: a comparison with fundus fluorescein angiography. *Eye* 29, 602–610; quiz 10. doi: 10.1038/eye.2015.44

Wu, Z., Ayton, L. N., Guymer, R. H., and Luu, C. D. (2014). Comparison between multifocal electroretinography and microperimetry in age-related macular degeneration. *Invest. Ophthalmol. Vis. Sci.* 55, 6431–6439. doi: 10.1167/iovs.14-14407

Yazdi, M. H., Faramarzi, M. A., Nikfar, S., Falavarjani, K. G., and Abdollahi, M. (2015). Ranibizumab and aflibercept for the treatment of wet age-related macular degeneration. *Expert. Opin. Biol. Ther.* 15, 1349–1358. doi: 10.1517/14712598.2015.1057565

Yu, D. C., Lee, J. S., Yoo, J. Y., Shin, H., Deng, H., Wei, Y., et al. (2012). Soluble vascular endothelial growth factor decoy receptor FP3 exerts potent antiangiogenic effects. *Mol. Ther.* 20, 938–947. doi: 10.1038/mt.2011.285

Zhang, S. X., and Ma, J. X. (2007). Ocular neovascularization: implication of endogenous angiogenic inhibitors and potential therapy. *Prog. Retin. Eye Res.* 26, 1–37. doi: 10.1016/j.preteyeres.2006.09.002

Zhang, M., Yu, D., Yang, C., Xia, Q., Li, W., Liu, B., et al. (2009). The pharmacology study of a new recombinant human VEGF receptor-fc fusion protein on experimental choroidal neovascularization. *Pharm. Res.* 26, 204–210. doi: 10.1007/s11095-008-9718-9

Zhang, M., Zhang, J., Yan, M., Luo, D., Zhu, W., Kaiser, P. K., et al. (2011). A phase 1 study of KH902, a vascular endothelial growth factor receptor decoy, for exudative age-related macular degeneration. *Ophthalmology* 118, 672–678. doi: 10.1016/j.ophtha.2010.08.008

frontiers | Frontiers in Neuroscience

TYPE Original Research
PUBLISHED 16 May 2023
DOI 10.3389/fnins.2023.1148950

OPEN ACCESS

EDITED BY
Wensi Tao,
University of Miami Health System,
United States

REVIEWED BY
Kofi Asiedu,
University of New South Wales, Australia
Driss Zoukhri,
Tufts University, United States

*CORRESPONDENCE
David J. Calkins
✉ david.j.calkins@vumc.org

RECEIVED 20 January 2023
ACCEPTED 21 April 2023
PUBLISHED 16 May 2023

CITATION
Wareham LK, Holden JM, Bossardet OL, Baratta RO, Del Buono BJ, Schlumpf E and Calkins DJ (2023) Collagen mimetic peptide repair of the corneal nerve bed in a mouse model of dry eye disease.
Front. Neurosci. 17:1148950.
doi: 10.3389/fnins.2023.1148950

Collagen mimetic peptide repair of the corneal nerve bed in a mouse model of dry eye disease

Lauren K. Wareham[1], Joseph M. Holden[1], Olivia L. Bossardet[1], Robert O. Baratta[2], Brian J. Del Buono[2], Eric Schlumpf[2] and David J. Calkins[1]*

[1]Department of Ophthalmology and Visual Sciences, Vanderbilt Eye Institute, Vanderbilt University Medical Center, Nashville, TN, United States, [2]Stuart Therapeutics, Inc., Stuart, FL, United States

The intraepithelial sub-basal nerve plexus of the cornea is characterized by a central swirl of nerve processes that terminate between the apical cells of the epithelium. This plexus is a critical component of maintaining homeostatic function of the ocular surface. The cornea contains a high concentration of collagen, which is susceptible to damage in conditions such as neuropathic pain, neurotrophic keratitis, and dry eye disease. Here we tested whether topical application of a collagen mimetic peptide (CMP) is efficacious in repairing the corneal sub-basal nerve plexus in a mouse model of ocular surface desiccation. We induced corneal tear film reduction, epithelial damage, and nerve bed degradation through a combination of environmental and pharmaceutical (atropine) desiccation. Mice were subjected to desiccating air flow and bilateral topical application of 1% atropine solution (4× daily) for 2 weeks. During the latter half of this exposure, mice received topical vehicle [phosphate buffered saline (PBS)] or CMP [200 μm (Pro-Pro-Gly)$_7$, 10 μl] once daily, 2 h prior to the first atropine treatment for that day. After euthanasia, cornea were labeled with antibodies against βIII tubulin to visualize and quantify changes to the nerve bed. For mice receiving vehicle only, the two-week desiccation regimen reduced neuronal coverage of the central sub-basal plexus and epithelial terminals compared to naïve, with some corneas demonstrating complete degeneration of nerve beds. Accordingly, both sub-basal and epithelial βIII tubulin-labeled processes demonstrated increased fragmentation, indicative of nerve disassembly. Treatment with CMP significantly reduced nerve fragmentation, expanded both sub-basal and epithelial neuronal coverage compared to vehicle controls, and improved corneal epithelium integrity, tear film production, and corneal sensitivity. Together, these results indicate that topical CMP significantly counters neurodegeneration characteristic of corneal surface desiccation. Repairing underlying collagen in conditions that damage the ocular surface could represent a novel therapeutic avenue in treating a broad spectrum of diseases or injury.

KEYWORDS

dry eye, ocular collagen, collagen mimetic peptides (CMPs), neuropathy, collagen reparative, extracellular matrix

Introduction

Innervation of the cornea is the densest in the human body (Zander and Weddell, 1951; Schimmelpfennig, 1982). Corneal nerves comprise both a sparse autonomic component and a far more abundant sensory component (Marfurt et al., 1989, 2010). The autonomic component represents some 10–15% of corneal nerve fibers and is nearly entirely sympathetic, involving axons from the superior cervical ganglion (Marfurt et al., 1989). These course through the ciliary nerves to form the limbal plexus (Al-Aqaba et al., 2019). Neurons that mediate sensory innervation of the cornea largely express two primary peptides, calcitonin gene–related peptide (CGRP) and substance P (Muller et al., 2003; He and Bazan, 2016). These send axons through the ophthalmic branch (V_1) of the trigeminal nerve to a sparse population of neurons in the trigeminal ganglion (Belmonte et al., 2017). The corneal nerve bed arises from large bundles of fibers entering the stroma at the limbus. These ramify extensively throughout the epithelium to form the intraepithelial corneal nerves (Stepp et al., 2020). As these converge centripetally, they form the tell-tale swirl pattern that also marks the pattern of corneal epithelial cells migrating from the limbus toward the apex of the cornea (Marfurt et al., 2010; Al-Aqaba et al., 2019). These fibers end as intraepithelial corneal nerve terminals that ramify in and between the apical cells of the epithelium. Thus, the basic structure of the nerve bed taken as a whole comprises two primary components that arise from the large stromal bundles penetrating at the limbus: the sub-basal, intraepithelial plexus, and the superficial terminals that characterize their endings (Marfurt et al., 2010; Al-Aqaba et al., 2019). Importantly, this basic architecture is conserved between human and mouse cornea (He and Bazan, 2016).

The dense corneal nerve plexus is critical to maintaining homeostatic function of the ocular surface (Asiedu, 2022; Vereertbrugghen and Galletti, 2022). Maintenance of a healthy tear film prevents surface desiccation and relies upon neurosensory information from the cornea that is essential for adequate blinking and tearing. The corneal nerve plexus also contributes to immune regulation of the ocular surface and to integrity of the corneal epithelial layer (Galletti and de Paiva, 2021; Asiedu, 2022; Wu et al., 2022). Damage to the corneal nerve bed can lead to enhanced epithelial permeability and diminished capacity for epithelial repair (Beuerman and Schimmelpfennig, 1980), while intact CGRP signaling within the nerve bed is essential to re-epithelialization (Mikulec and Tanelian, 1996; Hwang et al., 2021; Asiedu et al., 2022a). Nerve bed damage is endemic to dry eye disease (DED) (McKay et al., 2019; Guerrero-Moreno et al., 2020), which is the most prevalent progressive ocular surface disease, afflicting many millions of people worldwide (Belmonte et al., 2017; Farrand et al., 2017). Dysfunctional sensory nerves in dry eye exacerbate progression through reduced basal tearing and blinking and leads to neuropathic pain (Dieckmann et al., 2017; Vereertbrugghen and Galletti, 2022). Exposure to environmental desiccation in mice reduces sub-basal corneal nerve density and increases pro-inflammatory dendritic cells (Simsek et al., 2018). This effect has been demonstrated in human studies in systemic conditions such as diabetic chronic kidney disease and rheumatoid arthritis (Asiedu et al., 2022b; Bitirgen et al., 2023). Conversely, higher corneal nerve density in certain mouse strains is related to more efficient repair of wounds to the corneal epithelial layer (Pham et al., 2019).

Collagen accounts for some 90% of corneal thickness, distributing broadly across the various layers (Meek, 2009). Recently we hypothesized that a novel approach to repair corneal collagen, which is normally slowly replaced by mesenchymal and other cells, could offer a new therapeutic avenue to reduce ocular surface damage, inflammation, and neuropathic pain in DED (Baratta et al., 2022). In support of this idea, application of synthesized collagen peptides in animal models of dry eye disease promote corneal tear adherence and facilitate epithelium stabilization (Lee et al., 2017). Collagen mimetic peptides (CMPs) directly repair damaged collagen by intercalating into and reforming fragmented triple helices (Chattopadhyay et al., 2012, 2016; Chattopadhyay and Raines, 2014). Finally, we demonstrated that a type I collagen mimetic (CMP 03A) restored the corneal epithelium following acute damage (Baratta et al., 2021, 2022).

Therapies such as CMPs that restore the extracellular matrix (ECM) also have therapeutic potential by promoting repair of neurons (Ren et al., 2015; Song and Dityatev, 2018). We showed that intraocular delivery of a CMP (CMP 03A) protected and repaired neurons in both chronic and acute injury models of the visual system (Ribeiro et al., 2022). Here, we test whether topical application of this same CMP was efficacious in reducing damage to the ocular surface of the mouse eye induced by a combination of environmental and pharmaceutical (atropine) desiccation. We find that topical application of CMP improved integrity of the corneal epithelium, tear film production, and corneal sensitivity instigated by a two-week desiccation regimen compared to vehicle controls. CMP also prevented neuronal degeneration by reducing fragmentation and enhancing both sub-basal and epithelial neuronal coverage compared to vehicle controls. Together, our results indicate that topical CMP treatment reduces the neurodegenerative characteristic of corneal surface desiccation and that repairing underlying collagen in conditions that damage the ocular surface could represent a novel therapeutic avenue in treating ocular surface diseases.

Materials and methods

Animals

All experiments and procedures were conducted in accordance with the Association for Research in Vision and Ophthalmology (ARVO) statement for the use of animals in ophthalmic and vision research and were approved by the Vanderbilt University Institutional Animal Care and Use Committee. Mice were housed in a facility managed by Vanderbilt University Division of Animal Care, with *ad libitum* access to water and standard mouse chow and a 12 h light cycle (lights on at 6:30 a.m. and off at 6:30 p.m.). For all experiments, adult male and female C57/B6/J mice aged 8 weeks were obtained from Charles River Laboratory (Wilmington, MA, USA).

Corneal desiccation regimen

We modified a protocol designed for desiccation of the rabbit eye (Burgalassi et al., 1999). Mice were housed in standard cages in a light- and temperature-controlled room at 19 ± 1°C and 44 ± 4°C humidity. We prepared 1% atropine solution by dissolving 10 mg of atropine sulfate (Millipore Sigma, Burlington, MA, USA) in 1 ml 1× phosphate buffered saline (PBS). The solution was filter sterilized using a 0.22 μm filter (Millipore Sigma, Burlington, MA, USA) and stored at 4°C for no more than 3 days. During preliminary studies, we found that atropine alone for 2 weeks did reduce tear film production in mice but did not cause significant corneal nerve bed damage after 2 weeks. Thus, mice were randomized prior to baseline measurements and were then subjected to desiccating air turbulence using a fan directed into the cage for 9 h daily from 9 a.m. to 6 p.m. During hours of air turbulence, 4 μL of a 1% atropine solution was applied topically to the corneal surface at regular intervals for a total of 4 applications to both eyes daily. After 6 p.m., mice were returned to normal air flow and atropine dosage was stopped until 9 a.m. the following day. For atropine application, mice were anesthetized with 2% isoflurane in oxygen for 30 s for drop application and then incubated in the presence of 2% isoflurane for a further 30 s to increase atropine penetration. The regimen of combined desiccation and atropine application was continued for 14 days (**Figure 1**).

After baseline tear film wick test and corneal sensitivity measurements were taken, mice were subjected to the cornea desiccation protocol for 7 days. At day 5 and day 7, tear film wick test and corneal sensitivity measurements were taken (**Figure 1**). To assess whether CMP 03A [$(Pro\text{-}Pro\text{-}Gly)_7$] treatment prevented nerve damage induced by the desiccation regimen, at day 7 mice were randomly assigned to receive either vehicle or CMP bilaterally for an additional 7 days. Vehicle or CMP 03A was applied once daily via a 10 μL topical drop at least 1 h prior to the first atropine treatment for that day. Tear film wick test and corneal sensitivity measurements were taken at day 10 and day 14. Animals were euthanized at the end of day 14. For these experiments, N = 11–29 (vehicle), 11 (CMP 03A), and 13 (naïve), with additional animals added to the vehicle group from unrelated, parallel experiments.

Tear film wick test

Tear film production was measured via wick test using endodontic absorbent paper points (EAPP, World Precision Instrument, Sarasota, FL, USA) as previously described (Kilic and Kulualp, 2016). Awake animals were scruffed, and a single EAPP was placed using forceps into the lower lid of the right eye. The EAPP was left in place for 1 min before tear absorption was measured along the wick using a standard ruler. Tear production was measured in each animal at baseline, at 5 and 7 days prior to vehicle or CMP treatment, and again at day 10 and 14 prior to euthanasia.

Corneal sensitivity measurements

Corneal sensitivity was measured on the central cornea using a Cochet-Bonnet aesthesiometer (Luneau Ophtalmologie, Chartres Cedex, France) using a modified protocol previously described (Edwards et al., 2017; Stepp et al., 2018; Pham et al., 2019). The length of the monofilament was manually varied, and the following lengths were tested: 3.5, 2.5, 2, 1.5, 1- and 0.5-mm in each animal. Awake animals were scruffed, and the monofilament touched perpendicular to the central cornea 6 times at each length. A positive response was recorded if blinks occurred at a frequency of 50% (i.e., 3 blinks per a total of 6 taps) and the monofilament length was noted as the sensitivity threshold measurement. If no blink response could be elicited at a monofilament length of 0.5 cm then the sensitivity threshold was recorded as 0.

Corneal fluorescein staining

Corneal fluorescein staining was performed at baseline (day 0, i.e., naïve) and at the conclusion of the study (day 14). Mice were anesthetized with intraperitoneal injection of ketamine (135 mg/kg) and xylazine (7.5 mg/kg). Eyes were washed gently with sterile 1× PBS to remove surface debris. A 2 μl drop of a filtered 1% sodium fluorescein solution was then added to the surface of the cornea. The fluorescein solution was left for 1 min before excess solution was removed with a Q-tip at the outer cornea of the eye. The mouse was then placed under a Nikon AZ100 fluorescent microscope for imaging. Fluorescence images taken in the FITC channel using a 0.5× objective with 7× zoom and a 1 s exposure time.

Immunohistochemistry

Immediately after euthanasia, fresh cornea were dissected and placed into 4% paraformaldehyde (PFA) solution for 15 min at room temperature. Cornea were washed once in 1× PBS and then transferred to a 20% sucrose solution at room temperature for 30 min, and then into a 30% sucrose overnight at 4°C. The following day, cornea were subjected to 3 sets of 5 min freeze-thaw cycles before washing in 1× PBS. Cornea were then placed in a 1% Triton X-100 in 1× PBS solution for 3 h, shaking at room temperature. Cornea were blocked in a solution containing 2% normal donkey serum (NDS; 017-000-121, Jackson ImmunoResearch Laboratories, Inc., West Grove, PA, USA), 2% bovine serum albumin (BSA) and 1% Triton X-100/1× PBS for 2 h, shaking at room temperature. After blocking, corneas were placed in primary antibody solution (2% NDS/0.2% Triton X-100 in 1× PBS) with antibody [1:500 mouse anti-βIII tubulin (MAB5564, Millipore Sigma, Burlington, MA, USA)] for 3 days, shaking at 4°C. After 3 days of primary antibody incubation, cornea were washed 3× for 10 min per wash in 0.2% Triton X-100/1× PBS solution. Cornea were then placed in secondary antibody solution (1% NDS/0.2% Triton X-100 in 1× PBS) containing secondary antibody [Donkey anti-mouse Alexa Fluor-488 (715-546-150, Jackson ImmunoResearch Laboratories, Inc., West Grove, PA, USA)] for 2 h, shaking at room temperature. Cornea were then washed 3× in 1× PBS and mounted in DAPI Fluoromount-G (0100-20, SouthernBiotech, Birmingham, AL, USA) for imaging.

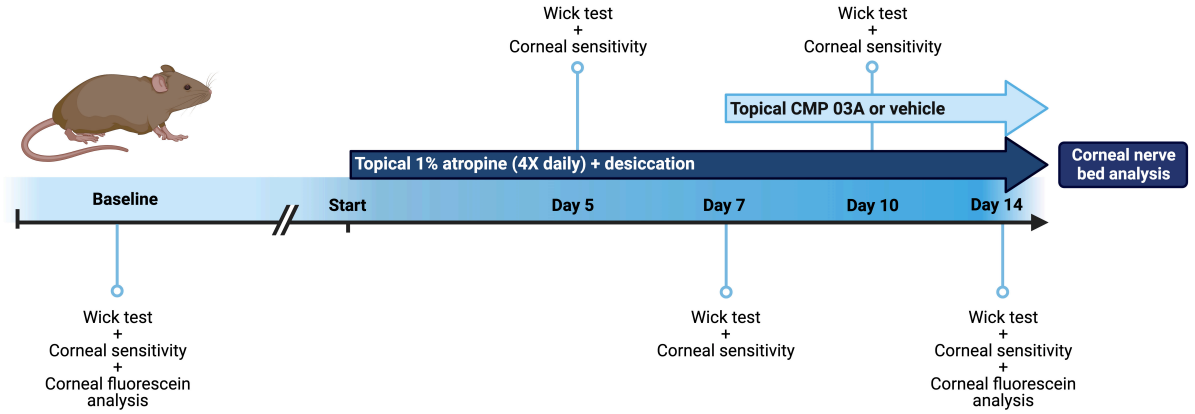

FIGURE 1
Schematic of dry eye desiccation model and treatment regimen. Baseline tear film production (wick test) and corneal sensitivity measurements were taken in all mice before commencement of the study (baseline = day 0). Animals were then treated bilaterally with topical 1% atropine 4× daily with desiccation for a total of 7 days. At day 5 and day 7, tear film and corneal sensitivity measurements were taken. At day 7, in addition to atropine + desiccation, mice were then treated topically with application of vehicle or CMP 03A (200 μm), 1× per day bilaterally for a further 7 days. Tear film production and corneal sensitivity measurements were carried out at day 10 and upon completion of the study at day 14. *In vivo* corneal fluorescein analysis was completed at baseline (day 0) and on day 14, after which mice from all cohorts were euthanized and corneal tissue processed for analysis.

Corneal tissue fluorescent imaging

Fluorescent whole corneal images were taken using a Nikon Ni fluorescent microscope and a 20× objective; whole corneal images were taken en montage. Central corneal stacked images were acquired using an Olympus FV-1000 inverted confocal microscope using a 40× oil objective.

Corneal nerve density and fragmentation analysis

Images were acquired in z-stacks through the entire central cornea using an Olympus FV1000 confocal microscope at 800 px^2 × 800 px^2 resolution on a 40× objective. Due to the curvature of the flattened cornea, different regions of the same corneal image had sub-basal nerves and epithelial nerve endings in different z-planes and thus needed to be stacked separately to compose the flattened final image. To aid in segmentation, a Python script was utilized to split the image into nine smaller z-stacked tiles that could be processed individually. The bounds for each tile sub-stack were manually chosen then flattened using the standard deviation z-stacking method in ImageJ. This produced a single stacked image each for the sub-basal plexus and epithelial terminal plexus. Each image was manually thresholded in ImageJ and the binary image saved. The python script re-stitched the binarized, flattened smaller tiles to give final stacked images of both the sub-basal nerve plexus and epithelial endings. The complete binarized images were then processed using a Python script that performed a flood-fill algorithm on every contiguous region, or fragment, identified in the binary image. Each unique, contiguous fragment was randomly assigned a red-greenblue (RGB) value, and an image generated to visually assess nerve fragmentation. The number of unique RGB values generated in this way was saved as a record of the number of fragments in each image. Fragmentation was then quantified as the number of fragments per image normalized to nerve coverage (area of binary image with nerve labeling).

Epithelial DAPI fluorescence intensity analysis

In ImageJ, stacked confocal images representing total central corneal epithelium were converted to 8-bit and a Gaussian filter applied to reduce speckle noise. Intensity line plots at 5 fixed, evenly spaced x-coordinates, and 5 fixed, evenly spaced y-coordinates were plotted; a total of 10 line plots across each image per animal were measured. Raw intensity line plots for each group were averaged and the first-derivative function plotted using GraphPad Prism version 9.0 (GraphPad Software, San Diego, CA, USA). Area under the curve (AUC) and number of peaks were generated using GraphPad from the first derivative curves in each group.

Statistical analysis

All data are presented as mean ± standard error of the mean (SEM) unless otherwise stated. Statistical analyses were performed, and graphs made using GraphPad Prism version 9.0 (GraphPad Software, San Diego, CA, USA) and SigmaPlot 15.0 (Systat-InPixon, Palo Alto, CA, USA). All data sets were checked for normality using a Shapiro–Wilk test. Significance in data comparisons was determined using parametric statistics if data passed normality (ANOVA: one-way analysis of variance, supplemented as needed with Students t-test); otherwise, we performed non-parametric statistics (ANOVA on ranks, Mann–Whitney or Welch's test). We defined statistical significance as $p \leq 0.05$.

Results

Collagen mimetic peptides improve tear film production and corneal sensitivity after desiccation stress

Patients with dry eye disease exhibit corneal hypoesthesia in addition to depletion of tear film. The extent of the corneal epithelial nerve damage positively correlates with decreased corneal sensitivity (Bourcier et al., 2005). Similarly, murine models of dry eye disease have shown reduced overall corneal sensitivity (Stepp et al., 2018). Atropine and desiccation reduced tear film production by 43% after 5 days and by 60% after 7 days compared to baseline day 0 ($p < 0.001$, Figure 2A). Following 7 days of vehicle treatment, tear production remained low (day 14 vs. day 7, $p = 0.07$); CMP 03A significantly improved tear production (day 14 vs. day 7, $p < 0.001$). We also used a Cochet-Bonnet aesthesiometer to determine the effect of desiccation on central corneal nerve sensitivity. After 7 days, corneal sensitivity threshold declined by 60% compared to baseline (1.08 ± 0.10 mm vs. 2.65 mm ± 0.10 mm; $p < 0.001$, Figure 2B). By day 10, after 3 days of vehicle treatment, corneal sensitivity continued to decline (day 7 vs. day 10, $p < 0.001$); CMP 03A reversed this trend (day 10 vs. day 7, $p = 0.29$). By day 14, after 7 days of CMP, sensitivity improved compared to day 7 ($p = 0.01$), while vehicle cornea still demonstrated reduced sensitivity ($p = 0.29$).

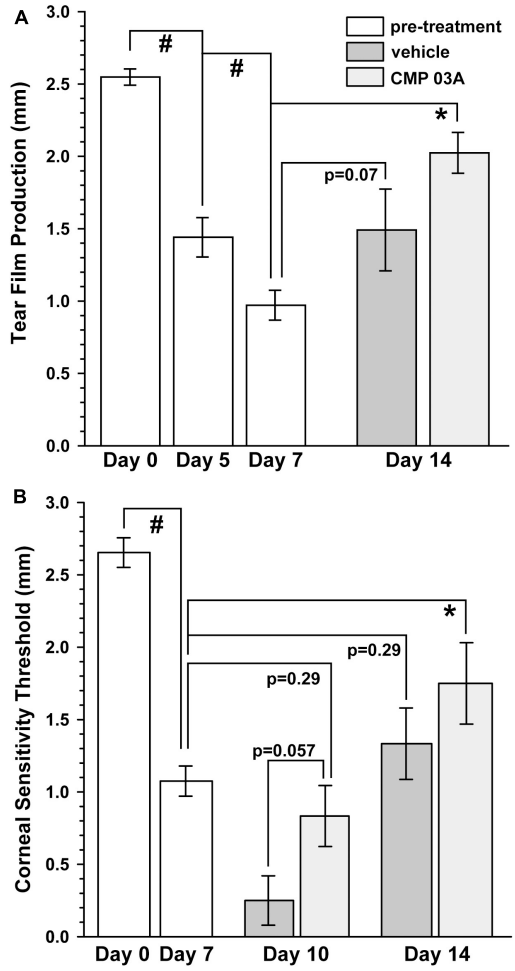

FIGURE 2
CMP 03A improves tear film production and corneal sensitivity. **(A)** The two-week desiccation regimen significantly reduced tear production in mice after 5 and 7 days (#, $p < 0.001$) compared to baseline (day 0). Tear film production did not improve in vehicle-treated mice (day 7 vs. day 14, $p = 0.07$), but did with CMP 03A treatment (day 7 vs. day 14; *, $p < 0.001$). **(B)** Corneal sensitivity was significantly reduced after 7 days of the desiccation regimen (#, $p < 0.001$). After 3 days of vehicle treatment, sensitivity was further reduced (day 10 vehicle vs. CMP 03A; $p = 0.057$), but not with CMP 03A ($p = 0.29$). On day 14 after 7 days, CMP 03A treatment improved sensitivity (*, $p = 0.01$), while vehicle did not ($p = 0.29$). $N = 11–29$ (vehicle), 11 (CMP 03A), and 13 (naïve).

Desiccation-induced corneal nerve bed damage is prevented by collagen mimetic peptide treatment

To assess central nerve structure, we labeled corneas with antibodies to βIII-tubulin (Figure 3). In naïve mice, central corneal nerve fibers in the sub-basal epithelial plexus exhibit an intact characteristic swirl pattern (sub-basal plexus; Figure 3A). These nerve fibers branch out at a 90-degree angle in the anterior direction and continue to extend up between apical cells of the epithelium where nerve terminals are evident (epithelial terminals). Desiccation and vehicle treatment led to reduced neuronal coverage in the sub-basal plexus, as evidenced by a decrease in nerve fibers and loss of the intact central nerve fiber swirl (Figure 3B). Epithelial nerve terminals also reduced in density compared to naïve. CMP 03A significantly improved corneal nerve bed survival at both the sub-basal and epithelial terminal plexus when compared to the vehicle treated group (Figures 3C vs. 3B).

Collagen mimetic peptide reduces nerve fragmentation

To assess the extent of nerve degeneration, we quantified fragmentation of βIII-tubulin-labeled nerve fibers. The number of contiguous nerve fragments in each sub-basal and epithelial terminal image were determined. Representative pseudo-colored fragmentation images are shown in Figure 4, where each contiguous nerve fragment is identified by a unique color. In naïve mice, sub-basal nerve fibers in the central swirl region were formed by long, contiguous fragments (Figure 4Ai). Similarly, epithelial terminals, although numerous, were intact; each nerve terminal was mostly unicolored (Figure 4Aiii, inset). In the vehicle group, there were a larger number of shorter, contiguous nerve fragments at the sub-basal plexus (Figure 4Bi), suggesting discontinuity. Compared to naïve animals, epithelial nerve terminals were reduced in number and highly fragmented (Figures 4Bii, iii; inset), indicating extensive degeneration. Interestingly, CMP treatment reversed this trend; nerves appeared to have greater continuity and were much less fragmented at the sub-basal (Figure 4Ci) and epithelial levels (Figures 4Cii, iii; inset), and exhibited levels of fragmentation similar to naïve mice.

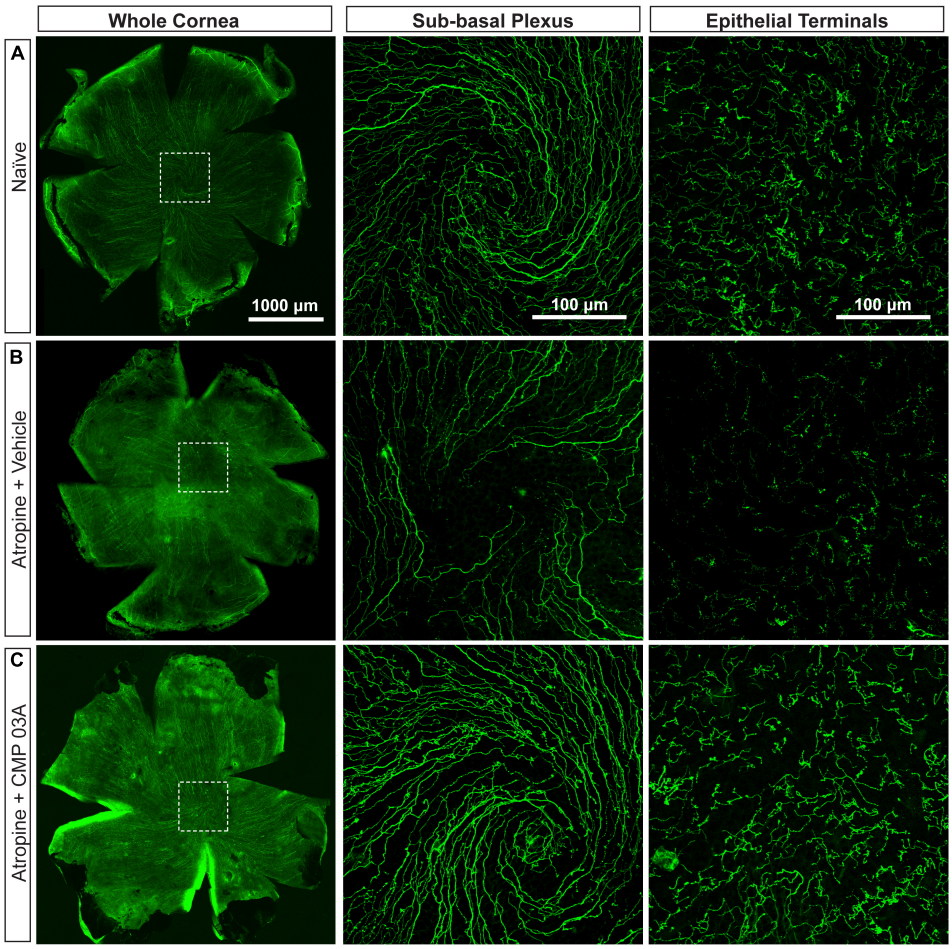

FIGURE 3
Central corneal nerve bed coverage in naïve, vehicle-, and CMP 03A-treated mice. Representative confocal images of βIII-tubulin-stained nerve fibers in the whole cornea with higher magnification images of the central sub-basal plexus and epithelial terminals. The dashed boxes indicate central swirl location. **(A)** Naïve animals have an intact central nerve fiber swirl and robust sub-basal plexus and nerve terminal coverage. **(B)** Desiccation with vehicle treatment only led to reduced sub-basal plexus and epithelial terminal coverage. **(C)** CMP 03A-treated mice did not exhibit a reduced nerve coverage at the sub-basal or terminal epithelial plexus.

We next quantified central nerve area coverage and fragmentation of the sub-basal plexus and epithelial terminal layers. In the vehicle cohort, the two-week desiccation regimen reduced neuronal coverage of the sub-basal plexus by 60 ± 5% ($p < 0.001$; Figure 5A), and epithelial terminals by 58 ± 5% compared to naïve cornea ($p < 0.001$; Figure 5B), with some corneas in the vehicle group demonstrating completely degenerated nerve beds. CMP treatment expanded both sub-basal (+72%) and epithelial (+42%) neuronal coverage compared to vehicle treatment ($p = 0.001$). Accordingly, both sub-basal and epithelial terminals demonstrated a 3-fold increase in fragmentation, indicative of degenerative disassembly ($p < 0.001$; Figures 5C, D). Treatment with CMP significantly reduced fragmentation by 40% in both zones ($p \leq 0.02$; Figures 5C, D). These results together suggest that topical CMP treatment preserves corneal nerve integrity during desiccating conditions.

The influence of CMP treatment in our regimen could be either restorative to damage occurring during the first week or protective of damage during the second. Although tear film production and corneal sensitivity were diminished after 1 week (Figure 2), βIII-tubulin-labeled nerve fibers in both the sub-basal plexus and layer of epithelial terminals appeared no different than naïve, without apparent increases in fragmentation using our algorithm (Figures 6A, B). When quantified, fragmentation of neither the sub-basal plexus nor epithelial terminals differed significantly from naïve (Figures 6C, D; $p \geq 0.30$). Compared with 1-week data, nerve fragmentation at 2 weeks showed significantly increased nerve degeneration in both the sub-basal and epithelial levels (Figures 6C, D; $p \leq 0.01$). These results suggest that CMP treatment in this regimen acts to preserve nerve structure in a protective rather than restorative manner.

Collagen mimetic peptide treatment preserves the integrity of the corneal epithelium

We determined *in vivo* how CMP treatment affected corneal epithelium with desiccation stress using sodium fluorescein staining (Figure 7). The surface of naïve eyes showed uniform

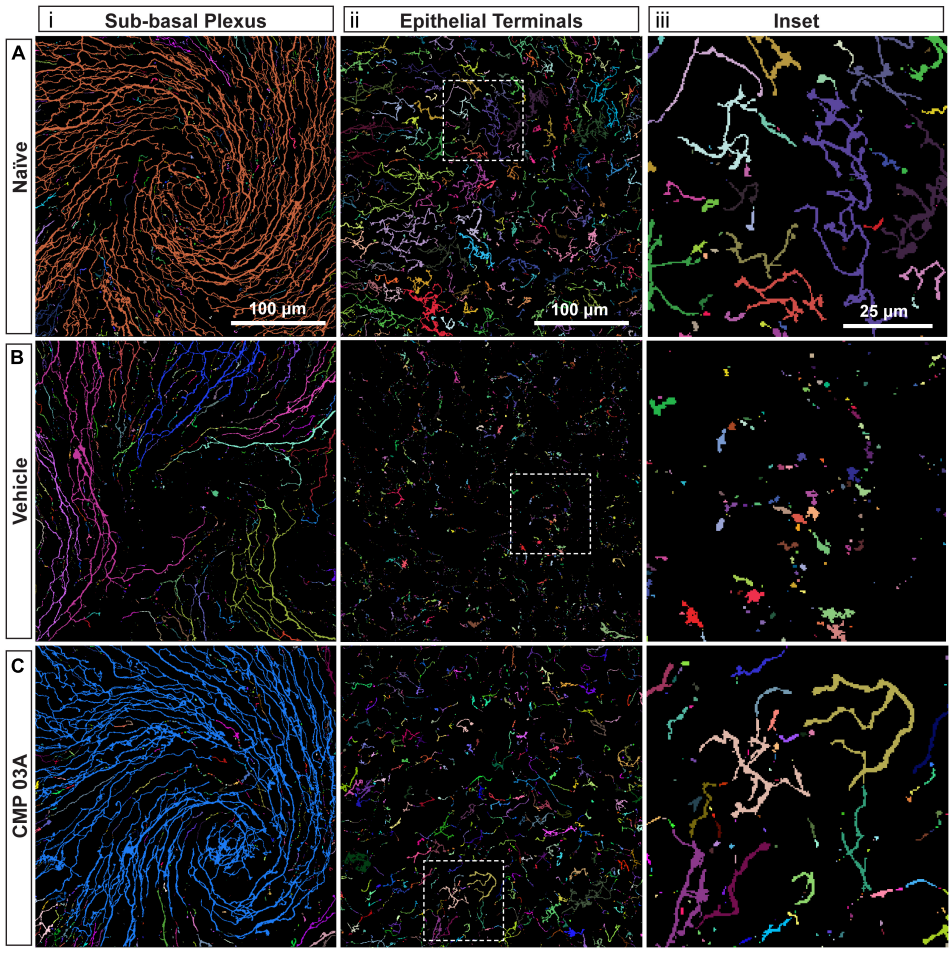

FIGURE 4
CMP reduces nerve fragmentation. Representative pseudo-colored nerve fragmentation images from **(A)** naïve, **(B)** desiccation + vehicle-, and **(C)** desiccation + CMP 03A-treated mice. Images show fragmentation in the **(i)** sub-basal plexus and **(ii)** epithelial terminals. Dashed boxes indicate location of enlarged inset images **(iii)**. Desiccation + vehicle increased nerve fragmentation as shown by the increase in frequency of distinctly colored fragments in the sub-basal plexus **(B,i)**. Although reduced in number, remaining epithelial terminals were more fragmented than in naïve and CMP 03A-treated mice (**B,ii**; inset). **(C)** CMP 03A-treated mice exhibited less nerve fragmentation in the sub-basal plexus **(C,i)** and in epithelial terminals **(C,ii)**. Scale bars as indicated.

staining with little to no imperfection (Figure 7A). Vehicle-treated cornea, however, exhibited uneven, pitted staining, indicative of epithelial damage (Figure 7B). CMP-treated animals did not exhibit as many imperfections and appeared similar to naïve animals (Figure 7C). These results suggest that the two-week desiccation regimen perturbs the cells of the corneal epithelium, a pathology prevented with topical CMP treatment.

Next, we assessed epithelial cell damage using DAPI-staining; representative images are shown in Figure 7. In naïve animals, the central epithelium was uniform, with clearly defined DAPI-stained nuclei (Figure 7D). In vehicle-treated animals, the integrity of the epithelium was diminished and definition between nuclei reduced with areas of epithelial cell loss, and also showed indications of localized damage (Figure 7E). However, CMP-treated mice resembled naïve animals; cell bodies were uniform and clearly defined with no evidence of damage (Figure 7F).

To further assess the integrity of the epithelium we analyzed the distribution of DAPI intensity in the central cornea. By drawing multiple fluorescence intensity line plots across each image, we extracted information regarding the uniformity and periodicity of DAPI-stained nuclei characteristic of naïve epithelium (Figure 8A). Intensity across space for naïve cornea shows regular intensity fluctuations, indicative of the pattern of higher intensity DAPI nuclei and lower intensity background in transitions between cells. In vehicle-treated animals, the amplitude of intensity fluctuations and their regularity were reduced (Figure 8B). However, CMP treatment increased amplitude and regularity, similar to naïve cornea (Figure 8C).

To better resolve the pattern of transition in DAPI staining, we calculated the first derivative of the intensity line plots (Figures 8D–F). A peak in the derivative corresponds to a transition to higher fluorescence (i.e., a cell nucleus), whereas a trough represents the transition from cell nucleus to background (i.e., the nucleus edge). The area under the curve of the derivative (AUC) gives the amplitude of the intensity of transitions in each group. Thus, a sample with clearly defined, high intensity epithelial nuclei will have large intensity transitions (larger AUC) compared to a sample with more ambiguous transitions (lower

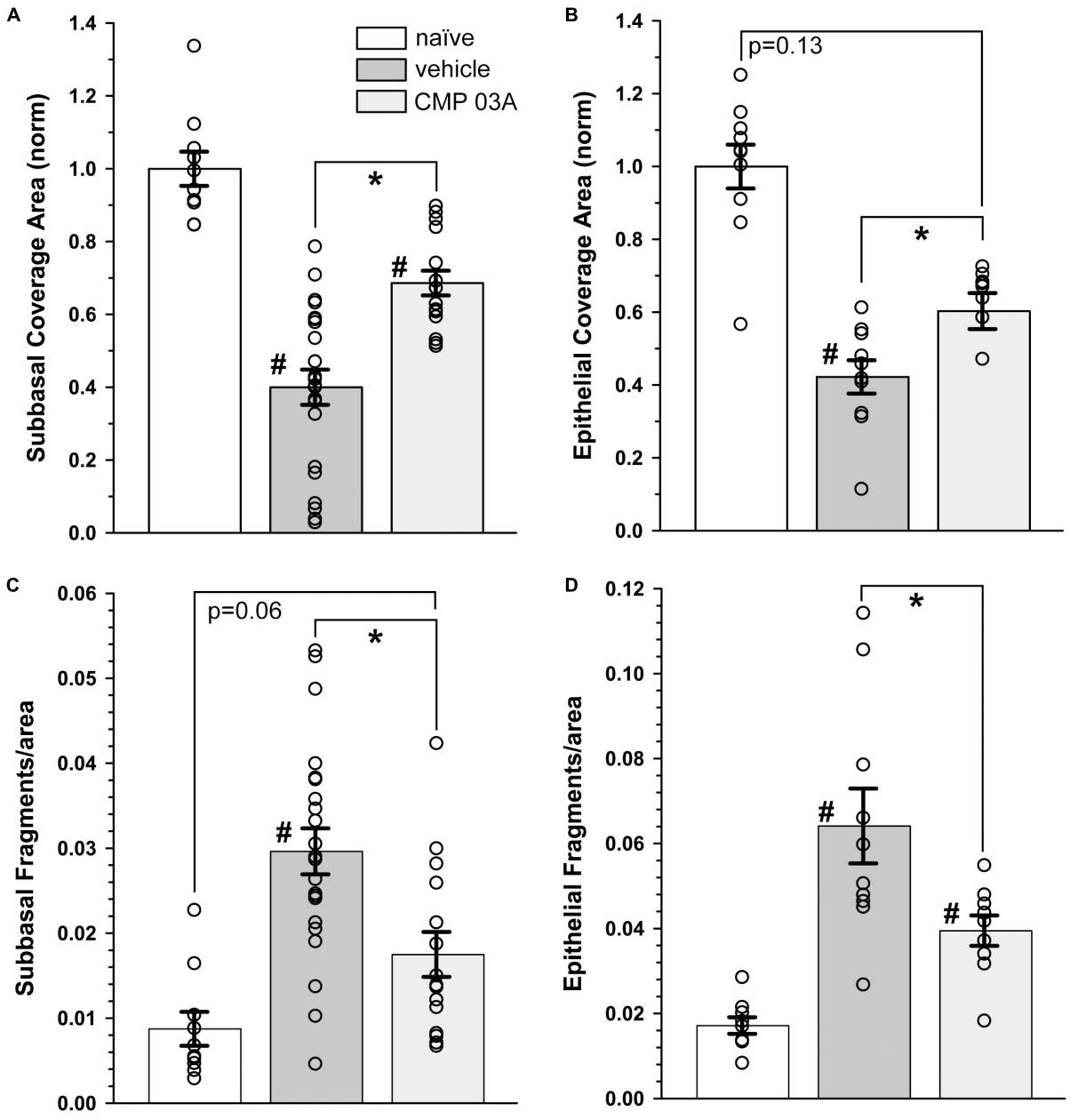

FIGURE 5
CMP 03A prevents desiccation-induced corneal nerve degeneration. **(A)** Desiccation regimen significantly reduced sub-basal nerve coverage in vehicle-treated mice compared to naïve (#, $p < 0.001$). CMP 03A improved coverage compared to vehicle ($p = 0.001$). **(B)** Vehicle significantly reduced epithelial coverage compared to naïve (#, $p = 0.001$). CMP 03A increased epithelial coverage compared to vehicle ($p = 0.001$) to a level that did not significantly differ from naïve ($p = 0.13$). **(C)** The desiccation regimen caused significantly higher sub-basal fragmentation in vehicle-treated mice compared to naïve (#, $p < 0.001$); CMP 03A reduced fragmentation (*, $p < 0.001$) similar to naïve levels ($p = 0.06$). **(D)** In the vehicle group, epithelial terminal fragmentation increased compared to naïve (#, $p < 0.001$); CMP 03A reduced this trend compared to vehicle (*, $p = 0.02$). Results obtained from imaging as described in Figures 3, 4 and replicated as follows: $n = 10$ (naïve), 22 and 10 (vehicle sub-basal and epithelial, respectively), and 15 and 9 (CMP 03A sub-basal and epithelial, respectively).

AUC). In vehicle-treated animals, the amplitude of transitions on the first derivative plot was reduced compared to naïve animals (Figure 8E); this trend was countered by CMP 03A treatment (Figure 8F). The absolute value of the difference in amplitude between peaks and troughs in the first derivative (the delta) was significantly lower in the vehicle group compared to naïve ($p = 0.01$, Figure 8G); CMP improved this outcome compared to vehicle ($p = 0.035$). Next, we calculated the combined AUC of peaks and troughs (Figure 8H) and the area apportioned to each transition in the derivative (Figure 8I). Vehicle-treated animals had a significantly lower AUC than naïve ($p = 0.002$) and CMP animals ($p < 0.001$). In the vehicle-treated group, the area per transition was reduced vs. naïve ($p = 0.008$); this was countered by CMP 03A ($p = 0.001$). By all three measures, CMP 03A restored epithelial integrity to naïve levels. Taken together, these data suggest that while desiccation effectively disrupts the epithelial

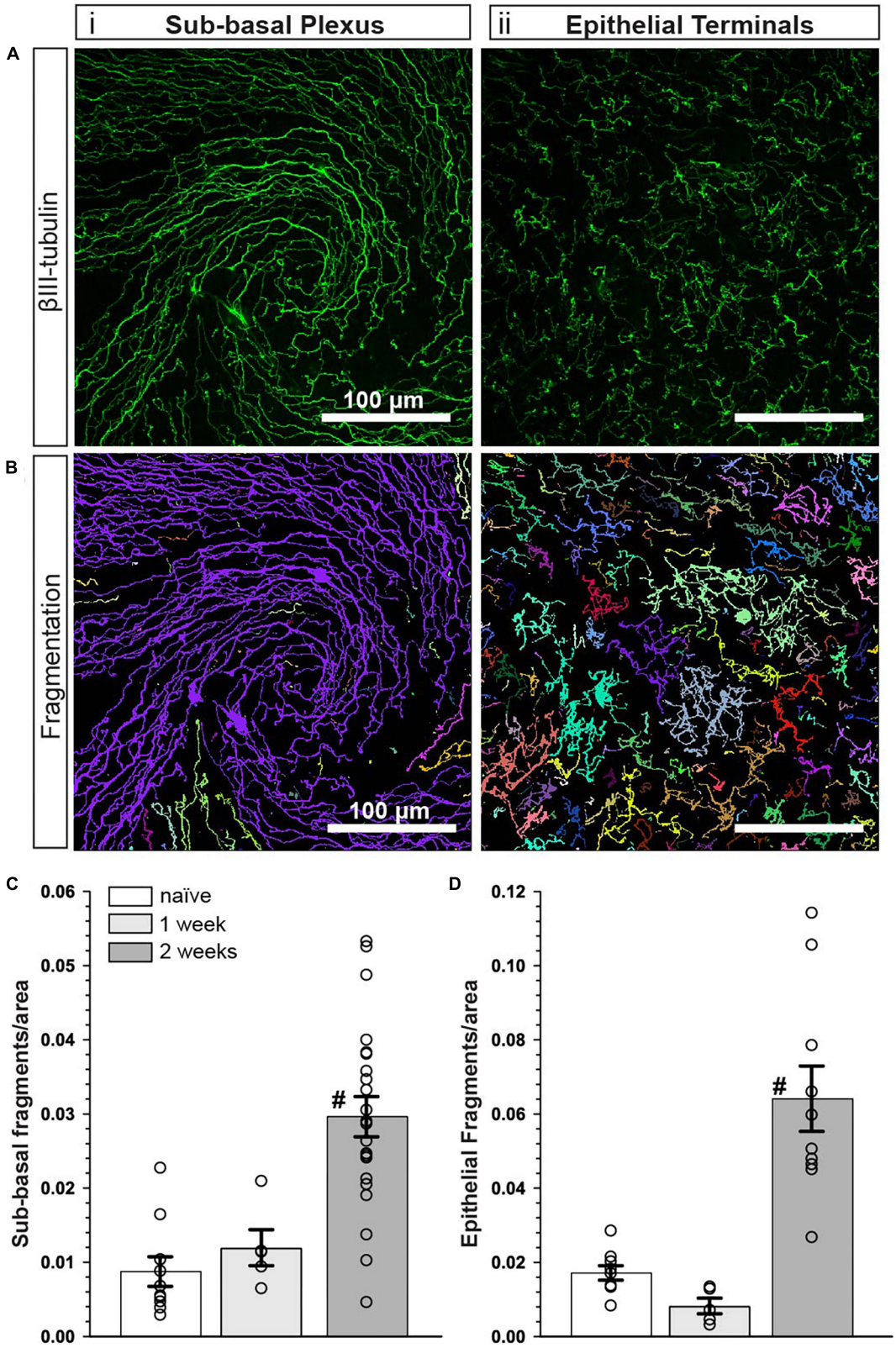

FIGURE 6
Corneal nerve bed is intact after 1 week of desiccation. **(A)** Representative confocal images of βIII-tubulin-stained nerve fibers in the **(i)** central sub-basal plexus and **(ii)** epithelial terminals after 1 week of desiccation. **(B)** Representative pseudo-colored nerve fragmentation images from the **(i)** central sub-basal plexus and **(ii)** epithelial terminals. **(C)** After 1 week, the desiccation regimen did not cause significant fragmentation in the sub-basal plexus compared to naïve (p = 0.60). **(D)** Similarly, there was no significant fragmentation of epithelial terminals (p = 0.30). Compared to 1 week, nerve fragmentation in both the sub-basal **(C)** and epithelial plexus **(D)** at 2 weeks with vehicle treatment was significantly increased ($^{\#}$, $p \leq 0.01$). Scale bars as indicated. Experiment replicated as in Figure 5 for naïve and vehicle (2 weeks); n = 5 (vehicle 1 week).

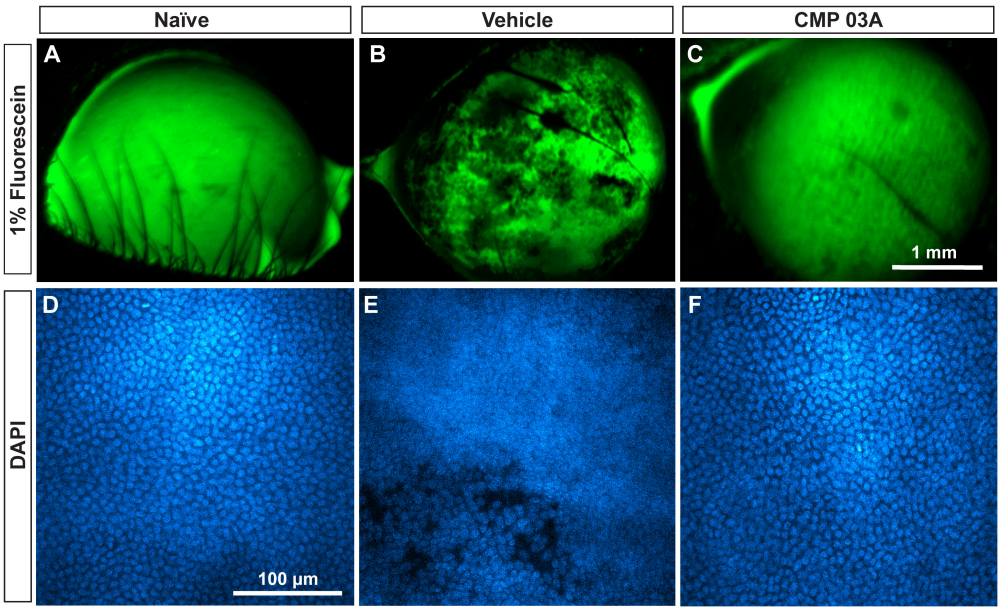

FIGURE 7
CMP 03A prevents desiccation-induced disruption of the corneal epithelium. Representative images of the corneal epithelial surface in **(A)** naïve, **(B)** vehicle- and **(C)** CMP-treated mice visualized *in vivo* by fluorescein staining. CMP 03A prevented corneal epithelial pitting observed in the vehicle group. Representative DAPI-stained confocal images of the epithelial layer in **(D)** naïve, **(E)** vehicle- and **(F)** CMP 03A-treated mice. Vehicle treatment caused epithelial disruption that is absent in the CMP 03A-treated cohort and comparable to naïve animals. Scale bars as indicated.

surface, topical CMP treatment acts to preserve the integrity of the epithelium.

Discussion

The densely innervated nerve bed of the cornea is a critical component in maintaining the homeostatic function of the ocular surface (Vereertbrugghen and Galletti, 2022). Corneal nerves aid in controlling tear film production that not only prevents surface desiccation, but also contributes to immune regulation of the ocular surface and to the integrity of the corneal epithelial layer (Galletti and de Paiva, 2021). In ocular surface diseases such as dry eye, damage to the corneal surface (including collagen itself) leads to a perpetual cycle of epithelial damage, increased inflammation, and progressive nerve degeneration (Beuerman and Schimmelpfennig, 1980). The cornea is a highly collagenous structure and damage to collagen has been strongly associated with age-related increases in susceptibility to injury or disease (Frantz et al., 2010; Sandhu et al., 2012). As such, targeting collagen to promote corneal healing may present a novel therapeutic avenue for the treatment of numerous ocular surface diseases. Our recent work demonstrated that CMPs show great promise in promoting corneal cellular integrity and function after acute injury (Baratta et al., 2022). Our results herein further this work and indicate that CMPs may also act to preserve corneal nerve bed structure and function during desiccating conditions.

In this study we combined pharmaceutical (atropine) and mechanical (air turbulence) desiccation to create a mouse model of ocular surface desiccation that recapitulates many of the features of dry eye disease. The two-week regimen effectively reduced tear film production (Figures 1, 2A). In addition, central corneal sensitivity was significantly diminished after 7 days of desiccation and even further by day 10 in the vehicle-only group (Figure 2B). Our results show that topical treatment with CMP for just 1 week during desiccation improved tear film production and partially restored corneal sensitivity (Figure 2).

Diminished corneal sensitivity is indicative of degenerative damage to the corneal nerve bed (Stepp et al., 2018), thus we visualized central corneal nerves with antibodies targeted to βIII-tubulin (Figure 3). Two weeks of desiccation in the vehicle-only group led to a reduction in the number of corneal sensory nerves and their terminals that extend apically into the epithelium. This loss presumably contributed to our observation of decreased corneal sensitivity (Figure 2B). Interestingly, mice that received topical CMP treatment during desiccation showed evidence of significant nerve bed preservation in both the sub-basal and terminal plexus (Figure 3) and had a significantly improved sensitivity threshold (Figure 2B), suggesting functional recovery. Fragmentation of peripheral nerve fibers such as those found in the cornea is an early feature of the axonal degeneration process (Cajal, 1928; Coleman and Hoke, 2020). In addition to expanding corneal nerve coverage, our results show that CMP treatment reduced the level of nerve fragmentation, which is indicative of degenerative assembly of neurons (Figure 4). This striking preservation of corneal nerve bed may be a consequence of damaged collagen repair by CMP which can impact both the structure and stability of nerves and the integrity of the epithelium through improvement of the extracellular matrix microenvironment.

Since CMP treatment preserved nerve integrity in our model, we sought to determine whether the actions of CMP were neuroprotective or restorative in nature. Corneal samples at day 7 did not show signs of nerve degeneration (Figure 6), suggesting

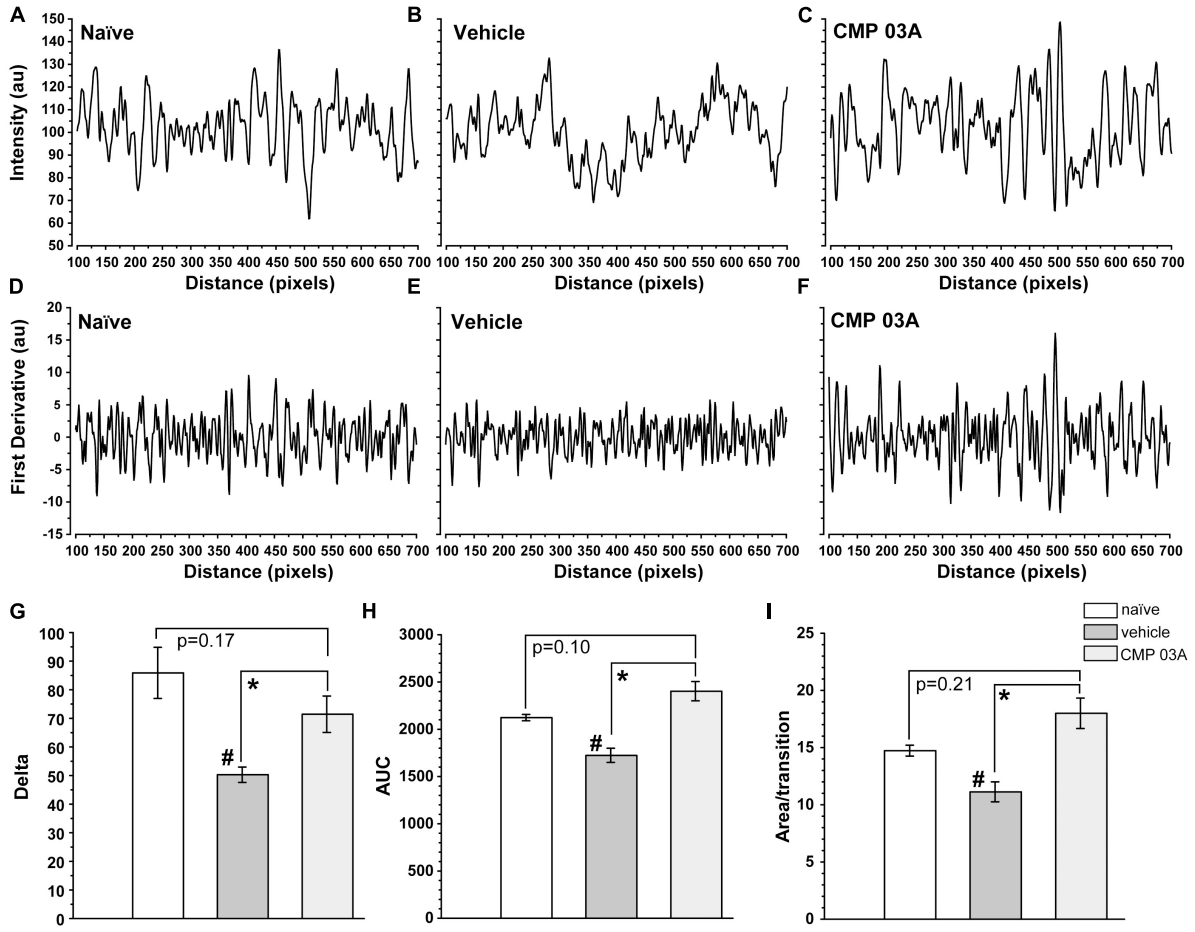

FIGURE 8
CMP 03A preserves the integrity of the corneal epithelial cell layer. Examples of fluorescence intensity and first-derivative line plots, respectively, in naïve **(A,D)**, vehicle **(B,E)**, and CMP-treated **(C,F)** mice. Desiccation reduces the amplitude of the derivative compared to naïve; CMP reverses this trend. **(G)** The transition delta is significantly reduced in the vehicle group compared to naive (#, $p = 0.01$), which is reversed by CMP 03A (*, $p = 0.035$). **(H)** The area under the curve (AUC) is significantly reduced by vehicle compared to naïve (#, $p = 0.002$); CMP 03A improves this trend compared to vehicle (*, $p < 0.001$), elevating to naïve levels. Similarly, the area under the curve per transition **(I)** is significantly reduced in vehicle compared to naïve (#, $p = 0.008$). CMP 03A improves this compared to vehicle ($p = 0.001$), once again to naïve levels. Results obtained from imaging as described in Figure 7 and replicated as follows: $n = 3$ (naïve), 6 (vehicle), and 8 (CMP 03A).

that CMP preserved, rather than restored nerve structure. Our results indicate that tear film and sensitivity measures were not fully restored to baseline levels (Figure 2), which suggests that the neuroprotective effect of CMP in this setting is tear-film independent. Since CMPs have a high affinity for collagen fragments, we hypothesize that the preservation of collagen structure may be facilitating the neuroprotective effects we observe. However, future studies testing the direct effects of CMP on collagen bioactivity and corneal nerve function are required to understand fully the mechanism of CMP action.

A mutual trophic support system exists in the avascular cornea whereby the health of nerves is supported by cells of the epithelium and vice versa (Labetoulle et al., 2019). The corneal epithelium shows signs of impairment and damage in patients with acute and chronic DED (Perez et al., 2020). While corneal nerves can stimulate epithelial cell differentiation, growth, proliferation, and the production of collagen through the release of neuropeptides and neurotrophins (Baker et al., 1993), epithelial cells can directly impact neuronal survival and growth through the release of trophic factors such as nerve growth factor (NGF) (Emoto and Beuerman, 1987). Application of topical CMP prevented disruption of the epithelium that occurred during desiccation (Figures 7, 8). By directly annealing to damaged collagen fragments, the effects of CMP in our model may be attributed to the repair of corneal collagen. This repair in turn can promote epithelial integrity and proliferation to recover epithelium damaged by desiccation stress (Baratta et al., 2021, 2022). Alternatively, preserving helical collagen structure is an important prerequisite in promoting homeostatic cell signaling (San Antonio et al., 2020). By repairing breaks in collagen strands that may trigger inflammation, CMPs may act to reduce local inflammation and further damage.

Our results overall suggest that CMP is multifaceted in its protection of the corneal surface during desiccation stress, acting to preserve central nerve bed structure and to improve epithelial integrity. CMPs may therefore show promise in promoting the health and function of nerves in the cornea in the treatment of dry eye disease.

Data availability statement

The raw data supporting the conclusions of this article will be made available by the authors, without undue reservation.

Ethics statement

This animal study was reviewed and approved by the Vanderbilt University Institutional Animal Care and Use Committee.

Author contributions

RB, BD, ES, LW, and DC conceived of the study. LW and DC designed the research and prepared the manuscript. LW, JH, and OB performed research. LW, JH, and DC analyzed data. All authors contributed to the article and approved the submitted version.

Funding

This study received funding from Stuart Therapeutics, Inc., which had no role in research design, data collection and analysis, interpretation of data, or in preparation of the manuscript and decision to publish, and from unrestricted funds (DC).

Conflict of interest

RB, BD, and ES were employed by Stuart Therapeutics, Inc., and DC served as a consultant for Stuart Therapeutics, Inc.

The remaining authors declare that the research was conducted in the absence of any commercial or financial relationships that could be construed as a potential conflict of interest.

Publisher's note

All claims expressed in this article are solely those of the authors and do not necessarily represent those of their affiliated organizations, or those of the publisher, the editors and the reviewers. Any product that may be evaluated in this article, or claim that may be made by its manufacturer, is not guaranteed or endorsed by the publisher.

References

Al-Aqaba, M. A., Dhillon, V. K., Mohammed, I., Said, D. G., and Dua, H. S. (2019). Corneal nerves in health and disease. *Prog. Retin. Eye Res.* 73:100762. doi: 10.1016/j.preteyeres.2019.05.003

Asiedu, K. (2022). Role of ocular surface neurobiology in neuronal-mediated inflammation in dry eye disease. *Neuropeptides* 95:102266. doi: 10.1016/j.npep.2022.102266

Asiedu, K., Markoulli, M., Bonini, S., Bron, A. J., Dogru, M., Kwai, N., et al. (2022a). Tear film and ocular surface neuropeptides: Characteristics, synthesis, signaling and implications for ocular surface and systemic diseases. *Exp. Eye Res.* 218:108973. doi: 10.1016/j.exer.2022.108973

Asiedu, K., Markoulli, M., Tummanapalli, S. S., Chiang, J. C. B., Alotaibi, S., Wang, L. L., et al. (2022b). Impact of chronic kidney disease on corneal neuroimmune features in type 2 diabetes. *J. Clin. Med.* 12:16. doi: 10.3390/jcm12010016

Baker, K. S., Anderson, S. C., Romanowski, E. G., Thoft, R. A., and Sundarraj, N. (1993). Trigeminal ganglion neurons affect corneal epithelial phenotype. Influence on type VII collagen expression in vitro. *Invest. Ophthalmol. Vis. Sci.* 34, 137–144.

Baratta, R. O., Del Buono, B. J., Schlumpf, E., Ceresa, B. P., and Calkins, D. J. (2021). Collagen mimetic peptides promote corneal epithelial cell regeneration. *Front. Pharmacol.* 12:705623. doi: 10.3389/fphar.2021.705623

Baratta, R. O., Schlumpf, E., Buono, B. J. D., Delorey, S., and Calkins, D. J. (2022). Corneal collagen as a potential therapeutic target in dry eye disease. *Surv. Ophthalmol.* 67, 60–67. doi: 10.1016/j.survophthal.2021.04.006

Belmonte, C., Nichols, J. J., Cox, S. M., Brock, J. A., Begley, C. G., Bereiter, D. A., et al. (2017). TFOS DEWS II pain and sensation report. *Ocul. Surf.* 15, 404–437. doi: 10.1016/j.jtos.2017.05.002

Beuerman, R. W., and Schimmelpfennig, B. (1980). Sensory denervation of the rabbit cornea affects epithelial properties. *Exp. Neurol.* 69, 196–201. doi: 10.1016/0014-4886(80)90154-5

Bitirgen, G., Kucuk, A., Ergun, M. C., Satirtav, G., and Malik, R. A. (2023). Corneal nerve loss and increased langerhans cells are associated with disease severity in patients with rheumatoid arthritis. *Eye*. [Epub ahead of print]. doi: 10.1038/s41433-023-02447-6

Bourcier, T., Acosta, M. C., Borderie, V., Borraìs, F., Gallar, J., Bury, T., et al. (2005). Decreased corneal sensitivity in patients with dry eye. *Invest. Ophthalmol. Vis. Sci.* 46, 2341–2345. doi: 10.1167/iovs.04-1426

Burgalassi, S., Panichi, L., Chetoni, P., Saettone, M. F., and Boldrini, E. (1999). Development of a simple dry eye model in the albino rabbit and evaluation of some tear substitutes. *Ophthalmic Res.* 31, 229–235. doi: 10.1159/000055537

Cajal, R. Y. (1928). *Degeneration and regeneration of the nervous system*. London: Oxford University Press.

Chattopadhyay, S., Guthrie, K. M., Teixeira, L., Murphy, C. J., Dubielzig, R. R., Mcanulty, J. F., et al. (2016). Anchoring a cytoactive factor in a wound bed promotes healing. *J. Tissue Eng. Regen. Med.* 10, 1012–1020. doi: 10.1002/term.1886

Chattopadhyay, S., Murphy, C. J., Mcanulty, J. F., and Raines, R. T. (2012). Peptides that anneal to natural collagen in vitro and ex vivo. *Org. Biomol. Chem.* 10, 5892–5897. doi: 10.1039/c2ob25190f

Chattopadhyay, S., and Raines, R. T. (2014). Review collagen-based biomaterials for wound healing. *Biopolymers* 101, 821–833. doi: 10.1002/bip.22486

Coleman, M. P., and Hoke, A. (2020). Programmed axon degeneration: From mouse to mechanism to medicine. *Nat. Rev. Neurosci.* 21, 183–196. doi: 10.1038/s41583-020-0269-3

Dieckmann, G., Goyal, S., and Hamrah, P. (2017). Neuropathic corneal pain: Approaches for management. *Ophthalmology* 124, S34–S47. doi: 10.1016/j.ophtha.2017.08.004

Edwards, R. G., Kopp, S. J., Ifergan, I., Shui, J. W., Kronenberg, M., Miller, S. D., et al. (2017). Murine corneal inflammation and nerve damage after infection with hsv-1 are promoted by hvem and ameliorated by immune-modifying nanoparticle therapy. *Invest. Ophthalmol. Vis. Sci.* 58, 282–291. doi: 10.1167/iovs.16-20668

Emoto, I., and Beuerman, R. W. (1987). Stimulation of neurite growth by epithelial implants into corneal stroma. *Neurosci. Lett.* 82, 140–144. doi: 10.1016/0304-3940(87)90118-2

Farrand, K. F., Fridman, M., Stillman, I. O., and Schaumberg, D. A. (2017). Prevalence of diagnosed dry eye disease in the united states among adults aged 18 years and older. *Am. J. Ophthalmol.* 182, 90–98. doi: 10.1016/j.ajo.2017.06.033

Frantz, C., Stewart, K. M., and Weaver, V. M. (2010). The extracellular matrix at a glance. *J. Cell Sci.* 123, 4195–4200. doi: 10.1242/jcs.023820

Galletti, J. G., and de Paiva, C. S. (2021). The ocular surface immune system through the eyes of aging. *Ocul. Surf.* 20, 139–162. doi: 10.1016/j.jtos.2021.02.007

Guerrero-Moreno, A., Baudouin, C., Melik Parsadaniantz, S., and Reaux-Le Goazigo, A. (2020). Morphological and functional changes of corneal nerves and their

contribution to peripheral and central sensory abnormalities. *Front. Cell Neurosci.* 14:610342. doi: 10.3389/fncel.2020.610342

He, J., and Bazan, H. E. (2016). Neuroanatomy and neurochemistry of mouse cornea. *Invest. Ophthalmol. Vis. Sci.* 57, 664–674. doi: 10.1167/iovs.15-18019

Hwang, D. D., Lee, S. J., Kim, J. H., and Lee, S. M. (2021). The role of neuropeptides in pathogenesis of dry dye. *J. Clin. Med.* 10:4248. doi: 10.3390/jcm10184248

Kilic, S., and Kulualp, K. (2016). Tear production rate in a mouse model of dry eye according to the phenol red thread and endodontic absorbent paper point tear tests. *Comp. Med.* 66, 367–372.

Labetoulle, M., Baudouin, C., Calonge, M., Merayo-Lloves, J., Boboridis, K. G., Akova, Y. A., et al. (2019). Role of corneal nerves in ocular surface homeostasis and disease. *Acta. Ophthalmol.* 97, 137–145. doi: 10.1111/aos.13844

Lee, H., Kim, C. E., Ahn, B. N., and Yang, J. (2017). Anti-inflammatory effect of hydroxyproline-gqdglagpk in desiccation stress-induced experimental dry eye mouse. *Sci. Rep.* 7:7413. doi: 10.1038/s41598-017-07965-4

Marfurt, C. F., Cox, J., Deek, S., and Dvorscak, L. (2010). Anatomy of the human corneal innervation. *Exp. Eye Res.* 90, 478–492. doi: 10.1016/j.exer.2009.12.010

Marfurt, C. F., Kingsley, R. E., and Echtenkamp, S. E. (1989). Sensory and sympathetic innervation of the mammalian cornea. A retrograde tracing study. *Invest. Ophthalmol. Vis. Sci.* 30, 461–472.

McKay, T. B., Seyed-Razavi, Y., Ghezzi, C. E., Dieckmann, G., Nieland, T. J. F., Cairns, D. M., et al. (2019). Corneal pain and experimental model development. *Prog. Retin. Eye Res.* 71, 88–113. doi: 10.1016/j.preteyeres.2018.11.005

Meek, K. M. (2009). Corneal collagen-its role in maintaining corneal shape and transparency. *Biophys. Rev.* 1, 83–93. doi: 10.1007/s12551-009-0011-x

Mikulec, A. A., and Tanelian, D. L. (1996). CGRP increases the rate of corneal re-epithelialization in an in vitro whole mount preparation. *J. Ocul. Pharmacol. Ther.* 12, 417–423. doi: 10.1089/jop.1996.12.417

Muller, L. J., Marfurt, C. F., Kruse, F., and Tervo, T. M. (2003). Corneal nerves: Structure, contents and function. *Exp. Eye Res.* 76, 521–542. doi: 10.1016/S0014-4835(03)00050-2

Perez, V. L., Stern, M. E., and Pflugfelder, S. C. (2020). Inflammatory basis for dry eye disease flares. *Exp. Eye Res.* 201:108294. doi: 10.1016/j.exer.2020.108294

Pham, T. L., Kakazu, A., He, J., and Bazan, H. E. P. (2019). Mouse strains and sexual divergence in corneal innervation and nerve regeneration. *FASEB J.* 33, 4598–4609. doi: 10.1096/fj.201801957R

Ren, T., Van Der Merwe, Y., and Steketee, M. B. (2015). Developing extracellular matrix technology to treat retinal or optic nerve injury. *eNeuro* 2, ENEURO.77–15.2015. doi: 10.1523/ENEURO.0077-15.2015

Ribeiro, M., Mcgrady, N. R., Baratta, R. O., Del Buono, B. J., Schlumpf, E., and Calkins, D. J. (2022). Intraocular delivery of a collagen mimetic peptide repairs retinal ganglion cell axons in chronic and acute injury models. *Int. J. Mol. Sci.* 23:2911. doi: 10.3390/ijms23062911

San Antonio, J. D., Jacenko, O., Fertala, A., and Orgel, J. (2020). Collagen structure-function mapping informs applications for regenerative medicine. *Bioengineering* 8:3. doi: 10.3390/bioengineering8010003

Sandhu, S. V., Gupta, S., Bansal, H., and Singla, K. (2012). Collagen in health and disease. *J. Orofac. Res.* 2, 153–159. doi: 10.5005/jp-journals-10026-1032

Schimmelpfennig, B. (1982). Nerve structures in human central corneal epithelium. *Graefes Arch. Clin. Exp. Ophthalmol.* 218, 14–20. doi: 10.1007/BF02134093

Simsek, C., Kojima, T., Dogru, M., and Tsubota, K. (2018). Alterations of murine subbasal corneal nerves after environmental dry eye stress. *Invest. Ophthalmol. Vis. Sci.* 59, 1986–1995. doi: 10.1167/iovs.17-23743

Song, I., and Dityatev, A. (2018). Crosstalk between glia, extracellular matrix and neurons. *Brain Res. Bull.* 136, 101–108. doi: 10.1016/j.brainresbull.2017.03.003

Stepp, M. A., Pal-Ghosh, S., Downie, L. E., Zhang, A. C., Chinnery, H. R., Machet, J., et al. (2020). Corneal epithelial "neuromas": A case of mistaken identity?. *Cornea* 39, 930–934. doi: 10.1097/ICO.0000000000002294

Stepp, M. A., Pal-Ghosh, S., Tadvalkar, G., Williams, A., Pflugfelder, S. C., and De Paiva, C. S. (2018). Reduced intraepithelial corneal nerve density and sensitivity accompany desiccating stress and aging in c57bl/6 mice. *Exp. Eye Res.* 169, 91–98. doi: 10.1016/j.exer.2018.01.024

Vereertbrugghen, A., and Galletti, J. G. (2022). Corneal nerves and their role in dry eye pathophysiology. *Exp. Eye Res.* 222:109191. doi: 10.1016/j.exer.2022.109191

Wu, M., Hill, L. J., Downie, L. E., and Chinnery, H. R. (2022). Neuroimmune crosstalk in the cornea: The role of immune cells in corneal nerve maintenance during homeostasis and inflammation. *Prog. Retin. Eye Res.* 91:101105. doi: 10.1016/j.preteyeres.2022.101105

Zander, E., and Weddell, G. (1951). Observations on the innervation of the cornea. *J. Anat.* 85, 68–99.

frontiers | Frontiers in Neuroscience

TYPE Original Research
PUBLISHED 01 June 2023
DOI 10.3389/fnins.2023.1204792

OPEN ACCESS

EDITED BY
Dan Wen,
Central South University, China

REVIEWED BY
FangJun Bao,
Affiliated Eye Hospital to Wenzhou Medical University, China
Ke Ma,
Sichuan University, China

*CORRESPONDENCE
Jing Zhao
✉ zhaojing_med@163.com
Xingtao Zhou
✉ doctzhouxingtao@163.com

†These authors have contributed equally to this work and share first authorship

RECEIVED 12 April 2023
ACCEPTED 15 May 2023
PUBLISHED 01 June 2023

CITATION
Ye Y, Zhang Z, Niu L, Shi W, Wang X, Yan L, Zhou X and Zhao J (2023) Binocular imbalance in patients after implantable collamer lens V4c implantation or femtosecond laser-assisted *in situ* keratomileusis for myopia with presbyopia. *Front. Neurosci.* 17:1204792. doi: 10.3389/fnins.2023.1204792

Binocular imbalance in patients after implantable collamer lens V4c implantation or femtosecond laser-assisted *in situ* keratomileusis for myopia with presbyopia

Yuhao Ye[1,2,3,4†], Zhe Zhang[1,2,3,4†], Lingling Niu[1,2,3,4], Wanru Shi[1,2,3,4], Xiaoying Wang[1,2,3,4], Li Yan[5], Xingtao Zhou[1,2,3,4*] and Jing Zhao[1,2,3,4*]

[1]Department of Ophthalmology and Optometry, Eye and ENT Hospital, Fudan University, Shanghai, China, [2]NHC Key Laboratory of Myopia (Fudan University), Key Laboratory of Myopia, Chinese Academy of Medical Sciences, Shanghai, China, [3]Shanghai Research Center of Ophthalmology and Optometry, Shanghai, China, [4]Shanghai Engineering Research Center of Laser and Autostereoscopic 3D for Vision Care (20DZ2255000), Shanghai, China, [5]National Engineering Research Center for Healthcare Devices, Guangzhou, China

Aim: To investigate the long-term safety, efficacy, and binocular balance of monovision surgery using Implantable Collamer Lens (ICL) V4c implantation and Femtosecond Laser-Assisted *in situ* Keratomileusis (FS-LASIK) for the treatment of myopic patients with presbyopia.

Methods: This case series study involved 90 eyes of 45 patients (male/female=19/26; average age:46.27±5.54 years; average follow-up time:48.73±14.65months) who underwent the aforementioned surgery to treat myopic presbyopes. Data on manifest refraction, corrected distance visual acuity, dominant eye, presbyopic addition, intraocular pressure, and anterior segment biometric parameters were collected. The visual outcomes and binocular balance at 0.4m, 0.8m, and 5m were documented.

Results: The safety index for the ICL V4c and FS-LASIK groups were 1.24±0.27 and 1.04±0.20 (p=0.125), respectively. Binocular visual acuity (logmar) for 0.4m, 0.8m, and 5m were−0.03±0.05, −0.03±0.02, and 0.10±0.03 for the ICL V4c group, and−0.02±0.09, −0.01±0.02, and 0.06±0.04 for the FS-LASIK group, respectively. The proportions of all patients with imbalanced vision at 0.4m, 0.8m, and 5m distances were 68.89, 71.11, and 82.22%, respectively (all p>0.05 between the two groups). There were significant differences in refraction between the balanced and imbalanced vision for patients at 0.4m distance (for non-dominant eye spherical equivalent [SE]: −1.14±0.17D and−1.47±0.13D, p<0.001), 0.8m distance (for preoperative ADD:0.90±0.17D and 1.05±0.11D, p=0.041), and 5m distance (for non-dominant SE: −1.13±0.33D and−1.42±0.11D, p<0.001).

Conclusion: ICL V4c implantation and FS-LASIK monovision treatment demonstrated good long-term safety and binocular visual acuity at various distances. After the procedure, the imbalanced patients' vision is primarily related to the age-related presbyopia and anisometropia progression caused by the monovision design.

KEYWORDS

myopia, presbyopia, monovision, implantable collamer lens V4c, femtosecond laser-assisted *in situ* keratomileusis, binocular balance, visual function

1. Introduction

Binocular vision integrates two slightly different images transmitted from each eye to the visual cortex. Effective cooperation between the eyes is crucial for obtaining high-quality images. A binocular imbalance may represent inhibitory binocular interactions by determining the signal strength inequality between the eyes (Kwon et al., 2014). It refers to intermittent partial suppression of monocular vision during binocular fusion (Tao et al., 2022). It shows processing defects in conditions such as autism spectrum disorder (Dunn and Jones, 2020), amblyopia (Mao et al., 2020; Webber et al., 2020), keratoconus (Marella et al., 2021), and glaucoma (Joao et al., 2021), as well as in normal individuals (Xu et al., 2019), which may result from periodic changes in visual cognition caused by neural oscillations in brain activity (Cha and Blake, 2019). Age is a major factor affecting binocular contrast sensitivity, indicating neural processes in binocular interactions (Ye et al., 2023). Further research is needed on the binocular interaction in aged patients, especially those with both myopia and presbyopia. Myopia is one of the most widespread visual impairments worldwide and causes significant disabilities (Wu et al., 2016; Modjtahedi et al., 2021). About one-third of the world's population currently suffers from myopia, with increasing numbers as the population ages (Holden et al., 2016). The projected increase in the number of older people affected by both myopia and presbyopia implies that society will bear substantial costs (Naidoo et al., 2019).

Monovision is commonly used to treat presbyopia because it is effective and relatively easy to apply in medical practice. It corrects far-sightedness in the dominant eye and near-sightedness in the non-dominant eye (Jain et al., 1996). Monovision refractive surgery is a good alternative for patients with myopia and presbyopia because it improves visual acuity at variable distances (Fu et al., 2018; Luft et al., 2018; Takahashi et al., 2018). However, few studies have assessed the long-term effects of a monovision design, particularly for Implantable Collamer Lens (ICL) V4c implantation and Femtosecond Laser-Assisted *in situ* Keratomileusis (FS-LASIK). Presbyopia progression may continue postoperatively. Furthermore, uneven refractive errors caused by monovision and age-related neural processing deficits may affect binocular balance. This could compromise patients' visual function and experience, highlighting the need for careful consideration of the potential benefits and drawbacks of this intervention (Yang et al., 2017).

Currently, few studies have evaluated the long-term inter-eye interactions following monovision refractive surgery utilizing ICL V4c implantation and FS-LASIK. Binocular balance and changes in the dominant and non-dominant eyes at different contrast sensitivities remain unclear. Age and anisometropia caused by monovision may be the significant contributing factors (Zheleznyak et al., 2015; Li et al., 2016). Therefore, the binocular balance may be related to presbyopic add and its changes or the intentional target residual myopia of the non-dominant eyes. In addition, it may also be affected by long-term refractive changes after surgery and the visual acuity of the dominant and non-dominant eyes at variable distances.

Thus, this study aimed to evaluate the long-term safety and effectiveness of a monovision design with ICL V4c implantation and FS-LASIK surgery and to assess binocular balance promptly and reliably. It will provide a reference for monovision refractive surgery from an inter-eye interaction perspective. This will help identify and monitor possible defects in inter-eye interactions, enabling clinically accurate evaluation of patient outcomes and prognosis beyond standard visual acuity.

2. Materials and methods

2.1. Subjects

This study enrolled 90 eyes in 45 patients (preoperative baseline data for all patients are shown in Table 1). The patient underwent FS-LASIK or ICL V4c surgery for myopia correction and presbyopia at the Fudan University Eye and ENT Hospital between June 2015 and August 2019. Age distribution and manifest refraction are shown in Figure 1A. Preoperative presbyopic ADD and at the last follow-up, and their differences are shown in Figure 1B. This case series study followed the regulations of the Ethics Committee of Fudan University Eye and ENT Hospital (Shanghai, China). It was conducted in accordance with the Helsinki Declaration. All procedures were performed with written informed consent from the patients. The studies inclusion criteria are (1) Age $\geq$ 40 years or above; (2) Stable spherical equivalent (SE) for the last 2 years ($\leq$0.5D/y); (3) Soft contact lenses should be discontinued for at least 2 weeks and rigid gas permeable lenses for at least 4 weeks before the examination. Exclusion criteria were (1) history of corneal diseases, cataracts, glaucoma, retinal detachment, neurological ophthalmic disease, or other ophthalmic diseases; (2) history of systemic diseases or severe psychological or psychiatric illness; and (3) unsuitable patients for ICL V4c implantation due to endothelial cell density (ECD) <2,000 cells/mm^2 or anterior chamber depth (ACD) <2.8 mm.

2.2. Examinations

The equipment used and measured parameters were as follows: (1) An RT-5100 phoropter (Nidek Technologies, Japan) was used to measure spherical equivalent (SE), corrected distance visual acuity (CDVA), uncorrected-distance visual acuity (UDVA), and presbyopic add power (ADD). The safety index (SI) was defined as the postoperative CDVA over the preoperative CDVA, and the efficacy index (EI) was defined as the postoperative UDVA over the preoperative CDVA. D-eyes and nD-eyes were determined using the card-hole method. ADD was measured using the Fusion Cross-Cylinder (FCC) method at a 33 cm distance with optimal distance visual acuity correction. (2) Intraocular pressure (IOP) was measured using a Canon Full Auto Tonometer TX-F (Canon, Inc., Tokyo, Japan). (3) Corneal thickness (CT), anterior chamber volume (ACV), ACD, anterior chamber angle (ACA), and white-to-white ratio (WTW) were measured using Pentacam HR (Oculus Optikgerate Wetzlar, Wetzlar, Germany). (4) Endothelial cell density (ECD) was measured using SP-2000P (Topcon Corporation, Kyoto, Japan). (5) White-to-white (WTW) measurements were performed using IOL Master 700 (Carl Zeiss AG, Germany). (6) Axial length (AL) was measured using IOL Master 500 (Carl Zeiss AG, Germany). Slit lamp and fundus examinations were conducted following pupillary dilation to evaluate lens transparency and exclude fundus lesions.

2.3. Monovision design

The D-eyes were targeted for −0.34 to 0.02 D and −1.25 to 0.25 D in the ICL V4c and FS-LASIK groups, respectively. The targeted nD-eyes were around −2.435 to −0.27 D and −2.75 to −0.25 D in the

TABLE 1 Preoperative patient demographics.

Characteristic	Mean±SD	Range	ICL V4c Group	FS-LASIK Group	*p*
Age (years)	46.27 ± 5.54	(40, 64)	43.17 ± 2.48	58.50 ± 7.73	**<0.001**
Gender (male/female)	19/26		6/12	13/14	-
Axial length (mm)	27.37 ± 1.96	(23.98, 32.11)	28.69 ± 2.09	26.54 ± 1.33	**<0.001**
Refraction sphere (D)	−8.90 ± 3.69	(−19.00, −2.25)	−12.12 ± 3.23	−7.14 ± 2.80	**<0.001**
Refraction cylinder (D)	−0.88 ± 0.80	(−3.25, 0)	−1.15 ± 1.05	−0.69 ± 0.52	0.161
SE (D)	−9.34 ± 3.78	(−19.00, −2.50)	−12.12 ± 3.23	−7.48 ± 2.80	**<0.001**
CDVA (LogMAR)	0.01 ± 0.08	(−0.18, 0.30)	0.05 ± 0.09	−0.01 ± 0.06	0.002
Dominant eye (OD/OS)	24/21		9/9	15/12	-
ADD (D)	1.00 ± 0.62	(0.25, 2.50)	0.64 ± 0.29	1.25 ± 0.67	**<0.001**
K-flat (D)	43.27 ± 1.38	(40.7, 46.60)	43.01 ± 1.59	43.44 ± 1.20	0.122
K-steep (D)	44.33 ± 1.52	(41.10, 47.20)	44.59 ± 1.93	44.16 ± 1.17	0.218

ICL, implantable collamer lens; FS-LASIK, femtosecond laser-assisted laser in situ keratomileusis; SE, spherical equivalent; CDVA, corrected-distant visual acuity; WTW, white to white. Values with statistical significance between ICL V4c group and FS-LASIK group are shown in bold.

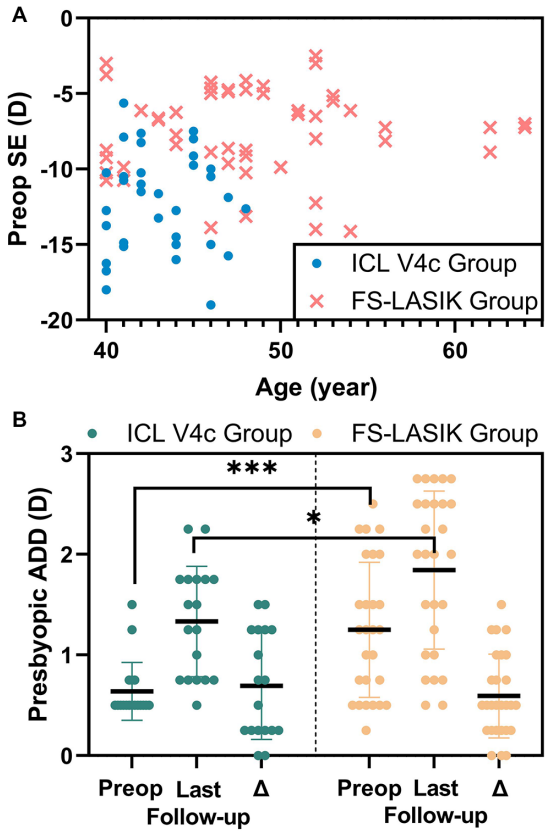

FIGURE 1
The preop SE and age distributions of the patients **(A)** and the change of presbyopic ADD **(B)** in implantable collamer lens V4c group and femtosecond laser-assisted laser *in situ* keratomileusis group.

two groups, respectively, according to each patient's presbyopic add power. In those with planned residual myopic diopters, the target refraction was on trial in-frame glasses preoperatively and was accepted by the patients.

2.4. Surgery

The choice of operation was confirmed by surgical indications after adequate communication with patients. For patients who met the two surgical indications at the same time, they could choose by themselves with the knowledge of the two surgeries. The same surgeon (XZ) performed all surgical procedures. The patients were administered antibiotic eye drops four times daily for 3 days before surgery. In FS-LASIK, a 500 kHz VisuMax femtosecond laser system (Carl Zeiss Meditec, Jena, Germany) with a pulse energy of 130 nJ was used for flap creation, followed by a MEL 90 excimer laser (Carl Zeiss Meditec) for stromal ablation, with a pulse energy of 185 nJ. The flap diameter and thickness were 7.5 mm and 100 μm, respectively, with standard 90° hinges and 90° side cut angles. The planned optic zone of 6.45 ± 0.20 mm (ranging from 6.00 to 6.80). After FS-LASIK, a soft contact lens was worn and removed on 1 day postoperatively. Topical levofloxacin, 0.1% fluorometholone solution, and non-preserved artificial tears were administered after FS-LASIK. The detailed steps have been previously described (Han et al., 2019).

The STAAR Surgical online calculator (Version 3.0)[1] was used to determine ICL power. ICL size calculation was based on the horizontal WTW, ACD, and ATA distances. For ICL sizing, we adjusted the WTW value obtained from the Pentacam and referred to the value obtained from the IOLmaster measurements. In the implantation surgeries, ICL V4c was implanted into the anterior chamber and pre-injected with a viscoelastic agent through the lateral corneal incision under topical anesthesia. After that, the ICL was adjusted using a manipulator, and the viscoelastic agent was replaced with a balanced salt solution. Postoperative antibiotics and steroid eye drops were administered 4 times daily for 2 weeks and tapered gradually. The detailed steps have been previously described (Chen et al., 2016).

1 http://en.informer.com/icl-power-calculation-software/

2.5. Follow-up

The patients were followed up for 4 years, with an average of 48.73 ± 14.65 months. At the last follow-up, the CDVA and UDVA (logMAR) of the D eyes, nD eyes, and both eyes at 0.4 m, 0.8 m, and 5 m were recorded. Measurements were performed using two trial frames and two tumbling E charts (VSK-VC-J 0.4 m/0.8 m, Wehen Vision, China) for the monocular and binocular VA at the distance of 0.4 m and 0.8 m, respectively. A phoropter was used for monocular and binocular distant VA at 5 m.

2.6. Binocular balance assessment

Binocular balance was assessed using a modified version of the dichoptic procedure proposed by Tao et al. (2022). The binocular contrast balance task consisted of the use of a sine bar. The images observed by the left and right eyes were divided into three-quarters of a sine function period at a glance y = sin (x)(x = [0, 3*pi/2]) grayscale image, and at a glance y = sin (x) (x = [pi/2, 2*pi]) grayscale image.

The stimulus image was presented on a three dimension (3D) gamma-corrected monitor (LGD2343P, with a resolution of 1920 × 1,080 pixels, the max luminance of 250 cd/m^2 and a refresh rate of 120HZ). All patients wore 3D polarized glasses to perform the BI tests at a distance of 0.4 m, 0.8 m, and 5 m; each eye was presented with either horizontal or vertical stripes individually, with 100% contrast (Supplementary Figure S1). The same size of stimuli were chosen to control the variables in different distances, because varies pixel size with distances decreases the effect of monovision design. The participants were asked to report whether they saw horizontal stripes, vertical stripes, or a grid. Binocular imbalance, they could not see the black-and-white cross grid. For participants with a binocular imbalance, the level of balance was recorded after reducing the contrast of the image of the dominant eye until the participants could see the grid. Next, the dominant and nondominant eyes of the patient presented with horizontal or vertical stripes at contrast level 1 (100% contrast), whereas the contrast of the opposite eye gradually decreased by 5% each time. The balance threshold range was observed and recorded.

2.7. Statistical analysis

All statistical analyses were performed using the Statistical Package for the Social Sciences version 25.0. (SPSS, Inc., Chicago, IL, USA). Results are expressed as mean ± standard deviation. The normality of the data was checked using the Kolmogorov–Smirnov test. Repeated ANOVA was used to compare the pre-and post-treatment and D- and nD eyes normally distributed data, while the paired t-test was used to compare the normally distributed data of the D and nD eyes at the last follow-up, and the Wilcoxon signed-rank test was used for non-normally distributed data. A generalized estimating equation was used to determine the correlation between binocular balance parameters (Balanced/Imbalanced, Level of balance, and range of balance [D-eye and nD-eye]) and refraction parameters (Visual acuity at 0.4-, 0.8, and 5.0 m distances, spherical equivalent, and presbyopic ADD). Differences were considered statistically significant at $p < 0.05$.

3. Results

All surgeries and examinations were performed, and no complications, such as cataracts or high intraocular pressure, occurred in any eye throughout the follow-up period. The data loss rate for all the types was <5%.

3.1. Safety and efficacy

At the last follow-up, the safety index of the ICL V4c and FS-LASIK groups were 1.24 ± 0.27 and 1.04 ± 0.20 ($p = 0.125$), respectively. Their efficacy indices were 0.77 ± 0.29 and 0.66 ± 0.34 ($p < 0.001$), respectively (Figure 2). The refractive parameter changes in the dominant and non-dominant eyes are presented in Table 2, and changes in the biological parameters are summarized in Table 3. The endothelial cell density (ECD) in the ICL V4c group decreased by an average of 549.42 ± 704.29/mm^2 (17.14 ± 14.88% and 3.59 ± 3.11% per year). The vault of all eyes after ICL V4c implantation was within the 150 ~ 850 μm range.

3.2. Monovision vision

The binocular visual acuity (logMAR) of the ICL V4c group were −0.03 ± 0.05 (0.4 m), −0.03 ± 0.02 (0.8 m), and 0.10 ± 0.03 (5 m). The corresponding figures were −0.02 ± 0.09, −0.01 ± 0.02, and 0.06 ± 0.04 in the FS-LASIK group. The two groups had no significant difference ($p > 0.05$; Figure 3). The percentages of binocular VA > 20/25 (Snellen Line) at the three distances were 78 and 85.19% in the ICL V4c and FS-LASIK groups, respectively. The percentage of non-dominant eyes with VA > 20/25 (Snellen Line) at 0.4 m was 88.89 and 85.19% for the ICL V4c and FS-LASIK groups, respectively; the percentage with VA > 20/32 (Snellen Line) was 100 and 96.30% for the two groups, respectively. At 5 m distance, for the ICL V4c and FS-LASIK groups, those with VA > 20/25 (Snellen Line) were 76.47 and 81.48%, respectively, and VA > 20/32 (Snellen Line) were 2.35 and 88.89%, respectively.

3.3. Binocular balance

Table 4 shows the binocular balance of both groups at various distances. The proportion of patients with binocular imbalance (balance) at near, intermediate, and distances were 68.89% (31.11%), 71.11% (28.89%), and 82.22% (17.78%), respectively. The difference in binocular imbalance and its level between the two groups was not significant. Additionally, the binocular balance within each group at different distances showed no significant difference. At 0.4 m, the proportions of patients with binocular balance levels 1–5 (contrast sensitivity) were 2.22, 6.67, 11.11, 4.44, and 6.67%, respectively; at 0.8 m, they were 4.44, 6.67, 11.11, 0.00, and 6.67%, respectively; and at 5.0 m, they were 2.22, 4.44, 4.44, 6.67, and 0.00%, respectively.

3.4. Contributing factors to binocular balance

3.4.1. Near distance (0.4m)

The SE of non-dominant eye (−1.14 ± 0.17D) for patients with binocular balance at 0.4 m significantly differs from that with binocular

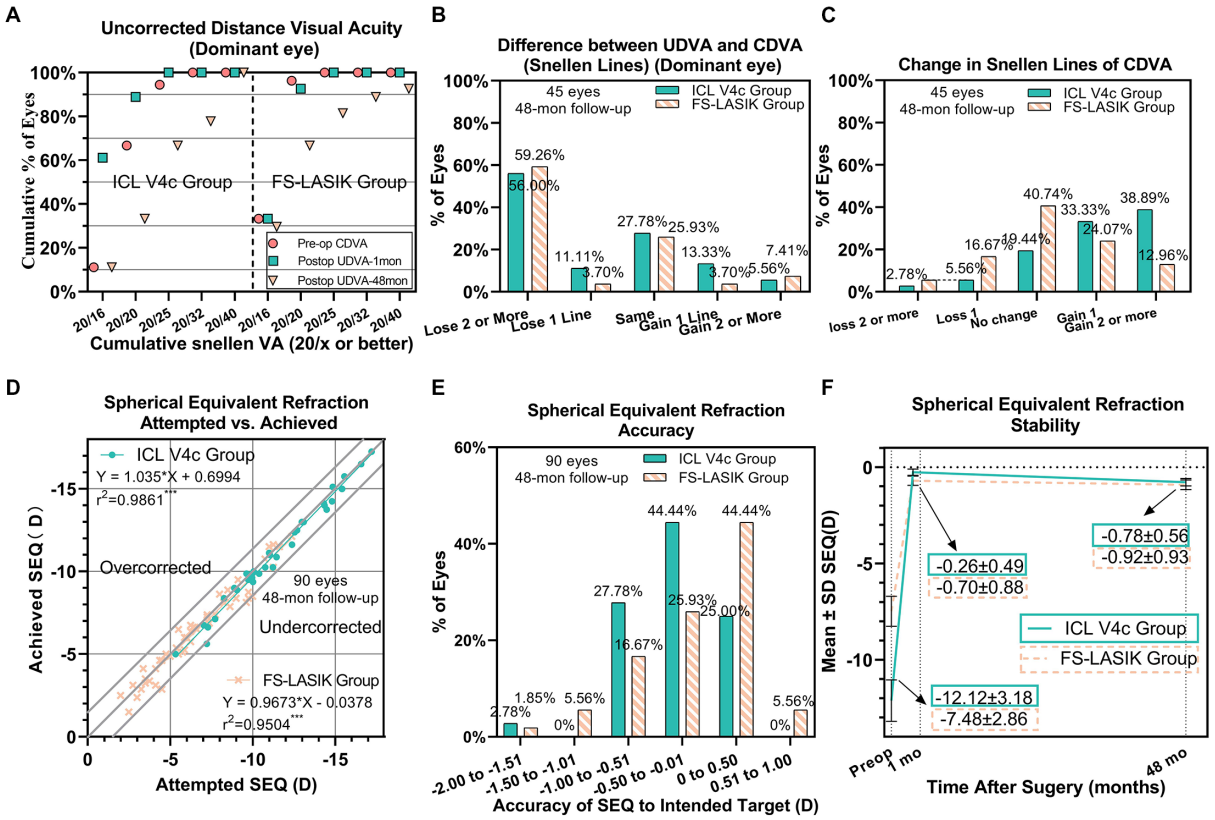

FIGURE 2
Clinical outcomes of 90 eyes with myopia and presbyopia at the last follow-up after Implantable collamer lens V4c implantation or femtosecond laser-assisted laser *in situ* keratomileusis. **(A)** Dominant eye: Postoperative uncorrected distance visual acuity (UDVA) vs. preoperative corrected distance visual acuity (CDVA); **(B)** Dominant eye: Difference between postoperative UDVA and preoperative CDVA; **(C)** Change in CDVA; **(D)** Attempted spherical equivalent refraction change versus the achieved spherical equivalent refraction change; **(E)** Distribution of postoperative spherical equivalent refraction accuracy; **(F)** Stability of spherical equivalent refraction up to 48 months. D = diopters; Postop = postoperative; Preop = preoperative; mo = month(s).

imbalance (−1.47 ± 0.13D) ($B = 6.617$, $p < 0.001$; Figure 4A). The degree of anisometropia between the non-dominant and dominant eyes did not differ between balanced and imbalanced patients ($B = -1.446$, $p = 0.145$). The binocular balance level was related to the monovision design and SE of the non-dominant eye at the last follow-up ($B = -27.289$, $p < 0.001$; $B = 28.386$, $p < 0.001$) (Figure 4B). The range of balance of the dominant eye may be related to the SE of the non-dominant eye ($B = 10.257$, $p = 0.027$) (Figure 4C), visual acuity at 0.4 m ($B = -3.172$, $p = 0.027$) (Figure 4D), and age ($B = -0.230$, $p = 0.030$) (Figure 4E).

3.4.2. Middle distance (0.8m)

There was a significant difference in preoperative ADD between the binocular balanced (0.90 ± 0.17D) and the imbalanced (1.05 ± 0.11D) patients at 0.8 m ($B = 2.72$, $p = 0.041$). Additionally, there was a significant difference in binocular visual acuity at 0.8 m between the binocular balanced patients (−0.01 ± 0.03) and the imbalanced (−0.02 ± 0.01D) at 0.8 m ($B = -27.077$, $p = 0.045$; Figure 5A) As shown in Figure 5B, The range of balance in the dominant eye might be correlated to the binocular visual acuity at 0.8 m of the non-dominant eye ($B = -5.086$, $p = 0.006$).

3.4.3. Far distance (5.0m)

There was a significant difference in SE of the non-dominant eye between the binocular balanced patients (−1.13 ± 0.33D) and the imbalanced (−1.42 ± 0.11D) at 5 m ($B = 30.524$, $p < 0.001$). Additionally, there was a significant difference in target SE of non-dominant eye between the binocular balanced patients (−0.78 ± 0.19D) and the imbalanced (−1.17 ± 0.13D) at 5.0 m ($B = -32.164$, $p < 0.001$; Figure 6A). As shown in Figure 6B, The range of balance in the non-dominant eye might be correlated to the visual acuity of the non-dominant eye at 5.0 m ($B = -13.89$, $p = 0.006$) and the real refraction of the dominant eye ($B = -4.375$, $p = 0.032$). The range of balance of the dominant eye may be correlated with age ($B = 0.386$, $p = 0.002$) and the visual acuity of the dominant eye at 5.0 m ($B = -2.291$, $p = 0.036$) (Figure 6C).

4. Discussion

This study elucidated the safety index of the two surgical procedures after 4 years postoperatively, which was 1.24 ± 0.27 and 1.04 ± 0.20, for the ICL V4c and FS-LASIK groups, respectively, while the efficacy index was 0.77 ± 0.29 and 0.66 ± 0.34, respectively. The efficacy index was lower owing to intentional undercorrection in the non-dominant eye than in conventional studies. However, considering good binocular visual acuity at near-to-far distances, monovision surgery using ICL V4c or FS-LASIK has good long-term safety and efficacy in myopic patients with presbyopia. With the increasing number of myopic patients and the aging of the population, the safety and efficacy of refractive surgery in people aged ≥40 years have received widespread attention (Levinger et al., 2013; Kamiya et al., 2017; Primavera et al.,

TABLE 2 The clinical parameters of the dominant eyes or non-dominant eyes before and after the implantable collamer lens V4c implantation or femtosecond laser-assisted laser *in situ* keratomileusis.

Characteristic	D-or nD-eye	Preoperative			1-mon follow-up			48-mon follow-up		
		ICL V4c Group	FS-LASIK Group	*p*	ICL V4c Group	FS-LASIK Group	*p*	ICL V4c Group	FS-LASIK Group	*P*
UDVA (Logmar)	D-eye	NA	NA	NA	−0.04 ± 0.07	**−0.02 ± 0.05***	0.506	0.12 ± 0.12▲	**0.07 ± 0.19***	0.501
	nD-eye				**0.03 ± 0.10**	**0.22 ± 0.18***	**<0.001**	**0.25 ± 0.17▲**	**0.44 ± 0.40*▲**	**0.018**
Refraction sphere (D)	D-eye	**−11.11 ± 3.07**	**−6.76 ± 2.36**	**<0.001**	**0.18 ± 0.34△**	**0.03 ± 0.22*△**	0.345	**−0.35 ± 0.39*△▲**	**−0.09 ± 0.70*△**	0.194
	nD-eye	**−11.97 ± 3.53**	**−7.52 ± 3.19**	**<0.001**	**−0.14 ± 0.41△**	**−1.23 ± 0.83*△**	**<0.001**	**−0.90 ± 0.59*△▲**	**−1.38 ± 0.73*△**	**0.016**
Refraction cylinder (D)	D-eye	−1.28 ± 1.04	−0.71 ± 0.53	**0.019**	**−0.44 ± 0.33△**	**−0.17 ± 0.31△**	**0.027**	**−0.39 ± 0.35△**	−0.40 ± 0.37	0.932
	nD-eye	−1.03 ± 1.07	−0.67 ± 0.51	0.130	−0.69 ± 0.72	**−0.24 ± 0.20△**	**<0.001**	**−0.49 ± 0.37△**	−0.32 ± 0.35	0.140
SE (D)	D-eye	**−11.75 ± 3.03**	**−7.12 ± 2.42**	**<0.001**	**−0.04 ± 0.29*△**	**−0.06 ± 0.25*△**	0.934	**−0.54 ± 0.39*△**	**−0.29 ± 0.66*△**	0.443
	nD-eye	**−12.49 ± 3.47**	**−7.85 ± 3.30**	**<0.001**	**−0.49 ± 0.57*△**	**−1.35 ± 0.83*△**	**<0.001**	**−1.15 ± 0.58*△▲**	**−1.54 ± 0.74*△**	**0.014**
CDVA (Logmar)	D-eye	**0.04 ± 0.08**	**−0.02 ± 0.05**	**0.008**	**−0.05 ± 0.06△**	−0.03 ± 0.05	0.252	**−0.06 ± 0.09△**	−0.04 ± 0.10	0.539
	nD-eye	**0.05 ± 0.11**	**−0.01 ± 0.07**	**0.018**	**−0.03 ± 0.07△**	−0.02 ± 0.07	0.740	**−0.01 ± 0.13△**	0 ± 0.11	0.763
ADD (D)		**0.64 ± 0.29**	**1.25 ± 0.67**	**0.001**	NA	NA	NA	**1.33 ± 0.55△**	**1.84 ± 0.78 △**	**0.021**
Safety indices	D-eye	NA	NA	NA	**1.27 ± 0.22**	**1.03 ± 0.08**	**<0.001**	**1.29 ± 0.29**	**1.06 ± 0.19**	**0.001**
	nD-eye				**1.23 ± 0.26**	**1.04 ± 0.08**	**<0.001**	**1.19 ± 0.24**	**1.01 ± 0.21**	**0.015**
Efficacy indices	D-eye	NA	NA	NA	**1.25 ± 0.24**	**1.01 ± 0.11***	**0.001**	**0.86 ± 0.29▲**	**0.88 ± 0.27*▲**	0.812
	nD-eye				**1.10 ± 0.33**	**0.64 ± 0.25***	**<0.001**	**0.68 ± 0.28▲**	**0.45 ± 0.25*▲**	**0.006**

ICL, implantable collamer lens; FS-LASIK, femtosecond laser-assisted laser in situ keratomileusis; D-eye, dominant eye; nD-eye, nondominant eye; UDVA, uncorrected distance visual acuity; ADD, presbyopic add power; SE, spherical equivalent; CDVA, corrected distance visual acuity. △ versus Preoperative, $p < 0.05$. ▲ versus the 1-month follow-up, $p < 0.05$. * dominant eye versus nondominant eye, $p < 0.05$. Values with statistical significance are shown in bold.

2020; Tañá-Rivero et al., 2020). The safety of ICL V4c implantation and FS-LASIK surgery in this population has been validated through comprehensive evaluations of multiple aspects, such as lens density (Ye et al., 2021) and monovision surgery for treating myopia combined with presbyopia (Kamiya et al., 2017; Takahashi et al., 2018; Ye et al., 2022). However, there has been little discussion on long-term effects. These results were similar to those after three years following monovision surgery using ICL V4c (1.22 ± 0.18 and 0.85 ± 0.29; Ye et al., 2022). Moreover, regarding biological parameters, ICL V4c implantation also exhibited long-term safety, with a similar decline in endothelial cell density to that reported in previous studies (Ye et al., 2021). The vault remained within a safe range (Gonvers et al., 2003).

Anisometropia between the dominant and non-dominant eyes caused by monovision may affect the visual function, which may affect their visual experience. A study has shown that anisometropia may lead to binocular imbalance and accommodative difficulties (Yang et al., 2017). This imbalance can cause the patients' vision to deteriorate at near or far distances, affecting visual comfort and quality. This study evaluated the balance of binocular vision and found that imbalances were common in this population at near, intermediate, and distant distances. Previous studies have shown that the binocular visual acuity of this population is often best at intermediate distances and that the dominant and non-dominant eyes have the largest overlap at this distance, making binocular vision at this distance have the greatest impact on binocular balance (Takahashi et al., 2018; Ye et al., 2022).

This study showed that at different distances, the balanced range of the dominant eye was related to the visual acuity or SE of the non-dominant eye and also showed a correlation with age at far and near distances. The correlation of visual acuity was that the closer the binocular visual acuity, the higher the balance range. The correlation between the dominant eye's balance range and the non-dominant eye's SE showed the opposite result. Thus, the higher the degree of under-correction of the non-dominant eye at near distances, the lower the degree of under-correction at far distances, and the higher the balance level of the dominant eye. This contrasts the extreme relationship between this parameter and eye balance. Previous studies have suggested that an increase in monocular blur may increase the stereo threshold at high spatial frequencies (Li et al., 2016) and that the increase in threshold may be related to suppression under binocular imbalance (Zheleznyak et al., 2015). An "adaptation phenomenon" in the binocular balance under monovision is speculated, which may increase binocular imbalance and the range of balance of the dominant eyes in the balanced eyes. This adaptation of the non-dominant eye after suppression indicates the potential feasibility of visual function training in this population.

People commonly experience binocular imbalance, with 65.9 and 62.89% experiencing low-and high-temporal-frequency stimuli, respectively (Xu et al., 2019). The proportion of binocular imbalance in this study at a 0.4 m distance was similar at 68.89%, while there was a certain degree of increase in the imbalance at intermediate and far distances (71.11 and 82.22%, respectively). Previous studies have demonstrated significant binocular balance and acuity differences between older individuals and those with myopia (Arani et al., 2019). It has been suggested that the binocular competition rate is lower in older individuals than in young people (Vera-Diaz et al., 2018), while binocular imbalance is more pronounced in myopic patients than in the emmetropic population. Therefore, this study's proportion of subjects with binocular imbalance may have been higher than that of age-matched individuals because of monovision. In simulated experiments in patients with anisometropia, visual acuity distribution at different distances from

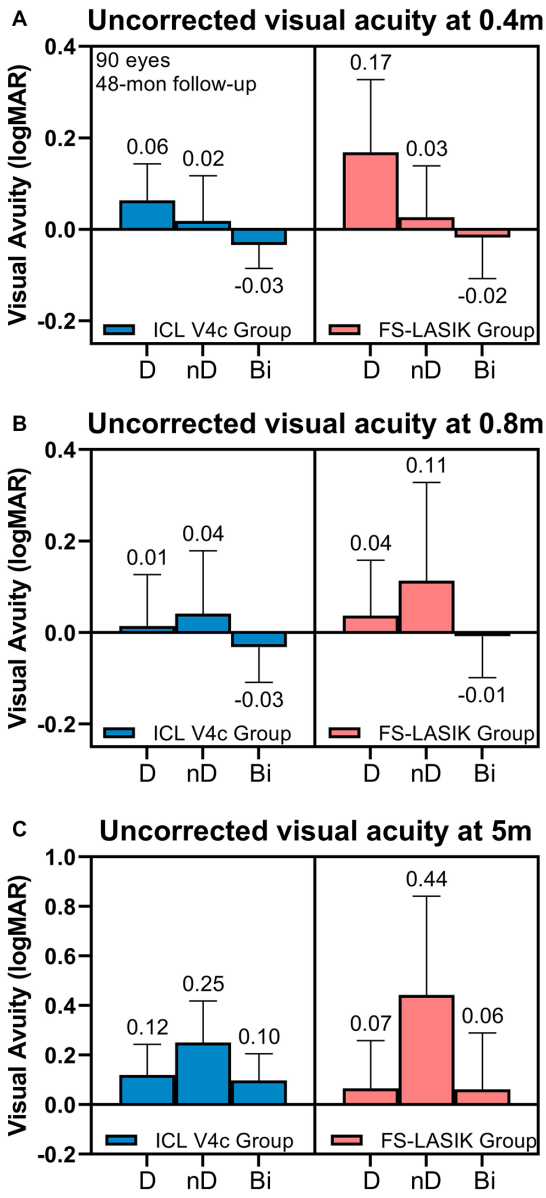

FIGURE 3
Uncorrected Visual Acuity at 0.4m **(A)**, 0.8m **(B)**, and 5.0m **(C)** at 48months after Implantable collamer lens V4c implantation or femtosecond laser-assisted laser *in situ* keratomileusis.

the dominant eye was an important factor affecting the contrast threshold performance (Zheleznyak et al., 2015). The increase in the imbalance proportion at intermediate and far distances may be related to changes in the contrast threshold or the gradual emergence of binocular imbalance with increasing testing time (Xu et al., 2019). Based on studies on neural rhythms, binocular imbalance may manifest as periodic changes in monocular dominance and dynamic fusion perception. Further research is necessary to determine whether these periodic changes are characteristic of monovision surgery. Treatment regimens that reduce suppression by promoting exposure to balanced binocular stimulation have improved visual acuity and stereo sensitivity (Kwon et al., 2014). Training in binocular balance stimulation after monocular design surgery may help further improve its efficacy.

Research conducted among myopic adolescents aged 6–18 years showed that an increase in binocular imbalance does not necessarily imply poorer SE or VA. Instead, an increase in anisometropia significantly correlated with an increase in binocular imbalance, and the dominant eye tended to have a more negative SE than the non-dominant eye (Tao et al., 2022). This study found that the balance of binocular vision at different distances was related to the refraction and visual acuity of both the dominant and non-dominant eyes. Unlike previous studies, this study showed no direct correlation between binocular balance and anisometropia. At a near distance of 0.4 m, the binocular balance was related to the SE of the non-dominant eye, while the balance threshold of the dominant eye depended on the non-dominant eye's worse visual acuity at a near distance. Therefore, the difference in results between the two studies at a near distance suggests that the balance vision of patients with myopia and presbyopia after monovision surgery is significantly related to the SE of the non-dominant eye under a monovision design compared with adolescents. A more negative SE in the non-dominant eye implies a more severe binocular imbalance. The more negative SE of the dominant eye (from the perspective of binocular balance) in adolescents may be related to the fact that the measurements were conducted at a near distance. Consequently, it suggests that binocular balance is not only a common and dynamic process (Xu et al., 2019) but is also closely related to the testing distance (Zheleznyak et al., 2015) and its corresponding accommodation.

This study had certain limitations. First, the preoperative binocular balance was not compared. However, with the advancement and optimization of detection methods for binocular balance, future studies can better evaluate the changes before and after monovision surgery. The short-term plasticity of visual perception training can also be added

TABLE 3 The biometric parameters before and after the implantable collamer lens V4c implantation or femtosecond laser-assisted laser *in situ* keratomileusis.

Parameters	Preoperative / 1-mon follow-up (Vault)			48-mon follow-up		
	ICL V4c Group	FS-LASIK Group	*P*	ICL V4c Group	FS-LASIK Group	*P*
ACD (mm)	**3.16 ± 0.35**	**2.98 ± 0.22**	**0.001**	**2.87 ± 0.34△**	**2.85 ± 0.21△**	0.728
ACV (μl)	180.89 ± 36.91	167.70 ± 26.46	0.177	**110.06 ± 24.82△**	**156.04 ± 26.98△**	**<0.001**
ACA (°)	36.55 ± 5.98	34.94 ± 5.13	0.083	**21.64 ± 4.39△**	**33.51 ± 4.87△**	**<0.001**
IOP (mmhg)	15.10 ± 2.31	16.05 ± 2.72	0.085	**16.13 ± 2.21△**	**11.36 ± 2.03△**	**<0.001**
AL (mm)	**28.69 ± 2.09**	**26.54 ± 1.33**	**<0.001**	**28.72 ± 2.04△**	**26.66 ± 1.37△**	**<0.001**
ECD (cell/mm^2)	3107.31 ± 585.84	NA	NA	**2557.89 ± 290.98△**	NA	NA
Vault (μm)	518.06 ± 196.13	NA	NA	**432.65 ± 208.03▲**	NA	NA

ACD, anterior chamber depth; ACV, anterior chamber volume; ACA, anterior chamber angle; IOP, intraocular pressure; ECD, endothelium cell density. △Versus preoperative, $p < 0.05$. ▲Versus the 1-month follow-up, $p < 0.05$. Values with statistical significance are shown in bold.

TABLE 4 Binocular imbalance in patients 48months after implantable collamer lens V4c implantation or femtosecond laser-assisted laser *in situ* keratomileusis.

Distance	Characteristic	ICL V4c Group	FS-LASIK Group	*p*
0.4 m	Balanced/Imbalanced	8/10	6/21	0.595
	Level of balance	1.50 ± 1.95	0.67 ± 1.36	0.454
	Range of balance (D-eye)	3.06 ± 1.63	2.93 ± 1.27	0.721
	Range of balance (nD-eye)	2.44 ± 1.76	2.93 ± 1.17	0.078
0.8 m	Balanced/Imbalanced	7/11	6/21	0.760
	Level of balance	1.11 ± 1.75	0.67 ± 1.36	0.665
	Range of balance (D-eye)	**2.67 ± 1.61***	2.81 ± 1.27	0.085
	Range of balance (nD-eye)	**1.89 ± 2.00***	**2.96 ± 1.19**	**0.025**
5.0 m	Balanced/Imbalanced	5/13	3/24	0.296
	Level of balance	0.89 ± 1.53	0.26 ± 0.86	0.233
	Range of balance (D-eye)	1.50 ± 1.69	1.37 ± 1.84	0.891
	Range of balance (nD-eye)	1.00 ± 1.33	0.74 ± 1.53	0.687

*Dominant eye versus nondominant eye, $p < 0.05$. Values with statistical significance are shown in bold.

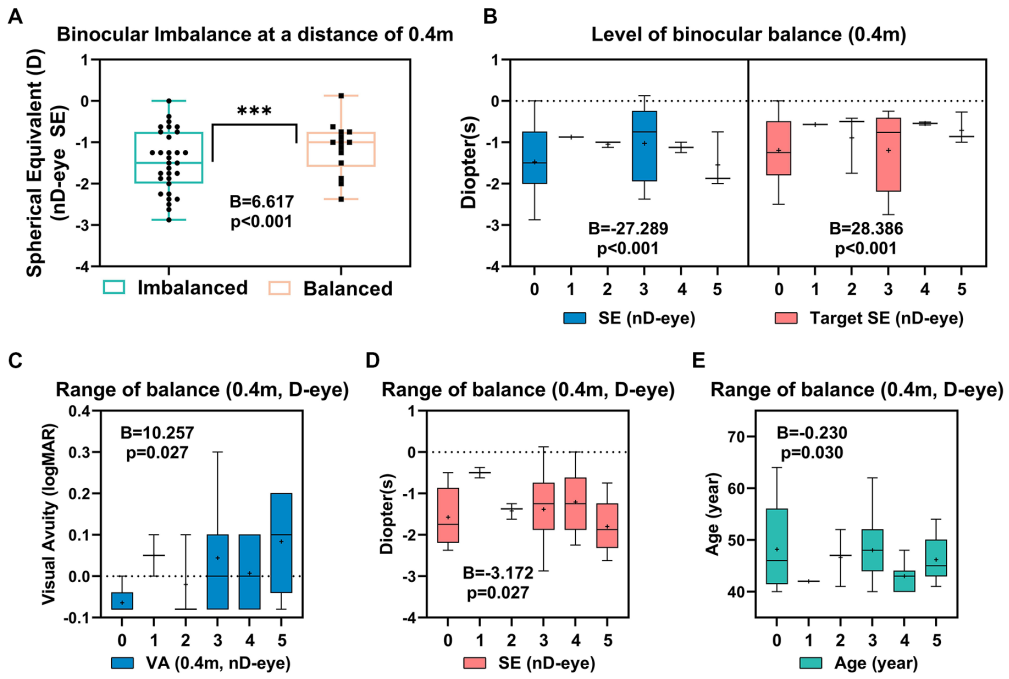

FIGURE 4
Correlated parameters of binocular imbalance **(A)**, level of binocular balance **(B)** and the range of balance **(C–E)** at 0.4m.

to increase data variability before and after training, which can provide valuable clinical support. Second, tests for stereo vision function were not applied in this study, and future research is needed as binocular imbalance and stereo vision are two different aspects of binocular interactions. Previous studies have shown that subjects with good binocular balance tend to have better stereo vision. Therefore, studying different aspects of binocular relationships, such as stereo vision, in this population will contribute to further evaluating the clinical effects of monovision surgery. Third, the binocular imbalance was not measured during different working hours, and transient binocular imbalance is likely a temporary physiological phenomenon (Xu et al., 2019). As time progresses, older adults may experience longer balance times and lower alternation probabilities than younger people (Arani et al., 2019; Wang et al., 2021). The binocular imbalance under different work lengths after monovision surgery may vary. Further research in this area will help assess functional defects, such as reading disorders, under prolonged binocular imbalance conditions. Fourth, this study had a relatively small sample size, and larger sample studies are required to evaluate binocular balance function. The proportions of two subpopulation were different, further researches are warranted including comparable subgroup cases.

In conclusion, the ICL V4c implantation and FS-LASIK monovision treatment demonstrated good long-term safety and

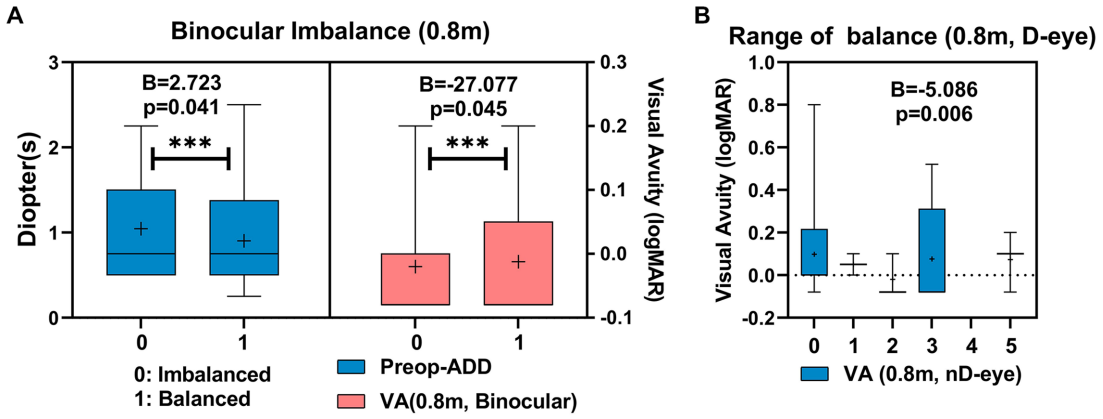

FIGURE 5
Correlated parameters of binocular imbalance **(A)**, and the range of balance **(B)** at 0.8m.

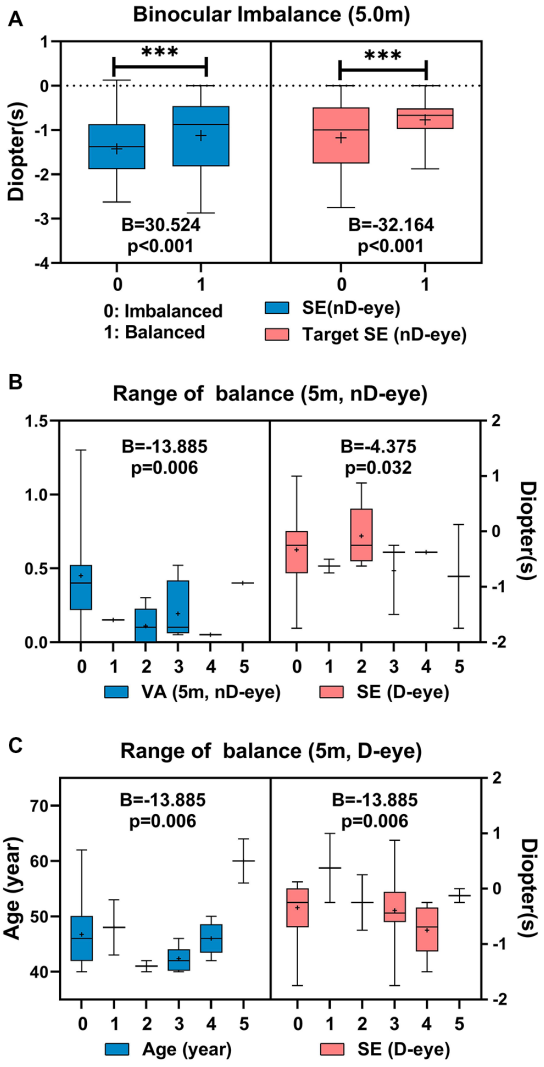

FIGURE 6
Correlated parameters of binocular imbalance **(A)**, and the range of balance **(B,C)** at 5m.

binocular visual acuity at various distances. The imbalanced patients' vision is primarily related to the age-related presbyopia and anisometropia progression caused by the monovision design. High levels of anisometropia may required careful consideration from the aspect of biocular balance.

Data availability statement

The raw data supporting the conclusions of this article will be made available by the authors, without undue reservation.

Ethics statement

This study followed the tenets of the Declaration of Helsinki and was approved by the Ethics Committee of Fudan University Eye and ENT Hospital Review Board (Shanghai, China; ID: 2013015, date: 2013/1/5). Informed consent was obtained from all participants. The patients/participants provided their written informed consent to participate in this study.

Author contributions

YY, ZZ, JZ, and XZ: study concept and design. YY, ZZ, LN, WS, XW, and JZ: data collection. YY: data analysis and interpretation. YY and JZ: drafting of the manuscript. LY, JZ, and XZ: critical revision of the manuscript. XZ: supervision. All authors read and approved the final manuscript.

Funding

This study was supported by National Natural Science Foundation of China (Grant no. 82271119), Shanghai Rising-Star Program (23QA1401000), Healthy Young Talents Project of Shanghai Municipal Health Commission (2022YQ015), Project of Shanghai Science and

Technology (Grant nos. 20410710100 and 21Y11909800), and Project of Shanghai Xuhui District Science and Technology (2020-015).

Acknowledgments

The authors would like to thank Editage (www.editage.cn) for English language editing.

Conflict of interest

The authors declare that the research was conducted in the absence of any commercial or financial relationships that could be construed as a potential conflict of interest.

Publisher's note

Supplementary material

The Supplementary material for this article can be found online at: https://www.frontiersin.org/articles/10.3389/fnins.2023.1204792/full#supplementary-material

References

Arani, E., van Ee, R., and van Wezel, R. (2019). Age-dependency in binocular rivalry is reflected by exclusive percepts, not mixed percepts. *Sci. Rep. UK* 9:55890. doi: 10.1038/s41598-019-55890-5

Cha, O., and Blake, R. (2019). Evidence for neural rhythms embedded within binocular rivalry. *Proc. Natl. Acad. Sci.* 116, 14811–14812. doi: 10.1073/pnas.1905174116

Chen, X., Miao, H., Naidu, R. K., Wang, X., and Zhou, X. (2016). Comparison of early changes in and factors affecting vault following posterior chamber phakic implantable collamer lens implantation without and with a central hole (ICL V4 and ICL V4c). *BMC Ophthalmol.* 16:161. doi: 10.1186/s12886-016-0336-8

Dunn, S., and Jones, M. (2020). Binocular rivalry dynamics associated with high levels of self-reported autistic traits suggest an imbalance of cortical excitation and inhibition. *Behav. Brain Res.* 388:112603. doi: 10.1016/j.bbr.2020.112603

Fu, D., Zeng, L., Zhao, J., Miao, H., Yu, Z., and Zhou, X. (2018). Safety and satisfaction of myopic small-incision lenticule extraction combined with monovision. *BMC Ophthalmol.* 18:131. doi: 10.1186/s12886-018-0794-2

Gonvers, M., Bornet, C., and Othenin-Girard, P. (2003). Implantable contact lens for moderate to high myopia. *J Cataract Refract Surg* 29, 918–924. doi: 10.1016/S0886-3350(03)00065-8

Han, T., Xu, Y., Han, X., Zeng, L., Shang, J., Chen, X., et al. (2019). Three-year outcomes of small incision lenticule extraction (SMILE) and femtosecond laser-assisted laser in situ keratomileusis (FS-LASIK) for myopia and myopic astigmatism. *Brit. J. Ophthalmol.* 103, 565–568. doi: 10.1136/bjophthalmol-2018-312140

Holden, B. A., Fricke, T. R., Wilson, D. A., Jong, M., Naidoo, K. S., Sankaridurg, P., et al. (2016). Global prevalence of myopia and high myopia and temporal trends from 2000 through 2050. *Ophthalmology* 123, 1036–1042. doi: 10.1016/j.ophtha.2016.01.006

Jain, S., Arora, I., and Azar, D. T. (1996). Success of monovision in presbyopes: review of the literature and potential applications to refractive surgery. *Surv. Ophthalmol.* 40, 491–499. doi: 10.1016/S0039-6257(96)82015-7

Joao, C. A. R., Scanferla, L., and Jansonius, N. M. (2021). Binocular interactions in Glaucoma patients with nonoverlapping visual field defects: contrast summation, rivalry, and phase combination. *Invest. Ophth. Vis. Sci.* 62:9. doi: 10.1167/iovs.62.12.9

Kamiya, K., Takahashi, M., Takahashi, N., Shoji, N., and Shimizu, K. (2017). Monovision by implantation of posterior chamber Phakic intraocular Lens with a central hole (hole ICL) for early presbyopia. *Sci. Rep. UK* 7:11539. doi: 10.1038/s41598-017-11539-9

Kwon, M., Lu, Z. L., Miller, A., Kazlas, M., Hunter, D. G., and Bex, P. J. (2014). Assessing binocular interaction in amblyopia and its clinical feasibility. *PLoS One* 9:e100156. doi: 10.1371/journal.pone.0100156

Levinger, E., Trivizki, O., Pokroy, R., Levartovsky, S., Sholohov, G., and Levinger, S. (2013). Monovision surgery in myopic Presbyopes: visual function and satisfaction. *Optometry Vision Sci.* 90, 1092–1097. doi: 10.1097/OPX.0000000000000002

Li, R. W., So, K., Wu, T. H., Craven, A. P., Tran, T. T., Gustafson, K. M., et al. (2016). Monocular blur alters the tuning characteristics of stereopsis for spatial frequency and size. *Roy. Soc. Open Sci.* 3:160273. doi: 10.1098/rsos.160273

Luft, N., Siedlecki, J., Sekundo, W., Wertheimer, C., Kreutzer, T. C., Mayer, W. J., et al. (2018). Small incision lenticule extraction (SMILE) monovision for presbyopia correction. *Eur. J. Ophthalmol.* 28, 287–293. doi: 10.5301/ejo.5001069

Mao, Y., Min, S. H., Chen, S., Gong, L., Chen, H., Hess, R. F., et al. (2020). Binocular imbalance in amblyopia depends on spatial frequency in binocular combination. *Invest. Ophth. Vis. Sci.* 61:7. doi: 10.1167/iovs.61.8.7

Marella, B. L., Conway, M. L., Suttle, C., and Bharadwaj, S. R. (2021). Contrast rivalry paradigm reveals suppression of monocular input in keratoconus. *Invest. Ophth. Vis. Sci.* 62:15. doi: 10.1167/iovs.62.2.12

Modjtahedi, B. S., Abbott, R. L., Fong, D. S., Lum, F., Tan, D., Ang, M., et al. (2021). Reducing the global burden of myopia by delaying the onset of myopia and reducing myopic progression in children. *Ophthalmology* 128, 816–826. doi: 10.1016/j.ophtha.2020.10.040

Naidoo, K. S., Fricke, T. R., Frick, K. D., Jong, M., Naduvilath, T. J., Resnikoff, S., et al. (2019). Potential lost productivity resulting from the global burden of myopia. *Ophthalmology* 126, 338–346. doi: 10.1016/j.ophtha.2018.10.029

Primavera, L., Canto-Cerdan, M., Alio, J. L., and Alio Del Barrio, J. L. (2020). Influence of age on small incision lenticule extraction outcomes. *Brit. J. Ophthalmol.* 106, 341–348. doi: 10.1136/bjophthalmol-2020-316865

Takahashi, M., Kamiya, K., Shoji, N., Kato, S., Igarashi, A., and Shimizu, K. (2018). Intentional Undercorrection by implantation of posterior chamber Phakic intraocular Lens with a central hole (hole ICL) for early presbyopia. *Biomed. Res. Int.* 2018, 1–5. doi: 10.1155/2018/6158520

Tañá-Rivero, P., Pastor-Pascual, F., Crespo, M., Rodríguez-Prats, J. L., Muñoz-Tomás, J. J., and Montés-Micó, R. (2020). Posterior-chamber Phakic intraocular Lens implantation in patients over 40 years of age. *J. Ophthalmol.* 2020, 1–8. doi: 10.1155/2020/7457902

Tao, Z., Deng, H., Chu, H., Wiederhold, M., Wiederhold, B. K., Zhong, H., et al. (2022). Exploring the relationship between binocular imbalance and myopia: Refraction with a virtual reality platform. *Cyberpsychol. Behav. Soc. Netw.* 25, 672–677. doi: 10.1089/cyber.2022.0162

Vera-Diaz, F. A., Bex, P. J., Ferreira, A., and Kosovicheva, A. (2018). Binocular temporal visual processing in myopia. *J. Vis.* 18:17. doi: 10.1167/18.11.17

Wang, X., Baldwin, A. S., and Hess, R. F. (2021). Balanced binocular inputs support superior stereopsis. *Invest. Ophth. Vis. Sci.* 62:10. doi: 10.1167/iovs.62.12.10

Webber, A. L., Schmid, K. L., Baldwin, A. S., and Hess, R. F. (2020). Suppression rather than visual acuity loss limits Stereoacuity in amblyopia. *Invest. Ophthalmol. Vis. Sci.* 61:50. doi: 10.1167/iovs.61.6.50

Wu, P., Huang, H., Yu, H., Fang, P., and Chen, C. (2016). Epidemiology of myopia. *Asia-Pacific J. Ophthalmol.* 5, 386–393. doi: 10.1097/APO.0000000000000236

Xu, L., Huang, M., Lan, J., Huang, W., Wang, X., Zhang, G., et al. (2019). Assessment of binocular imbalance with an augmented virtual reality platform in a Normal population. *Cyberpsychol. Behav. Soc. Netw.* 22, 127–131. doi: 10.1089/cyber.2019.0020

Yang, C., Li, X., Zhang, G., Lan, J., Zhang, Y., Chu, H., et al. (2017). Comparison of perceptual eye positions among patients with different degrees of anisometropia. *Medicine* 96:e8119. doi: 10.1097/MD.0000000000008119

Ye, Y., Aruma, A., Zhao, W., Lu, Z. L., Zhou, X., and Zhao, J. (2023). A novel quick contrast sensitivity function test in Chinese adults with myopia and its related parameters. *Graefes Arch. Clin. Exp. Ophthalmol.* Advance online publication. doi: 10.1007/s00417-023-06010-7

Ye, Y., Zhao, J., Niu, L., Shi, W., Wang, X., and Zhou, X. (2021). Long-term evaluation of anterior lens density after implantable collamer lens V4c implantation in patients with myopia over 40 years old. *Brit. J. Ophthalmol.* 106, 1508–1513. doi: 10.1136/bjophthalmol-2021-319205

Ye, Y., Zhao, J., Zhang, Z., Niu, L., Shi, W., Wang, X., et al. (2022). Long-term follow-up for monovision surgery by implantable collamer Lens V4c implantation for myopia correction in early presbyopia. *Graefe's Arch. Clin. Exp. Ophthalmol.* 260, 2763–2771. doi: 10.1007/s00417-021-05545-x

Zheleznyak, L., Alarcon, A., Dieter, K. C., Tadin, D., and Yoon, G. (2015). The role of sensory ocular dominance on through-focus visual performance in monovision presbyopia corrections. *J. Vision.* 15:17. doi: 10.1167/15.6.17

frontiers | Frontiers in Neuroscience

TYPE Original Research
PUBLISHED 12 June 2023
DOI 10.3389/fnins.2023.1207945

OPEN ACCESS

EDITED BY
Wensi Tao,
University of Miami Health System,
United States

REVIEWED BY
Bin Zhang,
Nova Southeastern University, United States
Chang-Bing Huang,
Chinese Academy of Sciences (CAS), China

*CORRESPONDENCE
E. Song
✉ songe@suda.edu.cn

RECEIVED 18 April 2023
ACCEPTED 15 May 2023
PUBLISHED 12 June 2023

CITATION
Wang Y, Zheng F, Zhou F and Song E (2023) Assessment of precision and reliability of a novel computerized heterophoria test. *Front. Neurosci.* 17:1207945. doi: 10.3389/fnins.2023.1207945

Assessment of precision and reliability of a novel computerized heterophoria test

Yuwen Wang[1,2], Fuhao Zheng[2], Fengchao Zhou[2] and E. Song[3]*

[1]Department of Ophthalmology, the Second Affiliated Hospital of Soochow University, Suzhou, Jiangsu, China, [2]Eye Hospital and School of Ophthalmology and Optometry, Wenzhou Medical University, Wenzhou, Zhejiang, China, [3]Department of Ophthalmology, Lixiang Eye Hospital of Soochow University, Suzhou, Jiangsu, China

Purpose: To assess the precision and reliability of a novel computerized heterophoria test (CHT).

Methods: One hundred and three subjects aged 20 to 48 (27.37±5.15) were recruited from Wenzhou Medical University. All subjects with corrected spectacles were examined with CHT and a prism-neutralized objective cover test (POCT) in a randomized order. They were then re-examined with CHT within 1week. Their heterophoria was measured at three different distances (3m, 0.77m and 0.4m); the average was recorded after three consecutive measurements. Inter-examiner repeatability, intra-examiner repeatability of CHT and agreement between CHT and POCT were evaluated.

Results: There was no significant difference among repeated measurements using CHT (all $p>0.05$). The difference between POCT and CHT was statistically significant at three distances (all $p<0.001$). However, the mean absolute difference was 1.20△, 1.93△, and 2.41△, all of which were significantly smaller than the permissible range of error (4△) at three different distances (all $p<0.001$).

Conclusion: The CHT demonstrated excellent inter- and intra-examiner repeatability, as well as good correlation with POCT. The differences between CHT and POCT were within the permissible range of error, indicating that CHT could provide a precise and reliable measurement for clinical applications.

KEYWORDS

heterophoria, repeatability, reliability, agreement, cover test, heterophoria method

Introduction

Visual fatigue is a global health concern, with a high prevalence among younger populations and university students worldwide. Studies have reported that 12.4–32.2% of individuals below 18 years of age (Ip et al., 2006; Tiwari, 2013) and 46–71% of university students suffer from visual fatigue (Han et al., 2013; Hashemi et al., 2019). Binocular vision anomaly has been identified as a leading cause of visual fatigue (Scheiman and Wick, 2014), and studies have suggested a correlation between binocular vision anomaly and visual fatigue (Garcia-Munoz et al., 2014; Sheppard and Wolffsohn, 2018; Zheng et al., 2021). Measuring heterophoria is crucial in evaluating binocular vision anomaly, as phoria at near and far distances can assist in the differential diagnosis of various types of binocular vision anomaly (Scheiman and Wick, 2014).

Many individuals experience visual fatigue due to prolonged use of digital devices, such as computers, for reading and writing purposes (Carmichael, 1947; Argiles et al., 2016). Some studies have suggested that the viewing distance during near work may vary depending on the nature of different tasks (Eastwood-Sutherland and Gale, 2011; Argiles et al., 2016). For example, a study that employed an ultrasound sensor device found that the viewing distances for game, text completion, and web search tasks were approximately 54.5 cm, which was shorter than that of a video task (62.3 cm) (Argiles et al., 2016). Similarly, the viewing distances for reading and writing tasks can also differ depending on the task and age, ranging from 25 cm to 40 cm (Yeo et al., 2013; Boccardo, 2021). Therefore, assessing heterophoria at different distances can provide valuable insights into the binocular vision anomalies of patients.

Several methods have been utilized to evaluate heterophoria, including the prism-neutralized objective cover test (POCT), the modified Thorington test (TH), and the Maddox rod test (MR). POCT is often regarded as a reliable test (Rainey et al., 1998a,b; Johns et al., 2004). However, its accuracy may be influenced by the examiner's experience, which introduces an external source of variance (Anderson et al., 2010; Hrynchak et al., 2010). TH is a popular method due to its simplicity (Schroeder et al., 1996; Cebrian et al., 2014). Nevertheless, the range of heterophoria and the measuring distance are limited by the length of the testing card (Cebrian et al., 2014). While MR allows for the measurement of heterophoria at any distance, its reliability and repeatability have been found to be inadequate (Rainey et al., 1998a,b; Cebrian et al., 2014).

To overcome the disadvantages of TH and MR, we developed the Computerized Heterophoria Test (CHT), which is based on the principle of TH and incorporates the advantages of MR. Heterophoria was measured by using Maddox rod to separate visual fields of two eyes and to scale the amplitude of heterophoria in the principle of TH. The goal of the study was to evaluate the reliability of CHT at different distances and its agreement with POCT, which is one of most popular tests for measuring heterophoria.

Methods

Subjects

The study recruited a total of 103 subjects (26 males and 77 females) from Wenzhou Medical University. All subjects underwent a comprehensive ophthalmic examination. Exclusion criteria included the history of eye surgery, trauma, strabismus, amblyopia, or any physical or mental impairment that could affect the test results. Subjects' refractive error ranged from +1.00 D to −6.00 D, astigmatism was less than −1.00 D, anisometropia was less than 1.00 D, and the best-corrected visual acuity was not worse than 20/20. The study adhered to the tenets of the Declaration of Helsinki and was approved by the Research Ethics Committee at Eye Hospital of Wenzhou Medical University. Each subject provided written informed consent.

Test methods

Heterophoria at three different distances were quantified using the CHT and POCT. Three distances were chosen based on clinical practice: 3 m, 0.77 m, and 0.40 m. The distance of 0.77 m (1.3D) represents an intermediate distance, as calculated by the average of the diopter of the distance (10 m, 0.1D) and near (0.4 m, 2.5D) based on Shibata's study (Shibata et al., 2011). Heterophoria was performed in two sessions, with an interval of less than 1 week between sessions.

Computerized heterophoria test

Equipment

The CHT was performed by a program which was written in MATLAB (MathWorks, Natick, MA) with PsychToolBox extensions (Kleiner et al., 2007). Stimuli were displayed on a 27-inch screen (ROG PG278QR, ASUS, Taiwan, China). The display had a spatial resolution of 2,560 × 1,440 pixels and a refresh rate of 60 Hz. An examinational spectacle with a white Maddox rod on right eye was used for examination (shown in Figure 1A).

Stimulus

In the visual test, a red stationary circle was displayed at the center of the screen. The diameter of the circle varied depending on the distance being measured, with a diameter of 15.15 mm at 3 m, and a diameter of 11.65 mm at 0.77 m and 0.40 m. A white horizontal line, 0.47 mm in width, was situated under the red circle. A white circle with the same size as the red one, was movable by the input of the mouse from the subjects.

Test procedure

Subjects viewed the display binocularly with their best corrections in a dim room. The spectacle for examination was worn throughout the entire measurement. Subjects were shown a red vertical line on the right eye, because through the Maddox rod (on the right eye of the glass in Figure 1A), a red fixed circle would become a red vertical line. Subjects were instructed to move the white circle to the cross point of the red vertical line and the white horizontal line (shown in Figure 1B), and to subsequently respond with the click using the mouse. After the click, the response would be recorded and the white point would move elsewhere randomly so that the positional bias could be removed. Subjects were then instructed to find the cross point and click again. The test was performed three times and the average was transformed into prism diopter and was outputted in the forms of the mean and standard deviation. The tests at distance of 3 m, 0.77 m and 0.40 m were performed in order. During the 0.40-meter test, subjects were asked to keep the sentence above clear to keep accommodation stable.

Prism-neutralized objective cover test (POCT)

Equipment

A prism bar with 2$^{\triangle}$ increment from 0$^{\triangle}$ to 20$^{\triangle}$ and 5$^{\triangle}$ increment from 25$^{\triangle}$ to 40$^{\triangle}$ was used in measurement.

Stimulus

The fixating targets used in the study were 20/30 letters, with their size determined by the respective distance. However, at distances of 0.77 m and 0.40 m, the same letters were used as the differences in size were negligible (less than 1 mm).

FIGURE 1
(A) An examinational spectacle with a horizontal Maddox rod on the right eye; **(B)** A schematic diagram of CHT. Subjects were asked to move the white point with the mouse to click the cross of red vertical line and white horizontal line. At 0.40-meter measurement, subjects were asked to keep the sentence clear during the test so that their accommodation would be stable.

Test procedure

Subjects were examined with corrected refractive errors, and they were told to keep the target letter clear. A prism bar was held no further than 1 cm from the right eye while the alternate cover test was performed. The test procedure followed that described by Johns et al. (2004), and the endpoint was determined as the midpoint of the first neutral and reversal points. Subjects repeated the test three times and the mean of their results was recorded as their final heterophoria value.

Study design

In light of the study by Bland and Altman (Martin Bland and Altman, 1986), we thought the best way to assess the repeatability of an instrument was to take several measurements in a series of subjects. In the first part of the study, the precision of the CHT was determined by inter- and intra-examiner repeatability. The first session was designed to determine inter-examiner repeatability, which refers to the reliability (agreement) of measurements between two different examiners. Three valid CHT tests were performed and considered independent since the white point was moved randomly. The time required to acquire three measurements was approximately 1 min. In the second session, intra-examiner repeatability was evaluated, which assesses the reliability of measurements between two sessions by the same examiner. The time interval between these two sessions varied from two to 7 days.

During the second part of the study, the agreement between the CHT and POCT was analyzed. Both tests were performed for each subject in the first session, and the order was randomized. CHT was administered by two novice optometrists, while POCT was conducted by an experienced optometrist who had more than 5 years of clinical experience. In the second session, all the examiners were blinded to the previous test results.

Statistical analysis

All data were analyzed using the SPSS for Windows software (version 22.0, SPSS, Inc.). A repeated-measures analysis of variance (ANOVA) with two factors (examiner and session) was conducted to examine the overall effects. $p < 0.05$ means statistical significance.

The repeatability of CHT between two examiners and two sessions, and the agreement between CHT and POCT were determined using the Bland–Altman method (Martin Bland and Altman, 1986; Zadnik et al., 1992). Comparison between CHT and POCT was analyzed with paired Student *t* tests. The variables used to evaluate were the mean difference (MD), the standard deviation of difference (SD), limits of agreement between two tests, the coefficient of repeatability (COR = ±1.96*SD), and Spearman correlation ratios between two tests.

Romano and von Noorden reported that the smallest eye movement detectable in a cover test is $2^{\triangle}$ (Romano and Von Noorden, 1971). In clinical practice, Rainey suggested that a difference of $\pm 4^{\triangle}$ or less between the 95% limits of agreement would be clinically acceptable (Schroeder et al., 1996). Therefore, a $\pm 4^{\triangle}$ difference should be considered as the standard for evaluating clinical agreement. A one-tailed Student t-test was used to compare the absolute difference between POCT and CHT and $4^{\triangle}$. $p < 0.05$ means statistical significance.

Results

A total of 103 subjects aged 20 to 48 (mean, 27.37 years; SD, 5.15 years) were enrolled in the study. The mean (SD) of spherical equivalent refractive errors for subjects were −3.47 (1.48) D.

Repeatability of CHT

The heterophoria measurements obtained by two examiners on two different days using the CHT did not show any statistical significance at three different distances. The results of the repeated-measures analysis of variance are presented in Table 1, and the heterophoria measurements were not significantly different between the two examiners at three different distances ($p > 0.05$). Moreover, there was no statistically significant difference in heterophoria measurements between the two sessions ($p > 0.05$), and the interactions between examiners and sessions were not significant ($p > 0.05$).

Inter- and intra-examiner repeatability coefficients for the different distance tests as well as Bland–Altman plots are shown in Figures 2, 3, respectively. The MD (COR) of inter-examiner repeatability were $-0.04^{\triangle}$ ($\pm 0.55^{\triangle}$) at 3 m, $-0.01^{\triangle}$ ($\pm 1.02^{\triangle}$) at 0.77 m, and $-0.08^{\triangle}$ ($\pm 1.21^{\triangle}$) at 0.40 m. The MD (COR) of intra-examiner repeatability were −0.05 ($\pm 1.83^{\triangle}$) at 3 m, −0.10 ($\pm 2.19^{\triangle}$) at 0.77 m, −0.03 ($\pm 3.04^{\triangle}$) at 0.40 m. The MD were smaller than $2^{\triangle}$ and COR was smaller than $4^{\triangle}$, indicating that the results were within a clinically acceptable range.

Agreement between CHT and POCT

The measurements of heterophoria using CHT and POCT showed a significant difference, but the difference was within a clinically acceptable range. Table 2 displays the description and agreement of heterophoria measurements by CHT and POCT, and Figure 4 shows the Bland–Altman plots. The differences between POCT and CHT at three different measurements were found to be significantly different ($p < 0.001$). However, there was a large correlation between CHT and POCT at 3 m ($r = 0.826$, $p < 0.001$), 0.77 m ($r = 0.823$, $p < 0.001$), and 0.40 m ($r = 0.855$, $p < 0.001$), as shown in Figure 5. Meanwhile, at 3 m, all differences between CHT and POCT were within ±4 △. At 0.77 m, 87 of 103 (84.47%) differences were within ±4△. At 0.40 m, 80 of 103 (77.67%) differences were within ±4△. The absolute difference between POCT and CHT was found to be smaller than 4△ at three different distances ($p < 0.001$). Additionally, the absolute difference between POCT and CHT was smaller than 2△ at 3 m ($t = -8.52$, $p < 0.001$).

TABLE 1 Statistic description of repeated measurements of CHT, *n*=103.

Test distance	3m	0.77m	0.40m
E1 S1	−0.47(−2.73, 0.02)	−1.23(−4.90, −0.12)	−3.07(−7.71, −0.18)
E2 S1	−0.42(−2.67, 0.04)	−1.37(−4.79, −0.01)	−2.74(−8.71, −0.21)
E1 S2	−0.95(−2.61, 0.05)	−1.36(−4.64, −0.05)	−3.30(−8.19, −0.17)
E2 S2	−0.82(−2.67, 0.03)	−1.12(−4.96, 0.00)	−3.28(−7.88, −0.09)
Examiner	$F = 1.974$, $p = 0.163$	$F = 0.044$, $p = 0.835$	$F = 1.890$, $p = 0.172$
Session	$F = 0.312$, $p = 0.577$	$F = 0.786$, $p = 0.377$	$F = 0.029$, $p = 0.866$
Examiner* Sessions	$F = 1.476$, $p = 0.227$	$F = 1.009$, $p = 0.317$	$F = 0.317$, $p = 0.575$

E1 means examiner 1; E2 means examiner 2; S1 means session 1; S2 means session 2; Examiner means repeated-measures analysis of variance based on the factor of examiner; Session means repeated-measures analysis of variance based on the factor of sessions; Examiner*Sessions means repeated-measures analysis of variance based on the interaction factor of the examiner and the session. The data are presented as medians and quartiles.

Discussion

In this study, we developed and validated the CHT by conducting repeated measurements with two different examiners across two different sessions. Our results demonstrate that the CHT has excellent inter- and intra-examiner repeatability. We then analyzed its repeatability and agreement with POCT. There was a strong correlation between the two methods, and the absolute difference between them was within a clinically acceptable range. Thus, the CHT could be considered as interchangeable with POCT. While POCT is generally considered reliable, its accuracy depends heavily on the experience of the examiner. In contrast, CHT demonstrated good reliability even with novice examiners. Additionally, CHT is a more convenient and efficient method of measuring heterophoria, which making it particularly suitable for use in settings such as outpatient triage and community screenings. Given these advantages, CHT has significant potential for improving the accuracy and efficiency of heterophoria measurements in clinical and community settings.

Repeatability of CHT

The results presented in Table 1 indicate excellent repeatability of the CHT test, with no significant differences observed between examiners or sessions. Additionally, the COR values were all less than 4△, which is an acceptable range for clinical measurements (Schroeder et al., 1996). This is due to the fact that the design of the CHT is based on TH, which is known for its high reliability in measurement (Cebrian et al., 2014). TH and POCT has been widely used for

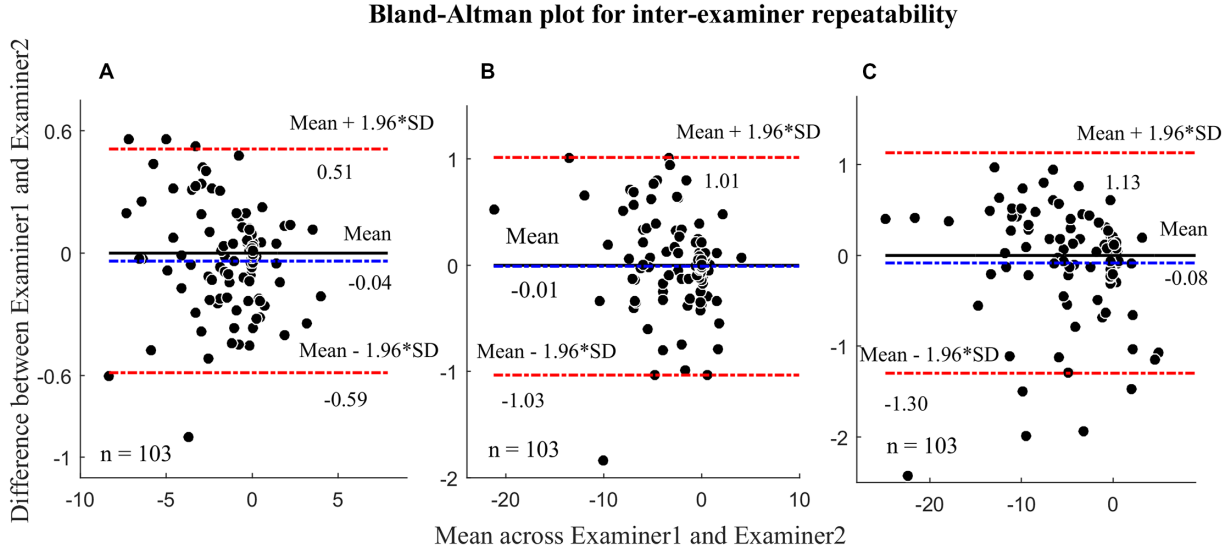

FIGURE 2
Bland-Altman plots illustrating the inter-examiner repeatability. **(A)** Heterophoria measured at 3 meters; **(B)** Heterophoria measured at 0.77 meters; **(C)** Heterophoria measured at 0.40 meters. The unit in the figure is prism diopters (Δ).

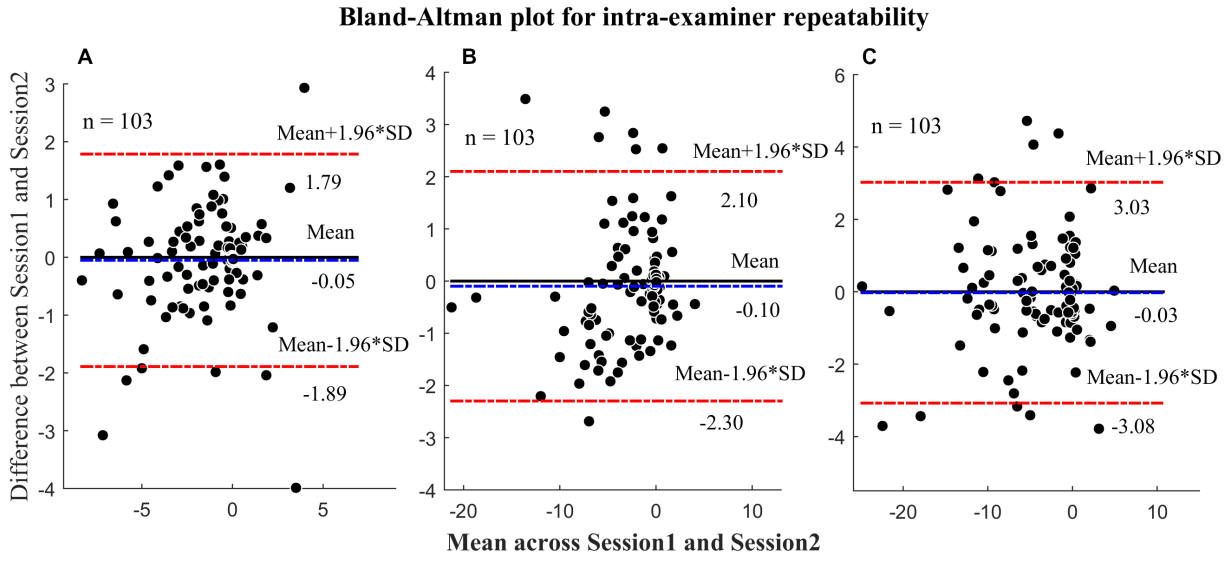

FIGURE 3
Bland-Altman plots illustrating the intra-examiner repeatability. **(A)** Heterophoria measured at 3 meters; **(B)** Heterophoria measured at 0.77 meters; **(C)** Heterophoria measured at 0.40 meters. The unit in the figure is prism diopters (Δ).

TABLE 2 Description of statistics and agreement of heterophoria measured by POCT and CHT, *n*=103.

Test distance	3m	0.77m	0.40m
CHT	−0.52(−2.22, 0.02)	−1.27(−4.18, −0.08)	−3.40(−7.41, −0.35)
POCT	−2.00(−3.83, −0.25)	−3.00(−6.00, −1.00)	−5.67(−8.00, −2.00)
CHT - POCT	0.77 ± 1.32 $t_1 = 5.93$, $p_1 < 0.001$	1.37 ± 2.18 $t_1 = 6.33$, $p_1 < 0.001$	1.57 ± 2.70 $t_1 = 5.87$, $p_1 < 0.001$
| CHT – POCT |	1.20 ± 0.95 $t_2 = -8.52$, $p_2 < 0.001$	1.93 ± 1.71 $t_2 = -12.28$, $p_2 < 0.001$	2.41 ± 2.00 $t_2 = -8.07$, $p_2 < 0.001$
COR	±2.59	±4.27	±5. 30

t_1 and p_1 denote the results of paired student *t* tests between CHT and POCT. t_2 and p_2 denote the results of student *t* tests between | CHT – POCT | and 4△, but the t_2 and p_2 at 3 m mean the result of student *t* tests between | CHT – POCT | and 2△. The data are presented as medians and quartiles. $p < 0.025$ means statistical significance.

measuring ocular deviations (Johns et al., 2004; Cebrian et al., 2014), and the inter-examiner COR were 1.43△ and ± 1.65△ for TH and POCT at distance, respectively. Our results showed the COR of CHT at distance was only 0.55△, which is better than TH and POCT. Similarly, the intra-examiner repeatability of CHT (±1.83△) was found to be comparable to that of TH (±1.28△) and POCT (±1.51△). These results were consistent at near as well. Thus, based on our findings, CHT demonstrates reliable repeatability at both 3 m and 0.40 m. Notably, there have been no previous investigations into the inter- and intra-examiner repeatability of heterophoria measurement at a middle distance (0.77 m). In this study, we found that the inter- and intra-examiner COR values at this distance were ± 1.02△ and ± 2.19△ respectively, both of which were less than 4△. These results indicate that the CHT exhibits good repeatability across near, middle, and far distances, making it comparable to TH and POCT methods.

Agreement

The results showed a strong correlation between CHT and POCT measurements, despite the CHT indicating greater esophoria compared to POCT. The significant differences between the POCT and other methods were also reported in other studies, for example, Cebrian et al. measured distance heterophoria using TH, MR, von Graefe (VG) method and POCT, and they found significant differences between any of the tests and POCT (Cebrian et al., 2014). Compared with Cebrian's study, the difference between CHT and POCT was comparable (0.77△ for CHT versus 0.63△, 0.44△, and 0.68△ TH, MR, and VG respectively). In our study, the mean absolute differences of two measurements at three different distances were smaller than 4△, as mentioned above, which is a clinical acceptable range. Additionally, the mean absolute difference at 3 m was less than the resolution of POCT (2△).

Our results indicated that the agreement between CHT and POCT is worse at near than far distance. Many studies concluded the variation of near heterophoria is much larger than far heterophoria (Schroeder et al., 1996; Canto-Cerdan et al., 2018). One of the reasons is accommodation. Canto-Cerdan and colleagues (Canto-Cerdan et al., 2018) analyzed the agreement between POCT and VG measurements for both non-presbyopic and presbyopic subjects. They found that the results for presbyopes showed better agreement, indicating that accommodation may play a role in phoria measurements. During the CHT test, subjects were instructed to maintain the sentences on the screen clear, which helped stabilize their accommodation at a constant level. Moreover, a previous clinical study

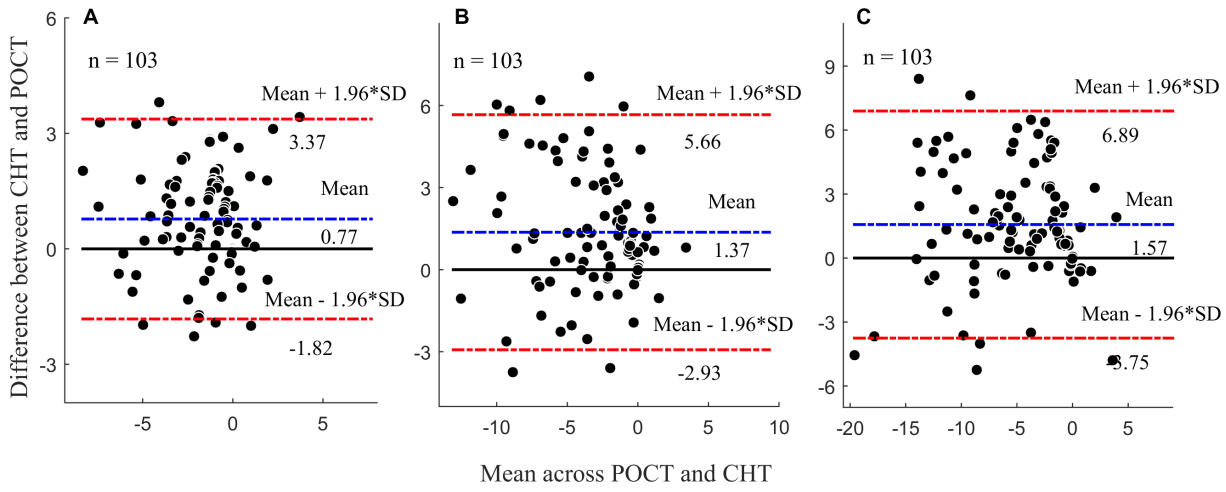

FIGURE 4
Bland-Altman plots illustrating the agreement between CHT and POCT. **(A)** Heterophoria measured at 3 meters; **(B)** Heterophoria measured at 0.77 meters; **(C)** Heterophoria measured at 0.40 meters. The unit in the figure is prism diopters (Δ). $p < 0.025$ means statistical significance.

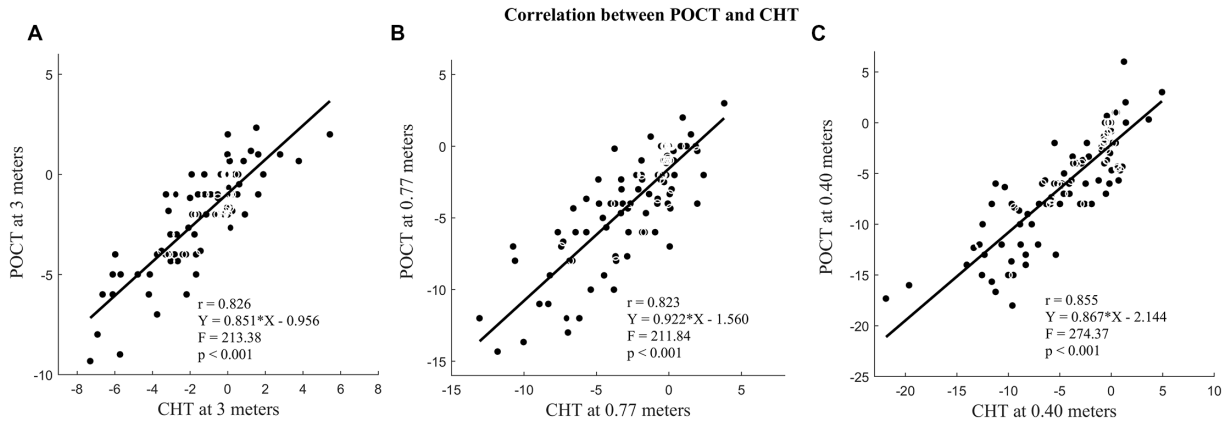

FIGURE 5
Correlation between POCT and CHT. **(A)** Heterophoria measured at 3 meters; **(B)** Heterophoria measured at 0.77 meters; **(C)** Heterophoria measured at 0.40 meters. The unit in the figure is prism diopters (Δ).

demonstrated that heterophoria measurement with the trial frame exhibited better repeatability than with the phoropter (Casillas and Rosenfield, 2006). The reason for this could be attributed to peripheral fusion, which can induce fusional vergence when retinal non-corresponding points are active spontaneously (Burian, 1939). Measuring with the trial frame was performed in free space and therefore provided a wide visual field, whereas the phoropter would restrict a relatively larger visual field. It is logical to infer that the presence of the peripheral stimuli, even under dissociate conditions, induced peripheral fusion when measuring heterophoria with trial frame. As a result, measuring heterophoria with the trial frame showed better repeatability than with the phoropter. Additionally, the previous study also demonstrated that TH had better repeatability than VG and MR at distance (Casillas and Rosenfield, 2006). Since the CHT combines the advantages of the trial frame and TH, it offers even greater repeatability.

Conclusion

CHT exhibits good test–retest repeatability and measurement agreement. Since CHT minimizes the measurement variances that can originate from examiners, results from CHT do not create external sources of measurement errors. Additionally, CHT is more flexible and user-friendly during measurement. Therefore, we believe that CHT can be considered interchangeable with POCT and is worthy of widespread use in clinical settings.

Data availability statement

The original contributions presented in the study are included in the article/supplementary material, further inquiries can be directed to the corresponding author.

Ethics statement

The studies involving human participants were reviewed and approved by the Ethics Committee of the Eye Hospital of Wenzhou Medical University. The patients/participants provided their written informed consent to participate in this study.

Author contributions

YW, FuZ, and ES contributed to conception and design of the study. FuZ performed the experiments, analyzed the data, and drafted the manuscript. FeZ revised the manuscript. All authors have reviewed and approved the final version for publication.

Conflict of interest

The authors declare that the research was conducted in the absence of any commercial or financial relationships that could be construed as a potential conflict of interest.

Publisher's note

All claims expressed in this article are solely those of the authors and do not necessarily represent those of their affiliated organizations, or those of the publisher, the editors and the reviewers. Any product that may be evaluated in this article, or claim that may be made by its manufacturer, is not guaranteed or endorsed by the publisher.

References

Anderson, H. A., Manny, R. E., Cotter, S. A., Mitchell, G. L., and Irani, J. A. (2010). Effect of examiner experience and technique on the alternate cover test. *Optom. Vis. Sci.* 87, 168–175. doi: 10.1097/OPX.0b013e3181d1d954

Argiles, M., Cardona, G., Perez-Cabre, E., Perez-Magrane, R., Morcego, B., and Gispets, J. (2016). Real-time non-intrusive assessment of viewing distance during computer use. *Optom. Vis. Sci.* 93, 1525–1531. doi: 10.1097/OPX.0000000000000995

Boccardo, L. (2021). Viewing distance of smartphones in presbyopic and non-presbyopic age. *J Optom* 14, 120–126. doi: 10.1016/j.optom.2020.08.001

Burian, H. M. (1939). Fusional movements: role of peripheral retinal stimuli. *Arch. Ophthalmol.* 21, 486–491. doi: 10.1001/archopht.1939.00860030092008

Canto-Cerdan, M., Cacho-Martinez, P., and Garcia-Munoz, A. (2018). Measuring the heterophoria: agreement between two methods in non-presbyopic and presbyopic patients. *J Optom* 11, 153–159. doi: 10.1016/j.optom.2017.10.002

Carmichael, L. (1947). Reading and visual fatigue. *Science* 106:628.

Casillas, E. C., and Rosenfield, M. (2006). Comparison of subjective heterophoria testing with a phoropter and trial frame. *Optom. Vis. Sci.* 83, 237–241. doi: 10.1097/01.opx.0000214316.50270.24

Cebrian, J. L., Antona, B., Barrio, A., Gonzalez, E., Gutierrez, A., and Sanchez, I. (2014). Repeatability of the modified Thorington card used to measure far heterophoria. *Optom. Vis. Sci.* 91, 786–792. doi: 10.1097/OPX.0000000000000297

Eastwood-Sutherland, C., and Gale, T. J. (2011). "Eye-screen distance monitoring for computer use." Annual International Conference of the IEEE Engineering in Medicine and Biology Society, Boston, MA, USA, pp. 2164–2167

Garcia-Munoz, A., Carbonell-Bonete, S., and Cacho-Martinez, P. (2014). Symptomatology associated with accommodative and binocular vision anomalies. *J Optom* 7, 178–192. doi: 10.1016/j.optom.2014.06.005

Han, C. C., Liu, R., Liu, R. R., Zhu, Z. H., Yu, R. B., and Ma, L. (2013). Prevalence of asthenopia and its risk factors in Chinese college students. *Int. J. Ophthalmol.* 6, 718–722. doi: 10.3980/j.issn.2222-3959.2013.05.31

Hashemi, H., Saatchi, M., Yekta, A., Ali, B., Ostadimoghaddam, H., Nabovati, P., et al. (2019). High prevalence of Asthenopia among a population of university students. *J. Ophthalmic Vis. Res.* 14, 474–482. doi: 10.18502/jovr.v14i4.5455

Hrynchak, P. K., Herriot, C., and Irving, E. L. (2010). Comparison of alternate cover test reliability at near in non-strabismus between experienced and novice examiners. *Ophthalmic Physiol. Opt.* 30, 304–309. doi: 10.1111/j.1475-1313.2010.00723.x

Ip, J. M., Robaei, D., Rochtchina, E., and Mitchell, P. (2006). Prevalence of eye disorders in young children with eyestrain complaints. *Am J. Ophthalmol.* 142, 495–497. doi: 10.1016/j.ajo.2006.03.047

Johns, H. A., Manny, R. E., Fern, K., and Hu, Y. S. (2004). The intraexaminer and interexaminer repeatability of the alternate cover test using different prism neutralization endpoints. *Optom. Vis. Sci.* 81, 939–946. doi: 10.1097/01.OPX.0000147675.67047.25

Kleiner, M. B., Brainard, D. H., Pelli, D. G., Ingling, A., and Broussard, C. (2007). What's new in Psychtoolbox-3? *Perception* 36, 301–307. doi: 10.1068/v070821

Martin Bland, J., and Altman, D. (1986). Statistical methods for assessing agreement between two methods of clinical measurement. *Lancet* 327, 307–310. doi: 10.1016/S0140-6736(86)90837-8

Rainey, B. B., Schroeder, T. L., Goss, D. A., and Grosvenor, T. P. (1998a). Inter-examiner repeatability of heterophoria tests. *Optom. Vis. Sci.* 75, 719–726. doi: 10.1097/00006324-199810000-00016

Rainey, B. B., Schroeder, T. L., Goss, D. A., and Grosvenor, T. P. (1998b). Reliability of and comparisons among three variations of the alternating cover test. *Ophthalmic Physiol. Opt.* 18, 430–437. doi: 10.1046/j.1475-1313.1998.00375.x

Romano, P. E., and Von Noorden, G. K. (1971). Limitations of cover test in detecting strabismus. *Am J. Ophthalmol.* 72, 10–12. doi: 10.1016/0002-9394(71)91585-6

Scheiman, M., and Wick, B. (2014). *Clinical management of binocular vision-heterophoric, accommodative, and eye movement disorders*. Philadelphia, Lippincott, Williams & Wilkins.

Schroeder, T. L., Rainey, B. B., Goss, D. A., and Grosvenor, T. P. (1996). Reliability of and comparisons among methods of measuring dissociated phoria. *Optom. Vis. Sci.* 73, 389–397. doi: 10.1097/00006324-199606000-00006

Sheppard, A. L., and Wolffsohn, J. S. (2018). Digital eye strain: prevalence, measurement and amelioration. *BMJ Open Ophthalmol* 3:e000146. doi: 10.1136/bmjophth-2018-000146

Shibata, T., Kim, J., Hoffman, D. M., and Banks, M. S. (2011). The zone of comfort: predicting visual discomfort with stereo displays. *J. Vis.* 11:11. doi: 10.1167/11.8.11

Tiwari, R. R. (2013). Eyestrain in working children of footwear making units of Agra, India. *Indian Pediatr.* 50, 411–413. doi: 10.1007/s13312-013-0117-x

Yeo, A. C., Atchison, D. A., and Schmid, K. L. (2013). Children's accommodation during reading of Chinese and English texts. *Optom. Vis. Sci.* 90, 156–163. doi: 10.1097/OPX.0b013e31827ce23a

Zadnik, K., Mutti, D. O., and Adams, A. J. (1992). The repeatability of measurement of the ocular components. *Invest. Ophthalmol. Vis. Sci.* 33, 2325–2333.

Zheng, F., Hou, F., Chen, R., Mei, J., Huang, P., Chen, B., et al. (2021). Investigation of the relationship between subjective symptoms of visual fatigue and visual functions. *Front. Neurosci.* 15:686740. doi: 10.3389/fnins.2021.686740

frontiers | Frontiers in Neuroscience

TYPE Original Research
PUBLISHED 28 June 2023
DOI 10.3389/fnins.2023.1209527

OPEN ACCESS

EDITED BY
Dan Wen,
Xiangya Hospital,
Central South University, China

REVIEWED BY
Meghah Vuppalapaty,
Surrozen, Inc., United States
Gottfried Martin,
University of Freiburg, Germany

*CORRESPONDENCE
Carol M. Troy
✉ cmt2@cumc.columbia.edu

RECEIVED 20 April 2023
ACCEPTED 05 June 2023
PUBLISHED 28 June 2023

CITATION
Avrutsky MI, Chen CW, Lawson JM, Snipas SJ, Salvesen GS and Troy CM (2023) Caspase-9 inhibition confers stronger neuronal and vascular protection compared to VEGF neutralization in a mouse model of retinal vein occlusion.
Front. Neurosci. 17:1209527.
doi: 10.3389/fnins.2023.1209527

Caspase-9 inhibition confers stronger neuronal and vascular protection compared to VEGF neutralization in a mouse model of retinal vein occlusion

Maria I. Avrutsky[1], Claire W. Chen[1], Jacqueline M. Lawson[1], Scott J. Snipas[2], Guy S. Salvesen[2] and Carol M. Troy[3,4,5]*

[1]Department of Pathology and Cell Biology, Vagelos College of Physicians and Surgeons, Columbia University, New York, NY, United States, [2]NCI-Designated Cancer Center, Sanford Burnham Prebys Medical Discovery Institute, La Jolla, CA, United States, [3]Department of Pathology and Cell Biology, Vagelos College of Physicians and Surgeons, Columbia University, New York, NY, United States, [4]Department of Neurology, Vagelos College of Physicians and Surgeons, Columbia University, New York, NY, United States, [5]The Taub Institute for Research on Alzheimer's Disease and the Aging Brain, Vagelos College of Physicians and Surgeons, Columbia University, New York, NY, United States

Purpose: Retinal vein occlusion (RVO) is a sight-threatening condition typically treated with intravitreal injection of vascular endothelial growth factor (VEGF) antagonists. Treatment response to anti-VEGF therapies is highly variable, with poor visual outcomes and treatment response in patients with significant retinal nonperfusion following RVO. Recently, caspase-9 has been identified as a potent regulator of edema, gliosis, and neuronal dysfunction during acute retinal hypoxia. The purpose of this study was to compare the therapeutic effect of caspase-9 inhibition against VEGF-neutralization in an established mouse model of RVO.

Methods: Adult male C57Bl/6J mice were randomized to induction of RVO and treatment with either vehicle, intravitreal injection of anti-VEGF antibody, topical administration of a selective caspase-9 inhibitor (Pen1-XBir3), or a combination therapy. Animals were followed on days 1, 2, and 8 after RVO with fundus retinal imaging, and with optical coherence tomography (OCT) to capture retinal swelling, capillary nonperfusion (measured by disorganization of retinal inner layers, DRIL), hyperreflective foci (HRF), and retinal atrophy. Focal electroretinography (ERG) measurements were performed on day 7. Histology was performed on retinal sections from day 8.

Results: Both VEGF neutralization and caspase-9 inhibition showed significant retinal protection from RVO compared to vehicle treatment arm. Retinal reperfusion of occluded veins was accelerated in eyes receiving caspase-9 inhibitor, but not significantly different from vehicle in the anti-VEGF group. Retinal edema was suppressed in all treatment groups, with approximately 2-fold greater edema reduction with caspase-9 inhibition compared to VEGF neutralization. HRF were reduced similarly across all treatment groups compared to vehicle. Retinal detachment was reduced only in eyes treated with caspase-9 inhibitor monotherapy. Caspase-9 inhibition reduced retinal atrophy and preserved ERG response; VEGF neutralization did not prevent neurodegeneration following RVO.

Conclusion: Caspase-9 inhibition confers stronger neuronal and vascular protection compared to VEGF neutralization in the mouse laser-induced model of RVO.

KEYWORDS

retinal vein occlusion, VEGF, caspase-9, cell penetrating peptide, neurodegeneration, neurovascular, edema, ischemia

1. Introduction

Retinal vein occlusion (RVO) occurs when a blockage in one of the major retinal veins obstructs blood outflow from the retina, causing accumulation of fluid, blood, and inflammatory cells. This condition affects between 1 and 2% of persons over the age of 40 (Ho et al., 2016), and can cause variable degrees of vision impairment, depending on the location (macular vs. peripheral), duration, and severity of ischemic injury.

Current treatments for RVO target retinal edema and neuroinflammation via anti-VEGF (vascular endothelial growth factor) treatments, or reduce broad-spectrum inflammation through corticosteroids (Ho et al., 2016). VEGF levels increase in response to hypoxia, and act on endothelial cells to promote vasodilation and increase vascular permeability (Apte et al., 2019). VEGF-neutralizing therapies can be highly effective at resolving retinal swelling and improving visual function, however individual treatment response is variable. Refractory edema persists in over 50% of eyes treated for RVO (Campochiaro et al., 2014), and over 20% of eyes experience visual acuity loss of >15 ETDRS [Early Treatment Diabetic Retinopathy Study] letters over 5 years (Wecker et al., 2017). RVO can damage retinal microvasculature, resulting in poor retinal perfusion and capillary ischemia. Ischemic RVO, typically defined as cases where the ischemic index (percent area of non-perfused retina) is ≥30%, is associated with worse visual outcomes, and poor treatment response (Khayat et al., 2018).

The laser-induced murine model of RVO has been used extensively to investigate mechanisms underlying RVO pathology (Khayat et al., 2017). In this model, an image-guided laser system is used to create a localized occlusion to one or more branch retinal veins. Optimized RVO induction and evaluation protocols enable highly reproducible measurement of retinal edema, inflammation, and neuronal injury (Colón Ortiz et al., 2021; Chen et al., 2022). Consistent with clinical findings, inhibiting VEGF signaling attenuates retinal edema and improves retinal nonperfusion following experimental RVO (Fuma et al., 2017). One novel mediator of retinal injury in RVO is caspase-9, which acts as a multimodal instigator of neurovascular and astroglial dysfunction (Avrutsky et al., 2020; Colon Ortiz et al., 2022). Selective *in vivo* inhibition of caspase-9 can be achieved through administration of Pen1-XBir3 (Akpan et al., 2011; Avrutsky et al., 2020), a formulation containing the caspase-9-inhibitory domain of XIAP protein (BIR3) (Denault et al., 2007) crosslinked to a cell penetrating peptide, Penetratin-1 (Dupont et al., 2011). Typically known for its role as an initiator of the intrinsic apoptosis pathway, caspase-9 mediates diverse inflammatory and degenerative pathologies through both apoptotic and nonapoptotic mechanisms (Avrutsky and Troy, 2021). In RVO, both VEGF and caspase-9 signaling modulate ischemic injury by regulating vascular endothelial cells.

Here, we compared the efficacy of VEGF-neutralization against a cell permeant topical caspase-9 inhibitor (Pen1-XBir3), following induction of RVO. Using an integrated panel of ophthalmic imaging readouts, we evaluated the progression of retinal ischemia, edema, and neurodegeneration in wild-type mice treated with either a VEGF-neutralizing antibody or a topical caspase-9 inhibitor.

2. Materials and methods

2.1. Randomization and masking

All animals were identified by ear punch, assigned alphanumeric IDs and randomized to treatment groups. RVO induction, retinal imaging, animal exclusions, ERGs, and image analysis was performed by investigators masked to treatment type. Different investigators were responsible for animal randomization, treatment administration, and RVO/retinal imaging procedures.

2.2. Animals

Male 2-month old C57Bl6/J mice were purchased from Jackson Laboratories, and allowed to acclimate in specific pathogen-free housing for at least 1 week prior to imaging.

All animals were handled in accordance with the Association for Research in Vision and Ophthalmology (ARVO) statement for the use of animals in ophthalmic and vision research and monitored by the Institutional Animal Care and Use Committee (IACUC) of Columbia University.

2.3. RVO procedure

RVO was induced by laser photocoagulation of all major retinal veins ($n = 3$–6 veins occluded/eye) 10–20 min following tail vein injection of Rose Bengal dye (37.5 mg/kg). Animals were anesthetized with intraperitoneal injection of a cocktail of ketamine (80–100 mg/kg) and xylazine (5–10 mg/kg). Eyes were dilated with tropicamide and phenylephrine chloride eye drops. Irradiation of retinal veins was to performed with the 532 nm Micron IV image guided laser system from Phoenix Research Labs by delivering three adjacent laser pulses (power: 100 mW, duration: 1 s, total energy 0.3 J) to each targeted vein at a distance of 375 μm from the optic nerve head. Occlusions were observed by fundus imaging for 1–2 min following laser treatment to record occlusions at Day 0. Exclusion criteria were applied by a masked investigator to identify eyes with fulminant retinal detachment, intravitreal hemorrhage, or reperfusion of all veins within 24 h. Detailed RVO procedure protocols are described in Colón Ortiz et al. (2021).

2.4. Anti-VEGF treatment

Animals were anesthetized by intra-peritoneal injection of ketamine (80 mg/kg) and xylazine (5-10 mg/kg), and one drop of 0.5%

alcaine was applied to the eye as a topical anesthetic. Sixteen hours prior to RVO mouse anti-VEGF antibody (200μg/ml; R&D Systems) was injected (2 μL) into the vitreous of both eyes using a sterile pulled capillary pipette attached to a Hamilton glass syringe. For controls, eyes were injected with 2 μL of sterile PBS 16 h prior to RVO. After injection, animals received 0.3% topical tobramycin to prevent infection.

2.5. Pen1-XBir3 treatment

His-tagged XBir3 was expressed in *Escherichia coli* and purified by nickel column. Pen1 (PolyPeptide Group) was mixed at a 2:1 molar ratio with purified XBir3 and incubated for 1–2 h at 37°C to generate disulfide-linked Pen1-XBir3 as described in Akpan et al. (2011) and Avrutsky et al. (2020). Eye drops containing 10 μg Pen1-XBir3 in sterile saline were administered immediately following RVO, and again at 24 h (Figure 1A). Equivalent volumes of saline containing unlinked Pen1, were administered as controls.

2.6. Treatment groups

There were 4 treatment groups. All animals received an injection and eyedrops. The vehicle group received saline injection and Pen1-saline eyedrops ($n = 23$ eyes). Anti-VEGF group received anti-VEGF injection and Pen1-saline eyedrops ($n = 20$ eyes). Pen1-XBir3 group received saline injection and Pen1-XBir3 eyedrops ($n = 18$ eyes). Combination group received anti-VEGF injection and Pen1-XBir3 eyedrops ($n = 19$ eyes).

2.7. OCT imaging and analysis

OCT images were captured using the Phoenix Micron IV image-guided OCT system, and layer segmentation was performed using InSight software. Four OCT scans were analyzed from each eye (two vertical and two horizontal scans) positioned approximately 75μm distal from the periphery of RVO burn areas. Intraretinal thickness was defined as GCL through IS/OS, and retinal detachment was quantified as the difference between IS/OS and the RPE (Figure 1B). Fundus images were captured at the time of OCT imaging on days 1, 2, and 8 post-RVO to monitor occlusion resolution following RVO.

HRF counts were measuring using Image J. OCT images were processed using 'Despeckle' function. HRF were selected by applying a threshold along the INL selection defined as [mode INL pixel intensity +2 standard deviations], and quantified using 'Analyze Particles' function.

DRIL (disorganization of retinal inner layers) was measured as the horizontal extent of each OCT B-scan lacking a distinct boundary between IPL/INL or INL/OPL.

Detailed OCT imaging and analysis protocols for the RVO model are described in (Chen et al., 2022).

2.8. ERG imaging

Animals were dark adapted, typically overnight, and subjected to electroretinogram recordings with the Micron IV Image-Guided Focal ERG system. A 1.5 mm flash spot size was centered on the optic nerve head, and a 10 ms white light LED was used to deliver stimulus intensities of −0.7 log (Cd s/m2) and 2.3 log (Cd s/m2). Ten ERG traces were averaged for each eye, and waveforms were analyzed with Labscribe3 ERG to calculate amplitudes of the a wave, b wave and oscillatory potentials (OPs). The sum of the first 6 OPs was used to calculate sum OP amplitude.

2.9. Histology

Mice were euthanized with overdose of Ketamine (160–200 mg/kg) plus Xylazine (10–20 mg/kg) and perfused with saline, followed by fixation with 4% paraformaldehyde. Eyes were enucleated, embedded in Optimal Cutting Temperature compound, and cryo-sectioned at 20 μm/section. For H&E staining, slides were submitted to the Columbia University Medical Center Molecular Pathology Shared Resource Histology Service. Ocular sections were imaged with a Nikon microscope (Nikon Instruments) and SPOT digital camera (SPOT Imaging), size bar = 20 μm.

2.10. Statistics

Statistical analyses were performed in Graphpad Prism. One-way and two-way ANOVA were used to determine statistical differences between groups. Statistical tests and *p*-values are depicted in figure legends. Data are presented as mean ± SEM. Significance was set to be $p < 0.05$.

3. Results

The standard of care for RVO is therapy with injections of anti-VEGF. We have shown that targeting caspase-9 in a mouse model of RVO provides substantial morphologic, cellular and functional protection (Avrutsky et al., 2020; Colon Ortiz et al., 2022). To compare the efficacy of inhibiting caspase-9, vs. blocking VEGF, mice were followed for 8 days following induction of RVO and treatment with either caspase-9 inhibitor eyedrops (Pen1-XBir3), or intravitreal injection of anti-VEGF antibody. We also evaluated a group that received combination therapy to determine if there were additive or potentiating effects of the treatment. Anti-VEGF/PBS administration was performed 16 h prior to induction of RVO to allow for screening out of animals with retinal morphological changes due to the intravitreal injection procedure. Caspase-9 inhibition was achieved by administration of 10 μg Pen1-XBir3 eyedrops immediately following RVO induction, followed by a second dose at 24 h as described in (Avrutsky et al., 2020). RVO-induced retinal pathology was measured by OCT imaging at 1, 2, and 8 days. ERG imaging was performed on dark-adapted animals at 7 days (Figure 1A). Occlusions induced by the laser RVO model typically last through 48 h, and resolve within 1 week. Consequently, the RVO model induces transient retinal detachment and intraretinal swelling characterized by thickening of GCL, IPL, INL and OPL layers at 24–48 h post RVO. By 8 days post-RVO, retinal edema resolves, revealing atrophy of retinal neuronal layers (Figure 1B).

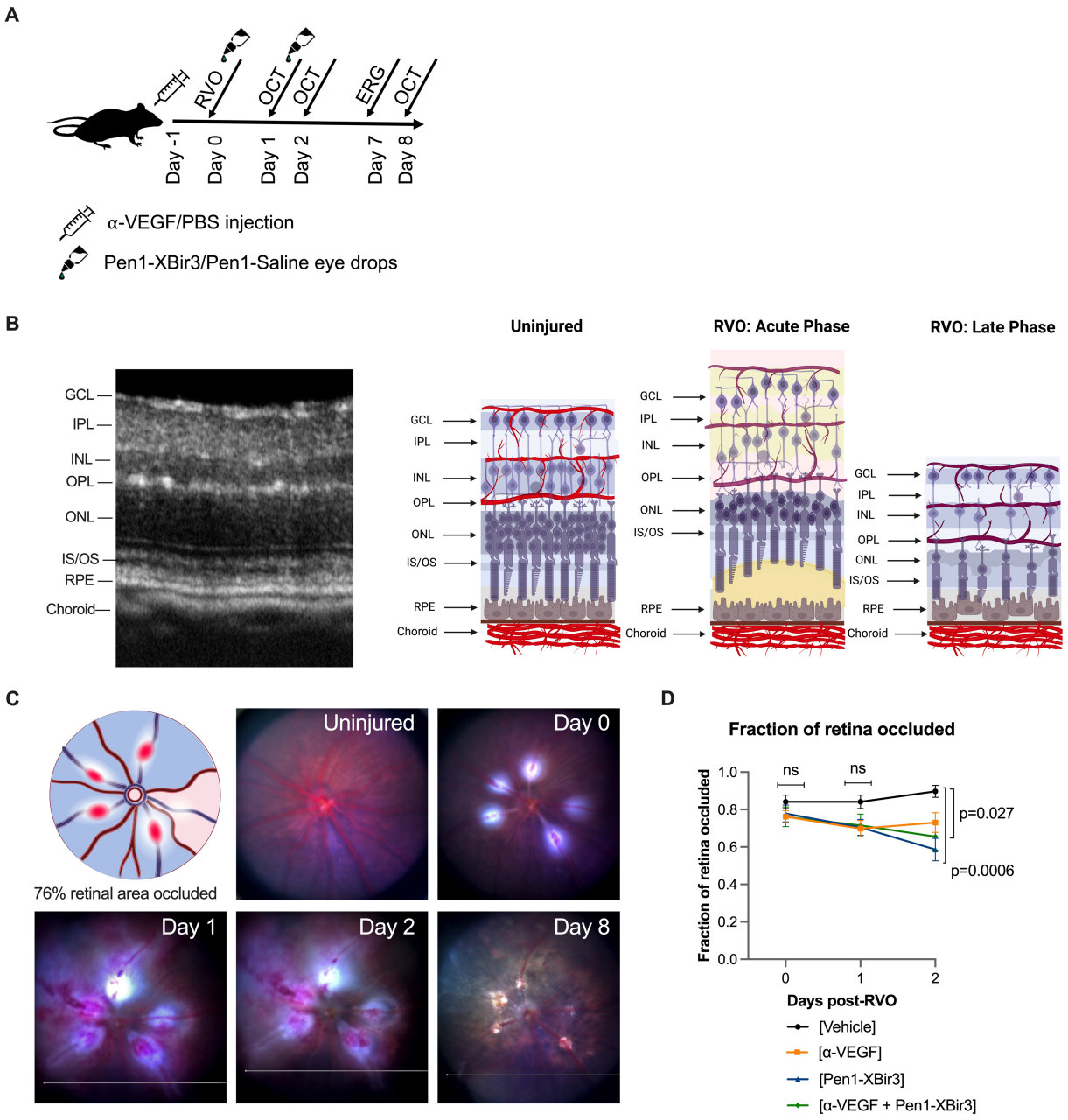

FIGURE 1
Mouse model of retinal vein occlusion. **(A)** Diagram depicts experimental plan showing timing of treatment administration and retinal imaging in a mouse model of RVO. **(B)** Representative image of an OCT retinal scan labeling retinal layers in an uninjured mouse. Diagram depicts retinal neuronal and vascular layers in uninjured animals and in acute and late phases of RVO. GCL; ganglion cell layer, IPL; inner plexiform layer, INL; inner nuclear layer, OPL; outer plexiform layer, ONL; outer nuclear layer, IS/OS; inner segment/outer segment, RPE; retinal pigment endothelium. Figure made with Biorender.com. **(C)** Fundus retinal imaging of a vehicle treated eye immediately prior to RVO, and at days 0, 1, 2, and 8 post-RVO. Diagram depicts location of occluded veins (red ovals), and shading of retinal occluded area in blue. Figure made with Biorender.com. **(D)** Quantification of the fraction of retina occluded in (n=16–23 eyes/timepoint/group) at days 0, 1, and 2 post-RVO. Graph shows mean±SEM. Differences between groups measured by Mixed-effects analysis with Tukey's multiple comparisons test for significance between groups at each timepoint. N eyes/group at 0/1/2days post-RVO: Vehicle (23/23/19), anti-VEGF (21/21/16), Pen1-XBir3 (18/18/18), anti-VEGF+Pen1-XBir3 (19/19/19).

3.1. Interventions improve retinal blood flow

Since both caspase-9 inhibition (Avrutsky et al., 2020) and VEGF neutralization (Fuma et al., 2017; Nishinaka et al., 2018) have been associated with improvements in retinal blood flow, we examined the development of retinal ischemia following induction of retinal vein occlusion. Murine retinal vasculature features alternating major retinal veins and arteries that emerge from the optic nerve whose branches dive into the retinal tissues to form three capillary plexi in the GCL, INL, and OPL (Figures 1B,C). The RVO procedure was performed on each

major retinal vein, resulting in an average occlusion rate of 77.6% ± 19.2% (mean ± SD) of retinal veins per eye. Retinal occlusion area was defined as the sector of fundus transcribed by the occluded vein and the two adjacent retinal arteries (Figure 1C). There were no significant differences in rates of retinal occlusion immediately after RVO, or at 1 day post-RVO between the treatment groups. However by day 2, we measured significant increase in retinal reperfusion in eyes treated with Pen1-XBir3, either with or without anti-VEGF (Figure 1D). Anti-VEGF treatment on its own was not significantly associated with occlusion resolution.

Retinal injury following RVO is significantly associated with microvascular ischemia. To evaluate the evolution of capillary nonperfusion, we analyzed retinal OCTs for DRIL (disorganization of retinal inner layers) (Avrutsky et al., 2020; Chen et al., 2022). DRIL measurements revealed inner retinal nonperfusion across approximately 51% of OCT B-scan length in vehicle treated animals, with no significant temporal trends across the duration of the study (Figures 2, 3A). All treatments were associated with improvement in DRIL, with significantly stronger effect among animals receiving Pen1-XBir3, either as a monotherapy or in conjunction with anti-VEGF.

3.2. Caspase-9 and VEGF inhibition regulate retinal edema through partially distinct mechanisms

During the edema phase of RVO, all treatments were associated with less retinal swelling (Figures 2, 3B–D). Representative OCT images are shown for 1, 2, and 8 days; representative H&E histology is shown for 8 days (Figure 2). Anti-VEGF treatment efficacy was most evident in the innermost retinal layers (GCL, IPL, INL), with no measured efficacy on OPL swelling (Figures 3C,D). Eyes treated with Pen1-XBir3 had significantly less swelling in all layers compared to anti-VEGF, and were additionally protected from retinal detachment (Figures 2, 3C; Table 1), however this effect was attenuated in eyes receiving both Pen1-XBir3 and anti-VEGF treatments. Retinal detachment post-RVO is caused by accumulation of subretinal fluid due to dysfunction of the outer blood-retinal barrier. The differential regulation of retinal detachment and intraretinal swelling by Pen1-XBir3 and anti-VEGF treatments suggests that distinct pathophysiological mechanisms may disrupt inner and outer blood retinal barrier in the murine RVO model. Retinal thickness measures in eyes receiving both Pen1-XBir3 and anti-VEGF treatment were not statistically different from either monotherapy, and generally measured an intermediate degree of retinal swelling with no additional benefit over Pen1-XBir3 alone.

3.3. Both caspase-9 inhibition and VEGF neutralization reduce HRF

Both in patients and in experimental models of RVO, retinal ischemia is associated with the appearance of hyperreflective foci (HRF) in the inner retina. While the etiology of HRF remains ambiguous, clinical data suggests a strong correlation between HRF, ocular inflammation, and visual prognosis outcomes (Chatziralli et al., 2016; Mo et al., 2017). We evaluated the number of HRFs detected in the INL; all treatments were associated with a 20.5–30.4% decrease in HRF counts compared to vehicle-treated eyes (Figure 4). Unlike the retinal ischemic measurements, there were no significant differences between any of the treatment groups.

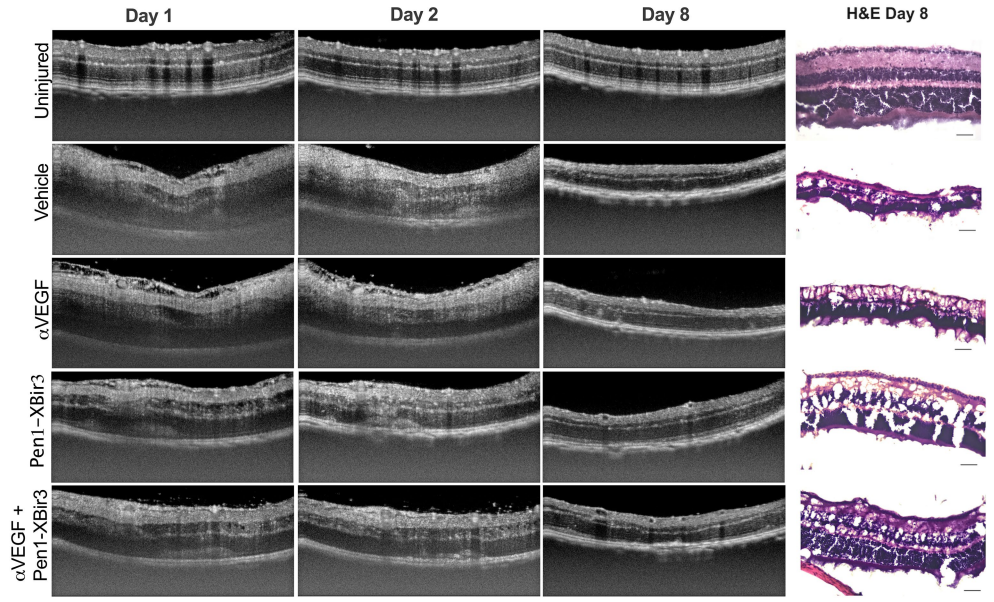

FIGURE 2
OCT representative images. Figure depicts representative longitudinal OCT scans from an uninjured animal and animals induced with RVO from each treatment group at days 1, 2, and 8. Representative H&E retinal histology sections depicted at right, scale bar=20μm.

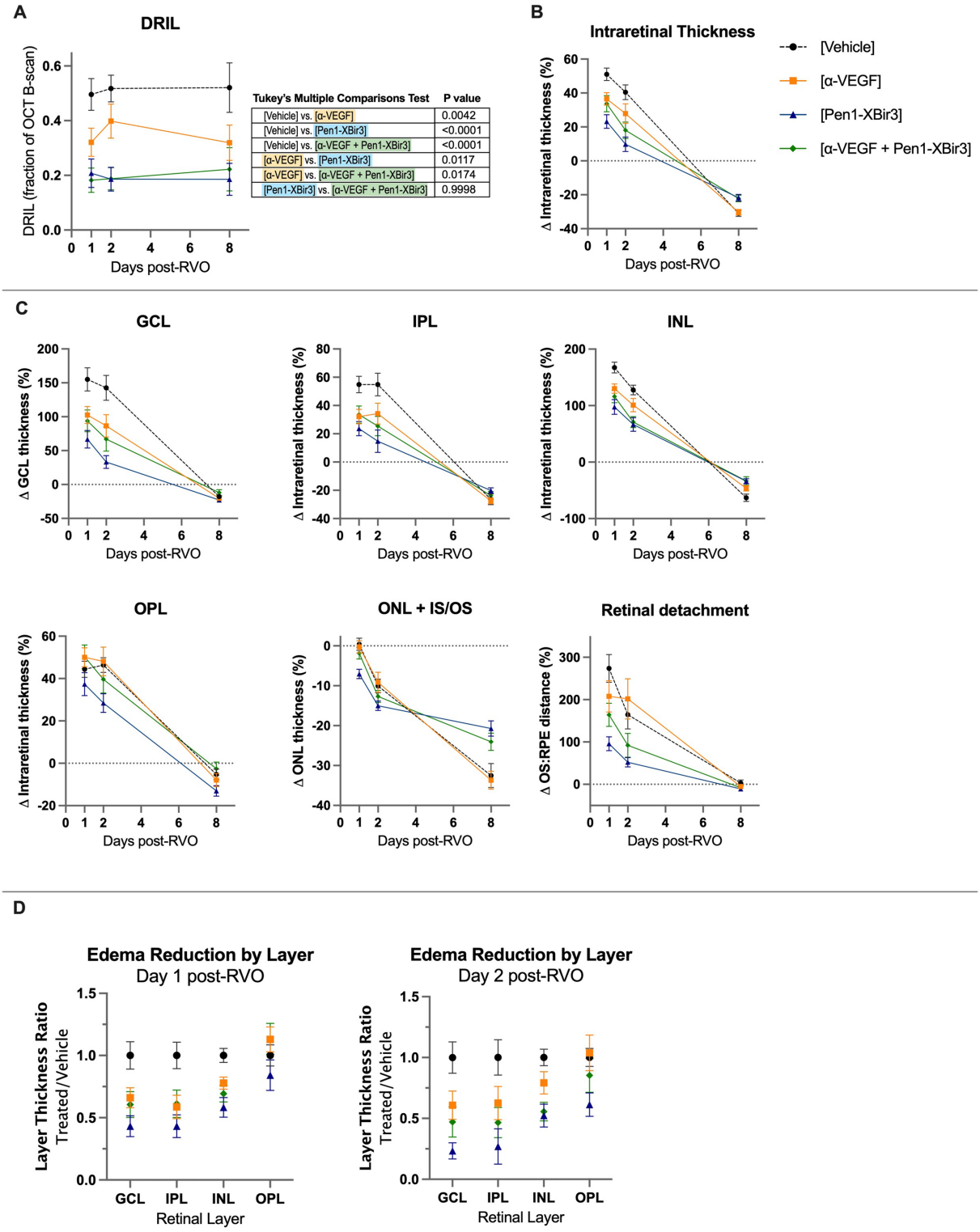

FIGURE 3
Quantification of DRIL and retinal thickness changes in OCT. **(A)** Quantification of DRIL measurements in (*n*=16–23 eyes/timepoint/group) each treatment group at days 1, 2, and 8 post-RVO. Graph shows mean±SEM. Differences between groups measured by 2Way ANOVA with Tukey's multiple comparisons test to compare main treatment group effect across all study timepoints (days 1/2/8 post-RVO). N eyes/group at 1/2/8days post-RVO: Vehicle (23/19/18), anti-VEGF (20/16/16), Pen1-XBir3 (18/18/18), anti-VEGF+Pen1-XBir3 (19/19/17). **(B)** Quantification of mean±SEM change in intraretinal thickness, measured by OCT between the GCL and the IS/OS of (*n*=16–23 eyes/timepoint/group) at days 1, 2, and 8 post-RVO for each treatment group. Differences between groups at each timepoint compared by 2Way ANOVA with Tukey's multiple comparisons, statistics shown in Table 1. N at 1/2/8days post-RVO: Vehicle (23/19/18), anti-VEGF (20/16/16), Pen1-XBir3 (18/18/18), anti-VEGF+Pen1-XBir3 (19/19/17). **(C)** Quantification of mean±SEM individual retinal layer thickness changes of OCT scans from panel **(B)**. Statistical comparisons from 2Way ANOVA shown in Table 1. **(D)** Quantification of mean±SEM of retinal thickness changes normalized to RVO/Vehicle treatment group of OCT scans from panels **(B,C)**.

TABLE 1 OCT measurement statistics table.

Tukey's multiple comparisons test	DRIL	Intraretinal thickness	GCL	IPL	INL	OPL	ONL	Retinal detachment
Day 1	**Adjusted *P* Value**	**Adjusted *P* Value**	**Adjusted *P* Value**	**Adjusted *P* Value**	**Adjusted *P* Value**	**Adjusted *P* Value**	**Adjusted *P* Value**	**Adjusted *P* Value**
[Vehicle] vs. [α-VEGF]	0.1283	0.0401	0.0799	0.028	0.0248	0.768	0.9908	0.5469
[Vehicle] vs. [Pen1-XBir3]	0.0036	<0.0001	0.0012	0.0013	0.0008	0.7206	0.0027	0.0002
[Vehicle] vs. [α-VEGF + Pen1-XBir3]	0.0007	0.0335	0.0602	0.0704	0.0059	0.8103	0.7182	0.0646
[α-VEGF] vs. [Pen1-XBir3]	0.4202	0.0875	0.2116	0.6445	0.183	0.2896	0.0073	0.0467
[α-VEGF] vs. [α-VEGF + Pen1-XBir3]	0.1959	0.9648	0.9734	0.9981	0.7383	>0.9999	0.8762	0.7774
[Pen1-XBir3] vs. [α-VEGF + Pen1-XBir3]	0.9822	0.3492	0.5634	0.5977	0.7134	0.3531	0.0466	0.1717
Day 2								
[Vehicle] vs. [α-VEGF]	0.4525	0.3218	0.1277	0.26	0.286	0.9956	0.9908	0.9194
[Vehicle] vs. [Pen1-XBir3]	<0.0001	<0.0001	<0.0001	0.0058	0.0014	0.0161	0.0976	0.0218
[Vehicle] vs. [α-VEGF + Pen1-XBir3]	<0.0001	0.0074	0.0262	0.04	0.0006	0.7932	0.6635	0.3636
[α-VEGF] vs. [Pen1-XBir3]	0.0451	0.0812	0.046	0.2948	0.1939	0.0963	0.1817	0.0325
[α-VEGF] vs. [α-VEGF + Pen1-XBir3]	0.043	0.5671	0.8494	0.8191	0.2211	0.8002	0.6351	0.2194
[Pen1-XBir3] vs. [α-VEGF + Pen1-XBir3]	>0.9999	0.5849	0.3514	0.7333	0.9929	0.4977	0.6055	0.5517
Day 8								
[Vehicle] vs. [α-VEGF]	0.29	0.9924	0.8562	0.9932	0.2009	0.9076	0.9891	0.7077
[Vehicle] vs. [Pen1-XBir3]	0.0209	0.0064	0.1077	0.4995	0.0052	0.1373	0.0128	0.2694
[Vehicle] vs. [α-VEGF + Pen1-XBir3]	0.0825	0.0102	0.6044	0.9515	0.0263	0.9062	0.1242	0.4683
[α-VEGF] vs. [Pen1-XBir3]	0.4297	0.0114	0.7913	0.0803	0.2647	0.5697	0.0007	0.4111
[α-VEGF] vs. [α-VEGF + Pen1-XBir3]	0.7782	0.018	0.3736	0.7348	0.4754	0.6221	0.0203	0.8784
[Pen1-XBir3] vs. [α-VEGF + Pen1-XBir3]	0.9819	0.9979	0.1182	0.7368	>0.9999	0.0614	0.6592	0.8501

Green = improvement. Light green = intermediate improvement. White = no significant effect over RVO.

3.4. Caspase-9 inhibition but not VEGF neutralization, protects against retinal atrophy

At 8 days post-RVO, retinal atrophy was measured in the GCL, IPL, INL, and ONL. Although anti-VEGF treatment effectively attenuated retinal swelling, it was not associated with protection from retinal atrophy (Figures 2, 3B,C). Conversely, both groups that received Pen1-XBir3 had significant protection of INL and ONL layers. The GCL/IPL complex, comprised of retinal ganglion neurons was not significantly protected by either treatment.

Consistent with OCT measures of retinal atrophy, ERG measurements showed functional neuroprotection with Pen1-XBir3 treatment, but not with anti-VEGF (Figure 5).

4. Discussion

This study represents a framework for comparing *in vivo* efficacy of experimental treatments against a clinically-established mechanism of action (VEGF-neutralization) in a mouse model of RVO. Our prior work has shown that non-apoptotic activation of caspase-9 regulates edema, gliosis and neuronal dysfunction in a well-defined mouse model of RVO (Avrutsky et al., 2020; Colon Ortiz et al., 2022). Here,

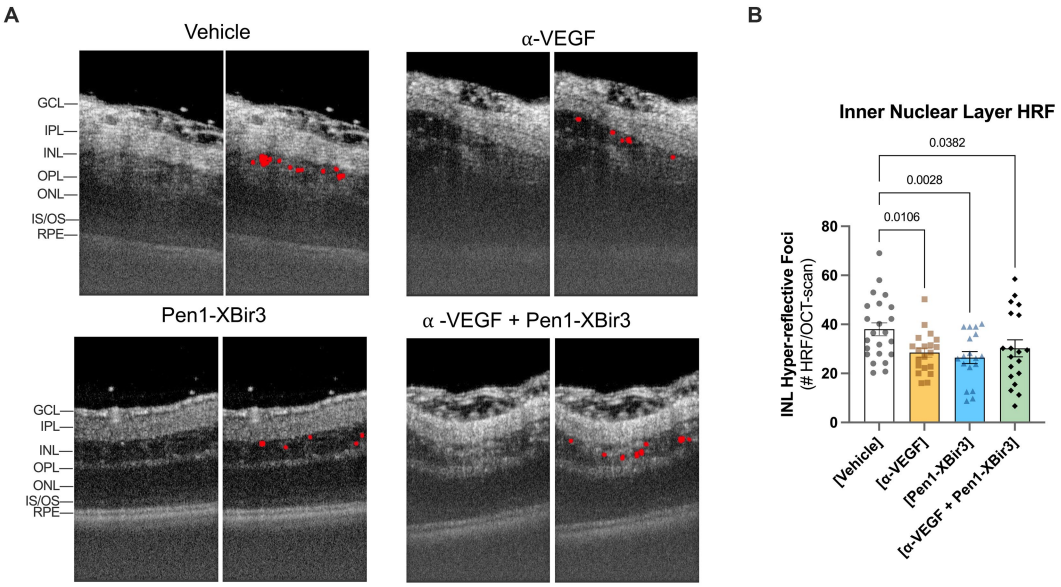

FIGURE 4
Quantification of hyper-reflective foci (HRF). **(A)** Closeup of representative OCT images at 1day post-RVO, with overlays showing automated detection of hyperreflective regions. **(B)** Quantification of mean±SEM number of hyperreflective foci detected in each treatment group at 1day post-RVO. Differences between groups measured by one-way ANOVA with Fisher's LSD test. N eyes/group: Vehicle (23), anti-VEGF (20), Pen1-XBir3 (18), anti-VEGF+Pen1-XBir3 (19).

we compare the functional efficacy of Pen1-XBir3, a caspase-9 inhibitor, with an established VEGF neutralizing treatment protocol. The data show that topical treatment with Pen1-XBir3 is equal or superior to intravitreal delivery of VEGF neutralizing antibodies across multiple *in vivo* measures.

Orthogonal measures capture different dimensions of RVO pathology in response to caspase-9 inhibition, VEGF-neutralization, or a combination treatment. Notably, our study was powered to capture therapeutic differences between Pen1-XBir3 treatment versus control, and was not powered to evaluate differences between the combination treatment and either monotherapy. Since neither therapy offers complete retinal protection by itself, a combination treatment was attempted to test the feasibility of using caspase-9 inhibition as an adjunct to VEGF neutralization. To maximize potential efficacy, both treatments were applied at maximal possible dose, based on limitations of intravitreal injection and eye-drop volumes. Stronger protection in eyes treated with the caspase-9 inhibitor suggest that caspase-9 signaling is a more critical target for treating retinal edema and capillary ischemia in RVO. Meanwhile the combination of the two therapies was more effective than anti-VEGF monotherapy, but did not show any improvement over the efficacy of Pen1-XBir3 alone. One limitation of this study is that this was the first attempt to co-administer caspase-9 and VEGF antagonists in a retinal injury model. The dosing levels and methods of delivering the respective treatments were not optimized for a combination therapy approach.

This study captured functional and morphological endpoints, and did not enable molecular profiling of signaling changes in response to the treatment arms. Future studies will be required to determine whether and how caspase-9 and VEGF signaling may interact in RVO. Both caspase-9 and VEGF are multimodal regulators of tissue injury and hypoxia response, with several intersecting mechanisms of action. Both proteins can regulate endothelial cell survival through modulation of autophagy and mitochondrial function (Domigan et al., 2015; An et al., 2019; Spengler et al., 2020). Additionally, both VEGF and caspase-9 have multiple immunomodulatory activities (Reinders et al., 2003; Avrutsky and Troy, 2021).

Using *in vivo* measures over time increases the translational relevance of preclinical models by utilizing techniques which are commonly used in the clinic to diagnose and follow the evolution of disease in persons receiving treatment for RVO. OCT measures retinal thickness, ischemia (using DRIL) and inflammation (tracking HRFs). Fundoscopic imaging follows resolution of retinal occlusions. ERGs reflect integrity of the retinal neuronal network. Efficacy of each treatment arm was equivalent with regard to HRFs but for all other measures Pen1-XBir3 provided superior efficacy compared to VEGF neutralization. Pen1-XBir3 protected neuronal function, while VEGF neutralization did not affect ERG response. These findings are consistent with clinical data noting extensive retinal degeneration after successful resolution of edema with anti-VEGF treatment (Hasegawa et al., 2017), and lack of functional improvements in retinal regions of severe nonperfusion at baseline (Rachima et al., 2020).

5. Conclusion

Comparison of VEGF-neutralization and caspase-9 inhibition strategies in a murine model of RVO demonstrate vascular protection by anti-VEGF, and both vascular and neuronal protection with inhibition of caspase-9. These data demonstrate comparison of an experimental therapy against a clinically-validated treatment modality, and support developing therapies to target pathways that are not VEGF-driven for the treatment of RVO.

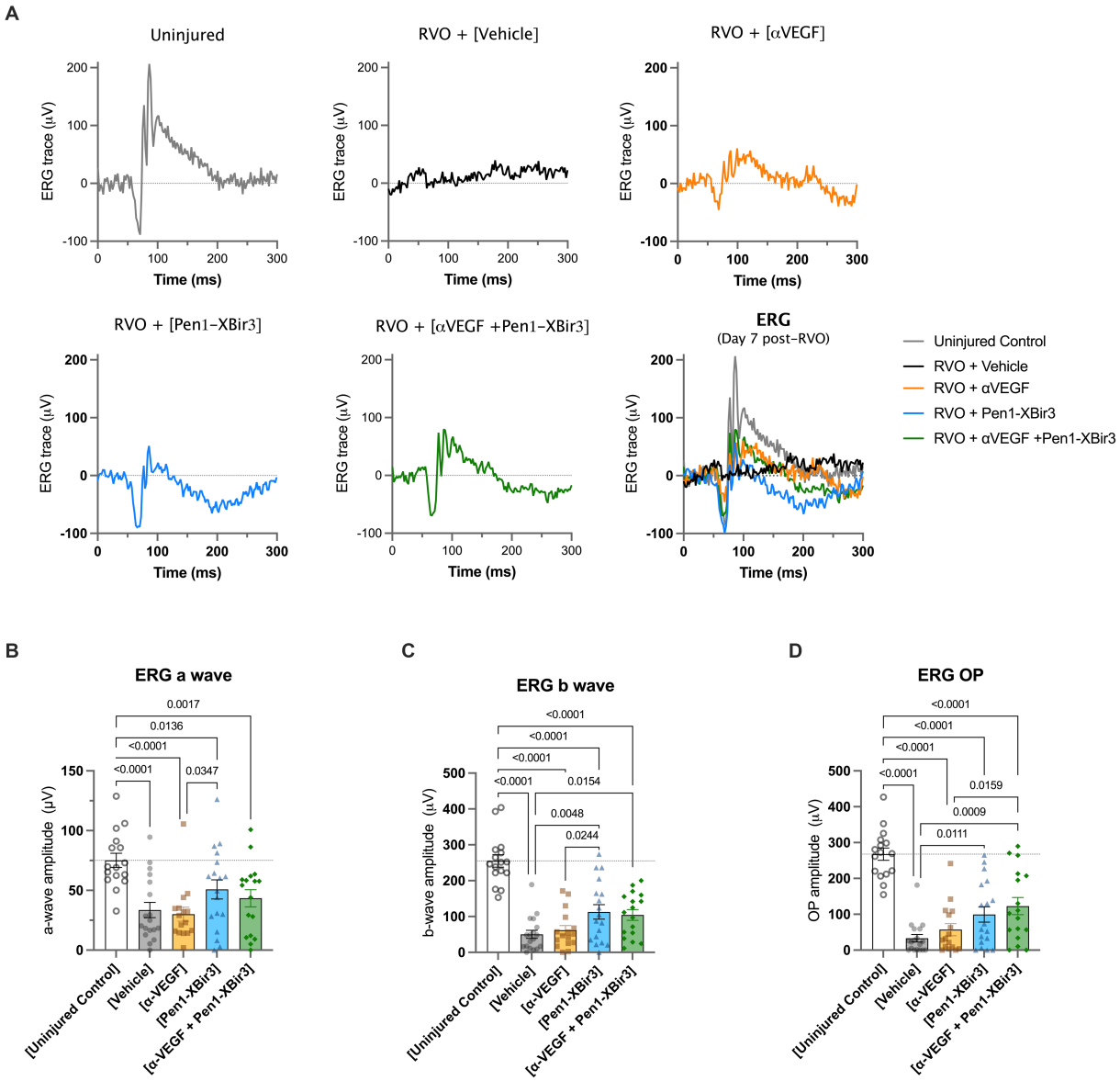

FIGURE 5
Retinal functional measure by focal ERG. **(A)** Depicts representative electroretinogram (ERG) traces in an uninjured control animal, and in each RVO treatment group. **(B)** Quantification of mean±SEM a wave amplitudes in (*n*=16–18 eyes/group) uninjured control mice and in each RVO treatment group. Difference between groups were measured by one-way ANOVA with Fisher's LSD test. N eyes/group: Vehicle (18), anti-VEGF (16), Pen1-XBir3 (18), anti-VEGF+Pen1-XBir3 (17), uninjured (16). **(C)** Quantification of mean±SEM b wave amplitudes in (*n*=16–18 eyes/group) uninjured control mice and in each RVO treatment group. Differences between groups were measured by one-way ANOVA with Fisher's LSD test. N eyes/group: Vehicle (18), anti-VEGF (16), Pen1-XBir3 (18), anti-VEGF+Pen1-XBir3 (17), uninjured (16). **(D)** Quantification of mean±SEM OP amplitudes in (*n*=16–18 eyes/group) uninjured control mice and in each RVO treatment group. Differences between groups were measured by one-way ANOVA with Fisher's LSD test. N eyes/group: Vehicle (18), anti-VEGF (16), Pen1-XBir3 (18), anti-VEGF+Pen1-XBir3 (17), uninjured (16).

Data availability statement

The original contributions presented in the study are included in the article/supplementary material, further inquiries can be directed to the corresponding author.

Author contributions

CT and MA contributed to the conception and design of the study. MA, CC, and JL performed the experimental procedures and data analysis. SS and GS generated XBir3 protein used in the study. CT, MA, and CC contributed to the writing, revision, and figures. CT acquired the funding. All authors contributed to the article and approved the submitted version.

Funding

This work was supported by a Sponsored Research Agreement with Opera Therapeutics to CT, by the National Institute of Neurological Disorders and Stroke (RO1 NS081333

to CT) and the Department of Defense Army/Air Force (DURIP to CT) and by the National Eye Institute (T32 EY013933 to MA).

Acknowledgments

We thank James Goldman, Columbia University for assistance with imaging H&E stained retinas.

Conflict of interest

CT and MA are listed as inventors on patent applications filed by the Trustees of Columbia University in the City of New York related to the therapeutic use of caspase-9 inhibitors. MA received consulting income from Opera Therapeutics.

The remaining authors declare that the research was conducted in the absence of any commercial or financial relationships that could be construed as a potential conflict of interest.

Publisher's note

All claims expressed in this article are solely those of the authors and do not necessarily represent those of their affiliated organizations, or those of the publisher, the editors and the reviewers. Any product that may be evaluated in this article, or claim that may be made by its manufacturer, is not guaranteed or endorsed by the publisher.

References

Akpan, N., Serrano-Saiz, E., Zacharia, B. E., Otten, M. L., Ducruet, A. F., Snipas, S. J., et al. (2011). Intranasal delivery of caspase-9 inhibitor reduces caspase-6-dependent axon/neuron loss and improves neurological function after stroke. *J. Neurosci.* 31, 8894–8904. doi: 10.1523/JNEUROSCI.0698-11.2011

An, H. K., Chung, K. M., Park, H., Hong, J., Gim, J. E., Choi, H., et al. (2019). CASP9 (caspase 9) is essential for autophagosome maturation through regulation of mitochondrial homeostasis. *Autophagy*, 16, 1–20. doi: 10.1080/15548627.2019.1695398

Apte, R. S., Chen, D. S., and Ferrara, N. (2019). VEGF in signaling and disease: beyond discovery and development. *Cells* 176, 1248–1264. doi: 10.1016/j.cell.2019.01.021

Avrutsky, M. I., Ortiz, C. C., Johnson, K. V., Potenski, A. M., Chen, C. W., Lawson, J. M., et al. (2020). Endothelial activation of caspase-9 promotes neurovascular injury in retinal vein occlusion. *Nat. Commun.* 11:3173. doi: 10.1038/s41467-020-16902-5

Avrutsky, M. I., and Troy, C. M. (2021). Caspase-9: a multimodal therapeutic target with diverse cellular expression in human disease. *Front. Pharmacol.* 12:701301. doi: 10.3389/fphar.2021.701301

Campochiaro, P. A., Sophie, R., Pearlman, J., Brown, D. M., Boyer, D. S., Heier, J. S., et al. (2014). Long-term outcomes in patients with retinal vein occlusion treated with ranibizumab: the RETAIN study. *Ophthalmology* 121, 209–219. doi: 10.1016/j.ophtha.2013.08.038

Chatziralli, I. P., Sergentanis, T. N., and Sivaprasad, S. (2016). Hyperreflective foci as an independent visual outcome predictor in macular edema due to retinal vascular diseases treated with intravitreal dexamethasone or ranibizumab. *Retina* 36, 2319–2328. doi: 10.1097/IAE.0000000000001070

Chen, C. W., Potenski, A. M., Colon Ortiz, C. K., Avrutsky, M. I., and Troy, C. M. (2022). In vivo vascular injury readouts in mouse retina to promote reproducibility. *J. Vis. Exp*. doi: 10.3791/63782

Colon Ortiz, C., Neal, A. M., Avrutsky, M. I., Choi, M., Smart, J., Lawson, J., et al. (2022). Neurovascular injury associated non-apoptotic endothelial caspase-9 and astroglial caspase-9 mediate inflammation and contrast sensitivity decline. *Cell Death Dis.* 13:937. doi: 10.1038/s41419-022-05387-3

Colón Ortiz, C., Potenski, A., Lawson, J. M., Smart, J., and Troy, C. M. (2021). Optimization of the retinal vein occlusion mouse model to limit variability. *J. Vis. Exp.* doi: 10.3791/62980

Denault, J. B., Eckelman, B. P., Shin, H., Pop, C., and Salvesen, G. S. (2007). Caspase 3 attenuates XIAP (X-linked inhibitor of apoptosis protein)-mediated inhibition of caspase 9. *Biochem J* 405, 11–19. doi: 10.1042/BJ20070288

Domigan, C. K., Warren, C. M., Antanesian, V., Happel, K., Ziyad, S., Lee, S., et al. (2015). Autocrine VEGF maintains endothelial survival through regulation of metabolism and autophagy. *J. Cell Sci.* 128, 2236–2248. doi: 10.1242/jcs.163774

Dupont, E., Prochiantz, A., and Joliot, A. (2011). Penetratin story: an overview. *Methods Mol Biol* 683, 21–29. doi: 10.1007/978-1-60761-919-2_2

Fuma, S., Nishinaka, A., Inoue, Y., Tsuruma, K., Shimazawa, M., Kondo, M., et al. (2017). A pharmacological approach in newly established retinal vein occlusion model. *Sci. Rep.* 7:43509. doi: 10.1038/srep43509

Hasegawa, T., Yamashita, M., Maruko, I., Koizumi, H., Kogure, A., Ogata, N., et al. (2017). Optical coherence tomographic predictor of retinal non-perfused areas in eyes with macular oedema associated with retinal vein occlusion. *Br. J. Ophthalmol.* 101, 569–573. doi: 10.1136/bjophthalmol-2016-308813

Ho, M., Liu, D. T., Lam, D. S., and Jonas, J. B. (2016). Retinal vein occlusions, from basics to the latest treatment. *Retina* 36, 432–448. doi: 10.1097/IAE.0000000000000843

Khayat, M., Lois, N., Williams, M., and Stitt, A. W. (2017). Animal models of retinal vein occlusion. *Invest. Ophthalmol. Vis. Sci.* 58, 6175–6192. doi: 10.1167/iovs.17-22788

Khayat, M., Williams, M., and Lois, N. (2018). Ischemic retinal vein occlusion: characterizing the more severe spectrum of retinal vein occlusion. *Surv. Ophthalmol.* 63, 816–850. doi: 10.1016/j.survophthal.2018.04.005

Mo, B., Zhou, H. Y., Jiao, X., and Zhang, F. (2017). Evaluation of hyperreflective foci as a prognostic factor of visual outcome in retinal vein occlusion. *Int. J. Ophthalmol.* 10, 605–612. doi: 10.18240/ijo.2017.04.17

Nishinaka, A., Inoue, Y., Fuma, S., Hida, Y., Nakamura, S., Shimazawa, M., et al. (2018). Pathophysiological role of VEGF on retinal edema and nonperfused areas in mouse eyes with retinal vein occlusion. *Invest. Ophthalmol. Vis. Sci.* 59, 4701–4713. doi: 10.1167/iovs.18-23994

Rachima, S., Hirabayashi, K., Imai, A., Iesato, Y., and Murata, T. (2020). Prediction of post-treatment retinal sensitivity by baseline retinal perfusion density measurements in eyes with branch retinal vein occlusion. *Sci. Rep.* 10:9614. doi: 10.1038/s41598-020-66708-0

Reinders, M. E., Sho, M., Izawa, A., Wang, P., Mukhopadhyay, D., Koss, K. E., et al. (2003). Proinflammatory functions of vascular endothelial growth factor in alloimmunity. *J. Clin. Invest.* 112, 1655–1665. doi: 10.1172/JCI17712

Spengler, K., Kryeziu, N., Große, S., Mosig, A. S., and Heller, R. (2020). VEGF triggers transient induction of autophagy in endothelial cells via AMPKα1. *Cells* 9:687. doi: 10.3390/cells9030687

Wecker, T., Ehlken, C., Buhler, A., Lange, C., Agostini, H., Bohringer, D., et al. (2017). Five-year visual acuity outcomes and injection patterns in patients with pro-re-nata treatments for AMD, DME, RVO and myopic CNV. *Br. J. Ophthalmol.* 101, 353–359. doi: 10.1136/bjophthalmol-2016-308668

frontiers | Frontiers in Neuroscience

TYPE Review
PUBLISHED 11 July 2023
DOI 10.3389/fnins.2023.1216489

OPEN ACCESS

EDITED BY
Dan Wen,
Central South University, China

REVIEWED BY
Michael Risner,
Vanderbilt University, United States
Francesco Di Virgilio,
University of Ferrara, Italy

*CORRESPONDENCE
Joanne A. Matsubara
✉ jms@mail.ubc.ca

RECEIVED 03 May 2023
ACCEPTED 26 June 2023
PUBLISHED 11 July 2023

CITATION
Molcak H, Jiang K, Campbell CJ and Matsubara JA (2023) Purinergic signaling via P2X receptors and mechanisms of unregulated ATP release in the outer retina and age-related macular degeneration.
Front. Neurosci. 17:1216489.
doi: 10.3389/fnins.2023.1216489

Purinergic signaling via P2X receptors and mechanisms of unregulated ATP release in the outer retina and age-related macular degeneration

Haydn Molcak[1], Kailun Jiang[1], Christopher J. Campbell[2] and Joanne A. Matsubara[1]*

[1]Matsubara Lab, Faculty of Medicine, Department of Ophthalmology and Visual Sciences, Eye Care Centre, Vancouver, BC, Canada, [2]Paragon Ventures Inc, Vancouver, BC, Canada

Age-related macular degeneration (AMD) is a chronic and progressive inflammatory disease of the retina characterized by photoceptor loss and significant central visual impairment due to either choroidal neovascularization or geographic atrophy. The pathophysiology of AMD is complex and multifactorial, driven by a combination of modifiable and non-modifiable risk factors, molecular mechanisms, and cellular processes that contribute to overall disease onset, severity, and progression. Unfortunately, due to the structural, cellular, and pathophysiologic complexity, therapeutic discovery is challenging. While purinergic signaling has been investigated for its role in the development and treatment of ocular pathologies including AMD, the potential crosstalk between known contributors to AMD, such as the complement cascade and inflammasome activation, and other biological systems, such as purinergic signaling, have not been fully characterized. In this review, we explore the interactions between purinergic signaling, ATP release, and known contributors to AMD pathogenesis including complement dysregulation and inflammasome activation. We begin by identifying what is known about purinergic receptors in cell populations of the outer retina and potential sources of extracellular ATP required to trigger purinergic receptor activation. Next, we examine evidence in the literature that the purinergic system accelerates AMD pathogenesis leading to apoptotic and pyroptotic cell death in retinal cells. To fully understand the potential role that purinergic signaling plays in AMD, more research is needed surrounding the expression, distribution, functions, and interactions of purinergic receptors within cells of the outer retina as well as potential crosstalk with other systems. By determining how these processes are affected in the context of purinergic signaling, it will improve our understanding of the mechanisms that drive AMD pathogenesis which is critical in developing treatment strategies that prevent or slow progression of the disease.

KEYWORDS

purinergic signaling, age-related macular degeneration, ATP, complement, inflammasome, P2X

Introduction

Purinergic signaling is a form of extracellular signaling involving purine and pyrimidine nucleotides and nucleosides that act on purinergic receptors to mediate numerous cellular functions (Burnstock, 2008). In total, there are three distinct classes of purinergic receptors known as P1, P2Y, and P2X receptors. P1 receptors are G protein-coupled receptors (GPCRs) that respond to adenosine (Burnstock, 2018). P2Y receptors are GPCRs that respond to nucleotides such as adenosine triphosphate (ATP), adenosine diphosphate (ADP), adenosine monophosphate (AMP), adenosine, uridine triphosphate (UTP), uridine diphosphate (UDP), and UDP-glucose (Burnstock, 2018). P2X receptors are unique and function as ligand-gated ion channels that respond exclusively to extracellular ATP (eATP) (Burnstock, 2018). Purinergic signaling represents a set of phylogenetically ancient pathways that play a critical role in numerous cellular processes, bodily systems, and developmental stages, including proliferation, differentiation, migration, apoptosis, embryogenesis, organogenesis, and aging (Burnstock and Dale, 2015; Huang et al., 2021). Within the eye, purinergic signaling has been investigated for its role in the development and treatment of ocular pathologies such as age-related macular degeneration (AMD), glaucoma, and diabetic retinopathy (Ye et al., 2021).

AMD is a leading cause of visual impairment and accounts for approximately 9% of all cases of blindness worldwide (Wong et al., 2014). The pathophysiology of AMD is complex and multifactorial, driven by a combination of non-modifiable risk factors (e.g., aging, genetic predisposition) and modifiable risk factors (e.g., smoking, hypertension, body mass index, hypercholesterolemia, nutritional intake, UV light) that contribute to overall disease onset, severity, and progression (Ambati and Fowler, 2012; Wong et al., 2014; Mitchell et al., 2018; de Jong et al., 2020; Stahl, 2020). AMD can be subdivided into early, intermediate, and advanced stages, with the advanced forms characterized by photoreceptor loss in the macula, the region of the retina responsible for central vision. There are two forms of advanced AMD. Wet (or exudative) AMD (~10% of cases) develops due to choroidal neovascularization (CNV), a form of abnormal angiogenesis in the choriocapillaris layers of the choroid, which results in the growth of neo-vessels breaching Bruch's membrane, causing photoreceptor death (Mitchell et al., 2018). Dry (or non-exudative) AMD (~90% of cases) is a slowly progressing degenerative process whereby regions of retinal pigment epithelium (RPE), a monolayer of cells that combine with Bruch's membrane and form the outer blood-eye barrier, undergo cell death leading to geographic atrophy (GA) (Mitchell et al., 2018). The early stages of both forms are characterized by the buildup of drusen deposits, which are composed of glycoproteins, lipids, and immunogenic factors. The drusen accumulate in the extracellular space between the RPE and Bruch's membrane and provoke a chronic proinflammatory milieu that triggers the development of AMD (Mitchell et al., 2018).

Despite the emergence of anti-vascular endothelial growth factor (VEGF) agents to treat wet AMD, there are currently no therapies available to prevent the development of dry AMD aside from nutritional supplementation (AREDS formulation) (Age-Related Eye Disease Study Research Group, 2001). However, in 2023, the FDA approved pegcetacoplan, a complement C3 inhibitor, to slow the progression of GA, providing some promise for those with late-stage GA. It is also possible for a portion of patients with wet AMD to develop severe vision loss and blindness by developing GA over time, further emphasizing the complex nature of AMD pathogenesis (Holz et al., 2014; Rasmussen and Sander, 2014; Agarwal et al., 2015; Chen and Kaiser, 2020). Thus, understanding the multiple mechanisms that drive AMD and the interplay between wet and dry forms, is crucial in developing treatment strategies that not only slow the progression of the disease, but ultimately prevent its development.

In the present review, we explore purinergic signaling and mechanisms of unregulated ATP release in the outer retina, and its potential significance in AMD pathogenesis. While there is evidence for an interplay between purinergic signaling and the mechanisms associated with AMD pathogenesis such as complement dysregulation, inflammasome activation, and sublytic membrane attack complex (MAC) deposition, few studies have addressed their detailed interactions. We first begin by identifying what is known about purinergic receptors in cell populations of the outer retina along with potential sources of eATP required to trigger purinergic receptor activation. Next, we examine evidence in the literature that the purinergic system accelerates AMD pathogenesis leading to apoptotic and pyroptotic cell death in RPE, photoreceptors, and choroidal cells.

Purinergic signaling

The purinergic system is a form of cell signaling in which both purine and pyrimidine nucleotides and nucleosides act on extracellular purinergic receptors (Burnstock, 2008). As outlined above, purinergic receptors are divided into two classes known as P1 and P2 receptors. P1 receptors are GPCRs that respond to the nucleoside adenosine (Burnstock, 2018). In contrast, P2 receptors are nucleotide receptors that are further subdivided into P2X and P2Y receptors. P2Y receptors are GPCRs that respond to several nucleotides such as ATP, ADP, AMP, UTP, UDP, and UDP-glucose (Burnstock, 2018). P2X receptors are ligand-gated ion channels that respond exclusively to eATP (Burnstock, 2018). This review will focus on P2X receptors which are composed of two transmembrane domains with cytoplasmic amino-and carboxyl-terminals that polymerize to form homotrimeric or heterotrimeric channels permeable to cations such as sodium, potassium, and calcium (Jacobson et al., 2020). In total, seven homotrimeric P2X receptors (P2X1-7) and several heterotrimeric P2X channels with hybrid properties exist (Ralevic and Burnstock, 1998; Jacobson et al., 2020; Santiago et al., 2020; Illes et al., 2021). Table 1 outlines the unique features of P2X1-7 receptors based on their functional and pharmacological properties (Illes et al., 2021). For a comprehensive review of purinergic signaling and current developments in this field, please see Burnstock (2006, 2017).

Due to its well-established role in several inflammatory processes, a significant quantity of research has been performed surrounding P2X7. However, normal extracellular concentrations of ATP are approximately 10 nM under steady-state conditions, and the half maximal effective concentration (EC50) for P2X7 receptor activation is approximately 100 μM. Furthermore, once ATP is released, it can be rapidly degraded by ecto-enzymes yielding ADP, AMP, and adenosine, further decreasing the concentrations of ATP available for P2X activation. This means that the concentration of ATP required to activate P2X7 receptors is considerably higher than that found under physiological conditions leading to past debate surrounding its

TABLE 1 P2X receptors showing their molecular, pharmacologic, and functional properties [Adapted from Illes et al. (2021)].

	P2X1	P2X2	P2X3	P2X4	P2X5	P2X6	P2X7
ATP EC50 (μM)	0.56–0.7	2–8	0.5–1	1–10	0.44–10	12	100
Desensitization	Rapid (<1 s)	Slow (>20s) or no desensitization	Rapid (<1 s)	Slow (>20s)	Slow (>20s)	Slow (>20s)	Slow (>20s)
Function	Non-selective cationic channel	Non-selective cationic channel	Non-selective cationic channel	Non-selective cationic channel Permeability for Ca2+ among highest in P2X family	Non-selective cationic channel Permeable to chloride ions	Non-selective cationic channel	Non-selective cationic channel
Large Pore	No	Yes	No	Yes	-	-	Yes
Functional Heterotrimers	P2X2, P2X4, P2X5	P2X1, P2X3, P2X5, P2X6	P2X2	P2X1, P2X6	P2X1, P2X2	P2X2, P2X4	P2X4
Location/ Cellular Expression Within the Retina	Inner plexiform layer, Muller cells, endothelial cells, glial cells	Amacrine cells, Muller cells, neurons	Amacrine cells, neurons	Glial cells, endothelial cells, neurons, horizontal cells of retina, amacrine and ganglion cells of the retina, Muller cells	Amacrine cells	Nerve fiber layer	Plexiform layers, horizontal cells, photoreceptors, amacrine cells, ganglion cells, glial cells, RPE, choroid, Muller cells

physiological relevance, especially in early stages of disease or inflammatory processes (Yang et al., 2011). However, with the novel introduction of plasma membrane luciferase (pmeLUC) which has made direct measurements of eATP possible, the concentration of eATP has been shown to reach 100–200 μM (Pellegatti et al., 2005, 2008; Morciano et al., 2017; Romagnani et al., 2020). Additionally, positive allosteric modulators acting at P2X7 are released into circulation during inflammation, thus further increasing the affinity of P2X7 for ATP (Tomasinsig et al., 2008; Kahlenberg and Kaplan, 2013; Di Virgilio et al., 2018). Secreted or membrane-bound ecto-kinases such as adenylate kinase, nucleoside monophosphokinases, and nucleoside diphosphokinases can also phosphorylate nucleosides to produce AMP, ADP, and ATP (Schwiebert and Zsembery, 2003). Taken together, there are several mechanisms whereby the concentration of eATP is capable of activating any and all of the P2X family of receptors. While questions remain surrounding the underlying pathways of P2X7 signaling in AMD, there is a significant gap in the literature surrounding other members of the P2X family of receptors, including novel and hybrid properties of heterotrimers, that may play an important role in various cellular and inflammatory processes.

Purinergic signaling in the retina

The organization of the retina has been well studied for its complex synaptic circuitry of retinal neurons, supported by two vascular beds, an inner (retinal) and outer (choroidal) retinal supply. The outer vascular bed is comprised of the choroidal circulation that supports the outer retina and plays an important homeostatic role for the retinal pigment epithelium (RPE) and photoreceptors (Figure 1). For cells of the inner neuroretina, RPE, choroid, and retinal vasculature, purinergic receptors from each receptor class are present (Yang et al., 2011; Wagner et al., 2013; Jacobson and Civan, 2016). This is important, as purinergic signaling has been implicated in the proliferation, survival, death, migration, and differentiation of retinal cells throughout development, aging, and in disease states. For a review on purinergic signaling in the inner retina, please see Ventura et al. (2019) and Sanderson et al. (2014). Here, we discuss the distribution and functions of purinergic receptors on cells present within the outer retina, including the RPE and choroid, that may influence and contribute to AMD pathogenesis (Figure 2).

Retinal pigment epithelium

The RPE is considered a primary site of pathology in AMD (Strauss, 2005; Bhutto and Lutty, 2012). It is supported by Bruch's membrane, an important extracellular matrix that separates the RPE from the choroidal blood supply. The RPE is positioned between the overlying outer segments of photoreceptors and the choroidal blood supply and combines the functions of epithelial and glial cells to act as both a barrier and supporting tissue for overlying photoreceptors (Strauss, 2005; Bhutto and Lutty, 2012). Indeed, communication between photoreceptors and the RPE is critical to retinal function and occurs through a small extracellular space that exists between the apical membrane of RPE cells and photoreceptors (Mitchell and Reigada, 2008). Located within this space is an abundance of enzymes and a highly structured extracellular matrix that allows for many functional interactions between the RPE and photoreceptors to take place (Mitchell and Reigada, 2008). For example, the RPE delivers nutrients from the choroidal blood supply to the photoreceptors, removes metabolic end products from photoreceptors, produces melanin granules to absorb stray light, and recycles molecules important for maintenance of the visual cycle (Strauss, 2005; Mitchell

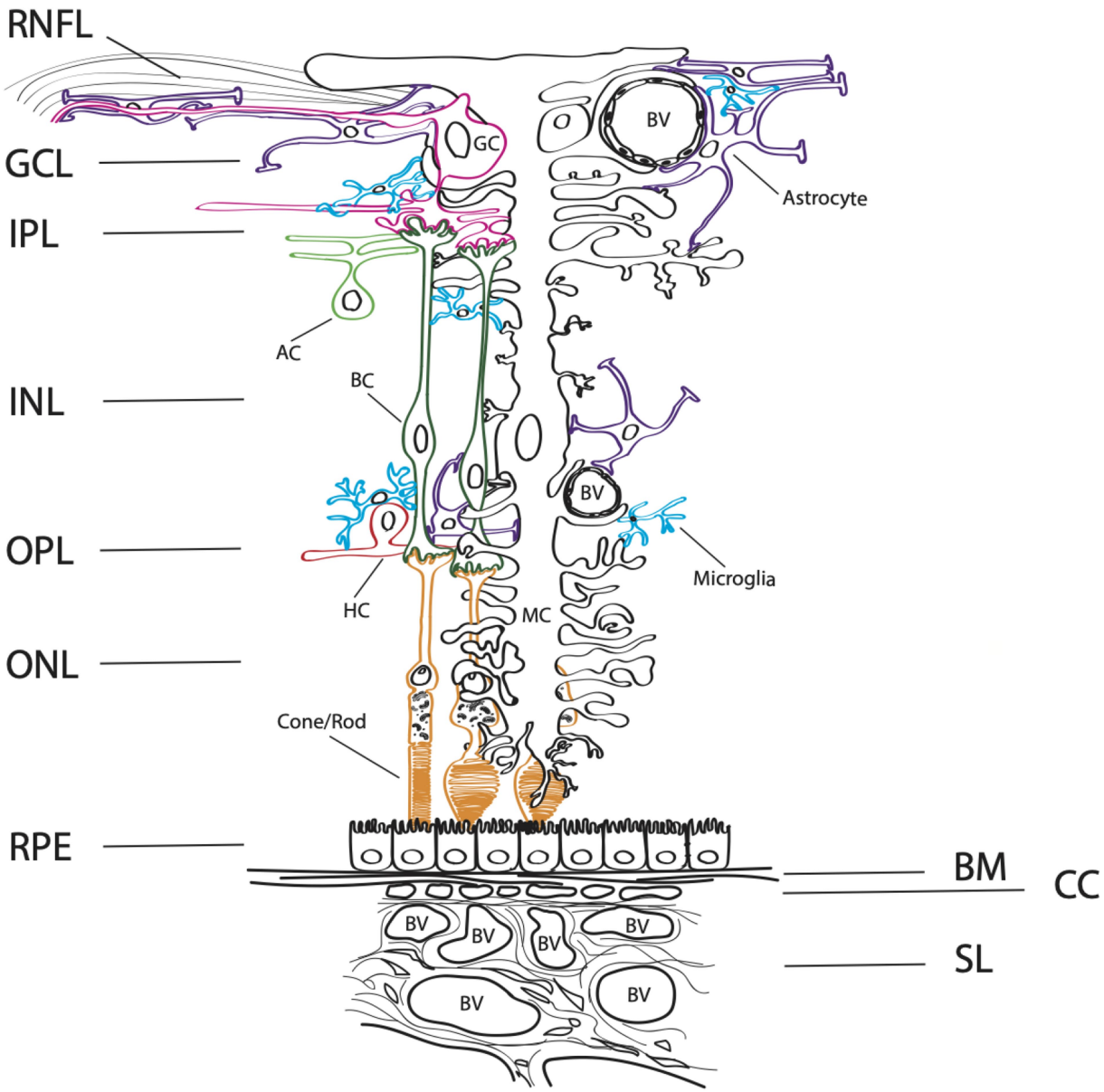

FIGURE 1
Complex architecture of the human retina. A schematic diagram of a cross-section through the retina. The layers of the neuroretina from inner to outer include: the retinal nerve fiber layer (RNFL), ganglion cell layer (GCL), inner plexiform layer (IPL), inner neuronal layer (INL), outer plexiform layer (OPL), and outer neuronal layer (ONL). Below the neuroretina is the retinal pigment epithelial layer (RPE) which is a monolayer of cells that sit on the extracellular matrix basement membrane, Bruch's membrane (BM). The outer retinal is supplied by the choroidal blood circulatory system, comprised of the choriocapillaris (CC), the small vessel layer (SL) and the large vessel layer (not shown). Blood vessels (BV) are depicted within the figure. The retinal neurons in the inner retina include bipolar cells (BC, dark green), ganglion cells (GC, pink), amacrine cells (AC, light green), horizontal cells (HC, red), and rod and cone photoreceptors (orange). Microglia (blue), astrocytes (purple) and the Muller cells, a specialized astrocyte (MC, black) are supportive glial cell types that provide homeostasis and metabolic support for the retina.

and Reigada, 2008; Bhutto and Lutty, 2012). The RPE also plays an integral role in the daily renewal of photoreceptors through the recycling and resynthesis of spent outer segments (Strauss, 2005; Mitchell and Reigada, 2008; Bhutto and Lutty, 2012).

While RPE cells have been found on exon level profiling to express all subtypes of purinergic receptors (Wagner et al., 2013), the distribution of P2X receptors in human RPE cells is not completely known and few studies have explored the role of P2X receptors within the outer retina. For example, Yang et al. (2011) found P2X7 receptor mRNA in human RPE cells and functional data indicating that in addition to P2X7, other P2X receptors such as P2X1, P2X2, P2X3, P2X4, and P2X5 may also be present. However, further studies are needed to understand the expression, localization, and functions of these receptors within RPE cells.

Perhaps the most well-characterized of these receptors in the RPE to date is the P2X7 receptor, which induces calcium signaling and the activation of numerous cellular pathways that lead to subsequent apoptosis in both native and cultured human RPE cells (Yang et al., 2011). RPE cell death also results in the release of proinflammatory cytokines and further unregulated release of ATP thereby increasing

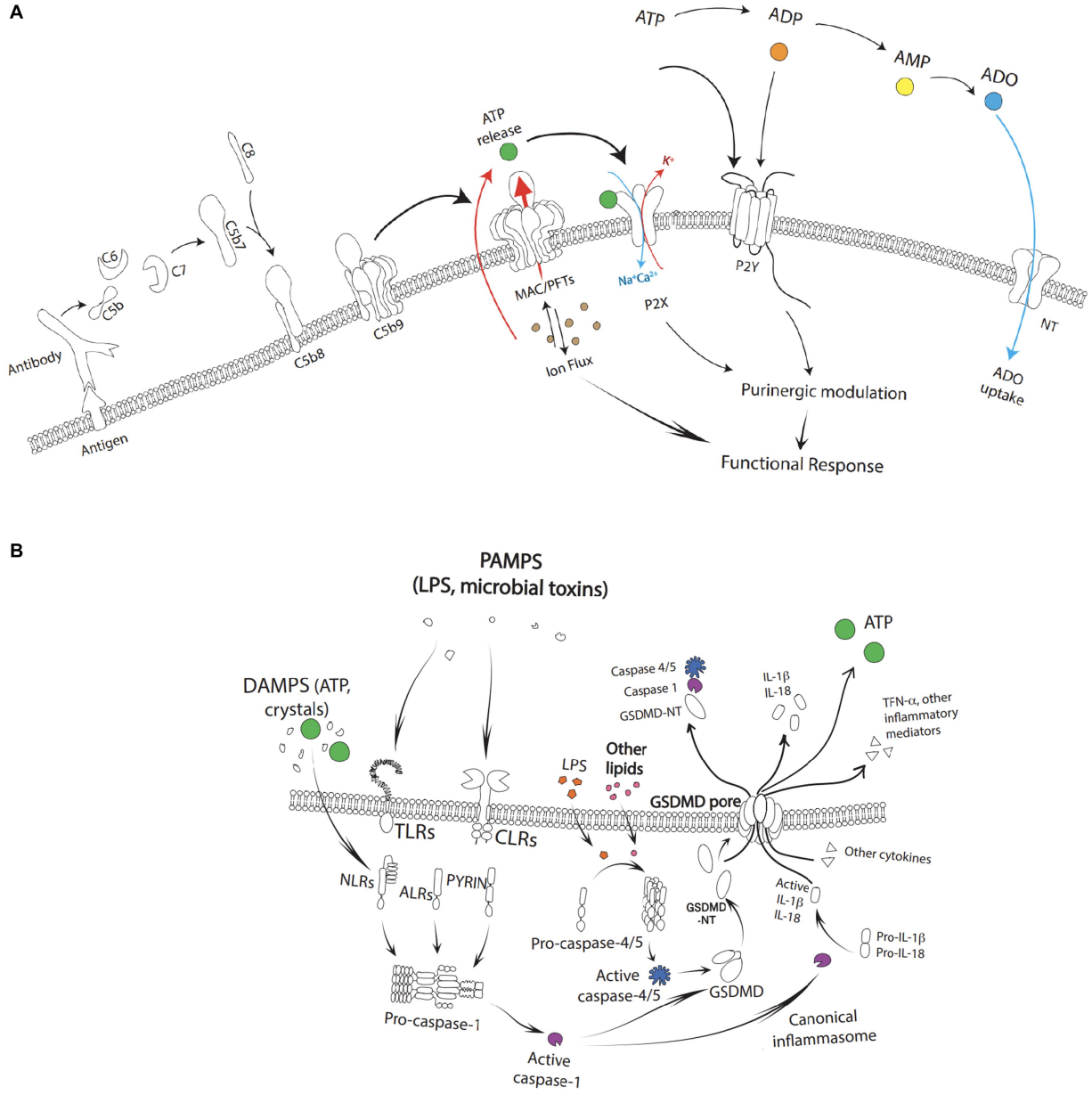

FIGURE 2
(A) Complement activation with the formation of the C5b-9(n) leading to the formation of a MAC/PFTs complex. The fully formed MAC creates large, 10nm-wide pores initiating an ion flux cumulating in a calcium dependent cell lysis. As a result of cell lysis, high concentrations of ATP may be released into the local environment which can simulate P2X and activate downstream purinergic modification. Extracellular ATP similarly can activate P2Y. Extracellular adenosine is re-cycled back into the cytoplasm via the nucleoside transporters (NT). **(B)** Pathogen-associated molecular patterns (PAMPs) and damage-associated molecular patterns (DAMPs) such as toxins, pathogens, metabolites, crystalline substances, nucleic acids, ion flux, reactive oxygen species, and ATP stimulate toll-like receptors (TLRs) and c type lectin receptors (CLRs) leading to activation of NF-κB followed by the subsequent transcriptional upregulation of NOD-like receptor family pyrin domain containing 3 (NLRP3) and pro-interleukin-1β. The cascade as depicted leads to the formation of gasdermin-D (GSDMD) and pyroptotic cell death through activation of caspase-4/5, capase-1, and GSDMD-NT along with release of ATP and other pro-inflammatory factors such as IL-1b, IL-18, and TFN-α.

the vulnerability of other cells to ATP-induced apoptosis (Yang et al., 2011). Increasing concentrations of eATP released from stressed, injured, or damaged outer retinal cells (in the case of AMD and other retinal diseases) also influence aspects of their overall function as support cells for the inner neuroretina through cytokine and growth factor release and as a stimulant for proliferation and differentiation (Notomi et al., 2011; Niyadurupola et al., 2013; Notomi et al., 2013; Clapp et al., 2019; Platania et al., 2019).

An important aspect of P2X signaling in RPE cells is that under physiological circumstances, these cells can maintain homeostasis and prevent ATP-induced apoptosis by expressing high levels of the enzymes CD39 and CD73 within their membranes. CD39 is an ectonucleoside triphosphate diphosphohydrolase (NTPDase) that rapidly hydrolyzes ATP and ADP to AMP, while CD73 is an ectonucleotidase that degrades AMP to adenosine (Kukulski et al., 2011; Dwyer et al., 2020). Interestingly, after being exposed to

inflammatory factors, Zhang et al. (2018) demonstrated that RPE cells can rapidly become CD73-negative. This was found to be the result of matrix metalloproteinase-9 (MMP-9)-mediated shedding of CD73 from the cell membrane of RPE after exposure to inflammatory factors *in vitro*, leading to impaired immune suppression, increased concentrations of eATP, and accelerated local inflammation in the AMD environment (Zhang et al., 2018).

Immune cells

All immune cells, whether of the myeloid or lymphoid lineage, express at least one P2X receptor subtype, and many express all seven subtypes (Burnstock, 2016). Within the outer retina and choroid, these immune cells include resident retinal microglia, mast cells, lymphocytes, monocytes, and dendritic cells (Sarma and Ward, 2011; Merle et al., 2015a,b; Di Virgilio et al., 2017; Behnke et al., 2020; Di Virgilio et al., 2020; Ogura et al., 2020).

Microglia

Microglia are resident professional phagocytes of the CNS, similar in function to blood-borne peripheral immune cells including monocytes, macrophages, and lymphocytes. They possess a high density of P2X7 receptors (Illes et al., 2017, 2020) in addition to P2X1 and P2X4 (Di Virgilio et al., 2020). Further, their ability to function as scavengers by migrating toward and clearing insoluble photo-oxidized material found in drusen has been shown to result from purinergic signaling interactions, such as in the case of ATP and P2X7 receptor activation (Gu and Wiley, 2018). Indeed, the heterogeneous expression of P2X1, P2X4, and P2X7 receptors on the surface of macrophages with varying ATP affinities may enable fine-tuning of macrophage responses to ATP (Guo et al., 2007; Adinolfi et al., 2018). This can result in distinct desensitization kinetics and diverse intracellular transduction pathways that contribute to numerous pro-inflammatory pathways in a concentration-dependent manner (Adinolfi et al., 2018).

Genetic association studies have also investigated this link by identifying a unique haplotype containing a heterotrimeric combination of P2X4 and P2X7 subunits that increases an individual's risk of developing AMD due to impaired P2X7 function. This results in reduced phagocytic capacity of macrophages, delayed clearance of apoptotic cells, and leakage of ATP from necrotic cells (Gu et al., 2013). Furthermore, P2X7-null mice models demonstrated reduced blood-borne macrophage phagocytosis activity resulting in thickening of Bruch's membrane, RPE dysfunction, and retinal stress at 12 months of age (Vessey et al., 2017), followed by Bruch's membrane thickening, RPE cell loss, retinal functional deficits, and signs of inflammation between the RPE and photoreceptors at 18 months of age – phenotypic characteristics consistent with early AMD (Vessey et al., 2017). Taken together, communication between macrophages occurs, in part, via purinergic signaling.

Other studies also support the role of ATP in regulating macrophage chemotaxis and macrophage activation (Kronlage et al., 2010; Junger, 2011; Sakaki et al., 2013). This outlines a potential mechanism for the role of purinergic signaling in the pathogenesis of AMD, whereby immune cells present within the outer retina are no longer able to manage the task of removing the constant supply of photoreceptor debris, leading to the progressive and damaging accumulation of drusen within Bruch's membrane, activation of bystander cells, worsening nutrient and oxygen support for the RPE, and a vicious cycle of RPE failure, neuronal cell death, and central vision loss (Strauss, 2005; Zumerle et al., 2019).

Mast cells

Mast cells (MCs) are recognized as key components of inflammatory reactions and are implicated in several inflammatory diseases. They are responsive to toxins and microbes, as well as substances such as advanced glycation end products, complement factors, C-reactive protein, and ATP, all of which are implicated in AMD (Ogura et al., 2020). Of the seven P2X receptors, only five (P2X1, P2X3, P2X4, P2X6, and P2X7) are expressed by MCs (Wareham et al., 2009; Wareham and Seward, 2016). These receptors play an important role in regulating MC activities, such as calcium influx and degranulation that results in the release of many pre-stored inflammatory mediators (Bulanova and Bulfone-Paus, 2010). Inflammatory mediators include IL-1β, Nuclear factor kappa B (NF-κB), tumor necrosis factor α (TNF-α), serotonin, and kinins, along with the synthesis and secretion of an array of cytokines, chemokines, prostaglandins, leukotrienes, and growth and angiogenesis factors (i.e., platelet-derived growth factor and VEGF) (Galli and Tsai, 2008; Bulanova and Bulfone-Paus, 2010; Kurashima et al., 2012; Theoharides et al., 2012; Shieh et al., 2014; Salcman et al., 2021). These MC components can modulate the activity of cells in their proximity and lead to the generation of reactive oxygen species (ROS), promotion of chemotaxis, altered phagocytosis, degradation of underlying extracellular matrix (ECM), and other events contributing to an overall increase in inflammation (Bhutto et al., 2016; Kempuraj et al., 2016; Caraffa et al., 2018).

In the pathogenesis of AMD, MC-derived tryptase release also results in the breakdown of collagens and activation of MMPs that degrade choroidal stroma and Bruch's membrane. This leads to thinning of the choroid and degeneration of the RPE, both of which are hallmarks of GA (Ogura et al., 2020). Additionally, MC activation has been implicated in choroidal neovascularization through granzyme B release through intracellular immune-mediated cell death and extracellular ECM degradation (Matsubara et al., 2020). This results in remodeling of the ECM in Bruch's membrane, breakdown of the blood-retina barrier, and slowing of metabolite transport between the choroidal blood supply and retina, which can contribute to drusen deposition, vascular leakage, disruption of choroidal endothelial cell function, and the release of sequestered VEGF from Bruch's membrane (Matsubara et al., 2020).

Choroid and retinal vasculature

The retina is nourished by two independent vascular supplies (Figure 1). The outer retina and photoreceptors are fed by the choroidal vasculature that lies directly beneath the photoreceptors and the RPE, while the inner retina is served by intrinsic retinal vasculature, branches of the central retinal artery that enter at the optic disc (Newman, 2015). As autonomic innervation is absent in the generation of retinal vascular tone, the tone of these vessels must

be generated by intrinsic mechanisms such as the release of vasoactive agents from neurons, glial cells, and vascular endothelial cells (Kur et al., 2012; Newman, 2015). For this reason, purinergic signaling involving ATP has been explored as a mechanism to generate tone in retinal arterioles (Kur and Newman, 2014). Indeed, experiments have demonstrated that a reduction of endogenous eATP levels leads to arteriole dilation, while an increase in eATP levels leads to vessel constriction through altered P2X1 receptor activity (Kur et al., 2012; Newman, 2015).

Purinergic signaling also results in choroidal and retinal neovascularization through remodeling of existing vasculature and proteolytic degradation of the endothelial basal membrane and surrounding extracellular matrix via MMP-2 and MMP-9 activation (Yancopoulos et al., 2000; Berglin et al., 2003). Additionally, stimulation of P2X receptors promotes VEGF release and alters endothelial barrier properties depending on the type of receptors present and the local concentration of the nucleotides within the vasculature (Adinolfi et al., 2018). For instance, chronic P2X receptor activation with ATP acting as a danger-associated molecular pattern (DAMP) at high concentrations leads to endothelial barrier destabilization and edema formation through impaired Müller cell function in the induction, maintenance, and proper functioning of the blood–retinal barrier (Shen et al., 2012; Wakx et al., 2016). Together, these processes can contribute to retinal degeneration under pathologic conditions such as the proinflammatory environment seen in AMD.

Mechanisms of ATP release

Broadly, mechanisms of intermittent ATP release can be the result of (1) cell damage or cell death (e.g., complement activation and MAC deposition, osmotic swelling, ischemia, inflammation, or apoptosis leading to the passive leakage of ATP from cells), (2) vesicular release, or (3) channel-mediated release (Bulanova and Bulfone-Paus, 2010). However, sustained ATP release which is likely the ATP release of pathophysiological significance can also result from a multiplicity of pathways (Lazarowski et al., 2003; Dale et al., 2023; Di Virgilio et al., 2023; Shinozaki et al., 2023). Within the outer retina, several processes that contribute to AMD pathogenesis lead to ATP release (Figure 2). For example, activation of the complement cascade results in ATP release from MAC deposition leading to inflammasome activation, the release of pore-forming gasdermins, and pyroptosis. ATP release can also act as a feedforward method to trigger P2X receptors and further promote cell degeneration in the AMD outer retina. Recently, apoptosis has also been shown to release ATP as a "find me" signal through Pannexin 1 channels (Medina et al., 2020).

Complement system

The complement system plays a central role in AMD pathogenesis, along with aspects of cellular immunity and homeostasis. It consists of a network of proteins that can be sequentially cleaved and activated through any of three distinct pathways: the classical pathway, the lectin pathway, and/or the alternative pathway (Ricklin et al., 2010; Sarma and Ward, 2011; Merle et al., 2015a,b). Each of these pathways converge in the terminal pathway of the complement system, which results in the formation of the C5b-9(n) MAC complex. Fully formed MAC creates large, 10 nm-wide, pores in the membranes of pathogens and vulnerable host cells and can result in calcium dependent cell lysis (Sarma and Ward, 2011; Merle et al., 2015a,b). For a comprehensive review of complement and its role in AMD, please see Armento et al. (2021).

As a result of cell lysis, high concentrations of ATP may be released into the local environment. This can stimulate P2X receptors and influence the recruitment and activation of numerous inflammatory cells such as retinal microglia, mast cells, and circulating lymphocytes, monocytes, and macrophages, as described above (Ricklin et al., 2010; Sarma and Ward, 2011; Merle et al., 2015a,b; Behnke et al., 2020; Ogura et al., 2020). Ultimately, this amplification loop can: (1) induce changes in the composition of Bruch's membrane, the choriocapillaris, and ECM, (2) impair transport properties, alter lipid metabolism, and result in the accumulation of drusen, and (3) lead to chronic inflammation, oxidative stress, and altered energy metabolism as seen in the pathogenesis of AMD (Armento et al., 2021).

These findings are echoed by genetic studies where over 33 different loci associated with aspects of the complement system, ECM remodeling, and other pathways such as cholesterol metabolism have demonstrated an increased risk for the development of AMD (Klein et al., 2005; Schramm et al., 2014; Black and Clark, 2016). Complement activation can also alter the expression of MMP-2 and MMP-9 in various cell types, including RPE (Bandyopadhyay and Rohrer, 2012). As discussed above, this can result in ECM turnover, neovascularization due to imbalances in VEGF secretion, altered ATP metabolism due to interactions with extracellular nucleosides, and increased purinergic signaling.

Sublytic MAC formation and pore forming toxins

MAC deposition does not always result in lysis of host cells due to the presence of regulatory proteins and active repair processes. For example, active repair processes such as MAC plugging, exocytosis, and endocytosis repair cell membranes and remove MAC pores before lysis can take place to limit sustained elevations in intracellular calcium (Kunchithapautham and Rohrer, 2011). Other regulatory processes include CD59, a membrane-bound GPI-anchored protein that inhibits the addition of C9 into the C5b-8/9 complex on host cells, which limits mean MAC lesion size (Kunchithapautham and Rohrer, 2011). Soluble inhibitors such as vitronectin or clusterin that bind to the C5b-7 structure of the MAC can also prevent its attachment to cell membranes, rendering it water-soluble and inactive (Kunchithapautham and Rohrer, 2011). Notably, these changes in MAC lesion size and binding affect the kinetics of ATP release and ion flux thereby influencing aspects of purinergic signaling.

Under sublytic conditions, several effects have been described that are hypothesized to contribute to the development and progression of both dry and wet forms of AMD. For instance, sublytic MAC formation can activate signaling pathways related to calcium, receptor tyrosine kinases, phospholipase C, protein kinase C, phospholipase 2α, and other extracellular signal-regulated kinases (Cybulsky et al., 2005; Fosbrink et al., 2005). This can lead to changes in cellular response including secretion, adherence, aggregation, chemotaxis, cell division, and impacts on membrane function (Bohana-Kashtan et al.,

2004). In RPE cells, sublytic MAC increases the production of cytokines IL-6, IL-8, and MCP-1, which may contribute to early AMD (Lueck et al., 2011). Increased expression of MMP-2 and MMP-9 and VEGF are also associated with sublytic MAC formation on RPE and correlate with both remodeling of the choriocapillaris and neovascular processes seen in wet AMD (Thurman et al., 2009; Lueck et al., 2011). This is because VEGF, present in granular vesicles, is secreted via exocytosis following depolarization of cell membranes through activation of voltage-gated calcium channels. Calcium influx also activates the Ras/Erk pathway known to be involved in the regulated secretion of VEGF (Kunchithapautham and Rohrer, 2011). Additionally, P2X7 receptor activation also triggers VEGF release (Hill et al., 2010; Adinolfi et al., 2012). Thus, sublytic MAC formation and purinergic signaling influences intracellular signaling pathways that result in growth factor secretion (Lueck et al., 2011).

Various membrane pore-forming toxins, such as α-haemolysin, leukotoxin, and α-toxin, have also been shown to exert their toxic effects through autocrine and paracrine signaling in human erythrocytes (Birke et al., 2013) leading to complement-mediated lysis amplified by ATP release and P2X receptor activation (Birke et al., 2013). Additionally, amyloid-β protein aggregates and other pore forming toxins may lead to sublytic membrane damage and subsequent release of cellular components such as ATP, IL-1β, and IL-18 (Sanz et al., 2009; Ciudad et al., 2020). However, the underlying mechanisms and processes surrounding complement amplification, MAC deposition, and P2X receptor activation are not yet fully understood. We hypothesize that MAC deposition leads to an increase in eATP and subsequent P2X receptor activation. This results in an enhancement of ion flux, which has an impact on mitochondrial potential, the formation of ROS, inflammasome activation, and other intracellular changes leading to a feedback loop that allows for more MAC deposition. Further research is needed to establish these connections.

Overall, sublytic MAC and pore formation results in the remodeling of the choriocapillaris which contributes to the buildup of drusen, enhances complement activation and NLRP3 inflammasome activity, and leads to increased inflammation through cytokine release and recruitment of immune cells. Chronic inflammatory changes impact the overlying RPE, and the outer retina responds through additional signaling resulting in CNV, or regression of the choriocapillaris forming "ghost" vessels, subsequent RPE loss, and photoreceptor death in GA (Kumar-Singh, 2019).

NLRP3 inflammasome activation

Inflammasomes are multimolecular complexes comprised of three protein constituents: a NOD-like receptor, the adaptor protein apoptosis-associated speck-like protein containing a caspase recruitment domain (ASC), and pro-caspase 1 (Latz et al., 2013). Their activation consists of a two-step process in which both an initial priming signal and an activating signal are required (Latz et al., 2013). The initial priming signal is initiated by pathogen-associated molecular patterns (PAMPs) that stimulate toll-like receptors (TLRs) leading to the activation of NF-κB followed by the subsequent transcriptional upregulation of NOD-like receptor family pyrin domain containing 3 (NLRP3) and pro-interleukin-1β (Latz et al., 2013; Kelley et al., 2019). This is especially important in non-immune cells such as the RPE where basal expression levels are considered insufficient to initiate inflammasome assembly (Tseng et al., 2013; Narendran et al., 2021). Next, an activation signal is provided by a broad variety of molecules classified as either PAMPs or damage-associated molecular patterns (DAMPs) such as toxins, pathogens, metabolites, crystalline substances, nucleic acids, ion flux, reactive oxygen species, and ATP (Latz et al., 2013; Malik and Kanneganti, 2017; Zheng et al., 2020). In the case of P2X7 activation, eATP acting as a DAMP is detected by P2X7. Following activation, inflammasomes lead to a unique inflammatory programmed cell death pathway known as pyroptosis (Kelley et al., 2019).

Pyroptosis is executed by a family of pore-forming proteins known as gasdermins (GSDMs) (Shi et al., 2015). In humans, the current members of the GSDM family include GSDMA, GSDMB, GSDMC, GSDMD, and GSDME, which contain an autoinhibitory carboxyterminal domain and a pore-forming amino-terminal domain responsible for perforating the plasma membrane of cells (Orning et al., 2019; Broz et al., 2020; Liu et al., 2021). Typically, pyroptotic cell death initiates following the activation of the NLRP3 inflammasome and most often results in GSDMD pore formation and release of ATP (He et al., 2015; Kayagaki et al., 2015; Shi et al., 2015). Proinflammatory cytokines such as IL-1β and IL-18 are also released through the nonselective 10–14 nM gasdermin pore (Latz et al., 2013; Yu et al., 2021) which induce both inflammatory an apoptotic effects (Martinon et al., 2002; Ambati et al., 2013). However, while there are cytotoxic effects of IL-18 and IL-1β on the RPE, studies have also shown beneficial effects of inflammasome-mediated IL-18 release through the inhibition of neovascularization in an acute laser-induced injury model of neovascular AMD (Doyle et al., 2012). These contrasting findings imply that a single factor (IL-18) or pathway (NLRP3 inflammasome activation) can be simultaneously anti-angiogenic and destructive to the RPE and that Toll-like receptor 3 (TLR3) activation may be beneficial in terms of decreasing choroidal neovascularization while also promoting RPE degeneration (Ambati et al., 2013). In contrast to the reported anti-angiogenic effects of IL-18, IL-1β promotes neovascularization (Lavalette et al., 2011).

Based on the mechanisms described above, activation of the NLRP3 inflammasome and various gasdermin proteins have been implicated in the pathogenesis of AMD and several pathways have been suggested to trigger inflammasome activation in the outer retina including lipofuscin component A2E, accumulated Alu RNA, drusen components, amyloid-β, lipid peroxidation products, photooxidative damage, lysosomal destabilizations, particulate matter, overexpression of VEGF, and eATP (Ambati et al., 2013; Kerur et al., 2013). For example, the formation of amyloid-β oligomers (AβOs), which are aggregates of amyloid-β peptides and a major proinflammatory component of drusen (Luibl et al., 2006), can lead to RPE degeneration and GA through AβO-induced priming, assembly, and activation of the NLRP3 inflammasome in RPE cells. This occurs through a P2X7-mediated pathway, in which amyloid-β protein aggregates form a conductivity pore resulting in membrane damage and subsequent release of cellular components such as ATP and inflammatory mediators (Sanz et al., 2009; Ciudad et al., 2020). Like other mechanisms of NLRP3 inflammasome activation, AβO-induced AMD models have been demonstrated to result in the expression of GSDMD (Sun et al., 2018), along with RPE cytotoxicity driven by mitochondrial dysfunction and ROS formation (Sorbara and Girardin, 2011; Zhou et al., 2011).

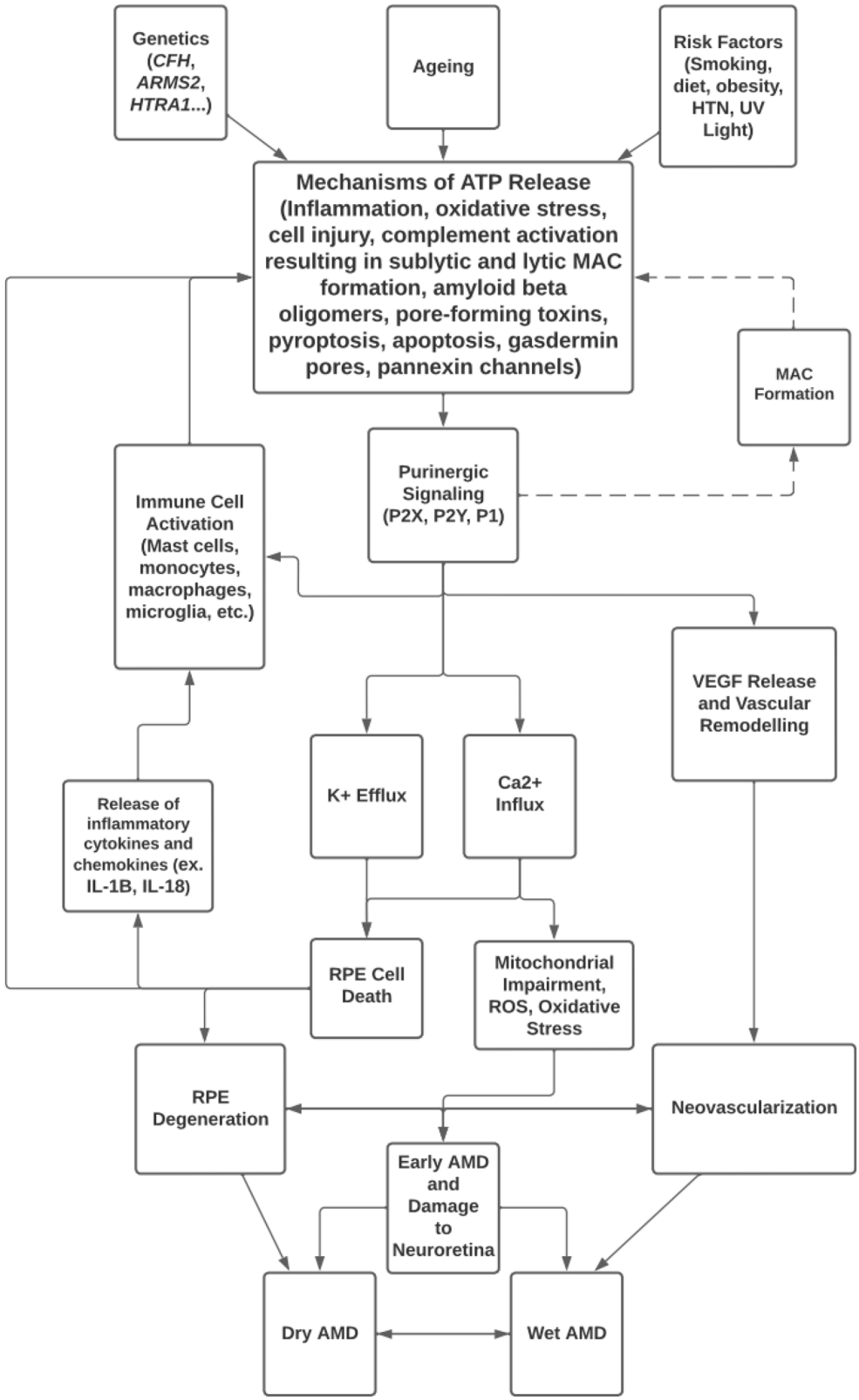

FIGURE 3
Overview of mechanisms of ATP release and purinergic signaling in the pathogenesis of AMD.

Additionally, repetitive element-derived *Alu* RNA transcripts, non-canonical targets of DICER1-mediated enzymatic degradation, accumulate in human GA following the loss of DICER1 expression and are capable of activating P2X7 and the NLRP3 inflammasome to cause cell death of the retinal pigment epithelium in GA (Fowler et al., 2014). This is because *Alu* RNA transcripts can function as both

priming and activating signals for inflammasome signaling (Ambati et al., 2013; Kerur et al., 2013). As a result of this pathway and the fact that *Alu* RNA transcripts require reverse transcriptase, multiple nucleoside reverse transcriptase inhibitors (NRTIs) have been investigated and found to be efficacious in inhibiting P2X7-mediated NLRP3 inflammasome activation in mouse models of GA, CNV, and other P2X7 driven diseases (Fowler et al., 2014).

Links between purinergic signaling and NLRP3 inflammasome activation are also well-defined as a result of ATP acting as a paracrine or autocrine signal in response to cell death or other stimuli (i.e., increased pressure, hypoxic injury, or complement-mediated damage). In these scenarios, the high amount of passive ATP release from cells activates the inflammasome through a P2X7R-dependent pyroptotic cell death pathway (Yang et al., 2015). Activated caspase-11 may also cleave pannexin-1 channels, inducing ATP release and P2X7R-related pyroptosis (Yang et al., 2015). Other nucleotide metabolites such as ADP, UTP, UDP, UDP glucose, and adenosine, along with other members of the purinergic receptor family (i.e., P2X, P2Y, and P1 receptors), may also contribute through complex purinergic signaling networks (Gombault et al., 2013).

Taken together, an increasing body of evidence suggests that the retina can respond to diverse danger signals including unregulated ATP release via purinergic signaling leading to NLRP3 inflammasome activation (Gombault et al., 2013; Gao et al., 2015; Yang et al., 2020), GSDM pore formation, and pyroptosis. Therefore, inhibition of P2X receptors and NLRP3 activation has been identified as putative drug targets in several models of AMD progression by delaying RPE degeneration in GA and/or slowing RPE barrier breakdown and neovascularization in CNV.

Conclusion

Purinergic signaling has been investigated for its role in the development of ocular pathologies such as AMD, glaucoma, and diabetic retinopathy. Despite the emergence of anti-VEGF agents to treat the wet form of late AMD, and the recently FDA-approved pegcetacoplan, a complement C3 inhibitor, to slow the progression of the dry form of late AMD, there are no approved drugs available to prevent the development of wet or dry AMD. For this reason, potential crosstalk between known contributors to AMD, such as complement dysregulation and inflammasome activation, and other cellular systems, such as purinergic signaling, must be considered (Figure 3).

As outlined in this review, the current literature surrounding purinergic signaling and AMD pathogenesis has focused primarily on the role of P2X7 receptor signaling. However, P2X7 has the highest EC50 for ATP in the P2X receptor family and may not be physiologically relevant throughout all stages of the development and progression of AMD, especially in the early stages of the disease. On the other hand, in advanced stages and under certain conditions, mechanisms may allow for P2X7 receptor activation through altered regulatory proteins, repair processes, and interactions between mediators such as MMPs and ectonucleosides leading to increased concentrations of ATP, increased purinergic signaling, and accelerated local inflammation contributing to the AMD pathogenesis.

To fully understand the potential roles that purinergic signaling plays in AMD, more research is needed surrounding the expression, distribution, functions, and interactions of P2X receptors with other systems, such as complement activation, within cells of the outer retina, RPE, choroid, retinal vasculature, and the immune system. This must include further characterization of both homotrimeric purinergic receptors, such as P2X1, P2X2, P2X3, P2X4, P2X5, and P2X6, along with heterotrimeric receptors that can exhibit novel properties and functions.

Finally, while there are numerous mechanisms for ATP release within the outer retina, the role of purinergic signaling in both lytic and sublytic processes should be explored in the context of how these processes may amplify complement-induced lysis, a mechanism that has not yet been fully elucidated. This may involve processes that make cells more vulnerable to MAC deposition following P2X activation, such as crosstalk between complement and P2X receptor signaling, MMP-9 activation, and other spatial and temporal aspects of ATP release. In determining how these processes can influence and be influenced by purinergic signaling, it will improve our understanding of the mechanisms that drive AMD pathogenesis, which is critical in developing treatment strategies that prevent or slow the progression of the disease.

Author contributions

HM performed the data collection and analysis. HM, KJ, and JM wrote the manuscript. JM and CC conceived the review, obtained funding, and critically revised the manuscript. All authors have read and approved the final manuscript.

Acknowledgments

The authors would like to thank Lucas Chang for help in data collection and analysis in early stages of the review process.

Conflict of interest

CC was employed by Paragon Ventures Inc.

The remaining authors declare that the research was conducted in the absence of any commercial or financial relationships that could be construed as a potential conflict of interest.

Publisher's note

References

Adinolfi, E., Giuliani, A. L., De Marchi, E., Pegoraro, A., Orioli, E., and Di Virgilio, F. (2018). The P2X7 receptor: a main player in inflammation. *Biochem. Pharmacol.* 151, 234–244. doi: 10.1016/j.bcp.2017.12.021

Adinolfi, E., Raffaghello, L., Giuliani, A. L., Cavazzini, L., Capece, M., Chiozzi, P., et al. (2012). Expression of P2X7 receptor increases in vivo tumor growth. *Cancer Res.* 72, 2957–2969. doi: 10.1158/0008-5472.CAN-11-1947

Agarwal, A., Rhoades, W. R., Hanout, M., Soliman, M. K., Sarwar, S., Sadiq, M. A., et al. (2015). Management of neovascular age-related macular degeneration: current state-of-the-art care for optimizing visual outcomes and therapies in development. *Clin. Ophthalmol.* 9, 1001–1015. doi: 10.2147/OPTH.S74959

Age-Related Eye Disease Study Research Group (2001). A randomized, placebo-controlled, clinical trial of high-dose supplementation with vitamins C and E, beta carotene, and zinc for age-related macular degeneration and vision loss: AREDS report no. 8. *Arch. Ophthalmol.* 119, 1417–1436. doi: 10.1001/archopht.119.10.1417

Ambati, J., Atkinson, J. P., and Gelfand, B. D. (2013). Immunology of age-related macular degeneration. *Nat. Rev. Immunol.* 13, 438–451. doi: 10.1038/nri3459

Ambati, J., and Fowler, B. J. (2012). Mechanisms of age-related macular degeneration. *Neuron* 75, 26–39. doi: 10.1016/j.neuron.2012.06.018

Armento, A., Ueffing, M., and Clark, S. J. (2021). The complement system in age-related macular degeneration. *Cell. Mol. Life Sci.* 78, 4487–4505. doi: 10.1007/s00018-021-03796-9

Bandyopadhyay, M., and Rohrer, B. (2012). Matrix metalloproteinase activity creates pro-angiogenic environment in primary human retinal pigment epithelial cells exposed to complement. *Investigative ophthalmology & visual science* 53, 1953–1961. doi: 10.1167/iovs.11-8638

Behnke, V., Wolf, A., and Langmann, T. (2020). The role of lymphocytes and phagocytes in age-related macular degeneration (AMD). *Cell. Mol. Life Sci.* 77, 781–788. doi: 10.1007/s00018-019-03419-4

Berglin, L., Sarman, S., van der Ploeg, I., Steen, B., Ming, Y., Itohara, S., et al. (2003). Reduced choroidal neovascular membrane formation in matrix metalloproteinase-2-deficient mice. *Invest. Ophthalmol. Vis. Sci.* 44, 403–408. doi: 10.1167/iovs.02-0180

Bhutto, I., and Lutty, G. (2012). Understanding age-related macular degeneration (AMD): relationships between the photoreceptor/retinal pigment epithelium/Bruch's membrane/choriocapillaris complex. *Mol. Asp. Med.* 33, 295–317. doi: 10.1016/j.mam.2012.04.005

Bhutto, I. A., McLeod, D. S., Jing, T., Sunness, J. S., Seddon, J. M., and Lutty, G. A. (2016). Increased choroidal mast cells and their degranulation in age-related macular degeneration. *Br. J. Ophthalmol.* 100, 720–726. doi: 10.1136/bjophthalmol-2015-308290

Birke, K., Lipo, E., Birke, M. T., and Kumar-Singh, R. (2013). Topical application of PPADS inhibits complement activation and choroidal neovascularization in a model of age-related macular degeneration. *PLoS One* 8:e76766. doi: 10.1371/journal.pone.0076766

Black, J. R., and Clark, S. J. (2016). Age-related macular degeneration: genome-wide association studies to translation. *Genet. Med.* 18, 283–289. doi: 10.1038/gim.2015.70

Bohana-Kashtan, O., Ziporen, L., Donin, N., Kraus, S., and Fishelson, Z. (2004). Cell signals transduced by complement. *Mol. Immunol.* 41, 583–597. doi: 10.1016/j.molimm.2004.04.007

Broz, P., Pelegrín, P., and Shao, F. (2020). The gasdermins, a protein family executing cell death and inflammation. *Nat. Rev. Immunol.* 20, 143–157. doi: 10.1038/s41577-019-0228-2

Bulanova, E., and Bulfone-Paus, S. (2010). P2 receptor-mediated signaling in mast cell biology. *Puriner. Signal.* 6, 3–17. doi: 10.1007/s11302-009-9173-z

Burnstock, G. (2006). Purinergic signalling-an overview. *Novartis Found. Symp.* 276, 26–281.

Burnstock, G. (2008). "Purinergic System" in *Encyclopedia of molecular pharmacology*. eds. S. Offermanns and W. Rosenthal (Berlin, Heidelberg: Springer)

Burnstock, G. (2016). P2X ion channel receptors and inflammation. *Purinergic Signal.* 12, 59–67. doi: 10.1007/s11302-015-9493-0

Burnstock, G. (2017). Purinergic signalling: therapeutic developments. *Front. Pharmacol.* 8:661. doi: 10.3389/fphar.2017.00661

Burnstock, G. (2018). Purine and purinergic receptors. *Brain Neurosci. Adv.* 2:2398212818817494. doi: 10.1177/2398212818817494

Burnstock, G., and Dale, N. (2015). Purinergic signalling during development and ageing. *Purinergic Signal.* 11, 277–305. doi: 10.1007/s11302-015-9452-9

Caraffa, A. L., Conti, C., D Ovidio, C., Gallenga, C. E., Tettamanti, L., Mastrangelo, F., et al. (2018). New concepts in neuroinflammation: mast cells pro-inflammatory and anti-inflammatory cytokine mediators. *J. Biol. Regul. Homeost. Agents* 32, 449–454.

Chen, E. R., and Kaiser, P. K. (2020). Therapeutic potential of the Ranibizumab port delivery system in the treatment of AMD: evidence to date. *Clin. Ophthalmol.* 14, 1349–1355. doi: 10.2147/OPTH.S194234

Ciudad, S., Puig, E., Botzanowski, T., Meigooni, M., Arango, A. S., Do, J., et al. (2020). Aβ(1-42) tetramer and octamer structures reveal edge conductivity pores as a mechanism for membrane damage. *Nat. Commun.* 11:3014. doi: 10.1038/s41467-020-16566-1

Clapp, C., Diaz-Lezama, N., Adan-Castro, E., Ramirez-Hernandez, G., Moreno-Carranza, B., Sarti, A. C., et al. (2019). Pharmacological blockade of the P2X7 receptor reverses retinal damage in a rat model of type 1 diabetes. *Acta Diabetol.* 56, 1031–1036. doi: 10.1007/s00592-019-01343-4

Cybulsky, A. V., Takano, T., Papillon, J., Bijian, K., and Guillemette, J. (2005). Activation of the extracellular signal-regulated kinase by complement C5b-9. *Am. J. Physiol. Renal Physiol.* 289, F593–F603. doi: 10.1152/ajprenal.00066.2005

Dale, N., Butler, J., Dospinescu, V. M., and Nijjar, S. (2023). Channel-mediated ATP release in the nervous system. *Neuropharmacology* 227:109435. doi: 10.1016/j.neuropharm.2023.109435

de Jong, E. K., Geerlings, M. J., and den Hollander, A. I. (2020). Age-related macular degeneration. *Genet. Genom. Eye Disease*, 1, 155–180. doi: 10.1016/B978-0-12-816222-4.00010-1

Di Virgilio, F., Dal Ben, D., Sarti, A. C., Giuliani, A. L., and Falzoni, S. (2017). The P2X7 receptor in infection and inflammation. *Immunity* 47, 15–31. doi: 10.1016/j.immuni.2017.06.020

Di Virgilio, F., Giuliani, A. L., Vultaggio-Poma, V., Falzoni, S., and Sarti, A. C. (2018). Non-nucleotide agonists triggering P2X7 receptor activation and pore formation. *Front. Pharmacol.* 9:39. doi: 10.3389/fphar.2018.00039

Di Virgilio, F., Sarti, A. C., and Coutinho-Silva, R. (2020). Purinergic signaling, DAMPs, and inflammation. *Am. J. Physiol. Cell Physiol.* 318, C832–C835. doi: 10.1152/ajpcell.00053.2020

Di Virgilio, F., Vultaggio-Poma, V., Falzoni, S., and Giuliani, A. L. (2023). Extracellular ATP: A powerful inflammatory mediator in the central nervous system. *Neuropharmacology* 224:109333. doi: 10.1016/j.neuropharm.2022.109333

Doyle, S. L., Campbell, M., Ozaki, E., Salomon, R. G., Mori, A., Kenna, P. F., et al. (2012). NLRP3 has a protective role in age-related macular degeneration through the induction of IL-18 by drusen components. *Nat. Med.* 18, 791–798. doi: 10.1038/nm.2717

Dwyer, K. M., Kishore, B. K., and Robson, S. C. (2020). Conversion of extracellular ATP into adenosine: a master switch in renal health and disease. *Nat. Rev. Nephrol.* 16, 509–524. doi: 10.1038/s41581-020-0304-7

Fosbrink, M., Niculescu, F., and Rus, H. (2005). The role of c5b-9 terminal complement complex in activation of the cell cycle and transcription. *Immunol. Res.* 31, 37–46. doi: 10.1385/IR:31:1:37

Fowler, B. J., Gelfand, B. D., Kim, Y., Kerur, N., Tarallo, V., Hirano, Y., et al. (2014). Nucleoside reverse transcriptase inhibitors possess intrinsic anti-inflammatory activity. *Science* 346, 1000–1003. doi: 10.1126/science.1261754

Galli, S. J., and Tsai, M. (2008). Mast cells: versatile regulators of inflammation, tissue remodeling, host defense and homeostasis. *J. Dermatol. Sci.* 49, 7–19. doi: 10.1016/j.jdermsci.2007.09.009

Gao, J., Liu, R. T., Cao, S., Cui, J. Z., Wang, A., et al. (2015). NLRP3 inflammasome: activation and regulation in age-related macular degeneration. *Mediat. Inflamm.* 2015, 1–11. doi: 10.1155/2015/690243

Gombault, A., Baron, L., and Couillin, I. (2013). ATP release and purinergic signaling in NLRP3 inflammasome activation. *Front. Immunol.* 3:414. doi: 10.3389/fimmu.2012.00414

Gu, B. J., Baird, P. N., Vessey, K. A., Skarratt, K. K., Fletcher, E. L., Fuller, S. J., et al. (2013). A rare functional haplotype of the P2RX4 and P2RX7 genes leads to loss of innate phagocytosis and confers increased risk of age-related macular degeneration. *FASEB J.* 27, 1479–1487. doi: 10.1096/fj.12-215368

Gu, B. J., and Wiley, J. S. (2018). P2X7 as a scavenger receptor for innate phagocytosis in the brain. *Br. J. Pharmacol.* 175, 4195–4208. doi: 10.1111/bph.14470

Guo, C., Masin, M., Qureshi, O. S., and Murrell-Lagnado, R. D. (2007). Evidence for functional P2X4/P2X7 heteromeric receptors. *Mol. Pharmacol.* 72, 1447–1456. doi: 10.1124/mol.107.035980

He, W. T., Wan, H., Hu, L., Chen, P., Wang, X., Huang, Z., et al. (2015). Gasdermin D is an executor of pyroptosis and required for interleukin-1β secretion. *Cell Res.* 25, 1285–1298. doi: 10.1038/cr.2015.139

Hill, L. M., Gavala, M. L., Lenertz, L. Y., and Bertics, P. J. (2010). Extracellular ATP may contribute to tissue repair by rapidly stimulating purinergic receptor X7-dependent vascular endothelial growth factor release from primary human monocytes. *J. Immunol.* 185, 3028–3034. doi: 10.4049/jimmunol.1001298

Holz, F. G., Schmitz-Valckenberg, S., and Fleckenstein, M. (2014). Recent developments in the treatment of age-related macular degeneration. *J. Clin. Invest.* 124, 1430–1438. doi: 10.1172/JCI71029

Huang, Z., Xie, N., Illes, P., Di Virgilio, F., Ulrich, H., Semyanov, A., et al. (2021). From purines to purinergic signalling: molecular functions and human diseases. *Signal Transduct. Target. Ther.* 6:162. doi: 10.1038/s41392-021-00553-z

Illes, P., Khan, T. M., and Rubini, P. (2017). Neuronal P2X7 receptors revisited: do they really exist? *J. Neurosci. Off. J. Soc. Neurosci.* 37, 7049–7062. doi: 10.1523/JNEUROSCI.3103-16.2017

Illes, P., Müller, C. E., Jacobson, K. A., Grutter, T., Nicke, A., Fountain, S. J., et al. (2021). Update of P2X receptor properties and their pharmacology: IUPHAR review 30. *Br. J. Pharmacol.* 178, 489–514. doi: 10.1111/bph.1529

Illes, P., Rubini, P., Ulrich, H., Zhao, Y., and Tang, Y. (2020). Regulation of microglial functions by purinergic mechanisms in the healthy and diseased CNS. *Cells* 9:1108. doi: 10.3390/cells9051108

Jacobson, K. A., and Civan, M. M. (2016). Ocular purine receptors as drug targets in the eye. *J. Ocul. Pharmacol. Therapeut.* 32, 534–547. doi: 10.1089/jop.2016.0090

Jacobson, K. A., Delicado, E. G., Gachet, C., Kennedy, C., von Kügelgen, I., Li, B., et al. (2020). Update of P2Y receptor pharmacology: IUPHAR review 27. *Br. J. Pharmacol.* 177, 2413–2433. doi: 10.1111/bph.15005

Junger, W. G. (2011). Immune cell regulation by autocrine purinergic signalling. *Nat. Rev. Immunol.* 11, 201–212. doi: 10.1038/nri2938

Kahlenberg, J. M., and Kaplan, M. J. (2013). Little peptide, big effects: the role of LL-37 in inflammation and autoimmune disease. *J. Immunol.* 191, 4895–4901. doi: 10.4049/jimmunol.1302005

Kayagaki, N., Stowe, I. B., Lee, B. L., O'Rourke, K., Anderson, K., Warming, S., et al. (2015). Caspase-11 cleaves gasdermin D for non-canonical inflammasome signalling. *Nature* 526, 666–671. doi: 10.1038/nature15541

Kelley, N., Jeltema, D., Duan, Y., and He, Y. (2019). The NLRP3 inflammasome: an overview of mechanisms of activation and regulation. *Int. J. Mol. Sci.* 20:3328. doi: 10.3390/ijms20133328

Kempuraj, D., Thangavel, R., Natteru, P. A., Selvakumar, G. P., Saeed, D., Zahoor, H., et al. (2016). Neuroinflammation induces neurodegeneration. *J. Neurol. Neurosurg. Spine* 1:1003.

Kerur, N., Hirano, Y., Tarallo, V., Fowler, B. J., Bastos-Carvalho, A., Yasuma, T., et al. (2013). TLR-independent and P2X7-dependent signaling mediate Alu RNA-induced NLRP3 inflammasome activation in geographic atrophy. *Invest. Ophthalmol. Vis. Sci.* 54, 7395–7401. doi: 10.1167/iovs.13-12500

Klein, R. J., Zeiss, C., Chew, E. Y., Tsai, J. Y., Sackler, R. S., Haynes, C., et al. (2005). Complement factor H polymorphism in age-related macular degeneration. *Science* 308, 385–389. doi: 10.1126/science.1109557

Kronlage, M., Song, J., Sorokin, L., Isfort, K., Schwerdtle, T., Leipziger, J., et al. (2010). Autocrine purinergic receptor signaling is essential for macrophage chemotaxis. *Sci. Signal.* 3:ra55. doi: 10.1126/scisignal.2000588

Kukulski, F., Lévesque, S. A., and Sévigny, J. (2011). Impact of ectoenzymes on p2 and p1 receptor signaling. *Adv. Pharmacol.* 61, 263–299. doi: 10.1016/B978-0-12-385526-8.00009-6

Kumar-Singh, R. (2019). The role of complement membrane attack complex in dry and wet AMD – from hypothesis to clinical trials. *Exp. Eye Res.* 184, 266–277. doi: 10.1016/j.exer.2019.05.006

Kunchithapautham, K., and Rohrer, B. (2011). Sublytic membrane-attack-complex (MAC) activation alters regulated rather than constitutive vascular endothelial growth factor (VEGF) secretion in retinal pigment epithelium monolayers. *J. Biol. Chem.* 286, 23717–23724. doi: 10.1074/jbc.M110.214593

Kur, J., and Newman, E. A. (2014). Purinergic control of vascular tone in the retina. *J. Physiol.* 592, 491–504. doi: 10.1113/jphysiol.2013.267294

Kur, J., Newman, E. A., and Chan-Ling, T. (2012). Cellular and physiological mechanisms underlying blood flow regulation in the retina and choroid in health and disease. *Prog. Retin. Eye Res.* 31, 377–406. doi: 10.1016/j.preteyeres.2012.04.004

Kurashima, Y., Amiya, T., Nochi, T., Fujisawa, K., Haraguchi, T., Iba, H., et al. (2012). Extracellular ATP mediates mast cell-dependent intestinal inflammation through P2X7 purinoceptors. *Nat. Commun.* 3:1034. doi: 10.1038/ncomms2023

Latz, E., Xiao, T. S., and Stutz, A. (2013). Activation and regulation of the inflammasomes. *Nat. Rev. Immunol.* 13, 397–411. doi: 10.1038/nri3452

Lavalette, S., Raoul, W., Houssier, M., Camelo, S., Levy, O., Calippe, B., et al. (2011). Interleukin-1β inhibition prevents choroidal neovascularization and does not exacerbate photoreceptor degeneration. *Am. J. Pathol.* 178, 2416–2423. doi: 10.1016/j.ajpath.2011.01.013

Lazarowski, E. R., Boucher, R. C., and Harden, T. K. (2003). Mechanisms of release of nucleotides and integration of their action as P2X-and P2Y-receptor activating molecules. *Mol. Pharmacol.* 64, 785–795. doi: 10.1124/mol.64.4.785

Liu, X., Xia, S., Zhang, Z., Wu, H., and Lieberman, J. (2021). Channelling inflammation: gasdermins in physiology and disease. *Nat. Rev. Drug Discov.* 20, 384–405. doi: 10.1038/s41573-021-00154-z

Lueck, K., Wasmuth, S., Williams, J., Hughes, T. R., Morgan, B. P., Lommatzsch, A., et al. (2011). Sub-lytic C5b-9 induces functional changes in retinal pigment epithelial cells consistent with age-related macular degeneration. *Eye* 25, 1074–1082. doi: 10.1038/eye.2011.109

Luibl, V., Isas, J. M., Kayed, R., Glabe, C. G., Langen, R., and Chen, J. (2006). Drusen deposits associated with aging and age-related macular degeneration contain nonfibrillar amyloid oligomers. *J. Clin. Invest.* 116, 378–385. doi: 10.1172/JCI25843

Malik, A., and Kanneganti, T. D. (2017). Inflammasome activation and assembly at a glance. *J. Cell Sci.* 130, 3955–3963. doi: 10.1242/jcs.207365

Martinon, F., Burns, K., and Tschopp, J. (2002). The inflammasome: a molecular platform triggering activation of inflammatory caspases and processing of proIL-beta. *Mol. Cell* 10, 417–426. doi: 10.1016/s1097-2765(02)00599-3

Matsubara, J. A., Tian, Y., Cui, J. Z., Zeglinski, M. R., Hiroyasu, S., Turner, C. T., et al. (2020). Retinal distribution and extracellular activity of granzyme B: a serine protease that degrades retinal pigment epithelial tight junctions and extracellular matrix proteins. *Front. Immunol.* 11:574. doi: 10.3389/fimmu.2020.00574

Medina, C. B., Mehrotra, P., Arandjelovic, S., Perry, J. S. A., Guo, Y., Morioka, S., et al. (2020). Metabolites released from apoptotic cells act as tissue messengers. *Nature* 580, 130–135. doi: 10.1038/s41586-020-2121-3

Merle, N. S., Church, S. E., Fremeaux-Bacchi, V., and Roumenina, L. T. (2015a). Complement system part I - molecular mechanisms of activation and regulation. *Front. Immunol.* 6:262. doi: 10.3389/fimmu.2015.00262

Merle, N. S., Noe, R., Halbwachs-Mecarelli, L., Fremeaux-Bacchi, V., and Roumenina, L. T. (2015b). Complement system part II: role in immunity. *Front. Immunol.* 6:257. doi: 10.3389/fimmu.2015.00257

Mitchell, P., Liew, G., Gopinath, B., and Wong, T. Y. (2018). Age-related macular degeneration. *Lancet* 392, 1147–1159. doi: 10.1016/S0140-6736(18)31550-2

Mitchell, C. H., and Reigada, D. (2008). Purinergic signalling in the subretinal space: a role in the communication between the retina and the RPE. *Purinergic signalling* 4, 101–107. doi: 10.1007/s11302-007-9054-2

Morciano, G., Sarti, A. C., Marchi, S., Missiroli, S., Falzoni, S., Raffaghello, L., et al. (2017). Use of luciferase probes to measure ATP in living cells and animals. *Nat. Protoc.* 12, 1542–1562. doi: 10.1038/nprot.2017.052

Narendran, S., Pereira, F., Yerramothu, P., Apicella, I., Wang, S. B., Ambati, K., et al. (2021). Nucleoside reverse transcriptase inhibitors and Kamuvudines inhibit amyloid-β induced retinal pigmented epithelium degeneration. *Signal Transduct. Target. Ther.* 6:149. doi: 10.1038/s41392-021-00537-z

Newman, E. A. (2015). Glial cell regulation of neuronal activity and blood flow in the retina by release of gliotransmitters. *Philos. Trans. R. Soc. Lond. Ser. B Biol. Sci.* 370:20140195. doi: 10.1098/rstb.2014.0195

Niyadurupola, N., Sidaway, P., Ma, N., Rhodes, J. D., Broadway, D. C., and Sanderson, J. (2013). P2X7 receptor activation mediates retinal ganglion cell death in a human retina model of ischemic neurodegeneration. *Invest. Ophthalmol. Vis. Sci.* 54, 2163–2170. doi: 10.1167/iovs.12-10968

Notomi, S., Hisatomi, T., Kanemaru, T., Takeda, A., Ikeda, Y., Enaida, H., et al. (2011). Critical involvement of extracellular ATP acting on P2RX7 purinergic receptors in photoreceptor cell death. *Am. J. Pathol.* 179, 2798–2809. doi: 10.1016/j.ajpath.2011.08.035

Notomi, S., Hisatomi, T., Murakami, Y., Terasaki, H., Sonoda, S., Asato, R., et al. (2013). Dynamic increase in extracellular ATP accelerates photoreceptor cell apoptosis via ligation of P2RX7 in subretinal hemorrhage. *PLoS ONE* 8:e53338. doi: 10.1371/journal.pone.0053338

Ogura, S., Baldeosingh, R., Bhutto, I. A., Kambhampati, S. P., Scott McLeod, D., Edwards, M. M., et al. (2020). A role for mast cells in geographic atrophy. *FASEB J.* 34, 10117–10131. doi: 10.1096/fj.202000807R

Orning, P., Lien, E., and Fitzgerald, K. A. (2019). Gasdermins and their role in immunity and inflammation. *J. Exp. Med.* 216, 2453–2465. doi: 10.1084/jem.20190545

Pellegatti, P., Falzoni, S., Pinton, P., Rizzuto, R., and Di Virgilio, F. (2005). A novel recombinant plasma membrane-targeted luciferase reveals a new pathway for ATP secretion. *Mol. Biol. Cell* 16, 3659–3665. doi: 10.1091/mbc.e05-03-0222

Pellegatti, P., Raffaghello, L., Bianchi, G., Piccardi, F., Pistoia, V., and Virgilioa, F.. (2008). Increased level of extracellular ATP at tumor sites: in vivo imaging with plasma membrane luciferase. *PloS one*, 3, e2599. doi: 10.1371/journal.pone.0002599

Platania, C. B. M., Lazzara, F., Fidilio, A., Fresta, C. G., Conti, F., Giurdanella, G., et al. (2019). Blood-retinal barrier protection against high glucose damage: the role of P2X7 receptor. *Biochem. Pharmacol.* 168, 249–258. doi: 10.1016/j.bcp.2019.07.010

Ralevic, V., and Burnstock, G. (1998). Receptors for purines and pyrimidines. *Pharmacol. Rev.* 50, 413–492.

Rasmussen, A., and Sander, B. (2014). Long-term longitudinal study of patients treated with ranibizumab for neovascular age-related macular degeneration. *Curr. Opin. Ophthalmol.* 25, 158–163. doi: 10.1097/ICU.0000000000000050

Ricklin, D., Hajishengallis, G., Yang, K., and Lambris, J. D. (2010). Complement: a key system for immune surveillance and homeostasis. *Nat. Immunol.* 11, 785–797. doi: 10.1038/ni.1923

Romagnani, A., Rottoli, E., Mazza, E. M. C., Rezzonico-Jost, T., De Ponte Conti, B., Proietti, M., et al. (2020). P2X7 receptor activity limits accumulation of T cells within tumors. *Cancer Res.* 80, 3906–3919. doi: 10.1158/0008-5472.CAN-19-3807

Sakaki, H., Tsukimoto, M., Harada, H., Moriyama, Y., and Kojima, S. (2013). Autocrine regulation of macrophage activation via exocytosis of ATP and activation of P2Y11 receptor. *PLoS One* 8:e59778. doi: 10.1371/journal.pone.0059778

Salcman, B., Affleck, K., and Bulfone-Paus, S. (2021). P2X receptor-dependent modulation of mast cell and glial cell activities in Neuroinflammation. *Cells* 10:2282. doi: 10.3390/cells10092282

Sanderson, J., Dartt, D. A., Trinkaus-Randall, V., Pintor, J., Civan, M. M., Delamere, N. A., et al. (2014). Purines in the eye: recent evidence for the physiological and pathological role of purines in the RPE, retinal neurons, astrocytes, Müller cells, lens, trabecular meshwork, cornea and lacrimal gland. *Exp. Eye Res.* 127, 270–279. doi: 10.1016/j.exer.2014.08.009

Santiago, A., Madeira, M., Boia, R., Aires, I., Rodrigues-Neves, A., Santos, P., et al. (2020). Keep an eye on adenosine: its role in retinal inflammation. *Pharmacol. Ther.* 210, 1–22. doi: 10.1016/j.pharmthera.2020.107513

Sanz, J. M., Chiozzi, P., Ferrari, D., Colaianna, M., Idzko, M., Falzoni, S., et al. (2009). Activation of microglia by amyloid {beta} requires P2X7 receptor expression. *J. Immunol. (Baltimore, Md.: 1950)*. 182(7), 4378–4385. doi: 10.4049/jimmunol.0803612

Sarma, J. V., and Ward, P. A. (2011). The complement system. *Cell Tissue Res.* 343, 227–235. doi: 10.1007/s00441-010-1034-0

Schramm, E. C., Clark, S. J., Triebwasser, M. P., Raychaudhuri, S., Seddon, J., and Atkinson, J. P. (2014). Genetic variants in the complement system predisposing to age-related macular degeneration: a review. *Mol. Immunol.* 61, 118–125. doi: 10.1016/j.molimm.2014.06.032

Schwiebert, E. M., and Zsembery, A. (2003). Extracellular ATP as a signaling molecule for epithelial cells. *Biochim. Biophys. Acta* 1615, 7–32. doi: 10.1016/s0005-2736(03)00210-4

Shen, W., Fruttiger, M., Zhu, L., Chung, S. H., Barnett, N. L., Kirk, J. K., et al. (2012). Conditional Muller cell ablation causes independent neuronal and vascular pathologies in a novel transgenic model. *J. Neurosci.* 32, 15715–15727. doi: 10.1523/JNEUROSCI.2841-12.2012

Shi, J., Zhao, Y., Wang, K., Shi, X., Wang, Y., Huang, H., et al. (2015). Cleavage of GSDMD by inflammatory caspases determines pyroptotic cell death. *Nature* 526, 660–665. doi: 10.1038/nature15514

Shieh, C. H., Heinrich, A., Serchov, T., van Calker, D., and Biber, K. (2014). P2X7-dependent, but differentially regulated release of IL-6, CCL2, and TNF-α in cultured mouse microglia. *Glia* 62, 592–607. doi: 10.1002/glia.22628

Shinozaki, Y., Saito, K., Kashiwagi, K., and Koizumi, S. (2023). Ocular P2 receptors and glaucoma. *Neuropharmacology* 222:109302. doi: 10.1016/j.neuropharm.2022.109302

Sorbara, M. T., and Girardin, S. E. (2011). Mitochondrial ROS fuel the inflammasome. *Cell Res.* 21, 558–560. doi: 10.1038/cr.2011.20

Stahl, A. (2020). The diagnosis and treatment of age-related macular degeneration. *Deutsch. Arztebl. Int.* 117, 513–520. doi: 10.3238/arztebl.2020.0513

Strauss, O. (2005). The retinal pigment epithelium in visual function. *Physiol. Rev.* 85, 845–881. doi: 10.1152/physrev.00021.2004

Sun, Y., Zheng, Y., Wang, C., and Liu, Y. (2018). Glutathione depletion induces ferroptosis, autophagy, and premature cell senescence in retinal pigment epithelial cells. *Cell Death Dis.* 9:753. doi: 10.1038/s41419-018-0794-4

Theoharides, T. C., Alysandratos, K. D., Angelidou, A., Delivanis, D. A., Sismanopoulos, N., Zhang, B., et al. (2012). Mast cells and inflammation. *Biochim. Biophys. Acta* 1822, 21–33. doi: 10.1016/j.bbadis.2010.12.014

Thurman, J. M., Renner, B., Kunchithapautham, K., Ferreira, V. P., Pangburn, M. K., Ablonczy, Z., et al. (2009). Oxidative stress renders retinal pigment epithelial cells susceptible to complement-mediated injury. *J. Biol. Chem.* 284, 16939–16947. doi: 10.1074/jbc.M808166200

Tomasinsig, L., Pizzirani, C., Skerlavaj, B., Pellegatti, P., Gulinelli, S., Tossi, A., et al. (2008). The human cathelicidin LL-37 modulates the activities of the P2X7 receptor in a structure-dependent manner. *J. Biol. Chem.* 283, 30471–30481. doi: 10.1074/jbc.M802185200

Tseng, W. A., Thein, T., Kinnunen, K., Lashkari, K., Gregory, M. S., D'Amore, P. A., et al. (2013). NLRP3 inflammasome activation in retinal pigment epithelial cells by lysosomal destabilization: implications for age-related macular degeneration. *Invest. Ophthalmol. Vis. Sci.* 54, 110–120. doi: 10.1167/iovs.12-10655

Ventura, A. L. M., Mitchell, C. H., and Faillace, M. P. (2019). Purinergic signaling in the retina: from development to disease. *Brain Res. Bull.* 151, 92–108. doi: 10.1016/j.brainresbull.2018.10.016

Vessey, K. A., Gu, B. J., Jobling, A. I., Phipps, J. A., Greferath, U., Tran, M. X., et al. (2017). Loss of function of P2X7 receptor scavenger activity in aging mice: a novel model for investigating the early pathogenesis of age-related macular degeneration. *Am. J. Pathol.* 187, 1670–1685. doi: 10.1016/j.ajpath.2017.04.016

Wagner, A. H., Anand, V. N., Wang, W. H., Chatterton, J. E., Sun, D., Shepard, A. R., et al. (2013). Exon-level expression profiling of ocular tissues. *Exp. Eye Res.* 111, 105–111. doi: 10.1016/j.exer.2013.03.004

Wakx, A., Dutot, M., Massicot, F., Mascarelli, F., Limb, G. A., and Rat, P. (2016). Amyloid β peptide induces apoptosis through P2X7 cell death receptor in retinal cells: modulation by marine Omega-3 fatty acid DHA and EPA. *Appl. Biochem. Biotechnol.* 178, 368–381. doi: 10.1007/s12010-015-1878-6

Wareham, K. J., and Seward, E. P. (2016). P2X7 receptors induce degranulation in human mast cells. *Purinergic Signal.* 12, 235–246. doi: 10.1007/s11302-016-9497-4

Wareham, K., Vial, C., Wykes, R., Bradding, P., and Seward, E. (2009). Functional evidence for the expression of P2X1, P2X4 and P2X7 receptors in human lung mast cells. *Br. J. Pharmacol.* 157, 1215–1224. doi: 10.1111/j.1476-5381.2009.00287.x

Wong, W. L., Su, X., Li, X., Cheung, C. M., Klein, R., Cheng, C. Y., et al. (2014). Global prevalence of age-related macular degeneration and disease burden projection for 2020 and 2040: a systematic review and meta-analysis. *Lancet Glob. Health* 2, e106–e116. doi: 10.1016/S2214-109X(13)70145-1

Yancopoulos, G. D., Davis, S., Gale, N. W., Rudge, J. S., Wiegand, S. J., and Holash, J. (2000). Vascular-specific growth factors and blood vessel formation. *Nature* 407, 242–248. doi: 10.1038/35025215

Yang, D., Elner, S. G., Clark, A. J., Hughes, B. A., Petty, H. R., and Elner, V. M. (2011). Activation of P2X receptors induces apoptosis in human retinal pigment epithelium. *Invest. Ophthalmol. Vis. Sci.* 52, 1522–1530. doi: 10.1167/iovs.10-6172

Yang, D., He, Y., Muñoz-Planillo, R., Liu, Q., and Núñez, G. (2015). Caspase-11 requires the Pannexin-1 channel and the purinergic P2X7 pore to mediate pyroptosis and endotoxic shock. *Immunity* 43, 923–932. doi: 10.1016/j.immuni.2015.10.009

Yang, M., So, K. F., Lam, W. C., and Lo, A. (2020). Novel programmed cell death as therapeutic targets in age-related macular degeneration? *Int. J. Mol. Sci.* 21:7279. doi: 10.3390/ijms21197279

Ye, S. S., Tang, Y., and Song, J. T. (2021). ATP and adenosine in the retina and retinal diseases. *Front. Pharmacol.* 12:654445. doi: 10.3389/fphar.2021.654445

Yu, P., Zhang, X., Liu, N., Tang, L., Peng, C., and Chen, X. (2021). Pyroptosis: mechanisms and diseases. *Signal Transduct. Target. Ther.* 6:128. doi: 10.1038/s41392-021-00507-5

Zhang, W., Zhou, S., Liu, G., Kong, F., Chen, S., and Yan, H. (2018). Multiple steps determine CD73 shedding from RPE: lipid raft localization, ARA1 interaction, and MMP-9 up- regulation. *Purinergic Signal.* 14, 443–457. doi: 10.1007/s11302-018-9628-1

Zheng, D., Liwinski, T., and Elinav, E. (2020). Inflammasome activation and regulation: toward a better understanding of complex mechanisms. *Cell Discov.* 6:36. doi: 10.1038/s41421-020-0167-x

Zhou, R., Yazdi, A. S., Menu, P., and Tschopp, J. (2011). A role for mitochondria in NLRP3 inflammasome activation. *Nature* 469, 221–225. doi: 10.1038/nature09663

Zumerle, S., Calì, B., Munari, F., Angioni, R., Di Virgilio, F., Molon, B., et al. (2019). Intercellular calcium signaling induced by ATP potentiates macrophage phagocytosis. *Cell Rep.* 27, 1–10.e4. doi: 10.1016/j.celrep.2019.03.011

frontiers | Frontiers in Neuroscience

TYPE Original Research
PUBLISHED 24 July 2023
DOI 10.3389/fnins.2023.1186025

OPEN ACCESS

EDITED BY
Wensi Tao,
University of Miami Health System,
United States

REVIEWED BY
Navneet Mehrotra,
Retina Foundation and Retina Care, India
Yong Koo Kang,
Kyungpook National University,
Republic of Korea

*CORRESPONDENCE
Heping Xu
✉ heping.xu@qub.ac.uk
Zhongping Chen
✉ chenzhongping@aierchina.com

†These authors have contributed equally to this work and share first authorship

RECEIVED 14 March 2023
ACCEPTED 29 June 2023
PUBLISHED 24 July 2023

CITATION
Zhou Y, Qi J, Liu H, Liang S, Guo T, Chen J, Pan W, Tan H, Wang J, Xu H and Chen Z (2023) Increased intraocular inflammation in retinal vein occlusion is independent of circulating immune mediators and is involved in retinal oedema.
Front. Neurosci. 17:1186025.
doi: 10.3389/fnins.2023.1186025

Increased intraocular inflammation in retinal vein occlusion is independent of circulating immune mediators and is involved in retinal oedema

Yufan Zhou[1,2†], Jinyan Qi[2,3†], Hengwei Liu[1,2], Shengnan Liang[1,2], Tingting Guo[1,4], Juan Chen[1], Wei Pan[3], Huanhuan Tan[1], Jie Wang[1], Heping Xu[2,3,5*] and Zhongping Chen[1,2,3,6*]

[1]Changsha Aier Eye Hospital, Changsha, China, [2]Aier School of Ophthalmology, Central South University, Changsha, China, [3]Aier Institute of Optometry and Vision Science, Changsha, China, [4]The First Clinical Medical College of Jinan University, Guangzhou, China, [5]Wellcome-Wolfson Institute for Experimental Medicine, School of Medicine, Dentistry and Biomedical Sciences, Queen's University Belfast, Belfast, United Kingdom, [6]School of Stomatology and Ophthalmology, Xianning Medical College, Hubei University of Science and Technology, Xianning, China

We aim to understand the link between systemic and intraocular levels of inflammatory mediators in treatment-naïve retinal vein occlusion (RVO) patients, and the relationship between inflammatory mediators and retinal pathologies. Twenty inflammatory mediators were measured in this study, including IL-17E, Flt-3L, IL-3, IL-8, IL-33, MIP-3β, MIP-1α, GRO β, PD-L1, CD40L, IFN-β, G-CSF, Granzyme B, TRAIL, EGF, PDGF-AA, PDGF-AB/BB, TGF-α, VEGF, and FGFβ. RVO patients had significantly higher levels of Flt-3L, IL-8, MIP-3β, GROβ, and VEGF, but lower levels of EGF in the aqueous humor than cataract controls. The levels of Flt-3L, IL-3, IL-33, MIP-1α, PD-L1, CD40 L, G-CSF, TRAIL, PDGF-AB/BB, TGF-α, and VEGF were significantly higher in CRVO than in BRVO. KEGG pathway enrichment revealed that these mediators affected the PI3K-Akt, Ras, MAPK, and Jak/STAT signaling pathways. Protein–Protein Interaction (PPI) analysis showed that VEGF is the upstream cytokine that influences IL-8, G-CSF, and IL-33 in RVO. In the plasma, the level of GROβ was lower in RVO than in controls and no alterations were observed in other mediators. Retinal thickness [including central retinal thickness (CRT) and inner limiting membrane to inner plexiform layer (ILM-IPL)] positively correlated with the intraocular levels of Flt-3L, IL-33, GROβ, PD-L1, G-CSF, and TGF-α. The size of the foveal avascular zone positively correlated with systemic factors, including the plasma levels of IL-17E, IL-33, INF-β, GROβ, Granzyme B, and FGFβ and circulating high/low-density lipids and total cholesterols. Our results suggest that intraocular inflammation in RVO is driven primarily by local factors but not circulating immune mediators. Intraocular inflammation may promote macular oedema through the PI3K-Akt, Ras, MAPK, and Jak/STAT signaling pathways in RVO. Systemic factors, including cytokines and lipid levels may be involved in retinal microvascular remodeling.

KEYWORDS

aqueous humor, inflammatory factors, plasma, optical coherence tomographic angiography, VEGF, PI3 K signaling pathway, JAK-STAT signaling pathway

1. Introduction

Retinal vein occlusion (RVO) is an obstruction of the retinal venous system that can occur in a branch of the retinal vein (branch retinal vein occlusion, BRVO) or the central retinal vein (central retinal vein occlusion, CRVO). The pathogenesis of the disease remains elusive. The risk factors of RVO include both local (e.g., glaucoma, short axial distance) and systemic (e.g., hypertension, arteriosclerosis, hypercholesterolemia, diabetes mellitus, systemic vascular disease or inflammation, inherited thrombophilia, increased coagulability, age, obesity, smoking, etc.; Marcinkowska et al., 2022). RVO causes retinal hemorrhage, ischemia, macular oedema, and neovascularization leading to visual impairment (Jung et al., 2014; Zeng et al., 2019). The mainstream therapies of RVO include intraocular injection of vascular endothelial cell growth factor (VEGF) inhibitors or dexamethasone, laser photocoagulation, and surgery (Soliman et al., 2022). Despite the successful outcomes of intraocular injection of anti-VEGF agents, up to 77.5% of RVO patients continue to suffer from refractory or recurring edema (Karagiannis et al., 2011). There is an urgent need to understand the pathogenesis of the disease and the mechanism of retinal damage, especially persistent macular oedema.

Blood vessel occlusion is caused by abnormal thrombosis, which can arise from abnormal activation of the platelets, circulating immune cells, and vascular endothelial cells (Rayes et al., 2020; Pilard et al., 2022). Previous studies have shown platelets response to thrombin and collagen (Leoncini et al., 2007) is increased in RVO patients. Higher circulating neutrophil counts and monocyte/high-density lipoprotein ratio have been reported in RVO patients (Duru et al., 2021; Pan et al., 2022). Patients with ocular tuberculosis have been reported to present as BRVO with (Yuksel and Ozdek, 2013) or without (O'Hearn et al., 2007) retinal vasculitis or uveitis, suggesting the involvement of local inflammation in RVO. Furthermore, higher levels of inflammatory mediators such as IL-6 (Yong et al., 2021), IL-8 (Yang et al., 2021), MCP-1 (Wei et al., 2020), placental growth factor (PIGF; Noma et al., 2014), platelet-derived growth factor (PDGF; Lee et al., 2012), and adhesion molecule ICAM-1 (Yi et al., 2020) have been reported in RVO patients. Inflammation and hypoxia are believed to play a critical role in the pathogenesis of RVO (Noma et al., 2020). How the systemic and local factors work together to lead to RVO remains unknown.

In this study, we measured the levels of 20 inflammatory mediators, including eight inflammatory cytokines (IL-17E, Flt-3 L, IL-3, IL-8, IL-33, MIP-3β, MIP-1α, and GRO β), six immunomodulatory cytokines (PD-L1, CD40L, IFN-β, G-CSF, Granzyme B, and TRAIL), and six growth factors involved in extracellular matrix remodeling and angiogenesis (EGF, PDGF-AA, PDGF-AB/BB, TGF-α, VEGF, and FGFβ) in both the plasma and the aqueous humor of RVO. We further investigated the relationship between the inflammatory mediators and clinical presentations (e.g., visual acuity, retinal thickness, and vascular density etc.) of RVO. Surprisingly, we found that increased intraocular inflammation in RVO is independent of systemic immune mediators.

2. Materials and methods

2.1. Patients

This prospective observational case–control study was performed under the Declaration of Helsinki. Informed consent was obtained from each participant and the Institutional Review Board (IRB) at the Changsha Aier Eye Hospital approved the study [Ethical approval number: (2020) KYPJ005]. Twenty RVO (six with CRVO and 14 with BRVO) treatment-naive patients were recruited from January 2021 to December 2021 in Changsha Aier Eye Hospital. Inclusion criteria were (1) RVO confirmed by fundus stereoscopy, optical coherence tomography angiography (OCTA), and fluorescein fundus angiography (FFA); (2) RVO with visual impairment who require medical attention [e.g., intravitreal anti-VEGF (ranibizumab) or dexamethasone (ozurdex) treatment]. Twenty patients with senile cataracts undergoing cataract surgery were used as controls. The inclusion criteria of the control group were elderly cataract patients who needed phacoemulsification. The exclusion criteria for all participants were (1) other retinal pathologies (e.g., glaucoma, diabetic retinopathy, and retinal neovascularization by other causes); (2) the existence or history of intraocular or systemic inflammatory diseases (e.g., uveitis, active pneumonitis); (3) the presence or history of cancer (e.g., breast cancer, colon cancer), autoimmune diseases (e.g., systemic lupus erythematosus), ocular trauma, severe liver, and kidney dysfunction; (4) history of intraocular surgery (e.g., vitrectomy，anti-VEGF, intraocular steroids) or laser treatment within 6 months.

2.2. Data collection and masking

All clinical examinations were conducted by two consultant ophthalmologists. Retinal images (FFA, OCT, and OCTA) were examined by two experienced retinal specialists. Researchers who carried out laboratory experiments and analysis were masked to the origin of the clinical samples to be analyzed.

2.3. Ocular examination

All RVO patients underwent a complete ocular examination including logMAR best corrected visual acuity (BCVA), slit lamp examination, intraocular pressure measurement, B-scan ocular ultrasound and fundus stereoscopic biomicroscopy, FFA (Spectralis™ HRA, Heidelberg Engineering, Heidelberg, Germany), and OCTA (RTVue-XR Avanti, Optovue, Fremont, CA, United States). OCTA images were used to collect the below parameters: CRT, foveal avascular zone (FAZ), perimeter (PERIM) of the fovea, ILM-IPL thickness, superficial vessel density (SVD), and deep vessel density (DVD).

All cataract patients underwent a comprehensive ophthalmic examination before surgery, including Log MAR BCVA, slit-lamp examination, intraocular pressure measurement, fundus stereoscopic biomicroscopy, B-scan ocular ultrasound, and optical coherence tomography (OCT; CIRRUS ™HD-OCT 5000, Carl Zeiss Meditec, Dublin, CA, United States).

2.4. Blood test

The following parameters were collected from routine blood tests: glucose (GLU), triglyceride (TG), total cholesterol (TC), high-density lipoprotein cholesterol (HDLC), low-density lipoprotein cholesterol

(LDLC), prothrombin time (PT), prothrombin time-international normalized ratio (PTINR), thrombin time (TT), activated partial thromboplastin time (APTT), and fibrinogen (FIB).

2.5. Demographic information

The following information was extracted from the medical records of each patient: age, gender, body mass index (BMI), the use of other medications (e.g., to control hypertension, diabetes, aspirin, and hormone supplements), smoking history, other eye diseases, history of systemic disease (e.g., hypertension, diabetes), history of allergy disease, autoimmune diseases, surgical history, history of drug allergy, and history of vaccinations.

2.6. Sample collection

The aqueous humor and plasma samples were collected as described previously (Luo et al., 2021). Briefly, in RVO patients, 60 μL of aqueous humor was extracted before intravitreal injection of ranibizumab or dexamethasone to relieve intraocular pressure. In cataract patients, 50 μL of aqueous humor was collected at the beginning of cataract surgery procedure. All procedures were conducted in an ophthalmology surgical operating room.

Fasting blood samples (5 mL) were loaded into a purple sterile vacuum blood collection tube with EDTAK2 anticoagulant (Huabo Technology, Haze, China) and were reversed several times immediately. Approximately, 2 mL of plasma samples were collected after centrifugation (3,000 r/min, 10 min at room temperature). Plasma and aqueous humor samples were kept in sterile Eppendorf and stored at −80°C until laboratory measurements.

2.7. Laboratory measurement

The levels of IL-17E, Flt-3 L, IL-3, IL-8, IL-33, MIP-3β, MIP-1α, GRO β, PD-L1, CD40 L, IFN-β, G-CSF, Granzyme B, TRAIL, EGF, PDGF-AA, PDGF-AB/BB, TGF-α, VEGF, and FGFβ in aqueous humor and plasma samples were measured using the Luminex® × MAP® technology following manufacturer's instructions (Luminex × Map Technology, Bio-Rad). A total of 25 μL of aqueous humor (1:2 dilution) and plasma (undiluted) from each sample were used in the study, respectively. The fluorescent intensity was measured using a plate reader with the Luminex® × PONENT® acquisition software (MAGPIX®). The concentration of target molecules was calculated using the MILLIPLEX® Analyst 5.1.

2.8. Bioinformatics analysis

Kyoto Encyclopedia of Genes and Genomes (KEGG) enrichment pathway analysis of differentially expressed proteins (DEPs) was performed using the online platform OmicShare[1] with adjusted $p < 0.05$. A protein–protein interaction (PPI) network of DEPs was searched in the STRING database with a confidence score > 0.4. The top 10 DEPs with the highest connection degree were calculated by the Cytohubba plugin and visualized in Cytoscape (Version3.9.1, Oracle, Redwood City, CA, United States).

2.9. Statistical analysis

Data were analyzed using the SPSS 20.0 software and plots were generated using GraphPad Prism v8.0. The Kolmogorov–Smirnov test was used to evaluate the data distribution. The non-normally distributed data were log-transformed into a normal distribution. The continuous variables were presented as mean ± SD and compared by the Student's *t*-test and One-way ANOVA. The chi-square test was used to compare categorical variables. Multivariable linear regression was used to check confounding factors when comparing the variables in different groups. The correlation between aqueous humor/plasma inflammatory factors levels and clinical parameters was assessed using the Pearson correlation method. $p < 0.05$ was considered statistically significant.

3. Results

3.1. Laboratory measurement rate

Cytokine levels were measured in 32 aqueous humor samples (13 controls and 19 RVO) and 40 plasma samples (20 controls and 20 RVO). All cytokines were within the measurement range. One sample in the cataract group was excluded from the analysis because 50% of the measurements were extremely high and the participant was later confirmed to suffer from rheumatoid arthritis.

3.2. Clinical characteristics

There was no significant difference in gender distribution, history of hypertension or diabetes, history of smoking, BMI, and BCVA between RVO patients and controls (Table 1). However, the average age of RVO, subgroup-BRVO patients was significantly younger than that of controls (Table 1). As expected, the CRT of RVO patients (including subgroup CRVO and BRVO) were significantly higher than controls (Table 1). There was no significant difference in age, RVO duration，CRT, FAZ, PERIM, ILM-IPL, SVD, and DVD between BRVO and CRVO (Table 1).

3.3. Inflammatory mediators in RVO patients and controls

In the aqueous humor, the levels of Flt-3 L, IL-8, MIP-3β, GROβ, PDGF-AA, and VEGF in the RVO patients were significantly higher while the level of EGF was significantly lower than in controls (Table 2). After adjusting for age, except for PDGF-AA, the differences remained (Table 2). Further subgroup analyses showed that the levels of Flt-3 L, IL-8, IL-33, MIP-1α, GROβ, G-CSF, PDGF-AA, PDGF-AB/BB, TGF-α, and VEGF in CRVO patients were

1 https://www.omicshare.com/tools

TABLE 1 Demographic and clinical characteristics of study participants.

Clinical variables	Control	RVO	Subgroups of RVO		
			CRVO	BRVO	*p* values
	N=19	*N*=20	*N*=6	*N*=14	BRVO vs. CRVO
Age (mean ± SD) years	66.63 ± 5.29	**59.55 ± 11.44**[*, a]	60.17 ± 11.04	**59.29 ± 12.00**[*, c]	1.000
Male (%)[b]	52.6	60.00	16.67	50.00	0.163
Hypertension (%)[b]	42.10	55.00	16.66	71.43	0.111
Diabetes (%)[b]	10.50	10.00	16.66	7.14	0.515
Smoking (%)[b]	26.30	15.00	16.66	14.29	0.891
BMI (mean ± SD) kg/m^2	22.13 ± 3.58	24.83 ± 3.21	23.7 ± 2.62	25.32 ± 3.40	1.00
BCVA (mean ± SD)	0.93 ± 0.85	0.92 ± 0.28	0.97 ± 0.24	0.90 ± 0.31	1.000
RVO duration (≤ 1-month) (%)[b]	\	50	50	50	1.000
CRT (mean ± SD) μm	222.22 ± 25.91	**588.85 ± 221.26**[**, a]	**660.50 ± 215.33**[**, c]	**558.14 ± 224.35**[**, c]	0.56
FAZ (mean ± SD) mm^2	\	0.24 ± 0.14	0.23 ± 0.13	0.24 ± 0.15	0.966
PERIM (mean ± SD) mm	\	1.93 ± 0.57	2.05 ± 0.58	1.89 ± 0.58	0.582
ILM-IPL (mean ± SD)	\	125.82 ± 96.88	169.11 ± 121.79	107.26 ± 82.33	0.199
SVD (mean ± SD)	\	44.75 ± 3.77	44.57 ± 3.21	44.82 ± 4.09	0.894
DVD (mean ± SD)	\	44.63 ± 3.23	45.91 ± 2.68	44.08 ± 3.37	0.255

[a]Independent sample *t*-test, between controls and RVO patients; [b]Chi-square test; [c]One-way ANOVA test analyzed controls, CRVO, and BRVO patients. *$p < 0.05$; **$p < 0.01$. Bold indicating *p* value was statistically significant. RVO, retinal vein occlusion; BRVO, branch retinal vein occlusion; CRVO, central retinal vein occlusion; BMI, body mass index; BCVA, best corrected visual acuity (expressed as LogMAR); CRT, central retinal thickness; FAZ, foveal avascular zone; PERIM, perimeter of fovea; ILM-IPL, inner limiting membrane-inner plexiform layer; SVD, superficial vessel density; and DVD, deep vessel density.

significantly higher than those in controls after adjustment for age (Table 2). The levels of Flt-3 L, IL-8, MIP-3β, and GROβ in BRVO patients were also significantly higher than in controls. However, the levels of PD-L1, CD40L, EGF, IL-3, and TRAIL in BRVO were significantly lower than in the controls (Table 2). Furthermore, patients with CRVO had significantly higher levels of Flt-3 L, IL-3, IL-33, MIP-1α, PD-L1, CD40L, G-CSF, TRAIL, PDGF-AB/BB, TGF-α, and VEGF than patients with BRVO (Table 2).

In the plasma, the levels of GROβ, EGF in the RVO patients were significantly lower than in controls. After adjusting for age, the difference in GROβ remained (Table 3). Further subgroup analysis showed that the level of GROβ in both CRVO and BRVO was significantly lower than that in controls (Table 3). The level of MIP-3β in BRVO patients was significantly higher than in controls after adjustment for age (Table 3). There was no significant difference in any of the variables between CRVO and BRVO patients (Table 3). We further found that the plasma levels of IL-17E, IL-8, IL-33, MIP-1α, TGF-α, and FGFβ in RVO positively correlated with disease duration, and patients with >1-month disease duration had significantly higher levels of these cytokines than patients with ≤1 month-disease duration (Supplementary Table S1). However, there was no significant difference in aqueous inflammatory mediators between disease duration >1-month and disease duration ≤1-month (Supplementary Table S1).

3.4. Correlation between inflammatory mediators and OCTA parameters in RVO patients

Pearson correlation analysis showed aqueous humor levels of GROβ and Granzyme B positively correlated with the CRT. The aqueous levels of Flt-3 L, IL-33, GROβ, PD-L1, G-CSF, and TGF-α positively correlated with the ILM-IPL thickness. G-CSF positively correlated and MIP-3β negatively correlated with DVD (Table 4). No correlation was observed between the aqueous humor levels of inflammatory factors and visual acuity, PERIM, FAZ, and SVD (Table 4). Our results suggest that intraocular levels of Flt-3 L, IL-33, GROβ, PD-L1, G-CSF, TGF-α, and MIP-3β may contribute to vascular leakage and retinal deep layer vascular degeneration in RVO.

The plasma levels of IL-17E, IL-33, INF-β, GROβ, and FGFβ positively correlated with the FAZ. No correlation was observed between the plasma levels of inflammatory mediators and visual acuity, PERIM, ILM-IPL, SVD, and DVD (Table 5).

We also found a positive correlation between blood GLU and retinal PERIM. The circulating levels of TC, HDLC, and LDLC positively correlated with FAZ. In addition, the level of APTT positively correlated with the CRT and the level of FIB positively correlated with the SVD (Table 6). Our results suggest a link between circulating levels of glucose, cholesterol, and coagulation factors and retinal structural alteration in RVO.

3.5. Correlation between plasma and aqueous humor levels of inflammatory mediators

The plasma level of EGF positively correlated with that in aqueous humor in all participants (Figure 1A), but the correlation became less significant in RVO patients (Figure 1). The plasma levels of GROβ, PDGF-AA, and PDGF-AB/BB negatively correlated with those in aqueous humor. No correlation was

TABLE 2 Aqueous humor levels of inflammatory factors in RVO patients and controls.

Variables	Control	RVO	Subgroups of RVO		
			CRVO	BRVO	*p* values
	(*n*=13, pg/mL)	(*n*=19, pg/mL)	(*n*=5, pg/mL)	(*n*=14, pg/mL)	BRVO vs. CRVO
IL-17E	21.15 ± 1.76	21.30 ± 2.60	22.14 ± 3.01	21.00 ± 2.49	0.445
Flt-3 L	30.53 ± 1.99	**40.95 ± 11.63**^{**,a}	**51.00 ± 11.11**^{**,c}	**37.36 ± 9.83**^{*,c}	**0.022**^{b}
IL-3	25.91 ± 2.79	24.26 ± 2.29	25.98 ± 3.46	**23.64 ± 1.41**^{*,c}	**0.047**^{b}
IL-8	13.86 ± 7.18	**101.40 ± 82.64**^{**,a}	**177.04 ± 103.40**^{**,c}	**74.38 ± 56.38**^{**,c}	0.063
IL-33	17.40 ± 1.31	17.96 ± 1.28	**19.22 ± 1.19**^{**,c}	17.50 ± 0.99	**0.006**^{b}
MIP-3β	6.30 ± 0.79	**13.19 ± 8.78**^{**,a}	9.6 ± 2.31	**14.47 ± 9.92**^{*,c}	0.388
MIP-1α	13.35 ± 2.04	13.29 ± 1.51	**14.94 ± 1.46**^{*,c}	12.69 ± 1.03	**0.002**^{b}
GRO β	14.70 ± 1.82	**21.64 ± 7.12**^{**,a}	**26.73 ± 7.46**^{**,c}	**19.83 ± 6.29**^{*,c}	0.065
PD-L1	109.26 ± 8.61	104.12 ± 12.76	119.10 ± 14.53	**98.78 ± 6.58**^{**,c}	**0.001**^{b}
CD40 L	1440.41 ± 162.50	1336.93 ± 129.86	1437.08 ± 137.22	**1301.17 ± 111.01**^{**,c}	**0.047**^{b}
IFN-β	3.87 ± 0.44	3.95 ± 0.40	3.77 ± 0.37	4.02 ± 0.41	0.254
G-CSF	10.11 ± 1.25	61.11 ± 151.63	**201.45 ± 264.60**^{**,c}	10.99 ± 3.23	**0.008**^{b}
Granzyme B	8.98 ± 2.12	9.60 ± 3.23	11.86 ± 5.46	8.80 ± 1.62	0.125
TRAIL	26.62 ± 1.53	26.28 ± 1.57	27.76 ± 1.81	**25.75 ± 1.21**^{*,c}	**0.01**^{b}
EGF	9.72 ± 1.47	**8.57 ± 1.95**^{*,a}	9.39 ± 1.24	**8.27 ± 2.11**^{*,c}	0.173
PDGF-AA	219.25 ± 36.00	292.94 ± 101.29	**371.61 ± 127.45**^{**,c}	264.84 ± 77.30	0.083
PDGF-AB/BB	3.85 ± 0.19	3.86 ± 0.26	**4.07 ± 0.29**^{*,c}	3.78 ± 0.21	**0.032**^{b}
TGF-α	9.84 ± 0.67	9.99 ± 0.79	**11.04 ± 0.53**^{**,c}	9.62 ± 0.47	**0.000**^{b}
VEGF	278.84 ± 123.40	**829.49 ± 892.55**^{*,a}	**1599.37 ± 1118.44**^{**,c}	554.53 ± 639.36	**0.014**^{b}
FGF β	12.80 ± 2.00	12.84 ± 2.56	13.14 ± 1.56	12.73 ± 2.88	0.641

[a]Multivariable linear regression analysis of inflammatory factors between controls and RVO patients after adjusting for age. [b]Independent sample *t*-test analysis between BRVO and CRVO patients; [c]Multivariable linear regression analysis of inflammatory factors between controls and CRVO, BRVO patients after adjusting for age. *$p < 0.05$; **$p < 0.01$. Bold indicating p value was statistically significant. RVO, retinal vein occlusion; BRVO, branch retinal vein occlusion; and CRVO, central retinal vein occlusion.

detected in other inflammatory mediators between the plasma and aqueous humor. Our results suggest that the majority of intraocular inflammatory mediators are independent of their counterparts in blood circulation.

3.6. PPI and enrichment analysis of measured inflammatory factors

To understand the pathways associated with RVO, we constructed a PPI network using the STRING database with the 17 differentially expressed proteins (DEPs) uncovered in our analysis. The analysis obtained 17 nodes and 78 edges with a confidence score > 0.4. Figure 2A showed the top 10 highest degree connection factors, namely, IL-8, VEGF, MIP-1α GROβ, CD40L, G-CSF, PD-L1, EGF, IL-3, and IL-33. VEGF appears to be the upstream protein that can affect all other proteins, whereas IL-8, G-CSF, and IL-33 are the downstream proteins affected by others in the PPI network (Figure 2A). KEGG analysis identified PI3K-Akt, EGFR tyrosine kinase inhibitor resistance, cancer, Ras, cytokine-cytokine receptor interaction, MAPK, Jak/STAT, glioma, prostate cancer, and bladder cancer as significantly enriched pathways (Figure 2B).

4. Discussion

In this study, we show that RVO patients had significantly higher intraocular levels of inflammatory mediators compared with senile cataract controls. Five (Flt-3 L, IL-8, MIP-3β, GROβ, and VEGF) out of 20 inflammatory mediators in the aqueous humor were significantly higher in RVO patients. The changes in intraocular cytokines were more pronounced in CRVO than in BRVO. Eleven out of 20 cytokines were significantly higher in CRVO than in BROV. KEGG enrichment analysis showed that the PI3K-Akt, Ras, MAPK, and Jak–STAT signaling pathways were affected by these cytokines. Importantly, we found that the alterations in intraocular cytokines were independent of systemic inflammation as none of the inflammatory cytokines was significantly increased in the plasma in RVO patients. Our results suggest that retinal pathologies in RVO may be driven primarily by dysregulation of intraocular immune response but not systemic immune mediators.

The RVO is due to abnormal thrombosis, which can arise from abnormal endothelial cell activation, misbehavior of circulating immune cells and platelets activation. The plasma IL-8, IL-17E, MIP-1α, MIP-3β, G-CSF, and IFNβ are most likely produced by circulating immune cells, and PDGF-AA and PDGF-AB/BB are known to be released by active platelets. The fact that none of them

TABLE 3 Plasma levels of inflammatory mediators in RVO patients and controls.

Variables	Control	RVO	Subgroups of RVO		
			CRVO	BRVO	*p* values
	(*n*=19, pg/mL)	(*n*=20, pg/mL)	(*n*=6, pg/mL)	(*n*=14, pg/mL)	BRVO vs. CRVO
IL-17E	6.22 ± 3.47	7.80 ± 6.96	7.63 ± 7.77	7.88 ± 6.89	0.81
Flt-3 L	66.15 ± 19.28	64.50 ± 28.82	63.23 ± 28.88	65.04 ± 29.86	0.987
IL-3	4.19 ± 3.90	5.35 ± 11.03	4.86 ± 3.90	5.55 ± 13.11	0.231
IL-8	2.87 ± 1.36	4.62 ± 8.21	1.76 ± 0.97	5.84 ± 9.63	0.394
IL-33	10.64 ± 4.51	9.75 ± 9.09	9.84 ± 7.98	9.71 ± 9.81	0.848
MIP-3β	61.91 ± 18.64	79.86 ± 34.22	68.44 ± 18.73	**84.76 ± 38.61***,c	0.413
MIP-α	20.12 ± 15.00	15.96 ± 10.40	15.04 ± 8.89	16.36 ± 11.27	0.992
GRO β	316.98 ± 170.94	**82.37 ± 102.26****,a	**71.67 ± 69.24****,c	**86.96 ± 115.61****,c	0.872
PD-L1	179.35 ± 433.37	118.37 ± 120.52	197.58 ± 147.27	84.42 ± 93.55	0.057
CD40 L	365.81 ± 195.71	562.85 ± 1179.37	483.26 ± 441.56	596.96 ± 1397.75	0.368
IFN-β	3.31 ± 4.18	3.42 ± 3.97	3.73 ± 5.51	3.28 ± 3.36	0.837
G-CSF	13.71 ± 7.74	11.89 ± 11.23	13.05 ± 13.56	11.39 ± 10.62	0.768
Granzyme B	3.40 ± 3.59	4.31 ± 8.90	5.08 ± 5.83	3.98 ± 10.11	0.225
TRAIL	43.28 ± 19.78	53.73 ± 32.19	60.96 ± 23.66	50.63 ± 35.56	0.301
EGF	15.24 ± 25.67	11.48 ± 22.61	11.22 ± 17.35	11.59 ± 25.12	0.548
PDGF-AA	1838.86 ± 1119.14	1690.93 ± 2137.33	1580.28 ± 2042.11	1738.36 ± 2250.46	0.961
PDGF-AB/BB	356.67 ± 291.63	299.83 ± 373.05	371.66 ± 516.67	269.05 ± 311.96	0.616
TGF-α	9.48 ± 6.44	9.10 ± 9.50	8.37 ± 8.91	9.41 ± 10.06	0.774
VEGF	56.57 ± 19.56	63.40 ± 53.77	78.57 ± 85.06	56.90 ± 35.93	0.601
FGF β	11.74 ± 6.34	11.29 ± 13.72	10.46 ± 11.55	11.65 ± 14.94	0.928

[a]Multivariable linear regression analysis of inflammatory factors between controls and RVO patients after adjusting for age. [b]Independent sample *t*-test analysis between BRVO and CRVO patients; [c]Multivariable linear regression analysis of inflammatory factors between controls and CRVO, BRVO patients after adjusting for age. *$p < 0.05$; **$p < 0.01$. Bold indicating *p* value was statistically significant. RVO, retinal vein occlusion; BRVO, branch retinal vein occlusion; and CRVO, central retinal vein occlusion.

was altered in RVO patients suggests that abnormal behavior of circulating immune cells and platelets is unlikely the cause of thrombosis. Surprisingly, the plasma level of GROβ was significantly lower in the RVO patients, particularly in those with less than 1-month disease duration (seven times lower than controls), suggesting a likely protective role of circulating GROβ in RVO. Interestingly, we found that the plasma levels of IL-17E, EGF, IL-33, MIP-1α, TGF-α, and FGFβ positively correlated with disease duration, indicating that these circulating factors may be an active response to RVO-mediated retinal ischemic injury.

We found that RVO (particularly CRVO) patients, had significantly higher intraocular levels of inflammatory cytokines/mediators including Flt-3 L, IL-8, IL-33, MIP-1α, RGOβ, G-CSF, PDGF-AA, PDGF-AB/BB, TGF-α, and VEGF. The higher intraocular inflammation may lead to retinal vascular endothelial activation, which may trigger abnormal thrombosis. The crosstalk between inflammation and coagulation and their involvement in thrombotic diseases is well recognized (Foley and Conway, 2016). For example, G-CSF and IL-8 can induce neutrophil extracellular traps (NETs), which can enhance coagulation (Demers et al., 2012; Alfaro et al., 2016; Thålin et al., 2019). TNF-α can facilitate the crosstalk between inflammation and thrombosis by triggering the NF-κB pathway (Muralidharan-Chari et al., 2016). VEGF can induce tissue factors in endothelial cells and tumor cells, activating coagulation and fibrin formation (Salgado et al., 2002). Although higher levels of intraocular inflammation can be explained by RVO-mediated retinal damage, it is possible that these eyes may also have higher basal levels of inflammatory cytokines, which may stimulate retinal vascular endothelial cells and contribute to the development of RVO.

We found positive correlations between parameters of macular oedema (i.e., CRT and ILM-IPL) and intraocular inflammatory mediators including GROβ, Granzyme B, Flt-3 L, IL-33, PD-L1, and G-CSF, suggesting that they may contribute to retinal vascular leakage, fluid accumulation, and neuronal damage in RVO. The aqueous level of MIP-3β negatively, but G-CSF positively correlated with DVD, an indicator of deep layer retinal vascular degeneration. G-CSF is an essential growth factor for microglia (Chitu et al., 2021). Retinal microglia in the inner retina are known to rely on IL-34 (O'Koren et al., 2019), whereas the microglia in the outer retinal layer are IL-34-independent, and they may rely on G-CSF. Microglia is an important component of neurovascular unit (Liu et al., 2020). Our results suggest that G-CSF may be protective, while MIP-3β may be detrimental to retinal microvasculature in RVO. Intravitreal injection of VEGF inhibitors is the standard of care for RVO-mediated macular

TABLE 4 Correlation between inflammatory factors and BCVA and OCTA parameters in aqueous humor RVO patients (n=19).

Variables	Log MAR	CRT	FAZ	PERIM	ILM-IPL	SVD	DVD
	r	*r*	*r*	*r*	*r*	*r*	*r*
IL-17E	0.12	−0.12	0.45	0.20	−0.11	−0.02	0.15
Flt-3 L	−0.02	0.34	−0.32	0.04	**0.57****	0.19	0.12
IL-3	−0.25	0.42	0.24	0.11	0.39	−0.13	0.14
IL-8	−0.06	0.27	−0.44	−0.04	0.41	0.01	0.12
IL-33	0.04	0.36	0.05	0.12	**0.53***	0.35	0.41
MIP-3β	0.11	0.24	−0.27	−0.14	−0.01	0.11	**−0.69****
MIP-1α	−0.23	0.41	0.23	0.16	0.32	−0.12	0.34
GRO β	−0.07	**0.54****	−0.29	−0.06	**0.50****	0.22	−0.08
PD-L1	0.12	0.36	0.19	0.16	**0.55****	−0.07	0.31
CD40 L	0.42	0.10	−0.09	0.01	−0.00	−0.00	0.10
IFN-β	−0.35	0.19	0.03	0.01	−0.18	−0.25	−0.13
G-CSF	0.10	0.16	−0.09	0.15	**0.67****	−0.01	**0.46***
Granzyme B	−0.06	**0.48***	0.31	0.23	0.38	0.25	0.23
TRAIL	0.12	−0.07	0.13	0.14	0.38	0.01	0.34
EGF	0.32	0.19	0.32	−0.04	0.12	−0.00	0.23
PDGF-AA	−0.21	0.24	−0.36	−0.12	0.14	0.09	−0.04
PDGF-AB/BB	−0.28	0.25	−0.09	0.00	0.42	0.07	0.09
TGF-α	0.13	0.34	0.02	0.18	**0.48***	0.15	0.14
VEGF	−0.21	−0.01	−0.18	0.03	0.24	0.03	0.05
FGF β	−0.36	−0.02	0.02	0.17	0.01	−0.14	−0.15

Pearson correlation analysis evaluated possible links between aqueous inflammatory factors and visual acuity, and OCTA parameters. *$p<0.05$; **$p<0.01$. Bold indicating p value was statistically significant. CRT, central retinal thickness; FAZ, foveal avascular zone; PERIM, perimeter of fovea; ILM-IPL, inner limiting membrane-inner plexiform layer; SVD, superficial vessel density; and DVD, deep vessel density.

oedema (Campochiaro et al., 2014a,b; Thach et al., 2014). Surprisingly, we did not detect any direct correlation between intraocular levels of VEGF and RVO-related macular changes. PPI analysis showed that VEGF is the upstream factor that can affect many other cytokines, including IL-8, IL-33, G-CSF, and GROβ (Figure 2A). Collectively, these cytokines can affect the PI3K-Akt, Ras, MAPK, and Jak–STAT signaling pathways (Figure 2B). The role of PI3K-Akt (Jacot and Sherris, 2011; Ma et al., 2022), Ras (Wang et al., 2015), MAPK (Supanji et al., 2013; Moustardas et al., 2023), and Jak–STAT (Chen et al., 2016, 2019; Hombrebueno et al., 2020; Cho et al., 2022) pathways in inflammatory and degeneration retinal diseases such as diabetic retinopathy and age-related macular degeneration has been well appreciated. Our results suggest that they may also be involved in RVO-mediated retinopathy.

Interestingly, we found positive correlations between FAZ and systemic factors, including the plasma levels of IL-17E, IL-33, GROβ, IFN-β, FGF β, and circulating lipid/cholesterols (TC, HDLC, and LDLC). FAZ is the most sensitive central area of the macula, and changes in its shape and size can pose great threats to vision. Progressive and irregular expansion of FAZ has been observed in RVO eyes (Fan et al., 2022), and changes in FAZ are related to capillary remodeling in the macular area (Tripathy et al., 2021). Our results suggest that circulating factors may be involved in retinal microvascular remodeling in RVO.

The strengths of the study include (1) the simultaneous measurement of inflammatory mediators in the blood and aqueous humor from the same participants; (2) comprehensive clinical and laboratory evaluations of the participants. The study has several limitations. First, the number of participants enrolled in this study was relatively small (e.g., six CRVO and 14 BRVO). Second, the OCTA parameters (e.g., FAZ, PERIM, and ILM-IPL) were only conducted in RVO patients but not in control cataract patients. Third, the study was conducted in a single center and the results can only reflect the biological feature of RVO in the local ethical population. Replication of the findings with a larger sample size and in multiple ethnic groups is necessary to confirm our results. However, it should be noted that single center study reduces procedure-related variation and increases the reliability of the results in small sample size studies.

In conclusion, we show that intraocular inflammation in RVO patients is driven primarily by local factors but not circulating immune mediators. Intraocular inflammation may be involved in the development of RVO and contribute to macular oedema through the PI3K-Akt, Ras, MAPK, and Jak/STAT signaling pathways. The blood levels of cholesterols and the levels of IL-17E, IL33, RGOβ, and FGF-b may affect retinal microvascular remodeling in RVO.

10.3389/fnins.2023.1186025

TABLE 5 Correlation between plasma inflammatory factors and BCVA and OCTA parameters in plasma levels of RVO patients (n=19).

Variables	Log MARr	CRT	FAZ	PERIM	ILM-IPL	SVD	DVD
	r	*r*	*r*	*r*	*r*	*r*	*r*
IL-17E	0.26	−0.09	**0.49***	0.15	−0.12	0.15	0.17
Flt-3 L	−0.18	−0.03	0.36	0.36	−0.17	−0.23	−0.10
IL-3	0.04	−0.01	0.34	−0.11	−0.14	−0.03	0.15
IL-8	−0.08	−0.20	−0.02	−0.08	−0.10	0.36	0.01
IL-33	0.32	−0.07	**0.50***	0.15	−0.11	0.12	0.14
MIP-3β	0.10	−0.17	0.12	0.36	0.02	0.18	−0.11
MIP-1α	0.20	0.23	0.26	0.04	0.10	0.35	0.06
GRO β	0.28	0.09	**0.50***	0.07	−0.03	0.13	0.17
PD-L1	0.13	0.18	0.22	0.07	0.00	0.05	−0.00
CD40 L	0.20	0.01	0.32	−0.08	−0.15	−0.01	0.13
IFN-β	0.41	−0.05	**0.47***	0.36	−0.10	0.13	0.05
G-CSF	0.29	−0.03	0.42	0.30	−0.05	0.11	0.13
Granzyme B	−0.14	0.20	0.41	−0.04	−0.14	−0.03	0.17
TRAIL	0. 31	0.00	0.32	0.11	−0.04	−0.04	0.05
EGF	0.26	0.01	0.37	0.10	−0.10	0.10	0.12
PDGF-AA	0.15	−0.14	0.37	0.15	−0.10	0.10	0.15
PDGF-AB/BB	−0.08	−0.04	0.37	0.26	−0.07	0.01	0.13
TGF-α	0.40	−0.10	0.40	0.12	−0.11	0.16	0.12
VEGF	0.20	0.06	0.43	0.33	−0.03	0.09	0.07
FGF β	0.37	−0.10	**0.49***	0.14	−0.10	0.14	0.12

Pearson correlation analysis evaluated possible links between plasma inflammatory factors and visual acuity, OCTA parameters. *$p < 0.05$; **$p < 0.01$. Bold indicating p value was statistically significant. CRT, central retinal thickness; FAZ, foveal avascular zone; PERIM, perimeter of fovea; ILM-IPL, inner limiting membrane-inner plexiform layer; SVD, superficial vessel density; and DVD, deep vessel density.

TABLE 6 Correlation between BCVA, OCTA parameters and blood test parameters in RVO patients (n=20).

Variables	Log MAR	CRT	FAZ	PERIM	ILM-IPL	SVD	DVD
	r	*r*	*r*	*r*	*r*	*r*	*r*
GLU	0.19	−0.18	0.22	**0.45***	−0.05	0.28	−0.12
TG	−0.11	0.08	0.30	0.44	0.00	0.42	0.09
TC	−0.15	−0.03	**0.52***	0.36	0.10	0.22	0.15
HDLC	−0.26	−0.08	**0.53***	0.07	−0.03	0.02	0.11
LDLC	−0.11	−0.03	**0.52***	0.27	0.04	0.14	0.13
PT	0.15	0.19	−0.27	−0.20	0.07	−0.14	0.03
PTINR	0.17	0.20	−0.26	−0.19	0.09	−0.12	0.03
TT	0.38	−0.16	−0.14	0.03	0.21	0.01	−0.02
APTT	0.06	**0.46***	0.03	−0.06	0.26	0.07	−0.09
FIB	0.12	−0.02	−0.04	0.20	0.02	**0.47***	0.19

Pearson correlation analysis evaluated possible links between blood test and visual acuity, OCTA parameters. *$p < 0.05$; **$p < 0.01$. Bold indicating p value was statistically significant. CRT, central retinal thickness; FAZ, foveal avascular zone; PERIM, perimeter of fovea; ILM-IPL, inner limiting membrane-inner plexiform layer; SVD, superficial vessel density; DVD, deep vessel density. GLU, glucose; TG, triglyceride; TC, total cholesterol; HDLC, high-density lipoprotein cholesterol; LDLC, low density lipoprotein cholesterol; PT, prothrombin time; PTINR, prothrombin time international normalized ratio; TT, thrombin time; APTT, activated partial thromboplastin time; and FIB, fibrinogen.

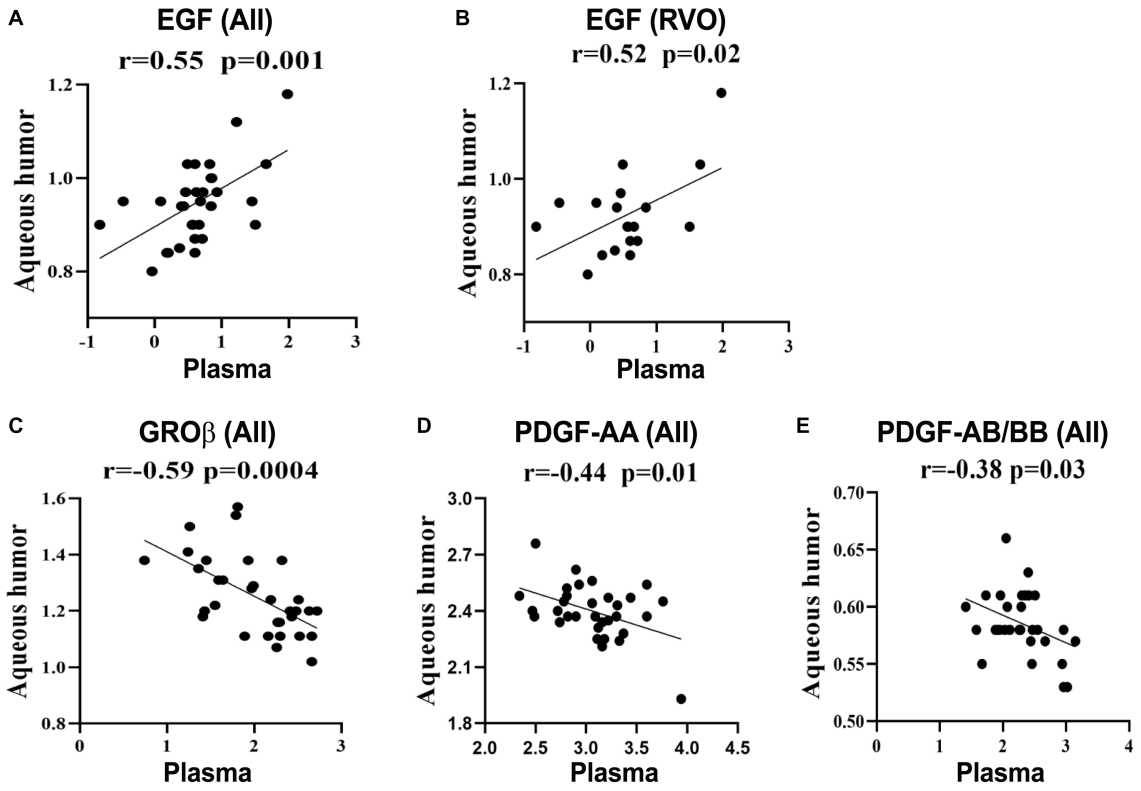

FIGURE 1
Correlations between the plasma and aqueous humor levels of immune mediators. Data were log-transformed and correlations were calculated as Pearson's correlation coefficient (*r*). **(A,C–E)** Correlation analysis of GROβ, EGF, PDGF-AA, and PDGF-AB/BB in RVO patients and cataracts. **(B)** Correlation analysis of EGF in RVO patients.

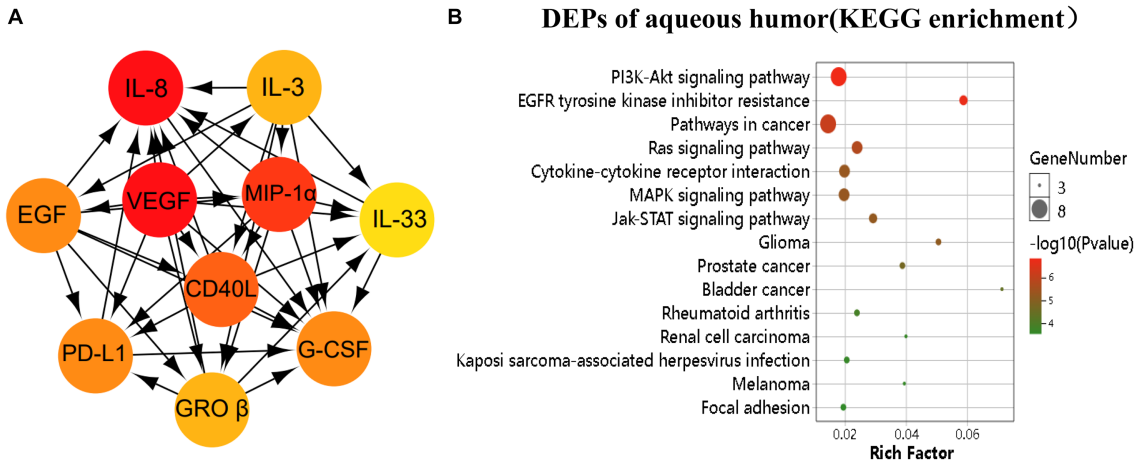

FIGURE 2
Pathway analysis of the differentially expressed proteins (DEPs). The DEPs were identified as $p<0.05$. **(A)** The image showed the top 10 highest degree of aqueous connection DEPs from Cytohubba. Arrows indicate the direction of protein–protein interaction. The darker the color, the higher degree of connectivity of the nodes. **(B)** The TOP 15 aqueous DEPs enriched pathways from KEGG analysis.

Data availability statement

The original contributions presented in the study are included in the article/Supplementary material, further inquiries can be directed to the corresponding authors.

Ethics statement

The studies involving human participants were reviewed and approved by Institutional Review Board (IRB) of the Changsha Aier Eye Hospital. The patients/participants provided their written informed consent to participate in this study.

Author contributions

HX and ZC conceived and designed the study. YZ, HL, JC, and HT acquired data. JQ, WP, and YZ analyzed the results. HX, ZC, JQ, and YZ discussed and interpreted the data. JQ, YZ, and HX wrote the manuscript, and YZ, JQ, HL, SL, TG, JC, WP, HT, JW, HX, and ZC reviewed the manuscript. All authors contributed to the article and approved the submitted version.

Funding

This research was supported by Research and Development Plan of Key Fields in Hunan Province (2020SKC2007), the Natural Science Foundation of Hunan Province (2021JJ30046), the Science Research Fund of AIER Eye Hospital Group (AF2201D12, AM2001D4, AM1913D1, and AR2003D1), Hunan Province Optometry Engineering and Technology Research Center, and Hunan Province International Cooperation Base for Optometry Science and Technology.

Acknowledgments

The authors thank the staff at the Changsha Aier Eye Hospital and Aier Institute of Optometry and Vision Science for their assistance in this research.

Conflict of interest

The authors declare that the research was conducted in the absence of any commercial or financial relationships that could be construed as a potential conflict of interest.

Publisher's note

Supplementary material

The Supplementary material for this article can be found online at: https://www.frontiersin.org/articles/10.3389/fnins.2023.1186025/full#supplementary-material

References

Alfaro, C., Teijeira, A., Oñate, C., Pérez, G., Sanmamed, M., Andueza, M., et al. (2016). Tumor-produced interleukin-8 attracts human myeloid-derived suppressor cells and elicits extrusion of neutrophil extracellular traps (nets). *Clin. Cancer Res.* 22, 3924–3936. doi: 10.1158/1078-0432.Ccr-15-2463

Campochiaro, P., Sophie, R., Pearlman, J., Brown, D., Boyer, D., Heier, J., et al. (2014a). Long-term outcomes in patients with retinal vein occlusion treated with ranibizumab: the RETAIN study. *Ophthalmology* 121, 209–219. doi: 10.1016/j.ophtha.2013.08.038

Campochiaro, P., Wykoff, C., Singer, M., Johnson, R., Marcus, D., Yau, L., et al. (2014b). Monthly versus as-needed ranibizumab injections in patients with retinal vein occlusion: the SHORE study. *Ophthalmology* 121, 2432–2442. doi: 10.1016/j.ophtha.2014.06.011

Chen, M., Lechner, J., Zhao, J., Toth, L., Hogg, R., Silvestri, G., et al. (2016). STAT3 activation in circulating monocytes contributes to neovascular age-related macular degeneration. *Curr. Mol. Med.* 16, 412–423. doi: 10.2174/1566524016666160324130031

Chen, M., Obasanmi, G., Armstrong, D., Lavery, N., Kissenpfennig, A., Lois, N., et al. (2019). STAT3 activation in circulating myeloid-derived cells contributes to retinal microvascular dysfunction in diabetes. *J. Neuroinflammation* 16:138. doi: 10.1186/s12974-019-1533-1

Chitu, V., Biundo, F., and Stanley, E. (2021). Colony stimulating factors in the nervous system. *Semin. Immunol.* 54:101511. doi: 10.1016/j.smim.2021.101511

Cho, C., Roh, K., Lim, N., Park, S., Park, S., and Kim, H. (2022). Role of the JAK/STAT pathway in a streptozotocin-induced diabetic retinopathy mouse model. *Graefes Arch. Clin. Exp. Ophthalmol.* 260, 3553–3563. doi: 10.1007/s00417-022-05694-7

Demers, M., Krause, D., Schatzberg, D., Martinod, K., Voorhees, J., Fuchs, T., et al. (2012). Cancers predispose neutrophils to release extracellular DNA traps that contribute to cancer-associated thrombosis. *Proc. Natl. Acad. Sci. U. S. A.* 109, 13076–13081. doi: 10.1073/pnas.1200419109

Duru, Z., Altunel, O., Alabay, B., Sirakaya, E., Sirakaya, E., Kucuk, B., et al. (2021). Elevated monocyte-to-high-density lipoprotein ratio as an indicator of systemic inflammation in patients with branch retinal vein occlusion. *Beyoglu Eye J.* 6, 212–216. doi: 10.14744/bej.2021.94547

Fan, L., Zhu, Y., and Liao, R. (2022). Evaluation of macular microvasculature and foveal avascular zone in patients with retinal vein occlusion using optical coherence tomography angiography. *Int. Ophthalmol.* 42, 211–218. doi: 10.1007/s10792-021-02015-5

Foley, J., and Conway, E. (2016). Cross talk pathways between coagulation and inflammation. *Circ. Res.* 118, 1392–1408. doi: 10.1161/circresaha.116.306853

Hombrebueno, J., Lynch, A., Byrne, E., Obasanmi, G., Kissenpfennig, A., Chen, M., et al. (2020). Hyaloid vasculature as a major source of stat3 (signal transducer and activator of transcription 3) myeloid cells for pathogenic retinal neovascularization in oxygen-induced retinopathy. *Arterioscler. Thromb. Vasc. Biol.* 40, e367–e379. doi: 10.1161/atvbaha.120.314567

Jacot, J., and Sherris, D. (2011). Potential therapeutic roles for inhibition of the PI3K/AKT/MTOR pathway in the pathophysiology of diabetic retinopathy. *J. Ophthalmol.* 2011:589813. doi: 10.1155/2011/589813

Jung, S., Kim, K., Sohn, S., and Yang, S. (2014). Association of aqueous humor cytokines with the development of retinal ischemia and recurrent macular edema in retinal vein occlusion. *Invest. Ophthalmol. Vis. Sci.* 55, 2290–2296. doi: 10.1167/iovs.13-13587

Karagiannis, D., Karampelas, M., Soumplis, V., Amariotakis, C., Georgalas, I., and Kandarakis, A. (2011). Recurrence of macular edema in retinal vein occlusions after treatment with intravitreal ranibizumab (Lucentis). *Canad. J. Ophthalmol.* 46, 486–490. doi: 10.1016/j.jcjo.2011.09.014

Lee, W., Kang, M., Seong, M., and Cho, H. (2012). Comparison of aqueous concentrations of angiogenic and inflammatory cytokines in diabetic macular oedema

and macular oedema due to branch retinal vein occlusion. *Br. J. Ophthalmol.* 96, 1426–1430. doi: 10.1136/bjophthalmol-2012-301913

Leoncini, G., Bruzzese, D., Signorello, M., Armani, U., Piana, A., Ghiglione, D., et al. (2007). Platelet activation by collagen is increased in retinal vein occlusion. *Thromb. Haemost.* 97, 218–227. doi: 10.1160/th06-05-0257

Liu, L., Liu, J., Bao, J., Bai, Q., and Wang, G. (2020). Interaction of microglia and astrocytes in the neurovascular unit. *Front. Immunol.* 11:1024. doi: 10.3389/fimmu.2020.01024

Luo, Y., Wan, J., Luo, C., Liu, H., Zhou, Y., Chen, J., et al. (2021). Higher aqueous levels of resistin and lipocalin-2 indicated worse visual improvement following anti-vegf therapy in patients with retinal vein occlusion. *Curr. Eye Res.* 46, 845–854. doi: 10.1080/02713683.2020.1842462

Ma, Q., Zhou, J., Yang, Z., Xue, Y., Xie, X., Li, T., et al. (2022). Mingmu Xiaoyao granules regulate the PI3K/Akt/mTOR signaling pathway to reduce anxiety and depression and reverse retinal abnormalities in rats. *Front. Pharmacol.* 13:1003614. doi: 10.3389/fphar.2022.1003614

Marcinkowska, A., Wolska, N., Luzak, B., Cisiecki, S., Marcinkowski, K., and Rozalski, M. (2022). Platelet-derived procoagulant microvesicles are elevated in patients with retinal vein occlusion (rvo). *J. Clin. Med.* 11:5099. doi: 10.3390/jcm11175099

Moustardas, P., Aberdam, D., and Lagali, N. (2023). MAPK pathways in ocular pathophysiology: potential therapeutic drugs and challenges. *Cells* 12:617. doi: 10.3390/cells12040617

Muralidharan-Chari, V., Kim, J., Abuawad, A., Naeem, M., Cui, H., and Mousa, S. (2016). Thymoquinone modulates blood coagulation in vitro via its effects on inflammatory and coagulation pathways. *Int. J. Mol. Sci.* 17:474. doi: 10.3390/ijms17040474

Noma, H., Mimura, T., Yasuda, K., and Shimura, M. (2014). Role of soluble vascular endothelial growth factor receptors-1 and -2, their ligands, and other factors in branch retinal vein occlusion with macular edema. *Invest. Ophthalmol. Vis. Sci.* 55, 3878–3885. doi: 10.1167/iovs.14-13961

Noma, H., Yasuda, K., and Shimura, M. (2020). Cytokines and pathogenesis of central retinal vein occlusion. *J. Clin. Med.* 9:3457. doi: 10.3390/jcm9113457

O'Hearn, T., Fawzi, A., Esmaili, D., Javaheri, M., Rao, N., and Lim, J. (2007). Presumed ocular tuberculosis presenting as a branch retinal vein occlusion in the absence of retinal vasculitis or uveitis. *Br. J. Ophthalmol.* 91, 981–982. doi: 10.1136/bjo.2006.100933

O'Koren, E., Yu, C., Klingeborn, M., Wong, A., Prigge, C., Mathew, R., et al. (2019). Microglial function is distinct in different anatomical locations during retinal homeostasis and degeneration. *Immunity* 50, 723–737.e727. doi: 10.1016/j.immuni.2019.02.007

Pan, M., Zhou, P., Guo, J., An, G., Liu, Z., Du, L., et al. (2022). Elevated neutrophil counts, triglycerides, monocyte/high-density lipoprotein (HDL) ratios, and lower HDL in patients with retinal vein occlusion. *Ophthalmic Res.* 66, 265–271. doi: 10.1159/000527446

Pilard, M., Ollivier, E. L., Gourdou-Latyszenok, V., Couturaud, F., and Lemarie, C. A. (2022). Endothelial cell phenotype, a major determinant of venous thrombo-inflammation. *Front. Cardiovasc. Med.* 9:864735. doi: 10.3389/fcvm.2022.864735

Rayes, J., Bourne, J., Brill, A., and Watson, S. (2020). The dual role of platelet-innate immune cell interactions in thrombo-inflammation. *Res. Pract. Thromb. Haemostasis* 4, 23–35. doi: 10.1002/rth2.12266

Salgado, R., Benoy, I., Weytjens, R., Van Bockstaele, D., Van Marck, E., Huget, P., et al. (2002). Arterio-venous gradients of IL-6, plasma and serum VEGF and D-dimers in human cancer. *Br. J. Cancer* 87, 1437–1444. doi: 10.1038/sj.bjc.6600655

Soliman, M., Zarranz-Ventura, J., Chakravarthy, U., McKibbin, M., Brand, C., Menon, G., et al. (2022). United Kingdom database study of intravitreal dexamethasone implant (ozurdex®) for macular edema related to retinal vein occlusion. *Retina* 43, 679–687. doi: 10.1097/iae.0000000000003698

Supanji, S. M., Hasan, M., Kawaichi, M., and Oka, C. (2013). HtrA1 is induced by oxidative stress and enhances cell senescence through p38 MAPK pathway. *Exp. Eye Res.* 112, 79–92. doi: 10.1016/j.exer.2013.04.013

Thach, A., Yau, L., Hoang, C., and Tuomi, L. (2014). Time to clinically significant visual acuity gains after ranibizumab treatment for retinal vein occlusion: BRAVO and CRUISE trials. *Ophthalmology* 121, 1059–1066. doi: 10.1016/j.ophtha.2013.11.022

Thålin, C., Hisada, Y., Lundström, S., Mackman, N., and Wallén, H. (2019). Neutrophil extracellular traps: villains and targets in arterial, venous, and cancer-associated thrombosis. *Arterioscler. Thromb. Vasc. Biol.* 39, 1724–1738. doi: 10.1161/atvbaha.119.312463

Tripathy, S., Le, H., Cicinelli, M., and Gill, M. (2021). Longitudinal changes on optical coherence tomography angiography in retinal vein occlusion. *J. Clin. Med.* 10:1423. doi: 10.3390/jcm10071423

Wang, B., Wang, F., Zhang, Y., Zhao, S., Zhao, W., Yan, S., et al. (2015). Effects of RAS inhibitors on diabetic retinopathy: a systematic review and meta-analysis. *Lancet. Diabet. Endocrinol.* 3, 263–274. doi: 10.1016/s2213-8587(14)70256-6

Wei, Q., Sun, T., Wan, Z., Zhang, Y., and Peng, Q. (2020). Cytokine and chemokine profile changes in patients after intravitreal conbercept injection for center macular edema due to branch retinal vein occlusion. *Am. J. Transl. Res.* 12, 4001–4008.

Yang, K., Sun, X., Sun, L., Li, J., Liu, Z., and Zhang, H. (2021). Aqueous humor cytokine levels and rebound macular edema after conbercept treatment in patients with central retinal vein occlusion. *Retina* 41, 834–843. doi: 10.1097/iae.0000000000002918

Yi, Q., Wang, Y., Chen, L., Li, W., Shen, Y., Jin, Y., et al. (2020). Implication of inflammatory cytokines in the aqueous humour for management of macular diseases. *Acta Ophthalmol.* 98, e309–e315. doi: 10.1111/aos.14248

Yong, H., Qi, H., Yan, H., Wu, Q., and Zuo, L. (2021). The correlation between cytokine levels in the aqueous humor and the prognostic value of anti-vascular endothelial growth factor therapy for treating macular edema resulting from retinal vein occlusion. *Graefes Arch. Clin. Exp. Ophthalmol.* 259, 3243–3250. doi: 10.1007/s00417-021-05211-2

Yuksel, E., and Ozdek, S. (2013). Unusual presentation of ocular tuberculosis: multiple chorioretinitis, retinal vasculitis and ischaemic central retinal vein occlusion. *Clin. Exp. Optom.* 96, 428–429. doi: 10.1111/cxo.12008

Zeng, Y., Cao, D., Yu, H., Zhuang, X., Yang, D., Hu, Y., et al. (2019). Comprehensive analysis of vitreous chemokines involved in ischemic retinal vein occlusion. *Mol. Vis.* 25, 756–765.

frontiers | Frontiers in Neuroscience

TYPE Original Research
PUBLISHED 12 October 2023
DOI 10.3389/fnins.2023.1227116

OPEN ACCESS

EDITED BY
Wensi Tao,
University of Miami Health System, Miami, United States

REVIEWED BY
岩 吴,
Tongji University, China
Xuezhi Zhou,
Central South University, China
Yi Shao,
Nanchang University, China

*CORRESPONDENCE
Richard K. Lee
✉ rlee@med.miami.edu

RECEIVED 22 May 2023
ACCEPTED 18 July 2023
PUBLISHED 12 October 2023

CITATION
Liu Y, Cheng He R, Munguba GC and Lee RK (2023) Parvalbumin expression changes with retinal ganglion cell degeneration. *Front. Neurosci.* 17:1227116. doi: 10.3389/fnins.2023.1227116

Parvalbumin expression changes with retinal ganglion cell degeneration

Yuan Liu[1], Rossana Cheng He[1,2], Gustavo C. Munguba[1,3] and Richard K. Lee[1]*

[1]Bascom Palmer Eye Institute, University of Miami Health System, Miami, FL, United States, [2]Department of Surgery, Mount Sinai Hospital, New York, NY, United States, [3]Envision Eye Specialists, Ocala, FL, United States

Background: Glaucoma is one of the main causes of irreversible visual field loss and blindness worldwide. Vision loss in this multifactorial neurodegenerative disease results from progressive degeneration of retinal ganglion cells (RGCs) and their axons. Identifying molecular markers that can be measured objectively and quantitatively may provide essential insights into glaucoma diagnosis and enhance pathophysiology understanding.

Methods: The chronic, progressive DBA/2J glaucomatous mouse model of glaucoma and C57BL6/J optic nerve crush (ONC) mouse model were used in this study. Changes in PVALB expression with RGC and optic nerve degeneration were assessed via gene expression microarray analysis, quantitative real-time polymerase chain reaction (qRT-PCR), Western blot and immunohistochemistry.

Results: Microarray analysis of the retinal gene expression in the DBA/2J mice at different ages showed that the expression of PVALB was downregulated as the mice aged and developed glaucoma with retinal ganglion cell loss. Analysis of qRT-PCR results demonstrated PVALB at the mRNA level was reduced in the retinas and optic nerves of old DBA/2J mice and in those after ONC compared to baseline young DBA2/J mice. PVALB protein expression measured by Western blot was also significantly reduced signal in the retinas and optic nerves of old DBA/2J mice and those eyes with crushed nerves. Immunohistochemical staining results demonstrated that there were fewer PVALB-positive cells in the ganglion cell layer (GCL) of the retina and staining pattern changed in the optic nerve from old DBA/2J mice as well as in mice eyes following ONC.

Conclusion: PVALB is abundantly expressed both by RGCs' soma in the retinas and RGCs' axons in the optic nerves of C57BL/6J. Furthermore, the expression level of PVALB decreases with RGC degeneration in the glaucomatous DBA/2J mice and after ONC injury of C57BL6/6J, indicating that PVALB is a reliable RGC molecular marker that can be used to study retinal and optic nerve degeneration.

KEYWORDS

retinal ganglion cell, glaucoma, optic nerve, microaaray, molecular marker, optic nerve crush

1. Introduction

Glaucoma is the second leading cause of irreversible blindness globally (Quigley and Broman, 2006). It was estimated that 64.3 million people were affected by glaucoma in 2013 and the study predicted that the number would reach 76 million in 2020 and 111.8 million in 2040 (Tham et al., 2014). Glaucoma is a group of optic neuropathies characterized by the progressive

death of RGCs and degeneration of the optic nerve, which result in visual field defects and blindness. RGCs, located in the innermost layer of the retina, function to integrate information from the photoreceptors via bipolar and amacrine cells and project into the brain for higher-order visual processing. RGC degeneration impairs information transmission in the optic pathway, rendering glaucoma a neurodegenerative disease.

Glaucoma is a multifactorial disease. A number of theories have been proposed for the pathogenesis and progression of glaucoma, which include intraocular pressure (IOP) elevation (Gordon et al., 2002; Heijl et al., 2002; Kass et al., 2002; Leske et al., 2007), neurotrophin deprivation (Pease et al., 2000; Quigley et al., 2000), vascular dysregulation (Hayreh, 1969; Chung et al., 1999; Hayreh et al., 2004), and neuroinflammation (Tezel, 2013; Kamat et al., 2016). Given the complex etiology of neurodegeneration in glaucoma, it is important to identify biomarkers that would allow for a better understanding of the disease, the monitoring of the disease progression, and the development of therapeutics.

PVALB is a calcium buffer that belongs to the large family of EF-hand calcium-binding proteins, which contain the classical EF-hand motif of helix–loop–helix that allows for calcium or magnesium binding (Kretsinger and Nockolds, 1973). Its calcium-binding capacity allows PVALB to regulate intracellular calcium concentration and thus, PVALB plays a role in various calcium-dependent signaling pathways (Schwaller, 2010). PVALB was first identified and characterized in carp muscle as a calcium-binding carp myogen (Konosu et al., 1965; Nockolds et al., 1972). Implicated in the process of muscle relaxation by binding and shuttling Ca^{2+} to the sarcoplasmic reticulum, PVALB's expression was also found in the fast-twitch muscles of most mammals, including mice, horses, and humans (Heizmann et al., 1982). Additionally, PVALB is expressed throughout the central and peripheral nervous system, including the cerebellum, hypothalamus, hippocampus, olfactory bulb, retina, and the spinal ganglia (Heizmann, 1984; Celio, 1990). PVALB, along with other EF-hand calcium-binding proteins such as calbindin D28K and calretinin, have been used as neuronal markers in various studies because of their abundance and specificity in neurons, which allow for the differentiation and characterization neuron subpopulations (Baimbridge et al., 1992). As a result, the function of a particular subpopulation of neurons in a neural circuitry can be further investigated and its susceptibility to neurodegenerative diseases can be assessed.

PVALB is expressed in the retina of various vertebrates; however, its immunoreactivity pattern varies across different species (Sanna et al., 1993). In the mammalian retina of rabbits, rats, and mice, PVALB has consistently showed immunoreactivity in the inner nuclear layer (INL) and the GCL, labeling amacrine cells and RGCs (Wäussle et al., 1993; Casini et al., 1995; Haverkamp and Wässle, 2000). In the retina of adult C57BL/6J mice, it was estimated that 85.93% of PVALB-immunoreactive cells were RGCs and 28.98% of RGCs expressed PVALB (Kim and Jeon, 2006). Furthermore, these PVALB-immunoreactive RGCs showed heterogeneity in their morphology, labeling different subpopulations of RGCs (Kim and Jeon, 2006).

In this study, we aimed to determine if PVALB is a reliable RGC marker in adult mouse eyes and if PVALB expression can be used to track progressive loss of RGCs, such as glaucomatous DBA/2J mouse model and optic nerve injury model. The ONC injury causes axonal degeneration and RGC death (Barron et al., 1986; Li et al., 1999; Leung et al., 2008). This experimental disease model allows for the study of mechanisms underlying axonal injury-induced RGC death and survival. On the other hand, the DBA/2J mice have become a widely used animal model for the study of glaucoma due to its similarities with the human disease. The DBA/2J mouse strain is mouse model of hereditary glaucoma; these mice spontaneously and progressively develop a number of ocular abnormalities with age. Starting at approximately 6 months of age, the DBA/2J mice develop pigment dispersion, iris transillumination, iris atrophy, and anterior synechia (John et al., 1998). Elevation in intraocular pressure (IOP) is detected from 9 to 12 months. By 12 months of age, the majority of animals have significant RGC loss and optic nerve degeneration (Libby et al., 2005). Using these two different animal models, we examined the changes in the expression of PVALB with retinal degeneration at both the transcript and protein level. Immunofluorescence experiments confirm that PVALB is preferentially expressed in non-crushed C57BL6/J and young DBA/2J mouse. Genechip analysis confirm by RT-PCR show that the expression of PVALB decreased with age in the DBA/2J mice and following ONC. Western blot results further supported our conclusion.

2. Methods

2.1. Animals

C57BL/6J and DBA/2J mice were purchased from the Jackson Laboratory (Bar Harbor, ME). They were bred and handled according to the ARVO Statement for the Use of Animals in Ophthalmic and Vision Research. All animal procedures were approved by the University of Miami Institutional Animal Care and Use Committee.

2.2. GeneChip microarray

Total RNA from 4 to 6 pooled whole retinas of C57BL/6J and DBA/2J mice was isolated using TRIzol Reagent and Qiagen RNeasy column purification. Samples were sent to Expression Analysis, Inc. (Durham, NC) for gene expression profile service using the Affymetrix GeneChip Mouse Genome 430 2.0 Array (see Munguba et al., 2013 for more details).

2.3. Optic nerve crush

The ONC was performed according to the method used by Li and colleagues with slight modifications (Li et al., 1999). 3-month-old C57BL/6J mice were anesthetized by intraperitoneal injection with 0.005 ml of anesthesia per gram of body weight, containing ketamine (15 mg/ml) and xylazine (3 mg/ml). An incision was made to the conjunctiva to allow access to the posterior region of the globe. The optic nerve was exposed through a small window made through blunt dissection. At a site approximately 2 mm posterior to the globe, the optic nerve was clamped with forceps for 8 s. The contralateral eye was used as the uncrushed control. The animals were sacrificed 1 month after the ONC.

2.4. Reverse transcription and quantitative real-time PCR

Whole retinas were isolated from glaucomatous DBA/2J and age-matched control C57BL/6J mice as well as from 1-month post-ONC mice. Four pooled retinas from each group were homogenized on ice with a mortar and pestle (Pellet Pestle Cordless Motor Tissue Grinder and Kimble Kontes Pellet Pestle, Kimble Chase, Rockwood, TN) and total RNA was isolated using TRIzol Reagent (Lot #54101, Invitrogen, Carlsbad, CA). cDNA was synthesized from 2 μg of total RNA using Superscript III Reverse Transcriptase (Lot #1517623, Invitrogen) according to the manufacturer's protocol. A 1:20 dilution was made to the resulting cDNA samples. All samples were stored at −20°C until qRT-PCR analysis.

The following primer pairs were designed using Primer-BLAST:

Gene	Forward primer (5′–3′)	Reverse primer (5′–3′)
PVALB	TCTTTTCGCACTTGCTCTGCC	TCAGAATGGACCCCAGCTCATC
Thy1	CAAGGTCCTTACCCTAGCCAA	CCAGCTTGTCTCTATACACACTG
β-actin	CAACGGCTCCGGCATGTGC	CTCTTGCTCTGGGCCTCG

The following components were added to each reaction well for a total volume of 20 μl per qRT-PCR reaction: 10 μl of iQ SYBR Green Supermix (Lot #010171B, Bio-Rad, Hercules, CA), 7.2 μl of diethylpyrocarbonate (DEPC)-treated water, 0.4 μl (an equivalent of 0.04 nmol) of forward primer, 0.4 μl (an equivalent of 0.04 nmol) of reverse primer, and 2 μl of the 1:20 dilution of the cDNA template. Samples were run in quadruplicates using the CFX Connect Real-Time PCR Detection System (Bio-Rad) and all samples were analyzed together on a single 96-well plate with CFX Manager Software (Bio-Rad). The qRT-PCR was repeated 5 times. All primer sets were exposed to identical three-step cycling conditions: 94°C for 5 min (initial denaturation and enzyme activation), followed by 40 cycles of 94°C for 30 s (denaturation), 55°C for 30 s (annealing), 72°C for 40 s (extension). β-actin was used as an endogenous control to normalize the mRNA expression of parvalbumin and Thy1 in each sample. The transcript levels were quantified by the comparative quantification method – the double delta Ct method – using β-actin as the reference gene and the C57BL/6J as the calibrator.

2.5. Immunofluorescence and confocal microscopy

After transcardial perfusion with phosphate-buffered saline (PBS) and 4% paraformaldehyde, eyes were enucleated from the following mice: 2.3- and 20-month-old DBA/2J, 3- and 20-month old C57BL/6J mice, and 1-month post ONC mice. The globes were fixed in 4% paraformaldehyde. Then, the globes were embedded in paraffin, sectioned at 4 μm thickness, and mounted onto glass slides. The tissue sections underwent deparaffinization with xylene overnight and rehydration during which they were subjected to an ethanol gradient wash (100% ethanol, 95% ethanol, 75% ethanol, 50% ethanol, and dH_2O; for 3 min each). To restore the immunoreactivity of the epitopes, the sections were steam-heated in 1× Rodent Decloaker (Biocare Medical, Concord, CA) for 40 min. Subsequently, the sections were blocked with Rodent Block M (Biocare Medical) for 20 min to reduce nonspecific antibody binding. Tissue slides were incubated for 2 nights with primary antibodies diluted in 1× PBS containing 0.5% Triton, washed with 1× PBS, incubated with secondary antibodies diluted in 1× PBS for 1 h, and washed with 1× PBS. Lastly, coverslips were mounted onto the slides using VECTASHIELD Antifade Mounting Medium with DAPI (Vector Laboratories, Burlingame, CA). Confocal microscopy images were taken using the Leica DM6000 B microscope (Leica Microsystems, Wetzlar, Germany) with a 40x oil immersion objective.

Primary antibodies used were: 1:200 rabbit polyclonal anti-parvalbumin antibody (Lot GR296273-1, Abcam, Cambridge, MA), 1:200 guinea pig polyclonal anti-RBPMS antibody (Lot NB916o, PhosphoSolutions, Aurora, CO), and 1:200 rat monoclonal anti-Thy1 antibody (Lot GR317580-1, Abcam). Secondary antibodies used were: 1:200 Cy3 donkey anti-rabbit IgG (Jackson ImmunoResearch, West Grove, PA), 1:200 Cy5 donkey anti guinea pig IgG (Jackson ImmunoResearch, West Grove, PA), and 1:200 Alexa Fluor 488 donkey anti-rat IgG (Jackson ImmunoResearch, West Grove, PA).

2.6. Western blots

Retinas from 4 mice in each group were homogenized and digested with RIPA buffer. Total protein extract (25 μg) was loaded on a 12% polyacrylamide gel. After electrophoresis, proteins were transferred onto polyvinyl difluoride (PVDF) membranes (ThermoFisher, Catalog number: 88518). Nonspecific bindings sites were blocked by immersing the membrane in 5% milk in Tris-buffered saline Tween (TBST) for 1 h at room temperature. Membranes were incubated with primary antibody overnight, washed 3 times with TBST for 15 min, incubated with secondary antibody for 1 h at room temperature, washed 3 times with TBST for 15 min and exposed with ECL (ThermoFisher, Catalog number: 32106). To quantify, the membranes were scanned by gel scanner using software.

Primary antibodies used were: 1:1000 rabbit polyclonal anti-parvalbumin antibody (Lot GR296273-1, Abcam, Cambridge, MA), 1:1000 mouse monoclonal anti-parvalbumin antibody (ab8245, Abcam, Cambridge, MA). Secondary antibodies used were 1:2000 HRP donkey anti-mouse IgG (Jackson ImmunoResearch, West Grove, PA), Secondary antibodies used were 1:2000 HRP donkey anti-rabbit IgG (Jackson ImmunoResearch, West Grove, PA).

2.7. Statistical analysis

Each animal was used in a single experiment and entered as an individual data point. Statistical analyses were performed using GraphPad Prism software (GraphPad Software, Inc., La Jolla, CA). Paired student *t*-test was used to compare two groups. *p* values less than 0.05 were considered statistically significant. Multiple comparison analyses were conducted using Analysis of Variance (ANOVA) with Tukey's *post hoc* test. *p* values less than 0.05 were considered statistically significant.

3. Results

3.1. Parvalbumin expression is reduced in mouse retina after optic nerve crush

In the 3-month-old C57BL/6J retina, PVALB demonstrated abundant expression in the GCL and NFL (Figure 1A) retinal layers. PVALB was also immunoreactive in the inner plexiform layer (IPL), thereby showing a three-band stratification pattern in the retina. Additionally, PVALB labeled a number of cells in the proximal inner nuclear layer. Antibodies specific for Tuj-1, a protein commonly used as a neuron marker (Barnstable and Dräger, 1984; Rodriguez et al., 2014), was used in conjunction with the antibody against PVALB in the immunohistochemical staining to further characterize the staining pattern of PVALB (Figures 1A,B). In the NFL, the majority of PVALB staining colocalized with Tuj-1 (Figure 1A). In the GCL, PVALB-positive cells showed colocalization with Tuj-1 (Figure 1A). In the IPL, PVALB labels showed very good lamination along this retinal layer. In the mice that underwent unilateral ONC, the crushed eye (Figure 1B) had fewer PVALB-positive cells in comparison to the contralateral, uncrushed control 1 month after the crush (Figure 1A).

To further examine the changes in the expression of PVALB with RGC degeneration, qRT-PCR and Western blot were performed. The qRT-PCR results showed that 4 weeks after the ONC injury, the transcript levels of PVALB in the crushed eyes significantly decreased in comparison to the uncrushed control. The level of PVALB expression was reduced to 21% of the control level (Figure 1C). The level of Thy1 expression, a recognized RGC marker, was also reduced to 30% of the control. When PVALB expression level was normalized to Thy1, no significant expression differences were observed between crushed and non-crushed control, indicating strong correlation with Thy1 and PVALB in RGCs. The protein expression of PVALB was significantly reduced in retinas from crushed eyes compared to the non-crushed contralateral eyes (Figure 1D) as demonstrated by Western blotting.

3.2. Parvalbumin expression change in mouse optic nerve after crush

In the 3-month-old C57BL/6J mice, we can observe positive PVALB staining in optic nerves and it colocalize with Tuj1 staining, which is a widely-used marker of nerve fibers (Figures 2A–C). After crush, nerve fibers underwent degeneration with diminished signal of both Tuj1 and PVALB (Figures 2D–F). The reduced expression of PVALB in optic nerves after crush was further verified by real-time PCR and Western blotting. Real time PCR show that the relative gene expression levels of PVALB significantly decreased at 4 weeks after crush compared to non-crushed controls (Figure 2G). Based upon western blot analysis, the amount of PVALB protein expression was significantly reduced in the optic nerves from crushed mice compared to non-crushed controls (Figure 2H).

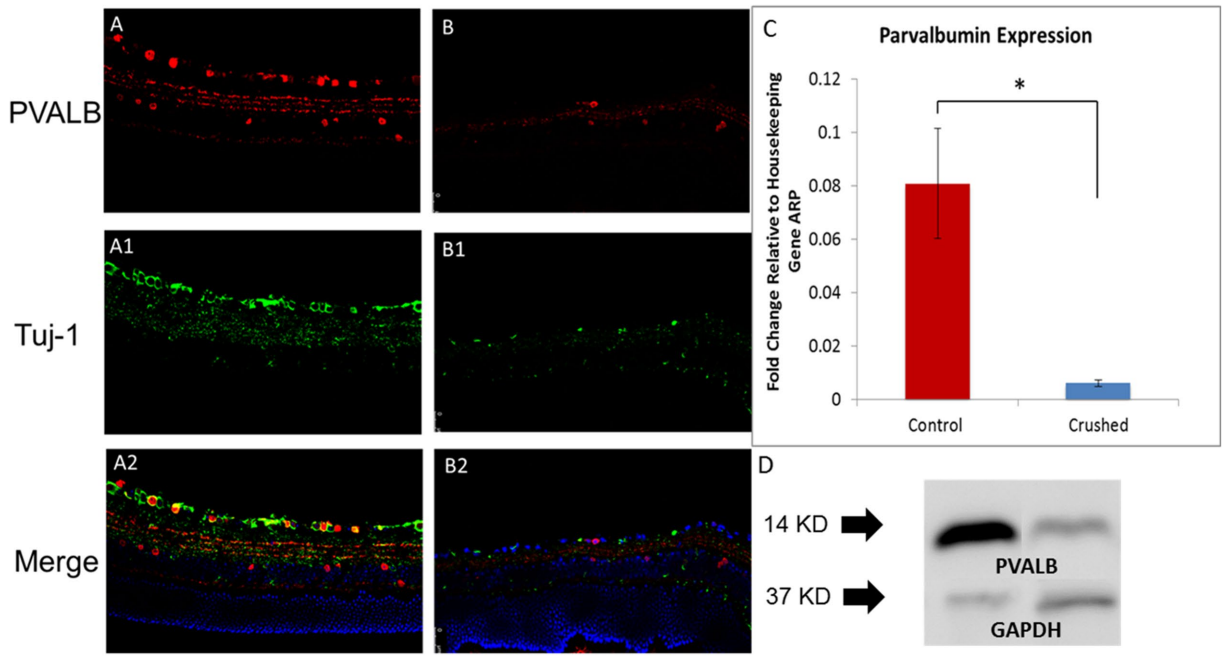

FIGURE 1
PVALB expression decreased in the retinas from mice that have been crushed. **(A)** PVALB immunohistochemistry (red) and its colocalization with neuronal markers, Tuj1(green), in a 3-month-old C57BL/6J mouse retina. PVALB mainly showed immunoreactivity in the NFL, GCL, and IPL. **(B)** Both PVALB and Tuj1 signal decreased after crush. **(C)** PVALB mRNA expression levels decreased 1 month after ONC by qRT-PCR. Using β-actin as the internal control, the expression levels of PVALB were reduced to 21% of the uncrushed control (*$p < 0.05$, student t test, $n = 10$ for each group). **(D)** Western blot results demonstrated decreased expression of PVALB in retinas from crushed mice. Left lane, retina extracts from mice have been crush for 4 weeks. Right lane, retina extracts from age-matched non-crushed mice. Bottom lane, GAPDH staining used as loading control ($n = 4$ for each group).

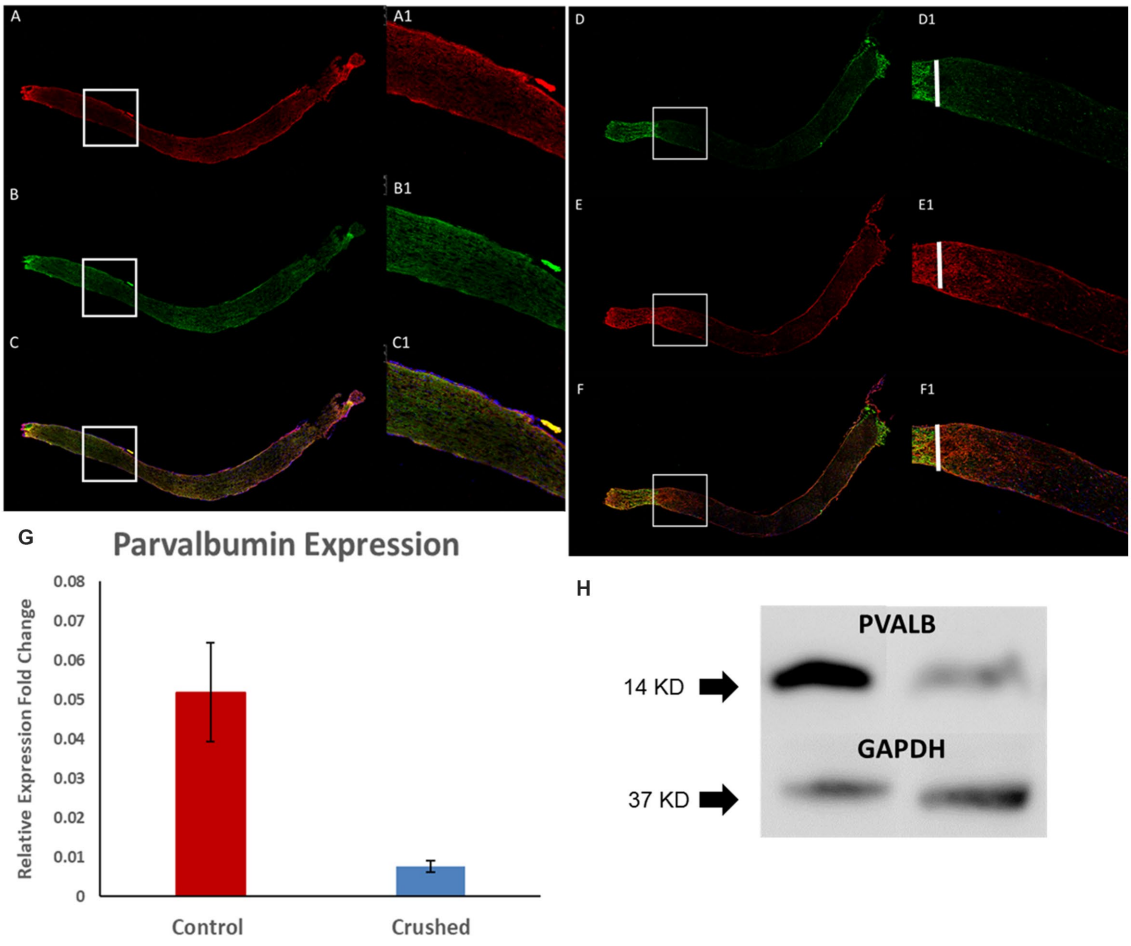

FIGURE 2
PVALB expression decreased in the optic nerves from mice that have been crushed. **(A–C)** PVALB immunohistochemistry (red) and its colocalization with neuronal fiber markers, Tuj1(green), in a 3-month-old C57BL/6J mouse optic nerve. **(D–F)** Both PVALB and Tuj1 signal decreased after crush. We can hardly observe PVALB and Tuj-1 signal after crush site. White bar labels crushed site. **(A1–F1)** are the amplified images from the square site. **(G)** PVALB mRNA expression levels decreased 1 month after ONC by qRT-PCR. Using β-actin as the internal control, the expression levels of PVALB were reduced to 23% of the uncrushed control (*$p < 0.05$, student t test, $n = 10$ for each group). **(H)** Western blot results demonstrated decreased expression of PVALB in optic nerves from crushed mice. Left lane, optic nerve extracts from mice have been crush for 4 weeks. Right lane, optic nerve extracts from age-matched non-crushed mice. Bottom lane, GAPDH staining used as loading control ($n = 4$ for each group).

3.3. Mouse glaucoma model shows reduced expression of parvalbumin in retina

PVALB expression in DBA/2J mice eyes changed as they aged. Fewer RGCs showed immunoreactivity for PVALB in the glaucomatous, 14-month-old DBA/2J mouse retina compared to age-matched C57BL6/J mice and young 4-month old DBA/2J mice (Figures 3A1-3,3B1-3). Compared to age matched C57BL6/J mice and young DBA/2J mice, a significantly diminished ganglion cell layer and inter plexiform layer was barely observed in the aged DBA/2J mice. The lamination of cells labeled by PVALB also disappeared.

A further analysis of the microarray data comparing the transcriptional profiles of pooled whole retinas from DBA/2J and C57BL6/J mice at different ages revealed PVALB to be a potential RGC marker. The signal level of PVALB from the Affymetrix microarrays decreased as the mice aged: the averaged relative signal intensity of PVALB in the young DBA/2J mice was significantly higher than that in the old mice (Figure 3C). The relative signal intensity of PVALB in C57BL6/J did not have any obvious trend decrease (Figure 3D).

To further examine the changes in the expression of PVALB with RGC degeneration, qRT-PCR was performed. No significant differences between the transcript levels of PVALB in DBA/2J mouse retinas at the age of 3 and 8 months was observed (Figure 3F, $p = 0.44$, $n = 20$; unpaired t-test). However, as the mice aged and developed glaucoma, the PVALB transcript levels showed a reduction from 8-month-old to 12-month-old mice (Figure 3F; $p < 0.0001$, $n = 20$; unpaired t-test). Although the expression level showed an increase at the age of 19 months, it was still significantly lower than that at 8 months of age (Figure 3F, $p = < 0.0001$, $n = 20$; unpaired t-test). We did not observe similar expression changes in the C57BL6/J mouse line (Figure 3E).

The expression of Thy1, a cell-surface glycoprotein commonly used as a RGC marker (Barnstable and Dräger, 1984), was also examined in this study. We found that the transcript levels of Thy1 in the DBA/2J mouse retinas at different ages showed a similar trend

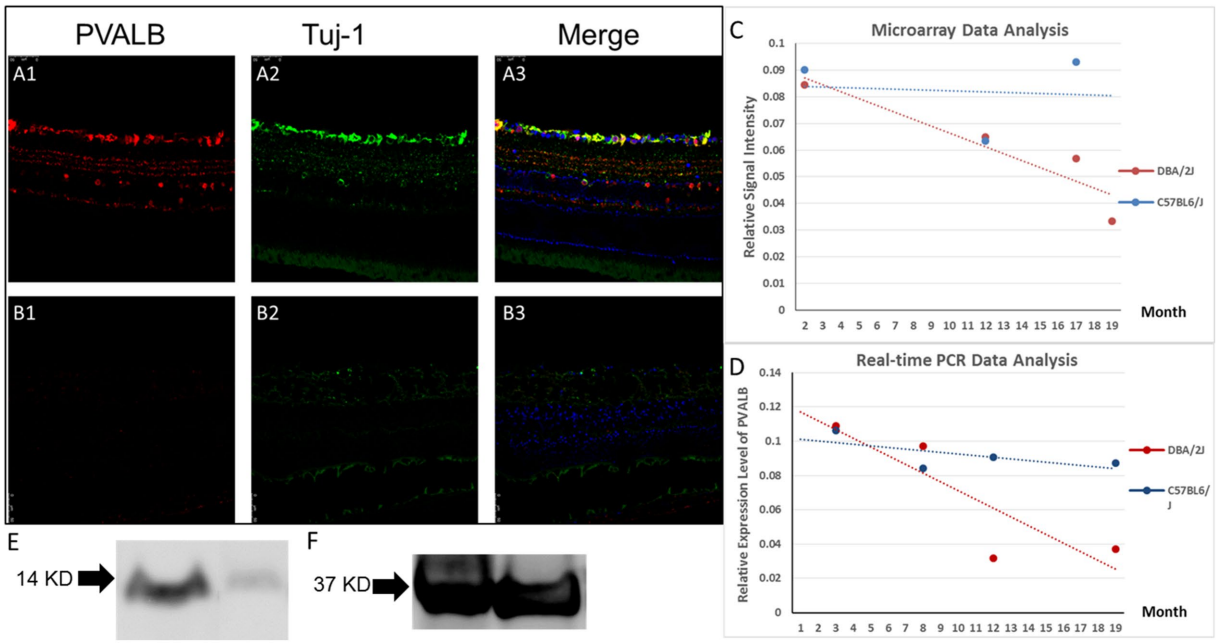

FIGURE 3
PVALB expression decreased in the retinas from aged DBA/2J mice. **(A1–A3)** PVALB immunohistochemistry (red) and its colocalization with neuronal markers, Tuj1 (green), in a 14-month-old C57BL/6J mouse retina. PVALB mainly showed immunoreactivity in the NFL, GCL, and IPL. **(B1–B3)** Both PVALB and Tuj1 signal decreased in 14-month-old DBA/2J mice. **(C,D)** Gene expression levels were measured from pooled whole retinas of the DBA/2J mouse model of glaucoma at different ages using the GeneChip Mouse Genome 430 2.0 Array. Signal levels of all Affymetrix probes for PVALB were averaged and plotted. Expression levels of PVALB were reduced as the DBA/2J mice aged **(C)**, while expression levels of PVALB in C57BL6/J mice did not have this decreasing trend. **(E)** Relative expression level of PVALB in C57BL6/J mice did not show decreasing trend. **(F)** PVALB mRNA expression levels decreased in aged DBA/2J mice quantified by qRT-PCR. Using β-actin as the internal control. **(G)** Western blot results demonstrated decreased expression of PVALB in retinas in aged DBA/2J mice. Left lane, retina extracts from 14-month-old DBA/2J mice. Right lane, retina extracts from age-matched C57BL6/J mice. Bottom lane, GAPDH staining used as loading control.

compared to PVALB, with a decrease from the age 8 to 12 months, followed by a slight increase from 12 to 19 months. The correlation analysis showed that the PVALB and Thy1 is strongly correlated ($r = 0.84$, $p = 0.051$).

Furthermore, Western blot was used to analyze the expression of PV at the protein level in the mouse retina. PVALB protein expression level in 14 months DBA/2J mice and age-matched C57BL/6J mice was quantified by Western blotting. We detected almost complete loss of PVALB protein signal in 14 months DBA/2J mice retina based on the Western blotting results (Figure 3G).

3.4. Effect of elevated pressure on the amount of parvalbumin in mouse optic nerve

Compared to control C57BL/6J mice optic nerve and young 4-month-old DBA/2J mouse, 14 months DBA/2J mice optic nerve demonstrated abnormal PVALB immunostaining pattern (Figures 4A1-3,4B1-3). We can find immunostaining positive deposits in the aged DBA/2J mice which were not seen in the wide type control and young DBA/2J mice. We quantified PVALB expression level in optic nerves by real-time PCR and Western blotting. Real-time PCR results demonstrated that the expression of PVALB sharply decreased at the age of 3.5 month, coinciding with the onset of glaucomatous retinal ganglion cell loss in the DBA/2J mouse line (Figure 4C). However, we did not observe same decreased expression of PVALB in C57BL6/J mice (Figure 4D). We also preformed western blot to detect PVALB protein expression change in the DBA/2J glaucomatous mouse line. The western blotting results demonstrated significantly reduced expression of PVALB in optic nerves of aged DBA/2J mice compared to age-matched BL6 control mice (Figure 4E).

4. Discussion

Glaucoma is a group of progressive optic neuropathies characterized by the degeneration of retinal ganglion cells (RGCs) and their axons, resulting in visual field loss. Early detection and timely intervention are crucial to prevent irreversible vision loss in glaucoma patients. Molecular markers offer valuable tools for improving the accuracy and efficiency of glaucoma diagnosis. Thus, identification of a reliable RGC marker to track disease progression is very important and a major focus of clinical research.

By utilizing molecular markers, clinicians can enhance the accuracy of glaucoma detection, monitor disease progression, and personalize treatment strategies. In the present study, we have identified PVALB as an effective marker with which to track RGC loss in both glaucoma animal model of disease and wide-used optic nerve injury model. We have demonstrated that PVALB is expressed by RGCs in both the C57BL/6J and DBA/2J mouse strains. Our findings are consistent with previous works, which showed that at least 8 different types of RGC in the mouse retina expressed PVALB (Kim and Jeon, 2006; Yi et al., 2012).

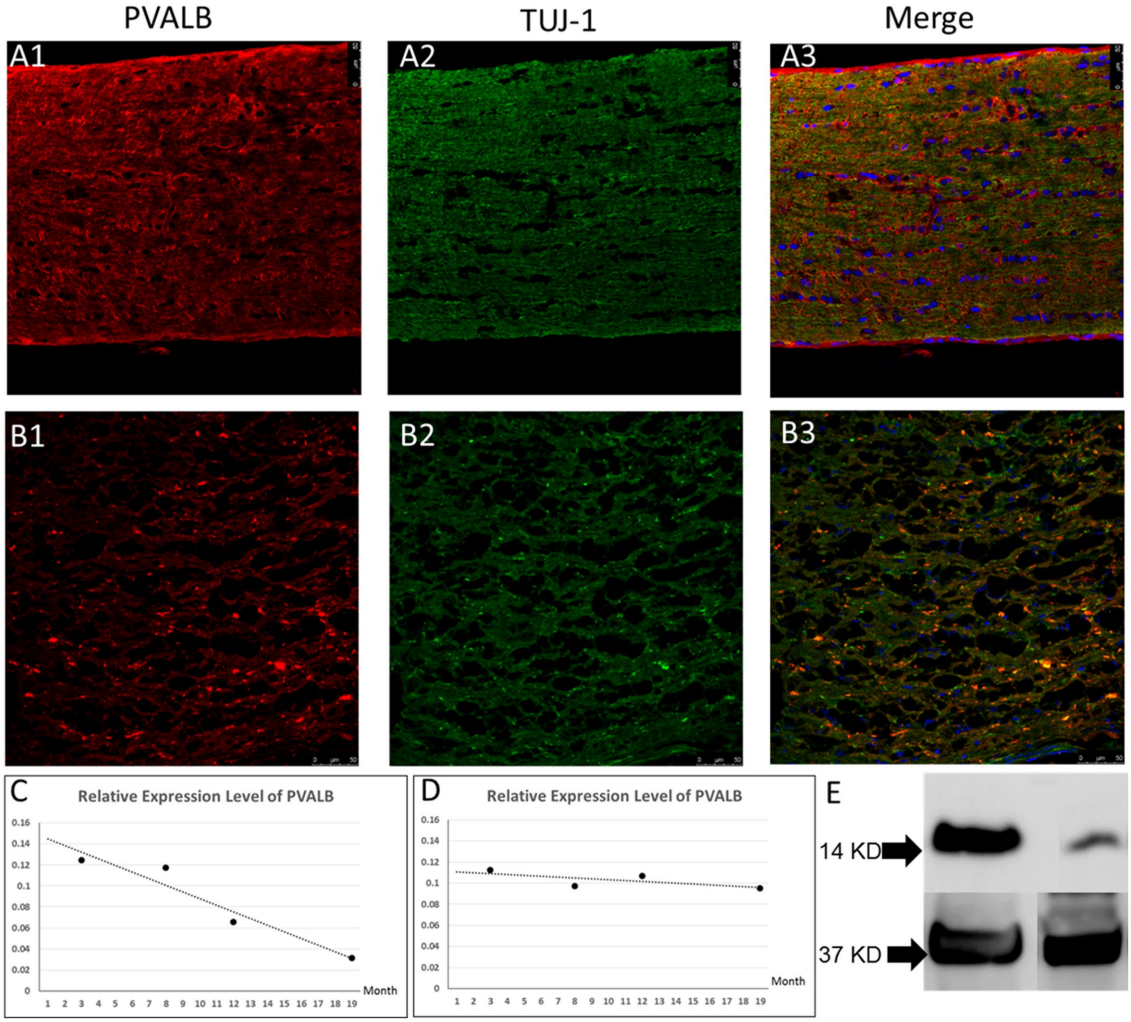

FIGURE 4
PVALB expression decreased in the optic nerves from aged DBA/2J mice. **(A1–A3)** Immunostaining of optic nerves from 4-month-old DBA/2J mouse. **(B1–B3)** Immunostaining of optic nerves from 14-month old DBA/2J mice. PVALB (red) and Tuj1 (green) were shown in the figures. We can observe immunostaining positive deposits in these optic nerves. **(C)** PVALB mRNA expression levels decreased in aged DBA/2J mice quantified by qRT-PCR. Using β-actin as the internal control. **(D)** Relative expression level of PVALB in C57BL6/J mice did not show decreasing trend. **(E)** Western blot results demonstrated decreased expression of PVALB in optic nerves from 14-month-old DBA/2J mice. Left lane, retina extracts from 14-month-old DBA/2J mice. Right lane, retina extracts from age-matched C57BL6/J mice. Bottom lane, GAPDH staining used as loading control.

More importantly, we have shown that the expression of PVALB decreased with RGC degeneration in the mouse retina and optic nerves. Previous studies have found that the expression of PVALB was decreased after the induction of retinal ischemia/reperfusion in rats (Kim et al., 2010), ONC in rats (Hong et al., 2016), and chronic elevation of IOP in mice (Gunn et al., 2011). Similarly, our results showed that PVALB expression was reduced in the mouse retina and optic nerves 1 month after ONC, an injury model that results in 46% of RGC loss 30 days after crush (Templeton et al., 2009). The expression change of PVALB is correlated with Thy1, a well-recognized RGC markers, indicating PVALB expression level may also serves as a marker for RGC degeneration.

Changes in PVALB expression have not been previously studied in the DBA/2J mouse genetic model of glaucoma. Here, we showed that the expression of PVALB decreased as the age of the DBA/2J mice increased. DBA/2J mice develop age-dependent progressive ocular abnormalities including elevated IOP, iris atrophy and secondary angle closure. Anterior chamber pathology in DBA/2J mice typically has its onset at approximately 6 months of age, followed by elevation of IOP between 8 and 9 months, and severe optic nerve damage and RGC loss by 12 months of age in the majority of animals. Our microarray data and real-time PCR results demonstrated these pathological changes. No significant difference was observed between PVALB expression level at 3 months and 8 months. However, after 8 months, the PVALB expression level sharply decreased and kept decreasing as mice age increased with progressive retinal ganglion cell loss. The slight increase in the expression level of PVALB and Thy1 in the 19-month-old DBA/2J mice seen in the qRT-PCR data may be due to the variable and asymmetric disease progression within and between animals in this model (John et al., 1998; Schlamp et al., 2006).

Calcium signaling underlies numerous, vital cellular processes including proliferation, metabolism, muscle contraction, and

neurotransmission (Brini et al., 2013). On the other hand, excessive intracellular Ca^{2+} can lead to cytotoxicity, triggering signaling cascades that result in cell death (Orrenius et al., 2003). Therefore, calcium-binding proteins are thought to play a protective role against neurodegeneration. Studies have demonstrated that the overexpression of PVALB offered protection to motor neurons against degeneration in amyotrophic lateral sclerosis (ALS; Elliott and Snider, 1995; Van Den Bosch et al., 2002). However, Laslo and colleagues found expression of parvalbumin within vulnerable motoneurons, suggesting that PVALB was not a reliable marker for resistance to degeneration in ALS (Laslo et al., 2000). The physiological function of PVALB in the retina is largely unclear and its potential neuroprotective role in retinal degeneration remains to be elucidated in future studies.

We proposed that PVALB may play a role in modulating calcium signaling in RGCs. Calcium signaling is crucial for neuronal function and survival, but excessive or dysregulated calcium levels can lead to cell damage or death. PVALB, as a calcium-binding protein, may help regulate calcium levels within RGCs and prevent calcium overload, which could be detrimental to their survival. Therefore, alterations in PVALB expression or function could disrupt calcium homeostasis and contribute to RGC degeneration.

Our study demonstrated that PVALB is abundantly expressed by RGCs' soma in the mouse retina and RGCs' axons in the optic nerve. Furthermore, the loss of RGCs seen in the transgenic DBA/2J mouse model of glaucoma as well as that induced by ONC injury was reliably identified by PVALB expression changes, demonstrating that PVALB may be used as a reliable RGC marker in different animal models of RGC degeneration to study the pathogenesis of various optic neuropathies.

Data availability statement

The datasets presented in this study can be found in online repositories. The names of the repository/repositories and accession number(s) can be found in the article/supplementary material.

Ethics statement

The animal study was reviewed and approved by the Institutional Animal Care and Use Committee, University of Miami.

Author contributions

YL and RL designed the research. YL, RC, and GM performed the research. YL and RC analyzed the data. YL and RL wrote the manuscript. All authors contributed to the article and approved the submitted version.

Funding

The Bascom Palmer Eye Institute is supported by NIH Center Core Grant P30EY014801 and a Research to Prevent Blindness Unrestricted Grant (GR004596-1). RL is supported by the Walter G. Ross Foundation. This work was partly supported by the Guitierrez Family Research Fund and the Camiener Foundation Glaucoma Research Fund.

Conflict of interest

The authors declare that the research was conducted in the absence of any commercial or financial relationships that could be construed as a potential conflict of interest.

Publisher's note

References

Baimbridge, K., Celio, M., and Rogers, J. H. (1992). Calcium-binding proteins in the nervous system. *Trends Neurosci.* 15, 303–308. doi: 10.1016/0166-2236(92)90081-I

Barnstable, C., and Dräger, U. (1984). Thy-1 antigen: a ganglion cell specific marker in rodent retina. *Neuroscience* 11, 847–855. doi: 10.1016/0306-4522(84)90195-7

Barron, K., Dentinger, M., Krohel, G., Easton, S., and Mankes, R. (1986). Qualitative and quantitative ultrastructural observations on retinal ganglion cell layer of rat after intraorbital optic nerve crush. *J. Neurocytol.* 15, 345–362. doi: 10.1007/BF01611437

Brini, M., Calì, T., Ottolini, D., and Carafoli, E. (2013). Intracellular calcium homeostasis and signaling. *Met Ions Life Sci.* 12, 119–68. doi: 10.1007/978-94-007-5561-1_5

Casini, G., Rickman, D. W., and Brecha, N. C. (1995). AII amacrine cell population in the rabbit retina: identification by parvalbumin immunoreactivity. *J. Comp. Neurol.* 356, 132–142. doi: 10.1002/cne.903560109

Celio, M. (1990). Calbindin D-28k and parvalbumin in the rat nervous system. *Neuroscience* 35, 375–475. doi: 10.1016/0306-4522(90)90091-H

Chung, H. S., Harris, A., Evans, D. W., Kagemann, L., Garzozi, H. J., and Martin, B. (1999). Vascular aspects in the pathophysiology of glaucomatous optic neuropathy. *Surv. Ophthalmol.* 43, S43–S50. doi: 10.1016/S0039-6257(99)00050-8

Elliott, J. L., and Snider, W. D. (1995). Parvalbumin is a marker of ALS-resistant motor neurons. *Neuroreport* 6, 449–452. doi: 10.1097/00001756-199502000-00011

Gordon, M. O., Beiser, J. A., Brandt, J. D., Heuer, D. K., Higginbotham, E. J., Johnson, C. A., et al. (2002). The ocular hypertension treatment study: baseline factors that predict the onset of primary open-angle glaucoma. *Arch. Ophthalmol.* 120, 714–720. doi: 10.1001/archopht.120.6.714

Gunn, D. J., Gole, G. A., and Barnett, N. L. (2011). Specific amacrine cell changes in an induced mouse model of glaucoma. *Clin. Exp. Ophthalmol.* 39, 555–563. doi: 10.1111/j.1442-9071.2010.02488.x

Haverkamp, S., and Wässle, H. (2000). Immunocytochemical analysis of the mouse retina. *J. Comp. Neurol.* 424, 1–23. doi: 10.1002/1096-9861(20000814)424:1<1::AID-CNE1>3.0.CO;2-V

Hayreh, S. S. (1969). Blood supply of the optic nerve head and its role in optic atrophy, glaucoma, and oedema of the optic disc. *Br. J. Ophthalmol.* 53, 721–748. doi: 10.1136/bjo.53.11.721

Hayreh, S. S., Zimmerman, M. B., Kimura, A., and Sanon, A. (2004). Central retinal artery occlusion.: retinal survival time. *Exp. Eye Res.* 78, 723–736. doi: 10.1016/S0014-4835(03)00214-8

Heijl, A., Leske, M. C., Bengtsson, B., Hyman, L., Bengtsson, B., and Hussein, M. (2002). Reduction of intraocular pressure and glaucoma progression: results from the early manifest glaucoma trial. *Arch. Ophthalmol.* 120, 1268–1279. doi: 10.1001/archopht.120.10.1268

Heizmann, C. (1984). Parvalbumin, and intracellular calcium-binding protein; distribution, properties and possible roles in mammalian cells. *Experientia* 40, 910–921. doi: 10.1007/BF01946439

Heizmann, C. W., Berchtold, M. W., and Rowlerson, A. M. (1982). Correlation of parvalbumin concentration with relaxation speed in mammalian muscles. *Proc. Nat. Acad. Sci. U. S. A.* 79, 7243–7247. doi: 10.1073/pnas.79.23.7243

Hong, C. J. H., Siddiqui, A. M., Sabljic, T. F., and Ball, A. K. (2016). Changes in parvalbumin immunoreactive retinal ganglion cells and amacrine cells after optic nerve injury. *Exp. Eye Res.* 145, 363–372. doi: 10.1016/j.exer.2015.11.005

John, S. W., Smith, R. S., Savinova, O. V., Hawes, N. L., Chang, B., Turnbull, D., et al. (1998). Essential iris atrophy, pigment dispersion, and glaucoma in DBA/2J mice. *Invest. Ophthalmol. Vis. Sci.* 39, 951–962.

Kamat, S. S., Gregory, M. S., and Pasquale, L. R. (2016). The role of the immune system in glaucoma: Bridging the divide between immune mechanisms in experimental glaucoma and the human disease. *Semin. Ophthalmol.* 31, 147–154. doi: 10.3109/08820538.2015.1114858

Kass, M. A., Heuer, D. K., Higginbotham, E. J., Johnson, C. A., Keltner, J. L., Miller, J. P., et al. (2002). The ocular hypertension treatment study: a randomized trial determines that topical ocular hypotensive medication delays or prevents the onset of primary open-angle glaucoma. *Arch. Ophthalmol.* 120, 701–713. doi: 10.1001/archopht.120.6.701

Kim, T., and Jeon, C. (2006). Morphological classification of parvalbumin-containing retinal ganglion cells in mouse: single-cell injection after immunocytochemistry. *Invest. Ophthalmol. Vis. Sci.* 47, 2757–2764. doi: 10.1167/iovs.05-1442

Kim, S., Jeon, J. H., Son, M. J., Cha, J., Chun, M., and Kim, I. (2010). Changes in transcript and protein levels of calbindin D28k, calretinin and parvalbumin, and numbers of neuronal populations expressing these proteins in an ischemia model of rat retina. *Anat. Cell Biol.* 43, 218–229. doi: 10.5115/acb.2010.43.3.218

Konosu, S., Hamoir, G., and Pechere, J. (1965). Carp myogens of white and red muscles. Properties and amino acid composition of the main low-molecular-weight components of white muscle. *Biochem. J.* 96, 98–112. doi: 10.1042/bj0960098

Kretsinger, R. H., and Nockolds, C. E. (1973). Carp muscle calcium-binding protein. II. Structure determination and general description. *J. Biol. Chem.* 248, 3313–3326. doi: 10.1016/S0021-9258(19)44043-X

Laslo, P., Lipski, J., Nicholson, L. F., Miles, G. B., and Funk, G. D. (2000). Calcium binding proteins in motoneurons at low and high risk for degeneration in ALS. *Neuroreport* 11, 3305–3308. doi: 10.1097/00001756-200010200-00009

Leske, M. C., Heijl, A., Hyman, L., Bengtsson, B., Dong, L., Yang, Z., et al. (2007). Predictors of long-term progression in the early manifest glaucoma trial. *Ophthalmology* 114, 1965–1972. doi: 10.1016/j.ophtha.2007.03.016

Leung, C. K., Lindsey, J. D., Crowston, J. G., Lijia, C., Chiang, S., and Weinreb, R. N. (2008). Longitudinal profile of retinal ganglion cell damage after optic nerve crush with blue-light confocal scanning laser ophthalmoscopy. *Invest. Ophthalmol. Vis. Sci.* 49, 4898–4902. doi: 10.1167/iovs.07-1447

Li, Y., Schlamp, C. L., and Nickells, R. W. (1999). Experimental induction of retinal ganglion cell death in adult mice. *Invest. Ophthalmol. Vis. Sci.* 40, 1004–1008.

Libby, R. T., Anderson, M. G., Pang, I., Robinson, Z. H., Savinova, O. V., Cosma, I. M., et al. (2005). Inherited glaucoma in DBA/2J mice: pertinent disease features for studying the neurodegeneration. *Vis. Neurosci.* 22, 637–648. doi: 10.1017/S0952523805225130

Munguba, G. C., Geisert, E. E., Williams, R. W., Tapia, M. L., Lam, D. K., Bhattacharya, S. K., et al. (2013). Effects of glaucoma on Chrna6 expression in the retina. *Curr. Eye Res.* 38, 150–157. doi: 10.3109/02713683.2012.724512

Nockolds, C. E., Kretsinger, R. H., Coffee, C. J., and Bradshaw, R. A. (1972). Structure of a calcium-binding carp myogen. *Proc. Natl. Acad. Sci. U. S. A.* 69, 581–584. doi: 10.1073/pnas.69.3.581

Orrenius, S., Zhivotovsky, B., and Nicotera, P. (2003). Regulation of cell death: the calcium–apoptosis link. *Nat. Rev. Mol. Cell Biol.* 4, 552–565. doi: 10.1038/nrm1150

Pease, M. E., McKinnon, S. J., Quigley, H. A., Kerrigan-Baumrind, L. A., and Zack, D. J. (2000). Obstructed axonal transport of BDNF and its receptor TrkB in experimental glaucoma. *Invest. Ophthalmol. Vis. Sci.* 41, 764–774.

Quigley, H. A., and Broman, A. T. (2006). The number of people with glaucoma worldwide in 2010 and 2020. *Br. J. Ophthalmol.* 90, 262–267. doi: 10.1136/bjo.2005.081224

Quigley, H. A., McKinnon, S. J., Zack, D. J., Pease, M. E., Kerrigan-Baumrind, L. A., Kerrigan, D. F., et al. (2000). Retrograde axonal transport of BDNF in retinal ganglion cells is blocked by acute IOP elevation in rats. *Invest. Ophthalmol. Vis. Sci.* 41, 3460–3466.

Rodriguez, A. R., Müller, S., Pérez, L., and Brecha, N. C. (2014). The RNA binding protein RBPMS is a selective marker of ganglion cells in the mammalian retina. *J. Comp. Neurol.* 522, 1411–1443. doi: 10.1002/cne.23521

Sanna, P. P., Keyser, K. T., Celio, M. R., Karten, H. J., and Bloom, F. E. (1993). Distribution of parvalbumin immunoreactivity in the vertebrate retina. *Brain Res.* 600, 141–150. doi: 10.1016/0006-8993(93)90412-G

Schlamp, C. L., Li, Y., Dietz, J. A., Janssen, K. T., and Nickells, R. W. (2006). Progressive ganglion cell loss and optic nerve degeneration in DBA/2J mice is variable and asymmetric. *BMC Neurosci.* 7:66. doi: 10.1186/1471-2202-7-66

Schwaller, B. (2010). Cytosolic Ca2+ buffers. *Cold Spring. Harb. Perspect. Biol.* 2:a004051. doi: 10.1101/cshperspect.a004051

Templeton, J. P., Nassr, M., Vazquez-Chona, F., Freeman-Anderson, N. E., Orr, W. E., Williams, R. W., et al. (2009). Differential response of C57BL/6J mouse and DBA/2J mouse to optic nerve crush. *BMC Neurosci.* 10:90. doi: 10.1186/1471-2202-10-90

Tezel, G. (2013). Immune regulation toward immunomodulation for neuroprotection in glaucoma. *Curr. Opin. Pharmacol.* 13, 23–31. doi: 10.1016/j.coph.2012.09.013

Tham, Y., Li, X., Wong, T. Y., Quigley, H. A., Aung, T., and Cheng, C. (2014). Global prevalence of glaucoma and projections of glaucoma burden through 2040: a systematic review and meta-analysis. *Ophthalmology* 121, 2081–2090. doi: 10.1016/j.ophtha.2014.05.013

Van Den Bosch, L., Schwaller, B., Vleminckx, V., Meijers, B., Stork, S., Ruehlicke, T., et al. (2002). Protective effect of parvalbumin on excitotoxic motor neuron death. *Exp. Neurol.* 174, 150–161. doi: 10.1006/exnr.2001.7858

Wäussle, H., Grüunert, U., and Röhrenbeck, J. (1993). Immunocytochemical staining of AII-amacrine cells in the rat retina with antibodies against parvalbumin. *J. Comp. Neurol.* 332, 407–420. doi: 10.1002/cne.903320403

Yi, C., Yu, S., Lee, E., Lee, J., and Jeon, C. (2012). Types of parvalbumin-containing retinotectal ganglion cells in mouse. *Acta Histochem. Cytochem.* 45, 201–210. doi: 10.1267/ahc.11061

Frontiers in Neuroscience

Provides a holistic understanding of brain function from genes to behavior

Part of the most cited neuroscience journal series which explores the brain - from the new eras of causation and anatomical neurosciences to neuroeconomics and neuroenergetics.

Discover the latest Research Topics

See more →

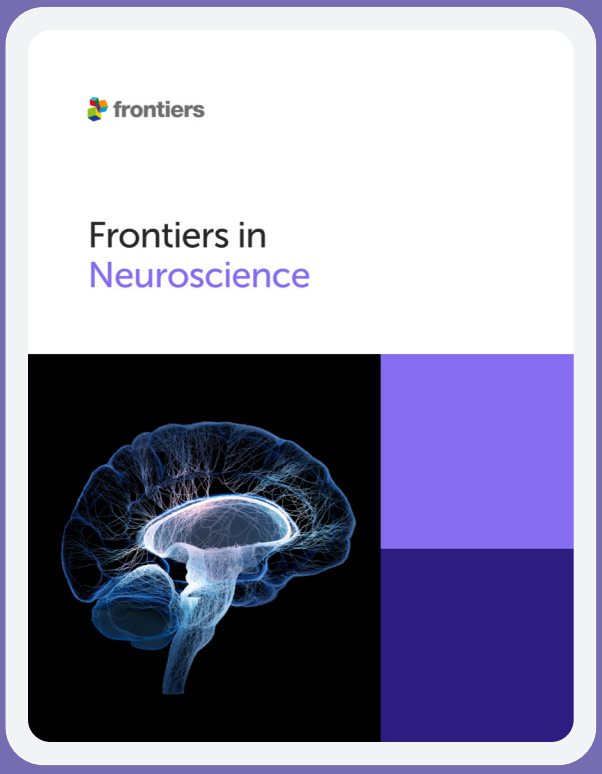

Frontiers

Avenue du Tribunal-Fédéral 34
1005 Lausanne, Switzerland
frontiersin.org

Contact us

+41 (0)21 510 17 00
frontiersin.org/about/contact